AD NUMBER

AD387189

CLASSIFICATION CHANGES

TO: unclassified

FROM: confidential

LIMITATION CHANGES

TO:

Approved for public release, distribution unlimited

FROM:

Distribution authorized to U.S. Gov't. agencies and their contractors; Adminstrative/Operational Use; Jan 1968. Other requests shall be referred to AFRPL [RPPR/STINFO], Edwards AFB, CA 93523.

AUTHORITY

AFRPL ltr dtd 15 Mar 1971; AFRPL ltr dtd 5 Feb 1986

CONFIDENTIAL

AFRPL-TR-67-280

(Unclassified Title)

FINAL REPORT ADVANCED CRYOGENIC ROCKET ENGINE PROGRAM, AEROSPIKE NOZZLE CONCEPT VOLUME I

F. B. Lary
Rocketdyne
A Division of North American Rockwell Corporation
6633 Canoga Ave.
Canoga Park, California

Technical Report AFRPL-TR-67-280

January 1968

Group 4
Downgraded at 3-Year Intervals
Declassified After 12 Years

In addition to security requirements which must be met, this document is subject to special export controls and each transmittal to foreign governments or foreign nationals may be made only with prior approval of AFRPL (RPPR/STINFO), Edwards, California, 93523.

Air Force Rocket Propulsion Laboratory
Air Force Systems Command
United States Air Force
Edwards Air Force Base, California

CONFIDENTIAL

When U.S. Government drawings, specifications, or other data are used for any purpose other than a definitely related Government procurement operation, the Government thereby incurs no responsibility nor any obligation whatsoever, and the fact that the Government may have formulated, furnished or in any way supplied the said drawings, specifications, or other data, is not to be regarded by implication or otherwise, or in any manner licensing the holder or any other person or corporation, or conveying any rights or permission to manufacture, use, or sell any patented invention that may in any way be related thereto.

In addition to security requirements which must be met, this document is subject to special export controls and each transmittal to foreign governments or foreign nationals may be made only with prior approval of AFRPL (RPPR/STINFO), Edwards, California 93523.

This material contains information affecting the national defense of the United States within the meaning of the espionage laws, Title 18 U.S.C., Sections 793 and 794, the transmission or revelation of which in any manner to an unauthorized person is prohibited by law.

ERRATA

1. Page 28, paragraph 2, line 4 (Unclassified)
2. Page 28, paragraph 3, line 25 (Confidential)
3. Page 94, paragraph 3, line 9 (Confidential)
4. Page 197, paragraph 2, line 10 (Confidential)
5. Page 197, paragraph 3, line 21 (Confidential)
6. Page 213, paragraph 4, line 13 (Confidential)
7. Page 287, Figure 125 (Confidential)
8. Page 379, paragraph 1, line 1 (Confidential)
9. Page 442, paragraph 2, line 14 (Confidential)
10. Page 549, line 31, title (Confidential)
11. Page 642, paragraph 3, line 12 (Confidential)
12. Page 642, paragraph 4, line 21 (Unclassified)
13. Page 765, paragraph 5, line 21 (Confidential)
14. Page 809, Figure 370 (Confidential)
15. Page 866, paragraph 2, line 9 (Confidential)

AFRPL-TR-67-280

(Unclassified Title)

FINAL REPORT, ADVANCED CRYOGENIC ROCKET ENGINE PROGRAM, AEROSPIKE NOZZLE CONCEPT

(VOLUME I)

F. B. Lary
Rocketdyne,
A Division of North American Rockwell Corporation
6633 Canoga Ave.
Canoga Park, California

Technical Report AFRPL-TR-67-280

January 1968

Group 4
Downgraded at 3-Year Intervals
Declassified After 12 Years

In addition to security requirements which must be met, this document is subject to special export controls and each transmittal to foreign governments or foreign nationals may be made only with prior approval of AFRPL (RPPR/STINFO), Edwards, California, 93523.

Air Force Rocket Propulsion Laboratory
Air Force Systems Command
United States Air Force
Edwards Air Force Base, California

FOREWORD

This report presents the work accomplished on Phase I of the Advanced Cryogenic Rocket Engine Program, Aerospike Nozzle Concept under Air Force Contract AF04(611)-11399. The work reported herein was conducted by Rocketdyne, A Division of North American Rockwell Corporation, 6633 Canoga Avenue, Canoga Park, California, under the Technical direction of Capt. Vernon L. Mahugh, Project Engineer, Air Force Rocket Propulsion Laboratory, Edwards, California. This report covers the contract period 1 March 1966 through 21 October 1967.

A portion of the design and tooling effort in Task II represents a joint effort with the Advanced Engineering Program, System and Dynamic Investigation (Aerospike), Contract NAS8-19.

Classified information has been extracted from documents listed under References.

This report, submitted January 1968, has been assigned Rocketdyne Report No. R-7168, Volumes I and II.

This technical report has been reviewed and is approved.

Vernon L. Mahugh
Capt, USAF
Project Engineer
Air Force Rocket Propulsion Laboratory

Ernie D. Braunschweig
Capt, USAF
Program Manager
Air Force Rocket Propulsion Laboratory

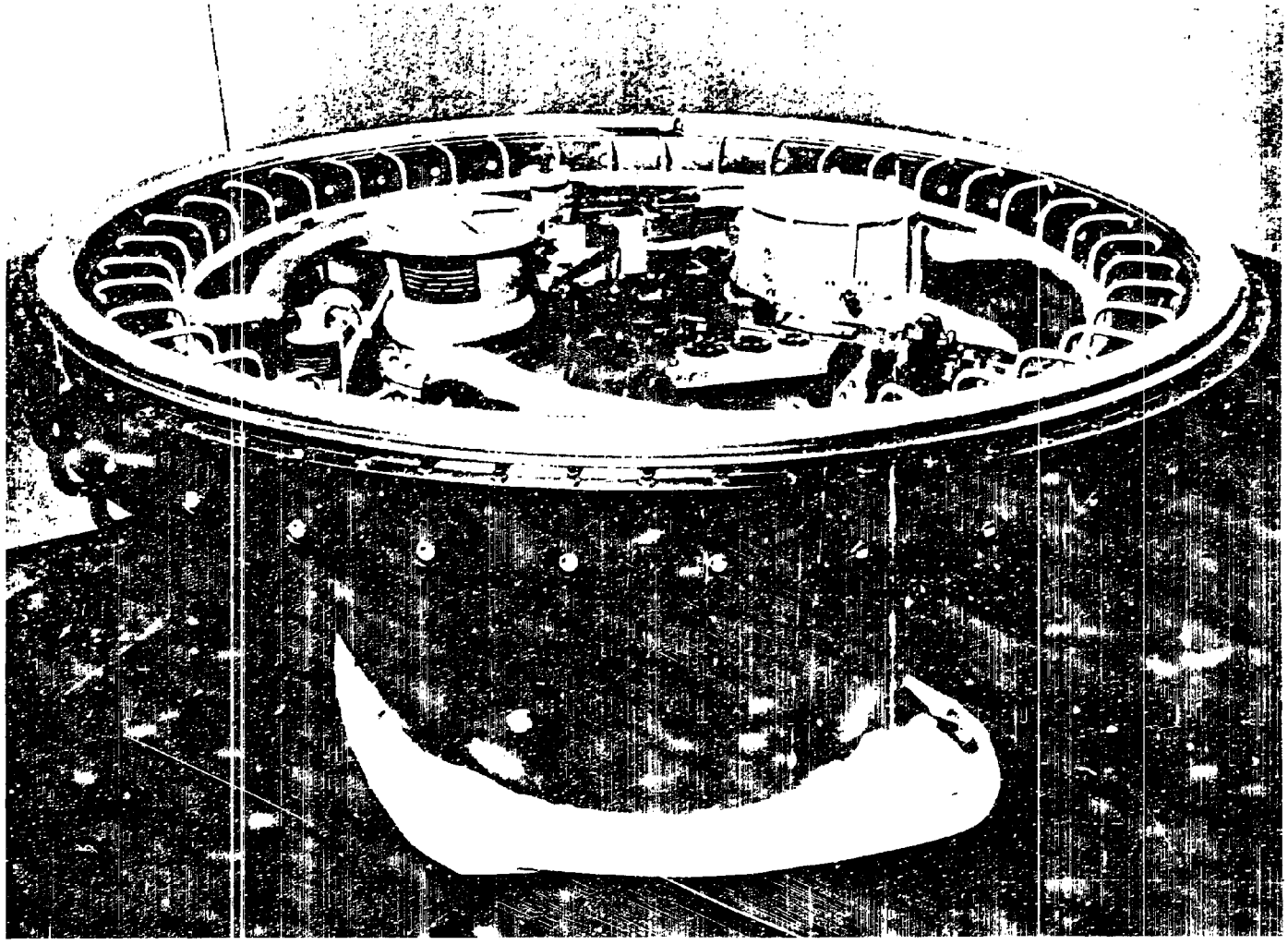

Frontispiece. Aerospike Flight Engine Mockup

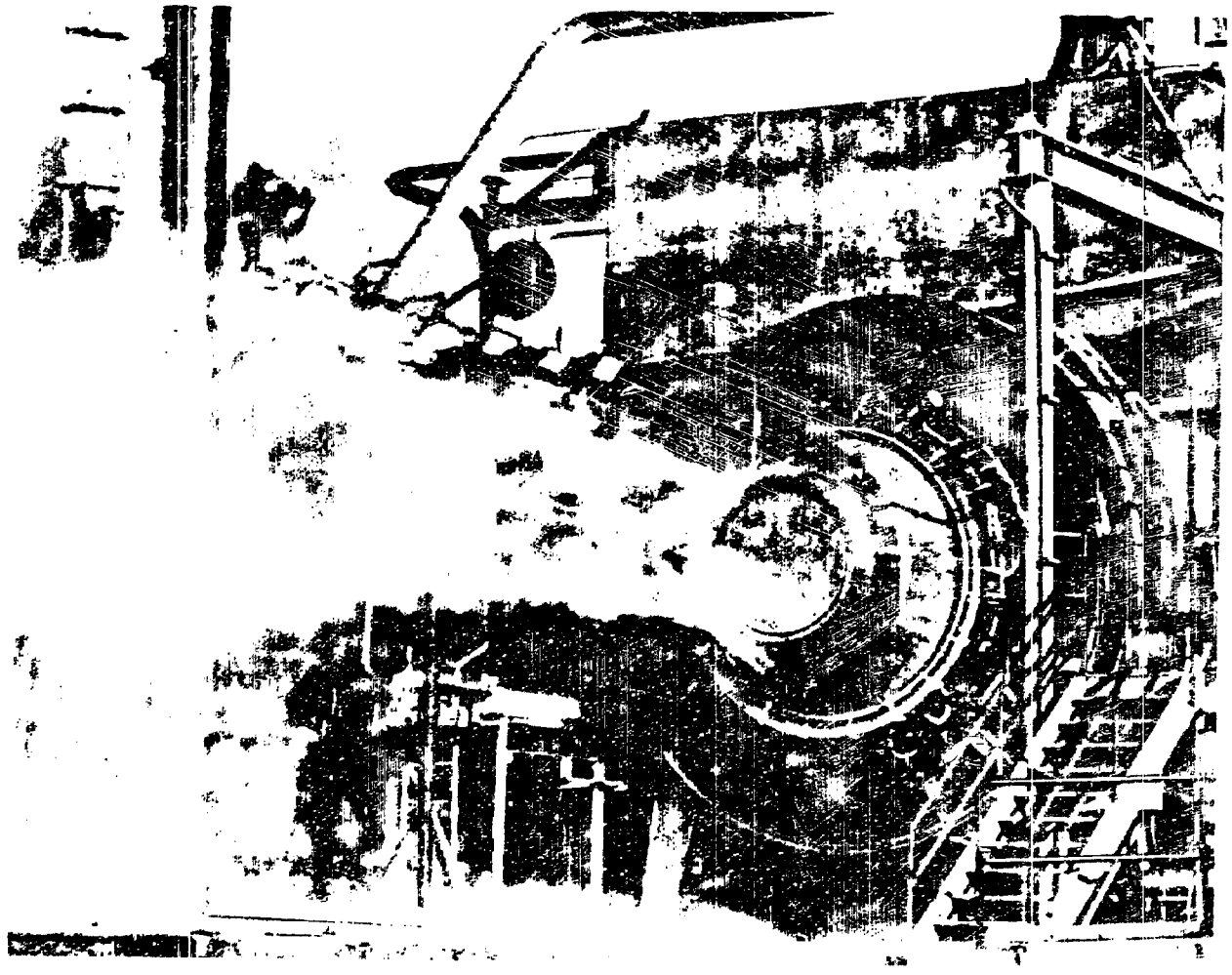

1XW24-9/29/67-R1*

Frontispiece: 250K Tube-Wall Test and Firing at Nevada Field Laboratory

ABSTRACT

(U) Technical results obtained at the completion of the contract effort are described for the Advanced Cryogenic Rocket Engine Program, Aerospike. This program includes analysis and preliminary design of an advanced rocket engine using an aerospike nozzle and experimental evaluation of critical technology related to the aerospike concept. Component and system features, physical arrangements, design parameters and details, operational characteristics, and performance have been established for an optimum demonstrator engine. Studies were made of application of a flight engine to certain vehicles. Experimental injector performance investigations and experimental cooling investigations on segment chambers were conducted, producing the target combustion performance. Various materials were studied for long life of thrust chamber cooling passages and the target life was demonstrated. Full-scale, cooled thrust chambers were fabricated and tested for overall combustor and nozzle performance demonstrations. Injector failure limited these tests; however, nozzle and combustor performance were as predicted when not influenced by excess leakage. Structural and cooling evaluations were conducted on a segment embodying essential elements of the Demonstrator chamber design.

CONTENTS

Volume I

Volume II

ILLUSTRATIONS

(This page is Unclassified)

TABLES

NOMENCLATURE

Symbol	Parameter	Units
A	area	$in.^2$
A*	aerodynamic threat area	$in.^2$
A_t	geometric throat area	$in.^2$
A_{otv}	oxidizer turbine throttle valve area	$in.^2$
A_{ttv}	tapoff throttle valve area	$in.^2$
C	turbine nozzle isentropic gas velocity	ft/sec
C_F	thrust coefficient	—
C_p	specific heat at constant pressure	Btu/lbm-R
C_T	overall nozzle efficiency	—
C_v	primary nozzle velocity coefficient	—
DN	bore diameter x speed	mm x rev/min
E	modules of elasticity	psi
F	thrust	lbf
F_{tu}	ultimate tensile strength	psi
F_{ty}	tensile yield strength	psi
G_c	coolant mass velocity	$lbm/in.^2$-sec
GPM	fluid flowrate	gal/min
GH_2	gaseous hydrogen	—
GN_2	gaseous nitrogen	—
GO_2, GOX	gaseous oxygen	—
HGI	hot-gas-ignition	—
I_s	specific impulse	lbf/sec/lbm
K	one thousand	(as noted)

Symbol	Parameter	Units
LH_2	liquid hydrogen	—
LO_2, LOX	liquid oxygen	—
MFV	main fuel valve	—
MR	mixture ratio, oxidizer-to-fuel	$(lbm)_o/(lbm)_f$
N, rpm	rotational speed	rev/min
N_{cy}	number of cycles to fatigue failure	—
NPSH	net positive suction head	feet
N_{NU}	Nusselt number	—
N_{PR}	Prandtl number	—
N_{RE}	Reynolds number	—
N_{ST}	Stanton number	—
OFHC	oxygen-free-high-conductivity	—
P	pressure	psia
P_c	nozzle throat stagnation pressure	psia
P_D	pump discharge	—
Q	volumetric flowrate	(as noted)
Q/A	local heat flux	$Btu/in.^2-sec$
$R_{dynamic}$	module dynamic envelop radius	in.
T	temperature	R, (as noted)
U	blade speed	ft/sec
c*	characteristic velocity	ft/sec
fps	—	ft/sec
g	gravitational constant (32.2)	$lbm-ft/lbf-sec^2$
h_g	gas-side heat transfer coefficient	$Btu/in.^2-sec-R$

Symbol	Parameter	Units
k	spring rate	lbf/in.
*cfm	standard flowrate	ft^3/min
t	wall thickness	inches
$\dot{w}$	mass flowrate	Btu/sec
α	coefficient of thermal expansion	in./in.-R
γ	specific heat ratio	—
ϵ	nozzle expansion area ratio	—
ϵ_R	surface roughness	microinches
η	efficiency	—
η_{Po}	injector-end stagnation pressure/ nozzle throat stagnation pressure	—
η_T	friction influence coefficient	—
θ^*	throat flow angle	degree
μ	Poisson's ratio	—
ρ	density	lbm/ft^3
σ	standard deviation	—
σ_{hyd}	hydraulic stress	psi
σ_y	yield strength	psi
τ	ratio of secondary-to-primary flow	(by weight)
φ_c	coolant curvature heat transfer enhancement factor	—
φ_E	coolant entrance heat transfer enhancement factor	—
φ_ϵ	coolant roughness heat transfer enhancement factor	—

Subscripts

B	bulk temperature
D	discharge
Ref	reference
Reg	regulator
a, amb	ambient
b	base
c	chamber
d	drag
e	exit
f	fuel
g	geometric
k	kinetic
o	oxidizer
p	primary
s	secondary
t	total flow
v, vac	cacuum
w	wall
cc	combustion chamber
ct	coolant
eng	engine
fc	film coolant
gg	gas generator
ie	injector end

Subscripts

inj	injector
pf	potential flow
tc	thrust chamber
to	tapoff
wc, wl	coolant-side-wall
wg	gas-side-wall
$\bar{}$(bar)	average
$'$(prime)	flight system

INTRODUCTION

(U) The Advanced Cryogenic Rocket Engine Program, Aerospike Nozzle Concept, started 1 March 1966 with a 17-month duration (later increased to 20 months). The objectives were to evaluate critical technology associated with the aerospike concept and produce the preliminary design of an advanced hydrogen-oxygen engine of the characteristics given in Table 1.

(U) Technology deemed critical to the aerospike concept for the foregoing engine were injector-combustor design, cooling tube life, full-scale combined chamber and nozzle performance and stability, throttling, ignition, and chamber structure. Several annular type injectors had been operated; however, the definition and characterization of an injector for the specified operating range and performance remained to be done. It was necessary to select a tube material for the specified life and operating requirements and demonstrate the ability to cool under these conditions. Several aerospike thrust chambers had proved the nozzle concept, and it was then desired to demonstrate the full performance potential of the nozzle at ground level and altitude over a wide throttling and mixture ratio range with a high-performance injector. Lastly, it was necessary to evaluate the ability of a lightweight structure to maintain a predictable throat area and the cooling and sealing of this structural tie across the chamber over the throttling range.

(U) The total effort was comprised of two major tasks:

Task 1, Analysis and Design

- A. Module Design
- B. Application Study

Task 2, Fabrication and Test

- A. Injector Performance Investigations
- B. Thrust Chamber Cooling Investigation
- C. Thrust Chamber Nozzle Demonstration
- D. Segment Structural Evaluation

TABLE 1

(C) ENGINE CHARACTERISTICS

Nominal Vacuum Thrust, pounds	250,000 at nominal mixture ratio
Minimum Delivered Specific Impulse	96% of theoretical shifting I_{sp} at rated thrust 95% of theoretical shifting I_{sp} during throttling
Throttling Range	Continuous down to 20 percent of rated thrust
Overall Mixture Ratio Range	Engine operation from 5.0 to 7.0 Nominal design point 6.0
Expansion Ratio	Aera ratio(s) representative of booster and upper-stage applications. Overall static engine diameter will not exceed 100 inches.
Durability	10 hours time between overhauls, 100 reuses, 300 starts, 300 thermal cycles, 10,000 valve cycles
Single Continuous Run Duration	Capability from 10 seconds to 600 seconds
Engine Starts	Multiple restart at sea level or altitude
Thrust Vector Control	Amplitude: ±7 degrees; Rate: 30 deg/sec; Acceleration: 30 rad/sec^2
Control Capability	+3 percent accuracy in thrust and mixture ratio at rated thrust. Excursions from extreme to extreme in thrust or mixture ratio within 5 seconds.
Propellant Conditions at Engine Inlets	LO_2: 16 feet NPSH from 1 atmosphere boiling temperature to 180 degrees LH_2: 60 feet NPSH from 1 atmosphere boiling temperature to 45 R
Environmental Conditions	Sea level to vacuum conditions Combined accelerations: 10 g axial with 2 g transverse, 6.5 g axial with 3 g transverse, 3 g axial with 6 g transverse
Engine Vehicle Interface Conditions	The engine will receive no external power, with the exception of normal electrical power and 3000 psia helium from the vehicle.

(U) As work progressed, the status and progress made was reported in (Ref. 1) quarterly progress reports, first through sixth. Technical effort on this contract terminated 31 October 1967. This report covers all of the technical work for the 20-month period supplemented as noted herein by two other special area reports. The first is a special report on the Application Study (Ref. 2), Task IB, and the second is the Materials and Process R&D report (Ref. 3) covering the fabrication techniques used during this program.

CONTENTS

SUMMARY

MODULE DESIGN

(U) The objective of this task was to formulate a preliminary design of an aerospike engine to provide: (1) demonstrated high performance over the specified thrust and mixture ratio range, (2) versatility to operate efficiently and repeatedly at any altitude, and (3) long-life capability sufficient to perform any missions between overhauls. The specific requirements are delineated in Table I. A functional analysis of the engine system and its requirements led to a series of tradeoff studies to establish the configuration.

(U) The cycle selection involved a tradeoff between the tapoff cycle and the gas generator cycle, and between a series and parallel turbine arrangement. A parallel turbine tapoff cycle was selected because it offered a simpler, lighter-weight system with better start characteristics and higher performance during throttling.

(C) The thrust chamber parameter selection included the selection of a straight-walled combustion chamber because of increased performance and simplified chamber construction. The chamber pressure was established at 1500 psia (nozzle stagnation pressure) based on advanced vehicle application studies, and heat transfer analysis confirmed that this was within the limits of regenerative cooling using nickel tubes. The nozzle area ratio is fixed by the prescribed 100-inch-diameter, the 250K thrust level, thrust chamber geometry, and the chamber pressure selection. The Demonstrator Engine area ratio is 74.1:1. The nozzle length was optimized on a performance-weight basis at 25 percent of the length of a 15-degree half-angle cone of the same area ratio.

(U) The throttling and mixture ratio control system selection involved a study of the possible control points, control logic, and operating envelopes Hot-gas valves located in series, one in the main tapoff duct

to control thrust and one in the oxidizer turbine inlet duct to control engine mixture ratio, were selected because of higher performance, lighter weight, and control flexibility. A closed-loop logic system was selected to meet the accuracy, safety, and response requirements of the engine system. A mixture ratio excursion at constant chamber pressure was selected instead of a constant-thrust excursion because of control system simplifications and more favorable vehicle application results.

(U) A hot-gas ignition system was selected for the thrust chamber because it promised light engine weight, rapid tank head start, unlimited restart capability, uniform ignition, and high reliability. A spark ignition system similar to the J-2 gas generator was selected for the central hot-gas igniter because it offered a simple, lightweight system with demonstrated reliability.

(U) A two-stage centrifugal design was selected for the fuel pump because it offered low weight and high efficiency together with good stall characteristics. A single-stage centrifugal design was selected for the oxidizer pump because the low head and medium flowrate are ideally suited to such a design. Axial flow preinducers were selected for both pumps, with hydraulic turbines used for the driving power. Because hydrodynamic considerations dictated different speed ratios, the hydraulic turbine was located behind the preinducer in the fuel pump, and in the preinducer hub in the oxidizer pump. Three-row, velocity-compounded turbines were selected to power the pumps because they offered the best performance vs weight tradeoff.

(U) A mechanical gimbal system was selected because it has the characteristics of high reliability, versatility, long life, and low cost.

Engine System

(U) The Demonstrator Module schematic, showing basic elements and propellant flow paths, is shown in Fig. 1. Individual oxidizer and fuel turbopumps are used with the turbines driven in parallel by hot gases tapped from the main combustion chamber during mainstage operation. The exhaust from the turbines is discharged through the base closure into the nozzle base region, producing an increase in base pressure that contributes to

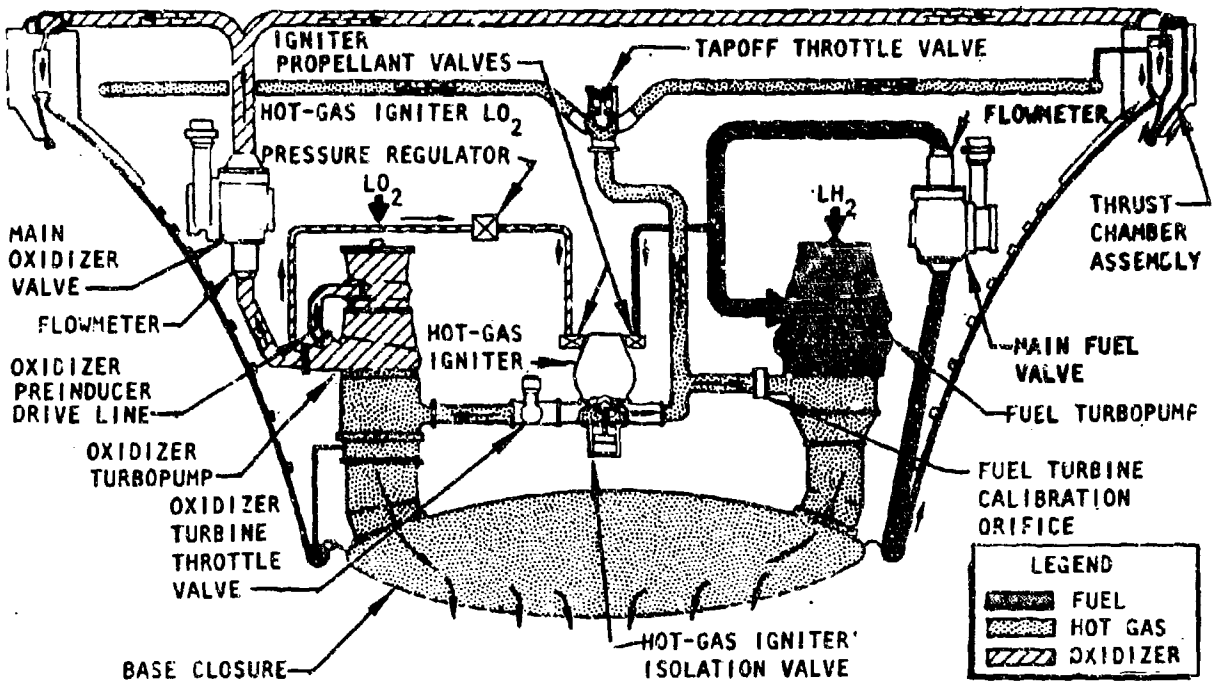

Figure 1. Demonstrator Module Schematic

total thrust. The complete thrust chamber and injector are regeneratively cooled with fuel. Thrust control is achieved with the tapoff throttle valve located at the Y-junction of the two tapoff hot-gas ducts. Engine mixture ratio is controlled by a throttle valve located at the oxidizer turbine inlet. Ignition is accomplished under tank head pressures with the use of a separate hot-gas igniter (HGI). This component produces hot

gases which are discharged into the turbine drive ducting and used to provide both the initial turbine spin and the ignition energy source for the main chamber. The temperature of the hot-gas igniter is controlled by an automatic oxidizer pressure regulator in the HGI inlet line. Once main chamber ignition is achieved, the HGI is shut down with its own liquid propellant shutoff valves, and the combustor body is isolated from the tapoff system by closing the HGI isolation valve. Engine shutdown is achieved simply by closing the oxidizer turbine valve and sequencing the main propellant valves to provide a fuel-rich cutoff.

(U) The projected operating parameters are shown in Table 2. The general arrangement of components and subsystems and major dimensions of the engine are shown in the layout, Fig. 2.

(U) The thrust structure provides support pads for the turbopumps hot-gas igniter, control components, and interface panels. Accessibility for system checkout and component repair has been provided in the design by making the thrust chamber easily removable from the thrust structure. This exposes all the major components, which are mounted directly to the six radial beams of the thrust structure. The base closure also is removable from the thrust chamber to provide access to the internal cavity from below without removal of the thrust chamber (Fig. 3).

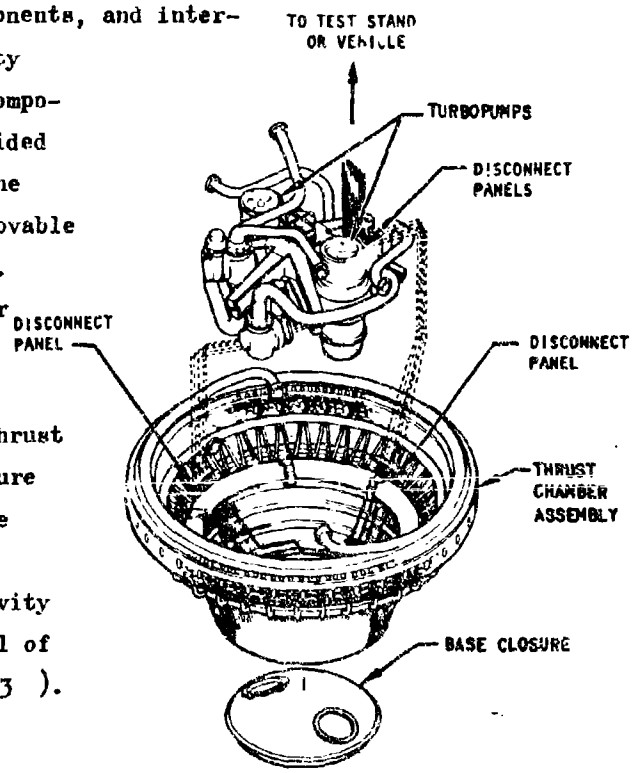

Figure 3. Engine Accessibility

TABLE 2A

(C) DEMONSTRATOR MODULE OPERATING CHARACTERISTICS

	Mixture Ratio, o/f = 5		Mixture Ratio, o/f = 6		Mixture Ratio, o/f = 7	
	Rated Thrust	20-Percent Thrust	Rated Thrust	20-Percent Thrust	Rated Thrust	20-Percent Thrust
Engine						
Vacuum Performance						
Thrust, pounds	244,200	48,700	250,000	50,000	254,500	50,850
Specific Impulse, seconds	455.0	446.1	450.1	443.8	441.7	431.8
Efficiency (Ref. Mixture Ratio Engine, Tank Conditions)	0.9731	0.960*	0.9701	0.960*	0.9618	0.947*
Sea Level Performance						
Thrust, pounds	205,000	31,200	206,000	32,400	208,000	33,100
Specific Impulse, seconds	376	287	371	289	362	282
Oxidizer						
Inlet Pressure, psia	37.5	37.5	37.5	37.5	37.5	37.5
Inlet Temperature, R	175.5	175.5	175.5	175.5	175.5	175.5
Flowrate, lb/sec	449.2	91.0	476.1	96.6	504.5	103.0
Fuel						
Inlet Pressure, psia	32	32	32	32	32	32
Inlet Temperature, R	41.7	41.7	41.7	41.7	41.7	41.7
Flowrate, lb/sec	89.8	18.2	79.3	16.1	72.1	14.7
Thrust Chamber Assembly						
Primary Nozzle **						
Chamber Pressure (Nozzle Stagnation), psia	1500	325	1500	325	1500	325
Mixture Ratio, o/f	5.40	5.18	6.50	6.23	7.62	7.30
Oxidizer Flowrate, lb/sec	443.3	90.4	470.8	96.0	499.6	102.5
Fuel Flowrate, lb/sec	82.2	17.4	72.4	15.4	65.6	14.0
Vacuum Thrust Coefficient	1.945	1.837	1.990	1.891	1.934	1.924
Characteristic Velocity, ft/sec	7797	7660	7540	7410	7246	7068
Throat Area, $in.^2$ (Geometric)	85.1	79.2	85.1	79.2	85.1	79.2
Expansion Area Ratio (Aerodynamic)	74.1	79.6	74.1	79.6	74.1	79.6
Percent Length of 15-Degree Cone	25	25	25	25	25	25
Vacuum Thrust Coefficient Efficiency (Nozzle)	0.9499	0.9430	0.9510	0.9414	0.9509	0.937
Characteristic Velocity Efficiency	0.996	0.980	0.996	0.985	0.996	0.980
Base Region						
Vacuum Pressure, psia	4.60	0.76	4.33	0.72	4.16	0.70
Flowrate, lb/sec	13.55	1.32	12.20	1.21	11.47	1.19

*Throttled engine efficiency referenced to full thrust throat area (ε = 74.1)

**Injector MR and flowrate are the same as for the engine. Differences between engine flowrates and MR above and primary nozzle shown below reflect tapoff requirements.

(C) TABLE 2B

DEMONSTRATOR MODULE OPERATING CHARACTERISTICS

	Mixture Ratio, o/f = 5		Mixture Ratio, o/f = 6		Mixture Ratio, o/f =	
	Rated Thrust	20-Percent Thrust	Rated Thrust	20-Percent Thrust	Rated Thrust	20-Percent Thrust
Fuel Turbopump						
Pump						
Inlet Pressure, psia	32	32	32	32	32	32
Inlet Temperature, R	41.8	41.8	41.8	41.8	41.8	41.8
NPSH (Minimum Required), feet	60	60	60	60	60	60
Discharge Pressure, psia	2942	601	2756	567	2542	547
Head, feet	90,800	18,800	85,600	17,800	81,800	17,200
Flowrate, lb/sec	89.8	18.2	79.3	16.1	72.1	14.7
Speed, rpm	36,800	15,500	35,000	15,100	33,600	14,500
Shaft Horsepower, bhp	19,860	999	16,560	875	14,460	805
Efficiency	0.75	0.641	0.75	0.610	0.747	0.584
Turbine						
Inlet Pressure (Total), psia	1166	113	1000	100	892	94.7
Inlet Temperature, R	1960	1960	1960	1960	1960	1960
Exit Pressure (Static), psia	76.9	8.2	66.7	7.4	61.1	7.2
Flowrate, lb/sec	10.34	1.00	8.86	0.89	7.93	0.84
Speed, rpm	36,800	15,500	35,000	15,100	33,600	14,500
Shaft Horsepower, bhp	19,860	999	16,560	875	14,460	805
Efficiency	0.637	0.337	0.622	0.337	0.611	0.33
Oxidizer Turbopump						
Pump						
Inlet Pressure, psia	37.5	37.5	37.5	37.5	37.5	37.5
Inlet Temperature, R	175.5	175.5	175.5	175.5	175.5	175.5
NPSP (Minimum Required), feet	16	16	16	16	16	16
Discharge Pressure, psia	1996	348	2060	350	2118	353
Head, feet	4020	650	4150	694	4263	660
Flowrate, lb/sec	449.2	91.0	476.1	96.6	504.5	103.0
Speed, rpm	24,400	9200	25,000	9250	25,600	935.0
Shaft Horsepower, bhp	4591	193	5019	199	5486	207
Efficiency	0.73	0.557	0.73	0.58	0.728	0.596
Turbine						
Inlet Pressure (Total), psia	715	69	750	71.9	795	78.5
Inlet Temperature, R	1960	1960	1960	1960	1960	1960
Exit Pressure (Static), psia	44.1	4.5	40	4.4	38.8	4.4
Flowrate, lb/sec	3.19	0.31	3.34	0.32	3.54	0.35
Speed, rpm	24,400	9200	25,000	9250	25,600	9350
Shaft Horsepower, bhp	4591	193	5019	199	5486	207
Efficiency	0.470	0.205	0.474	0.21	0.480	0.19

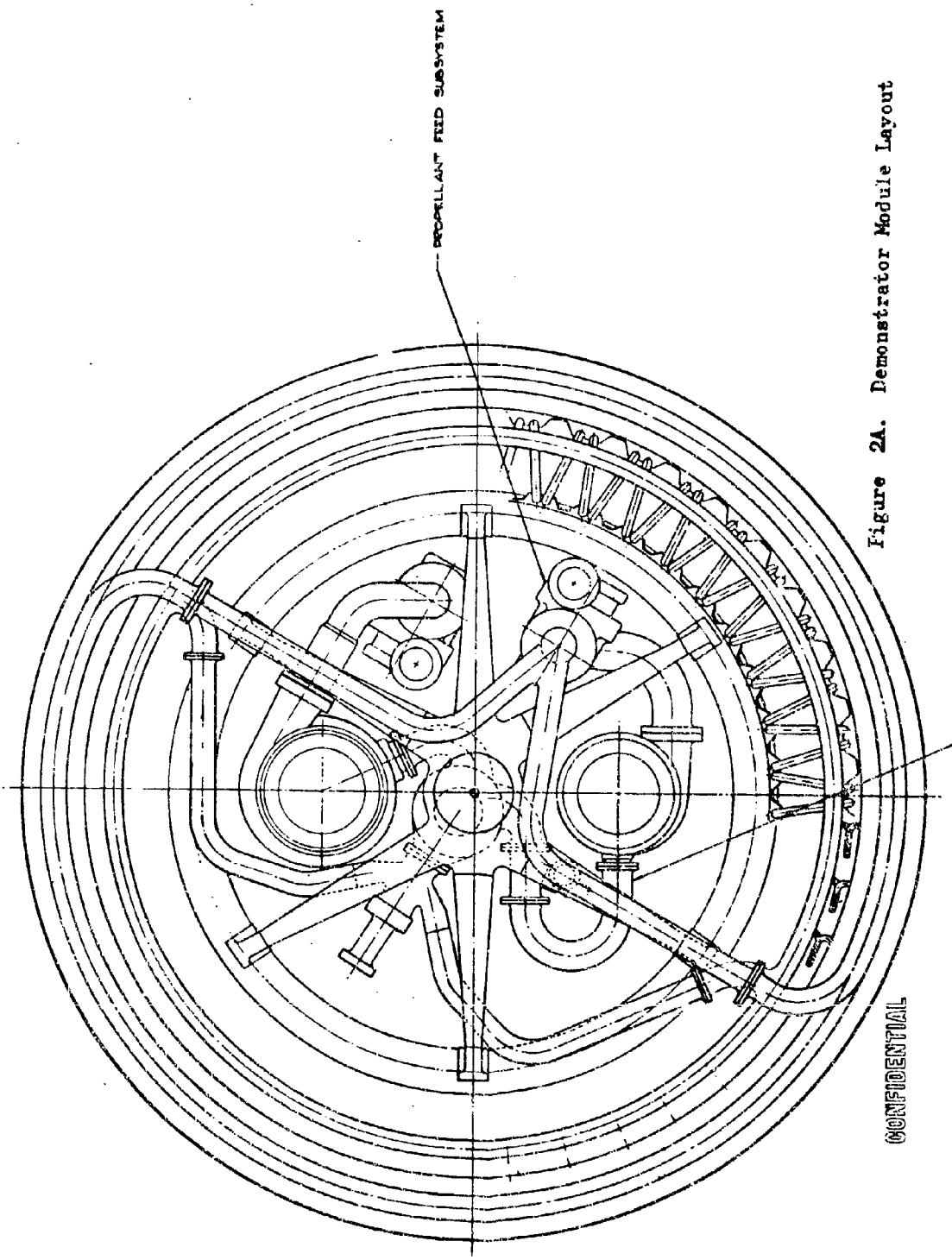

Figure 2A. Demonstrator Module Layout

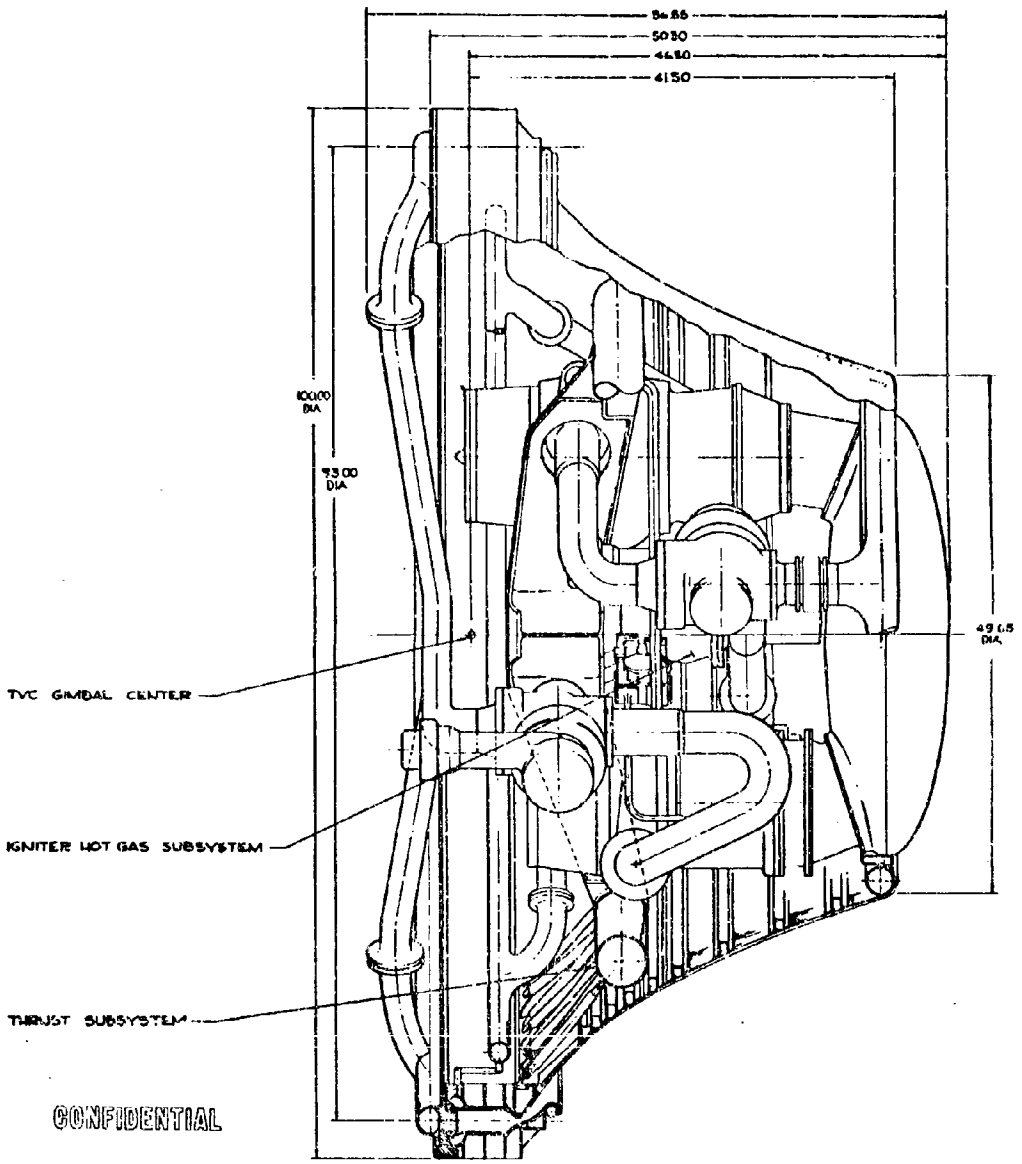

Figure 2B. Demonstrator Module Layout

(C) The total weight of the Demonstrator Module was calculated to be 3950 pounds, which represents a system with basic Flight Module design similarity, while incorporating test flexibility design features and design conservatism considered prudent to meet demonstration, cost, and schedule objectives.

(C) The combustion chamber performance for the Demonstrator Module was based upon tests conducted over a wide range of chamber pressure and mixture ratios during Task II. Based on the test data obtained, a c* efficiency of 99.6 percent has been predicted for the Demonstrator Module at full-thrust and 6:1 nominal mixture ratio. Analytical studies of a non-adiabatic nozzle determined that at the full-thrust, nominal mixture ratio design point, an overall engine specific impulse efficiency of 97.01 is achieved (including effects of heat loss, viscous drag, divergence losses, and kinetics losses). This yields an actual specific impulse equal to 450.1 seconds at 1500-psia chamber pressure and 6:1 mixture ratio. The specific impulse varies with thrust level and mixture ratio.

(U) The design of the aerospike engine includes allowances to account for performance variations that result from hardware tolerances and calibration inaccuracies. Because the aerospike engine is closed-loop controlled on chamber pressure and mixture ratio, the engine is first calibrated for design thrust to establish the exact nominal chamber pressure. Component variations, such as turbopump efficiencies, are compensated for by changing the turbine flowrate and hence the pump power required to meet the chamber pressure and mixture ratio input commands. These variations have virtually no effect on total thrust and less than a 1-second effect on specific impulse.

Thrust Chamber

(U) A summary of the thrust chamber design parameters is presented in Table 3. Materials and fabrication techniques utilized are state of the art with

(C)

TABLE 3

THRUST CHAMBER DESIGN PARAMETERS

Length as Percentage of Equivalent Area Ratio 15-Degree Cone, percent	25
Throat Area, $in.^2$	85.14
Overall Diameter, inches	100.0
Overall Height, inches	55.90
Contraction Area Ratio	7.13
Expansion Area Ratio	74.1
Mean Combustor Diameter, inches	93.0
Combustor Width, inches	2.0
Throat Gap, inch	0.281
Length Injector to Throat, inches	6.0
Tube Material	Nickel 200
Number Tubes Outer Body	4400
Number Tubes Inner Body	3240
Number Subsonic Struts	40

strong emphasis on cost and low weight. Features connected with critical technology evaluated in Task II embody the information gained and configurations proved successful in Task II experimentation. These include: combustor shape, nozzle contour, injector pattern, tapoff location and design, cooling tube material, structural arrangement and throat geometry, LO_2 manifold priming, assembly sealing, cooling tube heat transfer criteria, and accessibility provisions for thrust chamber and injector inspection during development testing.

(U) The thrust chamber design is shown in Fig. 4. Each of the combustor assemblies is fabricated of brazed nickel tubing which forms cylindrical sections with sealed manifolds at each end. The lightweight titanium support structure is subsequently adhesively bonded to the tubes. The bodies are connected by 40 regeneratively cooled subsonic struts, each radially installed in the annular combustion chamber area with two preloaded bolts.

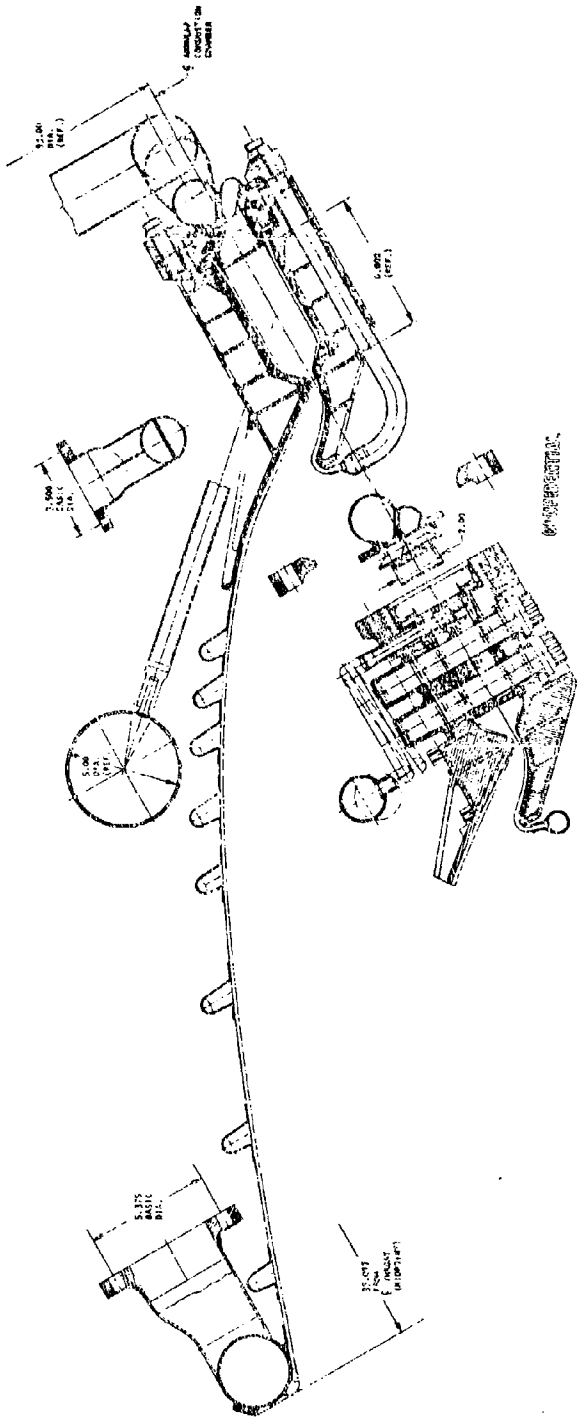

Figure 4. 25K Thrust Chamber Demonstrator Module

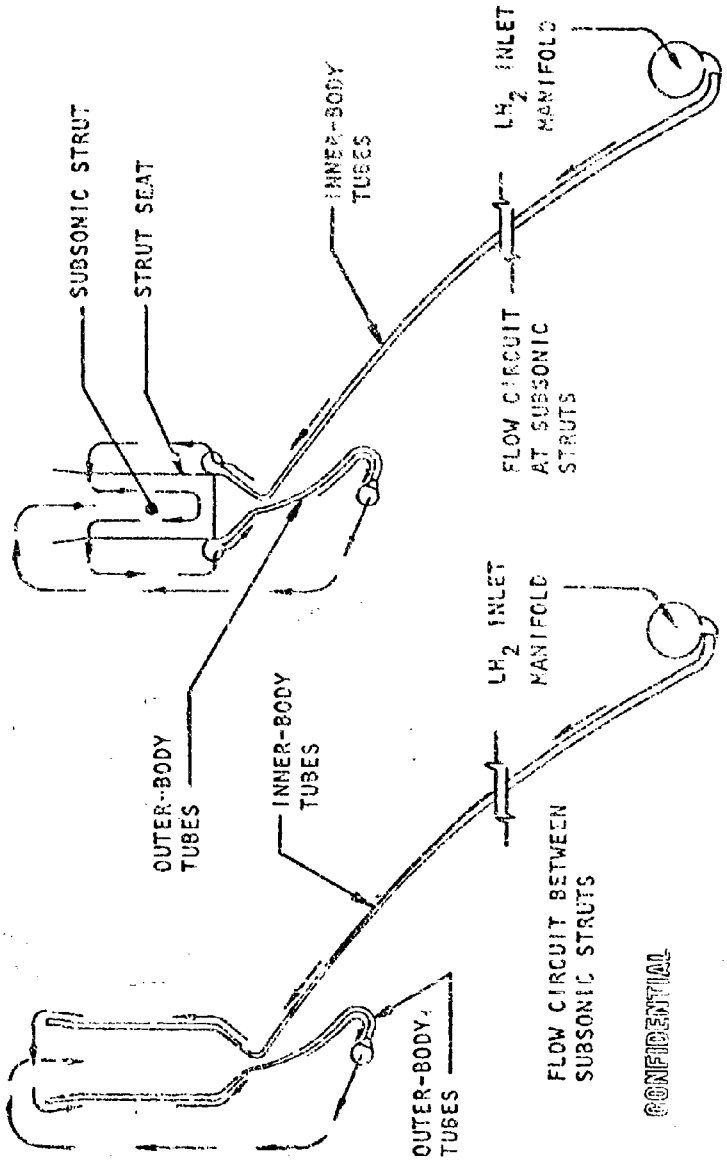

Figure 5. Regenerative-Coolant Flow Circuit

(U) The cooling circuit is shown on Fig. 5 . The tapoff manifold provides the dual function of (1) ducting hot gases from the igniter to each compartment of the combustion chamber at start, and (2) ducting hot gases from the combustion chamber to the turbines to provide power for the pumps during mainstage operation.

Turbopumps

(C) The fuel turbopump was designed to meet the maximum head and flowrates shown in Table 4 and provide not less than a 75 percent efficiency over the mixture ratio excursion at full thrust. The fuel turbopump consists of a two-stage centrifugal pump, a three-row turbine mounted on a common shaft, and a concentric integral, hydraulic turbine-driven preinducer. The main pump assembly and the preinducer assembly are both supported on propellant-lubricated, rolling-contact bearings. The main pump assembly operates at a nominal speed of 35,000 rpm, and the preinducer operates at a nominal speed of 14,535 rpm. The design layout of this turbopump is shown in Fig. 6 . Turbopump axial thrust is balanced by means of a hydraulic balance piston located between the two main impellers.

(U) Turbine discs are bolted together and torque is transmitted with curvic couplings, and a spline drive to the impellers. The turbine outboard bearing is mounted on six struts with pinned ends. The preinducer assembly is designed so that it can be developed independently of the main turbopump assembly.

(C) The oxidizer pump was designed to meet the maximum head and flowrates shown in Table 5 and to provide an efficiency not less than 73 percent over the mixture ratio excursion at full thrust.

TABLE 4

(C) SUMMARY OF FUEL TURBOPUMP DESIGN CHARACTERISTICS

(At Nominal Operating Point)

General	
Flow, Q, gpm	3450
Head Rise, ΔH, feet	84,300
Pressure Rise, ΔP, psi	2733
Discharge Pressure, P_d, psia	2735
Speed, N, rpm	35,000
Pump Horsepower	16,560
NPSH, feet	60
Suction Specific Speed, S_s	149,000
Pump Efficiency, η_p, percent	75
Turbine Efficiency, η_T, percent	62.2
Turbine Mass Flow, $\dot{W}_T$, lb/sec	8.86
Overall Diameter, D, inches	17.6
Overall Length, L, inches	32.8
Turbopump Weight, pounds	453
Turbine	
Inlet Pressure, P_t, psia	1000
Inlet Temperature, T_{t_1}, F	1500
Pressure Ratio, PR	15
Pitchline Velocity, U_m, fps	1360
Pitch Diameter, D_m, inches	8.9
Pump	
Number of Stages	2
Suction Specific Speed, N_{ss}	7313
Specific Speed, N_s	620
Stage Head Coefficient, Ψ	0.597
Impeller Blade Angle, β_2, degrees	60
Impeller Blade Width, inches	0.45

Pump (Cont.)	
Inlet Hub Diameters, inches	4.5
Impeller Diameter, d_t, inches	9.5
Impeller Inlet Eye Diameter, inches	6.3
Tip Speed, U_t, fps	1452
Number of Blades at Inlet	6
Number of Blades at Discharge	24
Preinducer	
Suction Specific Speed, S_s	62,000
Speed, N, rpm	14,535
Head Rise, ΔH, feet	883
Flow Coefficient, ϕ	0.07
Head Coefficient, Ψ	0.115
Inlet Tip Diameter, inches	9.5
Discharge Tip Diameter, inches	7.8
Number of Vanes	4 + 4
Turbine Head Drop, feet	1692
Turbine Inlet Tip Diameter, inches	6.83
Turbine Discharge Tip Diameter, inches	6.50
Main Inducer	
Suction Specific Speed, S_s	18,900
Speed, N, rpm	35,000
Head Rise, ΔH, feet	4000
Flow Coefficient, ϕ	0.081
Head Coefficient, Ψ	0.113
Inlet Diameter, inches	7.60
Discharge Tip Diameter, inches	6.90
Tip Speed, U_t, fps	1160

F = 250,000 pounds; P_c = 1500 psia; MR = 6.0

CONFIDENTIAL

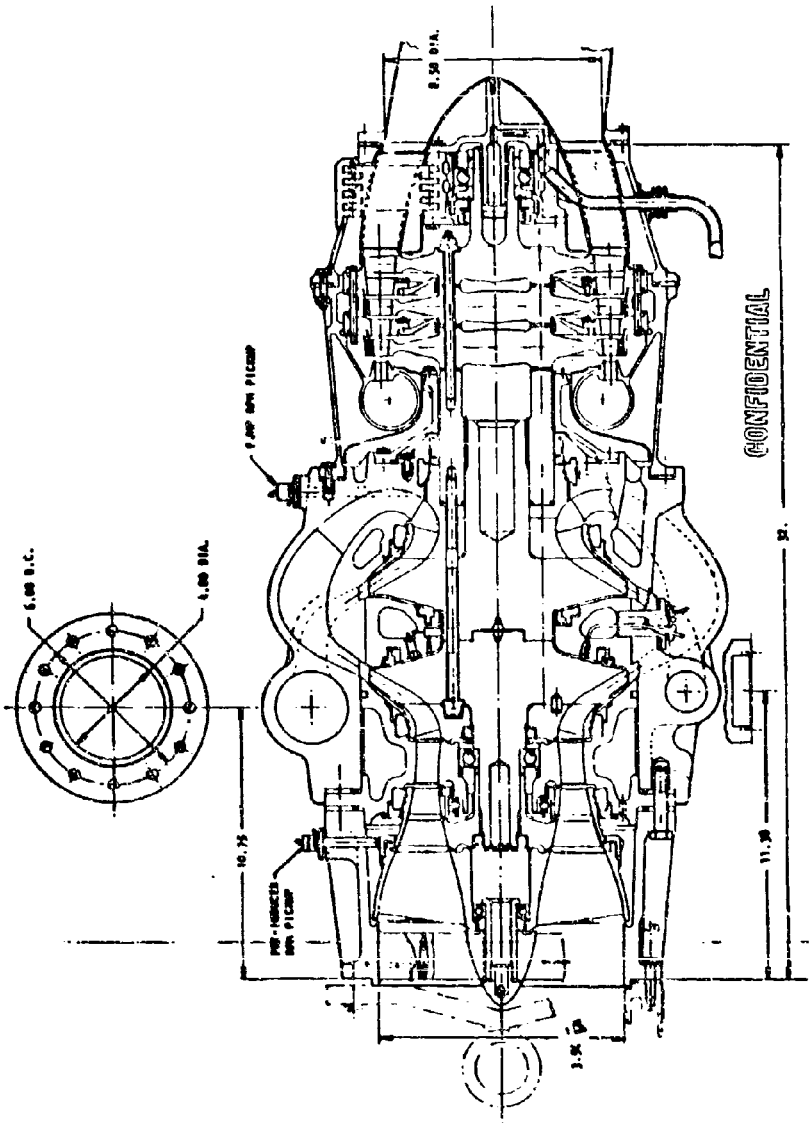

Figure 6. Demonstrator Engine Fuel Turbopump

TABLE 5

(C) SUMMARY OF OXIDIZER TURBOPUMP DESIGN CHARACTERISTICS

(At Nominal Operating Point)*

General	
Flow, Q, gpm	3126
Head Rise, ΔH, feet	4150
Pressure Rise, ΔP, psi	2023
Discharge Pressure, P_d, psia	2060
Speed, N, rpm	25,000
Pump Horsepower	5100
NPSH, feet	16
Suction Specific Speed, S_s	174,000
Pump Efficiency, η_p, percent	73
Turbine Efficiency, η_T, percent	47.4
Turbine Mass Flow, W_T, lb/sec	3.34
Overall Diameter, D, inches	15.0
Overall Length, L, inches	30.5
Turbopump Weight, pounds	343
Turbine	
Inlet Pressure, P_t, psia	730
Inlet Temperature, T_{t_1}, F	1500
Pressure Ratio, PR	18.7
Pitchline Velocity, U_m, fps	1090
Pitch Diameter, D_m, inches	10.0
Pump	
Suction Specific Speed, N_{ss}	17,300
Specific Speed, N_s	2640
Head Coefficient, Ψ	0.36
Impeller Blade Angle, β_2, degrees	35
Impeller Blade Width, inches	0.9

Pump (Cont.)	
Impeller Diameter, d_t, inches	5.5
Impeller Inlet Eye Diameter, t, inches	4.4
Tip Speed, U_t, fps	600
Preinducer	
Suction Specific Speed, S_s	42,000
Speed, N, rpm	6000
Head Rise, ΔH, feet	320
Flow Coefficient, ϕ	0.07
Head Coefficient, Ψ	0.250
Inlet Tip Diameter, inches	9.0
Discharge Tip Diameter, inches	7.75
Number of Vanes	4 + 4
Stator Inlet Tip Diameter, inches	7.75
Stator Discharge Tip Diameter, inches	6.75
Hub Turbine Pitch Diameter, inches	3.75
Passage Height, inches	0.29
Main Inducer	
NPSH, feet	3.36
Suction Specific Speed, S_s	18,200
Speed, N, rpm	25,000
Head Rise, H, feet	715
Flow Coefficient, ϕ	0.20
Head Coefficient, Ψ	0.100
Inlet Diameter, inches	4.65
Discharge Tip Diameter, inches	4.4
Tip Speed, U_t, fps	509

*Thrust = 250,000 pounds; P_c = 1500 psia; MR = 6.0

CONFIDENTIAL

(C) The oxidizer turbopump consists of a single-stage centrifugal pump and a three-row turbine mounted on a common shaft and a concentric integral hydraulic turbine driven preindicer, as shown in Fig. 7 . The hydraulic turbine-driven preinducer is made up of a four-stage hydraulic turbine mounted in the hub of the preinducer and driven by high-pressure (2000 psia) LO_2 that is tapped from the main pump discharge, flow through the turbine, and then returns to the main pump inlet. This turbine is mounted rigidly on two propellant-lubricated, rolling-contact bearings and is directly connected to the preinducer and rotates at a nominal speed at 6000 rpm. The main pump assembly is straddle-mounted on two rolling-contact bearings and runs at a nominal speed of 25,000 rpm. The pump bearing is lubricated with LO_2; however, because the environment downstream of the turbine bearing seal is hydrogen-rich, the turbine bearing is lubricated with GH_2 supplied from the thrust chamber fuel inlet manifold.

(U) The preinducer assembly is designed so that it not only can be developed separately from the main pump assembly, but can also be mounted remotely from the main pump assembly, if desired. The only connection needed is the high-pressure supply line to the preinducer turbine.

Igniter

(U) The specific design requirements for the hot-gas igniter (HGI) are taken from two points in the start sequence. Initiation of turbine spin (occurs immediately after ignition of the hot-gas igniter) and main chamber ignition.

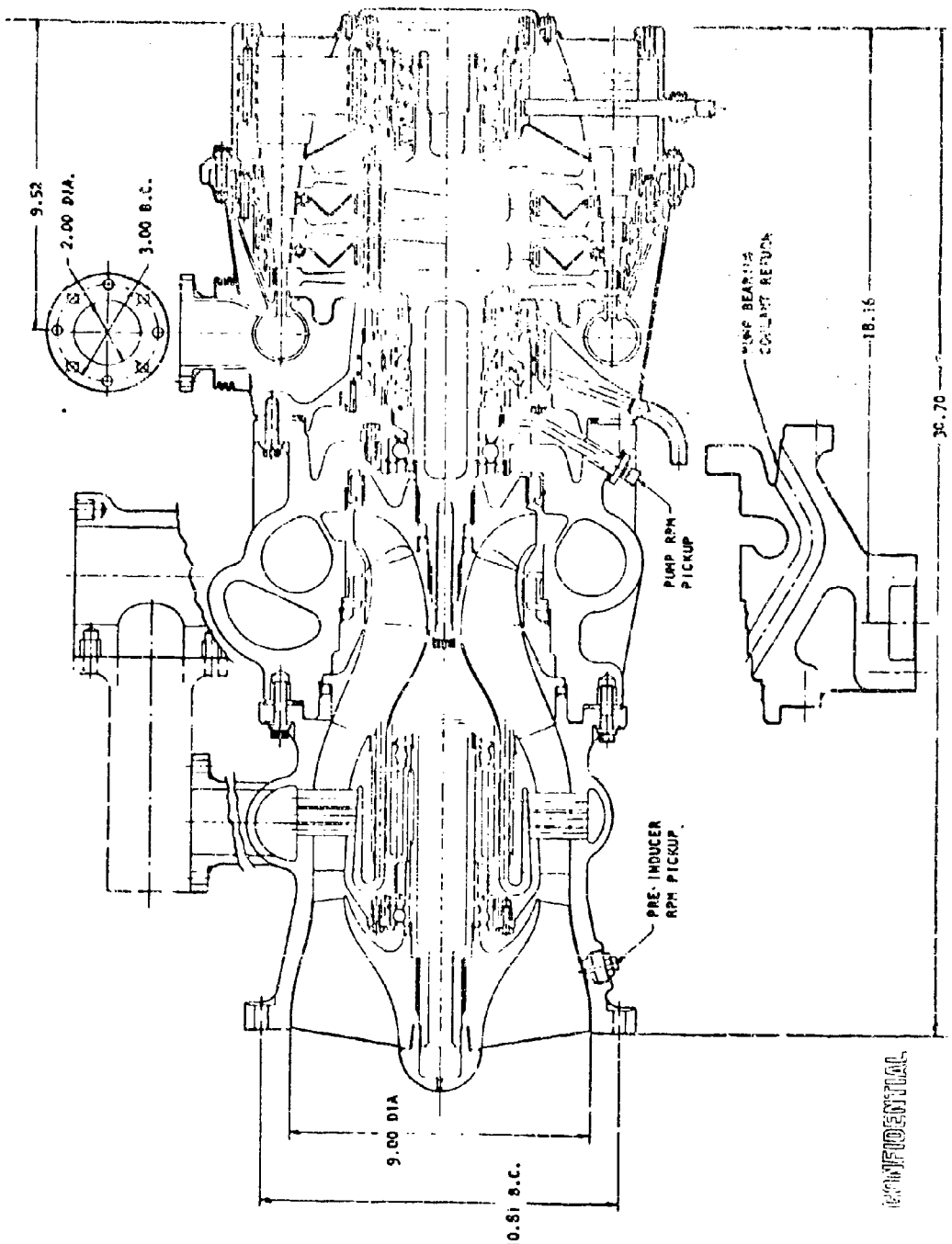

Figure 7. Demonstrator Engine Oxidizer Turbopump

(U) During the period of igniter operation, the propellant mixture ratio to the igniter must be controlled because of variations in oxidizer and fuel pump discharge pressure buildup. For this reason, an oxygen pressure regulator is included in the oxygen feed system to maintain a balanced inlet pressure to the igniter.

(U) The volume required in the igniter combustor is determined by the propellant stay time and is approximately the volume of an 8-inch-diameter sphere. Therefore, the maximum ID was set at 8 inches. The stay time in the combustor is 1.16 milliseconds at igniter start and 1.08 milliseconds at engine ignition.

Controls

(U) The total throttling and mixture ratio control system is shown schematically in Fig. 8 . Facility-mounted components are shown separated from engine-mounted components by the dashed line. Electrical signal flow is shown by the heavy lines connecting rectangular blocks identified in the schematic. Signal summation occurs at the circles with interior crosses in accord with the sign shown.

(U) The throttling valves will be driven by integral hydraulic actuators, which will be positioned by hydraulic servovalves. Integral with the valve actuators will be variable-reluctance-type position transducers producing modulated carrier signal feedback. Engine fuel flow and engine oxidizer flow are measured volumetrically by turbine flowmeters.

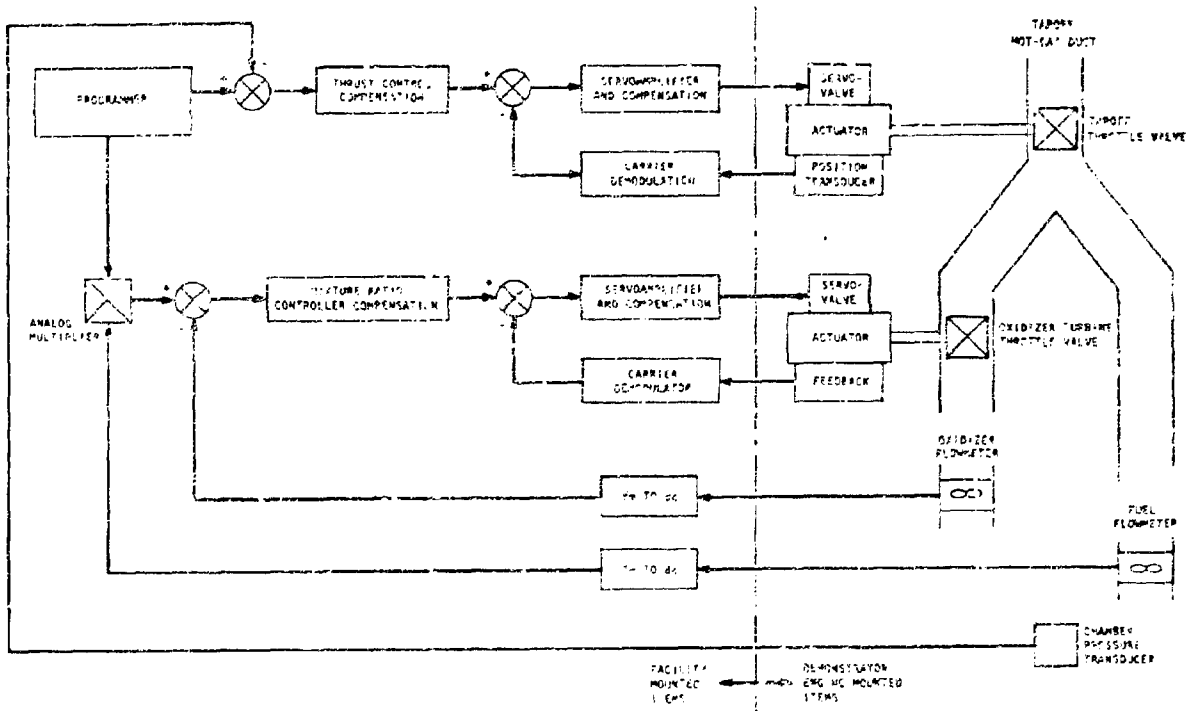

Figure 8. Demonstrator Engine Throttling and Mixture Ratio Control

(U) Tradeoff studies of the tapoff throttle valve were performed to select the optimum configuration, considering poppet, butterfly, and ball valves.

(U) A poppet valve was selected. The major advantages were the linearity of the actuator stroke vs flow area relationship, the ease in modifying that relationship by contouring the poppet, the good flow distribution during throttling, and the simple basic design.

(U) The tapoff throttle valve is a normally open pressure-balanced and contoured valve which is actuated by a hydraulic actuator. The actuator piston is attached directly to the poppet by a piston rod which eliminates all backlash.

(U) The main oxidizer valve is a normally closed "visor" valve which is installed in the high-pressure LO_2 line between the pump outlet and the thrust chamber. The valve is a modified ball which is operated by a pneumatic linear actuator through a link-lever mechanism. Valve position information is provided by a position transducer.

(U) The main fuel valve is identical in design to the main oxidizer valve with the possible exception of flow direction. The valve can be used with flow in either direction by modifying the bellows seal. The flow direction for both valves is selected to minimize the possibility of collecting condensed moisture in the valve, so the final selection of flow direction will be based on careful evaluation of the valve location in the system.

Flight Module

(C) The Flight Module differs from the Demonstrator Module in that nearly all subsystems and components employ welded interconnects and assemblies to minimize system weight and improve reliability. Component arrangements

within the engine have been modified to reflect the technological improvements and refinements characterizing the Flight Module. The configuration thus evolved employs a greater degree of symmetry regarding propellant feed ducting, hot-gas tapoff ducting and engine thrust mount. The separate turbine exhaust ducts are eliminated as a result of improvement modifications to the turbopumps, which allows recessing the turbopumps lower into the engine cavity, and which also aids in attaining engine thrust mount symmetry. The result is a shorter, lighter engine than the Demonstrator Module. The overall diameter remains the same at 100 inches; however, the length is reduced from 56.55 to 48.3 inches, and the weight is reduced from 3950 to 2939 pounds. An advanced, tapered-wall combustion chamber geometry was evolved from the parallel-wall Demonstrator Module, which permits an increase in the center line diameter from 93.0 to 94.0 inches, and a resultant area ratio increase from 74.1:1 to 75.8:1.

(C) Small improvements in the turbopump efficiencies are projected which, together with advancements in other component and system designs, result in an improvement in engine specific impulse from 450.1 to 452.0 seconds.

APPLICATION STUDY

(C) The prime objective of this study was to define a single engine module which provides a high preformance index for the vehicle applications defined by the Air Force. Six vehicles were defined for a 250K vacuum thrust module, and six vehicles were defined for a 350K vacuum thrust module. The different vehicle concepts illustrated the diversity of potential applications; including first and second stages, single-stage-to-orbit, single engine and clustered configurations, and reusable and expendable stages.

(U) Parametric performance index data were generated as a function of module diameter, mixture ratio, and chamber pressure. The analysis of these data led to the determination of the parameters of the optimum

module for each vehicle and the common module for each thrust level (250K and 350K).

(C) It was concluded from this study that the common module for the 250K vehicles should have a diameter of 78 inches and a rated thrust chamber pressure of 1300 psia. The module is truly common in that there are no engine changes or modifications required from vehicle to vehicle. The percent of the optimum performance index which can be achieved by the use of the common module as compared to the optimum module was determined for each case.

(C) Thus, common module parameters for the 350K vehicles were determined to be a diameter of 98 inches and a rated thrust chamber pressure of 1370 psia.

(C) In general, the lower-stage vehicle module optimizes at higher chamber pressure than the modules for the upper-stage vehicles, and the recoverable vehicle modules optimize at significantly lower chamber pressures than do those in the expendable vehicles. The optimum P_c never exceeds 2000 psia. For each case, 250K and 350K, the optimum pressures are approximately the same; as anticipated, the optimum diameters are larger for the 350K modules. This same trend appears in the common modules; namely, 1300- to 1370-psia chamber pressure for both, and the 250K common module has a diameter of 78 inches compared to the 98 inches diameter for the 350K common module.

(U) Additional perturbations considered, based on the selected common module for the 250K thrust class vehicles, were:

1. Constant thrust mode in lieu of the selected constant chamber pressure control mode
2. Nozzle percent length variation
3. Programmed mixture ratio

4. The use of a side gas injection thrust vector control system in lieu of a mechanical gimbaling system

FABRICATION AND TEST

(C) The objective of this large part of the contract effort was to demonstrate the technologies considered critical to the aerospike demonstrator engine. The Injector Performance Investigation Subtask was to provide a basis for the selection of a high-performing injector for the 250K testing, to evaluate heat flux generated by various injectors, to evaluate injector durability, to develop a gas tapoff technique that would yield a suitable working fluid for a turbine, and to evaluate the combustor shape for the 250K and Demonstrator Module chambers. The Thrust Chamber Cooling Investigation Subtask was to provide a basis for tube material selection for the Demonstrator Module, to define regenerative-cooling limits, to provide heat transfer design data, and to provide information on the life of the cooling tubes. Injectors from the Injector Subtask were to be used in the Cooling Investigations. The Thrust Chamber Nozzle Demonstration Subtask was to demonstrate performance of the complete, full-scale aerospike combustor and nozzle combination over the operating range, to evaluate base bleed effects, and to evaluate stability, operating characteristics, and preliminary structural effects. The Segment Structural Evaluation was to evaluate the lightweight structure of the Demonstrator as to its ability to maintain throat gap to verify cooling and sealing of the structural parts and performance over the operating range, and to obtain structural design data.

(U) A summary of the requirements for each subtask and the accomplishments is presented in Table 6 . All objectives of the Injector Performance Investigation subtask were achieved plus several items which were identified as valuable. The original goals were exceeded in the Cooling Investigation Subtask in the area of cyclic life evaluation and cooling

TABLE 6

(C) PHASE I DEMONSTRATION REQUIREMENTS AND ACCOMPLISHMENTS, TASK II FABRICATION AND TEST ITEMS

	Requirements	Accomplishments
Injector Performance Investigation (2.5" Solid-Wall Segment)		
Configuration Selection	Evaluation of promising candidate injector designs	Triplet injector configuration selected
Performance Evaluation	Effect of variations of combustion chamber dimensions and throttling	Parallel wall chamber configuration selected efficiencies of 0.96 to 1.00 were obtained between chamber pressures of 300 to 1500 psia at nominal mixture ratio
Durability	Full operating range	Single injector units have over 80 tests at chamber pressures from 600 to 1500 psia
Stability	Stable operation over mixture ratio range of 5:1 to 7:1	Stable operation throughout test series bomb test produced no sustained disturbance
Tapoff	Not required	Gas tapoff feasibility demonstrated.
Ignition	Compatibility with chamber and injector configuration	Hypergolic ignition achieved with TEAB and GF_2; Hot-gas ignition shown to be feasible
Throttling	5:1	10:1 throttling achieved and operating capabilities indicated by tests to 1700 psia
Alternate Configurations	Not required	Two injector configurations (fan, fan-reverse triplet) shown to provide high-performance capabilities
Number of Tests	50	128 injector test conducted (plus 300 tests on related programs)
Number of Test Hardware Items	Two solid-wall segments Four injectors	Two solid-wall segments plus replacement parts Eleven injectors with 31 modifications
Thrust Chamber Cooling Investigation		
Materials and Process Properties	Evaluate tube materials such as nickel, copper, and stainless steel	Nickel 200 selected for tube material, Be Cu--10 selected for possible future use.
Laboratory Fatigue Properties	Not required	Fatigue properties obtained to supplement analytical comparison of candidate materials; Nickel 200 found to have life expectancy of greater than 250 cycles
Tube Fatigue Testing	Temperature cyclic strain effects	Cyclic life of Nickel 200 demonstrated to be 312
Regenerative Cooling Capabilities	Maximum chamber pressure cooling capabilities--throttling effects of supplementary cooling on c^*	
Nickel Segment		Nickel 200--successfully cooled chamber pressure of 310 to 1550 psia
Copper Segment		Cu--successfully cooled chamber pressure of up to 1500 psia
Stainless Steel		Stainless eliminated, not suitable for life requirement. Film cooling found to reduce c^*, will not be used on demonstration engine
Segment Cycle Testing	Regenerative cooling capabilities plus 4 weeks of test for cycle evaluation of Nickel	Tests completed on Nickel segment, 313 cycles on one segment
Number of Tests	50 tests plus additional cycle testing	8 cooling tests plus 1; cyclic tests (313 cycles plus 15 cooling tests on related programs)
Number of Test Hardware Items	Three 2.5" tube-wall segments	Three tube-wall segments
25K Thrust Chamber Demonstration		
Injector and Facility Checkout		Nine tests with solid-wall chamber indicates satisfactory injector and facility operation
Tapoff	Hot gas tapoff on and combustion chamber tapoff to use common ports	Tapoff feasible
Ignition	Hot-gas ignition system feasibility demonstration, preliminary test using hypergol	Hypergolic ignition test conducted unsatisfactorily. Hot-gas ignition test not conducted
Priming	Not required	Uniform priming of oxidizer system achieved over full operating range
Stability	Demonstrate recovery of chamber pressures after tangential pulse	Two pulse tests with satisfactory results. No oscillations were experienced on subsequent tests
Combustion Efficiency	To be experimentally evaluated	Performance up to 98% psi P_c, one below goal
Nozzle Efficiency	To be experimentally evaluated	Tube-wall tests limited to 90% psi and solid-wall and tube-wall tests corresponds to theory
Throttling	Operation over 5:1 thrust range	Chamber pressure of 450 to 1700 psia completed on solid wall--60% to 90% on tube wall
Gas Bled	From 1 to 5 percent of total flow	GH_2 bleed gases from 0.3 to 1.0%
Altitude Effects	Testing to be conducted at simulated altitude conditions	Not conducted
Mixture Ratio Variation	5:1 to 7:1	Injector operation from 5:1 to 7:1 mixture ratio performance demonstrated at 5:1 and 6:1
Number of Tests	45 tests	14 completed
Number of Hardware Items	One solid-wall thrust chamber Two tube-wall thrust chambers Three injectors	One solid-wall thrust chamber Two tube-wall thrust chambers Two injectors
Segment Structural Evaluation (25K)		
Cooling (with Circuit for Demonstrator Thrust Chamber)	Cooling capability at design chamber pressure	Regenerative cooling demonstrated to 1100-psia P_c (facility limitation), 15% psia achieved at reduced mixture ratio
Throttling	Operation over 5:1 thrust range	From 1700-psi P_c at 5:1 to 350+ psi at 5:1 mixture ratio
Number of Tests	20	11 to date (plus 5 on related programs)
Number of Test Hardware Items	Two tube-wall segments Two injectors	Two tube-wall segments Two injectors
Performance	Verify	c^* efficiency verified 2.5" segment results
Structure	Evaluate lightweight structure	Demonstrated to 1700 psi; adhesive bond not achieved

limits on the selected material. The thrust chamber nozzle demonstration task was only partially completed due to the occurrence of a combustion oscillation which was not resolved during the contract period. Subsequent to the work on this contract, progress was made in reducing the combustion oscillations level on the NASA Advanced Engine Aerospike Program. Ground level performance was obtained at 600- and 900-psi chamber pressure. The objectives of the Structural Evaluation were achieved with the exception that maximum chamber pressure and regenerative-cooling operation at the maximum wall temperature were obtained on different tests because of facility limitations. Throttling demonstration was not attempted below 600-psi chamber pressure.

(U) Hardware items fabricated and tests conducted are summarized below.

Item	Planned	Actual
2.5K Solid-Wall		
Segments	2	2 and replacements
Injectors	4	11 and 31 modifications
Tests	50	128
2.5K Tube-Wall		
Segments	3	3 tested
Tests	52	25
250K Experimental		
Solid-Wall Chambers	1	1
Tube-Wall Chambers	2	2
Injectors	2	2
Tests	45	14
20K Structural Segment		
Segments	2	2
Injectors	2	2
Tests	20	11

Thrust Chamber Performance

(C) Performance results were obtained from the 2.5K injector investigation, the 2.5K tube-wall testing, the 20K segment testing, and 250K full-scale aerospike testing. Four different injectors were investigated, with many minor modifications of the most promising, from the standpoint of performance, durability, ignition, stability, throat heat flux, and tapoff gas properties. The triplet pattern shown in Fig. 9 was selected and developed to satisfy all requirements as determined by the segment testing. Each 2.5K injector unit was fabricated with four injection strips whereas the 250K injector used seven strips per baffle compartment. Combustion (c*) efficiency for this type over the operating range is shown in Fig. 10 and exceeds the values necessary to obtain the required 96-percent specific impulse efficiency at rated and 95 percent at throttled. This injector was tested in a 4-inch-long chamber as compared to 6-inch-long (2-inch-wide) chamber selected for the Demonstrator Module and experimental chamber, and only a small performance loss (less than 1 percent) was experienced.

(U) Performance data gathered during the 2.5K tube-wall segment testing with the identical combustion chamber and injector are summarized in Fig. 11 and corroborates the solid-wall test results. Performance data from the 20K segment testing with the same injector pattern, extended to cover three full compartments, are shown in Fig. 12 and adds confidence in the performance results. It is significant that this segment contains the Demonstrator Module baffle configuration indicating that the design produces no adverse effect on performance.

(U) The 250K injector utilized 280 of the strips defined in Fig. 13 arranged in 40 compartments, 7 strips per compartment (between baffles) as shown in Fig. 14. This injector was fired first in a solid-wall chamber, and then in tube-wall chambers. C* efficiency from the 250K

5AA34-8/24/66-S1A

Figure 9. 60-Degree LO_2 Impinging Triplet With Fuel Post Extended and Both Chamfered and Nonchamfered LOX Strips

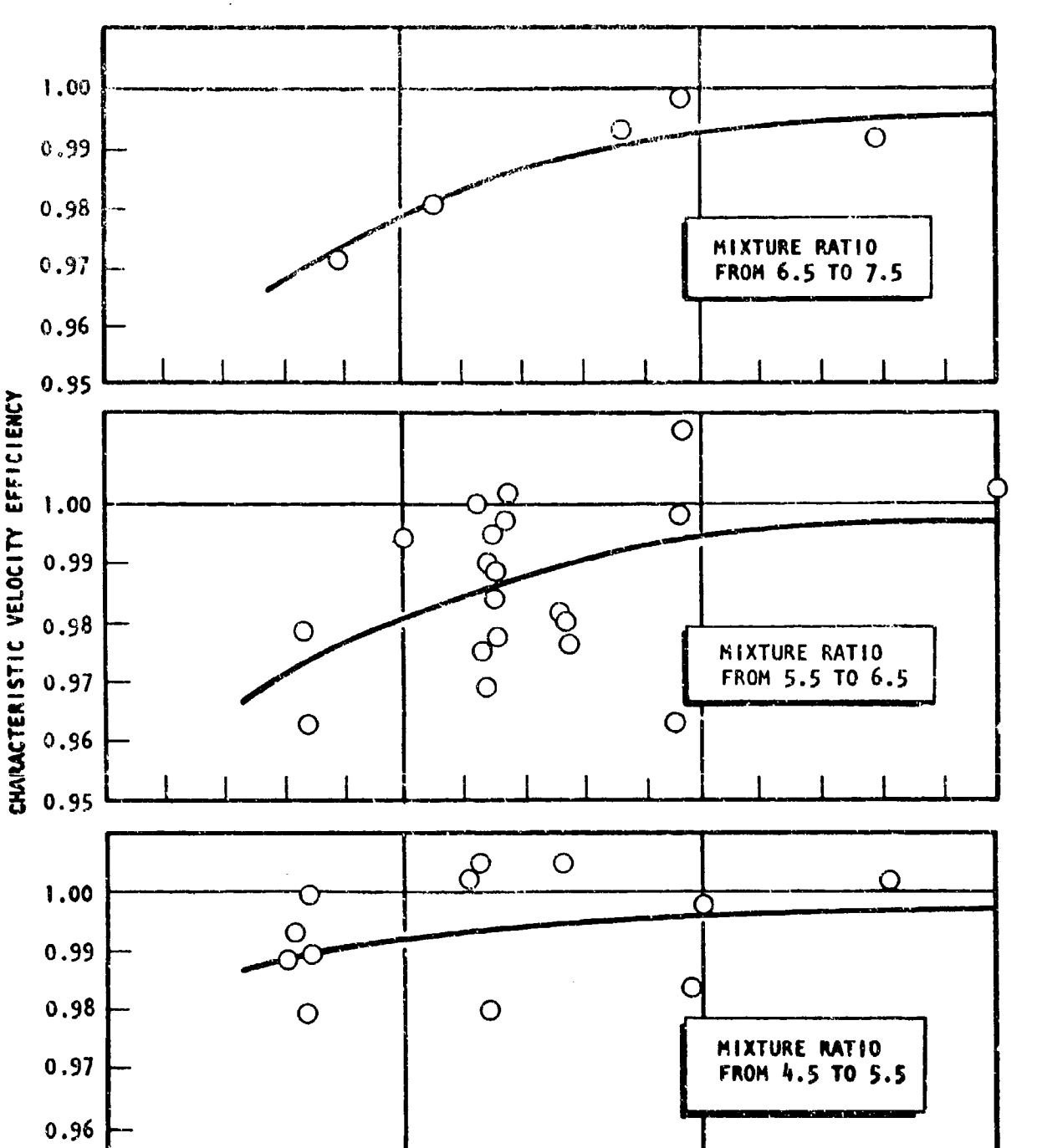

Figure 10. Triplet Injector Performance in the 2.5K Segment Thrust Chamber

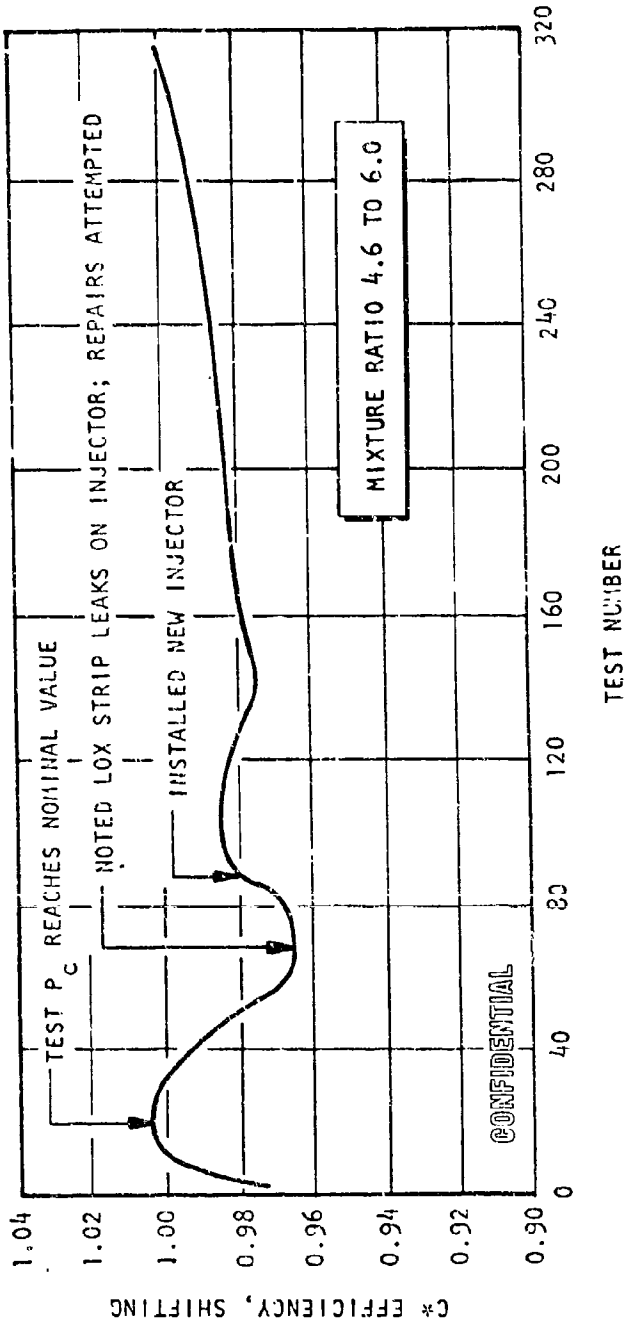

Figure 11. Combustion Efficiency vs Cyclic Test Number
Nickel Tube-Wall Segment Cycling Tests

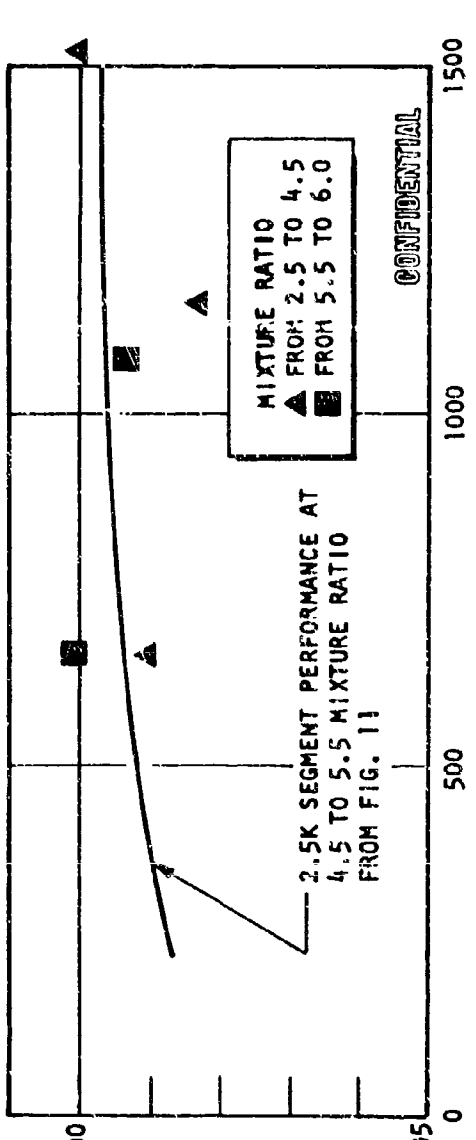

Figure 12. 20K Performance Compared to 2.5K Performance

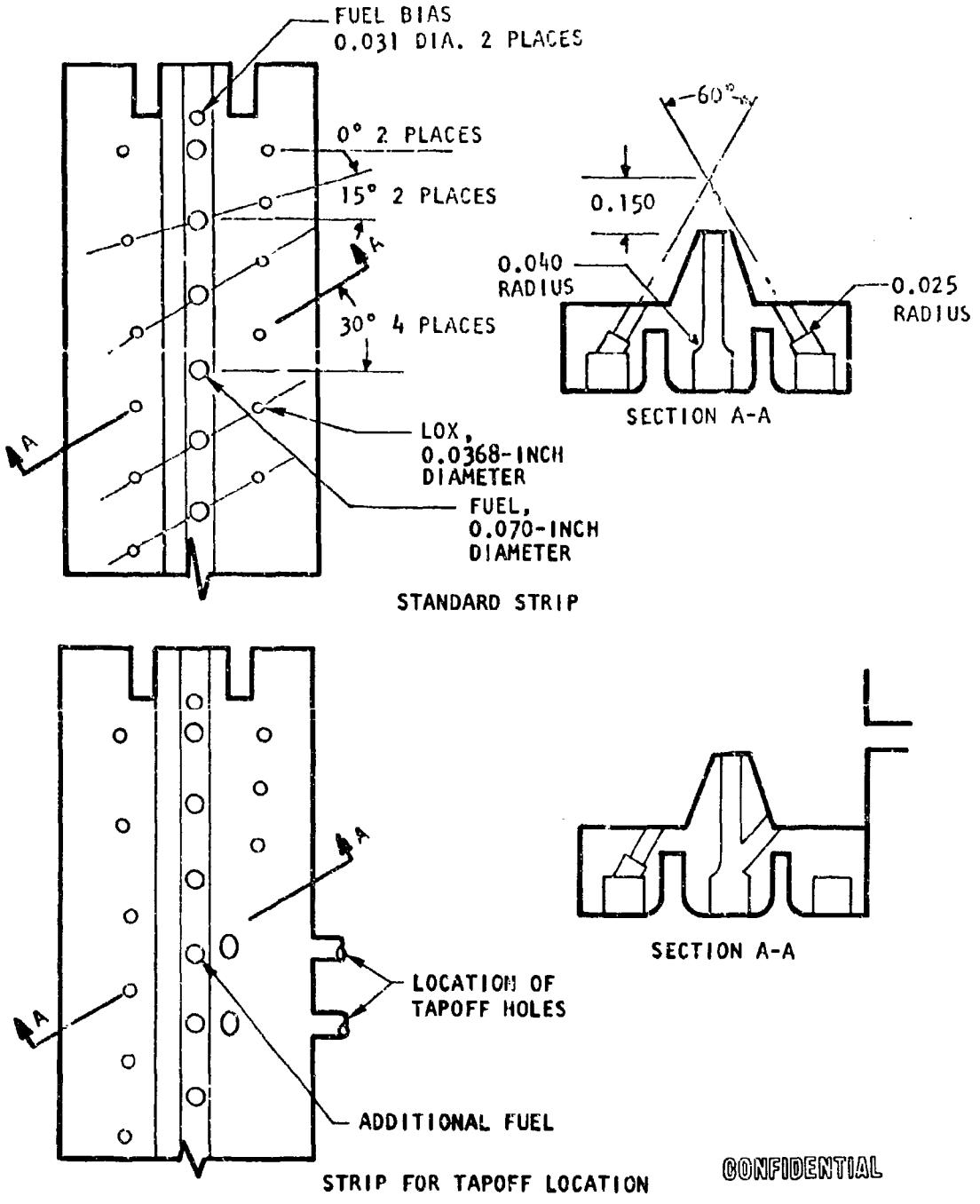

Figure 13. 250K Candidate Triplet With Fuel Post (No. 6-1A to 6-1D)

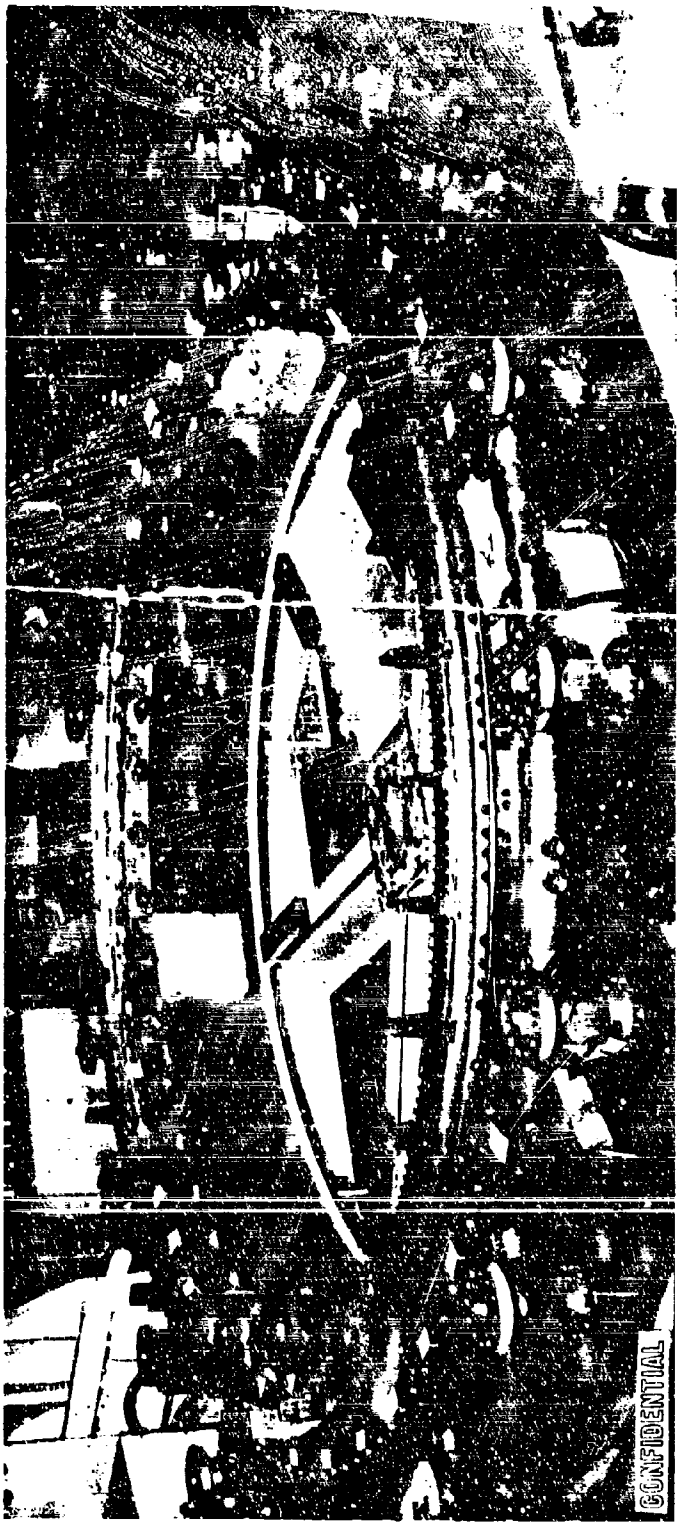

Figure 14 Injector After First Braze Cycle

solid-wall testing is not reliable because of the large effect of the water film coolant. Results from the limited 250K tube-wall testing are shown in Table 7 . The lower c^* values on tests 27 and 28 may have been caused by coolant leaks into the combustion chamber which develop during these two tests. These data indicate that the combustion performance obtained on the segments is obtainable on the full 250K chamber when the durability problem of this workhorse hardware is solved.

(U) Nozzle primary flow performance from both the solid wall and tube wall validates theoretical values and previous background data, as shown in Fig.15 . Nozzle base pressure also compared favorably with prediction, as shown in Fig. 16. Overall, impulse efficiency obtained met the contract goal on the one test in which coolant leaks did not occur; however, it was below target on the others because of the aforementioned coolant leakage and short duration. Correcting for the leakage on reasonable estimates of its effect brings the impulse performance to the goals. Furthermore, use of combustion efficiency from segment tests and nozzle performance from the full-scale tests shows that performance goals can be met. Figure 17 shows the three 250K tube-wall test points relative to performance predicted from nozzle hot-fire data and segment combustion data.

Thrust Chamber Cooling

(U) Cooling criteria are strongly tied to life requirements and the tube material. Accordingly, the cooling investigation encompassed gas-side heat transf , coolant-side enhancement, material conductivity, material properties related to processing, material fatigue resistance, tube fatigue life, overall segment cyclic life, and overall regenerative-cooling margin. An analytical model was established to relate the many variables, and experiments were conducted in the laboratory to obtain the necessary information.

TABLE 7

(C) TUBE-WALL THRUST CHAMBER PERFORMANCE DATA SUMMARY

	Test Number		
	023	027	028
Test Duration (90-90% P_c), seconds	0.40	0.275	0.800
Specific Impulse, seconds			
Flight System at Test Pressure	343.7	342.2	334.7
Flight System at Vacuum	443.6	435.1	425.8
Specific Impulse Efficiency			
Flight System at Vacuum (Based on Shifting Equilibrium)	0.9548	0.9340	0.9156
Combustion Efficiency (Based on Shifting Equilibrium)	0.9743	0.9623	0.9493
Nozzle Efficiency			
Flight System at Vacuum (Based on Shifting Equilibrium)	0.9615	0.9502	0.9508
Ambient Pressure*, psia	12.30	12.20	12.30
Injector End Pressure*, psia	608.8	824.7	897.9
Nozzle Stagnation Pressure, psia	605.9	821.2	894.1
Overall Engine Mixture Ratio*, o/f	4.720	4.852	5.277
Injector or Primary Mixture Ratio*, o/f	4.930	5.017	5.884
Measured Thrust*, pounds	76140	96611	109251
Total Oxidizer Flowrate*, lb/sec	185.72	238.41	278.15
Total Fuel Flowrate*, lb/sec	62.26	100.91	106.67
Fuel Dump Flowrate*, lb/sec	22.91	51.78	51.76
Centerbody Flowrate*, lb/sec	1.68	1.61	5.43
Total Coolant Flowrate*, lb/sec	60.58	99.30	102.85
Oxidizer Injection Temperature*, R	232.8	215.0	212.2
Fuel Injection Temperature*, R	469.6	381.9	416.5
Coolant Inlet Temperature*, R	100.3	105.3	103.0
Oxidizer Injection Pressure*, psia	640.0	890.5	995.8
Fuel Injection Pressure*, psia	766.8	975.5	1042.3
Coolant Inlet Pressure*, psia	1611.6	2080.1	2171.2
Oxidizer Injector Pressure Drop*, psi	31.2	65.8	97.9
Fuel Injector Pressure Drop*, psi	158.0	150.8	144.4
Geometric Throat Area*, $in.^2$	87.570	81.515	81.895
Nozzle Area Ratio	72.06	77.40	77.04

*Measured Values

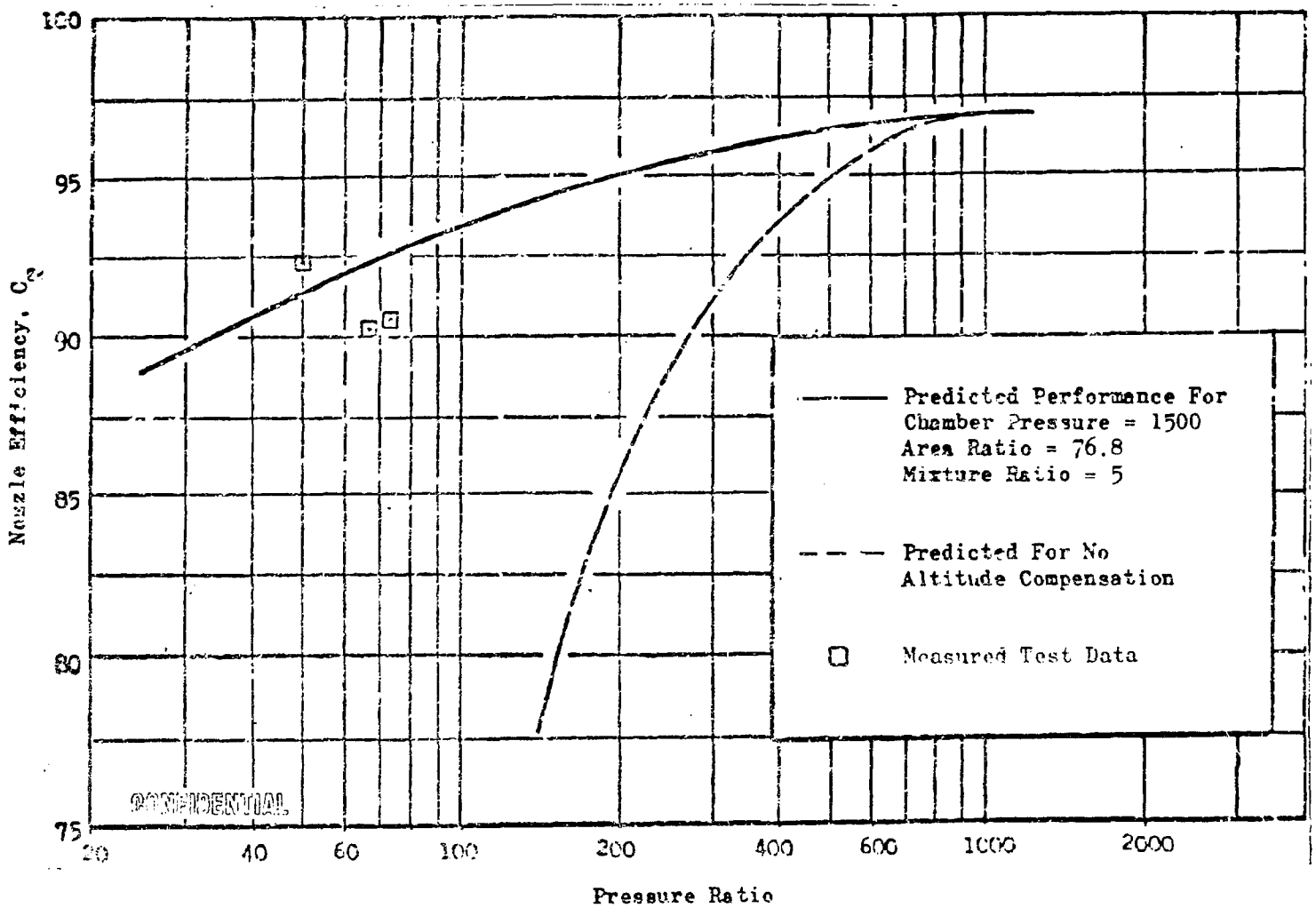

Figure 15. 25K Tube-Wall Thrust Chamber C_T Performance vs Pressure Ratio

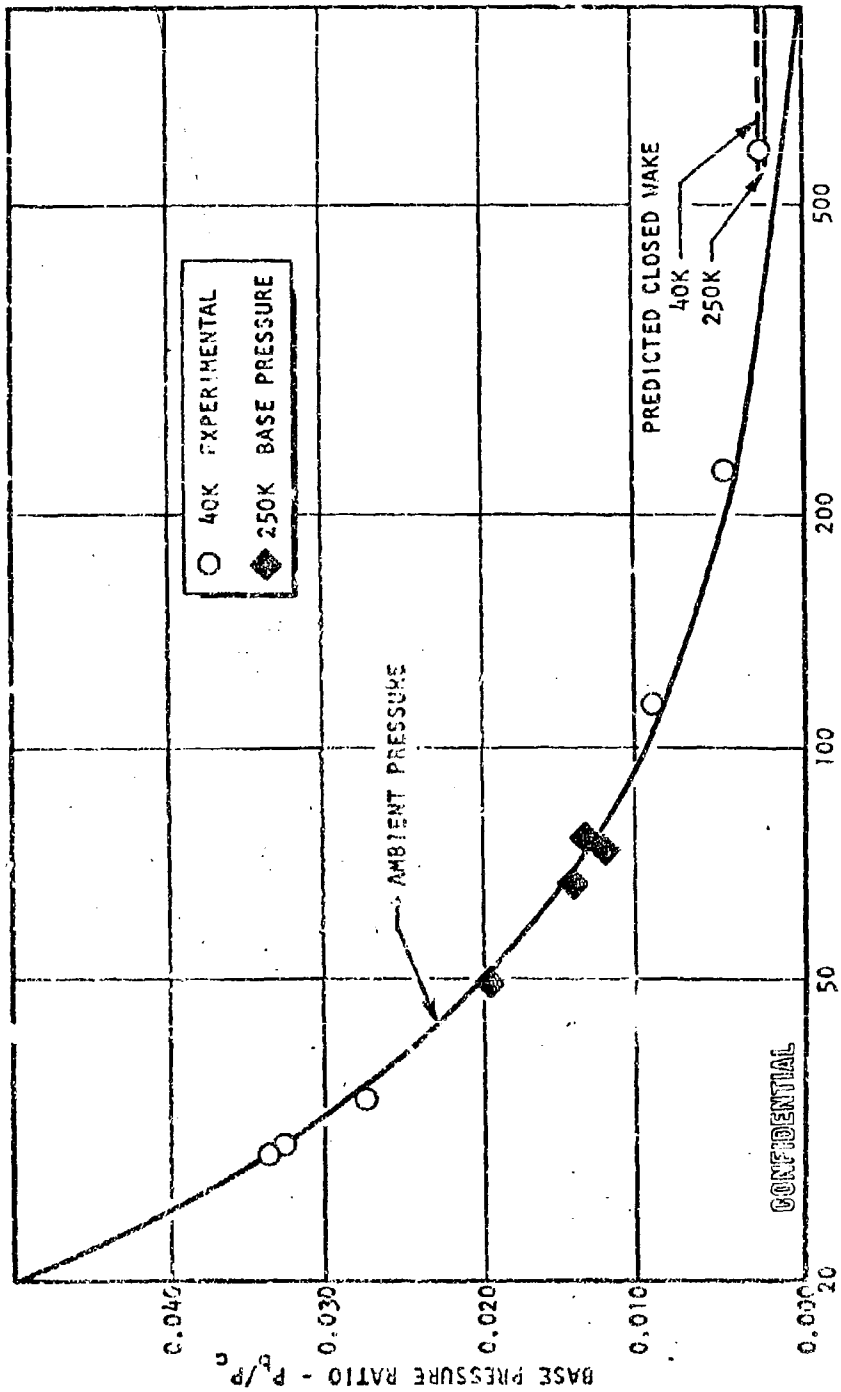

Figure 16. Experimental Base Pressure

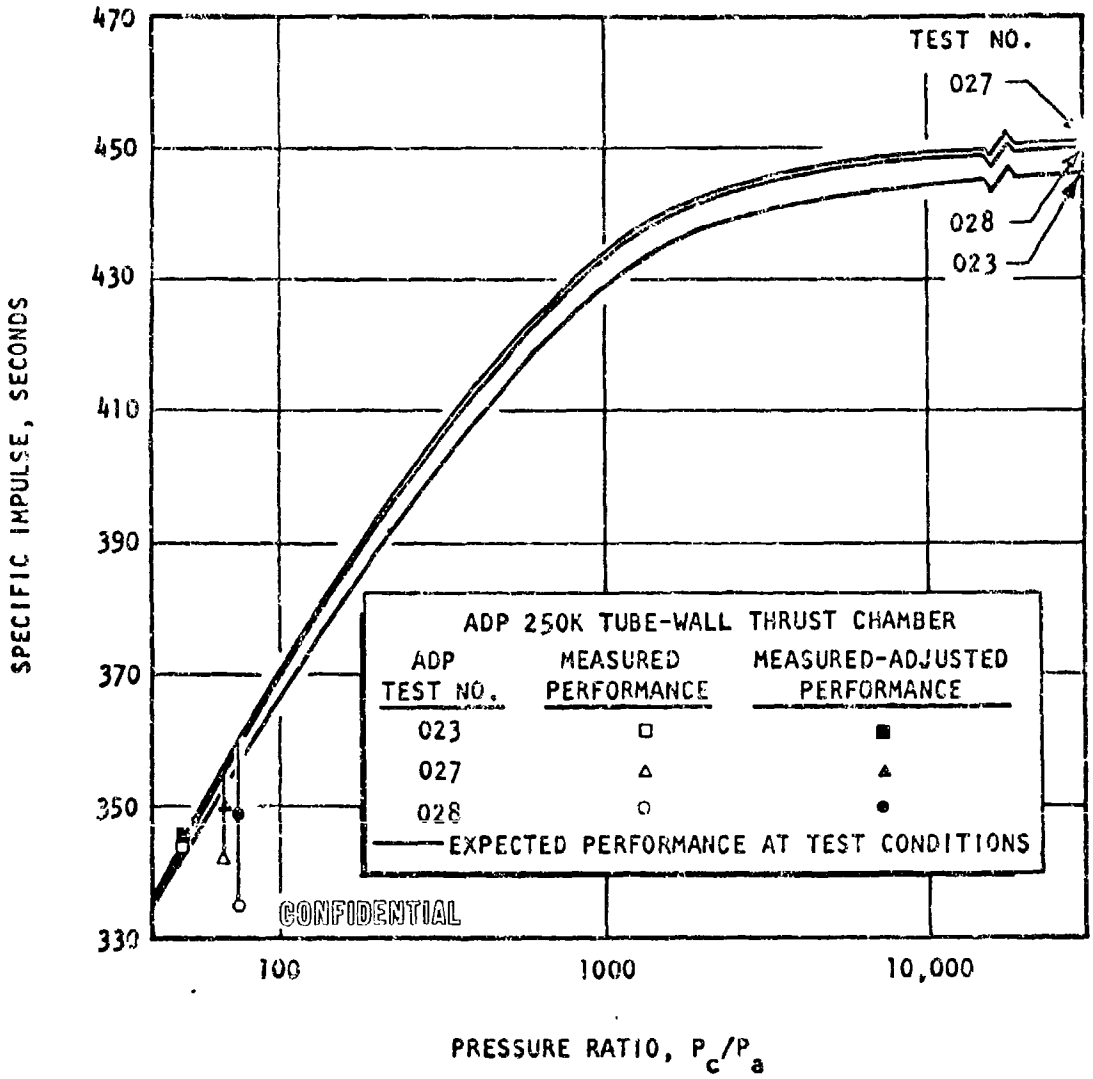

Figure 17. 250K Tube-Wall Thrust Chamber Specific Impulse vs Pressure Ratio

(C) Detailed heat transfer measurements at axial wall station locations were provided by highly instrumented water-cooled segment testing. Data were developed by calorimetric measurement of water temperature rises for a range in chamber pressure of 300 to 1580 psia and mixture ratio range of 3.31 to 9.71 in 120 tests. Data of the axial heat flux distribution vs length are shown in Fig. 18 for a nominal mixture ratio of 6.0 The nearly proportional increase of local heat flux with chamber pressure is shown. Isolation of the peak heat flux to a local region in the throat vicinity is illustrated. Experimental heat flux data (Fig. 19) defined a slope of 0.8 with chamber pressure which confirms that a turbulent boundary layer exists in the throat region.

(U) Confirmation of the water-cooled testing integrated heat input value for the combustion zone and throat region has been provided by tube-wall segment test data, as shown in Fig. 20. The anticipated slightly higher heat input values shown for the copper tube-wall segment are due to the lower wall temperatures provided by a higher wall thermal conductivity.

(C) On the coolant side, experimental values of the inner- and outer-body tube combined roughness and curvature factors ($\varphi_c \varphi_\epsilon$) determined from individual heated tube tests and segment tests are shown in Fig. 21 . At the throat locations indicated for the inner and outer body, combined factor experimental values of 3.0 and 2.5 are found.

(C) The analytical approach led to the selection of several candidate tube materials: Nickel 200, Nickel 270, boron deoxidized copper, beryllium copper alloy 10, type 347 stainless steel, and Hastelloy-X. The selection of this initial material candidate list was based on a preliminary cyclic life prediction obtained from the fatigue diagram, and fabrication and brazing confidence. The laboratory materials-evaluation effort, in conjunction with Rocketdyne's previous and concurrently generated

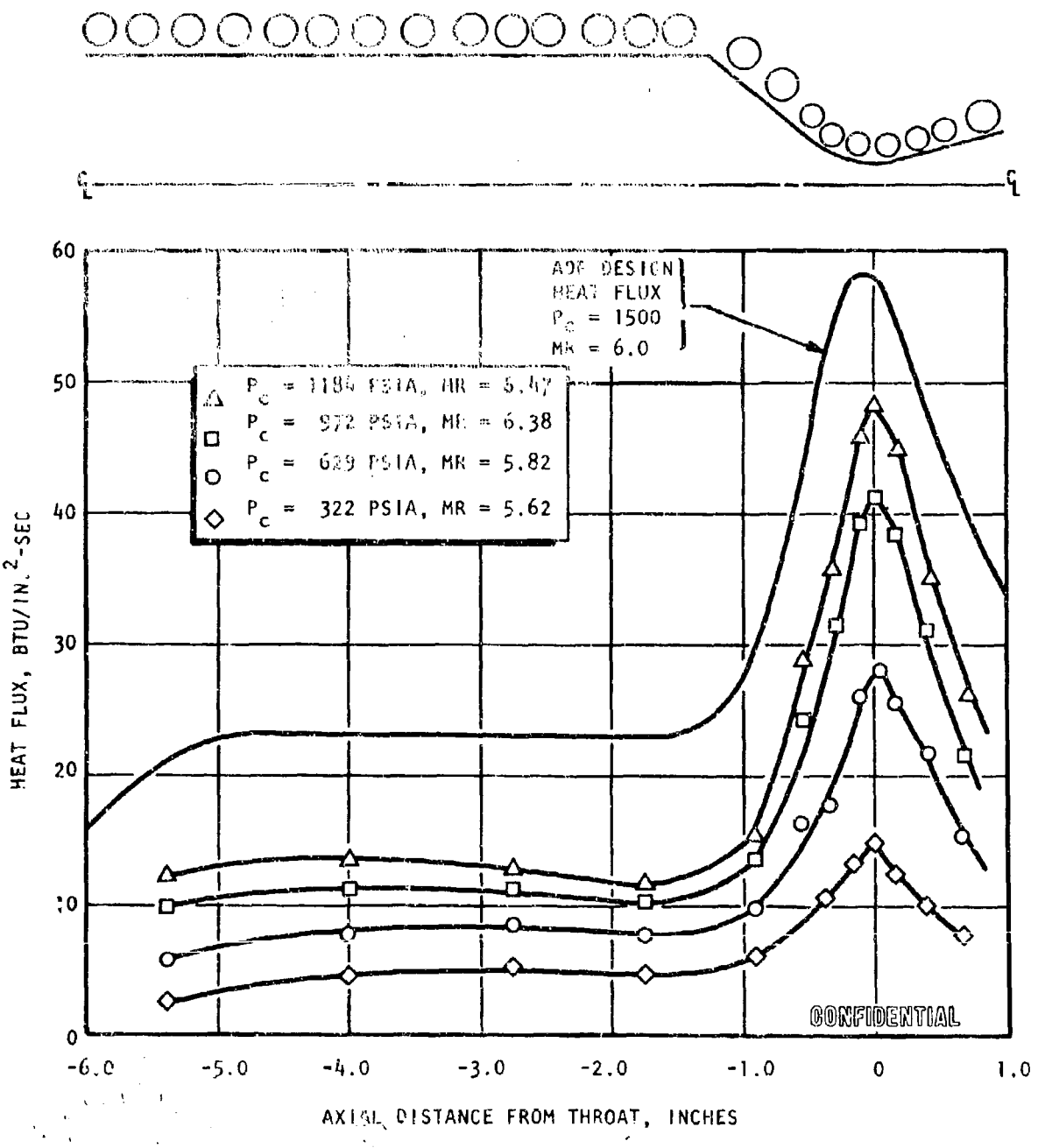

Figure 18. Experimental Heat Flux Distribution From 2.5K Water-Cooled Segment Tests

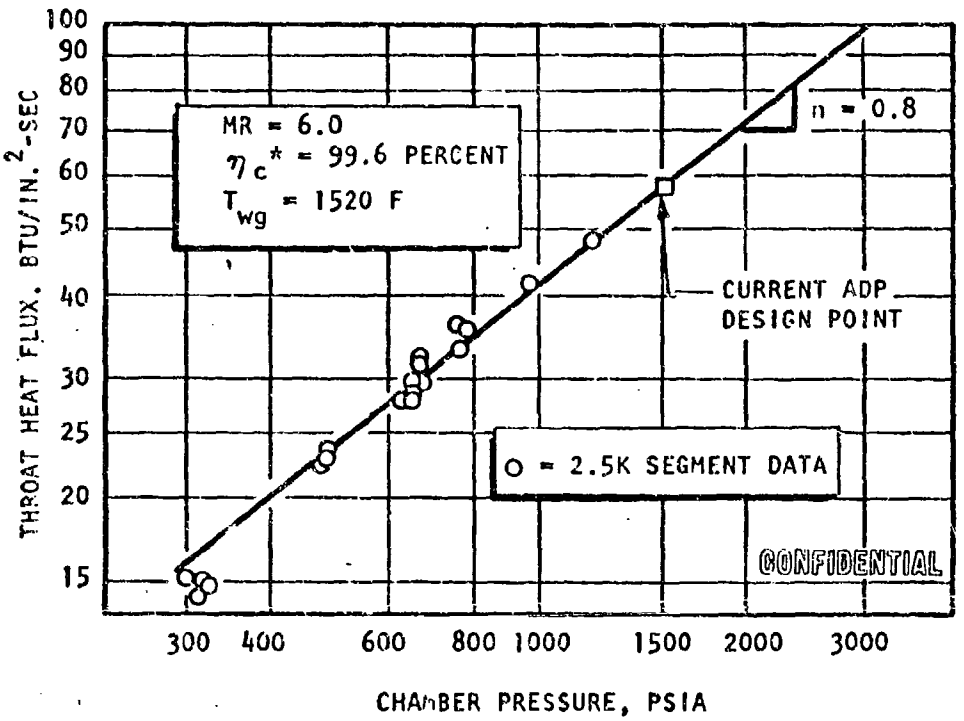

Figure 19. Throat Heat Flux vs Chamber Pressure

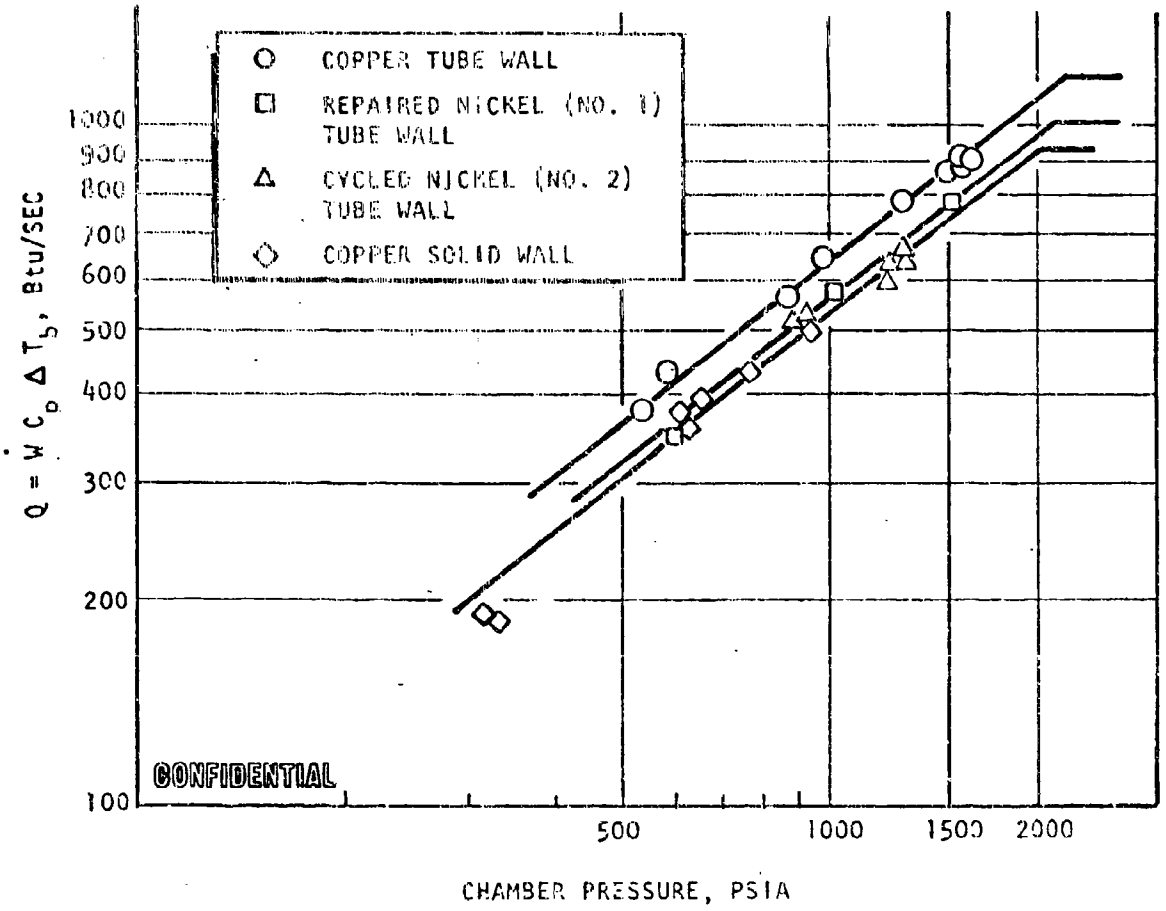

Figure 20. Contoured Tube Overall Heat Transfer Characteristics (2.5K ADP Copper and Repaired Nickel Segments)

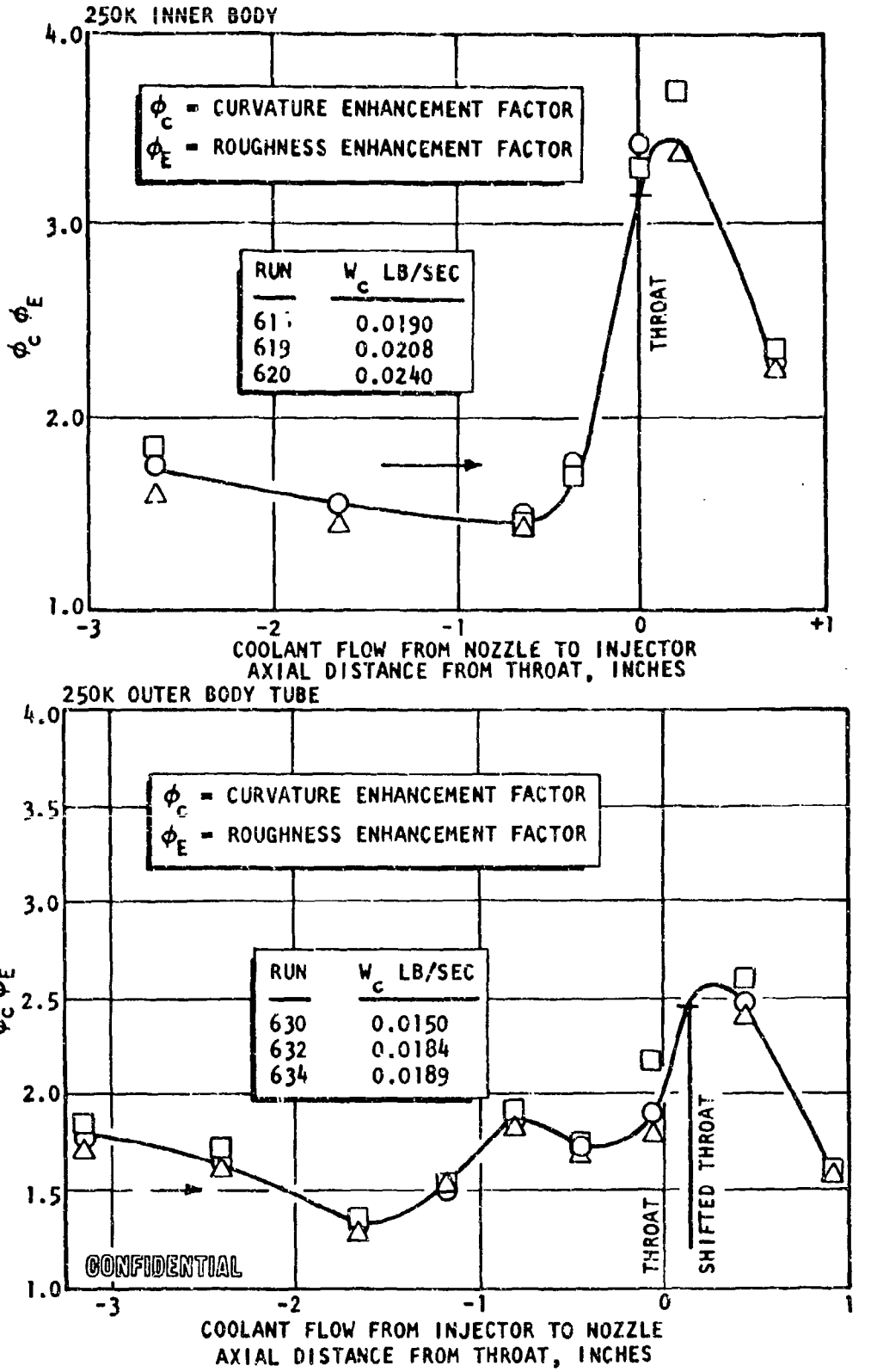

Figure 21. Experimental H_2 Coolant Heat Transfer Results for 250K Experimental Tubes Relative to Theoretical Straight Smooth Tube Heat Transfer Coefficient

fabrication and cost experience, led to the selection of Nickel 200 as the tube material for immediate and long-range application to the aerospike engine.

(U) A relationship between thermal analysis and mechanical fatigue was then used to obtain a thermal fatigue diagram (Fig. 22).

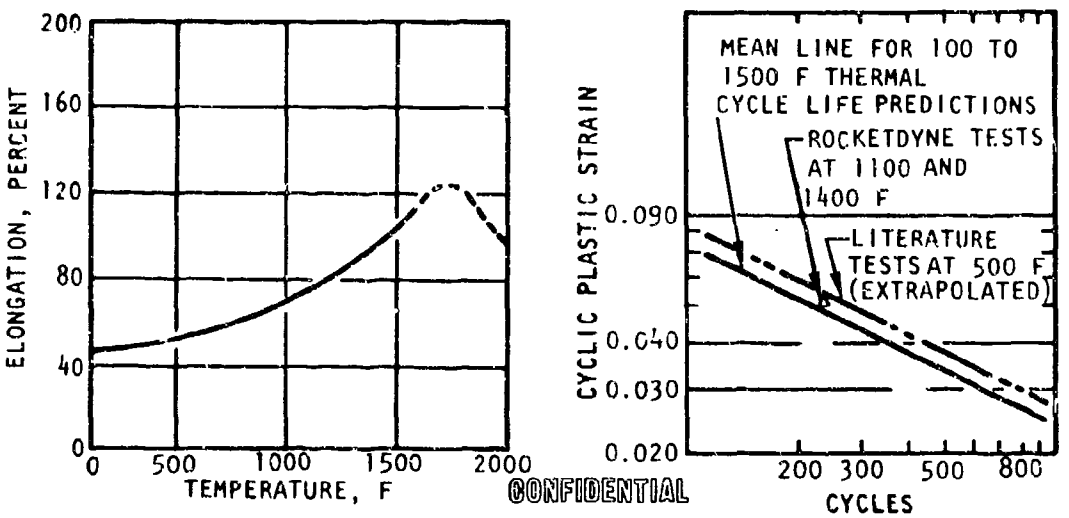

Figure 22. Low-Cycle Fatigue Characteristics (Nickel 200)

(C) Additional tests were conducted on an operating condition simulation tube tester to verify the life of Nickel 200 in fatigue creep. Results of these tests are shown in Table 8 .

(C) The most realistic demonstration of the cyclic life of a candidate tube material is afforded by hot-firing segment tests. The 2.5K nickel wall segment was fabricated to demonstrate this cyclic life. Three hundred and fifteen start-shutdown cycles have been successfully completed with no indication of tube erosion or overheating. These tests were conducted with a nominal tube-wall temperature of 1520 F.

TABLE 8

(C) THERMAL FATIGUE TUBE TESTER RESULTS ON NICKEL 200

Type of Test	Tubular Specimen Metallurgical Condition	Cyclic Gas Wall Temperature, F	Wall Temperature Drop, F	Hydraulic Stress in Heated Tube Crown, psi	No. of Thermal Cycles	Final Appearance of Heated Tube Crown	Equivalent Cycles at Demonstrator Conditions
Demo Module Start Simulation	As received	100 to 1400	74	1000	315	Intergranular and transgranular cracks, rupture	86
Demo Module Start Simulation	Furnace Processed	100 to 1400	65	1000	320	Intergranular and transgranular cracks, no rupture	94
Overtemperature Limit Test	Furnace Processed	100 to 1800	87	1000	142	Intergranular cracks, rupture	80
Overtemperature Limit Test	Furnace Processed	100 to 1800	92	1000	143	Intergranular cracks, rupture	86
Exploratory Limit Test	Furnace Processed	620 to 1140 100 to 900	200	3300 3300	800 193	No visible cracks, no leaks or rupture	Not applicable
Steady-State Limit Test	Furnace Processed	1365 to 1435	520	4500	22,500 over 7 hours	Cracks initiated, no leaks or rupture	22,500

CONFIDENTIAL

(C) A series of eight tests from chamber pressures of 310 to 2050 psia was also conducted on a related program with a 2.5K nickel tube-wall segment to extend available information on the regenerative-cooling capabilities of nickel tubular designs.

(C) The copper tube segment was operated to 1600 psi; however, it did not possess the fatigue, fabrication, and strength margin of the nickel. Operation of the 20K segments with nickel tubes, with the same cooling circuit as planned for the Demonstrator Chamber, to 1500-psi chamber pressure, and for 47 seconds duration at 1100 psi on a related program, serves to demonstrate further the regenerative-cooling capability.

(U) This cooling investigation provided data for design of long-life, high-chamber-pressure thrust chambers, and demonstrated both cooling margin and fatigue life of this type of chamber.

Lightweight Structural Evaluation

(U) The objective of this effort was to evaluate the selected structural arrangement in its ability to maintain predicted throat dimensions and to provide advanced structural, heat transfer, and fabrication data for a lightweight demonstrator module chamber design. To satisfy these conditions, a three-compartment rectangular segment was constructed. The segment includes two subsonic struts.

(U) The three-compartment segment approach provides close simulation of the maximum tube-wall thermal stress which occurs in the throat region, maximum coolant bulk temperature rise in the high heat flux area of the throat and combustion chamber, and a close approximation of pressure loads that will occur in the 250K module.

(U) Three compartments with two subsonic struts represent the shortest segment length required for continuous beam simulation. The rectangular combustor lengths are the equivalent arc length of the module at the throat diameter. Also, construction of all structural parts was closely simulated.

(U) To verify the calculated stresses acting on the lightweight backup structures on the 20K structural segment and the 250K demonstrator design, four strain gages were installed on each of two structural baffle bolts, and additional strain gages were installed on the horizontal and vertical ribs of the titanium backup structure. The location of these gages was selected to provide data on load distribution paths, maximum stresses, and resultant moments.

(C) During the series of 20K hot-firing tests, a range of chamber pressures from 600 psi to excess of 1500 psi were achieved. The baffle bolt stresses were measured on each of the tests. Results indicated excellent agreement between the measured and calculated bolt load.

(U) The throat gap was monitored throughout the test series by taking measurements with a ball-type gage inserted into the gap. These measurements indicate that the backup structure had no signs of plastic yielding and therefore was quite predictable. Even after the hardware was partially disassembled and reassembled, the throat gap returned to its original position.

(U) An analysis of the 20K structural segment was conducted to determine the manner in which throat area would change as a function of external loads (chamber pressure). The loads, stresses, and deflections of the 20K segment structure were modeled on a computer program.

(C) These analytical stress predictions were shown to be in good agreement with the measured values. The same analysis predicted throat deflections which result in approximately 1-percent throat area increases per 100-psi chamber pressure. This increase in throat area is favorable to performance of a full-scale engine. At full-thrust conditions, the Demonstrator Module would operate at the design area ratio. As the chamber is throttled, throat area would decrease, and the expansion area ratio of the thrust chamber would be increased accordingly. Based on the analysis of the 20K structural segment, the area ratio of the full-scale chamber would be increased approximately 12 percent at the full-throttled condition.

(U) Cooling and sealing of the structural ties across the combustion chamber were entirely satisfactory with two complete assemblies. Likewise, there was no adverse effect of these structural ties on performance or on cooling of the throat downstream of them. The 20K Segment Structural Evaluation demonstrated conclusively the ability of a lightweight-type structure to hold throat dimensions with satisfactory cooling of all parts and with no performance effect.

Operation

(C) Experiments were conducted on the 2.5K segments to obtain gas suitable for powering turbines by tapoff from the thrust chamber. Mixture ratio of local areas at the compartment ends was altered by selecting injection orifice areas to produce the desired temperature, and by variations in tapoff port locations. Three tests with the final configuration produced tapoff temperatures of 1000 to 1400 F over the operating ranges.

(C) Ignition of the segments by means of CTF and by TEAB was satisfactory. Likewise, CTF injection into each compartment on the 250K and verifying a pilot flame proved entirely successful. Hot-gas ignition was proved feasible in a related segment test program, and now only the combination of hot-gas ignition with tapoff ports remains to be completed. Hot-gas ignition was not accomplished on the 250K chamber because of damage to the injector which had those provisions.

(U) Priming of the full circumferential oxidizer manifold on start was even and symmetrical and verified an analytical model of the filling process.

(C) The 2.5K segment testing revealed no instability or significant combustion oscillations over a chamber pressure range from 300 to 1500 psi and mixture ratio from 4 to 8. Moderate oscillations were experienced at approximately 1200 and 1300 cps on the 20K segment, thought to be associated with the oxidizer feed system. No damage or performance effects were found in long-duration testing.

(U) A rotating mode of combustion oscillation was observed on the 250K tube-wall chamber tests. Even though the amplitude was not severe, the oscillation had the effect of increasing heat transfer around the baffles and bringing about coolant leaks in baffles and tubes behind baffles. Attenuation of this mode of oscillation remains to be accomplished at the end of the contract. Subsequent to the work on this contract, work on the NASA Advanced Engine Aerospike Program produced results on this

combustion oscillation. Modifications to the LO_2 feed system and to the baffles to produce better compartmentation attenuated the oscillation. Damage was reduced to a level such that long (7 second) duration tests were conducted.

(C) Major damage was experienced on the No. 1 250K tube-wall assembly because of overheating of the injector edges resulting from braze joint leakage in combination with hot-gas recirculation in the injector-to-chamber gap and the circumferential combustion oscillation. Filling of these gaps on subsequent assemblies solved this problem. Basic durability of the strip-type, triplet pattern injector was demonstrated by 225 start-stop cycles on one injector unit and 80 tests of 11 different units on the 2.5K segment test program.

Fabrication

(U) Tapering, forming, and brazing of stainless steel, nickel, and copper tubes of the small, highly tapered aerospike configuration was accomplished. Furnace-braze tooling and processes were developed so that four inner and four outer bodies were successfully completed on this and a related NASA program. Techniques for ensuring balanced coolant passages and repairing damage were employed. These chambers are illustrated in Fig. 23 and 24. Likewise, valuable experience was gained in successfully completing and firing three injectors (including NASA unit) with several improved processes for close control and reduced cost.

(U) The fabrication of the 20K lightweight structure segment proved the workability of the demonstrator baffle seat, baffle, and tube-wall design. Experience with adhesive bonding of the titanium structure to the nickel tubes was gained, pointing up areas requiring close control such as assembly fit up and cleaning--priming of the two surfaces to be joined.

IXE32-4/12/67-C1B

Figure 23. Completed 250K Tube Wall Outer Body

Figure 24. Completed 250K Tube Wall Inner Body

CONCLUSIONS AND RECOMMENTATIONS

(U) 1. The Demonstrator Module design evolved in this effort meets all requirements to demonstrate the aerospike capability in late 1969 to provide a base for development of a high-performance, flexible, longlife Flight Module.

(U) 2. Thrust and mixture ratio excursion requirements can be met with a relatively simple system design using only two hot-gas valves as points of control: one valve to control total tapoff gas flowrate and one valve to control oxidizer turbine gas flowrate. A closed-loop control system is simpler, lighter, and more complementary to vehicles and test requirements than other alternatives. The aerospike engine will, however, operate satisfactorily open loop.

(C) 3. It is concluded that the Demonstrator Module can be designed to operate regeneratively cooled at 1500 psia and deliver, and a mixture ratio of 6:1, theoretical shifting specific impulse efficiencies in excess of 96 percent at rated thrust and 95 percent at throttled conditions.

(C) 4. From the application study, the common 250K aerospike engine should have a design chamber pressure of 1300 psia and a diameter of 78 inches. There is no significant performance index advantage to increasing the 250K or 350K aerospike engine design chamber pressure to a value greater than 1500 psia for any one of the six Air Force defined vehicles and missions. The reusable vehicles all require significantly lower engine chamber pressures to maximize performance index than do the expendable vehicles.

(C) 5. Performance testing of the selected triplet injector pattern in both one-half compartment (2.5K) and three-compartment (20K) segments indicates this injector delivers a combustion (c^*) efficiency sufficient to meet the overall specific impulse requirements for the engine for the nominal mixture ratio. Complete chamber (250K) results at 40-percent chamber pressure verified segment findings.

(C) 6. Segment testing is an effective and low-cost means of evaluating aerospike thrust chambers and injectors for performance, injector durability, cooling life, and ignition. The limits of application of segments should be enlarged to cover thrust chamber durability, stability, and reliability by duplicating the propellant feed passages and combustion compartments of the complete chamber.

(C) 7. Combustion was oscillatory and damaging on the full-scale chamber. Since combustion was stable over a broad operating range, on the one-half compartment (2.5K) segments, was oscillatory but not damaging on the three-compartment (20K) segment, and injector propellant feed passages and degree of compartmentation of combustion varied widely among the three, it is concluded that these factors are connected with the degree of stability achieved. Feed system and baffle modifications were helpful in attenuating the combustion oscillations on the 250K thrust chamber on the NASA Advanced Engine Aerospike Program subsequent to work on this contract.

(C) 8. Based on the tangential oscillations experienced during testing of the full-scale annular chamber, it is recommended that subsequent aerospike engines consider the segmentation of the propellant manifolds to avoid feed system combustion process coupling. It is further recommended that the thrust chamber baffles be sealed to the thrust chamber walls and be of sufficient length to ensure that the combustion energy is released within the baffled compartment.

(U) 9. Nozzle performance results for the selected design from 250K solid-wall and tube-wall testing were close to predicted values from cold-flow models, 10K, and 40K hot-firing tests. Nozzle performance is sufficient to meet the overall specific impulse requirements for the engine.

(U) 10. Injector durability has been demonstrated by one 2.5K-segment injector undergoing 229 tests with no leaks, the many 2.5K units fired, and a 20K injector undergoing repeated tests up to 47 seconds duration. 250K testing has shown the necessity to minimize intercompartmental and local gas circulation.

(U) 11. Hot-gas tapoff from the combustion chamber for turbine drive with the compartmented aerospike thrust chamber has been demonstrated to be feasible. The feasibility of hot-gas ignition of a chamber segment, with the tapoff ports serving as hot-gas entry ports for ignition, has been demonstrated on a chamber segment (on a related program).

(U) 12. The NASA System and Dynamics Investigation manifold studies and 250K hot-firing tests have shown that the current aerospike liquid oxygen manifold design will fulfill thrust chamber start and shutdown requirements. Priming times are predictable with a developed analytical model for all required flow conditions, and ignition and buildup are satisfactory. Shutdown characteristics with gaseous nitrogen purge have been shown to be controllable and acceptable.

(U) 13. Successful completion of furnace braze of four outer-body and four inner-body 250K tube-wall assemblies (two each on the NASA System and Dynamics Investigation program) demonstrates the workability of this tooling and fabrication procedure. As the demonstrator module tube bundle is designed to use this same tooling, modified for detailed differences, it is believed that a similar one-for-one success can be achieved for that chamber. Many techniques for dimensional control, checks of details before assembly, and multiple-station tooling, particularly applicable to annular injectors and chambers, were developed for reduced cost of future units.

(C) 14. Testing of both copper and nickel tube wall segments to 1500 psi chamber pressure illustrates the capability of regenerative cooling

of the demonstrator chamber combustor shape with a high-performing injector. Testing of a nickel tube segment with a 99-percent c* efficiency injector to 2050 psi chamber pressure on a related program with no damage to the tubes demonstrates a measure of cooling margin available.

(C) 15. From analytical studies, laboratory materials fatigue tests, brazing tests, tube tester simulation tests, and hot-fire experience, it is concluded that Nickel 200 is superior to stainless steel and pure (OFHC) copper as a Demonstrator Module thrust chamber tube material. However, beryllium-copper shows great long-range promise as a superior material to nickel when available in tube form.

(C) 16. Testing of a second nickel tube-wall segment for 314 start-stop cycles has demonstrated adequate fatigue life of nickel tube material. Over 280 of these cycles were from ambient to maximum tube-wall temperature with material plastic strain as predicted for the Demonstrator Module. This conclusion is supported by materials testing, tube-tester simulation tests for the same number of cycles, and an analytical model of the heating and strain-producing process.

(C) 17. Testing of the 20K segment from 600- to 1540-psi chamber pressure and for a duration of 47 seconds, regeneratively cooled, demonstrates the capability of a lightweight structure with structural ties through the combustion chamber to maintain a predictable throat gap through the operating range. Ability to cool the structure and seal the cooling circuit was also demonstrated. Combustion performance and overall heat flux measured on the 20K segment tests compare favorably to 2.5K segment results and, therefore, to the data used as a basis for Demonstrator thrust chamber predictions. The use of adhesive bonding will require special care during fabrication.

TASK I, DESIGN AND ANALYSIS

DEMONSTRATOR MODULE DESIGN

Objectives and Requirements

(U) The requirements for this subtask were as follows:

(U) Module Design was to include preliminary designs of the Demonstrator Module and the generation of parametric data required in the application study. Therefore, this effort was to include a comprehensive analysis of performance, cooling, system control, and engine weight. An analysis was also to be performed to identify features needed to enhance the versatility of the module design for use in a broad range of vehicle applications. From the preliminary module design, detailed component designs were to be derived for the test articles to be used in testing.

(U) Detailed designs were to be conducted for long-lead time items required for fabrication of Demonstrator Module turbopumps. An analysis of the control system was to be conducted to define control system and servo loop requirements. Preliminary design of control system components were to be completed.

(U) The objective then of the Phase I Demonstrator Module Design and Analysis Task was to define design requirements for a full scale engine to be built in Phase II and used in a demonstration test series at sea level and altitude conditions. The test series will demonstrate performance, operating characteristics, combustion stability, durability, altitude restart, start and cutoff behavior, and control characteristics. Specific design goals are listed in Table 9. Sufficient detailed hardware design was to be made on the engine system and critical components such as the thrust chamber, turbopumps, and control elements to permit initiation of long-lead item procurement within 4 to 6 months after Phase II go-ahead.

(C)

TABLE 9

DEMONSTRATOR MODULE DESIGN REQUIREMENTS

Nominal Vacuum Thrust	250,000 pounds at nominal mixture ratio
Minimum Delivered Specific Impulse	96% of theoretical shifting I_s at rated thrust 95% of theoretical shifting I_s during throttling
Throttling Range	Continuous down to 20% of rated thrust
Overall Mixture Ratio Range	Engine operation from 5.0 to 7.0 Nominal design point 6.0
Expansion Ratio	Area ratio(s) representative of booster and upper-stage applications. Overall static engine diameter will not exceed 100 inches
Durability	10 hours time between overhauls, 100 reused, 300 starts, 300 thermal cycles, 10,000 valve cycles
Single Continuous Run Duration	Capability from 10 to 600 seconds
Engine Starts	Multiple restart at sea level or altitude
Control Capability	Plus or minus 3% accuracy in thrust and mixture ratio at rated thrust. Excursions from extreme to extreme in thrust or mixture ratio within 5 seconds
Propellant Conditions at Engine Inlets	LO_2: 15 feet NPSH from 1 atmosphere boiling temperature to 180 R LH_2: 60 feet NPSH from 1 atmosphere boiling temperature to 45 R
Environmental Conditions	Sea level to vacuum conditions. Combined accelerations: 10 g axial with 2 g transverse, 6.5 g axial with 3 g transverse, 3 g axial with 6 g transverse
Engine/Vehicle Interface Conditions	Flight Module design without requirements for external power, with the exception of nominal electrical power and 3000-psia helium from the vehicle

Summary of Work Accomplished

(U) The effort expended on Task I during the contract period was defined by the objectives to include the Demonstrator Module analysis and design portions of the contract. Under the analysis portions, the effort was broken down into system trade studies and design support analysis. The trade studies included a re-evaluation of the pump power cycle (tapoff vs gas generator) and the turbine arrangement (series vs parallel), an investigation and selection of the optimum module control points (liquid vs hot-gas valves control) and control logic (open loop vs closed loop), and a selection of the optimum operating envelope (constant thrust vs constant chamber pressure mixture ratio excursions).

(U) The design analysis began with an initial estimate of the system engine balance. This defined preliminary engine parameters to be used in the first preliminary system and component designs. Feedback from the design groups then provided a better basis for more accurate system balances. These data were then used in predicting the system performance and in formulating a system start model. The sensitivity of the system to design changes was studied, and the effect of manufacturing tolerances was incorporated into the calculation of the system design parameters. Final engine performance and weight calculations were then made for both a Demonstrator Module and a projected Flight Module.

(U) Under the design portion of work, the effort was broken down into system design, turbomachinery design, thrust chamber design, and controls design. The system design included an investigation of alternative thrust structure concepts which considered different types of structural members (solid beams, trusses, honeycomb) as well as different locations of the

gimbal point. The major component locations and interfaces were determined and the available envelopes defined. The system design integration function included the preliminary design of all of the interconnect ducting and component support mounts. An overall module design layout was then completed together with separate subsystem layouts.

(U) The turbomachinery design effort began with basic design trade studies in order to select the pump, preinducer, and turbine configuration. Centrifugal and radial designs were studied for the pumps, separate- and integral-drive arrangements were studied for the preinducers, and different numbers of wheels were studied for the hot-gas turbines. After the basic design concepts were selected, analytical studies were conducted to optimize such design features as the impeller blade profile, the turbine wheel configuration and attachment, the axial thrust balance mechanism, and the bearing support design. Finally, a rotodynamics analysis was conducted to ensure that the turbopumps operated safely away from the critical speeds. Pump and turbine performance was predicted in support of the system analysis effort. The task was concluded with the preparation of detail design layouts including the selection of materials, bearings, and seals.

(U) The thrust chamber design effort included performance, structural, and heat transfer studies of the combustor and nozzle, thrust chamber support structure, injector design, and base closure design. Heat transfer analysis of the combustor and nozzle included the selection of an appropriate cooling circuit and tube material, and the prediction of the regenerative-cooling circuit pressure drop. In addition, the tube design had to be optimized with respect to size, contour, and thickness in order to meet the performance and life goals. Several alternative combustor support structure designs comparing different materials and bonding concepts were studied in an effort to minimize weight. The injector design

was studied to optimize combustion performance as well as ensure satisfactory tapoff and ignition characteristics. Alternative injector mounting concepts were studied in conjunction with the subsonic structural tie design. Design considerations for the latter included structural requirements, tapoff port provisions, and cooling circuit requirements. Different base closure designs were studied with different mounting concepts in order to attain maximum performance with minimum weight. A detail thrust chamber layout was completed.

(U) The controls design effort was conducted in two basic areas, performance controller logic and valve mechanical design. The former consisted of formulating controller logic and functional design and then performing system control analyses on an analog model. The mechanical design effort included an evaluation of different design concepts for the liquid propellant valves (poppet, butterfly, and visor) and the hot-gas throttle valves (balanced poppet, conventional poppet, butterfly, and visor). After the concept selection was made, design layouts were completed for the two main liquid propellant valves and, also, for the hot-gas tapoff throttle valve.

Demonstrator Module Design Summary

(U) The major trade studies that served to establish the basic Demonstrator Module configuration included the power cycle evaluation, the selection of the throttling and mixture ratio control system, the turbomachinery design selection, and the thrust chamber combustor configuration selection.

(U) The cycle trade study involved a comparison of the tapoff and the gas generator cycles, and a series and parallel turbine arrangement. A tapoff cycle with parallel turbines was confirmed superior because it offered a simpler, lighter-weight system with better start characteristics and higher performance during throttling.

(U) The throttling and mixture ratio control system selection involved a study of the possible control points, control logic, and operating envelopes. Hot-gas valves located in series, one in the main tapoff duct to control thrust and one in the oxidizer turbine inlet duct to control engine mixture ratio, were selected because of higher performance, lighter weight, and control flexibility. A closed-loop logic system was selected to meet the accuracy, safety, and response requirements of the engine system. A mixture ratio excursion at constant chamber pressure was selected instead of a constant-thrust excursion because of control system simplifications and more favorable vehicle application results.

(U) A two-stage centrifugal design was selected for the fuel pump because it offers low weight and high efficiency together with good stall characteristics. A single-stage centrifugal design was selected for the oxidizer pump because the low head and medium flowrate are ideally suited to such a design. Axial flow preinducers were selected for both pumps with hydraulic turbines used for the driving power. Because hydrodynamic considerations dictated different speed ratios, the hydraulic turbine was located behind the preinducer in the fuel pump, and in the preinducer hub in the oxidizer pump. Three-row, velocity-compounded turbines were selected to power the pumps because they offer the best performance vs weight tradeoff.

(U) The thrust chamber design analysis included the selection of a straight-walled combustion chamber because of increased performance and simplified chamber construction.

(U) The final Demonstrator Module design has a maximum overall diameter of 100 inches and a length of 56.55 inches, and the dynamic envelope diameter is equal to the static envelope diameter because the gimbal point is located in the plane of the maximum diameter. The overall engine dimensions and the physical relationships of the components are shown in Fig. 25 .

(U) The Demonstrator Engine schematic, showing basic elements and propellant flow paths, is shown in Fig. 26 . Individual oxidizer and fuel turbopumps are used with the turbines driven in parallel by hot gases tapped from the main combustion chamber during mainstage operation. The exhaust from the turbines is discharged through the base closure into the nozzle base region, producing an increase in base pressure that contributes to total thrust. The complete thrust chamber and injector are regeneratively cooled with fuel. Thrust control is achieved with the tapoff throttle valve located at the Y-junction of the two tapoff hot-gas ducts, and engine mixture ratio is controlled by a throttle valve located at the oxidizer turbine inlet. Ignition is accomplished under tank head pressures with the use of a separate hot-gas igniter (HGI). This component produces hot gases which are discharged into the turbine drive

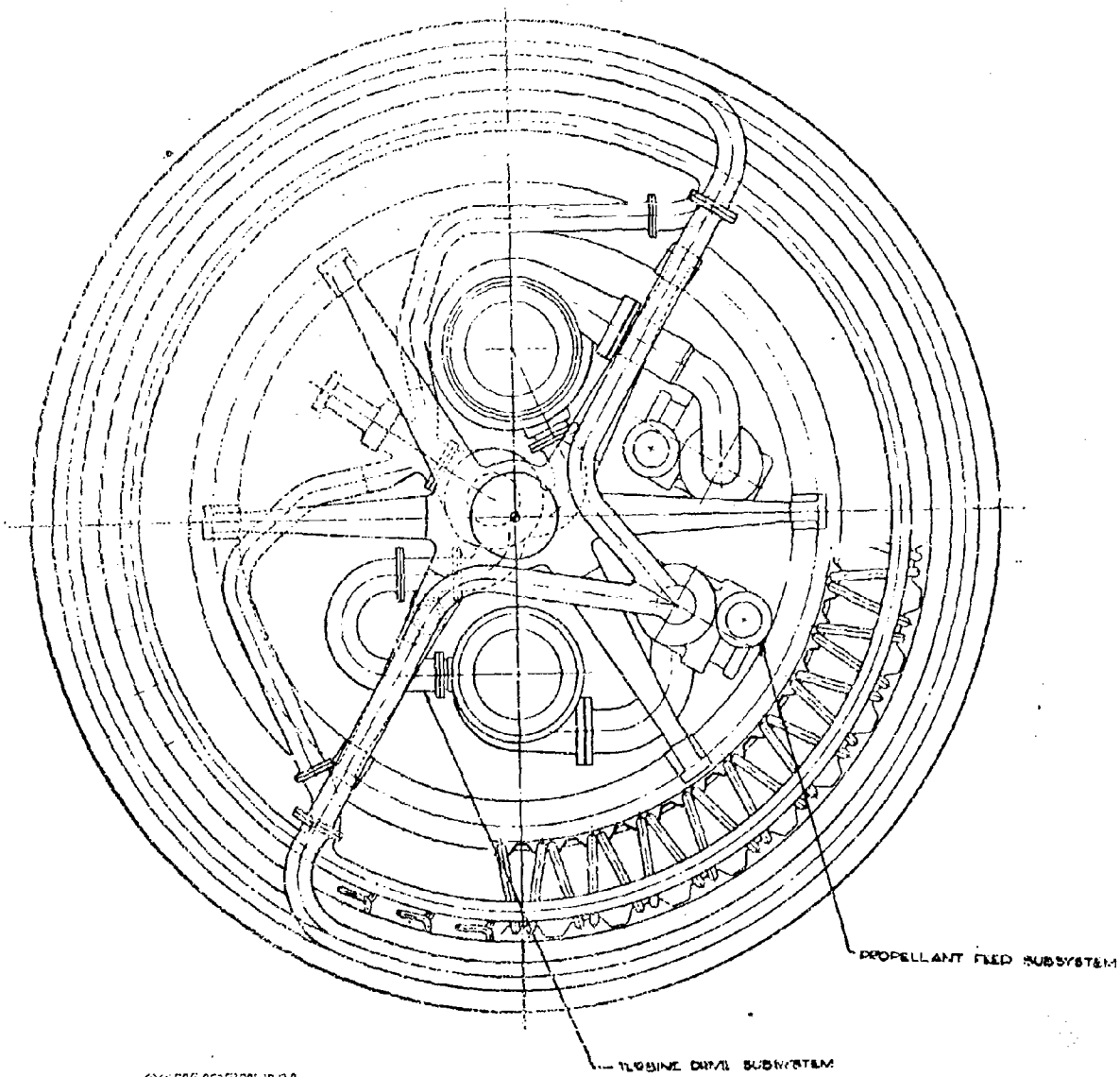

CONFIDENTIAL

Figure 25A. Demonstrator Module Layout

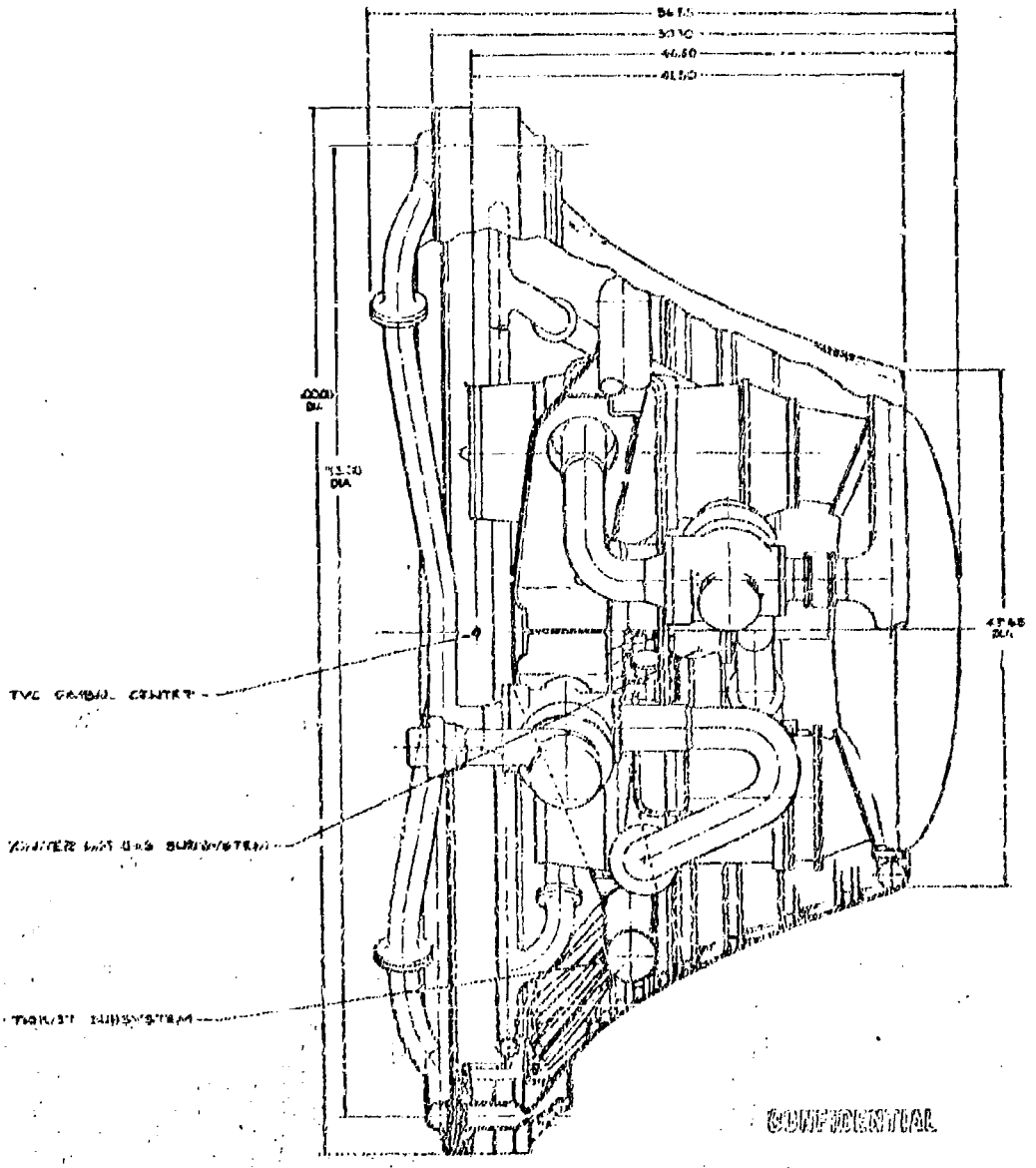

Figure 25a. Demonstrator Module Layout

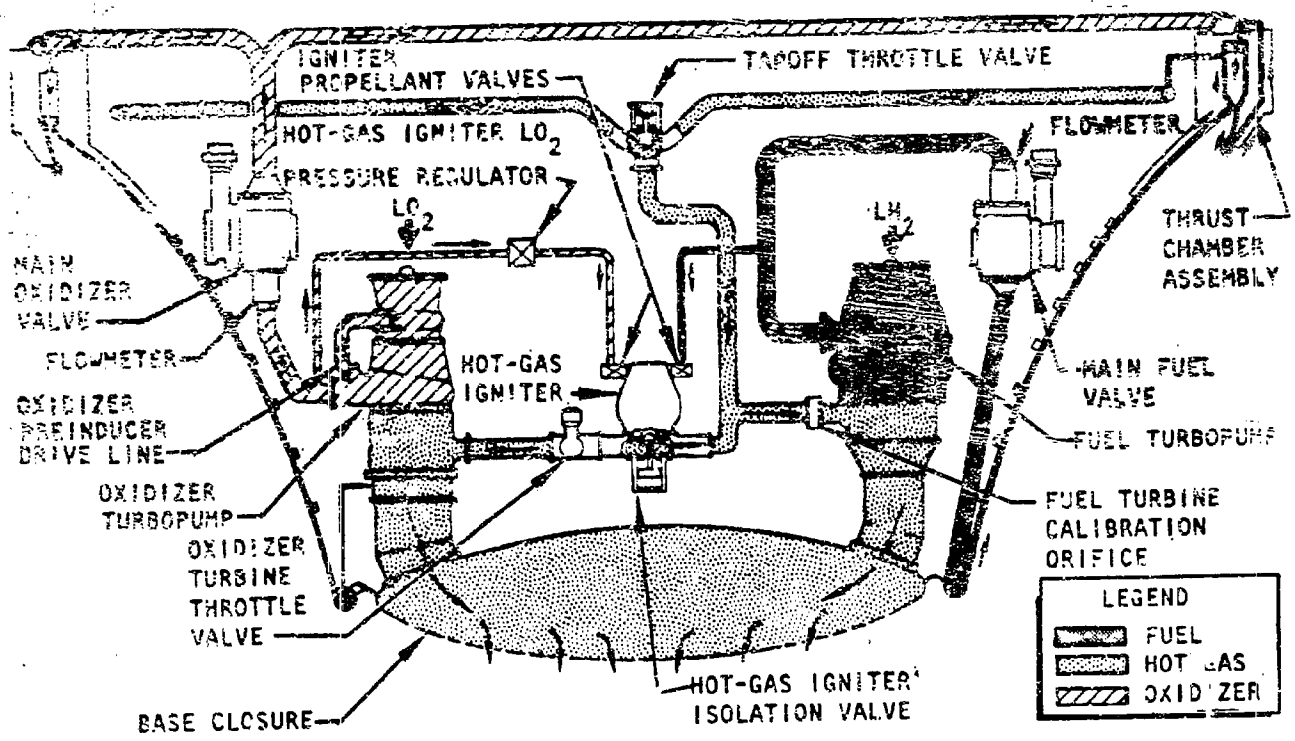

Figure 26. Demonstrator Module Schematic

ducting and used to provide both the initial turbine spin and the ignition energy source for the main chamber. The temperature of the hot-gas igniter is controlled by an automatic oxidizer pressure regulator in the HGI inlet line. Once main chamber ignition is achieved, the HGI is shut down with its own liquid-propellant shutoff valves, and the combustor body is isolated from the tapoff system by closing the HGI isolation valve. Engine shutdown is achieved simply by closing the oxidizer turbine valve and sequencing the main propellant valves to provide a fuel-rich cutoff.

(C) Using a systems engineering approach, the engine mechanical design was divided into the following four functional subsystems: thrust, propellant feed, turbine drive, and hot-gas ignition. The thrust subsystem is comprised of the thrust chamber and injector, the thrust structure, and the base closure. The thrust chamber consists of two regeneratively cooled nickel tube subassemblies, referred to as the inner body and the outer body, connected by 40 regeneratively cooled subsonic struts. The inner-body tubes have a 2:1 splice approximately 4 inches downstream of the throat with nickel used in both sections. The injector is formed by radially mounting 240 copper injector strips on an Inconel 625 structural body. Each strip is 2 inches long and 3/4 inch wide, and contains eight triplet patterns with two oxidizer orifices for each fuel orifice (same triplet pattern as demonstrated in Task II). The thrust chamber tubes are supported by a mechanically jointed segmented titanium structure adhesively bonded to the tube bundle in the area of the combustion zone, and by eight Inconel 718 compression rings mounted between the throat and the nozzle exit on the inner body. The engine thrust structure transmits thrust from the thrust chamber to the gimbal bearing mounting pad located on the engine centerline. It is comprised of a radial beam/hub assembly and a truss cone/intermediate ring assembly, which is bolted to the backside structure of the combustion chamber body. The thrust structure also provides support pads for the turbopumps, hot-gas igniter, control components, and interface panels.

(C) The propellant feed subsystem is comprised of the liquid-propellant ducts, valves, and turbopumps. The main valves are visor (modified ball)-type valves which provide on-off control only. The oxidizer pump is a single-stage centrifugal type driven by a three-row, velocity-compounded, hot-gas turbine operating at a nominal speed of 25,000 rpm. It is provided with a preinducer driven by a hub-mounted hydraulic turbine using LO_2 tapped off the pump discharge. The pump is sealed from the fuel-rich turbine gases with a triple-seal package consisting of two hydrodynamic liftoff secondary seals and a primary, purged-shaft riding seal. The fuel pump is a two-stage centrifugal type driven by a three-row, velocity-compounded, hot-gas turbine operating at a nominal speed of 35,000 rpm. The fuel pump preinducer is driven by an internal, through-flow hydraulic turbine. The turbine area is sealed from high-pressure pump fluids by a combination of labyrinth seals and a hydrostatic liftoff seal. Propellant-lubricated roller bearings were selected for both pumps.

(U) The turbine drive subsystem includes the hot-gas ducts and the two hot-gas throttle valves. A trade study resulted in the selection of a poppet-type valve for the tapoff throttle valve.

(U) The hot-gas ignition subsystem consists of a small combustion chamber for LO_2 and LH_2, and injector, igniter propellant valves, a spark ignition device, and an isolation valve located at the combustor outlet in the distribution manifold which interfaces with the turbine drive subsystem.

(C) The engine thrust and mixture ratio controls consist of the two hot-gas throttle valves, which are the only servocontrolled valves in the system. These are hydraulically actuated using facility-supplied hydraulic power. All other valves are sequenced by four-way solenoid valves, and are hydraulically actuated. The servovalves utilize an outer closed-loop control system on the desired performance parameter (chamber pressure

for the tapoff throttle valve and mixture ratio for the oxidizer turbine throttle valve) and an inner closed-loop control system on valve position using both integral and proportional control. This type of control ensures dynamic stability and safety while meeting the response (5 seconds between any two points) and accuracy (±3 percent) requirements of the engine system.

(U) Accessibility for system checkout and component repair has been provided in the design by making the thrust chamber easily removable from the thrust structure. This exposes all the major components, which are mounted directly to the six radial beams of the thrust structure. The base closure also is removable from the thrust chamber to provide access to the internal cavity from below without removal of the thrust chamber.

(U) The Demonstrator Module is designed to interface with test facility attach points, and gimbal actuators will be replaced by nongimbaling stiff arms.

(C) The total weight of the Demonstrator Module was calculated to be 3950 pounds, which represents a system with basic Flight Module design similarity while incorporating test flexibility design features and design conservatism considered prudent to meet demonstration, cost, and schedule objectives.

(C) Performance analysis predicted an actual specific impulse equal to 450.1 seconds at a 1500-psia chamber pressure and a 6:1 mixture ratio. Based on analytical studies of a nonadiabatic nozzle, this yielded an overall engine specific impulse efficiency of 97.01 percent (including effects of heat loss, viscous drag, divergence losses, and kinetics losses). The combustion chamber performance for the Demonstrator Module was based upon 39 segment tests conducted over an operating range in excess of

the required mixture ratio and throttle range during Phase 3 of this program. Based on the test data obtained, a c* efficiency of 99.6 percent was predicted for the Demonstrator Module at full-thrust conditions.

(U) The design of the Demonstrator Module includes allowances to account for performance variations that result from hardware tolerances and calibration inaccuracies. Individual 3-σ component variations were established from previous Rocketdyne engine fabrication and test experience. These then were used in the performance prediction model to determine the maximum design conditions required on each component to meet the maximum thrust and mixture ratio excursion requirements of the engine system. Because the Demonstrator Module is closed-loop controlled on chamber pressure and mixture ratio, the engine is first calibrated for design thrust to establish the exact nominal chamber pressure and nominal mixture ratio. Thrust calibration accuracies and thrust chamber fabrication variations therefore determine the maximum chamber pressure the engine might experience. Other component variations, such as turbopump efficiencies, are compensated for by changing the turbine flowrate and hence the pump power required to meet the chamber pressure and mixture ratio input commands. These variations have virtually no effect on total thrust and less than a 1-second effect on specific impulse.

System Analysis

(U) Operation and Performance. The aerospike engine system formulated during this effort utilizes an advanced nozzle concept in conjunction with a simple advanced power cycle. The advanced nozzle has an annular combustion chamber with the primary hot gas expanding over a truncated spike. A secondary gas flow is injected through the base plane of the nozzle to enhance the engine performance. The advanced power cycle

utilizes turbines driven by hot gases tapped from the main combustion chamber. The system analysis effort was concentrated primarily upon determining and optimizing the critical parameters associated with this cycle and thereafter determining the performance of the complete system.

(C) Engine Schematic and Operation. The schematic shown in Fig. 27 represents the Demonstrator cycle configuration, and the pressures and flowrates correspond to the nominal design point of 250K thrust, 6:1 mixture ratio, and 1500-psia chamber pressure. Individual oxidizer and fuel turbopumps are used with separate turbines driven in parallel by hot gases tapped from the main combustion chamber during mainstage operation. The exhaust from the turbines is discharged through the base closure into the nozzle base region, producing an increase in base pressure that contributes to total thrust. The complete thrust chamber and injector are cooled entirely by the fuel flowing through a regenerative cooling circuit before it is injected into the main combustion chamber. The oxidizer flow is pumped directly to the injector.

(U) Engine control is achieved in the hot-gas lines feeding the turbines rather than in the high-pressure liquid lines. Thrust is varied with a tapoff throttle valve (located in the Y junction of the two tapoff hot-gas ducts) which controls the power to both turbines. Engine mixture ratio is controlled by a throttle valve located at the oxidizer turbine inlet. Some interaction between these two valves is required to throttle at constant mixture ratio, or vary the mixture ratio at constant thrust.

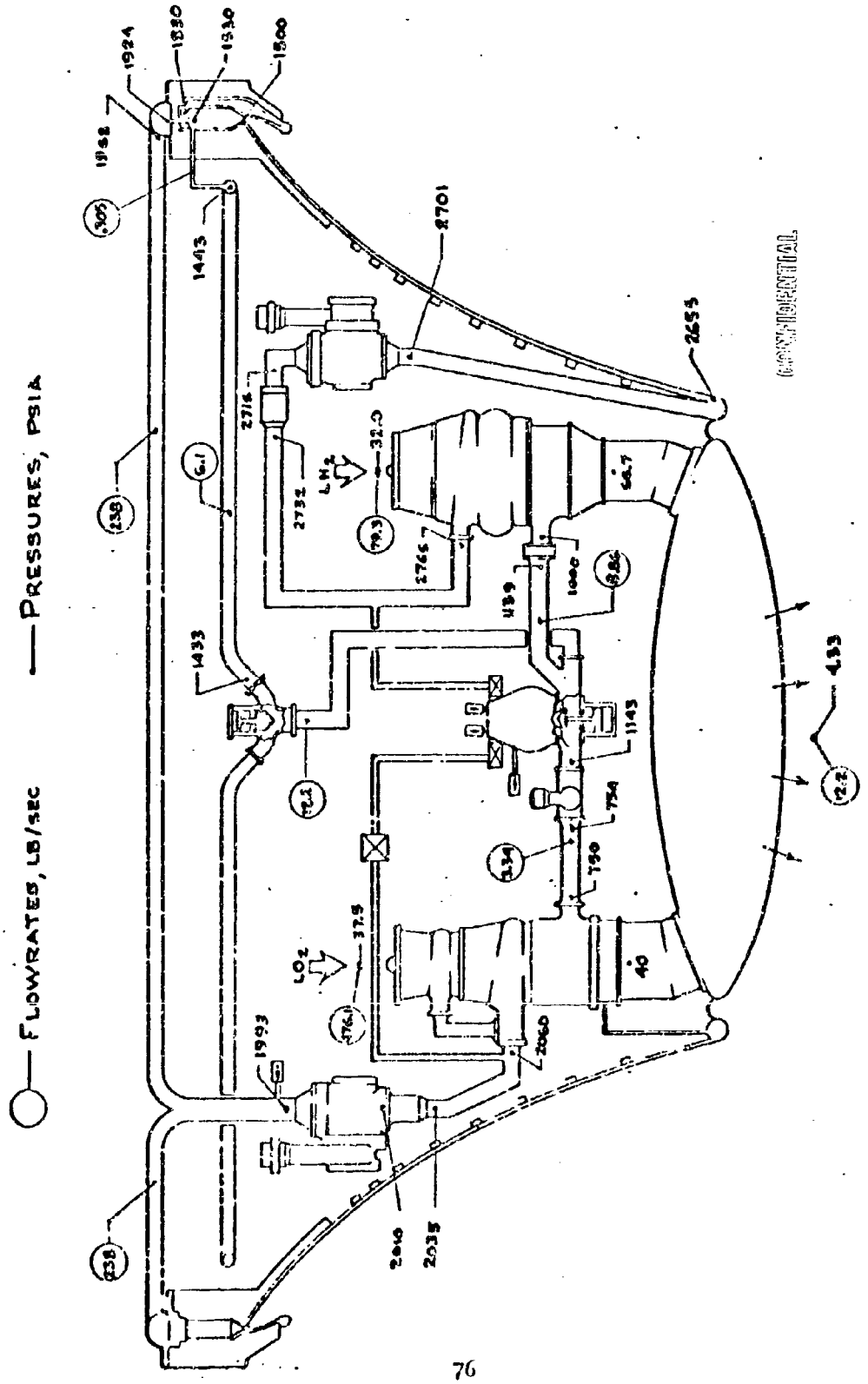

Figure 27. Demonstrator Engine (F = 250K, P_c = 1500 psia, MR = 6:1, I_s = 450.1 seconds)

This interaction is achieved with a closed-loop control system. The tap-off throttle valve is closed-loop controlled around chamber pressure, and the oxidizer turbine valve is closed-loop controlled around engine mixture ratio. The latter is sensed with turbine-type flowmeters in the pump discharge lines.

(C) The thrust and mixture ratio control valves are the only servocontrolled valves in the system. They are actuated by hydraulic fluid supplied by the facility at high pressure. All other valves are sequenced by four-way solenoid valves and hydraulically actuated. The servovalves utilize an outer closed-loop control system on the desired performance parameter and an inner closed-loop control system on valve position, coupled with a logic system which provides both integral and proportional control. This type of control ensures dynamic stability and safety while meeting the response (< 5 seconds between any two points) and accuracy (±3 percent) requirements of the engine system.

(U) Provision for off-design component performance resulting from manufacturing tolerances is made by inserting an orifice in the fuel turbine inlet line. The oxidizer turbine throttle valve is used as the calibrating device on the oxidizer side.

(C) Ignition is accomplished under tank head pressures with the use of a separate hot-gas igniter (HGI). This component produces hot gases which are discharged into the turbine drive ducting and used to provide both the initial turbine spin and the ignition energy source for the main chamber.

(C)

TABLE 10A

DEMONSTRATOR MODULE OPERATING CHARACTERISTICS

	Mixture Ratio, o/f = 5		Mixture Ratio, o/f = 6		Mixture Ratio, o/f = 7	
	Rated Thrust	20-Percent Thrust	Rated Thrust	20-Percent Thrust	Rated Thrust	20-Percent Thrust
Engine						
Vacuum Performance						
Thrust, pounds	244,200	48,700	250,000	50,000	254,800	50,850
Specific Impulse, seconds	453.0	446.1	450.1	443.8	441.3	431.8
Efficiency (Ref. Mixture Ratio Engine, Tank Conditions)	0.9731	0.9604*	0.9701	0.9604*	0.9618	0.9479*
Sea Level Performance						
Thrust, pounds	205,000	31,200	206,000	32,400	208,800	33,100
Specific Impulse, seconds	376	287	371	289	368	282
Oxidizer						
Inlet Pressure, psia	37.5	37.5	37.5	37.5	37.5	37.5
Inlet Temperature, R	175.5	175.5	175.5	175.5	175.5	175.5
Flowrate, lb/sec	449.9	91.0	476.1	96.6	504.5	103.0
Fuel						
Inlet Pressure, psia	32	32	32	32	32	32
Inlet Temperature, R	41.7	41.7	41.7	41.7	41.7	41.7
Flowrate, lb/sec	89.8	18.2	79.3	16.1	72.1	14.7
Thrust Chamber Assembly						
Primary Nozzle **						
Chamber Pressure (Nozzle Stagnation), psia	1500	325	1500	325	1500	325
Mixture Ratio, o/f	5.40	5.38	6.50	6.23	7.62	7.30
Oxidizer Flowrate, lb/sec	463.3	90.4	470.8	96.0	499.6	102.5
Fuel Flowrate, lb/sec	82.2	17.4	72.4	15.4	65.6	14.0
Vacuum Thrust Coefficient	1.845	1.837	1.896	1.891	1.934	1.924
Characteristic Velocity, ft/sec	7797	7650	7540	7410	7266	7088
Throat Area, $in.^2$ (Geometric)	85.1	79.2	85.1	79.2	85.1	79.2
Expansion Area Ratio (Aerodynamic)	74.1	79.6	74.1	79.6	74.1	79.6
Percent Length of 15-Degree Cone	25	25	25	25	25	25
Vacuum Thrust Coefficient Efficiency (Nozzle)	0.9499	0.9430	0.9510	0.9474	0.9509	0.937
Characteristic Velocity Efficiency	0.996	0.980	0.996	0.985	0.996	0.980
Base Region						
Vacuum Pressure, psia	4.60	0.76	4.33	0.72	4.16	0.70
Flowrate, lb/sec	13.53	1.32	12.20	1.21	11.47	1.19

*Throttled engine efficiency referenced to full thrust throat area (ε = 79.1)

**Injector MR and flowrate are the same as for the engine. Differences between engine flowrate and MR above and primary nozzle shown below reflect tap off requirements.

(c)

TABLE 10B

DEMONSTRATOR MODULE OPERATING CHARACTERISTICS

	Mixture Ratio, o/f = 5		Mixture Ratio, o/f = 6		Mixture Ratio, o/f = 7	
	Rated Thrust	40-Percent Thrust	Rated Thrust	40-Percent Thrust	Rated Thrust	40-Percent Thrust
Fuel Turbopump						
Pump						
Inlet Pressure, psia	32	32	32	32	32	32
Inlet Temperature, R	41.8	41.8	41.8	41.8	41.8	41.8
NPSH (Minimum Required), feet	60	60	60	60	60	60
Discharge Pressure, psia	2742	601	2756	587	2542	547
Head, feet	90,800	18,800	85,600	17,800	81,800	17,200
Flowrate, lb/sec	89.8	18.2	79.3	16.1	72.1	14.7
Speed, rpm	36,800	15,500	35,000	15,100	33,600	14,500
Shaft Horsepower, bhp	19,860	999	16,560	875	14,460	805
Efficiency	0.75	0.641	0.75	0.610	0.747	0.584
Turbine						
Inlet Pressure (Total), psia	1166	115	1000	100	892	94.7
Inlet Temperature, R	1960	1960	1960	1960	1960	1960
Exit Pressure (Static), psia	76.9	8.2	66.7	7.4	61.1	7.2
Flowrate, lb/sec	10.34	1.00	8.86	0.89	7.93	0.83
Speed, rpm	36,800	15,500	35,000	15,100	33,600	14,500
Shaft Horsepower, bhp	19,860	999	16,560	875	14,460	805
Efficiency	0.637	0.537	0.622	0.537	0.611	0.53
Oxidizer Turbopump						
Pump						
Inlet Pressure, psia	37.5	37.5	37.5	37.5	37.5	37.5
Inlet Temperature, R	175.5	175.5	175.5	175.5	175.5	175.5
NPSH (Minimum Required), feet	16	16	16	16	16	16
Discharge Pressure, psia	1096	348	2080	350	2418	369
Head, feet	4020	650	4150	650	4267	660
Flowrate, lb/sec	469.2	91.0	476.1	96.6	504.5	103.0
Speed, rpm	24,400	9200	25,000	9250	25,500	9350
Shaft Horsepower, bhp	4591	193	5013	199	5486	209
Efficiency	0.75	0.557	0.73	0.58	0.728	0.596
Turbine						
Inlet Pressure (Total), psia	715	69	730	71.5	795	78.5
Inlet Temperature, R	1960	1960	1960	1960	1960	1960
Exit Pressure (Static), psia	44.1	5.6	45	6.0	50.8	6.4
Flowrate, lb/sec	5.10	0.31	5.34	0.32	5.54	0.33
Speed, rpm	24,400	9200	25,000	9250	25,500	9350
Shaft Horsepower, bhp	4591	193	5013	199	5486	209
Efficiency	0.470	0.205	0.474	0.21	0.440	0.19

CONFIDENTIAL

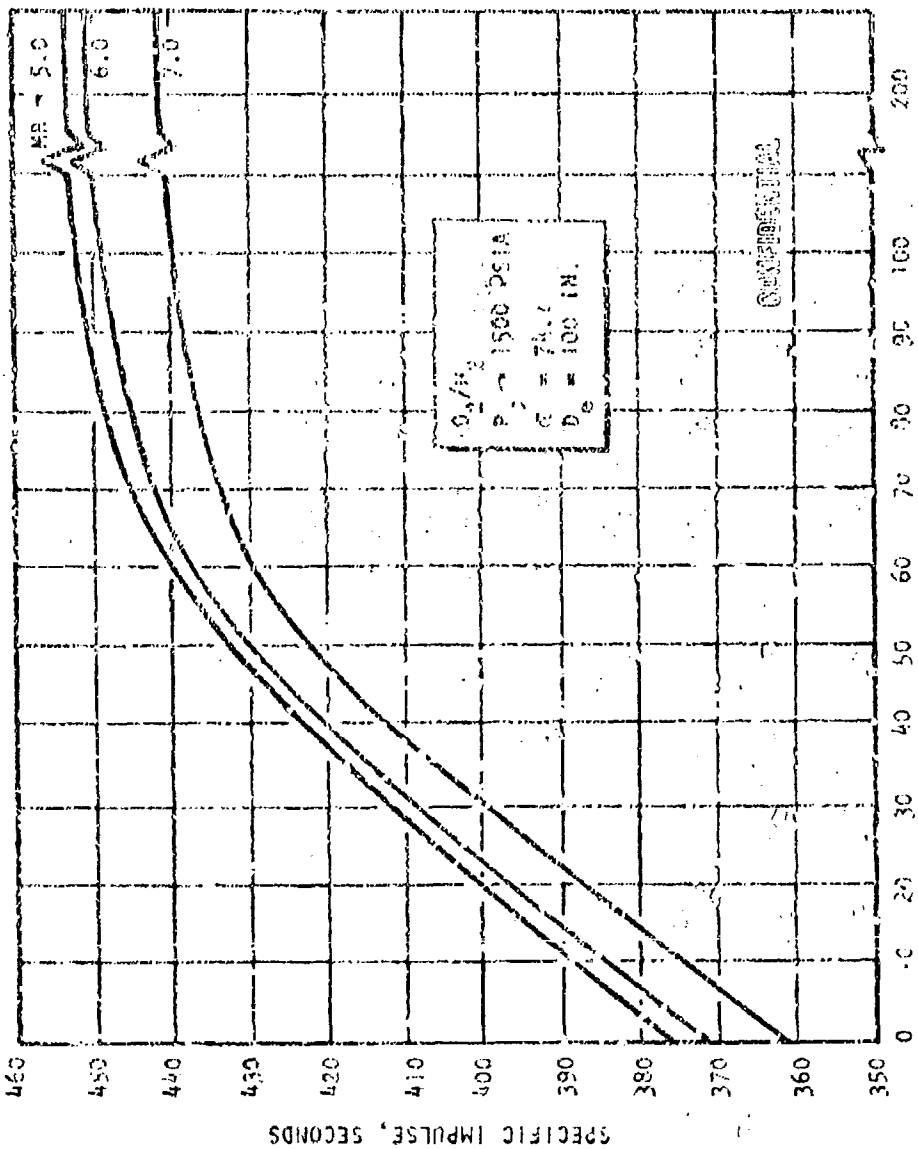

Figure 28. Demonstrator Engine I_s vs Altitude

The temperature of the HGI is controlled by an automatic oxidizer pressure regulator in the inlet line maintaining a combustion temperature of approximately 1500 F. Once main chamber ignition is achieved, the HGI is shut down with its own liquid-propellant shutoff valves, and the combustor is isolated from the tapoff system by closing the HGI isolation valve. Engine shutdown is achieved simply by closing the oxidizer turbine valve and sequencing the main propellant valves to provide a fuel-rich cutoff.

(C) Engine Balance and Performance. System and component performance is shown in Table 10 at rated thrust and minimum thrust for engine mixture ratios of 5, 6 and 7. The variation of engine specific impulse with altitude for engine mixture ratios of 5, 6, and 7 is shown in Fig. 28, and the variation with thrust level is shown in Fig. 29.

(C) Transient Operation. The valve sequence and engine transients for a vacuum start are shown in Fig. 30. To start the engine, a mainstage thrust command signal, mainstage mixture ratio command signal, and a start signal are required. The time sequencing of the propellant and hot-gas control valves will then follow as shown in Fig. 30a. The main fuel valve is opened first to establish fuel flow and to ensure liquid propellant to the pump inlet and to the hot-gas igniter line. At 1.0 second (0.5 to 1.0 second of fuel lead will probably be required), the hot-gas igniter valves are opened, and combustion is established in the HGI. The tapoff control valve and the oxidizer turbine throttle valve are positioned full open until thrust chamber prime. The oxidizer turbine throttle valve is

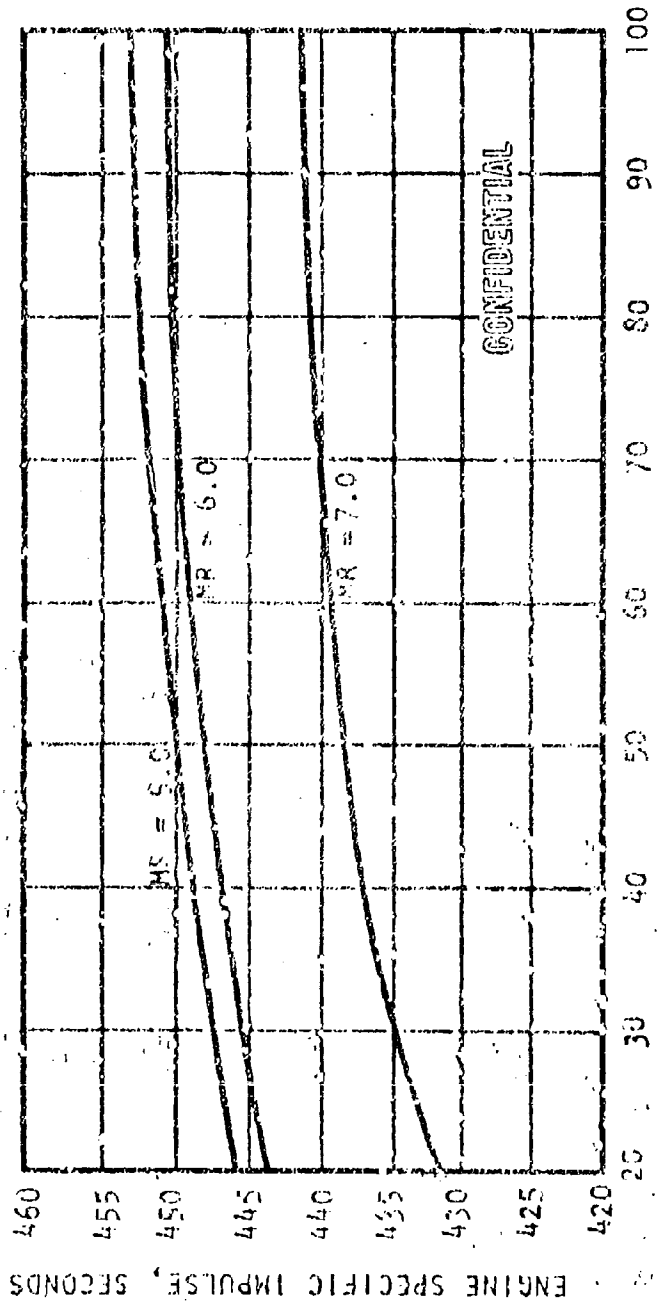

Figure 29. Demonstrator Engine Throttling Performance

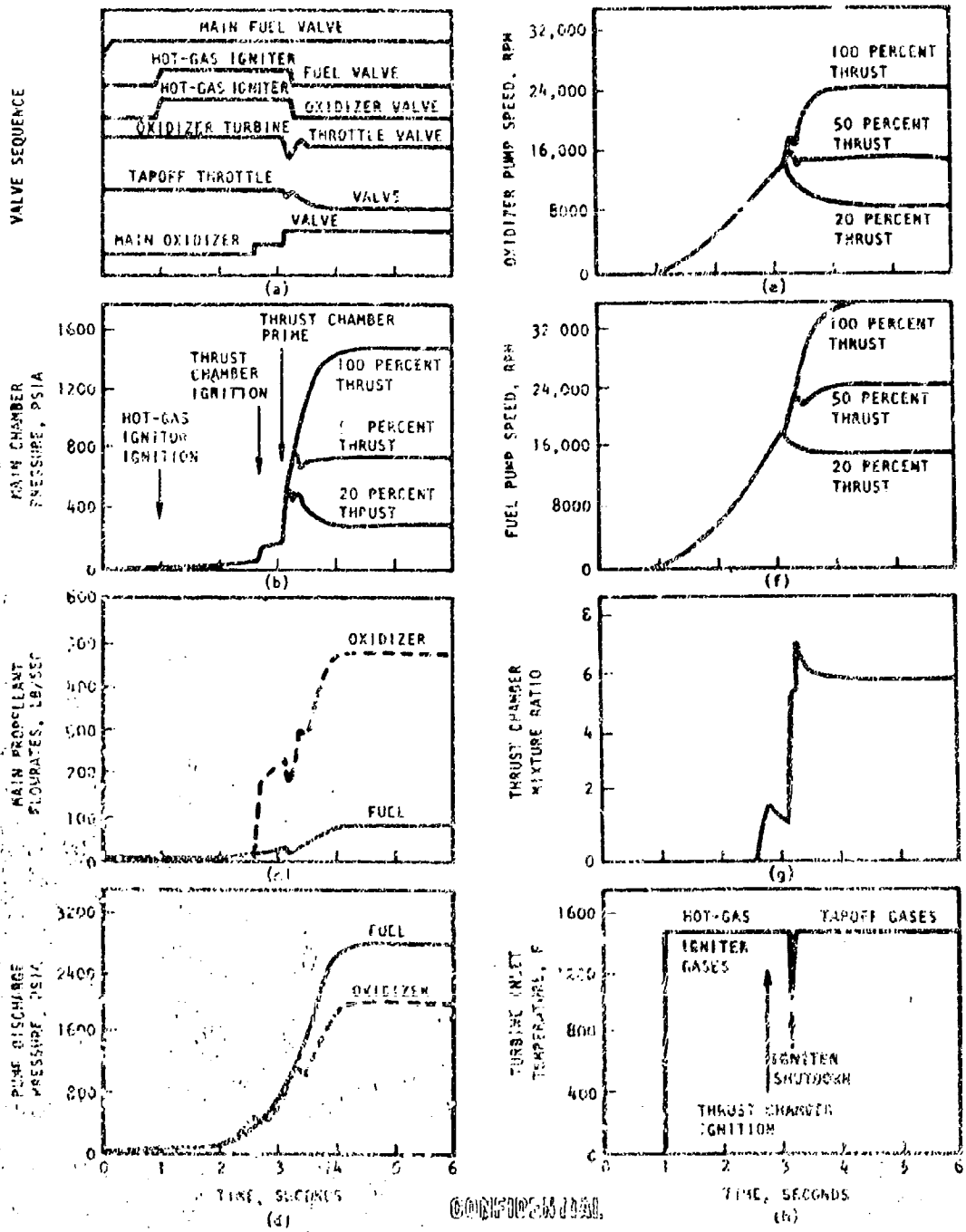

Figure 30. Engine Vacuum Start Transients

full open to eliminate excessive valve movement when the main oxidizer valve opens to the first position (20 degrees), and to provide maximum oxidizer turbine breakaway torque. The tapoff throttle valve is full open to maximize the hot-gas ignition flow to the thrust chamber.

(U) While oxidizer turbine breakaway is achieved with HGI flow, fuel turbine breakaway is predicted when the main fuel valve opens and is due to windmilling through the pump. If higher breakaway torques occur, the fuel turbopump will break away with the oxidizer turbopump under HGI gas flow.

(C) When the HGI pressure reaches 190 psi (to ensure sufficient hot-gas flow to the thrust chamber for ignition), the main oxidizer valve is opened to a throttle position of 20 degrees.

(C) Main propellant ignition will be achieved with oxygen in the gaseous state being injected shortly after the main oxidizer valves leaves the full-closed position. While the LO_2 dome is priming with liquid oxygen, chamber mixture ratio is maintained greater than 1.0 (Fig. 30g) and chamber pressure will be maintained above 100 psi. After approximately 600 milliseconds, full LO_2 dome prime will be achieved and chamber pressure will rise to about 500 psi. The hot-gas ignition valves are signalled to close when thrust chamber pressure passes 250 psi to prevent excessive power to the turbines. After this time, turbine flow is provided by tapoff gases from the main chamber. Approximately 100 milliseconds after LO_2 dome prime is achieved, the main oxidizer valve is ramped to full open in approximately 100 milliseconds. At the same time, the thrust and mixture ratio control systems are activated. The remainder of the transient to command thrust and mixture ratio is governed by the control systems. The entire transient from start signal to 90-percent thrust is accomplished in 3.6 seconds at vacuum.

(U) The engine transients shown in Fig. 30 give a graphic representation of the system dynamics at several of the key points in time during the

start transient. The data reveal that the fuel pump has a very smooth buildup over the entire transient and is virtually unaffected by disturbances in the oxidizer system such as main oxidizer valve opening. It should be pointed out that no thrust chamber bypass during start is required for the fuel. This is an advantage which the aerospike engine has over a conventional regeneratively cooled bell engine because of the significant reduction in thrust chamber tube volume (short-length nozzle).

(U) The oxidizer pump discharge pressure buildup (Fig.30d) reflects the movement of the oxidizer valve and the oxidizer turbine throttle valve and also the occurrence of thrust chamber oxidizer manifold priming. The buildup is nevertheless seen to be well ordered and under control.

(U) The HGI temperature (Fig.30h) is maintained at the design level until after thrust chamber ignition by the oxidizer pressure regulator. The temperature dips during the fuel-rich HGI shutdown.

(C) The thrust chamber mixture ratio (Fig.30g) rises to approximately 1.7:1 under gaseous oxygen flow, during which time main chamber ignition is achieved. (Hot-gas ignition tests have indicated that mixture ratios in excess of 1.0 are required.) After oxidizer manifold prime occurs, the mixture ratio rises rapidly to a value of 5.7:1 (thrust chamber) by the activation of the mixture ratio control valve.

(C) Start transients to levels other than 100 percent were studied, and the chamber pressure and pump speed traces for these cases are shown in Fig.30b, 30e, and 30f. A small overshoot is seen to occur for a start of 20 percent. The following three engine control variations were studied to eliminate the thrust chamber pressure overshoot when starting the low thrust levels:

1. Move the location of the thrust control valve so that it is between the central igniter and the turbines

2. Add a flow controller to the central igniter fuel line

3. Add a control valve in the fuel turbine inlet line

All of these variations provide the capability to control the individual pump buildup rates and thereby eliminate the overshoot; however, the control complexity will be increased. Deeper studies of these alternatives will need to be made should subsequent vehicle studies indicate that the overshoot is undesirable.

(C) The transients for a sea level start are shown in Fig.31 . The only difference between this start and a vacuum start is the time to reach an HGI pressure of 190 psia (time at which the main oxidizer valve is signaled open). For sea level, this occurs at 4.4 seconds as opposed to 2.6 seconds at vacuum. After this time, the transients are virtually identical, and the model predicted a sea level start time of 5.6 seconds to reach 90-percent thrust.

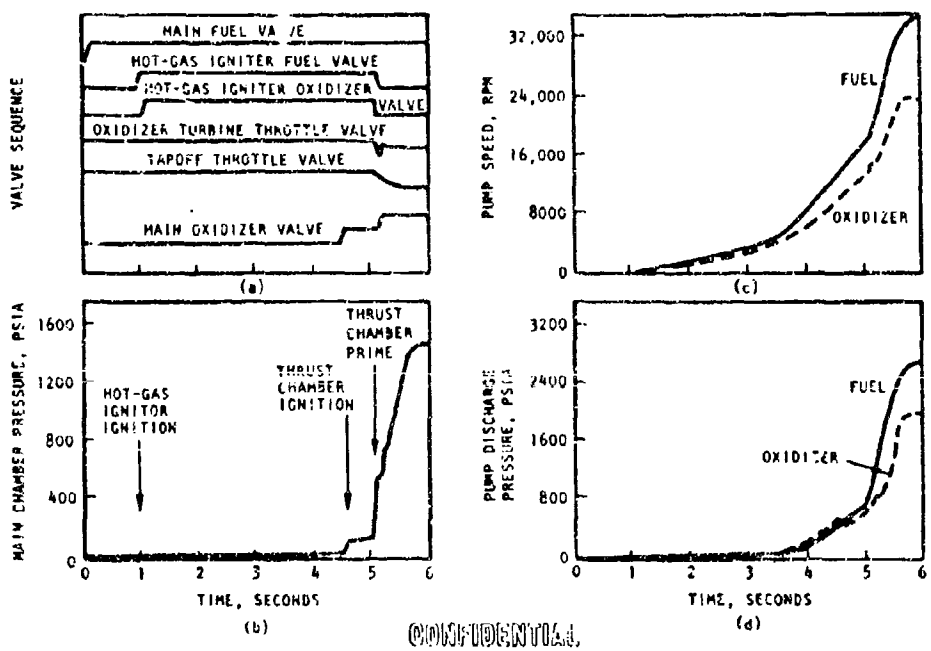

Figure 31. Engine Sea Level Start Transients

(C) In all the start transients, a fully preconditioned pump was assumed with liquid propellants up to the main valves. However, the effects of different thrust chamber preconditions were studied. The initial thrust chamber temperature used for the transients shown in Fig. 30 and 31 was ±165 F. This was considered the maximum temperature anticipated at sea level or at vacuum, and hence represented the fuel system stability worst condition. Other starts were calculated with a thrust chamber precondition temperature of -65 F. Only minor differences in fuel flow resulted, and other transients were almost completely unaffected. This indicates that no hardware system dynamics problem can be expected as a result of an unconditioned thrust chamber.

(U) A simple cutoff of the Demonstrator Module is achieved with a single signal to the engine sequencer which signals the two main propellant valves and the oxidizer turbine throttle valve. The cutoff transients and valve timing sequence are shown in Fig. 32 on an expanded time scale.

(C) At cutoff signal, the oxidizer turbine throttle valve and main oxidizer propellant valve are signaled to close; the tapoff throttle valve and main fuel valve remain open. When the oxidizer injection pressure reaches 300 psia, an oxidizer system purge commences and continues until the oxidizer volume is completely purged. This sequence maintains power to the fuel pump during the purge period to ensure a fuel-rich cutoff.

(C) Thrust chamber pressure drops to approximately 60 psi in 150 milliseconds as a result of the loss of oxidizer pump power and flow. When the main oxidizer valve reaches full closed, a surge is caused at the pump inlet and discharge, but because oxidizer pump discharge is already down, the surge at the pump discharge is not important. A surge of 26 psi above oxidizer tank pressure produced at the pump inlet would occur using an inlet duct 7 inches in diameter and 41 inches long. The magnitude of the surge is approximately proportional to duct length divided by the area; therefore, a longer duct or a smaller area duct would produce a proportionately larger

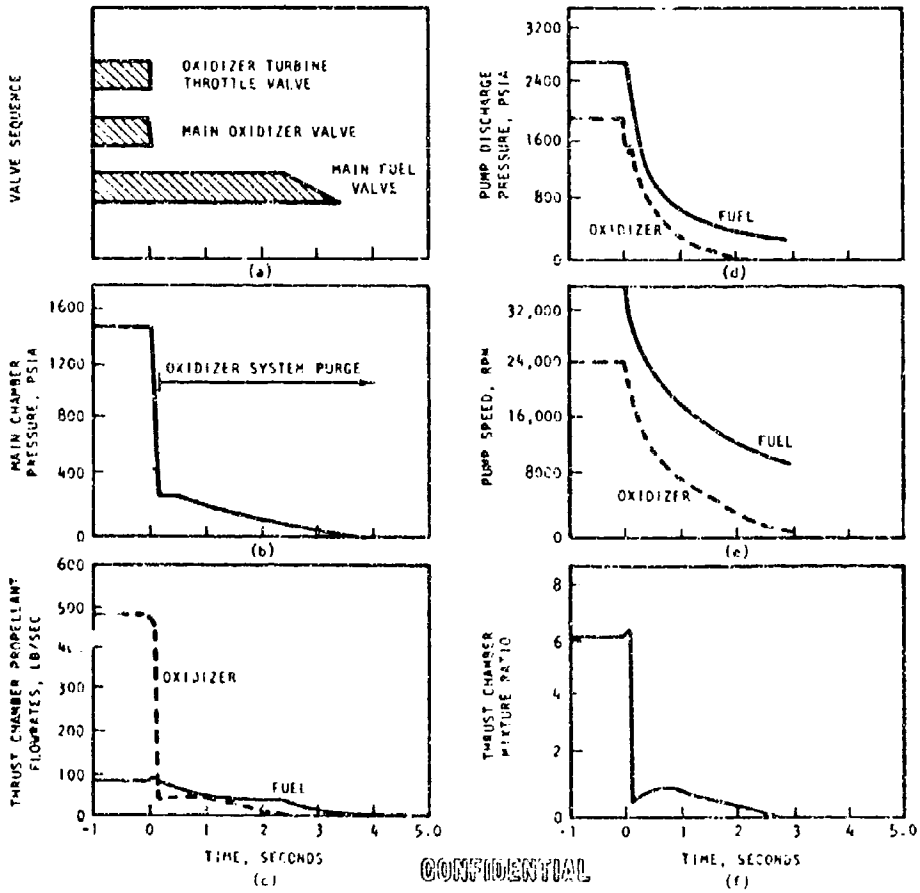

CONFIDENTIAL

Figure 32 . Engine Cutoff Transients

surge. After a 2.5-second delay, the main fuel valve is closed and the shutdown is completed. For the Demonstrator Module, no optimization of the purge timing was conducted; therefore, the tailoff transient data are merely a projection. A system purge and vent will also be required on the HGI to prevent ice formation in the igniter injector and valves. This purge will be continuous during engine operation as a safety measure against possible leakage of the isolation valve.

(U) The Demonstrator Module is so designed that no additional requirements are imposed for a restart; the sequence is identical to that described above.

Analysis.

(C) Pressure Budgets. In order to establish the nominal design point parameters, the system pressure losses were carefully studied. Liquid-line losses directly affect pump discharge pressure and hot-gas-line losses affect the turbine inlet pressure. The former is a measure of the pump power requirements and the latter affects the turbine specific horsepower through pressure ratio. Therefore, both areas directly affect the magnitude of the turbine flowrate, and since this is used as the secondary flowrate in the aerospike nozzle, engine specific impulse is influenced. Close coordination with the design effort was necessary to perform weight and performance tradeoffs in order to optimize the total system. The hot-gas pressure schedule for a mixture ratio of 6:1 and nominal manufacturing tolerances is shown in Table 11. Additional schedules for the $+3\sigma$ manufacturing tolerances are also shown for mixture ratios of 5:1 and 7:1. These latter are used to define the calibration orifice requirements and to define the operating range of the tapoff throttle valve (Table 12, Fig. 33) and the oxidizer turbine throttle valve (Table 13, Fig. 34). Liquid-propellant feed pressure schedules are shown in Tables 14 and 15 for the nominal design point (P_c = 1500 psia, MR = 6:1).

(U) Design Tolerances. The design of rocket engine components must include allowances to account for the performance variation due to hardware variation and calibration inaccuracies as well as any expected variations in test or flight conditions. This approach assigns realistic design margins to all components, but it does not impose added weight penalties by unnecessary "design pads." Tolerances are assigned to all variables such as line and injector resistances, pump and turbine efficiencies, and calibration accuracy. Then the change in engine operating conditions is found for each independent variable through the use of a digital computer program which rebalances the engine to find the new operating point. The total expected component variation is then found by statistically summing the

(C) TABLE II

HOT-GAS SYSTEM PRESSURE SCHEDULE

Parameter	ΔP, psi	$P_{upstream}$, psia	$\dot{w}$, lb/sec
(MR_E = 6:1; Nominal Manufacturing Tolerances)			
Tapoff			
Injector End Pressure	--	1530	12.20
Thrust Chamber and Manifold	87	1530	12.20
Tapoff Duct	16	1443	12.20
Control Valve	273	1433	12.20
Fuel Turbine Drive			
Distribution Plenum	21	1160	8.86
Calibration Orifice	139	1139	8.86
Turbine Inlet Pressure	--	1000	8.86
Oxidizer Turbine Drive			
Distribution Plenum	17	1160	3.34
Control Valve	389	1143	3.34
Turbine Inlet Duct	4	754	3.34
Turbine Inlet Pressure	--	750	3.34
(MR_E = 5:1; +3σ Manufacturing Tolerances)			
Tapoff			
Injector End Pressure	--	1530	14.91
Thrust Chamber and Manifold	129	1530	14.91
Tapoff Duct	15	1401	14.91
Control Valve	75	1386	14.91
Fuel Turbine Drive			
Distribution Plenum	29	1311	11.45
Calibration Orifice	0	1282	11.45
Turbine Inlet Pressure	--	1282	11.45
Oxidizer Turbine Drive			
Distribution Plenum	16	1311	3.46
Control Valve	510	1295	3.46
Turbine Inlet Duct	3	785	3.46
Turbine Inlet Pressure	--	782	3.46
(MR_E = 7:1; 3σ Manufacturing Tolerances)			
Tapoff			
Injector End Pressure	--	1530	12.46
Thrust Chamber and Manifold	92	1538	12.46
Tapoff Duct	11	1438	12.46
Control Valve	420	1427	12.46
Fuel Turbine Drive			
Distribution Plenum	25	1007	8.74
Calibration Orifice	0	982	8.74
Turbine Inlet Pressure	--	982	8.74
Oxidizer Turbine Drive			
Distribution Plenum	23	1007	3.90
Control Valve	104	984	3.90
Turbine Inlet Duct	5	880	3.90
Turbine Inlet Pressure	--	875	3.90

(C) TABLE 12

TAPOFF THROTTLE VALVE REQUIREMENTS

Chamber Pressure, psia	Mixture Ratio	$\dot{w}$, lb/sec	ΔP, psi	P, psia
1500 (~100% F)	5 (3σ)	14.91	75	1491
	5	13.53	61	1413
	6	12.20	273	1435
	7	11.47	413	1447
1200 (~80% F)	5	9.17	209	1144
	6	8.35	361	1157
	7	7.84	451	1163
900 (~60% F)	5	5.68	294	868
	6	5.15	332	876
	7	4.83	435	879
600 (~40% F)	5	2.96	285	585
	6	2.71	328	589
	7	2.55	352	490
325 (~20% F)	5	1.32	186	319
	6	1.20	202	320
	7	1.19	208	320
Open Flow	--	13.53	15	1413
Life: 10 hours TBO, 10,000 cycles				
Maximum hot-gas temperature: 2112 R				

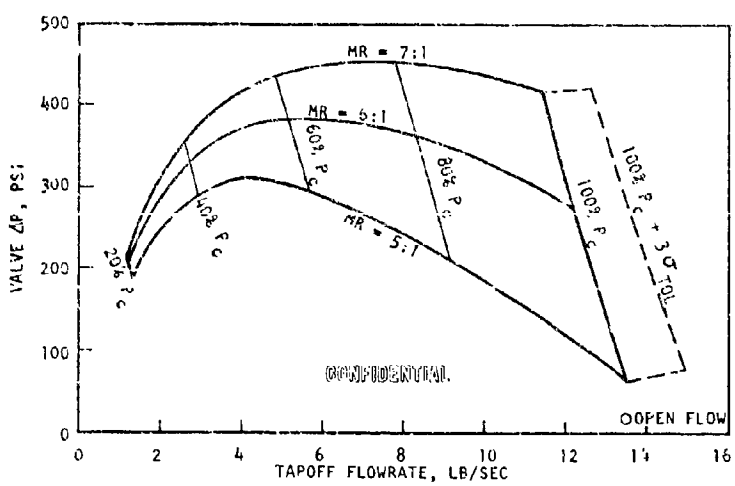

Figure 33. Tapoff Throttle Valve Δ P vs Flowrate

(C)

TABLE 13

OXIDIZER TURBINE THROTTLE VALVE REQUIREMENTS

Chamber Pressure, psia	Mixture Ratio	ẇ, lb/sec	ΔP, psi	P, psia
1500 (~100% F)	5 (R)	3.19	621	1339
	6	3.34	389	1143
	7	3.54	217	1016
	7	3.90	104	984
1200 (~80% F)	5	2.11	449	926
	6	2.25	276	784
	7	2.38	161	699
900 (~60% F)	5	1.31	271	568
	6	1.37	177	487
	7	1.44	110	436
600 (~40% F)	5	0.70	137	295
	6	0.72	94	257
	7	0.74	66	234
325 (~20% F)	5	0.31	61	131
	6	0.32	44	116
	7	0.35	30	110
Open Flow	—	3.54	15	1016
Life: 10 hours TBO, 10,000 cycles				
Maximum hot-gas temperature: 2112 R				

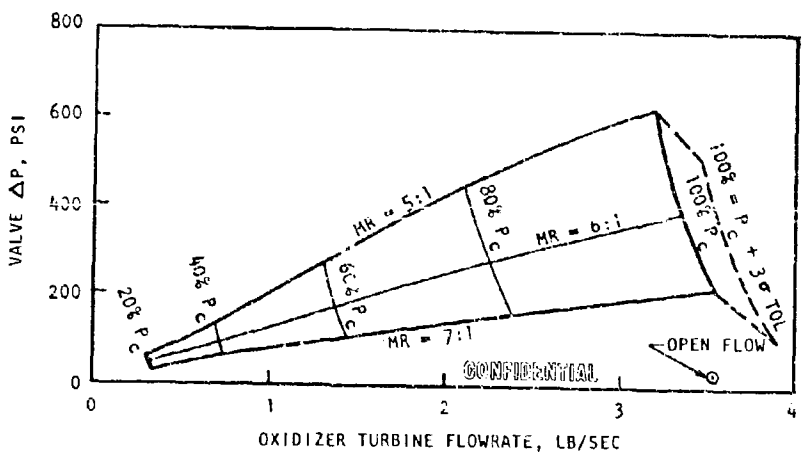

Figure 34. Oxidizer Turbine Throttle Valve Δ P vs Flowrate

(C) TABLE 14

LIQUID-OXIDIZER PROPELLANT FEED PRESSURE SCHEDULE

(Nominal MR = 6:1; $\dot{w}_{ox}$ = 476.1 lb/sec)

Parameter	Upstream Pressure psia	ΔP, psia
P_D	2060	-
Pump Discharge Duct	2060	25
Flowmeter	2035	25
MLV	2010	17
Branch Lines	1993	25
TC Manifold	1968	44
Injector	1924	394
TC Injector End Pressure	1530	-

(C) TABLE 15

LIQUID-FUEL PROPELLANT FEED PRESSURE SCHEDULE

(Nominal MR = 6:1; $\dot{w}_F$ = 79.3 lb/sec)

Parameter	Upstream Pressure, psia	ΔP, psia
P_D	2766	-
Discharge Duct	2766	34
Flowmeter	2732	16
MFV	2716	15
TC Inlet Manifold	2701	46
TC Tube Bundle	2655	823
Injector	1839	300
TC Injector End Pressure	1530	-

effects of the independent variables. The assumption is made that all of the tolerances exhibit a normal Gaussian distribution and that all of the independent variables do not depend upon any other variable for their value.

(U) Since the Demonstrator Module will have an active control system for thrust and mixture ratio, the component operating range will not be as large as for an engine which does not have an active control system.

(U) Table 16 lists the hardware variations and expected variations in test conditions which were used to determine the component operating ranges.

(U) The maximum expected operating condition was found by rebalancing the engine at the extremes of the mixture ratio range (5.0 and 7.0) and selecting the maximum condition for each parameter. Then the 3σ variations are added to find the maximum expected operating condition for each component. The results are shown in Table 17. These results do not represent an engine operating point because all of the component maximum operation conditions cannot occur simultaneously. As an example, the LO_2 turbine flowrate is a maximum at an engine mixture ratio of 7.0 and the fuel turbine flowrate is a maximum at an engine mixture ratio of 5.0, and thus these two maximums cannot occur together at a single operating point.

(C) The effect of manufacturing tolerances on the power cycle must also be considered in the design of the hot-gas system. Turbomachinery inefficiencies were found to demand higher turbine flowrates which can be met only with higher turbine inlet pressures. Therefore, the system must be designed to provide this additional capability. Since the turbine drive gases are tapped from the main chamber at a fixed chamber pressure (1530 psia maximum), the turbine inlet pressure can be raised only by the removal of some resistance between the turbine and the main chamber. A possible method of providing this capability is to design the control valves with an additional nominal ΔP and use these valves as the calibrating device. However, because of the series arrangement of the tapoff and oxidizer

(C) TABLE 16

INDEPENDENT VARIABLE ±3σ VARIATIONS

	±3σ Variation, percent
Hardware Variations	
Main Fuel Line Resistance	19.5
Valve Resistance	19.5
Thrust Chamber Resistance	19.5
Injector Resistance	19.5
Main LO_2 Line Resistance	19.5
Valve Resistance	19.5
Manifold Resistance	19.5
Injector Resistance	19.5
Tapoff Duct Resistance	15.0
Control Valve Resistance	15.0
LO_2 Turbine Control Valve Resistance	15.0
Exhaust Resistance	15.0
Efficiency	4.5
Nozzle Area	4.5
Fuel Turbine Exhaust Resistance	15.0
Efficiency	4.5
Nozzle Area	4.5
LO_2 Pump Efficiency	3.51
Head	3.0
Fuel Pump Efficiency	3.66
Head	7.20
Thrust Chamber c*	1.17
C_F	1.17
Throat Area	6.0
Base Closure Flow Area	4.50
Expected In Test Variations	
Fuel Pump Inlet Pressure	15.0
Temperature	0.9
LO_2 Pump Inlet Pressure	9.0
Temperature	0.9
Thrust Chamber Pressure	3.0
Engine Mixture Ratio	3.0

(C) TABLE 17

PREDICTED MAXIMUM PARAMETER VARIATIONS

Parameter	Maximum Off Design	3σ Variation	Maximum
Engine Thrust, pounds x 10^3	254.5	7.5	262.0
Engine Mixture Ratio	7.000	0.21	7.21
Thrust Chamber Injector End Pressure (total), psia	1530	105	1635
Thrust Chamber Fuel Flow, lb/sec	89.8	4.02	93.82
Thrust Chamber LO_2 Flow, lb/sec	499.6	24.0	523.6
Tapoff Pressure (total) psia	1515	105	1620
Tapoff Fuel Flow, lb/sec	7.67	1.71	9.38
Tapoff LO_2 Flow, lb/sec	5.80	1.31	7.17
Tapoff Gas Temperature, R	1960	152	2112
Fuel Turbine Out Temperature, R	1619	127	1746
Fuel Turbine In Pressure (total), psia	1166	117	1283
Fuel Turbine Speed, rpm	36,800	1560	38,360
Fuel Turbine Out Pressure, psia	76.90	8.23	85.13
Fuel Turbine Torque, ft-lb	2839	223	3062
Fuel Turbine Flow, lb/sec	10.34	1.11	11.45
LO_2 Turbine Out Temperature, R	1726	133	1859
LO_2 Turbine In Pressure (total), psia	795	87.8	882.8
LO_2 Turbine Out Pressure, psia	44.1	4.32	48.42
LO_2 Turbine Speed, rpm	25,600	1060	26,660
LO_2 Turbine Torque, ft-lb	1122	95	1217
LO_2 Turbine Flow, lb/sec	3.54	0.41	3.95
Fuel Pump Out Pressure (total), psia	2942	210	3152
Valve In Pressure (total), psia	2877	204	3087
Thrust Chamber In Pressure (total), psia	2858	204	3062
Injector In Pressure (total), psia	1900	133	2033
LO_2 Pump Out Pressure (total), psia	2118	166	2284
Valve In Pressure (total), psia	2056	163	2219
Manifold In Pressure (total), psia	2004	160	2164
Injector In Pressure (total), psia	1970	156	2126
Fuel Pump Head, feet	90,800	6170	96,970
Volume Flow, gpm	9560	483	10,043
Horsepower	19,860	2000	21,860
LO_2 Pump Head, feet	4263	347	4610
Volume Flow, gpm	3295	160	3455
Horsepower	5486	643	6129
Base Thrust, pounds	9200	556	9756
Base Flow, lb/sec	13.53	1.42	14.95

turbine throttle valves, such a scheme would not allow each turbine to be calibrated independently, and the oxidizer turbine nominal design point would be adversely affected. Therefore, a modified scheme was adopted wherein a calibration orifice was placed in the fuel turbine inlet line, while the oxidizer turbine throttle valve was retained as the calibrating device for the oxidizer turbine. The design requirements for these components were then determined from engine balances at the operating envelope extremes, as discussed in the preceding section.

(U) Performance Analysis. The system performance analysis has been divided into five areas: (1) combustion chamber, (2) nozzle, (3) base region, (4) tapoff gas properties, and (5) the performance model. These are discussed below.

(C) The combustion chamber efficiency, η_{c*}, for the Demonstrator Module was based on the 2.5K injector test results which are discussed in detail in the Task II section (page 428). These test results indicate a combustion efficiency of greater than 99 percent at 1500-psia chamber pressures and nominal mixture ratio with a drop in efficiency at lower pressures and higher mixture ratio. The predicted combustor chamber efficiency is shown in Fig. 35 , as a function of chamber pressure and engine mixture ratio. The effect of extracting fuel-rich tapoff gases causes the thrust chamber mixture ratio to shift as shown in Fig. 36 . These efficiencies are based on theoretical c* values which are computed from the propellant enthalpy levels existing at the injector inlet, which are equal to the propellant enthalpies at tank conditions raised by the enthalpy increase from the pump work and heat input to the coolant through the boundary layer.

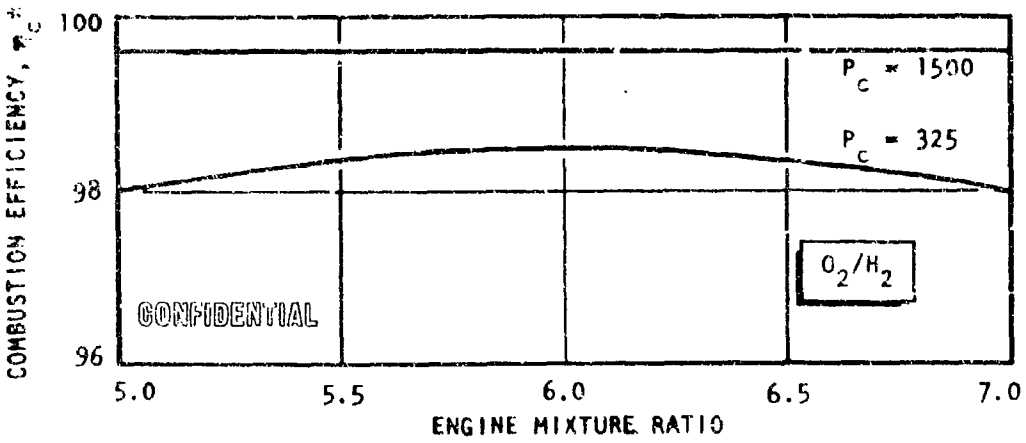

Figure 35. Variation of η_{c^*} With Mixture Ratio

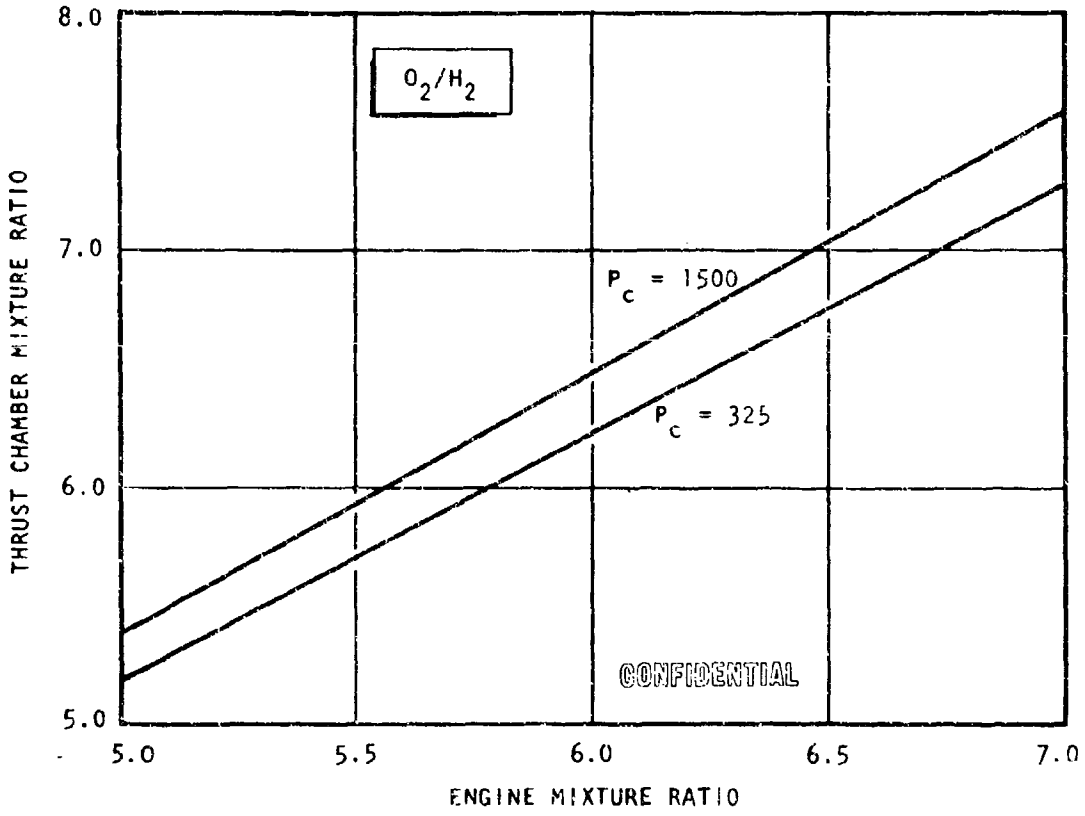

Figure 36. Variation of Thrust Chamber Mixture Ratio With Engine Mixture Ratio

(C) The thrust chamber contour was optimized based on iterative aerodynamic, viscous drag, chemical kinetics, and heat transfer studies. The aerodynamic analysis was based on chemical equilibrium properties. The optimization included both the inner spike contour and the outer shroud contour. Early designs incorporated a relatively short outer shroud and a corresponding effective nozzle diameter (measured from the shroud tip) of 90.5 inches. However, at low-pressure ratios, theoretical flow field calculations have subsequently indicated that the short shroud would produce a recompression shock of sufficient strength to exceed the cooling capacity of the inner wall tubes during throttled sea level runs. A cold-flow test series was conducted to measure the recompression wall pressure profiles for the full-length shroud and a truncated shroud, and to verify the calculated results. Results are discussed in the Thrust Chamber Assembly section (page 177).

(C) The long shroud configuration decreases the effective nozzle exit diameter from 90.5 to 89.5 inches, which results in a decrease in vacuum I_s of 0.4 second. However, sea level performance increases by 0.3 second.

This configuration was therefore selected to provide the capability of engine cooling at low-pressure-ratio operation since the resultant effect on performance was small.

(U) A chemical kinetic analysis of the nozzle was performed to determine the performance loss resulting from the nonequilibrium flow. This loss is shown in Fig. 37 as a function of chamber pressure and mixture ratio. The kinetic losses are lowest at low mixture ratios and high chamber pressures.

(U) The boundary layer on viscous drag analysis was computed from a numerical solution of the boundary layer equations accounting for the wall temperature, pressure gradient, turbulent velocity profile, and heat

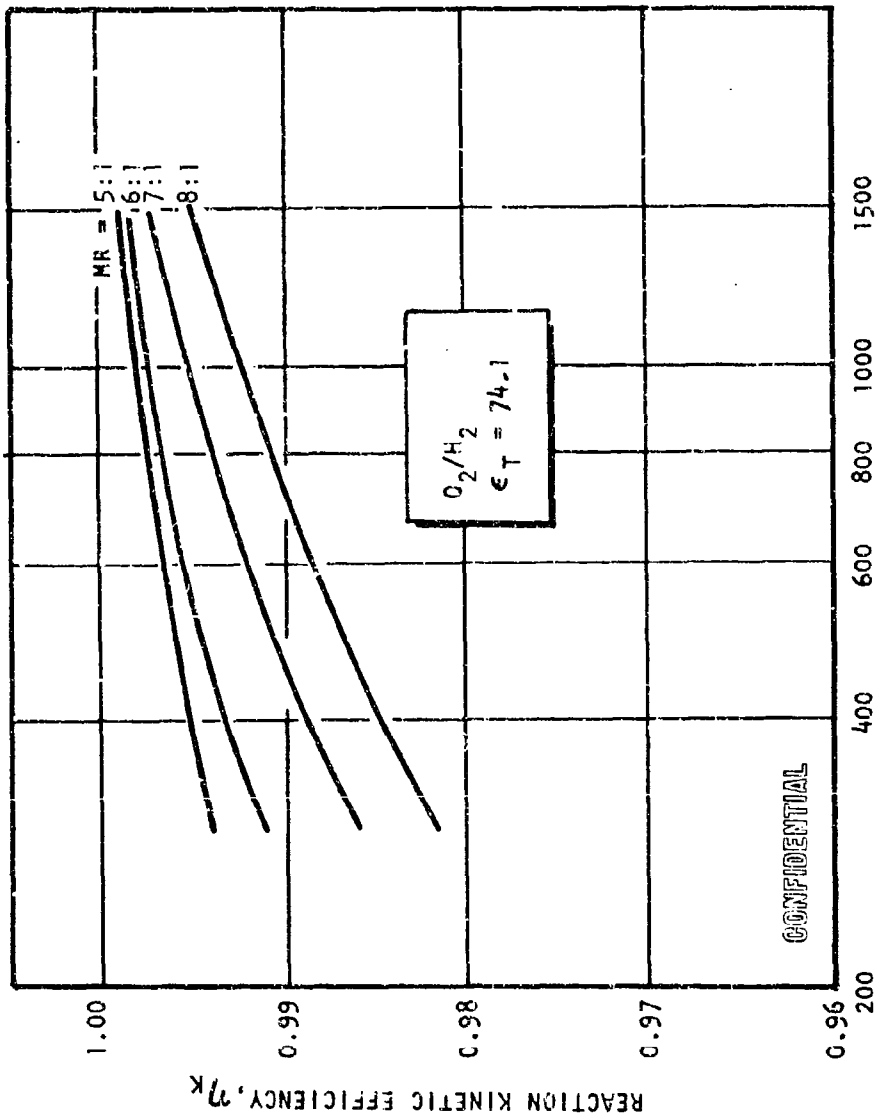

Figure 37. Demonstrator Engine I_s vs Altitude

flux in the boundary layer. The results are shown in Fig. 38 as a degradation of thrust coefficient as a function of chamber pressure.

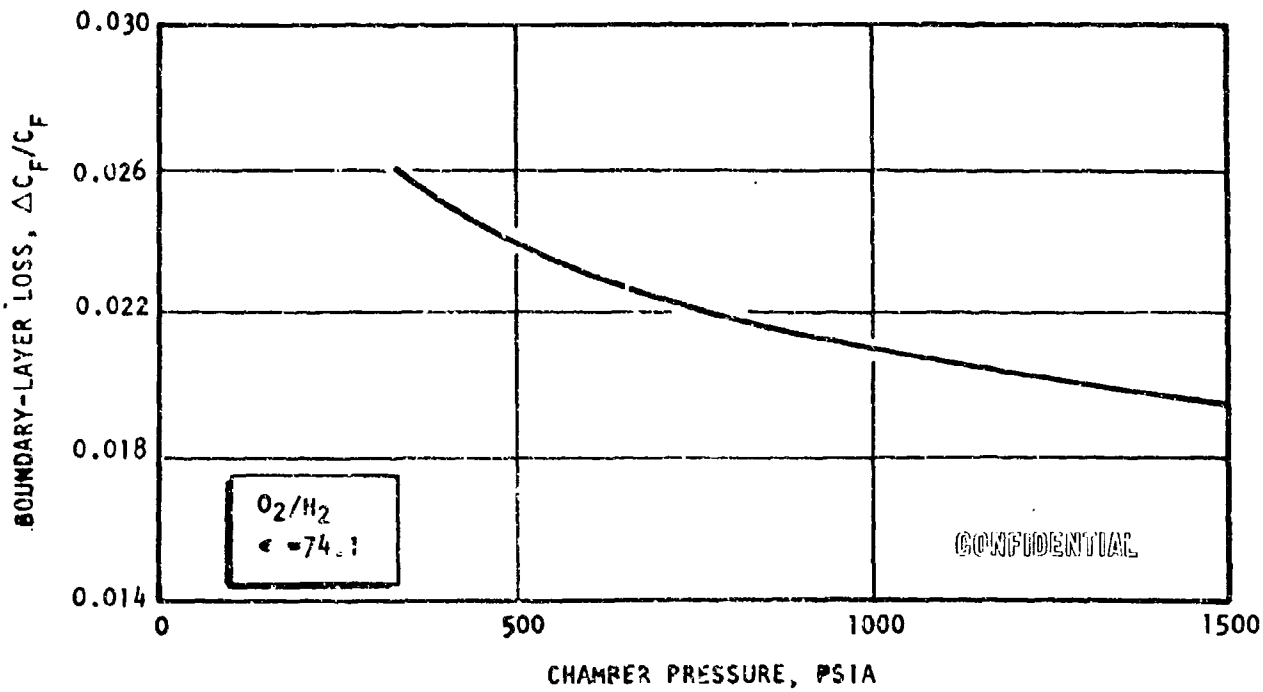

Figure 38. Demonstrator Engine Throttling Performance

(U) The geometric efficiency of the nozzle is a function of the nozzle contour and the gas properties. The gas properties are a function of the propellant mixture ratio, and thus, the nozzle geometric efficiency varies with mixture ratio as shown in Fig. 39.

(U) The base region of an aerospike nozzle allows highly efficient use of the turbine exhaust since these gases can be used to increase the base pressure. Experimental investigations and theoretical analysis have determined that the base pressure for a fixed nozzle geometry design is a function of chamber pressure, secondary flowrate, the properties of the secondary gases, and ambient pressure. The base pressure increases with increasing

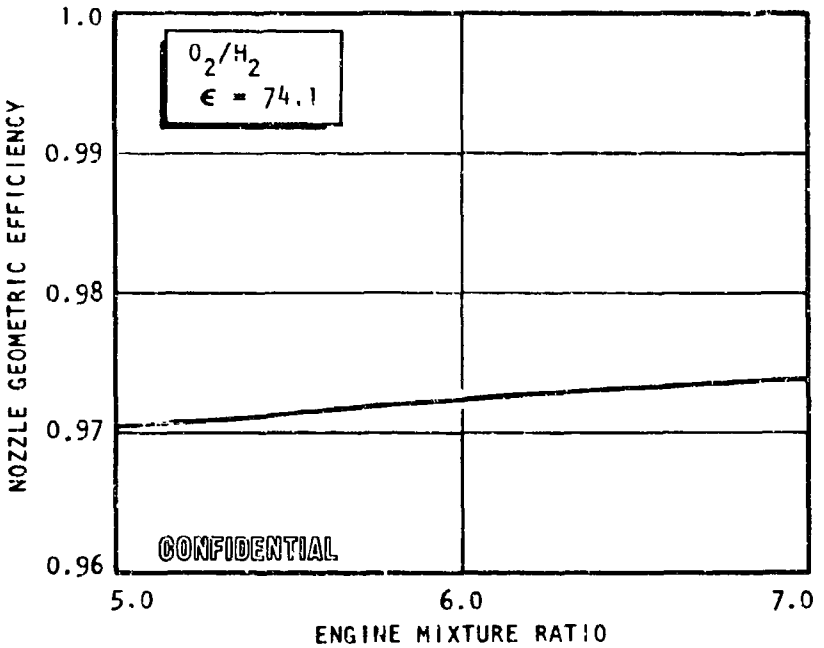

Figure 39. Nozzle Geometric Efficiency vs Mixture Ratio

secondary gas flowrate and ambient pressure. The relationship with secondary flow is shown in Fig. 40. However, there is a secondary flowrate which produces maximum overall engine performance. The variation of engine performance with secondary flow for the Demonstrator Module nominal design point is shown in Fig. 41. (It should be noted that Fig. 40 and 41 assume a constant thrust chamber mixture ratio.)

(C) Tapoff gas properties such as heat capacity (C_p), molecular weight (M), ratio of heat capacities (γ), and characteristic velocity (c*) can be determined by analytical methods if the tapoff gas temperature and propellant injector inlet conditions are known. The Rocketdyne free-energy propellant program can then be used to calculate the resultant combustion products and their properties. The tapoff gas mixture ratio required to give a temperature of 1960 R decreases as the hydrogen inlet temperature increases as shown in Fig. 42. The higher hydrogen content of the low-mixture-ratio gases results in higher energy (i.e., Btu/lb of gas) for the same temperature because of the higher heat capacity of the mixture.

(C) The feasibility of obtaining the desired tapoff temperature has been demonstrated by the 2.5K segment test program. The results are summarized in Fig. 43.

(C) The known tapoff gas temperature (1500 F) and the known hydrogen inlet temperature (630 R) result in a tapoff gas mixture ratio of 0.764 as shown in Fig. 42. The physical properties of the tapoff gases are then fixed by the temperature, pressure, and composition. These properties are listed below:

Mixture Ratio, o/f	0.764
Molecular Weight	3.556
Heat Capacity, Btu/lb-R	2.13
Ratio of Specific Heats	1.3557
Characteristic Velocity (c*), ft/sec	7730

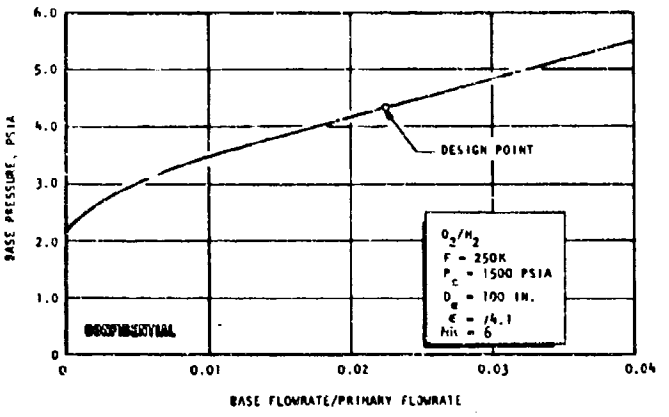

Figure 40. Variation of Base Pressure With Flowrate at Vacuum Conditions

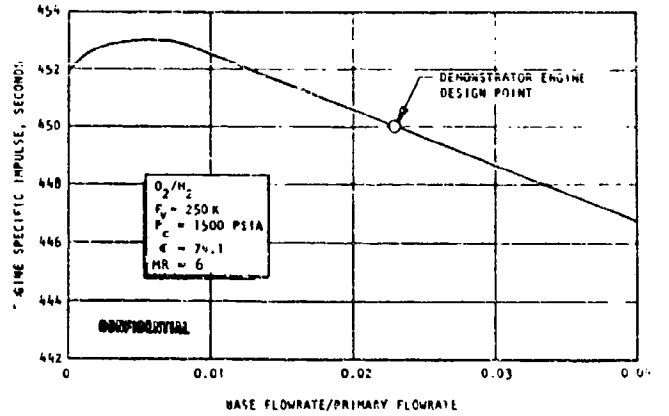

Figure 41. Variation of Engine Vacuum I_s With Secondary Flowrate at Vacuum Conditions

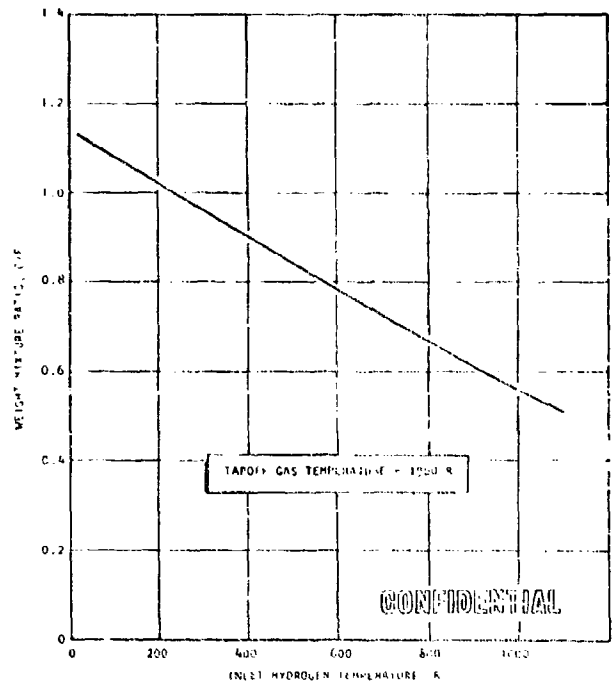

Figure 42. Tapoff Gas Mit vs Hydrogen Inlet Temperature

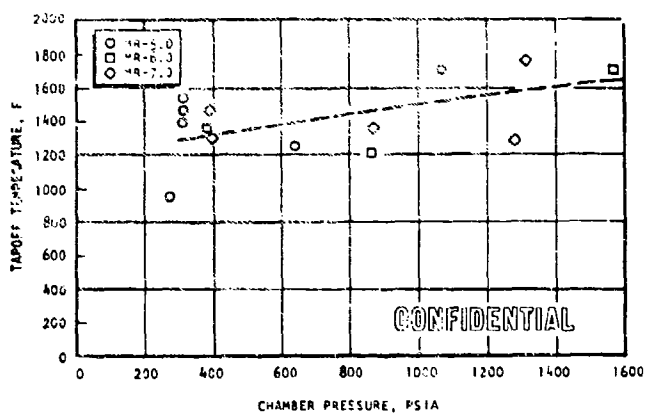

Figure 43. 2.5K Segment Tapoff Temperature vs Chamber Pressure

(U) The procedure for calculation of delivered performance is similar to the performance model under consideration by the ICRPG Performance Standardization Group. The major calculations and sequence in the Rocketdyne technique is illustrated in Fig. 44. Included in this procedure are the effects of advanced pump-fed systems and nozzles, which extend it beyond the current ICRPG investigation. Rocketdyne's developed and verified technology provides the base for analyses of these special aspects.

(U) Rigorous performance calculation requires a series of iterations to converge on the final performance prediction, primarily as a result of first-order interactions between processes which occur simultaneously in the engine. As an example, the flow field and boundary layer analyses must be completed before propellant injection temperature is known, but they, in turn, are dependent on injection temperature. First estimates must therefore be made and an iterative analysis conducted by adjusting the estimates until a converging answer is obtained.

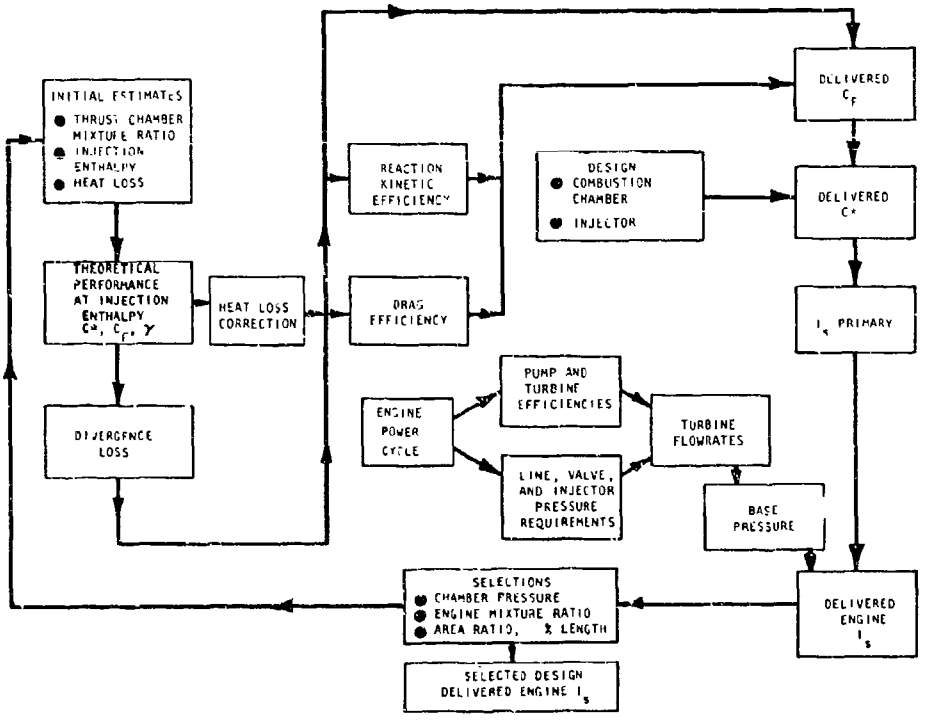

Figure 44. Delivered Performance Calculation Procedure

(U) All primary interactions between loss mechanisms and most secondary interactions are accounted for in the procedure shown in Fig. 44. All of the primary and secondary effects considered by the ICRPG are included with the exception of the effects of finite reaction rates on the boundary layer and combustion efficiency losses. In the current state of the art, no method is available for computing the effects of kinetics on the boundary layer loss. As for combustion efficiency losses, it is not necessary to account for them analytically because the combustion efficiency is determined directly from hot-fire test data. The Rocketdyne procedure therefore includes virtually every computable effect that is believed by the ICRPG to influence the performance by 0.2 percent or more. In addition, the effects of one-dimensional heat loss and secondary flow, not considered by the ICRPG, are included.

(C) Sensitivity. Figures 45 through 47 illustrate the sensitivity of specific impulse to several engine design and operating parameters for the engine operating at 250K and a mixture ratio of 6. Figures 45 and 56 present the sensitivity of the engine to turbine inlet temperature and turbomachinery efficiencies as a function of chamber pressure. These indicate that the engine is more sensitive at a higher pressure. This is explained by the fact that the engine performance is a function of the hot-gas flowrate extracted from the chamber to drive the turbines, and this flowrate is proportional to the pump power requirements and, thus, the chamber pressure. Therefore, a given percent change in efficiencies or turbine inlet temperature causes a larger absolute change in turbine flowrate at high pressure, and hence has a larger effect on delivered specific impulse. Figure 45 shows the effect of turbine inlet temperature and Fig. 46 the effect of turbomachinery efficiencies. The latter is plotted as gain factors which are applied to all four nominal turbopump efficiencies. Thus, the 90-percent gain line reflects a 20-percent increase in turbine flowrate. Figure 47 shows also the individual effects of the pumps and turbines at a chamber pressure of 1500 psia. The data reveal that the

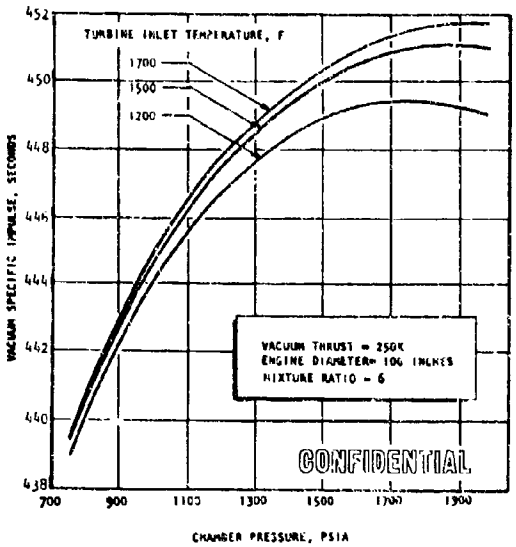

Figure 45 . Vacuum Specific Impulse vs Chamber Pressure, Effect of Turbine Inlet Temperature

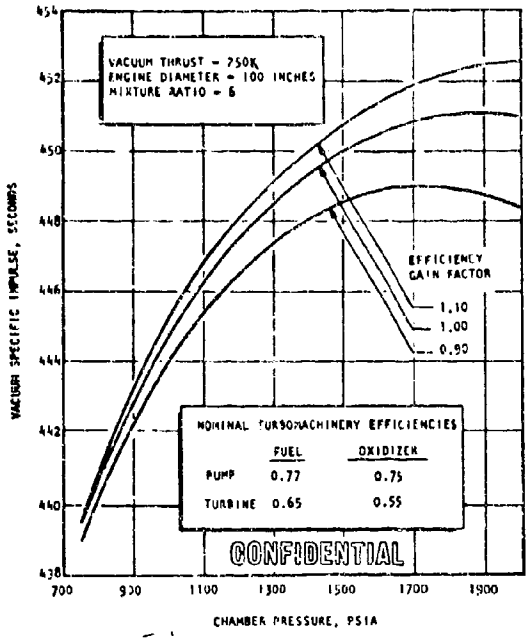

Figure 46 . Vacuum Specific Impulse vs Chamber Pressure, Effect of Turbopump Efficiencies

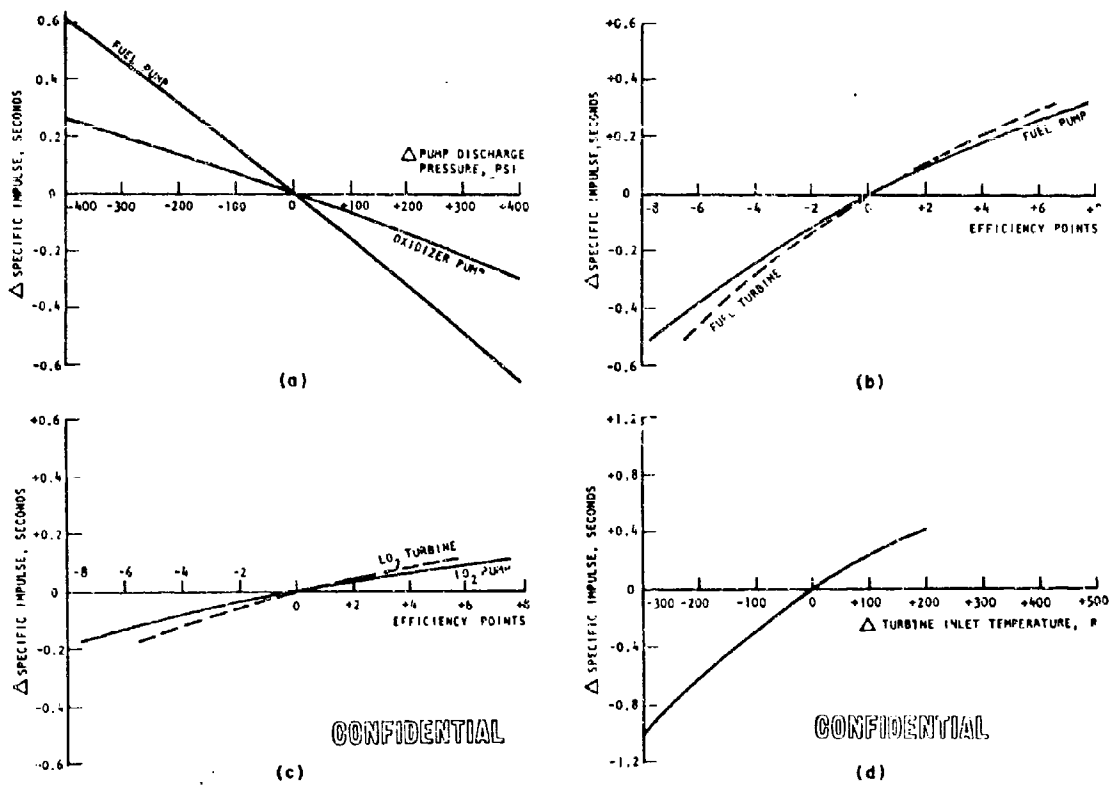

Figure 47. Engine Sensitivity with Turbomachinery Parameters

aerospike engine performance is relatively insensitive even to large changes in the turbomachinery performance. The effect of pump discharge pressure also is included in this figure. Changes in the fuel pump discharge pressure reflect changes in the cooling jacket pressure drop, and these, too, are seen to have a very small effect on specific impulse.

(U) Start Model. The start transients shown in Fig. 30 were determined from a mathematical model formulated to simulate the low-frequency dynamic behavior of the Demonstrator Module system. This model is an analytical formulation and numerical solution of a set of equations that simulate the engine system. The formulations include the nonlinear partial differential equations that describe, over the entire region encountered during start, the liquid, gas, and supercritical propellant in the feed systems. The feed system descriptions also include pumps, ducting, and distributed parameter cooling tubes with two-dimensional heat transfer. The engine system description also incorporates the nonlinear differential and algebraic equations required to describe the low-frequency combustion process, hot-gas flow, and turbine power generation. The analytical formulations have control logic and nonlinearities that are representative of the engine sequencing and control valves. The entire system of equations is solved simultaneously with the aid of computer technology developed as a result of the start model experience at Rocketdyne.

(C) The HGI flow transient shown in Fig. 48 indicates a smooth operating range from ignition (1.0 second) to cutoff (3.5 seconds) During this period, the temperature is held constant by the automati oxidizer pressure regulator which maintains a constant HGI mixture ratio. The start model assumed a simple control device which makes the oxidizer regulator out pressure equal to a reference hydrogen pressure just upstream of the HGI injector. By proper design of the HGI injector resistances, this will ensure a constant mixture ratio of 1.12 which yields a temperature of 1500 F. The reference hydrogen pressure was taken at a point between the

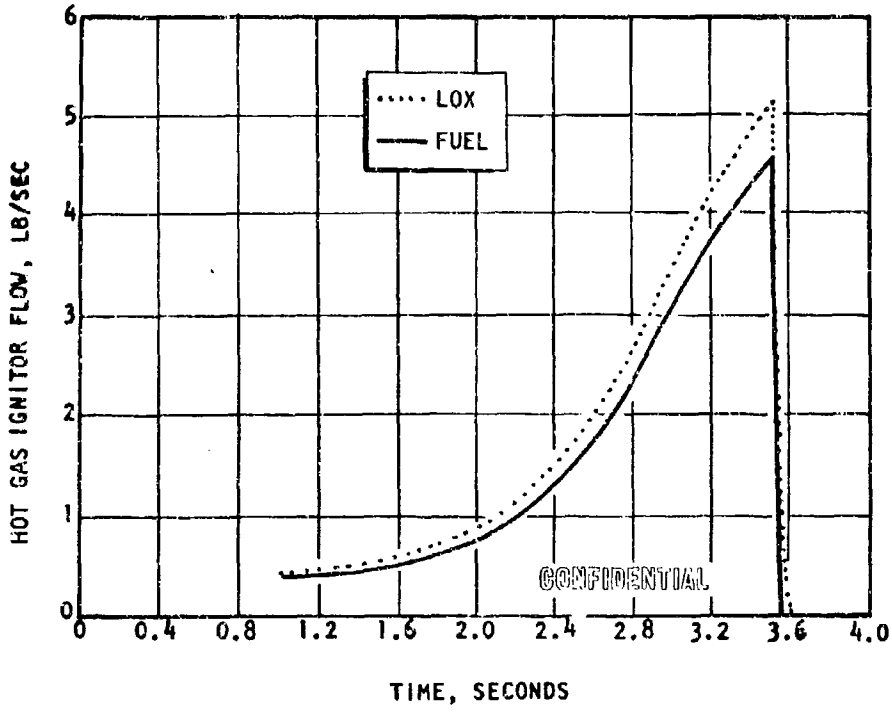

Figure 48. Start Model, HGI Flow Transient

HGI and the pump discharge with an arbitrary resistance equal to that of the HGI injector inserted upstream of the reference point. This particular division of the fuel-side resistance was found by trial and error to permit temperature control during the entire HGI operation while providing a rapid, smooth start. In order to accomplish this, it may be necessary to orifice the fuel-side feed system since the injector resistance does not necessarily represent one-half of the total resistance. A check on the resulting available injection pressure drops determined that both the fuel and oxidizer ΔP's were adequate for satisfactory HGI operation.

(U) Figure 49 shows the resultant oxidizer pressure regulator requirements. The shaded region between the oxidizer pump discharge pressure and the regulator reference pressure defines the regulator ΔP transient (Fig.49a). This is plotted directly in Fig.49b together with a relative resistance curve determined by dividing by the flowrate squared. Because the flowrate is so small at the start, the maximum regulator resistance occurs at this time. Specific transient data listing pressures, flowrates, and ΔP's are presented in Table 18.

(C) The Demonstrator Module start model defined regulator requirements with a 6:1 resistance range. This is not anticipated to present any design problems. A regulator based on the same back-to-back pressure reference principle is currently being studied for a possible application on the J-2 engine. This regulator has a resistance range of roughly 1000:1 and a response of 85 cps. While the accuracy requirements for the J-2 application are not very stringent (temperature control within 500 F), the design appears to offer reasonable control that might well be capable of meeting possible Demonstrator requirements of approximately ± 50 F.

(C) The transition from HGI operation to tapoff operation occurs as the HGI is shut down. At this time, the HGI pressure decays while the main chamber pressure is rising, thereby creating a positive driving pressure for the tapoff gases, and a smooth reversal in the flow direction. There

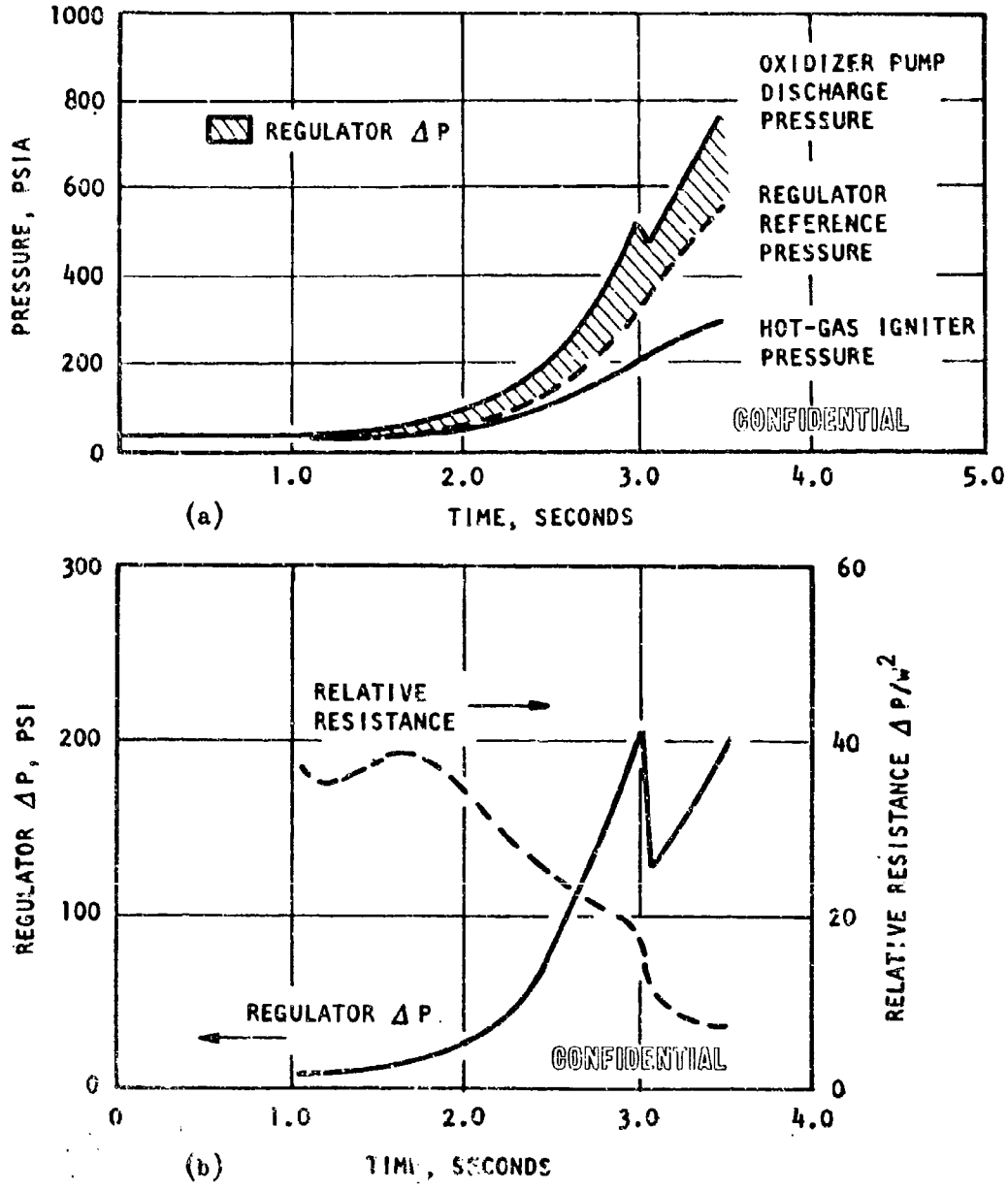

Figure 49. HGI Oxidizer Pressure Regulator Requirements

(C)

TABLE 18

HGI OXIDIZER PRESSURE REGULATOR DATA

Time, seconds	P_{D_f}	P_{D_o}	P_{HGI}	$\dot{w}_{F_{HGI}}$	$\dot{w}_{o_{HGI}}$	$P_{Reg_{Ref}}$	ΔP_{Reg}	Relative Resistance
1.05	31.9	37.5	27.4	0.418	0.466	29.6	7.9	36.4
1.20	33.2	38.9	28.4	0.431	0.482	30.8	8.1	34.9
1.40	36.2	43.3	30.6	0.467	0.520	33.4	9.9	36.6
1.60	41.8	51.5	34.6	0.528	0.588	38.2	13.3	38.5
2.00	67.7	86.0	51.7	0.788	0.880	59.7	26.3	34.0
2.40	136.6	172.9	89.1	1.36	1.52	112.9	60.0	26.0
2.60	204.1	256.8	119.2	1.82	2.03	161.6	95.2	23.1
2.80	305.9	384.0	157.7	2.41	2.69	231.8	152.2	21.0
3.00	447.0	528.0	202.8	3.09	3.45	324.9	203.1	17.1
3.20	613.3	579.5	248.9	3.78	4.22	431.1	148.4	9.3
3.40	768.1	707.8	286.6	4.34	4.86	527.4	180.4	7.7
3.50	830.3	767.8	300.8	4.55	5.10	565.6	202.2	7.8

is a small finite time (a few milliseconds) when both HGI and tapoff gases are flowing to the turbines. During this period, the turbine inlet temperature takes a sharp drop. This results from the fuel-rich shutdown sequence of the HGI. A 50-millisecond hot-gas igniter oxidizer valve closing time and a 100-millisecond hot-gas igniter fuel valve closing time were assumed in the start model. Therefore, there is a period of 50 milliseconds when virtually pure fuel is being mixed with the 1500 F tapoff gases. This causes the turbine inlet temperature to drop momentarily to roughly 1000 F. Since main chamber ignition has already been accomplished, the only effect the temperature drop might have is on the turbopump speed buildup. However, the short duration of the transition and the inertia of the turbopumps minimize the effect on the start transient, and other system effects are considered more significant during this period.

(U) No effects of the isolation valve resistance were considered in the start model. This is equivalent to assuming a small time lag in the closing time of this valve after the hot-gas igniter fuel valve is closed, which is a valid and realistic assumption.

(U) The start model transients were calculated using tapoff gases having gas generator properties. Therefore, the temperature drop was a simple calculation reflecting the effects of a change in mixture ratio. However, if a new start transient were calculated based on preheated hydrogen tapoff gas properties, the temperature drop would be somewhat less. Because of the higher specific heat of the tapoff gases, cooling with pure hydrogen has a smaller temperature effect.

(U) No provision was made in the start model for a HGI purge. This could extend the time during which the turbine inlet temperature is depressed if the isolation valve is left open and the purge gases are exhausted through the turbine drive system.

Alternatives Studied.

(U) Cycle Trade Study. Early in the contract period, a trade study was conducted to re-evaluate the selection between the two low turbine flow cycles (gas generator vs tapoff).

(U) Schematics for these two cycles are shown in Fig. 50. The tapoff cycle utilizes hot gases from the main chamber during mainstage to drive the turbines, which are shown in a parallel arrangement. (A trade study comparing the series and parallel arrangements is presented on page 118). Engine thrust is controlled with the tapoff throttle valve located in the main tapoff duct, while engine mixture ratio control is accomplished with the oxidizer turbine throttle valve. Main chamber ignition is achieved with hot gases generated during the start transient in the hot-gas igniter. (See page 155 for the ignition system study.) Some of these gases are utilized to drive the turbine until main chamber tapoff operation can be commenced.

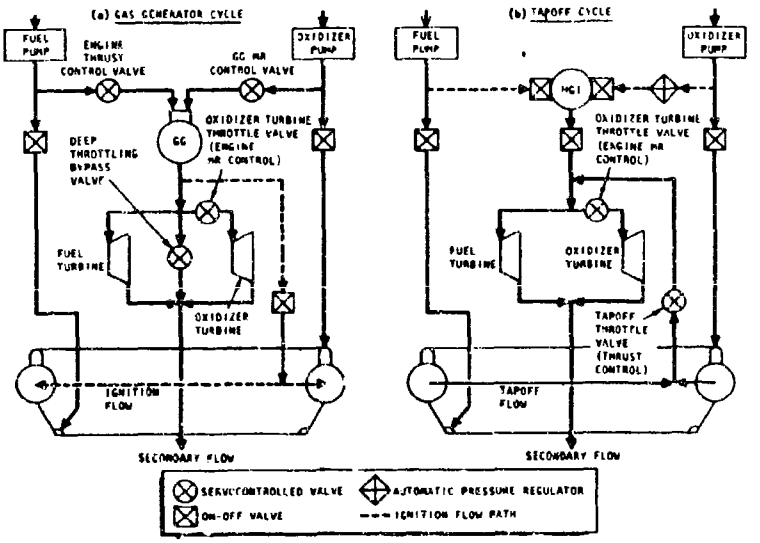

Figure 50. Aerospike Cycle Comparison

(C) The gas generator cycle (Fig. 50a) utilizes hot gases from the gas generator to drive the turbines throughout the engine operation. Thus, control is accomplished with a valve in the gas generator liquid fuel line, while engine mixture ratio is varied with an oxidizer turbine hot-gas throttle valve. The gas generator mixture ratio is controlled by a valve in the gas generator liquid oxidizer line. A hot-gas ignition system,

basically the same as for the tapoff cycle, is also incorporated. The 5:1 throttling requirement on the engine requires that the turbine drive gases be throttled greater than 10:1. This design goal requires either additional gas generator development or employment of an alternate turbine bypass at the throttled condition. Because 10:1 throttling of a gas generator would not be demonstrated during Phase I, the bypass was used in the tradeoff study.

(U) Four major factors were considered: (1) performance, (2) weight, (3) complexity, and (4) development problem areas. The two cycles were compared at a common chamber pressure; both utilized a similar hot-gas ignition system. Because the exact properties of tapoff gases had not yet been demonstrated, the two cycles were compared using similar turbine drive gases with properties equal to those of the gas generator. This assumption tends to lower the specific impulse of the tapoff cycle, but does not alter the conclusion of the study. Except for the turbine drive component arrangement and control, the two systems are identical, and therefore, only the effects of this portion of the system had to be studied.

(C) The specific impulse of the two systems will differ only if the secondary flowrates are different. These are a direct result of turbine performance and pump horsepower requirements. The fuel pump discharge pressure for a gas generator system will be slightly higher than for a tapoff system because of an increased coolant pressure drop, thereby raising the pump power requirement. A higher pressure drop is required because the fuel used in the gas generator is not available for thrust chamber cooling. However, this effect was found to be insignificant because the increase in fuel pump discharge pressure was calculated to be only 60 psia, which reduces specific impulse only 0.1 second compared to the tapoff system.

(C) The fuel turbine inlet pressure for the tapoff system is determined by the main chamber pressure, the hot-gas pressure drop, and manufacturing tolerances. For the gas generator system, the fuel turbine inlet pressure

is limited by the oxygen pump discharge pressure, pressure drops in the gas generator feedlines and injector, the hot-gas pressure drop, and manufacturing tolerances. To ensure stable gas generator operation at the throttled level using a fixed-area injector design, a large gas generator injector pressure drop is necessary at the full-thrust point. This requirement, together with an added liquid control valve pressure loss, is sufficient to bring the fuel turbine inlet pressure for the gas generator cycle down to the approximate level of that for the tapoff system, and thus, no significant increase in turbine pressure ratio can be achieved. The study therefore indicated that the full-thrust specific impulses of the two systems were nearly identical. However, at the throttled condition, the tapoff system specific impulse is significantly higher than the gas generator system. This results from the throttling requirements on the gas generator. Ten-to-one throttling of the turbine flow is necessary to meet the power requirements of the engine at 20-percent thrust; however, only 5:1 throttling of a gas generator was considered feasible for the Demonstrator Module at this time. The excess gas generator flowrate was then bypassed into the base region, with a corresponding specific impulse reduction of 3 to 4 seconds.

(U) The weight study of the two systems found the two to be quite comparable. Most of the components are practically identical, and the difference in weight lies solely in the ignition and turbine drive subsystems. The elimination of the turbine bypass duct and control valve for the tapoff system amounted to a small weight saving over the gas generator.

(C) The complexity of the two systems was measured in terms of the control requirements. Here, the tapoff cycle offers a simple system with only two servocontrolled valves, the tapoff hot-gas throttle valve and the oxidizer turbine hot-gas throttle valve, whereas the gas generator cycle requires four servocontrolled valves, two in the gas generator liquid lines and two in the turbine hot-gas system. Another small disadvantage to the gas generator cycle also was attributed to the fact that the engine thrust

control was not accomplished at the turbine inlets, but upstream of the gas generator in the liquid lines. Thus, the gas generator oscillations become coupled with the thrust chamber oscillations and impose more stringent requirements on the control system.

(U) A limited evaluation of the development areas required for each system was conducted. Control of the tapoff properties for turbine drive gases in the tapoff cycle will require extensive testing, and the tapoff port design will have to serve a dual function to include ignition. This latter consideration was felt at first to favor the gas generator cycle thrust chamber development; however, it must be noted that the gas generator ignition port design must also be located in a cool-temperature region to prevent burning out the ignition ports and manifold during mainstage operation. Therefore, the development of a satisfactory port design is roughly the same for either system. The tapoff property control development in the tapoff system is offset in the gas generator system with a gas generator throttling development; therefore, the area of development was considered a standoff.

(U) On the basis of the foregoing factors, the tapoff cycle was judged to be the superior cycle, exhibiting higher overall performance and lower weight with a simpler and therefore more reliable system.

(C) Turbine Arrangement. The tradeoff between a series and parallel turbine arrangement was studied because of the potential reduction in turbine flowrate that the series arrangement offers. A more detailed analysis determined that the series arrangement produced a higher engine specific impulse (0.6 second at full thrust); however, the parallel arrangement was a simpler and lighter system. These latter considerations are discussed in more detail in the following paragraphs.

(U) The parallel arrangement offers simplicity in packaging because the turbine inlet lines for both turbines can be designed small in size as

a result of the high density of the gases at the inlets. The series arrangement, on the other hand, requires a large-diameter crossover duct between the two turbines to handle the low-density fuel turbine exhaust gas, reducing accessibility to the other components. Furthermore, thermal growth in the crossover duct imposes side loads between the two turbopumps. Designs to accommodate these loads would entail increased structural requirements or incorporation of undesirable flexible joints.

(U) With the requirement of tank head starts, it was found that the series turbine arrangement was marginal in producing sufficient torque for breakaway which was estimated to be between 15 to 50 in.-lb for each turbopump. Hence, extended start times would result at sea level. It therefore is necessary to design a fuel turbine bypass for the start transient. This additional ducting, valve, and control network adds weight and complexity to the series design. The parallel arrangement, however, exhibits completely satisfactory start transients without any additional turbine drive gas start controls (see the Engine Operation section, page 75).

(U) The final results of the study therefore led to the conclusion that the simpler control system, simpler component packaging, and lighter weight of the parallel arrangement more than compensated for the slightly lower performance of this system.

(U) Control Point Selection. A trade study to determine the best choice of control points for the tapoff cycle was conducted. Control concepts utilizing multiple controllers for one function (e.g., rough thrust control with one hot-gas valve and trimming with two liquid line valves) were eliminated because of the adverse effect upon system reliability. Therefore, only those concepts with two-point control were retained for study in detail. These are listed below with the numbers in parentheses corresponding to the control points shown schematically in Fig. 51.

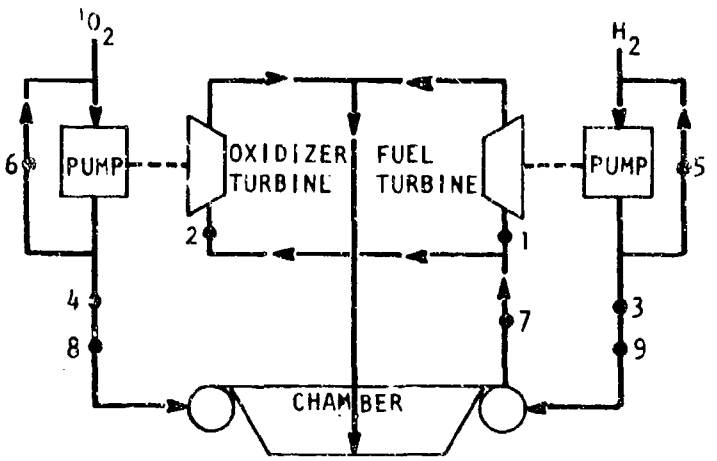

1. FUEL TURBINE THROTTLE VALVE (HOT GAS)
2. OXIDIZER TURBINE THROTTLE VALVE (HOT GAS)
3. MAIN FUEL VALVE
4. MAIN OXIDIZER VALVE
5. FUEL PUMP BYPASS VALVE
6. OXIDIZER PUMP BYPASS VALVE
7. TAPOFF THROTTLE VALVE (HOT GAS)
8. OXIDIZER VARIABLE-AREA CAVITATING VENTURI
9. FUEL VARIABLE-AREA CAVITATING VENTURI

Figure 51. Candidate Engine Control Points

1. Fuel turbine and oxidizer turbine throttle valves (1, 2)
2. Tapoff and oxidizer turbine throttle valves (2, 7)
3. Main fuel valve and main oxidizer valve (3, 4)
4. Two variable-area cavitating venturis (8, 9)
5. Tapoff throttle valve and main oxidizer valve (7, 4)
6. Tapoff throttle valve and fuel pump bypass valve (7, 5)
7. Tapoff throttle valve and oxidizer pump bypass valve (7, 6)
8. Main oxidizer valve and fuel pump bypass valve (4, 5)
9. Main fuel valve and oxidizer pump bypass valve (3, 6)

(U) The study was performed using steady-state operating levels at the extreme points of the operating envelope. Constant-temperature tapoff gas was assumed.

(U) The effects of each control system on the critical engine operating parameters are summarized in Table 19. Undesirable levels of each parameter are shown with an asterisk. (Since this study was completed early in the contract, the numbers in the summary table do not agree precisely with the latest engine balance; however, the conclusions of the study remain valid.)

(U) The systems using two hot-gas valves have lower pump discharge pressures or lower pump flowrates (or both) than all of the systems using liquid side control. Therefore, the hot-gas control systems have lower engine weights and/or higher engine specific impulse.

(C) A dynamic analysis of control system response favors liquid control over the hot-gas systems. Nevertheless, the hot-gas system response was still satisfactory in meeting the engine requirements, even at 20-percent throttling. However, if the throttling range should be extended, this

TABLE 19

COMPARISON OF SIGNIFICANT ENGINE PARAMETERS AT STEADY STATE

Control System	Significant Engine Parameter									Remarks
	P_{d_o}	$\dot{w}_o$	N_o	P_{d_f}	$\dot{w}_f$	N_f	I_s	F	MR	
1 and 2	2030	486	25000	2420	69.4	33600	441.2	246K	7	300-psi tapoff differential pressure
	2056	476	25016	2634	79.3	35986	450.2	250K	6	
	1800	405	23065	2560	81	36000	354.5	224K	5	
3	2118	505	25646	3031*	72.5	36948	440.2	254K	7	Maximum differential pressure: 200 psi oxidizer 670 psi fuel
	2242	447	25914	3284*	79.6	38873	449	250K	6	
	2391	456	26342	2891*	91.3*	38854	453	248K	5	
4	2750	482	28400*	3870*	80.3*	41700*	445	250K	6	
5	2064	482	23650	2498	70.9	34344	449.9	248K	6.84	Nominal oxidizer valve differential pressure = 400 psi
	2425	476	27614	2635	79.4	36000		250K	6	
	2706*	427	25500	2566	82.8	36000		230K	5.18	
6 and 8	2054	476	25013	2650	99.5*	38701	449.3	250K	6	
	2163	486.3	25640	2916	98.1*	39440*	452.5	261K	5.36	
7 and 9	2516	589.3*	27850*	2918	83.7*	37830*	441.7	292K	6.9	
	2055	606.4*	25442	2634	79.4	35992	449.8	250K	6	

*Denotes Undesirable Magnitude

P_{d_o} = oxidizer pump out pressure

$\dot{w}_o$ = oxidizer pump weight flow

N_o = oxidizer pump speed

P_{d_f} = fuel pump out pressure

$\dot{w}_f$ = fuel pump weight flow

N_f = fuel pump speed

I_s = specific impulse

F = thrust

MR = mixture ratio

CONFIDENTIAL

factor must be seriously reviewed. Another advantage of the hot-gas control systems is that they can be used to control pump power during the start and shutdown transients. The liquid-side control systems cannot be used for these applications because they also control flow to the thrust chambers. Therefore, it was concluded that a system utilizing hot-gas control was preferable to concepts utilizing liquid-side control, and a further study between the series or parallel hot-gas valve arrangement was made.

(U) The series arrangement tends to separate the functions of each valve. The common upstream valve is used for thrust control, and the oxidizer turbine valve is used for mixture ratio control. This separation of functions characteristic of system 2 will simplify development of the engine system because it will be possible to operate the engine and components with one valve and an orifice equivalent of the other valve. This characteristic also gives this system the potential for open-loop operation (valve position control only), and provides a measure of safety since the failure of one valve does not destroy the functional effectiveness of the other. The parallel arrangement will give greater start transient control versatility; however, satisfactory start characteristics for the series arrangement are predicted.

(U) Furthermore, a unique design incorporating the tapoff valve (poppet type) of system 2 into a Y in the tapoff ducting provides design advantages for this system over system 1, and the control characteristics of such a valve will be superior to that of a conventional poppet valve.

(U) The conclusion of this study was that hot-gas valves arranged in series (system 2) should be selected because of control flexibility, superior design features, and safety advantages.

(U) Control Logic. After selecting the system control points, the control logic for the Demonstrator Module was investigated. The two candidates considered were open-loop thrust and mixture ratio control, and closed-loop thrust and mixture ratio control. Both systems were analytically designed to meet the specific requirements for the thrust and mixture ratio controls. The closed-loop system was selected because of its superior control characteristics. Hybrid systems (such as open-loop thrust and closed-loop mixture ratio control) were eliminated from consideration for the same reasons presented for the pure open-loop system.

(U) The closed-loop system has a separate control loop for each valve. The tapoff valve loop is closed on chamber pressure (the selection of which is discussed on page 344), and the oxidizer turbine valve loop is closed on engine mixture ratio. Interior closed loops on valve position are also utilized.

(U) The open-loop system functions upon a valve position command and incorporates interior closed loops on valve position together with function generators relating the two valve positions. The function generators are necessary to protect the engine since throttling of one valve leads to an undesirable operating region unless the other valve is also repositioned.

(U) The closed-loop system exhibits much greater versatility than the open-loop system. Extensions in either thrust or mixture ratio range are possible with the closed-loop system with recalibration of the system, and components can be replaced in the engine system without system recalibration. Furthermore, programming of the closed-loop system for test purposes will be simplified because the path followed between two operating points will more closely follow a predictable straight line. The closed-loop system can be run in the open-loop mode, while the open-loop system cannot be run in the closed-loop mode.

(C) The requirements for engine self-protection also create doubt that an open-loop system may be simpler than a closed-loop system. Safety for either control scheme cannot be implemented by the location of fixed mechanical stops on the hot-gas valves since mechanical stops on the tap-off throttle valve limit the use of this valve during start and shutdown, and mechanical stops on the oxidizer turbine throttle valve will not allow full traverse at nominal thrust or will allow burnout and flameout at 20-percent thrust. Both systems are therefore dependent upon signal limiting and upon reliable feedback signal maintenance to ensure that the engine is operating at a desirable point. This is accomplished automatically with the closed-loop system and by function generators in the open-loop system. However, the dynamics of the engine cause a problem with the open-loop system when traversing from point to point. This can be seen in Fig. 52. In the traverse from 20-percent thrust and mixture ratio of 7 to 50-percent thrust and mixture ratio of 7, a dynamic excursion of mixture ratio to 8.5 is observed. This results from the ability of the oxidizer turbopump system to accelerate more rapidly than the fuel system.

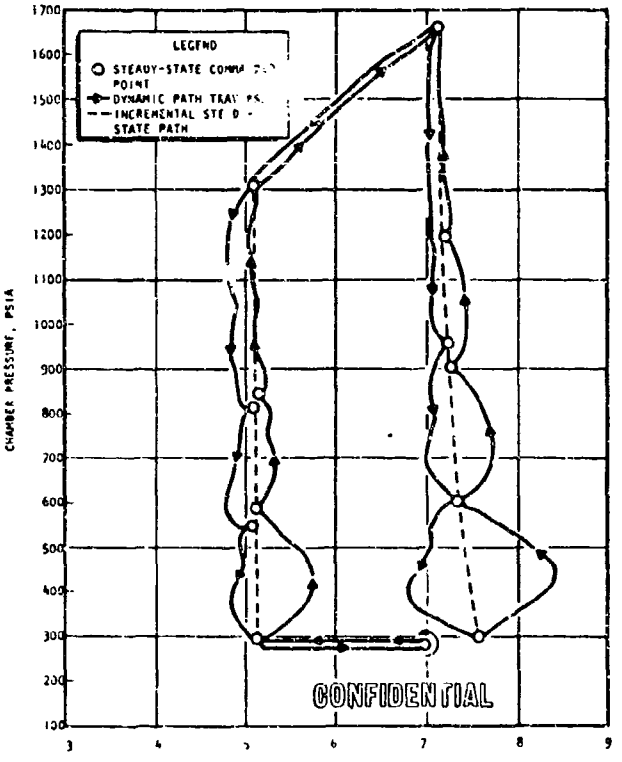

Figure 52. Dynamic Performance Path for an Open-Loop Control System

(C) The additional components to solve this problem will either make the open-loop system more complex than the closed-loop system or require programming at slower than the 5-second maximum excursion rate.

(U) Furthermore, the accuracy of the closed-loop system will be much better than that of the open loop because it is not dependent as much upon component calibrations and engine calibrations.

(U) Therefore, the closed-loop system was selected for the Demonstrator Module.

(U) Operating Envelope. The upper thrust level definition of the engine operating envelope was fixed at a constant thrust during the Phase I proposal; however, subsequent analysis suggested that other criteria may possibly lead to engine and vehicle advantages. Therefore, a study was made comparing a constant-thrust mixture ratio excursion against a maximum pump speed limitation and against a constant-chamber-pressure mixture ratio excursion.

(U) Each of the different candidates defines a different maximum thrust vs mixture ratio variation resulting in different pump speeds. The three candidates are shown graphically in Fig. 53, which shows the trends of these parameters with mixture ratio. Table 20 summarizes the characteristics of each method.

TABLE 20

(C) THRUST VS MIXTURE RATIO COMPARISON

Consideration	Constant F	Constant P_c	Maximum Pump Speed
Specific Impulse, Δ seconds	0.1	<0.1	0
Engine Weight, pounds	+30	<30	0
Engine Versatility	Excellent	Excellent	Good
Maximum Fuel Pump Speed (MR=5), rpm	38,900	38,300	36,000
Maximum LO_2 Pump Speed (MR=7), rpm	25,330	25,700	25,000
$Thrust_{vac}$ (MR=5), pounds	250K	244K	244K
$Thrust_{sl}$ (MR=5), pounds	208K	203K	186K
System Complexity	Greater than constant P_c	Simplest	Greater than constant P_c

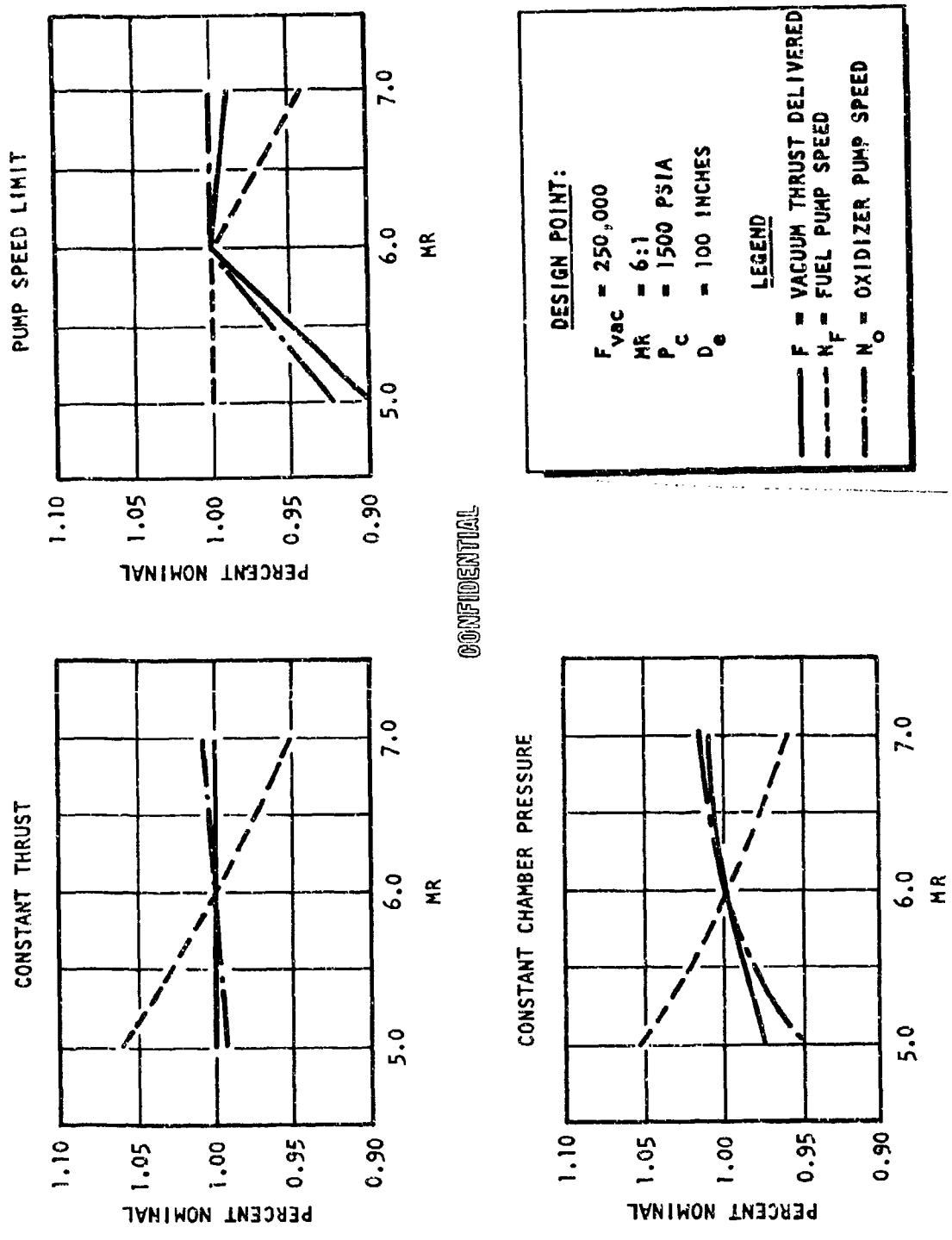

Figure 53. Operating Envelope Comparisons

(C) The constant-thrust criterion is slightly more complicated than the other two because the control system does not sense thrust directly. The constant-pump-speed criterion eases the turbopump design requirements but has the disadvantage of a 26,000-pound reduction in thrust at a mixture ratio of 5:1. The constant-chamber-pressure criterion is easier to control, and only a small decrease in thrust (4000 pounds) occurs at a mixture ratio of 5:1. At the throttled condition (P_c = 325 psia), the variation in vacuum thrust for the constant-chamber-pressure method is even less pronounced with a decrease of 1050 pounds at 5:1 and an increase of 850 pounds at 7:1.

(C) A comparison of the constant-thrust and constant-chamber-pressure methods was made in the applications study to determine the control method effect upon the optimum vehicle mixture ratio. This comparison is shown in Fig. 54 for a typical application, an expendable first-stage engine. The comparison showed the constant-chamber-pressure method to have approximately equal maximum index, but more importantly, the optimum mixture ratio shifted to a higher value. This shift is faborable with regard to vehicle propellant tank construction costs since it will result in a smaller fuel tank.

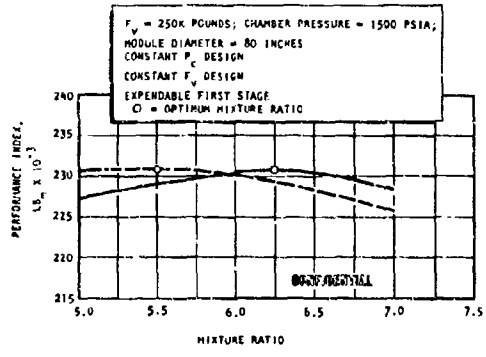

Figure 54. Comparison of Effect of Mixture Ratio on Performance Index

Similar trends were found for all six vehicle applications studied during Phase I. It was therefore decided to operate the Demonstrator Module closed loop on chamber pressure.

(U) Ignition Systems. While no tradeoff study of alternative ignition systems was made specifically for the tapoff cycle, several different candidates were re-evaluated in conjunction with the tapoff/gas generator cycle comparison. This study compared the hot-gas source with hypergolic, propellant additive, spark igniter, and catalytic systems.

(U) The hot-gas source ignition system utilized for the gas generator cycle is identical to the system used for the tapoff cycle. This has been described on page 152.

(U) The hypergolic ignition system utilizes a third propellant, which is hypergolic with liquid hydrogen, as a lead in the oxidizer system during start. Separate hypergol cartridges with explosive valves are provided for each start. Hypergols considered were chlorine trifluoride (ClF_3), Compound A, a mixture of Compund A and trifluoride, and fluorine.

(U) The propellant additive ignition system utilizes an additive injected into the oxidizer propellant during the start sequence which makes it hypergolic with the fuel. The main difference between an additive and a hypergol is the manner of injection. The additive becomes integral with the oxidizer propellant, while the hypergol slug is used as a propellant lead. The additive system would utilize a start tank with a metering control valve at the pump inlet.

(U) Two possible spark ignition systems were considered. The first was simply a series of spark plugs, mounted around the chamber at or near the injector face, which ignite the main propellants directly. The second was a multiple augmented spark ignition system (ASI) which utilizes plugs

recessed in the combustion zone with their own propellant feed independent of the main chamber. Each ASI unit produces a small hot-gas source which in turn ignites the main propellants. The ASI system has a higher ignition energy than individual spark plugs, and fewer units would therefore be required.

(U) The catalytic ignition technique makes use of an H_2 and O_2 reaction, promoted by a catalytic surface, which gives off hot gases. The gases are used to ignite the main propellants. The catalyst is chemically unaltered during the reaction and resists degradation due to thermal effects. Individual catalytic packs would be required at several points around the chamber, and separate propellant feed systems would be necessary for each pack.

(C) In the preparation for Phase 1, these candidate ignition concepts were studied and the central igniter hot-gas source was selected as the most promising. This system offered many desirable attributes including low weight, rapid start, unlimited restart capability, uniform ignition, and high reliability. Its biggest drawback was the lack of experience associated with hot-gas ignition. A feasibility test study was conducted on a related program to demonstrate hot-gas ignition. Results of the test series were encouraging, and satisfactory segment ignition was demonstarted with hot-gas temperatures as low as 1400 F and ignition delays below 40 milliseconds. Test ignition pressures ranged between 118 and 195 psia which are comparable to the design chamber ignition pressure of 100 to 150 psia.

(U) All alternate systems exhibit slower starts than the central hot-gas igniter system because the turbopump buildup rate is dependent upon the main chamber pressure buildup rate. Provision for an alternate turbine spin gas source was considered but it would have added an unduly large weight and complexity penalty.

(C) Of the four hypergolic ignition system candidates, gaseous fluorine injection into the combustor proved to be the most desirable. The major problem with the ClF_3 and Compound A systems is the environmental temperature control. ClF_3 will freeze at -105 F and Compound A at -155 F,

probably necessitating temperature control through use of heaters. Further undesirable features of each of the four hypergolic ignition systems are the additional storage space, feedlines, and controls required.

(C) The propellant additive system is most attractive when a single start tank is used rather than separate cartridges to provide accurate metering of the additive. Of the additive candidates, only ozone difluoride meets the performance requirements. However, ozone difluoride is not considered feasible because of its stability characteristics. Ozone difluoride freezes at LN_2 temperatures, and decomposes rapidly above LO_2 temperatures, presenting only a narrow band for stability. In addition, ozone difluoride is subject to detonation and would present an unsafe condition should it become isolated in an LO_2 start system. Therefore, this additive system was eliminated because it requires more stringent control than the hypergolic system without offering any advantages.

(C) The direct spark igniter system was considered and found to be impractical because of the extremely small energy source. This would mean many spark plugs would be mounted in the main chamber compartments, requiring multiple sets of electrical harness and exciter equipment. The complexity of this system together with spark location design and development problems and probable high weight were additional negative factors.

(U) The multiple augmented spark igniter system mounted in the main chamber showed little improvement over the direct spark igniter system. The hot gases it generates provide a higher energy source, thereby reducing the number of spark locations required, but each ASI unit is more complicated than the simple plug. It nevertheless is preferred over simple spark plugs because it produces smoother, more repeatable starts. However, the high weight, electrical complexity, and chamber design problems for this system restrict its application.

(U) The catalyst ignition systems were analyzed from both the adaptability and the state-of-the-art standpoint. The incorporation of this design into a toroidal chamber is extremely complicated and the state of the art was not considered adequate for this application.

(U) The results of the study therefore led to the conclusion that the hot-gas source ignition system was the best for either a tapoff or gas generator cycle aerospike engine.

System Preliminary Design

(U) The Demonstrator Module design is based upon the requirement to design, fabricate, and test a full-scale, high-performance LO_2/LH_2 engine at 250K thrust and over the operating range anticipated for a Flight Engine. Specific demonstration and design requirements are presented in Table 9 (page 62). The system and component designs duplicate the Flight Module configuration as closely as practicable within the constraints of cost, schedule, safety, and development test flexibility. However, none of the deviations from the Flight Module configuration affect the technical integrity of the concept demonstration.

(U) The mechanical design is divided functionally into four subsystems: (1) thrust, (2) propellant feed, (3) turbine drive, and (4) hot-gas ignition. These are shown schematically in Fig. 55. Organization into the subsystems facilitates the system engineering concept by providing overall control of the technical logic process, by promoting function identification, by defining function grouping, and by allocation of requirements for engine system and component design, analysis, evaluation, and test. The integrated system is shown in Fig. 55 and the individual subsystem considerations are discussed below.

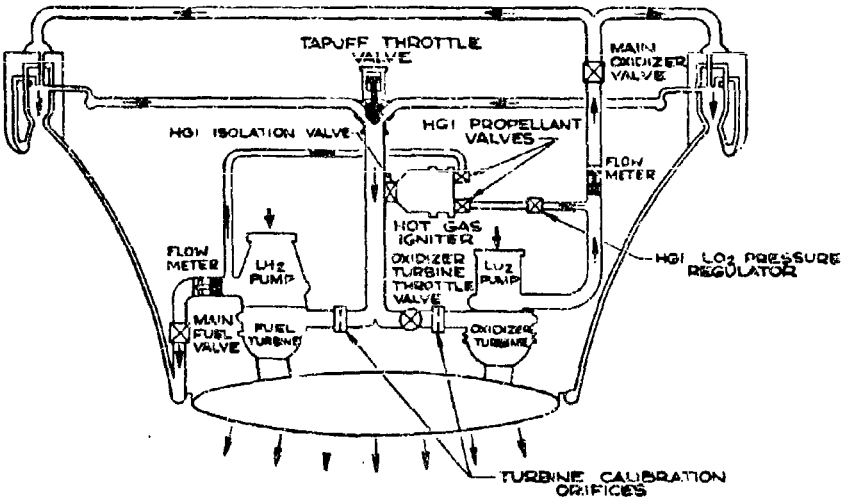

DEMONSTRATOR MODULE SCHEMATIC

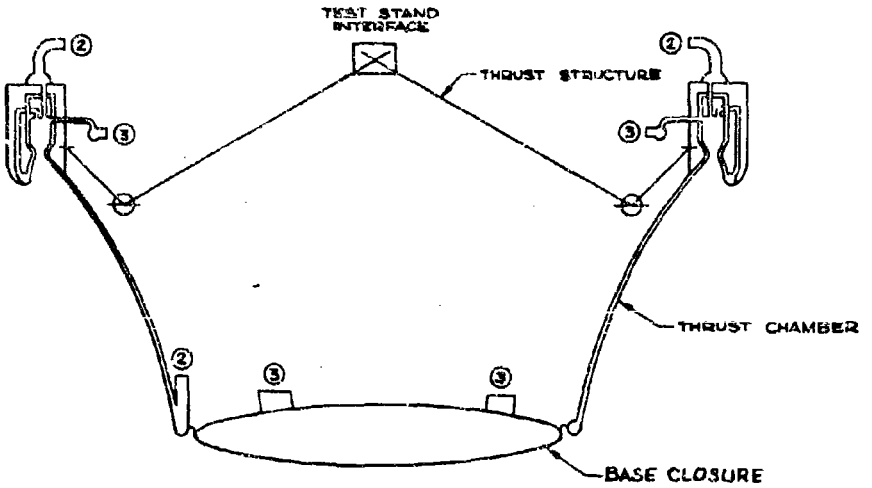

①—THRUST SUBSYSTEM

Figure 55A. System and Subsystem Schematic

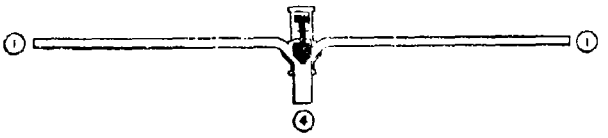

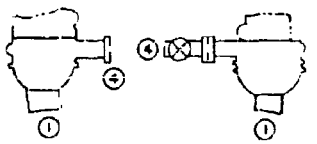

③ TURBINE DRIVE SUBSYSTEM

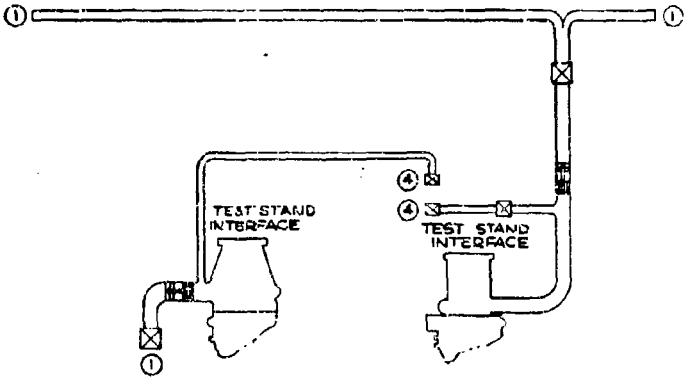

②PROPELLANT FEED SUBSYSTEM

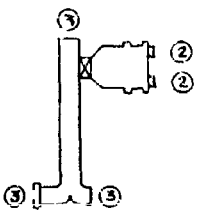

④IGNITER HOT GAS SUBSYSTEM

SYSTEM INTERFACE LEGEND:

①THRUST SUBSYSTEM
②PROPELLANT FEED SUBSYSTEM
③TURBINE DRIVE SUBSYSTEM
④IGNITER HOT GAS SUBSYSTEM

Figure 55B. System and Subsystem Schematic

(U) Thrust Subsystem. The function of the thrust subsystem is to develop and transmit the thrust of the engine system to the gimbal point, to provide structural and mounting support for the engine components, and to provide hot gases to drive the turbines.

(U) Description and Analysis. The design requirements for the thrust subsystem are defined by the overall engine performance requirements and the interface relationships with other subsystems.

(U) The Demonstrator Module thrust subsystem (Fig. 56) is composed of the following components: a thrust chamber, a base closure, a thrust structure, and pump mounts. The thrust structure is assembled to the thrust chamber at 40 points located in the plane of the 40 subsonic struts, thereby providing a load path from the outer to the inner body. The thrust is then transmitted through the thrust structure to the gimbal point which is located in the plane of the maximum diameter, thereby making the dynamic envelope equal to the static envelope. The thrust chamber is described in detail in a separate section, page 160.

(C) The perforated base closure used with aerospike thrust chambers provides the means for introduction and distribution of turbine exhaust gases into the inner-body base region to increase base thrust. The basic design approach consists of mounting the base closure assembly rigidly to the turbopump exhaust flanges with a flexible coupling between the closure and the nozzle fuel inlet manifold capable of accepting thermally induced differential expansions and providing torsional restraint for lateral pump support. The thrust load of the closure is transmitted directly through the pump casings into the thrust structure. A minor axis dimension of 6.00 inches was determined to provide a minimum weight compatible with envelope considerations. The aft surface of the closure extends 5.00 inches below the chamber exit plane; however, this additional height does not affect the gimbal excursion, while the weight and internal flow advantages offset the increased height. Turbine exhaust ducts are required between the turbopumps and the closure utilizing bolted flange couplings.

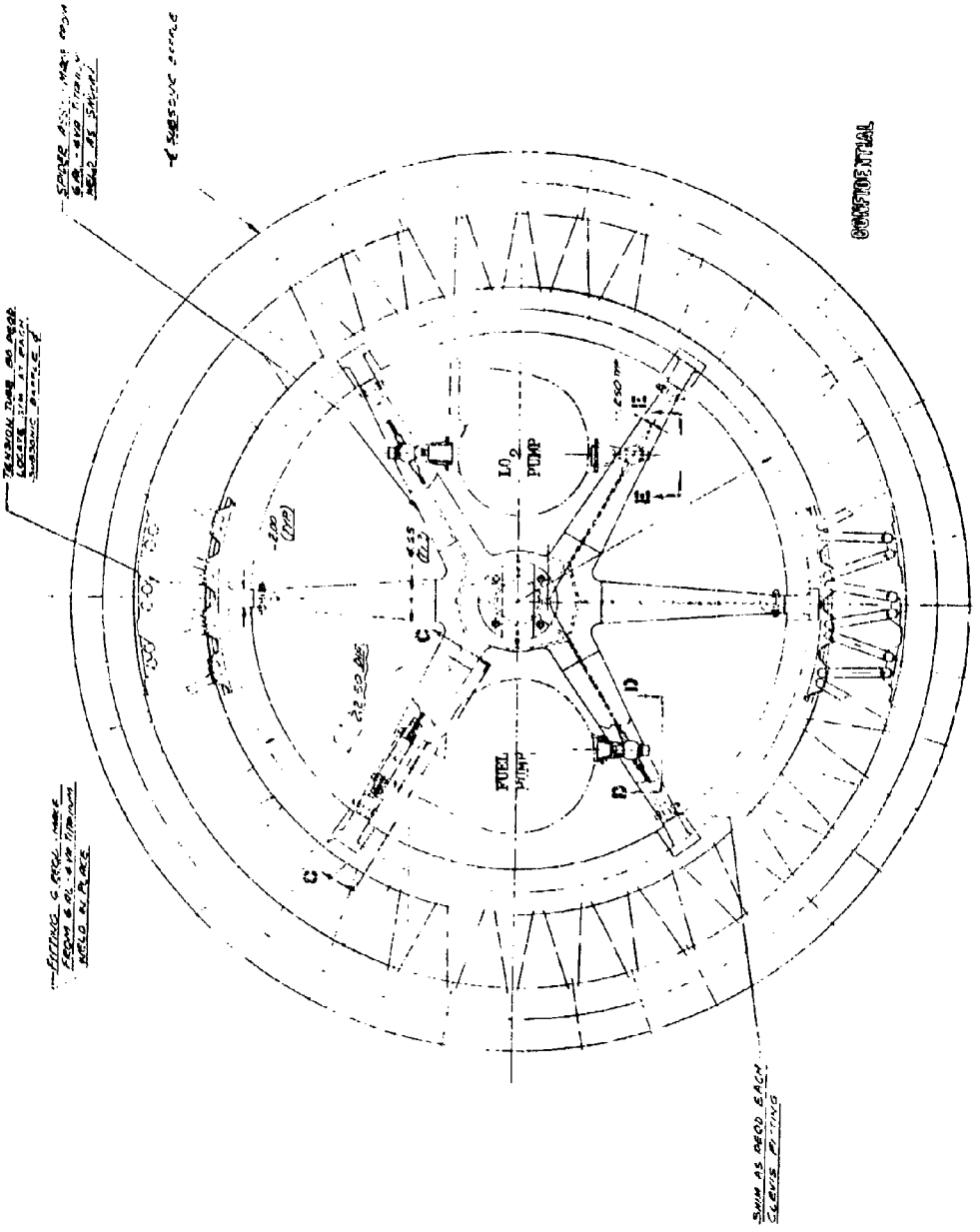

Figure 564. Thrust System Layout

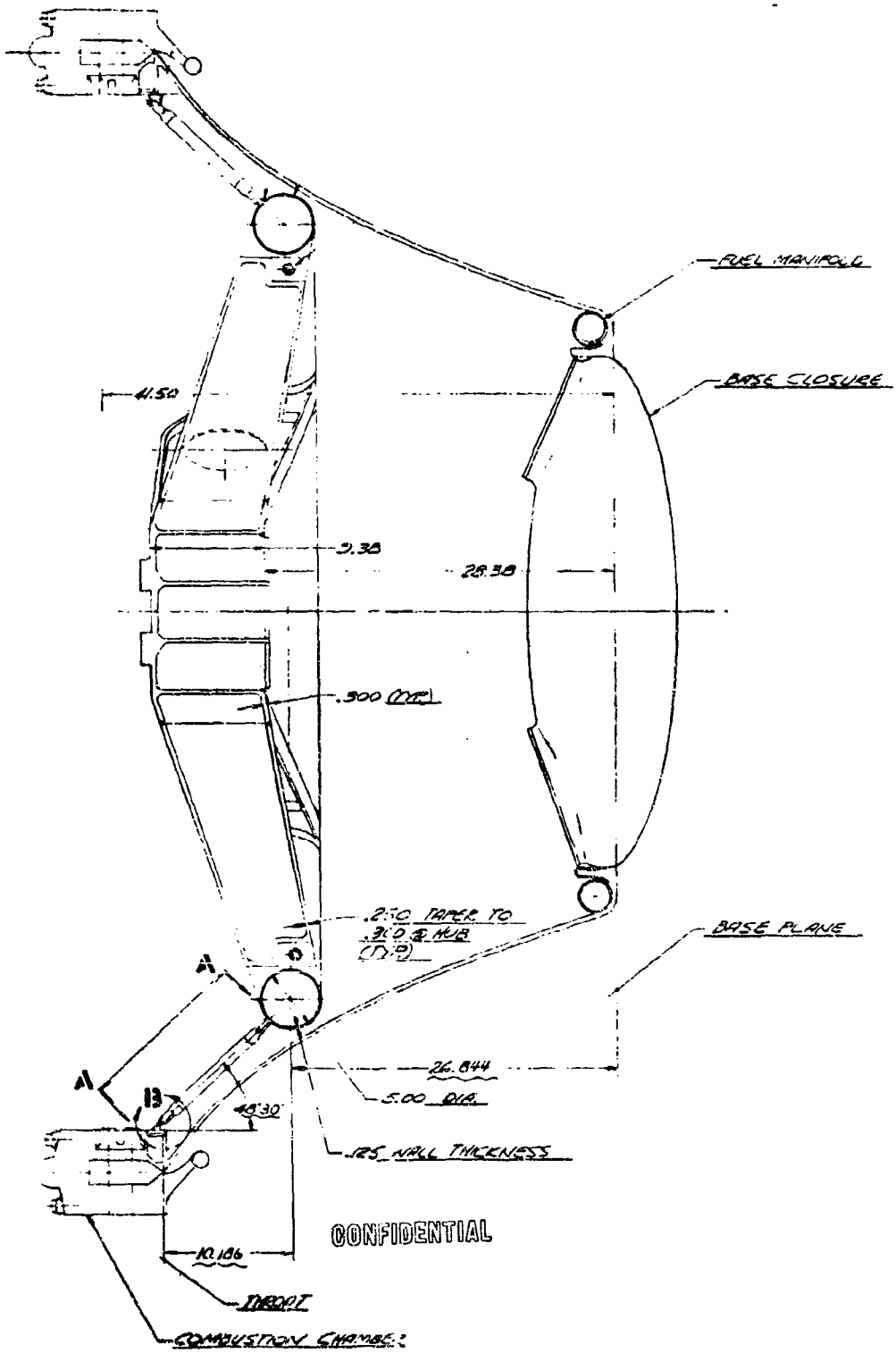

Figure 56B. Thrust System Layout

(U) An internal bolting arrangement on the base closure flange is used with access for insertion of the bolts provided by holes in the perforated aft shell. Cone-shpaed orifice plates are utilized at the inlet to the base closure from each turbine to distribute gas flow within the closure as well as reducing the fuel and oxidizer turbine exhaust discharge pressure from 70 and 40 psia respectively, to the nominal 30-psia closure internal pressure. A flexible coupling, consisting of a laminate of Inconel 625 sheet steel with a total thickness of 0.020 inch, is provided for sealing the closure to the nozzle and to provide the aft stabilizing support for the turbopump system.

(U) The thrust structure (Fig. 57) is a truss-ring-beam-hub structure which attaches to the inner periphery of the thrust chamber. It is designed with an open radial beam structure to allow accessibility for maintenance and inspection. The center radial beam thrust mount can be removed easily from the truss-ring and lifted out (with the pumps, valves, ducting, and hot-gas igniter attached) by removing six bolts at the ring-beam interface. The turbine exhaust ducts, and LH_2, LO_2, and hot-gas ducts will be disconnected before the assembly is removed. The truss cone and ring assembly is not removable from the thrust chamber.

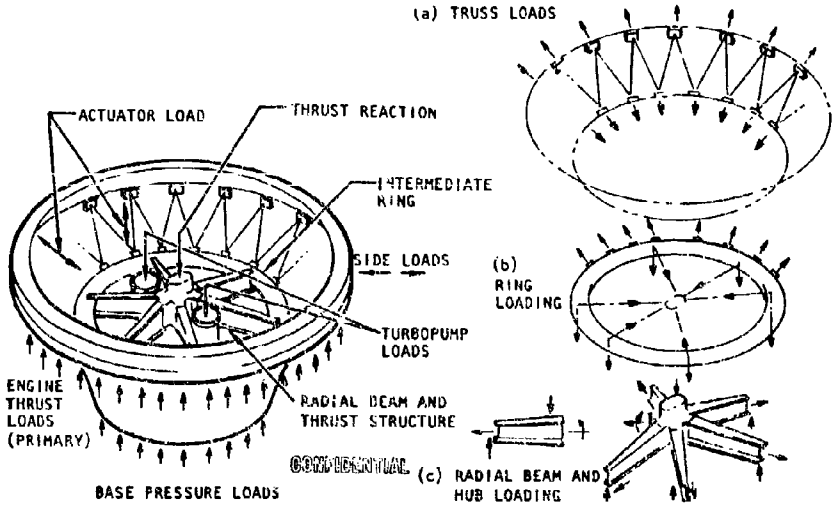

Figure 57. Aerospike Engine Thrust Load Diagram

(U) A graphic representation of the thrust structure load distribution is also shown in Fig. 57. All engine thrust loads are transmitted through the combination truss-ring and radial beam thrust mount to a single, simulated gimbal block located on the engine's longitudinal axis. The thrust cone truss is attached to the chamber inner body at 40 attach points, and transmits the thrust load (in tension) to the circular ring which, in turn, transmits the load into the radial beams through a combination of bending, ring torsion, and hoop loading. The six symmetrically spaced radial beams transmit the thrust load, in shear and bending, to the centrally located hub.

(U) The design is not deflection limited, and stress levels are within normal design safety factors. The thrust structure beams are designed to withstand a maximum bending moment as a cantilever beam. The entire thrust load is carried in bearing through the shelf at the six clevis fittings (Fig. 56). The 1/2-inch-diameter shear bolt is sized to take the thrust chamber weight multiplied by a ground-handling load factor of 10 g.

(U) The thrust structure is fabricated from 6Al4V titanium. The thrust beam and hub assembly is machined from hand-forged billets. The torus ring utilizes seam-welded tubing made from strip sheet stock and the T ring is a contour roll forged ring. The six beam attach fittings that assemble to the torus ring are made from titanium bar stock or small hand forgings. The 80 tension tubes that form the truss structure are welded assemblies made of bar stock or forged fittings welded to seamless tubing.

(U) Trunnion-type mounts were selected for attaching both turbopumps to the thrust structure. In this design, the fuel turbopump is provided structural support from the thrust structure at the fuel discharge flange (Section C-C, Fig. 56) and by a structural pad and fitting (Section D-D) on the fuel volute opposite the discharge flange. To accomplish this, fittings with spherical surfaces permitting angular misalignment are

incorporated on the centerlines of the radial beams adjacent to the pump. The fitting at the flange provides a fixed point of support, and the opposite fitting is fixed in two directions allowing motion in a radial direction from the pump centerline through the fitting. A third support point is provided by the turbine exhaust duct, base closure, and the pump shell to prevent motion of the pump about the axis found by the two fittings on the thrust structure. The trunnion design for the oxidizer pump provides structural support at two structural pads and fittings 180 degrees apart on the volute in the manner shown in Fig. 56. The other aspects of the oxidizer pump mounts are identical to those of the fuel pump. In addition to the turbopump loads, the turbopump mounts transmit the base closure thrust loads to the thrust structure.

(U) Alternatives Studied. A detailed trade study was conducted to establish the optimum thrust structure configuration, and an alternate pump mounting design was considered. These two studies are presented below.

(U) A thrust structure trade study was made to evaluate the weight, assembly, and accessibility aspects of this component assembly. Twenty five basic concepts were evaluated in three basic categories using the module gimbal point as a means of classification. These categories were: (1) designs with the gimbal point at the elevation of the injector face, (2) variations of category 1 designs but locating the gimbal point 5 inches above the injector face, and (3) designs for a gimbal point located at the maximum elevation of 24 inches. Because of volume requirements for components within the thrust chamber inner-body cavity, structure designs were limited to an envelope extending less than 13 inches below the injector face. The upper limit was established by dynamic envelope and engine length requirements from module application considerations. Out of the 25 concepts, four candidates (Fig. 58) were selected for more extensive evaluation preparatory to the final selection. Figure 59 shows the plot of weight vs height for the truss configuration and is the same

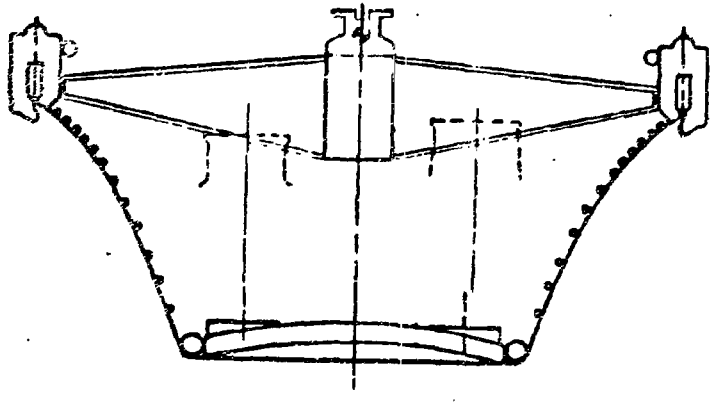

Design C
Beam

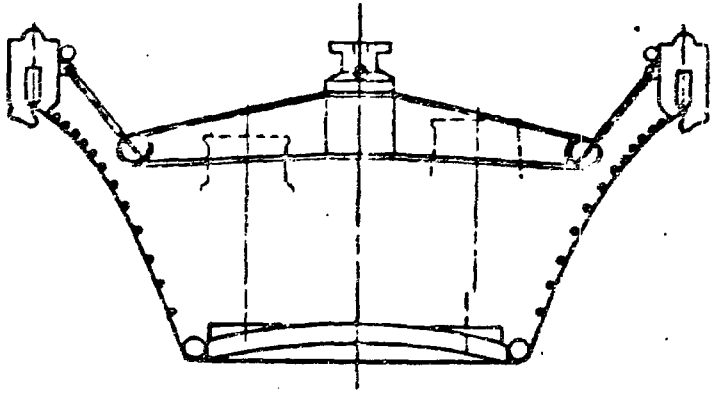

Design F
Beam-Ring-Cone

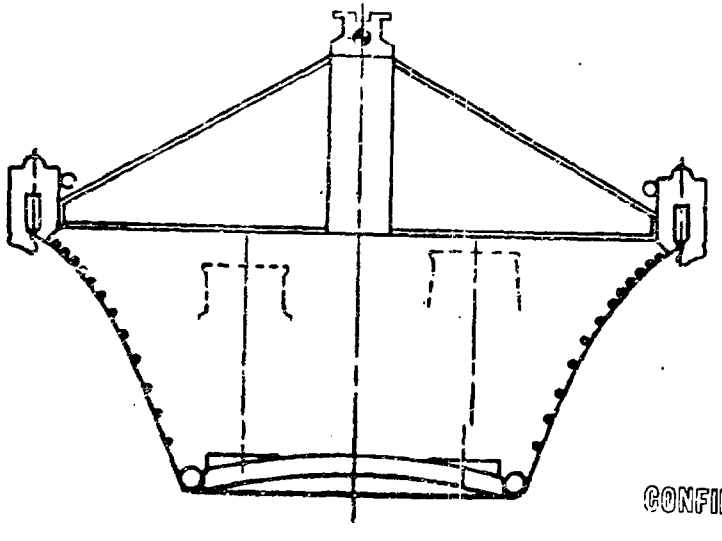

Design Q
Beam

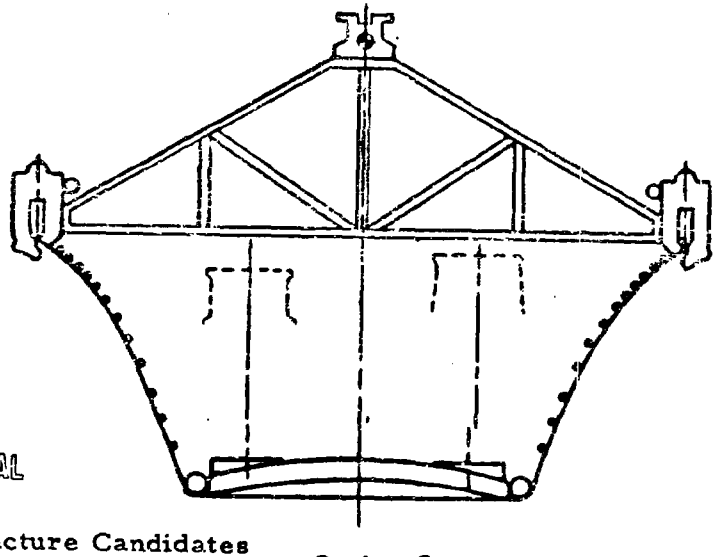

Design R
Truss

Figure 58. Thrust Structure Candidates

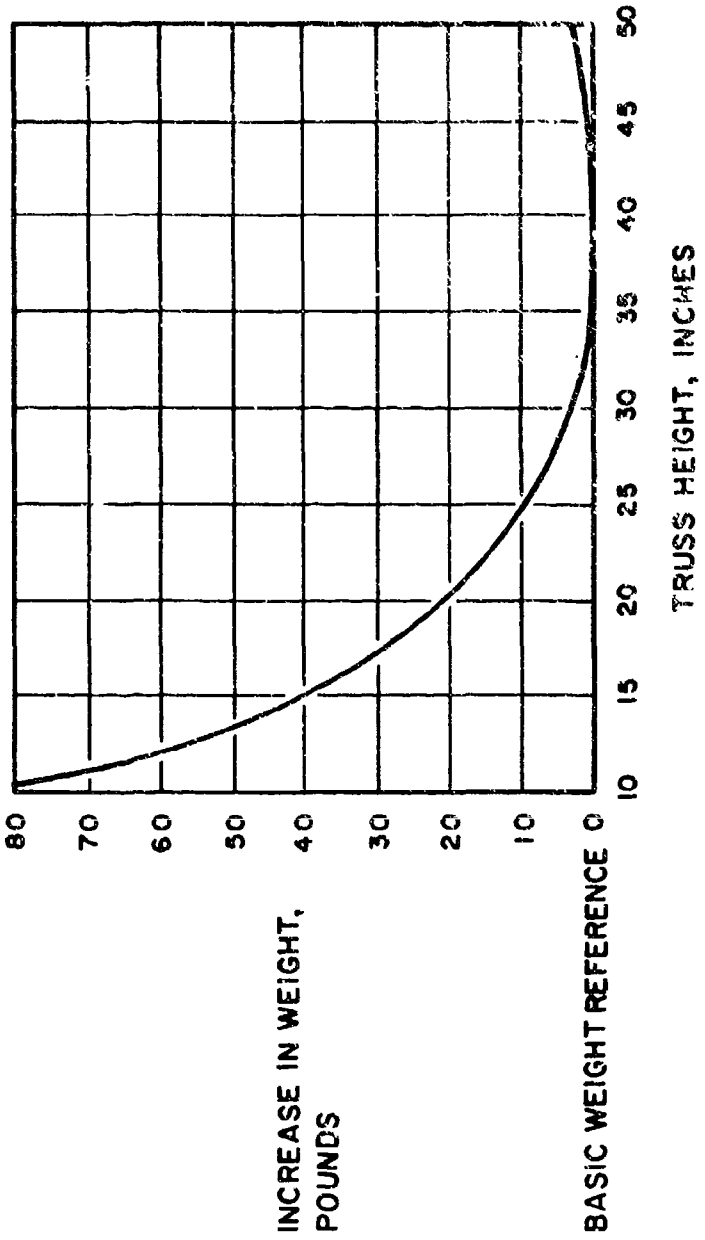

Figure 59. Titanium Thrust Structure Weight vs Depth of Truss Structure

in general for the beams. Figure 60 shows the dimensional geometry of the module related to available space for the thrust structure. A plot of the module dynamic envelope radius vs gimbal point elevation is shown in Fig. 61 for the 7-degree circular gimbal pattern.

(U) These four remaining candidate thrust structures were subjected to deeper analysis. The final design selection is a modification of concept F. The major factors in the selection of the final structure were weight, the size of the module static and dynamic envelopes, the structural considerations at the thrust chamber interface, component mounting and space considerations, manufacturing, assembly, and accessibility. Table 21 presents the evaluation of the four candidates in terms of the above factors. As indicated in Table 21 , thrust chamber weight and thrust structure weight for the selected structure were rated 4 and 3, respectively. Through the truss cone arrangement of configuration F, 40 points of attachment to the thrust chamber are made possible, thus providing excellent load distribution to the thrust structure. Configuration F, though somewhat lower in structural efficiency than the truss arrangement of configuration R, is more efficient than configurations C and Q because of the tension-type structure and shortened beam span. Relative ratings were assigned to each candidate on a numerical basis of 1 through 4 with higher numbers indicating better ratings.

(U) The module static and dynamic envelope with the selected structure is rated 4. Through this structural arrangement, a minimum module length is achieved and the dynamic envelope is no greater than the static envelope. Module length and dynamic envelopes are greater with the other candidates.

(U) The structure interface with the thrust chamber rates (4) for the selected candidate by providing a more uniform load distribution through 40 attach points as compared to 6 attach points with the other candidates.

(U) Facility for component mounting is equally provided for by the candidate and the shallow beam structure (configuration C), based upon access to the structure for this purpose and space within the module envelope for the components.

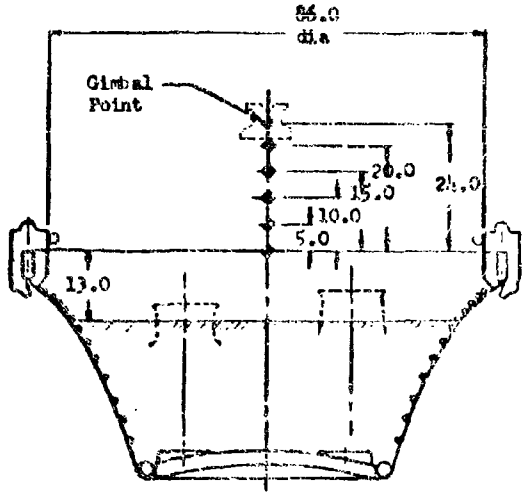

Figure 60. Gimbal Height and Thrust Structure Space Limitation Diagram

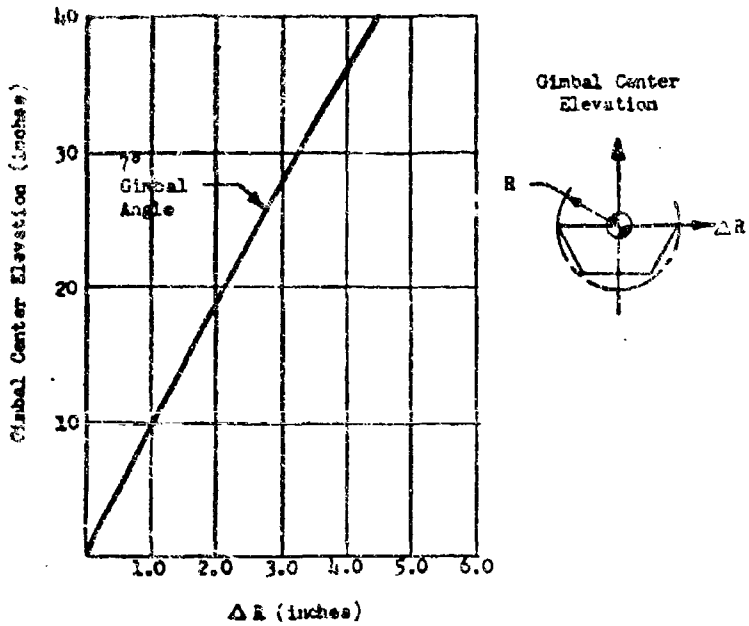

Figure 61. Increase in Dynamic Envelope Requirement With Gimbal Center Elevation Above Position Where $R_{static} = R_{dynamic}$

TABLE 21

RELATIVE RANKING OF CANDIDATE THRUST STRUCTURE DESIGNS*

Rating Factor \ Candidate Configuration	Selected Configuration 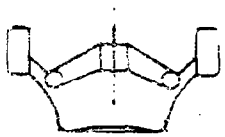 F-Cone-Ring Beam	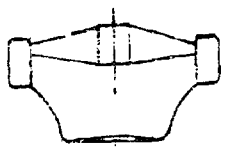 C-Shallow Beam	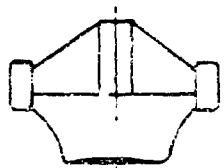 Q-Deep Beam	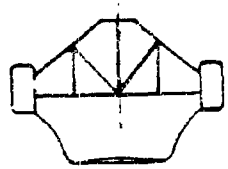 R-Truss
Weight				
Thrust Chamber	4	2	2	2
Thrust Structure	3	1	2	4
Module Envelope	Static = Dynamic			
Static	4	3	2	2
Dynamic	4	3	2	2
Thrust Chamber Structural Connection	4 40 point attachment	2 6 point attachment	2 6 point attachment	2 6 point attachment
Facility for Component Mounting	4	4	3	2
Manufacturing Simplicity	3	4	4	2
Access and Assembly Provision	4	4	2	2

*Relative rating 1 through 4; the higher the number the better the rating.

(U) Configuration F is rated 3 for manufacturing simplicity, while the simple beams of configurations C and Q are both rated 4. The pure truss arrangement of configuration R is the most complex and is rated 1. Access and assembly of configurations F and C are both rated 4. The volume accessible from the rim of the thrust chamber caused by the low profile of the thrust structure is substantial, while the deep structures used in configurations Q and R tend to impair accessibility.

(U) In conclusion, the configuration F type was selected. This structure consists of six radial beams, a torus ring, and truss cone arrangement (Fig.56). The features that mark the principal difference between the selected structure and that originally proposed for the demonstrator module are the thrust cone which is replaced by a series of individual truss members, the weldment of the truss members to the torus ring and thrust chamber, and the radial beam arrangement. The radial beams and hub are a removable assembly by virtue of mechanical joints between the radial beam ends and the torus ring. The beams are of continuous shear web and cap construction tapering to bolted fittings at the torus ring. The preliminary layout was completed with the arrangement of truss members between the torus ring and the thrust chamber. They lie in a conical plane joined to the torus with weld fittings. This assembly in turn is welded to the periphery of the thrust chamber inner body. The material throughout is 6AlAV titanium for light weight and weld compatibility. Preliminary results of the thermal analysis show a 0.070-inch thermal contraction of the thrust chamber structure at start from introducing LH_2 into the regenerative cooling circuit prior to main chamber ignition. This contraction is accommodated by the thrust structure by deflection of the truss cone arrangement and is minimized by location of the attachment to the thrust chamber.

(U) Two turbopump mounting concepts were studied. The first, for both fuel and oxidizer pumps, features adjustability in the X, Y, and Z planes provided by a yoke fitting and a stabilizing rod shown in Fig. 62. Attachment to the turbopump is made through four clevis fittings machined on the

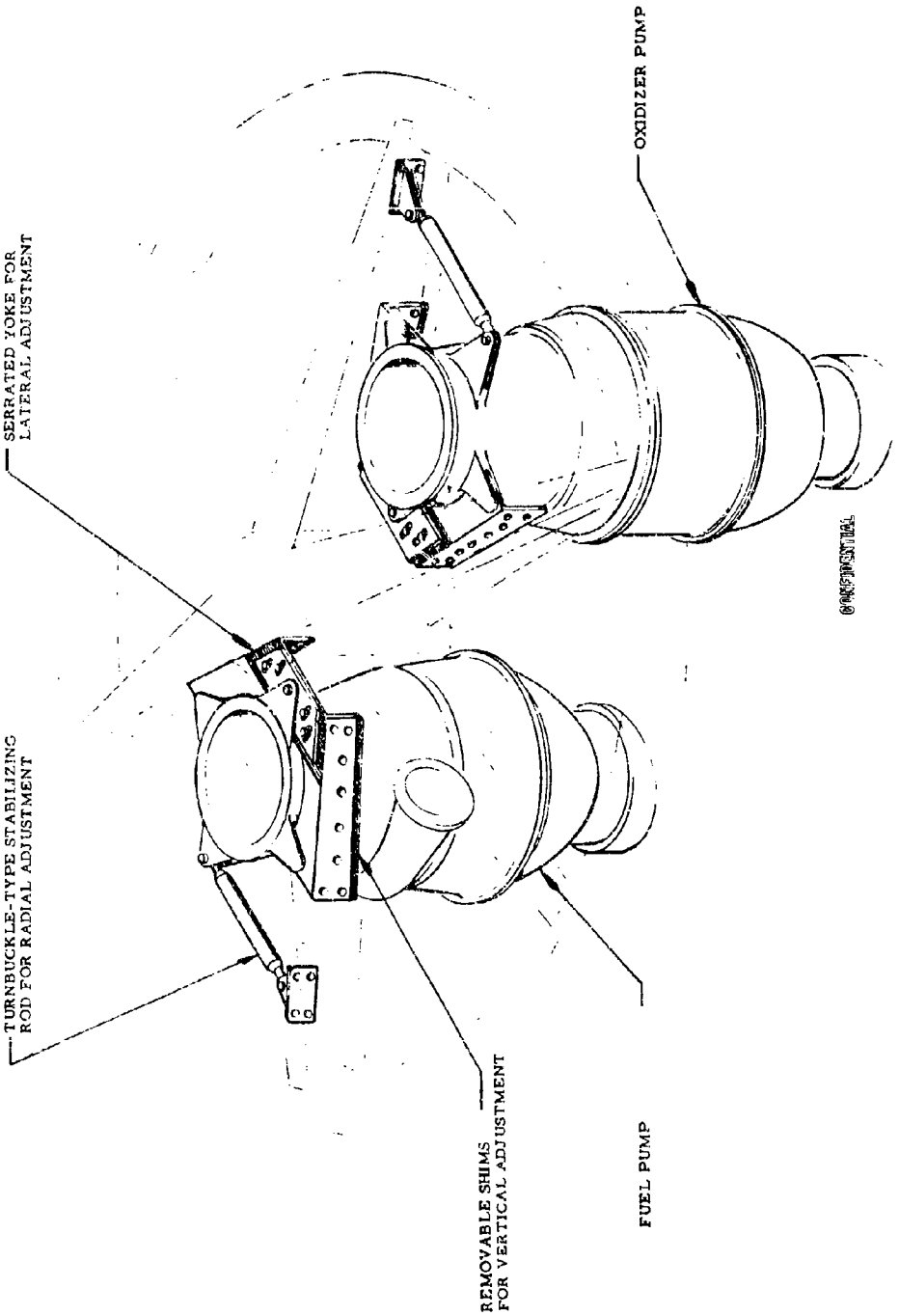

Figure 62. Proposed Adjustable Pump Mounting Concept

pump shell. Adjustment in two of the planes is accomplished by the serrated plate and stabilizing rod, allowing the turbopump to be rotated about the pinned clevis by the stabilizing rod and adjusted radially by positioning the serrated plate. Adjustment in the vertical plane is accomplished by use of the removable shims.

(U) The second concept was the trunnion-type mount described on page 139. The trunnion-type mount was selected because of the more efficient, bolted-type pad connection to the turbopump, the better section characteristics of the trunnion fitting, and manufacturing simplicity.

Propellant Feed Sybsystem.

(U) Description and Analysis. The Demonstrator Module propellant feed subsystem consists of the following components: (1) oxidizer and fuel turbopumps, (2) oxidizer and fuel liquid-propellant line assemblies, (3) main fuel and oxidizer valves, (4) oxidizer and fuel system flowmeters and flow straighteners, and (5) hot-gas igniter liquid-propellant feed lines. The complete subsystem is shown in Fig 63. Turbopump details are discussed on pages 243 through 330 of this report.

(U) A single discharge line carries the oxidizer from the pump discharge port to the flowmeter and main valve. Downstream of the control valve is a Y fitting which splits and directs the flow to two branch lines of equal diameter to two ports, 180 degrees apart on the injector oxidizer manifold. A single discharge line also is used for the fuel from the pump through the flowmeter to the main valve. The outlet flange of the main fuel valve is the fuel feed system interface with the thrust chamber fuel manifold inlet flange. The hot-gas igniter fuel and oxidizer are supplied by tapping off the main propellant lines below the pump outlet flanges. The oxidizer and fuel turbopumps are mounted to the thrust structure beams, and the turbine exhaust ducts attach directly to the base closure

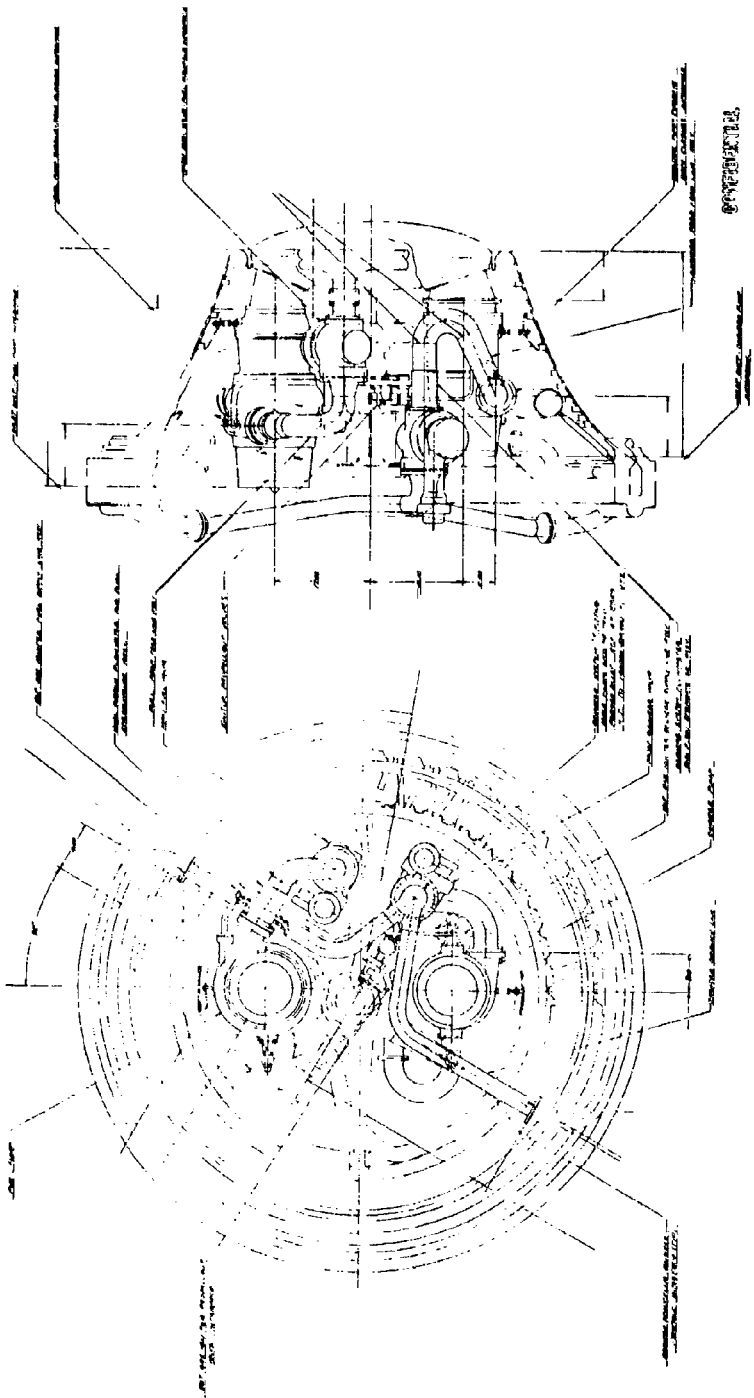

Figure 63. Propellant Feed Subsystem Layout

assembly. Pump axial dimensional variation is compensated for by the use of a flexible, U-shaped, hot-gas seal between the nozzle and the base closure assembly.

(U) The main fuel and oxidizer valves are quick-response, flight-type, pneumatically actuated visor (modified ball)-type units, and are located downstream of the turbopumps to control propellant flow to the fuel and oxidizer manifolds.

(U) Turbine-type flowmeters with flow straighteners similar to those used on the J-2 engine are installed in each propellant line. Both flowmeter assemblies are installed in their respective systems at a point upstream of the propellant valve inlet ports.

(C) The oxidizer flow dividing the Y fitting is located above the thrust structure to permit routing the oxidizer branch lengths to the injector oxidizer manifold to aid priming and equalize line ΔP. The routing of the main oxidizer line from the pump discharge to the main oxidizer valve provides a straight section of line upstream of the main oxidizer valve to contain the oxidizer flowmeter. The main oxidizer line and branch line sizes are 4.0 and 2.75-inch ID, respectively, which establishes 80 ft/sec oxidizer flow velocity at the system nominal operating point. The main fuel line routing provides a straight section immediately downstream of the fuel pump discharge to contain the fuel flowmeter. This fuel line passes through the shear web of the thrust structure radial beam adjacent to the fuel pump discharge. It is provided with a spherical surface collar fitting providing one of the support points for mounting the fuel turbopump. The fuel line size is 3.75-inch ID, which establishes 200 ft/sec fuel flow velocity at the system nominal operating point.

(U) All line assemblies are made of Inconel 718 sheet stock, rolled, seam welded, roll planished, and sized to the required inside diameter. All flanges, flowmeter housings, and the oxidizer Y fitting are machined from Inconel 718 forgings. After completion of butt welding, each line assembly is heat treated to 175,000 to 200,000 psi ultimate tensile strength, and

final required dimensional control is obtained by a final post heat-treat machining operation. The oxidizer branch lines are designed as symmetrical as possible to equalize injector manifold propellant distribution. The lines are designed to deflect as the injector manifold/thrust chamber expands or contracts during its thermal excursion. The line deflections will not cause bending stresses that will exceed the allowable material yield value. Inconel 718 nickel base alloy was selected for this application because of its high strength-to-weight ratio.

(U) The propellant duct structural sizing is based on internal pressure, bending stresses imposed by thermal loads, and material thinning in metal-forming operations such as tube bending and sheet forming. The system was then optimized to yield the lightest weight and lowest pressure loss configuration.

(U) Many different types of commercially available static seals were considered during studies of static-sealing methods. On the basis of proved satisfactory operation and experience, the Naflex seal was selected for usage on both the fuel and oxidizer systems.

(U) Alternatives Studied. Design alternative studies were conducted to select the duct materials and fabrication processes, and to select the best flange static seal. These evaluations are discussed below.

(U) A design evaluation study conducted to select the material for the main oxidizer and fuel high-pressure propellant feed ducts resulted in the selection of Inconel 718 for both systems. Other candidates in the study were 6061-T6 aluminum, 347 CRES, and Inconel 718. Inconel 718 was selected because of its higher strength-to-weight ratio and its superior capability to resist thermal stresses and deflections.

(U) A design evaluation study was likewise performed on the manufacturing approach to be used to produce the oxidizer branch line Y fitting. Three-dimensional machining of a one-piece forged billet, a formed sheet stock, four-piece weldment, and a one-piece precision investment casting were considered. The three-dimensional, machine-forged billet approach was selected. The selection factors influencing the decision were weight, reliability, tooling, and cost for limited initial production.

(U) The Naflex pressure-actuated seal was selected for use in all the flanged (static seal) applications. Elastomer O-rings, metal O-rings (vented and pressurized types), K seals, and Cono-seals were among the other types of seals evaluated in an independent survey of cryogenic, static face seals where the Naflex seal showed best performance.

Turbine Drive Subsystem.

(U) Description and Analysis. The Demonstrator module turbine drive subsystem consists of (1) tapoff hot-gas ducts, (2) oxidizer turbine inlet duct, (3) turbine discharge ducts, (4) tapoff throttle valve, (5) oxidizer turbine throttle valve, and (6) fuel turbine calibration orifice. The subsystem integration is shown in Fig. 64.

(U) The tapoff hot-gas ducts interconnect the two ports on the combustio chamber tapoff manifold with the tapoff hot-gas throttle valve which effectively forms a Y joining the two ducts. The discharge port of the tapoff throttle valve interfaces with the distribution manifold that is part of the igniter subsystem. The oxidizer turbine throttle valve is located at the oxidizer turbine port of the distribution manifold and the oxidizer turbine inlet duct connects the valve with the oxidizer turbine. The fuel turbine calibration orifice is located at the interface between the distribution manifold and the fuel turbine. Engine thrust control is achieved with the tapoff throttle valve and engine mixture ratio is controlled by the oxidizer turbine throttle valve.

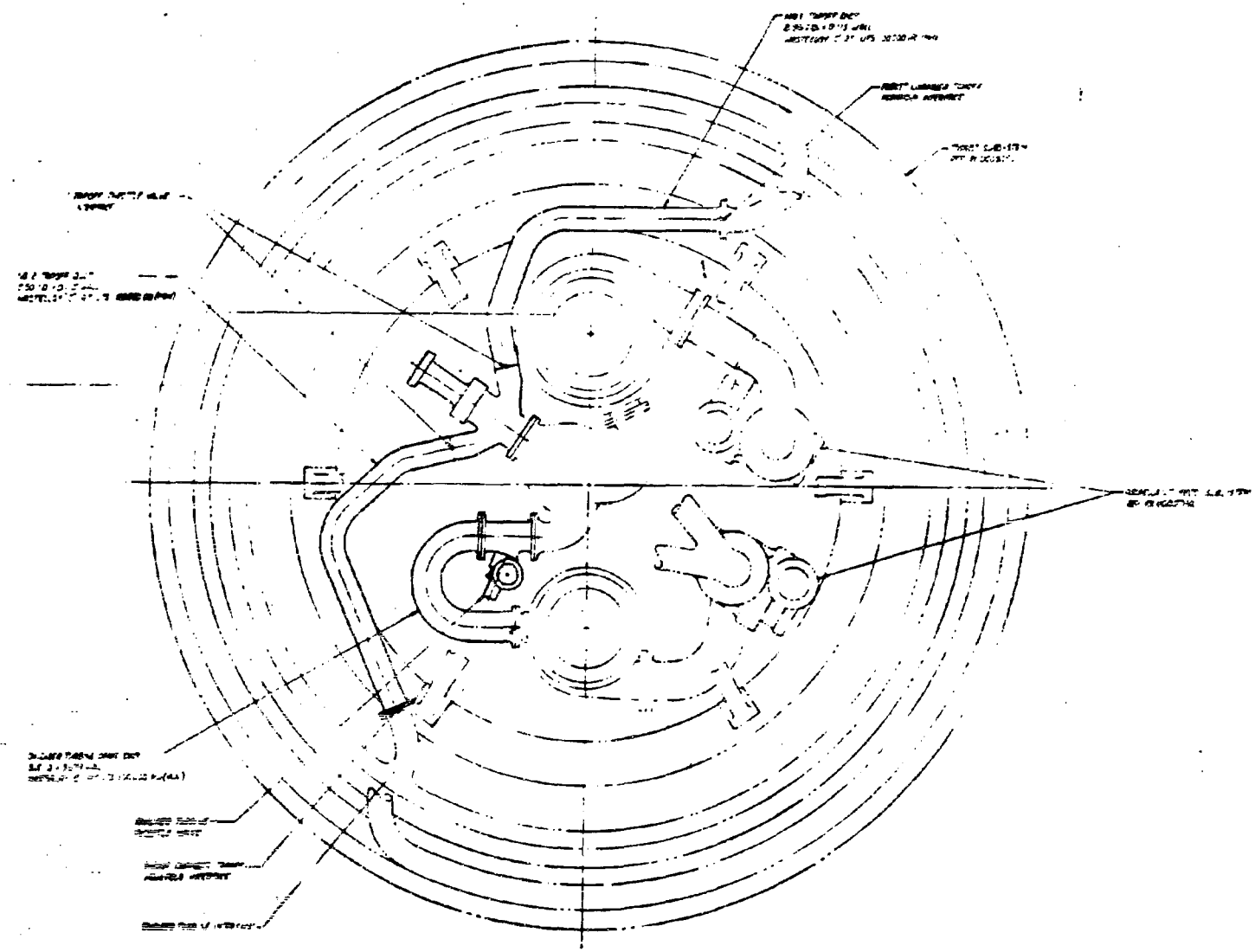

Figure 6.1. Demonstrator Module Turbine Drive Subsystem

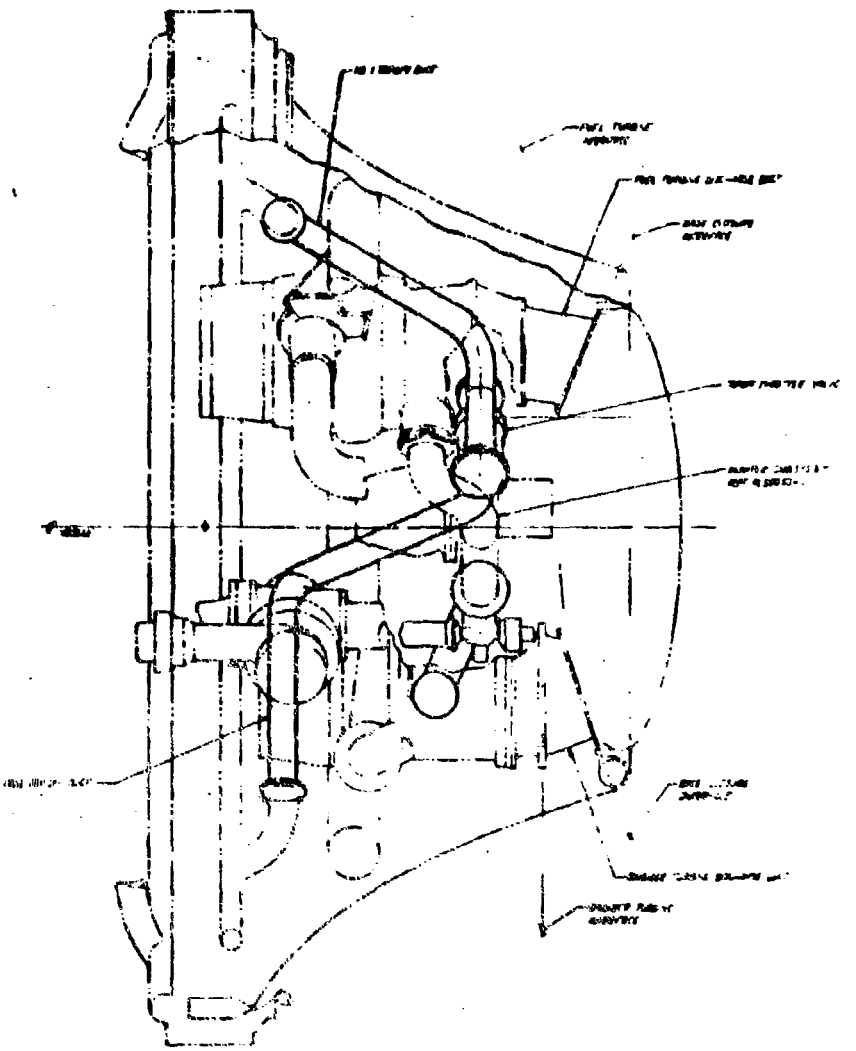

Figure 64B. Demonstrator Module Turbine Drive Subsystem

(U) The concept of combining the tapoff throttle valve and the Y joining the two tapoff ducts permitted the selection of a poppet-type valve which has a lower pressure loss than conventional 90-degree poppet valves. The turbine-drive hot-gas ducts and manifolds are sized for the start condition in order to provide a maximum turbine inlet pressure for the tank head start. The tapoff ducts are sized for steady state and have a 2.50-inch ID; the oxidizer turbine inlet duct is 3.15-inch ID, and the nominal interface between the distribution manifold and the fuel turbine is 3.15-inch ID. The shape of the ducts interconnecting the two tapoff manifold flanges to the tapoff throttle valve are designed to permit deflection during thermal growth. The length and shape of the oxidizer turbine inlet duct is likewise designed to permit thermal deflection. All high-pressure duct assemblies are made of Hastelloy C, selected because of its high strength at elevated temperatures.

(U) The fuel and oxidizer turbine discharge ducts interconnect their respective turbines with the nozzle base closure. These ducts are sized for internal pressure and base closure thrust loads, and are made of Inconel 718 material selected for its high strength-to-weight ratio and its capability to resist thermal stresses.

Hot-Gas Ignition Subsystem.

(U) Description and Analysis. The Demonstrator Module hot-gas ignition subsystem consists of (1) igniter assembly, (2) isolation valve, (3) distribution manifold, (4) liquid propellant valves, (5) LO_2 pressure regulator, and (6) purge and vent check valves. The location of the hot-gas ignition subsystem within the Demonstrator Engine is shown in Fig. 65.

(U) The hot-gas distribution manifold serves as the interface between the hot-gas igniter subsystem and turbine drive subsystem. This manifold has four ports. One port interfaces directly with the fuel turbine inlet,

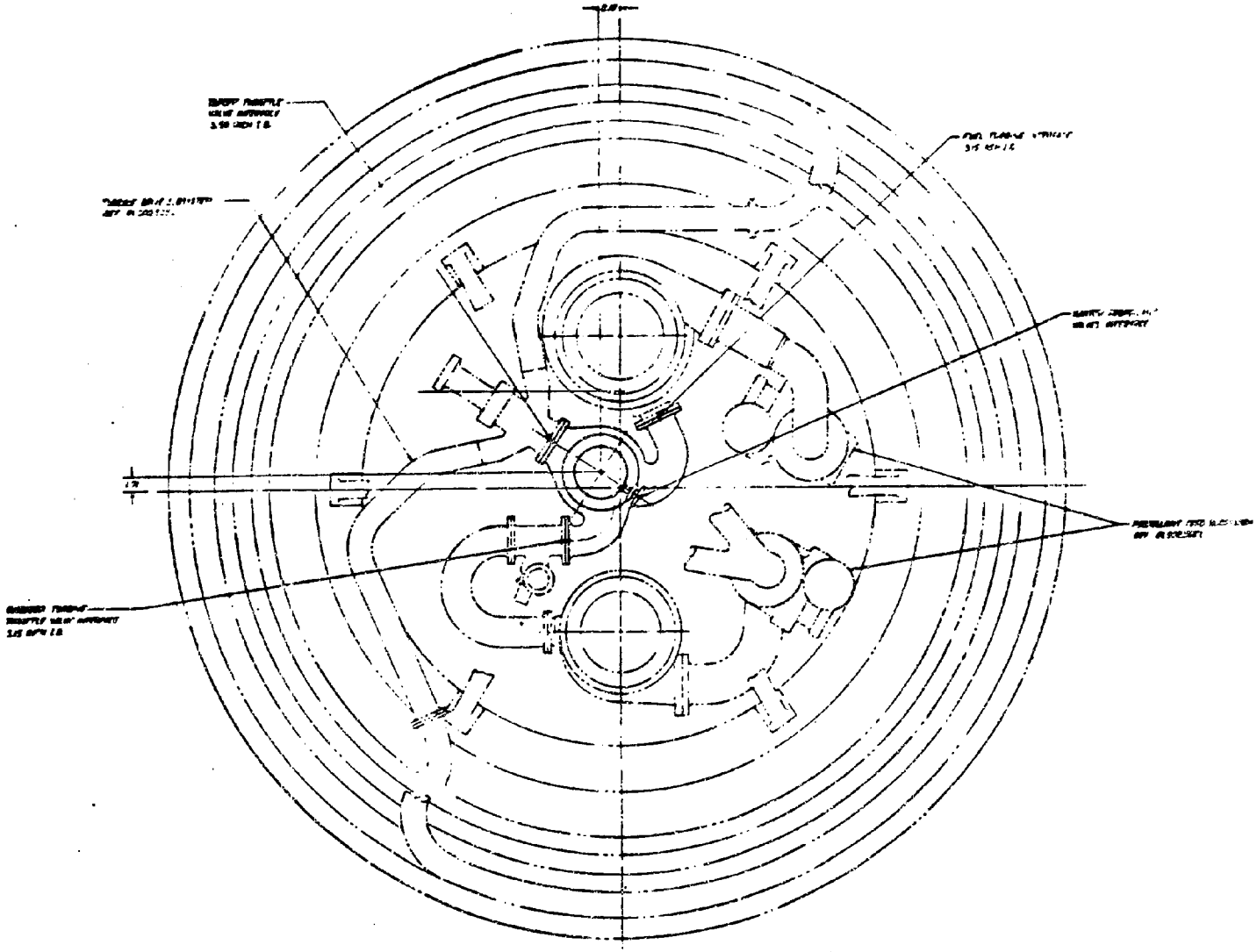

Figure 65A. Demonstrator Module Ignition Hot-Gas Subsystem

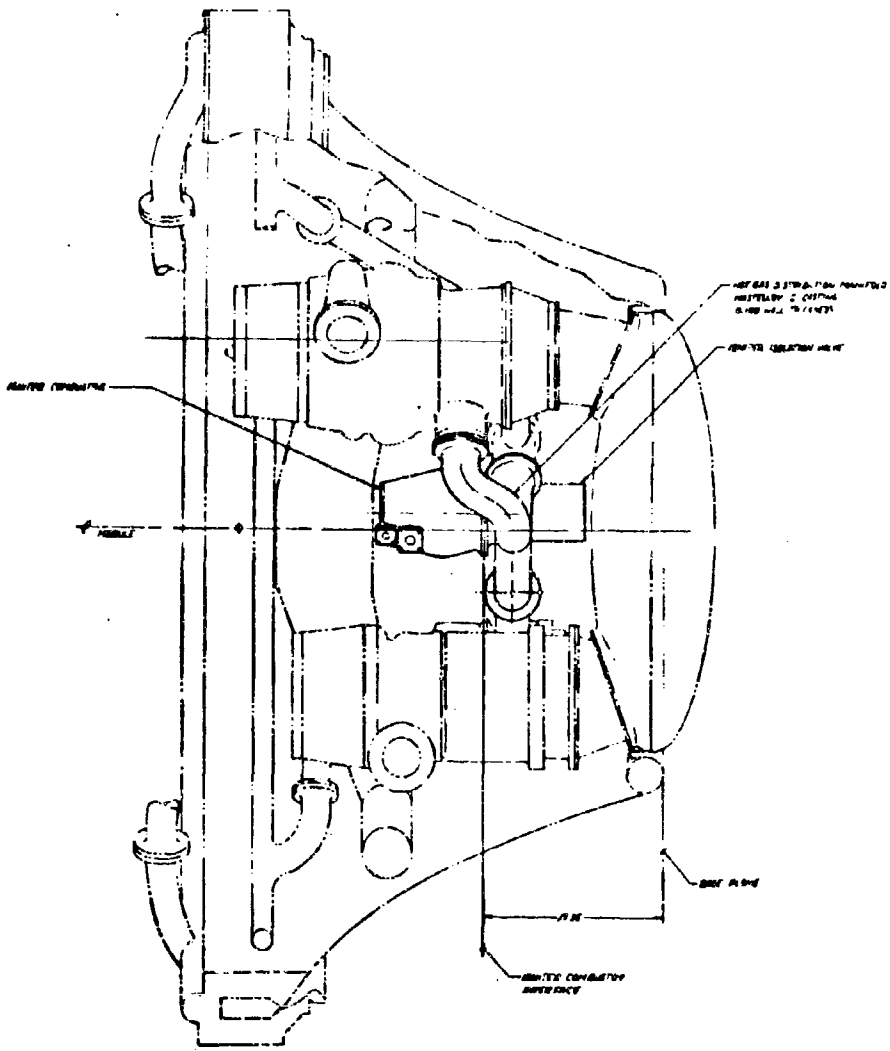

Figure 65B. Demonstrator Module Ignition Hot-Gas Subsystem

another port interfaces with the oxidizer turbine throttle valve, and a third port interfaces with the tapoff throttle valve. The isolation valve, a poppet-type valve located in the base of the distribution manifold, seats on the fourth port and mates with the igniter combustor body.

(U) To provide multiple starts, the hot-gas igniter uses a spark ignition system and is monitored by an ignition detection device. The hot-gas igniter isolation valve prevents tapoff gas backflow into the igniter. The igniter fuel and oxidizer valves are mechanically linked together to provide more reliable valve timing during start and shutdown. Hot-gas igniter temperature is controlled by an oxidizer pressure regulator which maintains the oxidizer manifold pressure at the proper level relative to the fuel manifold pressure. Hot-gas igniter purge and vent check valves are provided to prevent steam and contaminant backflow through the hot-gas igniter combustor and injector.

(U) Since the hot-gas igniter operates only during start, the propellant lines and hot-gas lines for the igniter subsystem are sized for low resistance for turbine spin and ignition under tank head conditions. Line sizes for the hot-gas igniter subsystem are as follows: tapoff throttle valve interface 3.50-inch ID, fuel turbine interface 3.15-inch ID, and oxidizer turbine throttle valve interface 3.15-inch ID.

(C) "Hastelloy C" material was selected for the distribution manifold because of its high strength characteristics at the 1500 F operating temperature of the system. Casting was selected as the manufacturing approach for the manifold because it is best suited to produce the internal passages required in the manifold and porting for attachment of the igniter combustor and the igniter isolation valve.

(U) Accessibility. Accessibility considerations assumed a major role in the design of the Demonstrator Module system. In this area, accessibility

for leak, functional, and electromechanical checkout is a primary consideration. The systems design provided access for and gave preferred locations to critical components. The engine design thus provides for component replacement.

(U) Locations of leak, functional, and electrical checkout panels have not been finalized on the engine; however, electrical, mechanical, and leak check connectors will be brought to the top of the engine package for easy access. Accessible disconnect panels are shown in Fig. 66 .

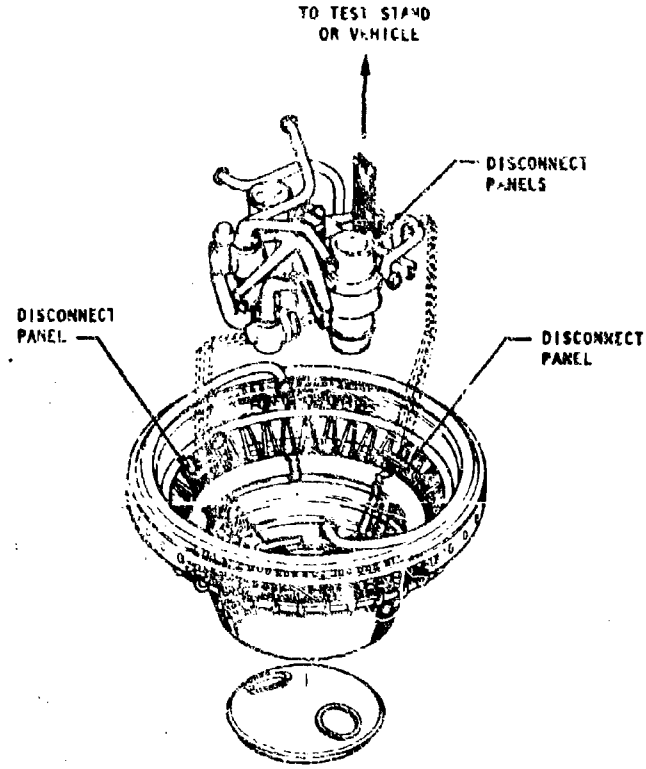

Figure 66. Engine Accessibility

Two are located within the inner body; the other spans the thrust structure beams and is for engine-to-vehicle or test facility interface. The turbopumps, valves, and igniter are arranged with mounting connections made to the radial beam and hub assembly of the thrust structure such that these components may be installed and removed together with their interconnecting ducts as a subassembly. This design feature makes it possible to replace any major component after removing the hub and beam subassembly from the thrust chamber.

CONFIDENTIAL

(This page is Unclassified)

(C) Demonstrator Module Weight. A very important aspect of the Demonstrator Module design is Flight Module similarity. The Demonstrator Module components and system are designed to be as near flightweight as is economically prudent without compromising the high confidence level and test flexibility that must be ensured for the demonstrator program. In many cases, further weight reductions will be achieved through development efforts and design refinements that would be impractical for incorporation in the Demonstrator Module. For example, flanged fittings are used through the Demonstrator Engine to reduce development time and cost, whereas the Flight Module will have all welded fittings resulting in significant weight savings. The Demonstrator Module weight was calculated to be 3950 pounds. A detailed weight breakdown is shown in Table 25.

(U) Interface Requirements. The Demonstrator Module is designed to be interchangeable with all test facility attachment points. Thrust vector control may be accomplished by means of a J-2 type gimbal bearing actuated by hydraulic actuators attached to the thrust mount. While this capability is inherent in the basic design, it is not intended to incorporate an active system in the engine design. The test stand-to-engine interface areas include (1) thrust and stabilizer connections, (2) fuel and oxidizer low pressure inlet ducts, (3) electrical supply lines, and (4) pneumatic supply lines.

Thrust Chamber Design

(U) Thrust Chamber Assembly Requirements. The initial thrust chamber assembly design requirements, which were derived from the contractual thrust, performance, and operational requirements and the pressure requirements defined by the systems analysis, are shown in Table 23. Thrust chamber design details are shown in the layouts of Fig. 67, and the weight breakdown was presented in Table 22 .

(C)

TABLE 22

SUMMARY OF DEMONSTRATOR MODULE WEIGHTS

Thrust Subsystem	(2675 pounds)*	
Injector and Manifold		352
Injector Clamp Rings		144
Structural Tie		474
Inner Body		772
Outer Body		431
Base Closure		72
Tapoff Manifold		60
Thrust Structure		300
Attach Parts		70
Turbine Drive Subsystem	(106 pounds)	
Tapoff Lines		26
Inlet Duct Oxidizer Turbine		6
Exhaust Duct, Turbine		18
Tapoff Throttle Valve		36
Oxidizer Turbine Throttle Valve		18
Calibration Orifices		2
Hot-Gas Igniter Subsystem	(112 pounds)	
Combustor and Injector		47
Hot Gas Distribution Manifold		33
Hot-Gas Igniter Isolation Valve		28
Propellant Feed Line		2
Oxidizer Pressure Regulator		2
Propellant Feed Subsystem	(1028 pounds)	
Oxidizer Turbopump		343
Fuel Turbopump		453
Propellant Ducting		61
Propellant Flow Sensors		9
Main Oxidizer Valve		60
Main Fuel Valve		59
Igniter Propellant Control Valve		11
Mounts Turbopump		2
Vent and Purge Subsystem	(29 pounds)	
Gimbal Bearing		
Controls Electrical		
Controls Pneumatic		
Total Engine Weight	(3950 pounds)	

*Thrust chamber assembly weight (thrust subsystem minus thrust structure) = 2375 pounds

(C) TABLE 23

THRUST CHAMBER ASSEMBLY DESIGN REQUIREMENTS

Performance	Commensurate with meeting engine requirements of 96% theoretical I_s at full thrust, 95% I_s during throttling
Maximum Engine Thrust	262,000 pounds
Maximum Pressure Limits	Injector End, psia 1635 Fuel Manifold Inlet, psia 3062 Oxidizer Manifold Inlet, psia 2164
Critical Cooling Conditions	P_c, psia / MR_{eng} / MR_{tc} / $\dot{\omega}LH_2$, lb/sec / LH_2 manifold Pr, psia 1500 / 5.8:1 / 6.50 / 79.3 / 2655 325 / 7:1 / 7.30 / 14.7 / 544
Base Closure	Maximum Thrust, pounds 9756 Maximum Flowrate, lb/sec 14.95
Tapoff Manifold	1500 F Gases at MR = 0.764 Maximum Manifold ΔP = 129 at $\dot{\omega}$ = 14.95 lb/sec
Life	300 thermal cycles, 10 hours TBO
Durability	Maximum single run duration: 100% F: 600 seconds 20% F at sea level: 20 seconds

(U) The three major subcomponents, i.e., combustor and nozzle, injector, and base closure, are discussed in more detail in the following paragraphs.

(U) Materials and fabrication techniques utilized are state of the art, with strong emphasis on cost and low weight. Features connected with critical technology embody the information gained and configurations proved successful in the Task II experimentation. These include: combustor shape, nozzle contour, injector pattern, tapoff location and design, cooling tube material, structural arrangement and throat geometry, LO_2 manifold priming features, assembly seal features, cooling tube heat transfer criteria, and accessibility provisions for thrust chamber and injector inspection during development testing.

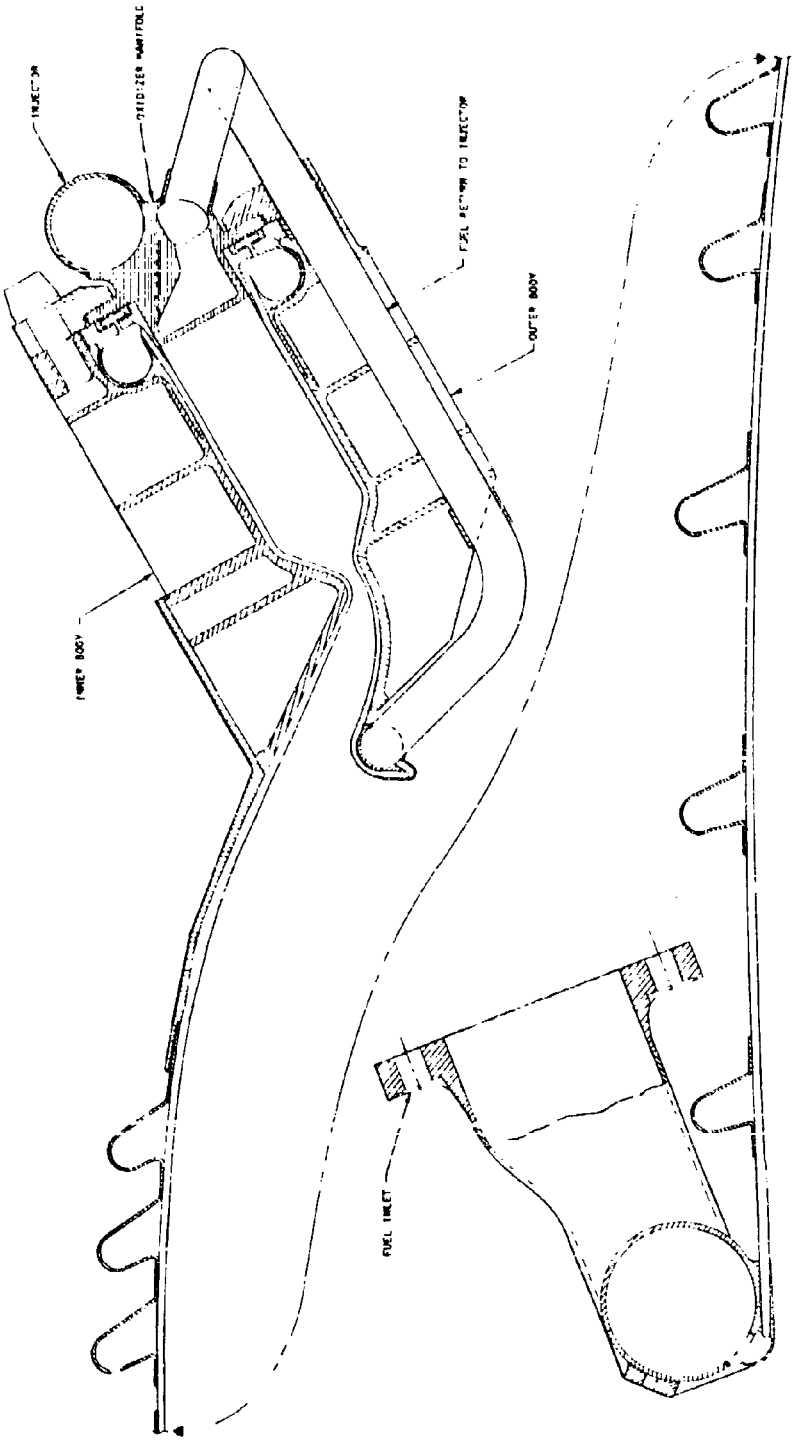

Figure 67. 250K Thrust Chamber Demonstrator Module

(C) The thrust chamber for the Demonstrator Module has evolved from design analysis and Phase I testing, and represents the best compromise between concept evaluation, cost, schedule, and weight. It is designed with a nozzle length equivalent to 25 percent the length of a 15-degree, half-angle cone of the same area ratio, and consists of concentric regeneratively cooled inner and outer combustor assemblies; an annular injector; a perforated base closure; thrust mount attach provisions; and interfaces for fluid and gaseous ducting from the turbopumps. The combustor assemblies form an annular chamber leading to a converging throat, a shrouded outer tubular nozzle wall to the exit plane. These elements are shown in Fig.68.

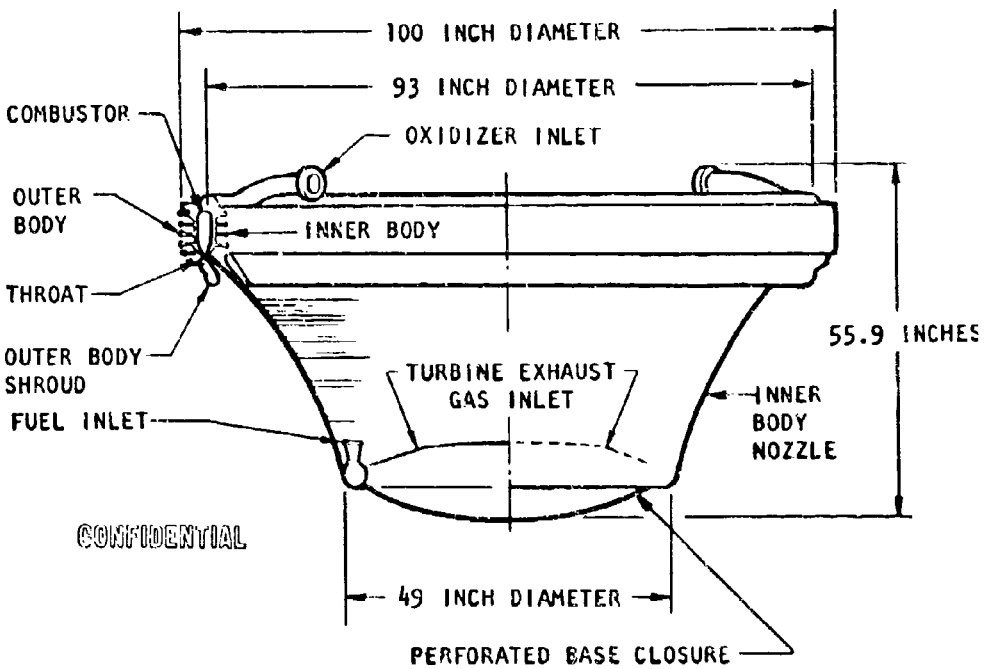

Figure 68. Demonstrator Engine Thrust Chamber Assembly

(U) Each combustor assembly is fabricated of brazed tubing which forms cylindrical sections with sealed manifolds at each end. The support structure is subsequently adhesively bonded to the tubes. The bodies are connected by 40 regeneratively cooled subsonic struts, each installed radially in the annular combustion chamber area with two preloaded bolts. The combustion chamber is closed at the top of an injector ring assembly, axially

bolted to each combustor assembly. Provision is made to attach a thrust structure assembly to the backside surface of the inner combustor. The base closure attaches at the inner-body nozzle exit. Each subassembly can be readily removed for replacement or interchangeability.

(U) To effect cost savings and provide for flexibility in development test operations, some design features are not flight type. The design concept, however, has not been affected, and a logical growth to the Flight Module will follow from the selected thrust chamber design. Although minimum weight has been a design objective, a weight penalty has been accepted for the demonstrator thrust chamber if:

1. It can be logically shown that the weight can be removed from the flight chamber
2. A significant cost saving can be ensured in Phase II
3. The technical integrity of the concept demonstration is maintained
4. The development test flexibility is improved

Specific areas affected by these considerations are the tube design, injector design, and fuel risers.

(U) Combustor and Nozzle Description. The combustor and nozzle description can be separated into discussions of the thrust chamber construction, the regenerative-cooling circuit, and the hot-gas manifold design. Each is discussed in the following paragraphs.

(U) Thrust Chamber Construction. The combustion chamber and nozzle of the Demonstrator Module thrust chamber are formed by two regeneratively cooled subassemblies, inner body and outer body, and 40 regeneratively cooled subsonic struts with the design parameters shown in Table 24 .

(C)

TABLE 24

THRUST CHAMBER DESIGN PARAMETERS

Length as Percentage of Equivalent Area Ratio 15-Degree Cone, percent	25
Throat Area, $in.^2$	85.14
Overall Diameter, inches	100.0
Overall Height, inches	55.90
Contraction Area Ratio	7.13
Expansion Area Ratio	74.1
Mean Combustor Diameter, inches	93.0
Combustor Width, inches	2.0
Throat Gap, inch	0.281
Length Injector to Throat, inches	6.0
Tube Material	Nickel 200
Number Tubes Outer Body	4400
Number Tubes Inner Body	4240
Number Subsonic Struts	40

(C) The inner body which forms one side of the combustor wall consists of a 4-1/2-inch straight wall which converges to the throat and diverges to a truncated spike contour (nozzle) upon which combustion gases act. The outer body forms the second side of the combustor wall and consists of a 4-1/2-inch straight section, a convergent section to the throat, and the contoured shroud. Both inner and outer bodies consist of regeneratively cooled, tubular systems to which the external support structure is adhesively bonded. The coolant circuit is formed by nickel tubes (4400 on the outer body and 4240 on the inner body), furnace brazed to form 360-degree assemblies.

(U) Seats are provided at 40 locations, equally spaced on the inner and outer bodies (on the straight walls of the combustor zone), for attaching subsonic struts that carry separating loads and stabilize the throat gap.

(U) The nozzle exit of the inner body contains a single inlet distribution manifold into which hydrogen propellant from the turbopump is introduced. Provisions are also made at this point to attach the perforated base closure. Regeneratively cooled tubes carry propellant to a collection manifold at the injector end. The truncated spike nozzle of the inner tubular wall (below the combustion chamber and throat area) is supported against buckling and side loads by eight circumferentially placed "hat" bands.

(U) The injector end of the outer body contains a propellant collection manifold similar to the inner body. Fuel is accepted at this point and distributed through regenerative-coolant tubes to the collection manifold brazed to the end of the shroud. Provision is made at this point for attachment of 40 transfer tubes that duct the propellant to the injector.

(U) Structural restraint against chamber pressure, thermal and operational loads, and excessive throat deflection is provided the Demonstrator Module thrust chamber by means of titanium (6Al-4V) shells, fabricated in segments, and adhesively bonded to the tube bundle. The segments are fabricated with thin webs on the outer periphery to provide a maximum moment of inertia and to resist bending with a minimum of weight. The segments are bolted to each other and adhesively bonded to the brazed tube bundle.

(C) Forty subsonic struts maintain the inner and outer bodies at their design radial locations and produce a rigid annular structure with a mean diameter of 93.0 inches. Each strut is secured in position by two bolts passing through its center and through the inner and outer bodies.

(C) Each inner- and outer-body shell is fabricated in segments (four outer and four inner) and mechanically joined at segment interfaces to provide a continuous 360-degree structure. The assembled combustor diameter at the tube-wall interface of the outer shell is approximately 95 inches and that of the inner shell is 91 inches.

(U) The four outer-body segments (Fig. 69) are of identical geometry and extend from the injector end to a plane just above the collection manifold at the shroud end. Each is fabricated with a continuous contour on the tube mating surface, integrally attaching to four peripheral sections spaced for maximum structural efficiency. At 10 equally spaced locations on each quadrant, bearing surfaces for seating subsonic struts are machined and holes for insertion of structural tie bolts are drilled.

(C) The inner body (Fig. 69) is formed from four segments, three of which are identical units, each representing a 117-degree arc of a 91-inch-diameter circle, and the fourth is a 9-degree segment. Each unit extends from the injector end to a point on the nozzle approximately 6 inches (measured axially) from the throat plane, and includes a nozzle support structure and provisions for thrust mount attachment. Bearing surfaces, radially opposite those on the outer body, are provided for seating struts.

(U) Regenerative-Cooling System. The regenerative-cooling system consists of the brazed tube bundle, the various manifolds and ducts, the subsonic struts, and all elements that provide flow paths for, and are cooled by, the fuel during its passage from the inlet of the thrust chamber to the injector inlet manifold.

(C) The basic cooling circuit for the inner and outer bodies was optimized early in the contract for the lowest pressure loss with reasonable tube sizes. This procedure resulted in the selection of cooling the inner body in series with the outer body.(Fig. 70). In this scheme, the coolant enters a manifold at the exit end of the inner body, cools the inner body, flows through the injector, cools the outer body, and then is injected into the chamber. The total regenerative-cooling pressure loss including inlet and exit manifolds was predicted to be 825 psi.

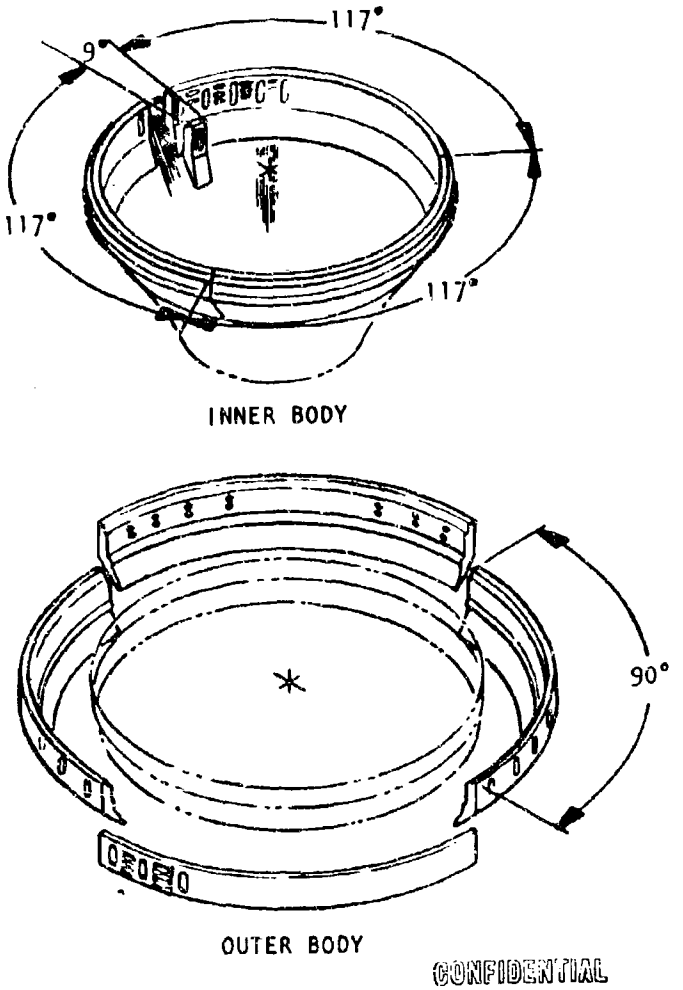

Figure 69. Demonstrator Module Thrust Chamber Segmented Titanium Structural Shell

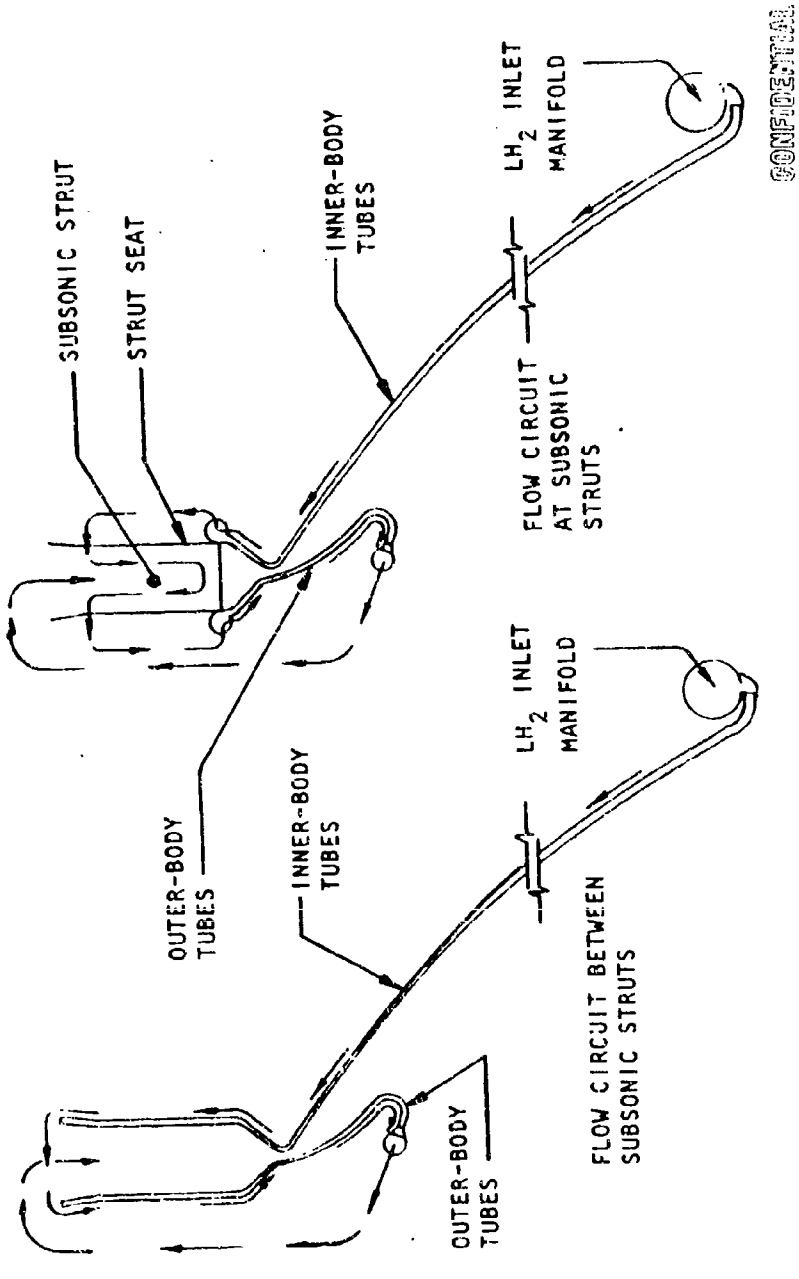

Figure 70. Regenerative-Coolant Flow Circuit

(U) Total fuel flow is introduced into a single-inlet, nontapered manifold located at the exit plane of the inner tube-wall nozzle. A single-pass circuit feeds 2120 tubes spliced 2:1 to 4240 tubes toward the injector end. At the start of chamber convergence to the throat in the combustion zone of the inner body, two paths must be described for clarity, that through the baffle seat and baffle and that through the remainder of the system.

(U) The inner-body tubes intersecting each of the 40 equally spaced subsonic strut seats (extending from the start of the convergence system to the injector end) discharge their flow into manifolding within the seat. Part of this flow is directed within this manifold into the strut across the sealed strut-seat interface. The remainder of flow in the seat is directed to a collection manifold at the injector end of the inner body.

(U) Hydrogen flow through the remainder of the system (between strut seats) continues from the start of convergence to the throat of the inner body to the same collection manifold mentioned above.

(C) At each of the 40 strut locations, passages connect the collection manifold to the strut across the sealed strut-seat interface. Total fuel flow is thus directed into the subsonic strut where approximately 25 percent is used to cool the copper strut face in a single-pass regenerative circuit. The remaining 75 percent of flow is directed across the baffle where the total is discharged into a manifolding system at the injector end of the outer body, identical to that of the inner body. From this point, single-pass flow through the outer body and shroud tubes occurs.

(U) A collection manifold at the exit of the outer-body shroud combines the flow from the circuits described. Transfer to the injector hydrogen manifold is made through 40 riser tubes connecting the shroud to the injector. Disassembly during the development program is accomplished by cutting the fuel risers, and reassembly is done by orbit welding or induction brazing of 40 connections. The orbit welder has been successfully employed on the J-2 engine for assembly of engine tubing. It is an automatic device which rotates a welding head around a tube joint according to preset condition to produce consistant welded joints.

(C) The regeneratively cooled wall of the inner body is composed of 2120 assemblies of 2:1 spliced tubes, e.g., 2120 tubes in the nozzle, to a point approximately 4.0 inches downstream of the throat, each brazed as a subassembly to two tubes in the combustor region. Tube-wall thickness throughout the inner body is 0.012 inch. Nickel 200 was selected as the basic tube material, operating at a maximum temperature of 1450 F. Inconel 625 was selected as a long-range substitute, pending the accrual of brazing and formability data for this material. Substantial weight savings are available through use of the latter material.

(C) The outer body consists of 4400 tubes of 0.010-inch Nickel 200 material. To achieve wall temperatures under 1520 F (based on 300 cycle life requirement), the inner body was displaced 3/16-inch downstream, starting at the beginning of the chamber convergence. This effectively moves the sonic point on the outer body 3/16-inch downstream. This change permits utilization of the maximum obtainable coolant curvature enhancement at the high heat flux region of the throat (59 Btu/in.^{2}-sec for a 1450 F wall temperature).

(U) Subsonic Struts. In addition to its function to space and structurally tie the inner and outer bodies, the subsonic strut serves as a fluid passage to transfer the hydrogen propellant from the inner body to the outer body, as a fluid passage for introducing ignition gases into the chamber (or extracting tapoff gases from the chamber), and as a stabilizing influence to the combustion process.

(C) Each of the 40 struts extends from the injector face to the start of convergence to the throat, approximately 4.5 inches. Located within the combustion zone, the external surface of each baffle is exposed to combustion gases and must be cooled. This is done regeneratively, utilizing the transfer propellant mentioned previously.

(C) The exposed periphery of each strut is composed of 0.25-inch OFHC copper containing five coolant passages, 0.156 inch in diameter. The copper plate is furnace brazed to a baffle body of Inconel which is suitably compartmented to provide the differential pressure required to sustain the regenerative-coolant flow through the copper surface plate. Provision is made to "bleed" hydrogen into the strut bolt cavities to provide coolant to surround the bolt. In the event of seal leakage at the strut interface, coolant would flow from the bolt cavity into the combustion chamber, ensuring that combustion gases do not leak into the bolt cavity.

(U) Installation of seats for subsonic struts on inner and outer tube-wall bodies is accomplished after the bodies have been through their initial braze cycle. With this technique, the criticality of stack tolerances and tube number and orientation in body fabrication is reduced. A pictorial definition of the installation process is presented in Fig. 71. Step 1 shows the seats applied to inner and outer contours of a 360-degree brazed body assembly. Steps 2 and 3 indicate the electrical discharge machining (EDM) processes for forming manifolds internally and step 4 installation of the final seat by welding.

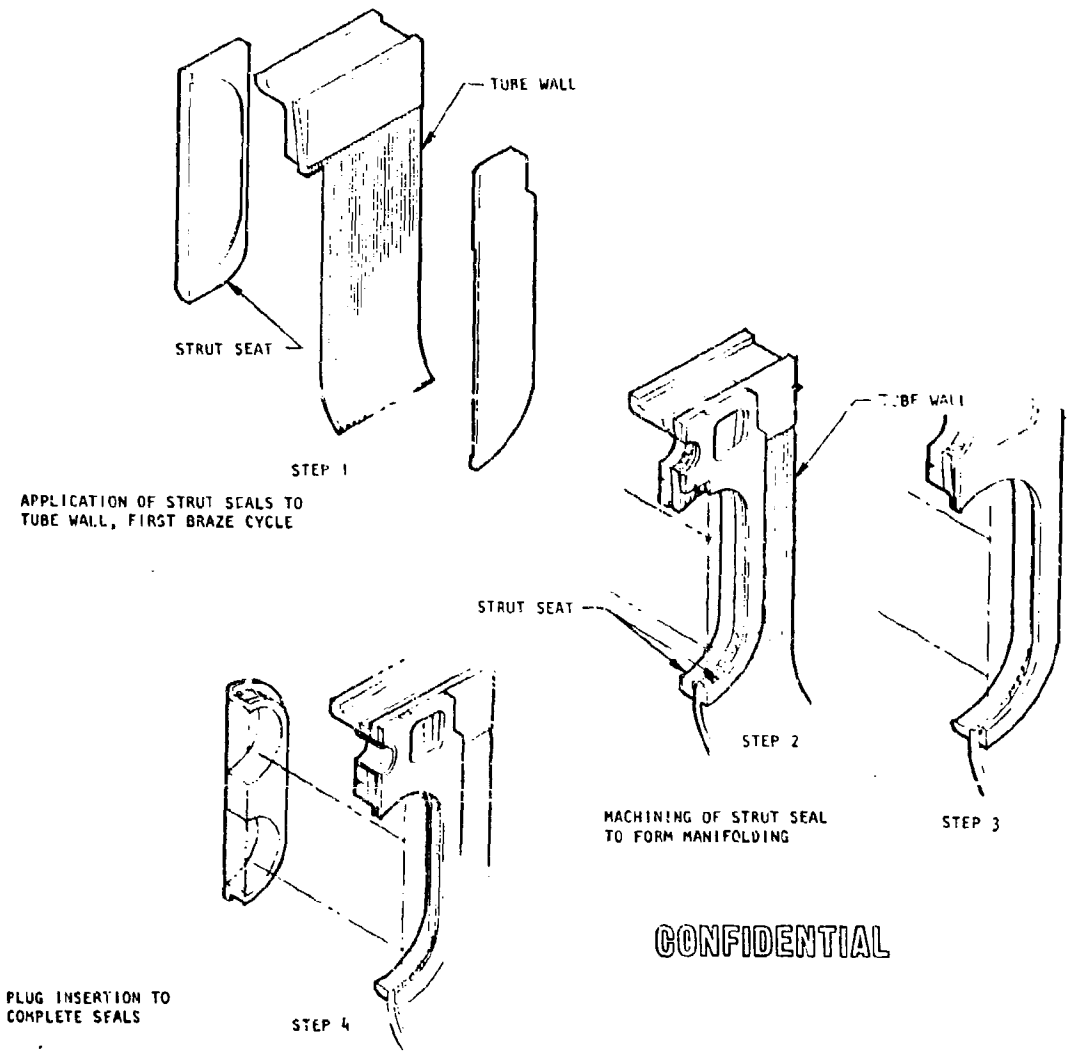

Figure 71. Application, Machining, and Plug Insertion

Installation of the strut seat by this technique prevents plugging of tubes under the seat during the braze cycle.and enables pressure check of the joint and realloying.

(U) Hot-Gas Manifold. The tapoff manifolding provides the dual function of: (1) ducting hot gases from the hot-gas igniter to provide ignition of the propellants within the thrust chamber, and (2) ducting hot gases from the thrust chamber to provide power to the engine turbines.

(U) The tapoff manifold consists of a large torus collection manifold and 40 riser tubes. The collection manifold is made from a tube 1.88 inches in diameter and rolled into a torous 79.25 inches in diameter. It is mounted inboard of the inner body just above the centerline of the throat. The 40 risers, each 0.626 inch in diameter, mount the torus to the inner body. The risers are fabricated with multiple bends to provide the flexibility necessary when the manifold system undergoes dimensional changes due to temperature extremes. The torus and the risers are lined with a thin sheet that is held from the outer walls by a mesh of stainless steel, providing the insulation necessary to keep ignition gases hot and structural materials cool enough to function with integrity.

(U) Each riser is connected to a pass-through pipe that lines up with the hot-gas tapoff hole in each baffle seat. This tapoff hole, in turn, lines up with the hot-gas entrance ports in each subsonic strut.

(U) For ignition, the hot gases from the hot-gas igniter are ducted to and through the manifold, up the risers, through the strut seat, through the strut hot-gas passages, and are injected into each compartment of the combustor. For tapoff, the flow is reversed and the hot gases are taken from the chamber and ducted through the system to the turbines.

Combustor and Nozzle Analysis.

(U) Combustor Configuration Selection. The performance and heat transfer characteristics of the thrust chamber are determined by the shape and contour of the various portions of the assembly. During the contract period, data useful to the thrust chamber design were generated through this program and complementary programs conducted in parallel. Analytical studies, cold-flow tests, and hot-firing tests were conducted to optimize combustor shape, throat flow angle, shroud length, and nozzle contour. The results of this work have been integrated into the demonstrator thrust chamber design.

(C) Selection of the combustor shape is based on the requirements of high combustion efficiency and low heating loads while maintaining low weight. The selected chamber geometry is 2 inches wide at the injector and has a 6-inch length from injector face to throat. The chamber walls are parallel down to a point approximately 4.5 inches downstream of the injector face, and then converge at a 40-degree angle. This parallel wall design (evolved from the previously proposed curved wall design as a result of 2.5K segment tests on several different combustor shapes) offers reduced weight and improved structural characteristics. It also results in a smaller combustor cross section and allows the exit throat to be moved outboard nearer the 100-inch diameter. This change results in increased performance associated with an increased area ratio and simplifies combustion chamber construction. In addition, subsonic struts are much easier to incorporate into this configuration. This combustor has a characteristic length (L*) of approximately 40 inches, which is sufficient for achieving high combustion efficiency. The throat radius of curvature of the outer body is 0.7 inch while that of the inner body is 0.51 inch, which, in conjunction with the 40-degree throat convergence angle, provides beneficial coolant-side curvature enhancement.

(C) Extensive water-cooled segment testing of this configuration in Task II yielded parametric performance and heat transfer data, and combustion efficiences of >99 percent were demonstrated. Heat transfer tests on curved

tubes have also shown good correlation with the predicted curvature. Phase I testing experience (combustor shape, heat flux, enhancement) has demonstrated that measured throat heating rates and total heat inputs can be handled by regenerative cooling, using conventional tube materials.

(U) Nozzle Contour Selection. The shroud and nozzle contour used on the proposed Aerospike Engine employs a double-expansion shroud configuration coupled with a modified ideal spike inner-body contour. This type of design (Fig. 72) was developed as a means of obtaining all Aerospike performance advantages while maintaining design flexibility. Of particular advantage is the ability to orient the throat at any desired angle, as distinguished from the unshrouded spike nozzle for which the throat angle is a function of area ratio. Therefore, at high area ratios, the unshrouded spike nozzle throat angle would be approximately radial as opposed to the more desirable axial position.

(C) The contour design analysis was based upon chemical equilibrium expansion of oxygen/hydrogen products of combustion, and the nozzle area ratio defined by the engine diameter limit of 100 inches, and the required thrust of 250K. The mean flow angle and radius of curvature (r) at the nozzle throat were selected based on an attempt to minimize shroud length, and simultaneously minimize the difference between the angle of flow at the injector and at the throat, and provide adequate curvature on the inner wall to enhance regenerative cooling at the throat. A throat flow angle of 4.5 degrees and a radius of curvature of 0.510 inch was found to be the best compromise between the three considerations.

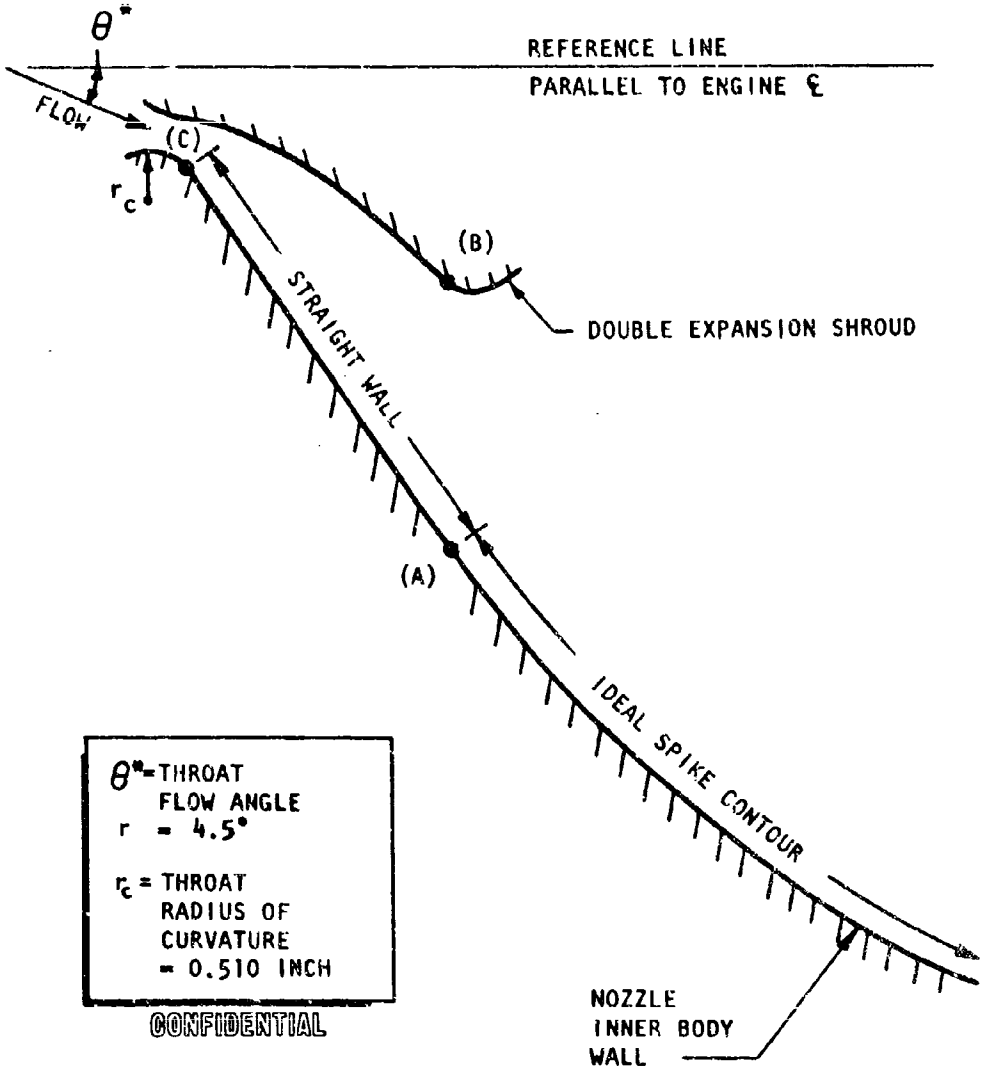

Figure 72. Double-Expansion Shroud Nozzle Design Schematic

(U) The design procedure consists of starting with an ideal spike exit flow field and computing the unshrouded nozzle contour required to give this flow field. The regulations of the flow field are solved by the method of characteristics. The mean flow angle selected for the geometric throat, (θ^*), established three critical points in the nozzle design: (1) the point on the inner wall at which the ideal spike contour will end, (2) a corresponding point on the shroud exit, and (3) the point of tangency to the throat curvature.

(U) The inner body wall contour is then completed by joining the ideal spike contour and the throat with a straight line tangent to the ideal contour at point (1). The shroud contour is completed by using the nozzle design procedure beginning with the known flow field between (1) and (3).

(U) The nozzle thus developed has aerodynamic performance identical to that of the truncated ideal spike nozzle, since the modification leaves the exit flow undisturbed.

(U) During the nozzle selection study, the possibility of reducing the shroud length was examined as a means of reducing weight, cooling load, and friction loss on the outer wall. Theoretical calculations and cold-flow model tests showed that negligible changes in base pressure, geometric performance, and kinetic performance occurred for high pressure ratios when the nozzle shroud was truncated to half the original length. However, at low pressure ratios, theoretical flow field calculations indicated that the truncated shrouds would produce a recompression shock of sufficient strength to exceed the cooling capacity of the inner-wall tubes during throttled sea level runs.

(U) A comparison of wall pressure profiles for a short and long shroud is presented in Fig. 73 for low pressure ratio (P_c/P_a) conditions. The wall pressure profiles for the long shroud configuration are the result of isentropic recompression, while the short-shroud wall pressure profiles

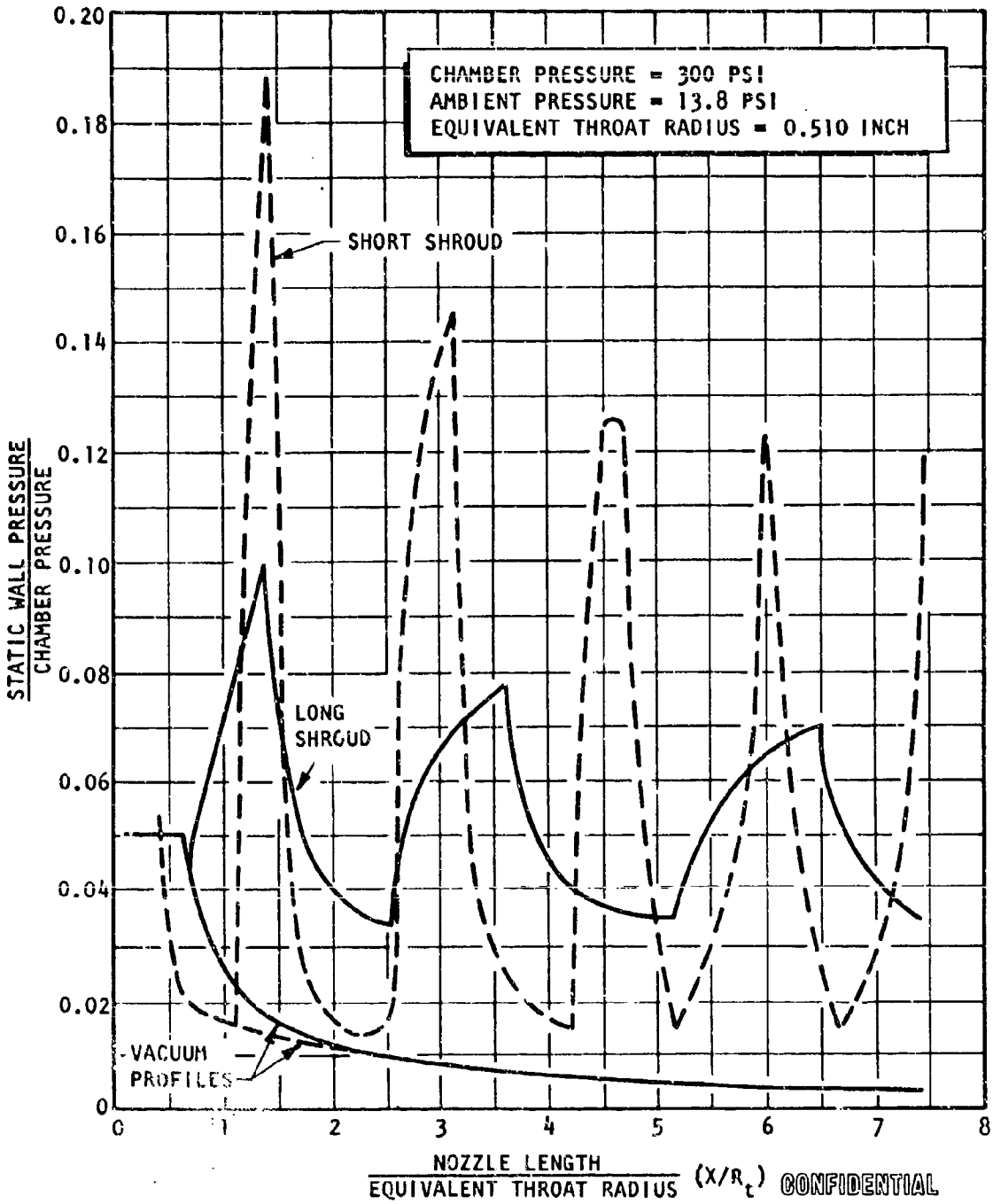

Figure 73. Sea Level Inner Body Wall Pressure Profile

are the result of the impingement of oblique shocks on the nozzle wall. A sufficiently strong shock can result in local separation and reattachment of the boundary layer. The Mager criterion has indicated that separation could occur for the short-shroud configuration, but the long-shroud configuration will not separate.

(U) A cold-flow test series was conducted to measure the recompression wall pressure profiles for the full-length, shroud, and to verify the calculated results. The model employed in this test series was a two-dimensional quarter-scale segment of the 250K thrust chamber. Good agreement was obtained between computed and measured pressure profiles for the cold-flow model, as shown in Fig. 74. The full-length shroud configuration was selected for the demonstrator thrust chamber to minimize the heat fluxes on the nozzle wall during sea level operation.

(U) Structural Analysis. The thrust chamber structure resists the pressure loads and transmits the resultant useful thrust to the thrust structure. The sea level and altitude gas pressure distribution on the nozzle structure is shown in Fig. 75. Because of the rapid decrease in pressure downstream of the throat, it is only necessary to support the nozzle tube bundle uniformly for a short distance. Beyond this point, the nozzle tube bundle is adequately supported by intermittently spaced compression rings. The radially inward component of the nozzle pressure distribution is transmitted as a compressive load to the rings by the tube wall. The thrust generated by the nozzle pressure axial component is carried by axial compression in the tube bundle.

(U) The compression ring spacing is determined by consideration of the stresses imposed by bending of the tubes, the compression from thrust loading, and tension due to the tube internal coolant pressure. The cross sections of the rings are governed by the moment of inertia required to resist buckling and ring bending.

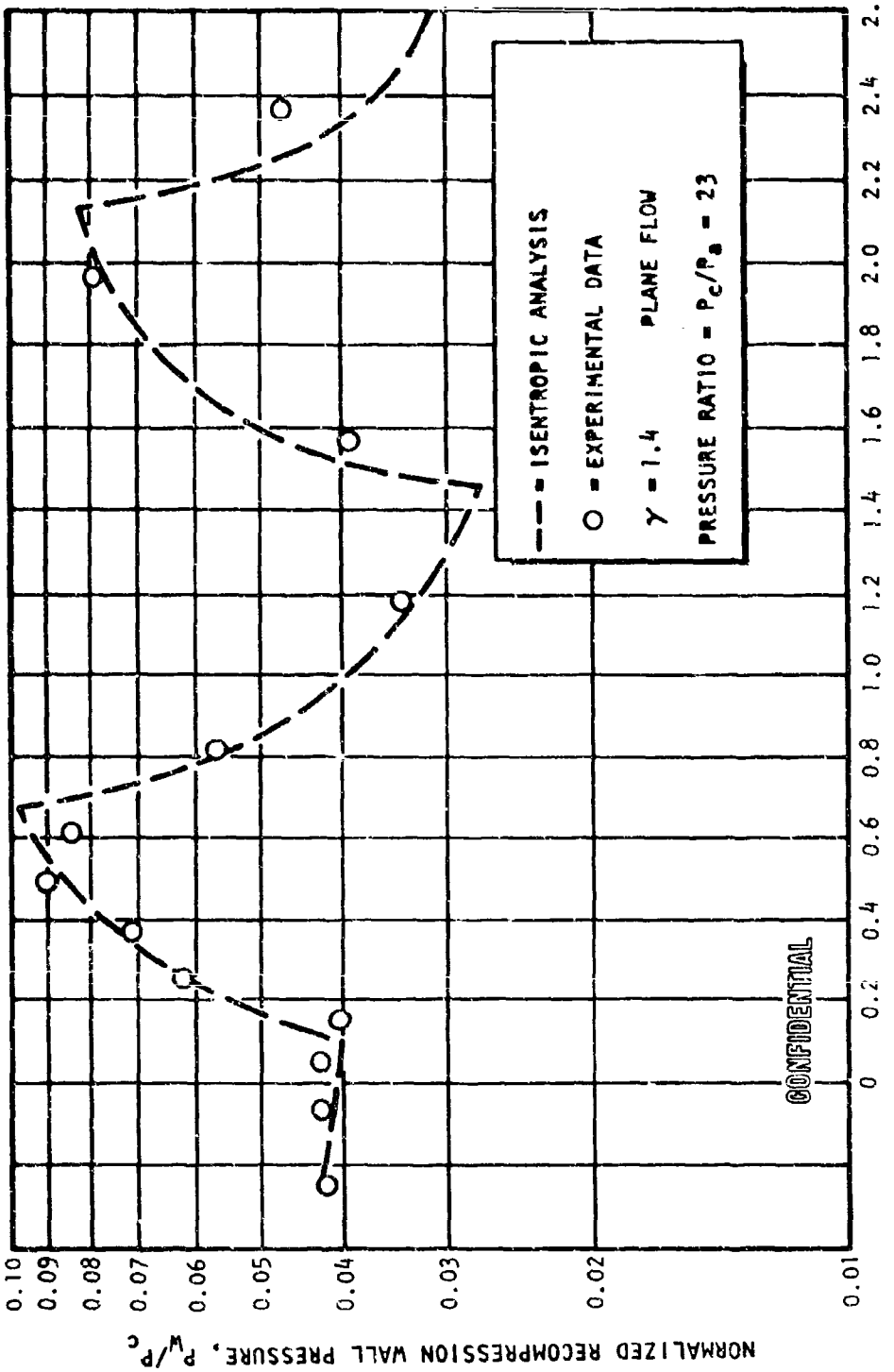

Figure 74. Full-Length Shroud Pressure Profile

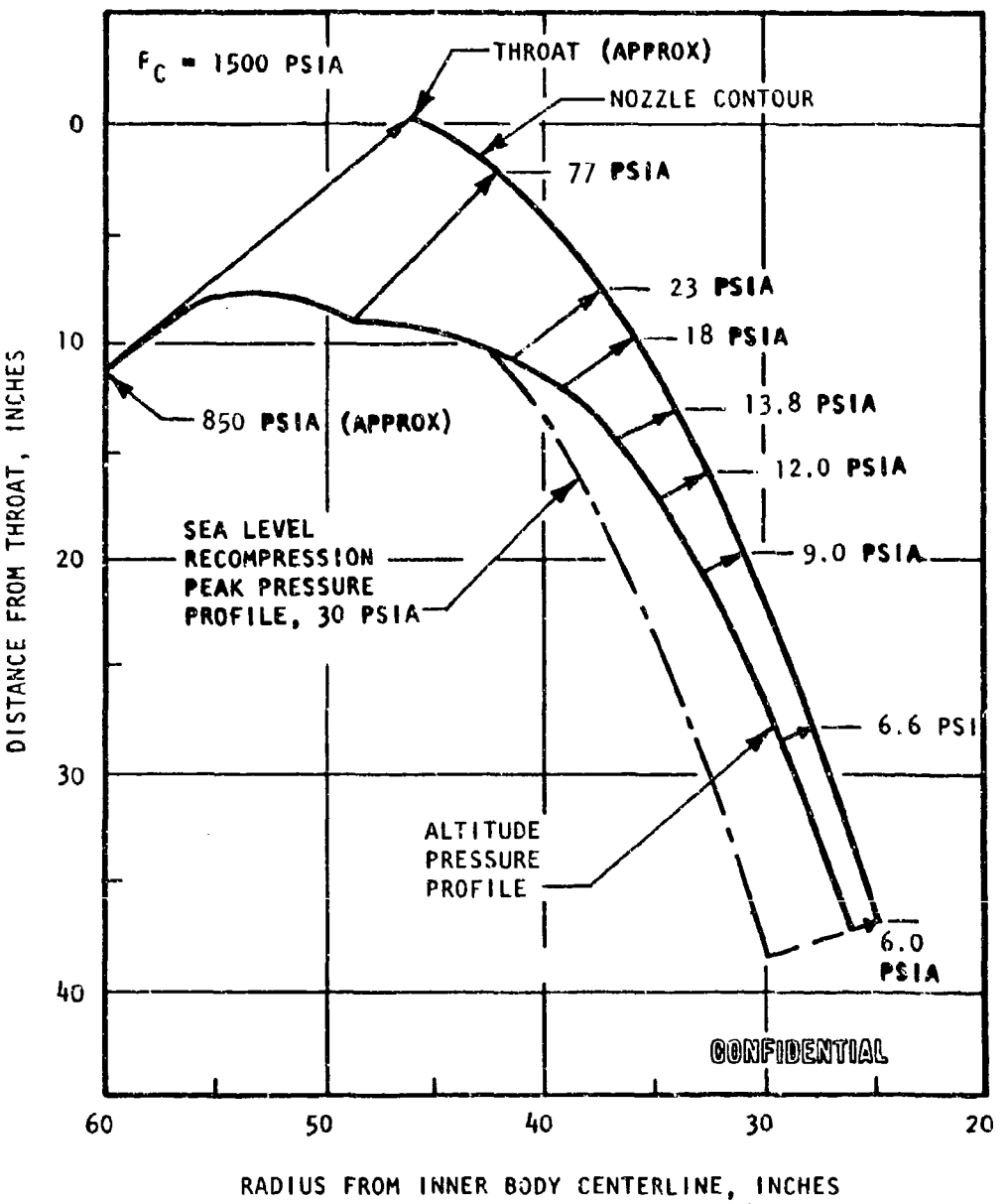

Figure 75. Sea Level and Altitude Nozzle Pressure Profile

(U) The thrust in the tube bundle and the thrust from the combustion chamber throat are transmitted to the thrust structure through 40 structural members. Because these 40 attach points cannot be located in the plane of the resultant thrust, and because they are not reacting the thrust uniformly, bending moments, twisting moments, and shear forces are developed at the combustion chamber. The combustion chamber structure reacts these in addition to the chamber pressure (Fig. 76).

(C) The annular combustion zone was analyzed for a chamber pressure of 1530 psia, a nominal thrust of 250K, a maximum gimbal acceleration rate of 30 rad/sec^2, and longitudinal and lateral accelerations as outlined in Table 9 . The main loads are carried by the titanium combustor bodies and the Inconel baffles. The combustor body structure is of open web design to facilitate fabrication, and the pressure is contained by the outer and inner bodies through beam action between the baffles. The outer and inner combustor bodies are tied together by two Inconel 718 bolts in each baffle with a total of 40 baffles located every 9 degrees around the circumference of the annular thrust chamber. The injector is used to contain the pressure in the forward direction.

(C) The selection of titanium for the backup structure precludes a brazed assembly. For this reason, a study was conducted to select the optimum adhesive for attaching the structure to the brazed tube bundle. The operating regime of the thrust chamber dictates that the adhesive must be capable of withstanding thermal cycling from chilldown to throttling temperatures and must also have insulating capability to keep the temperature of the lightweight structure within reasonable limits. Adhesive strength properties are not required below the outer-body throat, since two mechanical joints support the tubes in this region. Among the important requirements for the adhesive were:

1. Retention of suitable strength from tube temperatures to 600 F. Below the outer body (where the temperature exceeds 600 F at throttled sea level operation), the adhesive has no strength requirement and need act as an insulation barrier only.

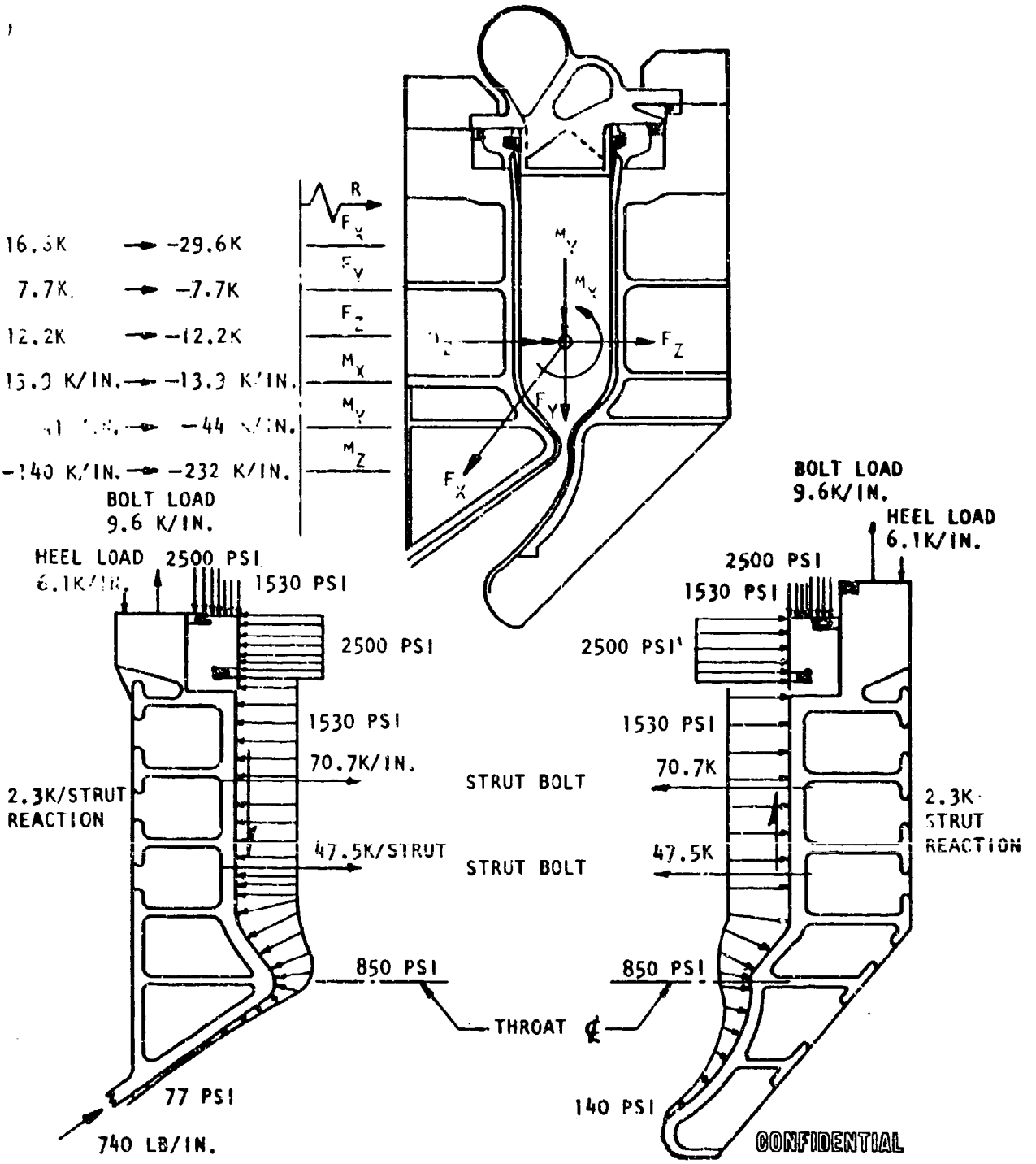

Figure 76. Combustor Body Loads Due to Thrust and Pressure

2. Ability to withstand up to 300 thermal shock cycles over the same temperature extremes
3. Excellent bond development to nickel, aluminum, and titanium
4. Workability characteristics consistent with thrust chamber fabrication, i.e., long pot life to permit assembly and bonding pressure requirements of less than 100 psi

(C) Mechanical property tests of bonded joints for butt tension, lap shear, and peel were initiated at temperatures from -300 to 650 F, after 50, 150, and 300 cycles. Several materials were utilized as the base structure for comparative results.

(U) The end results of the test program indicated that although certain adhesives displayed good performance within certain temperature ranges and under specific conditions, only one consistently met the requirements as set forth earlier in the program. American Cyanamid's HT 424 Epoxy Phenolic film on a glass fabric carrier exhibited the best all-around characteristics of all adhesives tested. Room temperature and cryogenic lap shear values were both moderately high, while 600 F strengths were slightly lower (Fig. 77). Most other adhesives tested were high at one temperature range and low at others.

(U) The epoxy phenolic bond showed only slight degradation due to cryogenic cycling and a 1/2-hour soak at 600 F before testing. It can be stated that the strength levels of the HT 424 will be satisfactory even after repeated thermal shock cycling in the thrust chamber.

(C) The change in throat area during operation is a function of the chamber pressure, the rigidity of the chamber structure, and the temperature. Analysis indicates that the maximum change in throat area is 9.25 percent. Tests conducted on similar chamber structures showed excellent

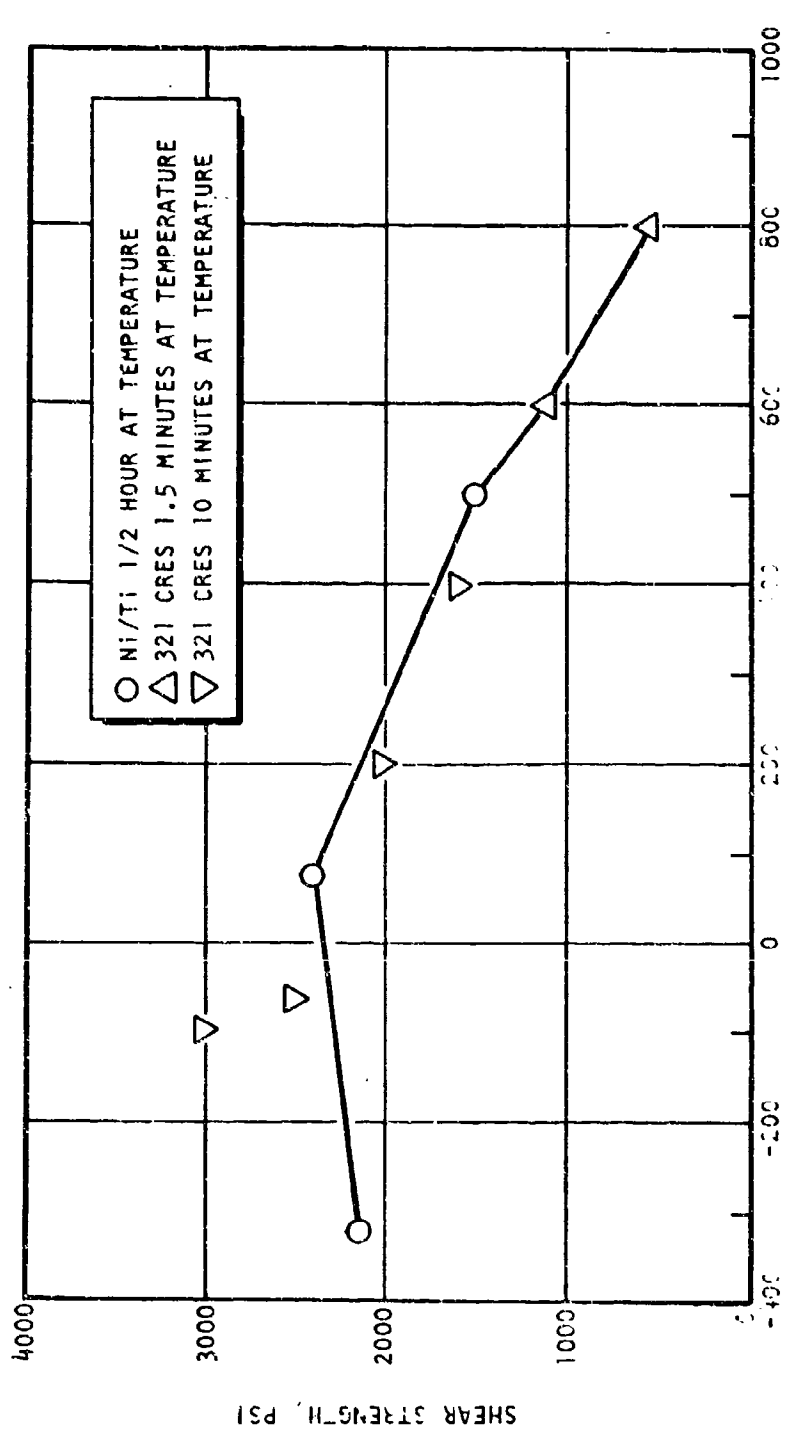

Figure 77. Shear Strength vs Temperature HT 424 Film Adhesive

correlation between test and analytical predictions (Fig. 78). The change in throat gap is repeatable and has the desirable attribute of increasing performance at throttled levels because the throat gap closes and the nozzle area ratio increases.

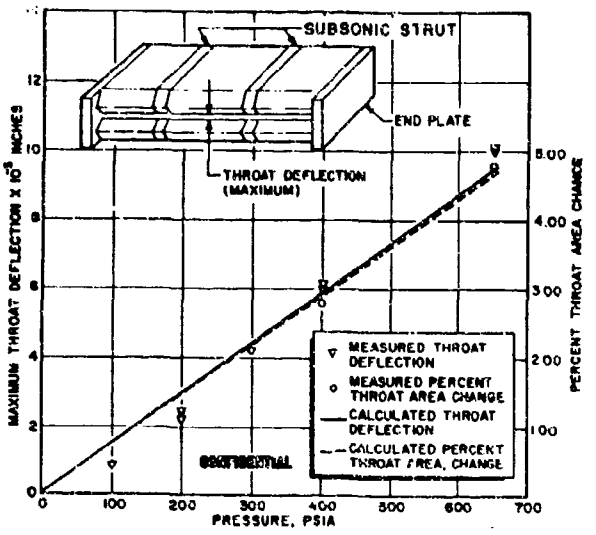

Figure 78. Throat Deflections for Center Compartment at Several Chamber Pressures

(U) Tube Material Selection. With the targeted engine life goals in mind, an effort was made to obtain an indication of the life capability of many thrust chamber tube materials. Special consideration was given to those materials that had received usage in production thrust chambers, and also those materials that had received some thrust chamber usage and were of high thermal conductivity. The latter requirements were very desirable because of the high peak heat flux at the throat of the thrust chamber.

(C) A recently developed tube-wall, plastic strain analysis was used in conjunction with a heat transfer analysis to predict the cyclic plastic strain incurred in many candidate tube materials operating as throat tubes during an ambient to 1500-psia chamber pressure start sequence. This analysis and experimental verification is discussed under Task II, Thrust Chamber Cooling Investigation.

(C) The materials evaluation effort described above, in conjunction with Rocketdyne's previous and concurrently generated fabrication and cost experience, led to the selection of Nickel 200 as the tube material for immediate and long-range application to the Aerospike Engine.

(C) Recent and past experience at Rocketdyne has shown that Nickel 200 tubing has excellent tube-tapering and forming properties in the sizes required for the Demonstrator Module thrust chamber. Nickel 200 oxides are easily reduced in a dry hydrogen atmosphere, affording excellent alloy flow during furnace brazing. Recent laboratory tests have shown the rigidity of Nickel 200 tubes at 2000 F to be more than adequate, permitting the use of efficient pressure bag tooling for dimensional control during the furnace brazing process. A full-scale Nickel 200 chamber has been successfully furnace brazed for the SDI program with the same tooling used to braze the stainless-steel, tube-wall thrust chamber.

(C) A series of eight tests, from chamber pressures of 310 to 2050 psia, were also conducted with a 2.5K nickel tube-wall segment to extend available information on the regenerative-cooling capabilities of nickel tubular designs.

(U) Tube Design. Figure 67 shows the tube profile for the inner- and outer-body tubes. The cross-sectional areas were established from the heat transfer analysis to provide adequate cooling and life with a minimum pressure loss.

(C) The tube splice was studied in a heat transfer/pressure drop/hydraulic stress tradeoff analysis. The tube upstream of the splice is designed to a mixture ratio of 6:1 at a 1500-psia chamber pressure, which will produce slightly reduced wall temperatures at MR = 7:1. The tube below the splice is designed to operate at a 300-psia chamber pressure and a mixture ratio of 7:1 at sea level conditions, this being the most stringent condition for this part of the inner body. This results from the recompression which occurs at sea level in conjunction with the low coolant flowrates.

(U) Heat Transfer Analysis. The thrust chamber design is firmly based on experimental and analytical heat transfer data developed during this and other related programs. Study support effort has been provided for the areas of both gas-side and coolant-side detailed heat transfer measurements and in the definition of the wall material requirements to provide long life and low wall temperatures. The life aspects were described in detail in the Tube Material Selection section, and the following discussions treat the aspects of heat transfer and wall thermal conduction.

(C) Heat Input Definition. Detailed heat transfer measurements at axial wall station locations have been provided by highly instrumented water-cooled segment testing during this program and related programs. Data were developed by calorimetric measurement of water temperature rises for a range in chamber pressure of 150 to 1580 psia and a mixture ratio range of 3.31 to 9.71 in 170 tests.

(C) Data of the axial heat flux distribution vs length are shown in Fig. 79 for a nominal MR = 6:0. The nearly proportional increase of local heat flux with chamber pressure is shown. Isolation of the peak heat flux to a local region in the throat vicinity is also illustrated.

(C) Experimental heat flux data (Fig. 80) defined a slope of 0.8 with chamber pressure, which confirms that a turbulent boundary layer exists in the throat region. This results in an excellent throttling capability over the planned 5:1 range because of the nearly linear reduction of heat flux with chamber pressure. Throat heat flux is shown to vary from 58 Btu/in.^{2}-sec at a 1500-psia chamber pressure to 15 Btu/in.^{2}-sec at the 300-psia throttled condition. A mixture ratio of 6:0 is shown to result in the peak heat flux input to the thrust chamber wall surface as predicted by experimental and theoretical predictions, shown in Fig. 81. At mixture ratio values below and above 6:1, the combustion

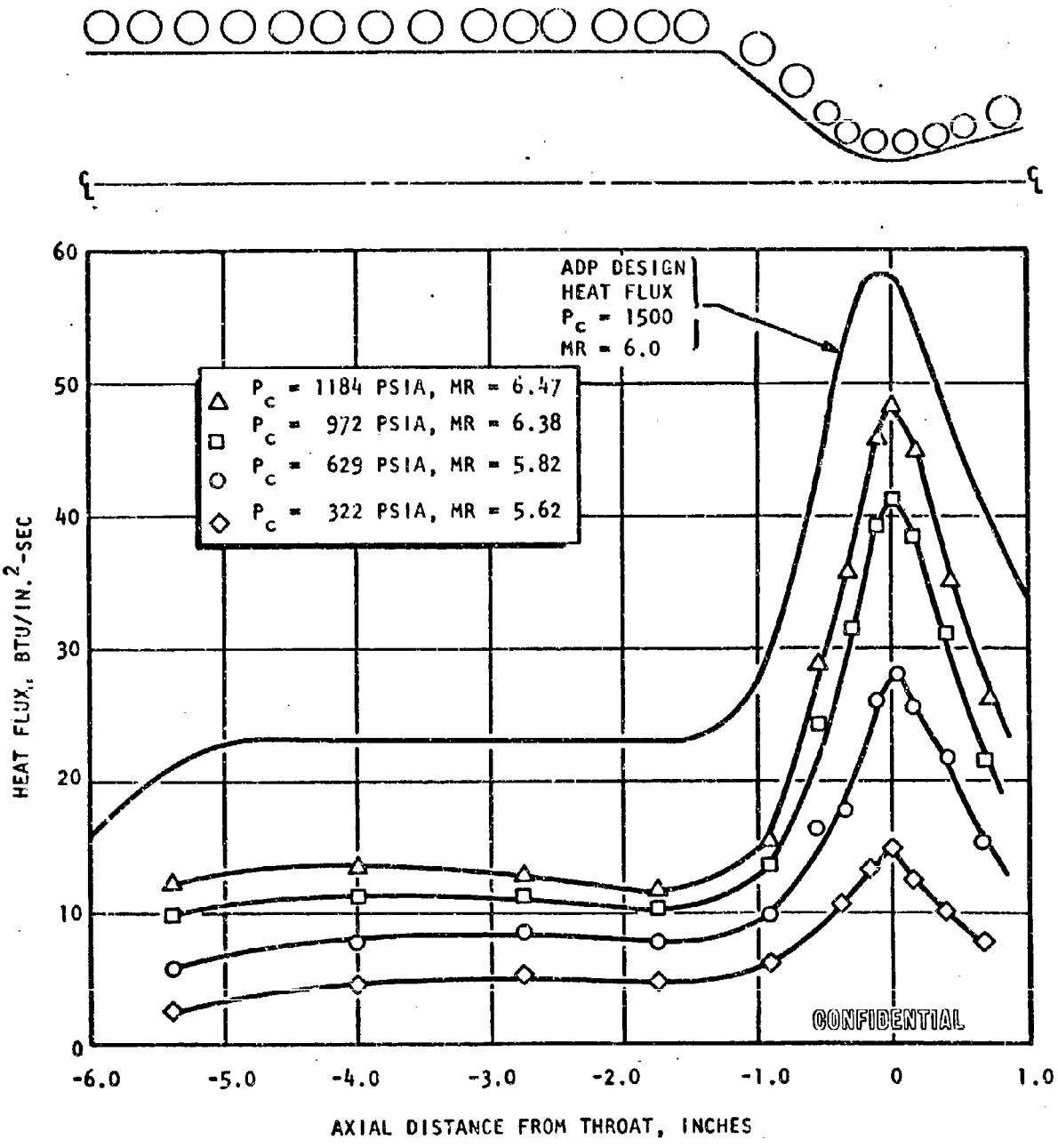

Figure 79. Experimental Heat Flux Distribution From 2.5K Water-Cooled Segment Tests

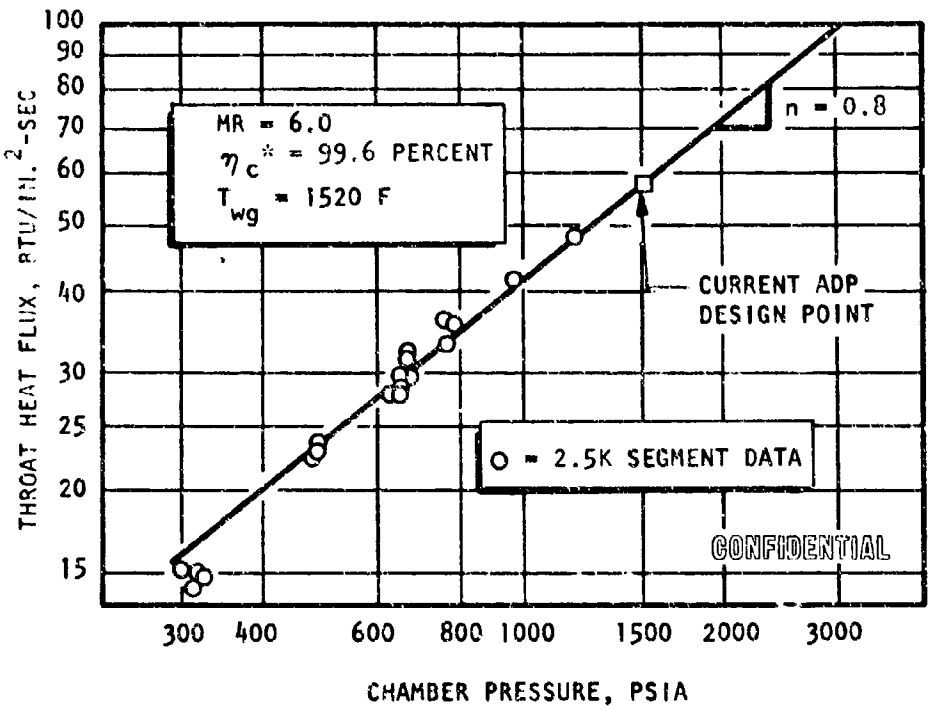

Figure 80. Throat Heat Flux vs Chamber Pressure

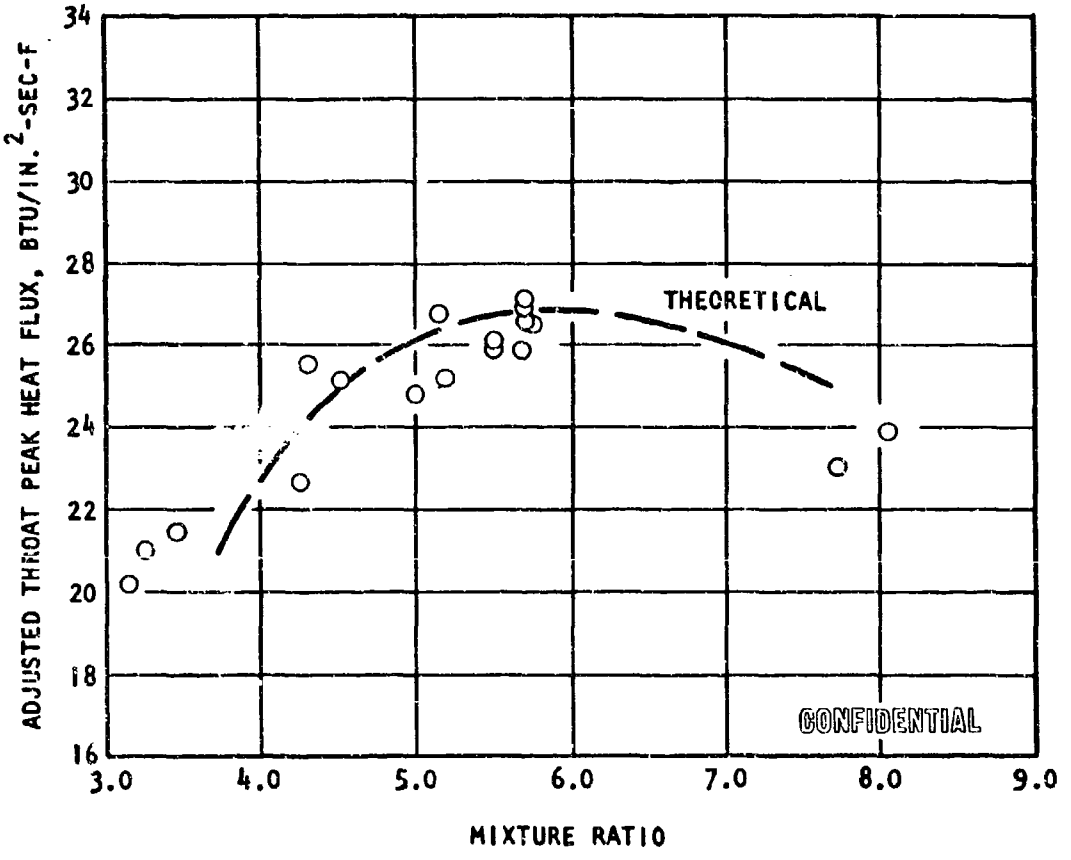

Figure 81. Effect of Mixture Ratio on Throat Peak Heat Flux With O_2/H_2 Propellants

gas enthalpy decreases with an attendant related decrease in heat transport enthalpy from the combustion gas to the chamber wall surface. Consequently, off-design operation at the low mixture ratio side poses no problems due to rapidly decreasing wall temperatures. Operation at a high mixture ratio (MR = 7.0) will theoretically result in a nearly constant wall temperature because the decrease in heat flux and boundary layer resistance is approximately proportional to the decrease in fuel flowrate. Variation of theoretical relative coolant mass velocity and flow areas required are shown in Fig. 82.

(U) Confirmation of the water-cooled testing integrated heat input value for the combustion zone and throat region has been provided by the tube-wall segment tests of Task II. The excellent agreement with the heat input data for both the hydrogen-cooled copper and nickel tube-wall chambers is illustrated in Fig. 83. The anticipated slightly higher heat input values shown for the copper tube-wall segment are due to the lower wall temperatures provided by a higher wall thermal conductivity. Approximately 60 percent of the total heat input profile (excluding the nozzle region, including the highest heat flux regions of the combustor and throat) has been verified during this program.

(U) Coolant Heat Absorption. Detailed analysis and experimental study of the influences of tube internal surface roughness and throat region tube curvature on the enhancement of the hydrogen-cooling capability were carried on during the program. Substantial improvements in the hydrogen-cooling capability (Nusselt number), expressed in the equation below

$$N_{NU_B} = 0.025 \, (N_{RE_B})^{0.8} \, (N_{PR_B})^{0.4} \, (T_B/T_{w\ell})^{0.55} \, \varphi_c \, \varphi_\epsilon$$

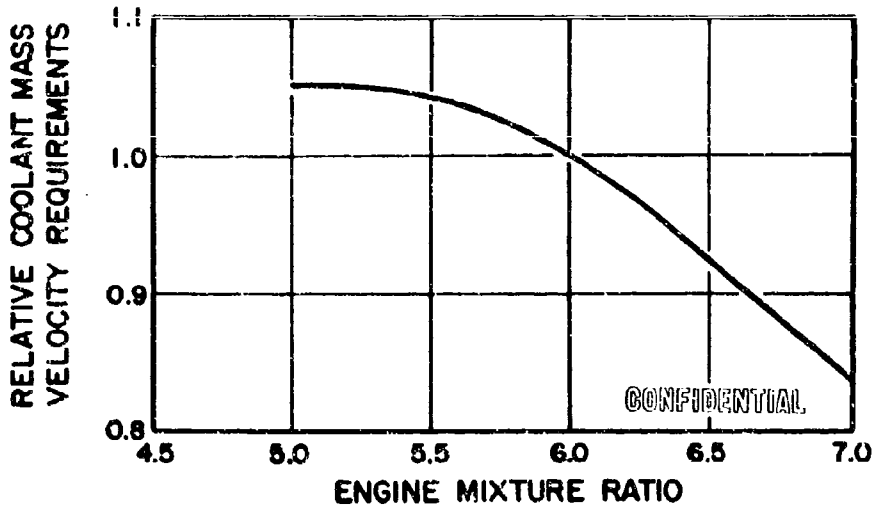

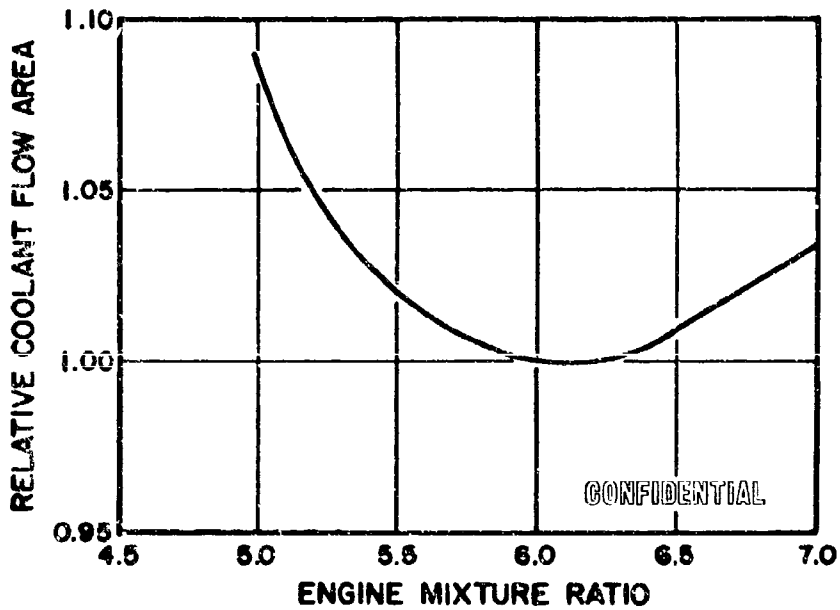

Figure 82. Effect of Mixture Ratio on Coolant Mass Velocity and Flow Area Requirements O_2/H_2, 1500 P_c, Constant Combustion Gas Flowrate 0.008 Inch 347 CRES Tube, T_{wg} = 1600 F

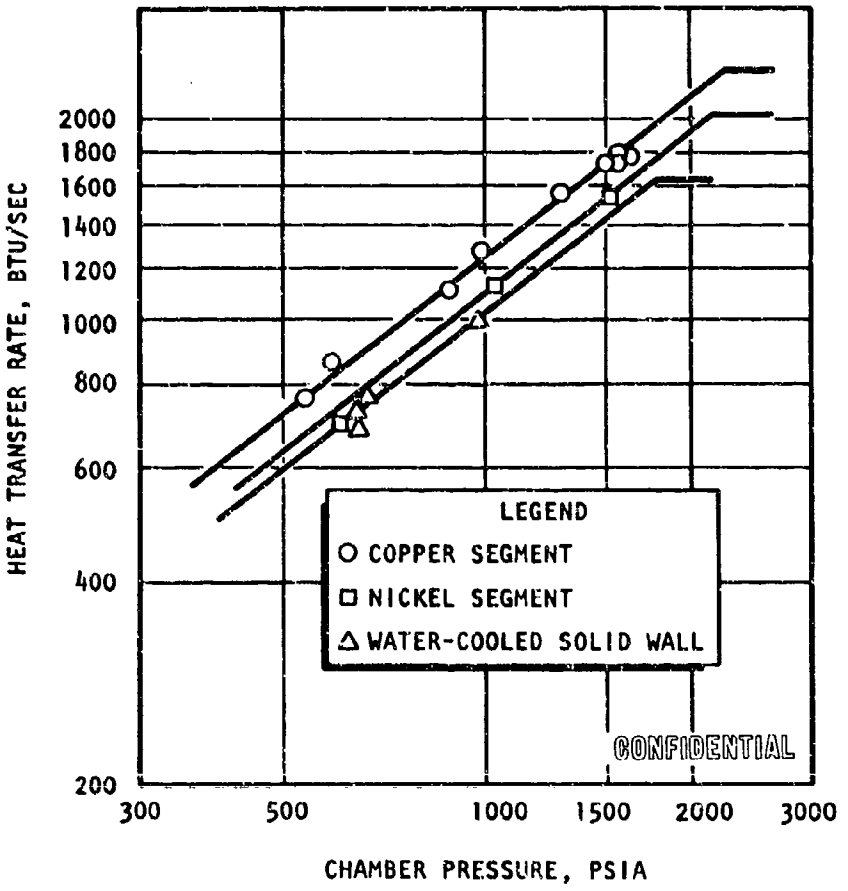

Figure 83. Contoured Tube Overall Heat Input Characteristics

are provided by the curvature and roughness factors φ_c and φ_ϵ. Figure 84 illustrates the variation in curvature enhancement predicted with tube turn L/D. Improvements of 40 to 50 percent over the noncurved tube case are noted for the outer- and inner-body design, respectively. Figure 85 illustrates the improvement factor, φ_ϵ, predicted for the proposed tube internal surface roughness and coolant mass velocity. With the natural tube manufacturing roughness and the tube-tapering and forming effects of fabrication, a considerable enhancement factor is predicted.

(U) Experimental values of the inner- and outer-body tube combined roughness and curvature factors $(\varphi_c\varphi_\epsilon)$ were determined in Task II, Thrust Chamber Cooling Investigation. At the throat locations indicated for the inner and outer body, combined factor experimental values of 3.0 and 2.5 are found. These are somewhat higher than the respective values of 2.0 and 1.85 which were predicted early in this effort. However, the lower predicted values have been used for the Demonstrator Module design, thereby providing an added design margin. Curvature enhancement effects on the wall temperature for the inner and outer body of the demonstrator are shown in Fig. 86. A reduction in wall temperature of over 300 F as a result of the curvature enhancement is shown.

(U) Wall Thermal Conduction. Selection of Nickel 200 as a tube-wall material for the Demonstrator Engine was based partly upon long-life characteristics discussed in the Tube Material Selection section of this report. However, from a heat transfer standpoint, the allowable wall temperature of 1520 F, combined with the excellent thermal conduction (2.5 times that of 347 CRES), is very advantageous in maintaining coolant velocity conditions below a Mach number of 0.5 to prevent coolant-flow choking.

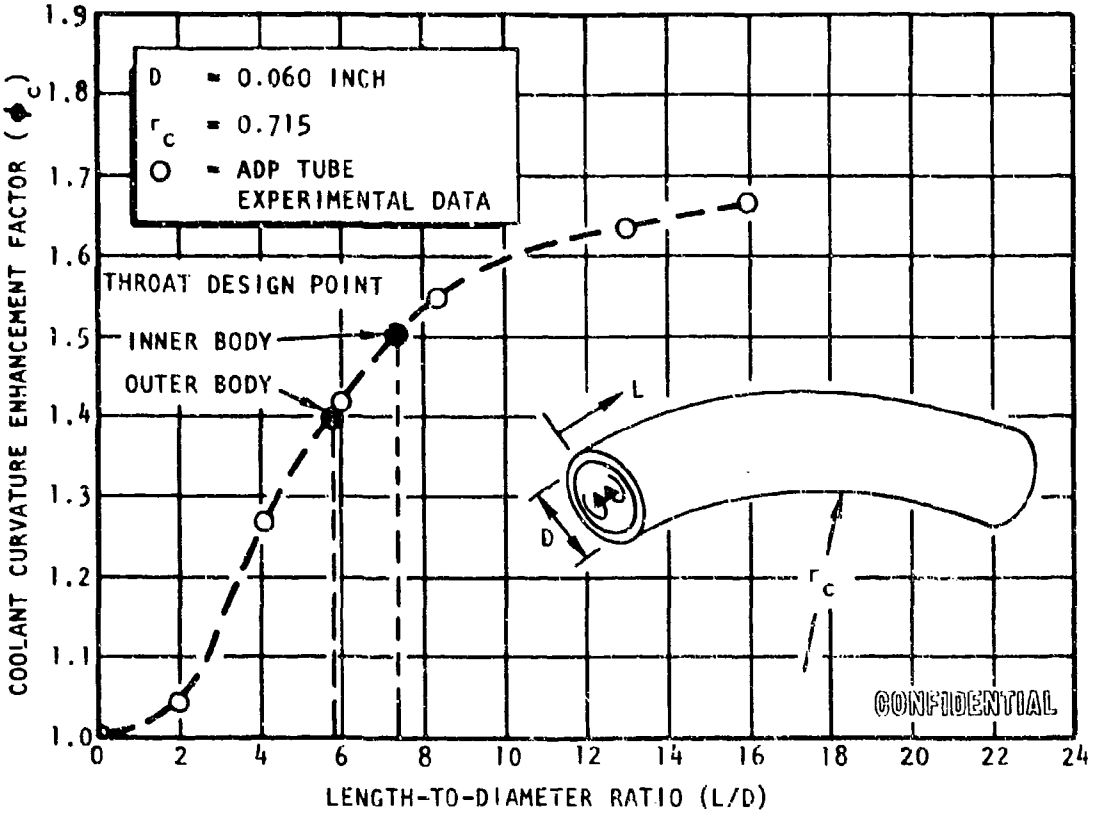

Figure 84. Design Coolant-Side Curvature Enhancement Factor

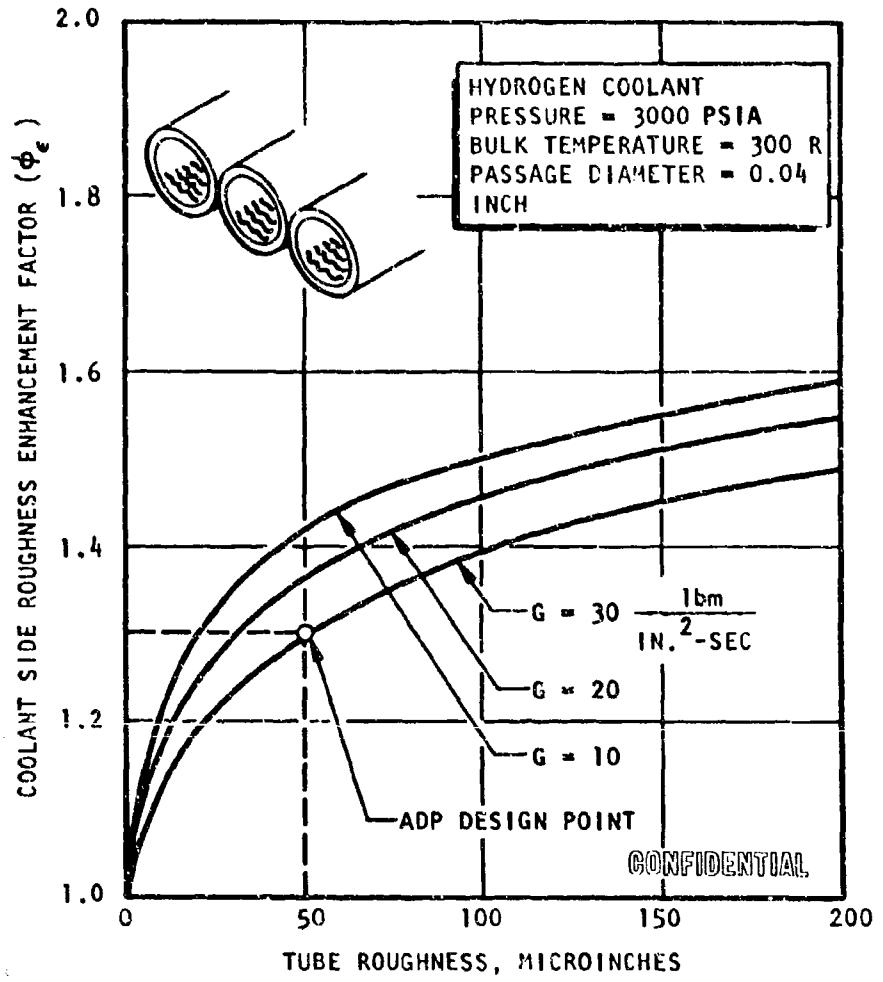

Figure 85. Coolant-Side Roughness Enhancement Factor

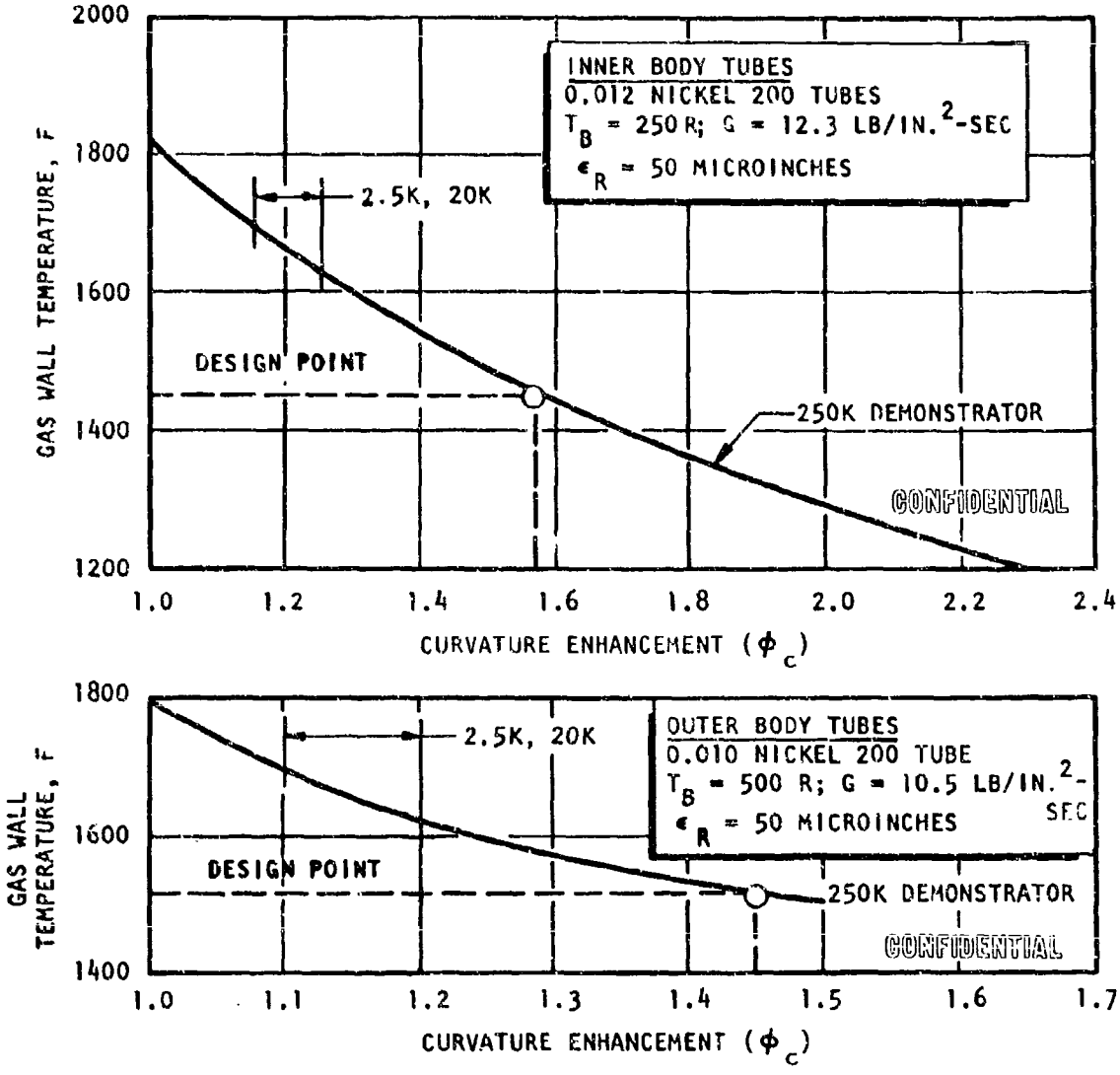

Figure 86. Gas-Wall Temperature vs Coolant Curvature Enhancement

(U) The theoretical predictions for the gas-side heat flux and the corresponding coolant-side film coefficient relationships for the analysis of the demonstrator design conditions are discussed presently.

(U) Heat Transfer Design Conditions. The thrust chamber tube geometry has been optimized on the basis of the most current heat transfer data, both analytical and experimental, obtained during the program. All analytical correlations have been checked against the test data, and this information has been used to make refinements in the cooling system to achieve a minimum coolant pressure loss.

(C) The combustion zone tube geometry has been optimized at the maximum heat flux condition (MR = 6) for the 250K Demonstrator Module. The procedure used involves achieving a wall thickness and tube flow area that yields a maximum wall temperature that is consistent with life cycle requirements and is capable of withstanding the internal pressure stresses. The minimum tube flow area occurs at the throat and must be designed for a 1500-psia chamber pressure and a mixture ratio of 6.0. The nozzle tube geometry designed for the nominal chamber conditions must be modified to accept heat flux levels predicted for sea level operation at throttled conditions. Because of recompression effects at sea level, the maximum heat flux on the nozzle is nearly independent of chamber pressure with the location of the peak heat flux shifted toward the throat as chamber pressure is decreased. Since the impingement point shifts with chamber pressure, the maximum design condition for each chamber pressure must be incorporated into the tube design at all axial locations.

(C) Inner-Body Tubes. The design of the inner body must be divided into two parts. The portion of the inner body downstream of the shroud exit is to be designed to meet sea level operation over the full range of

chamber pressure (principally between 300 and 600-psia P_c) at MR = 7.0. The throat and combustion zone are designed for 1500-psia P_c, MR = 6.

(C) The inner-body design parameters are shown in Fig. 87 through 89 . The heat flux profiles for both inner and outer bodies are shown in Fig. 87. The peak heat flux at the throat is 58 Btu/in.^{2}-sec, based on 1500-psia P_c, MR = 6.0, 100-percent η_{c^*}. The heat flux profile between the injector and throat is based on 2.5K solid-wall data and has been verified in terms of overall heat load by the 2.5K copper and nickel tube-wall test data shown previously. Theoretical nozzle heat fluxes, based on aerodynamic analysis, are about the same at nominal conditions and throttled sea level conditions, making the latter a more severe cooling problem because of less coolant flow at lower chamber pressure.

(C) Figure 88 shows the nozzle contour, the hydrogen bulk temperature profile at 1500-psia P_c (MR = 6), and the gas-side wall temperature profiles at sea level and vacuum. About 60 percent of the bulk-temperature rise is seen to occur between the injector and shroud exit plane when operating at 1500-psia P_c vacuum.

(C) Under vacuum conditions, the maximum wall temperature occurs in the throat, where the design temperature is 1450 F. The combustion zone is designed for a 1250 F wall temperature. It is seen that the throttled condition in a vacuum results in lower wall temperatures than the nominal 1500-psia chamber pressure condition. However, at sea level, the nozzle wall temperatures approach 1450 F, based on the current theoretical analysis of the recompression strengths and locations, and the resulting heat fluxes. The wall temperature peaks match the heat flux peaks in Fig. 87, which, in turn, line up with recompression zones at a chamber pressure of 300 psia. The first and strongest recompression is seen to occur within 4 inches of the shroud exit plane at a 300-psia chamber pressure.

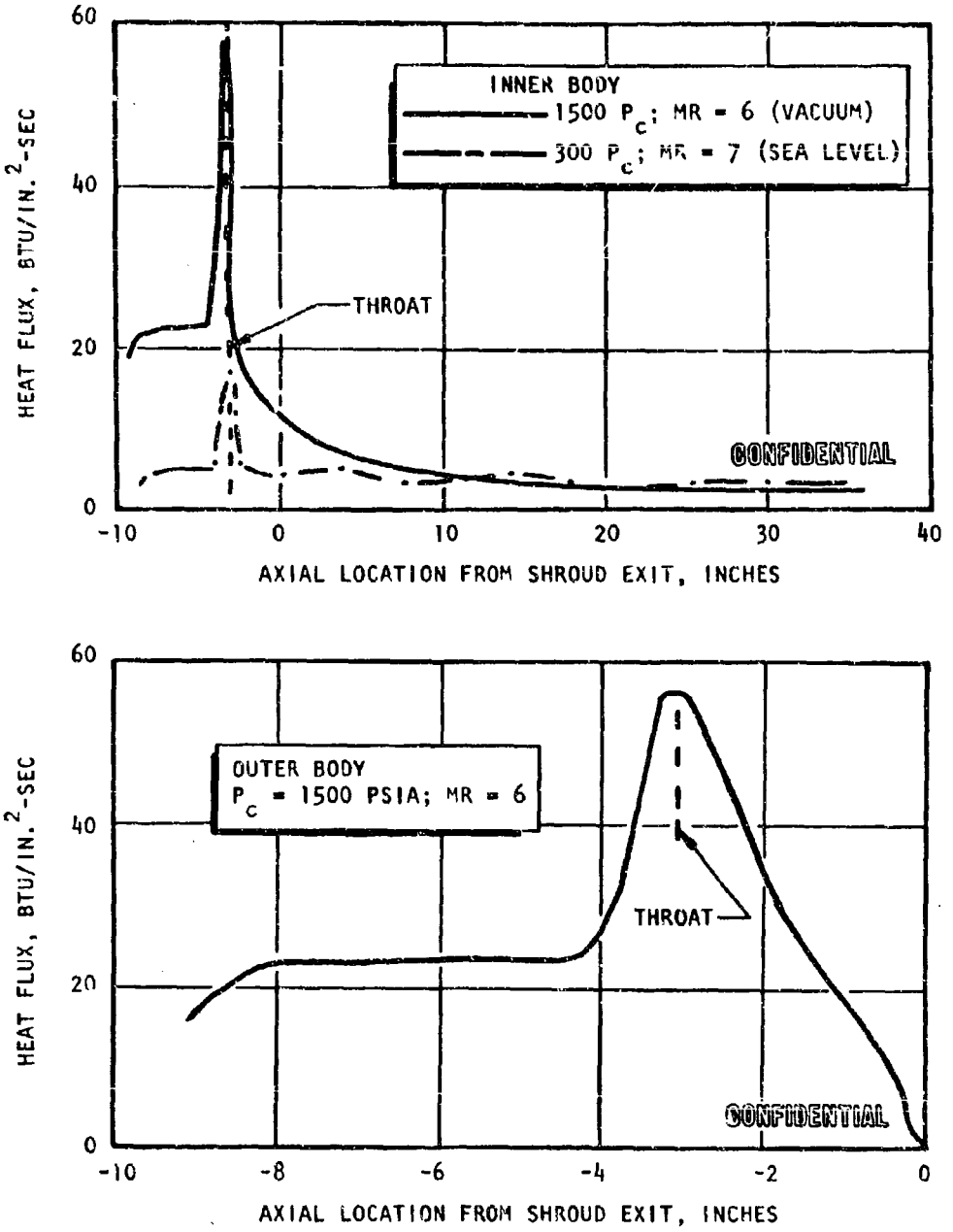

Figure 87. 250K Demonstrator Heat Flux Profiles

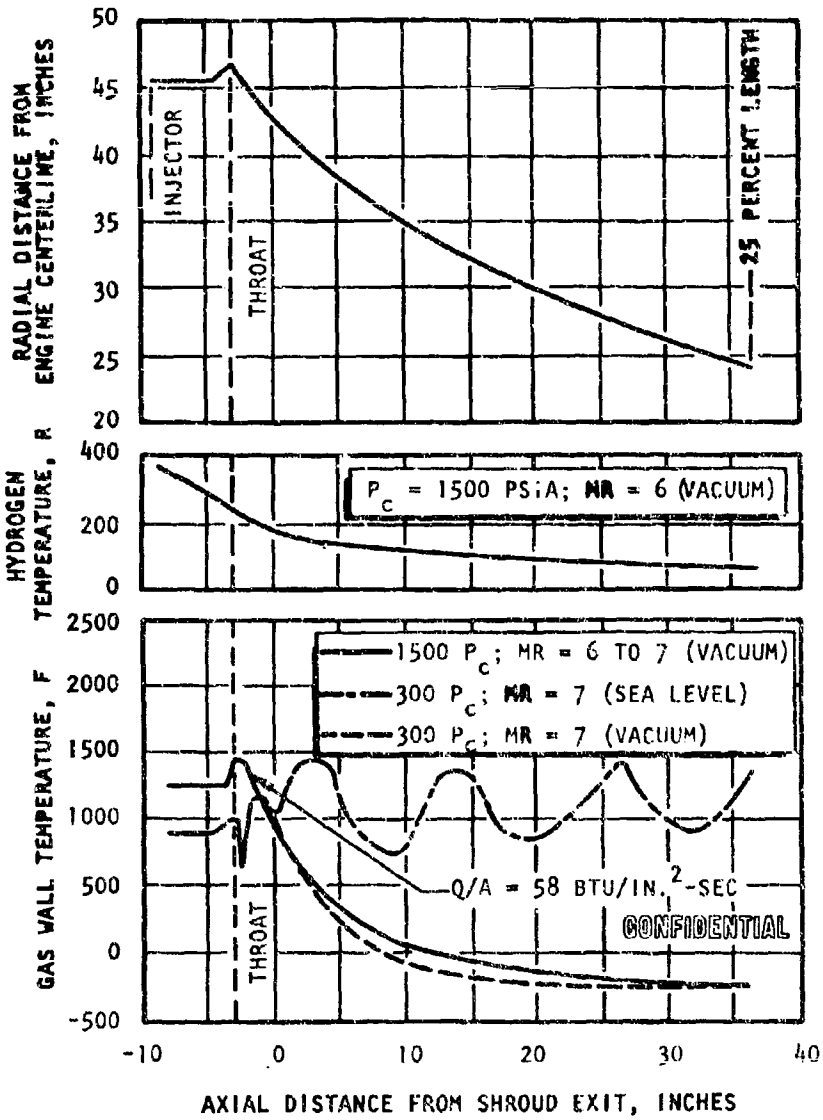

Figure 88. Demonstrator Engine Inner Body, 0.012-Inch Nickel 200 Tube

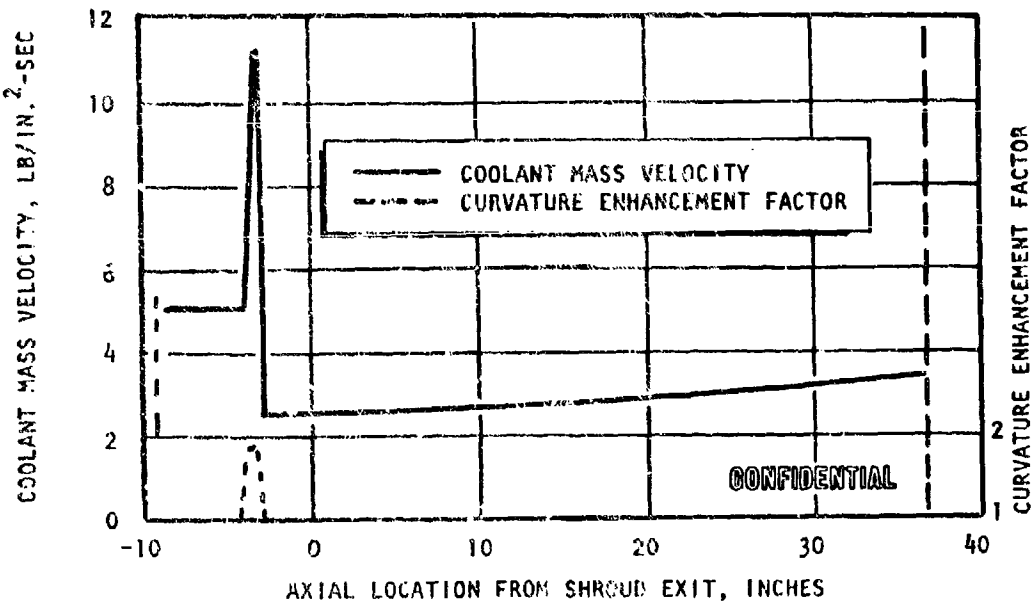

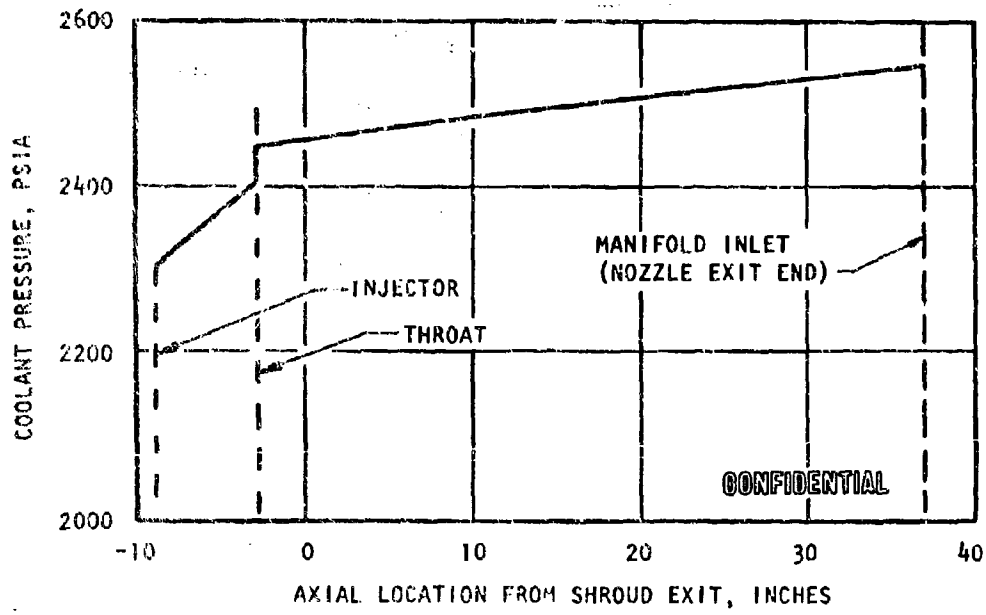

Figure 89. 250K Demonstrator Inner Body Coolant Mass Velocity and Total Pressure Profiles (P_c = 1500 psia, MR = 6)

(C) The coolant mass velocity profile is shown in Fig. 89 for the nominal operating condition. The mass velocity peak value of 12.3 $lb/in.^2$-sec occurs in the throat and is based on 1500 chamber pressure operation with a coolant curvature enhancement of 1.5 at the throat.

(U) The coolant total pressure profile is also shown in Fig. 89. There is about a 50-psi loss in the first 15 inches of tube. The principal pressure drop occurs in the throat (about 150 psi) with about 60 psi in the straight section of the combustion zone.

(C) As indicated earlier, higher heat fluxes occur at sea level because of recompression regions on the spike. While this results in higher wall temperatures, it also results in higher hydrogen bulk temperatures. Figure 90. shows the coolant bulk temperature profile for a chamber pressure of 300 and mixture ratio of 7 under vacuum and sea level conditions. The inner body tube exit temperature is predicted to be 375 R (Fig. 88) in vacuum at nominal conditions. This increases to about 520 R and 800 R at a chamber pressure of 300 psia for vacuum and seal level operation, respectively. This increase in hydrogen temperature will affect inner and outer body wall temperatures and pressure drops, as well as injector pressure drop. The difference in bulk temperature between vacuum and sea level operations becomes less at lower mixture ratios and high chamber pressures because of: (1) more coolant flow, (2) peak nozzle region heat flux is nearly independent of chamber pressure, and (3) less of the nozzle is affected by recompression zones.

(U) Outer-Body Tubes. Sea level operation should not affect the heat flux profile for the outer body (Fig. 87) except at the very shroud exit for the required engine throttling range. The outer body operating conditions are shown in Fig. 91 and 92.

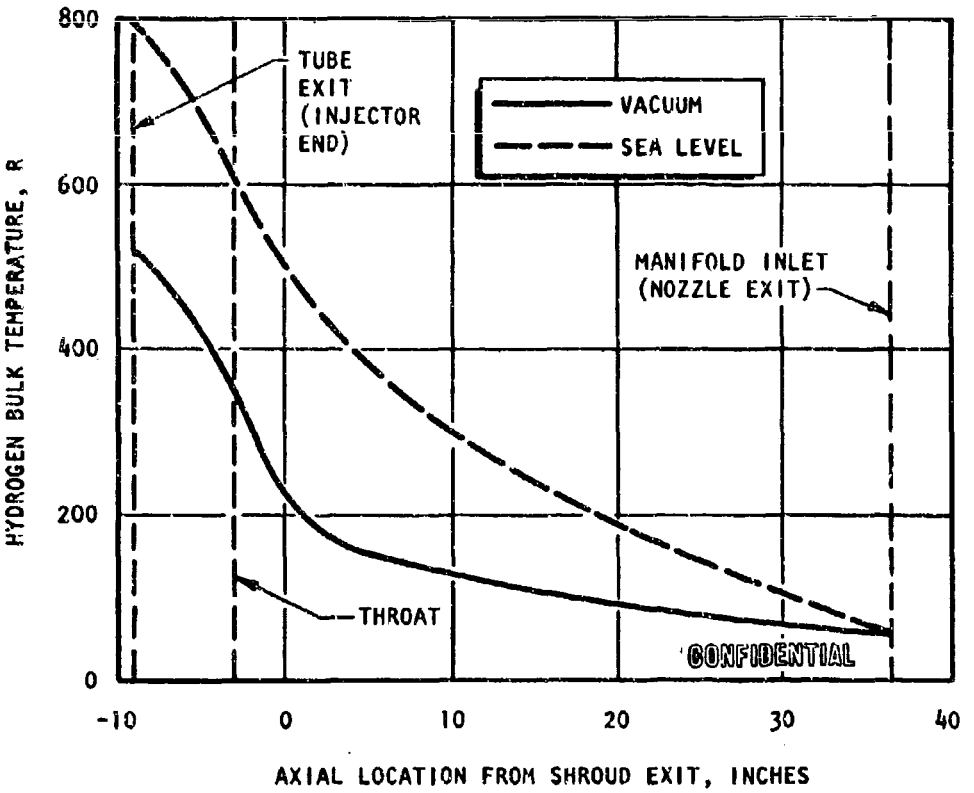

Figure 90. 250K Demonstrator Hydrogen Temperature Profile, Inner Body (P_c = 300 psia, MR = 7)

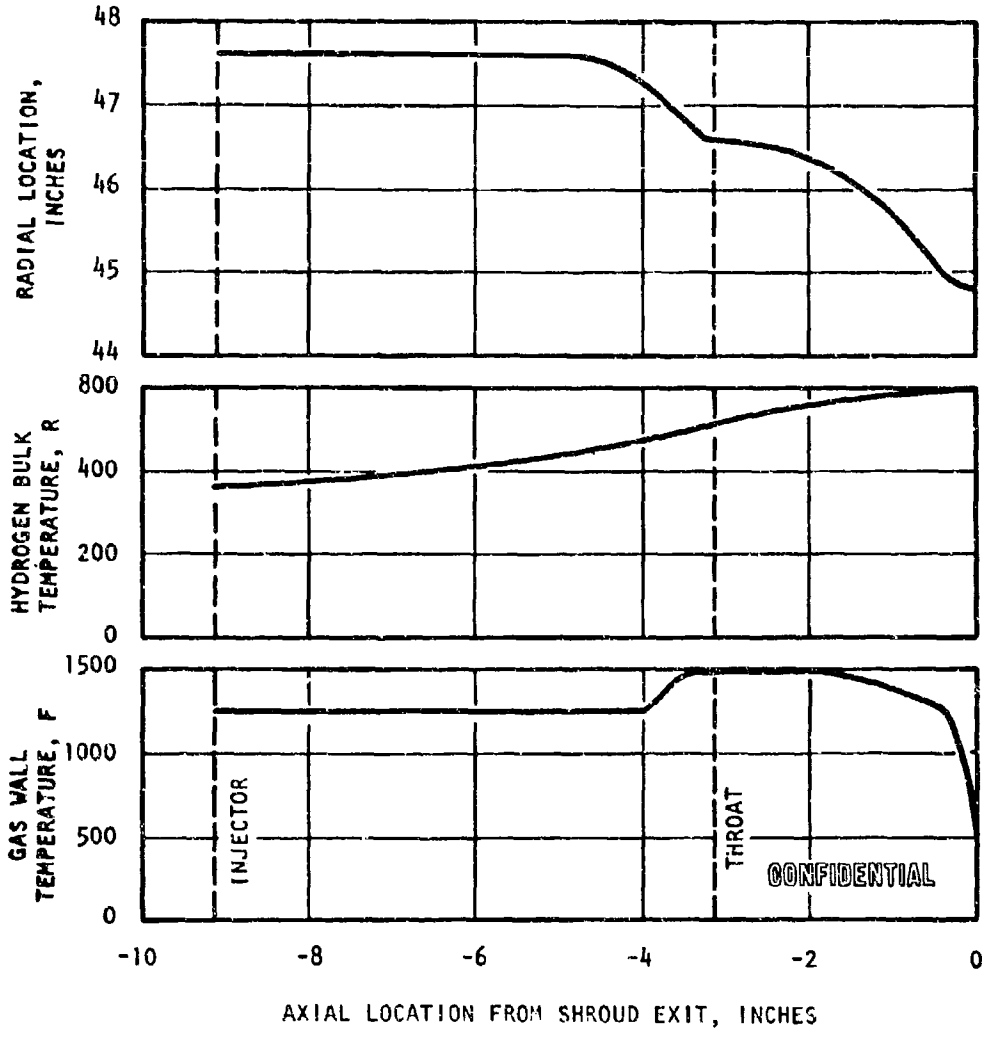

Figure 91. 250K Demonstrator Outer Body (0.010-Inch Nickel 200 Tubes)

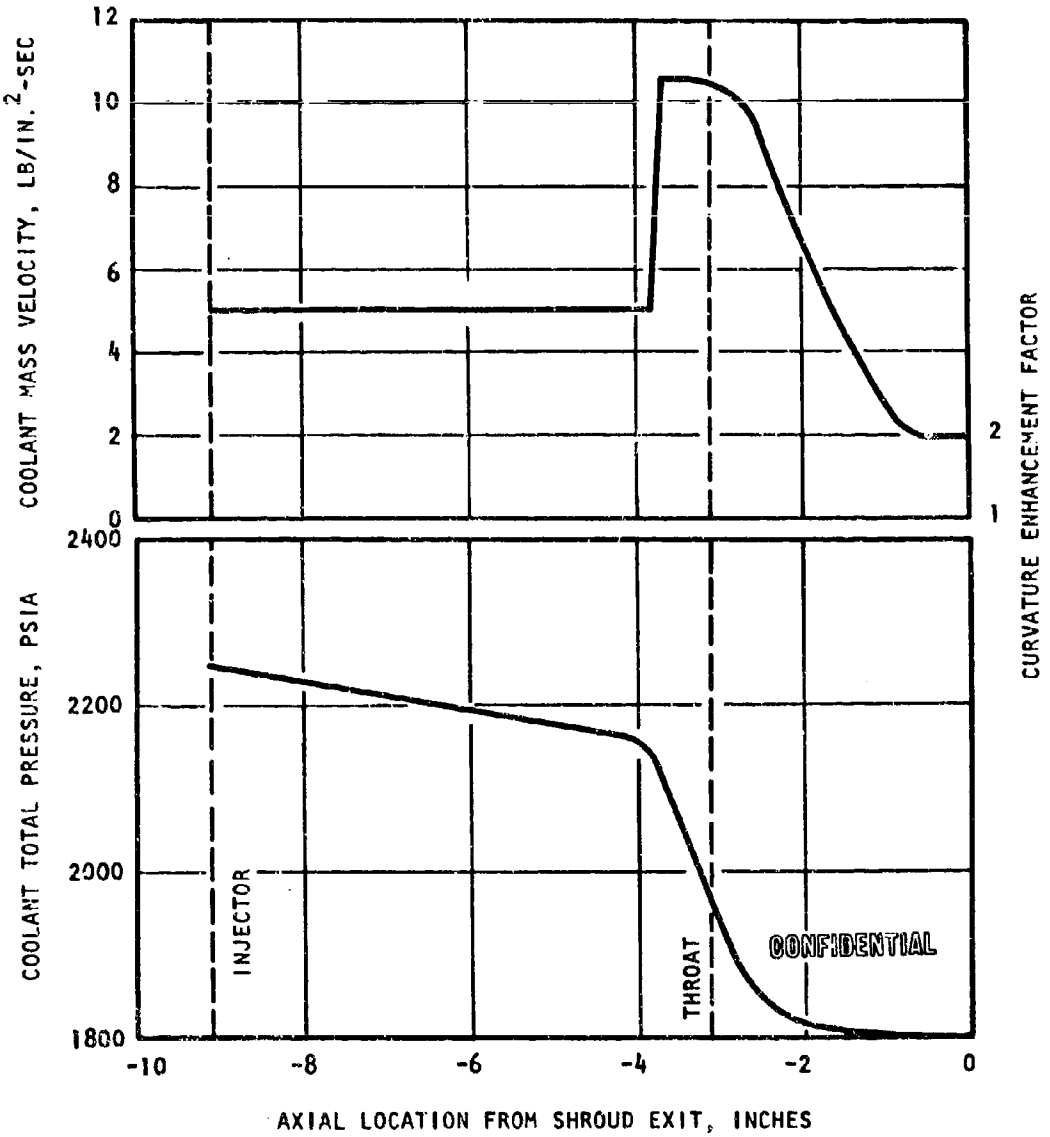

Figure 92. 250K Demonstrator Outer-Body Coolant Total Pressure and Mass Velocity Profiles

(C) The combustion chamber gas wall temperature profile shown in Fig. 91 is similar to that for the inner body upstream of the throat, with a design value of 1250 F. However, the maximum coolant mass velocity in Fig. 92 is limited on the outer body by choking considerations. A mass velocity of 10.5 lb/in.^{2}-sec was chosen which provides a peak coolant Mach number of 0.50 for a coolant throat bulk temperature of 520 R (Fig. 91) and tube exit pressure of approximately 1800 psi. Based on this mass velocity, the throat wall temperature is approximately 1520 F, assuming a curvature enhancement of 1.4 for the shifted throat design. This curvature value is based on the ratio of film coefficients between the outside and inside of the curve as measured in heated tube tests discussed previously.

(U) The pressure drop shown in Fig. 92 is somewhat higher for the outer body than the inner body because of the slower expansion, higher hydrogen bulk temperature, and lower coolant pressure.

(C) The hydrogen temperature at the injector is shown in Fig. 93 as a function of chamber pressure and mixture ratio. For a mixture ratio of 6.0, the injection temperature is approximately 600 R at full thrust and 790 R at 300 P_c for vacuum operation. At sea level, the temperature becomes 1105 R for MR = 6.0 and 1250 R for MR = 7.0 at 300 P_c. The bulk temperature of the hydrogen at P_c = 300 psia and MR's = 5, 6, and 7 is shown in Fig. 94.

(C) Subsonic Struts. Because the subsonic struts are made of copper, the maximum gas wall temperature is limited to 1000 F. The heat flux in this region of the chamber is quite low (23 Btu/in.^{2} and there is therefore no difficulty in cooling the struts with only 25 percent of the hydrogen flow. The selected orientation for the baffle cooling passages is parallel to the flow of hot gases, which results in a cooling pressure drop of 104 psi including frictional, rounded entrance, and exit losses. The inlet

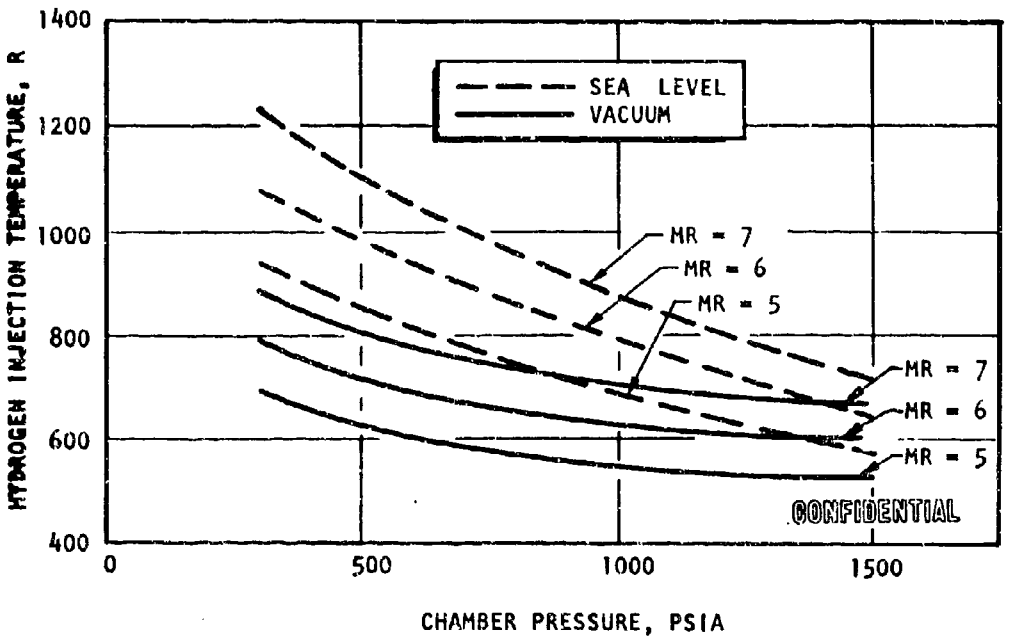

Figure 93. H_2 Injection Temperature vs Chamber Pressure (T_{inlet} = 60 R)

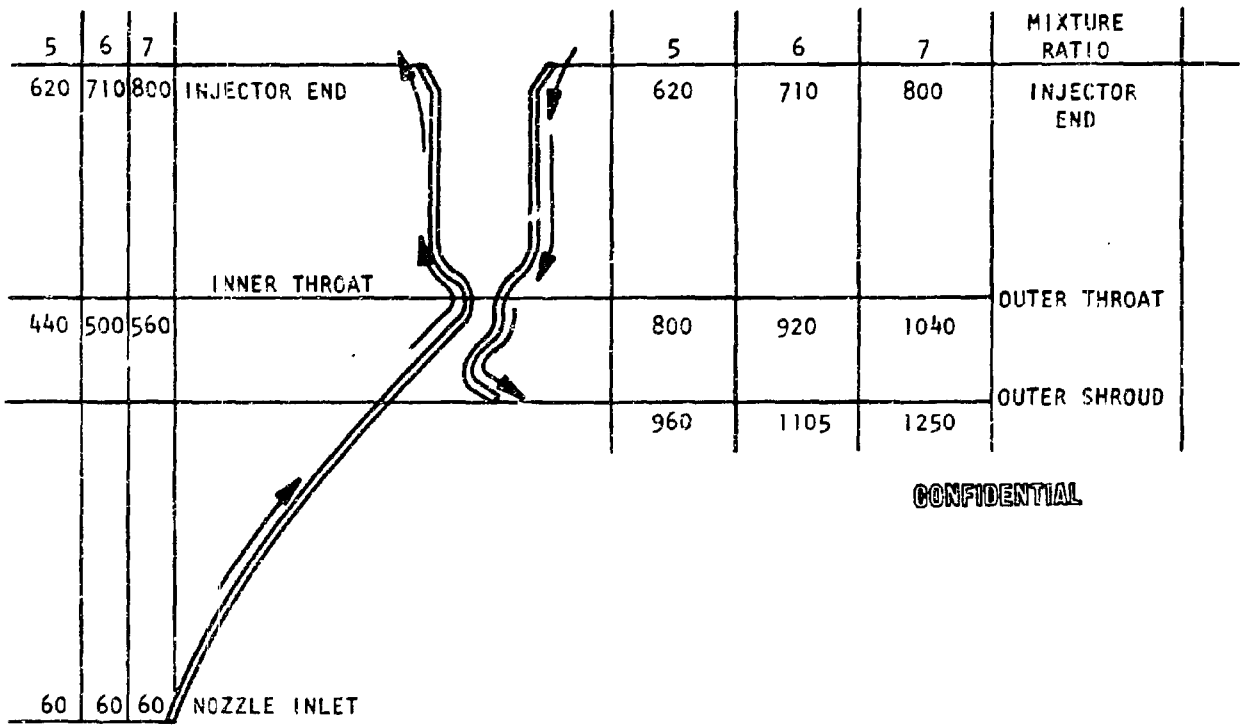

Figure 94. Bulk Temperature (R) of Hydrogen in Coolant Tubes vs MR (P_c = 300 psia, Sea Level Operation)

bulk temperature for the design condition (P_c = 1500, MR = 6) is 300 R with a temperature rise through the strut circuit of 155 R.

(U) The strut is also charged with the pressure losses associated with intercepting the flow from the inner body tubes and passing through the strut seat transfer passages. The data shown in Fig. 95 and 96 were used to determine the pressure losses through the seat and to size the transfer passage areas.

(U) Combustor and Nozzle Alternatives Studied. Tradeoff studies were conducted to select the support structure material, the support structure assembly technique, the cooling circuit design, and the possible incorporation of a tube splice in the inner body nozzle. These are discussed in the following paragraphs.

(U) Support Structure Material. The chamber wall structure has been defined as titanium alloy (6Al-4V). Nickel coolant tubes will be brazed to a thin nickel backup member (either bands or a complete sheet), which, in turn, will be epoxy-bonded to the titanium structural wall. In addition, the chamber walls will be linked together by bolting through the 40 chamber baffles. This structural tie will maintain the throat gap within acceptable limits during firing, and will result in a significantly lower chamber weight over an unlinked design.

(U) This design approach resulted from a parallel and competitive design study which compared a conventional Inconel 718 structure (Fig. 97), and more advanced structural concepts of honeycomb (Fig. 98), and press diffusion-bonded titanium (Fig. 99) with the selected configuration (Fig. 67, page 163). The criteria for selection in this design study were weight, manufacture and assembly, cost, and experience. The conclusions are presented in Table 25. The more advanced honeycomb and diffusion-bonded titanium designs will require development of the specific

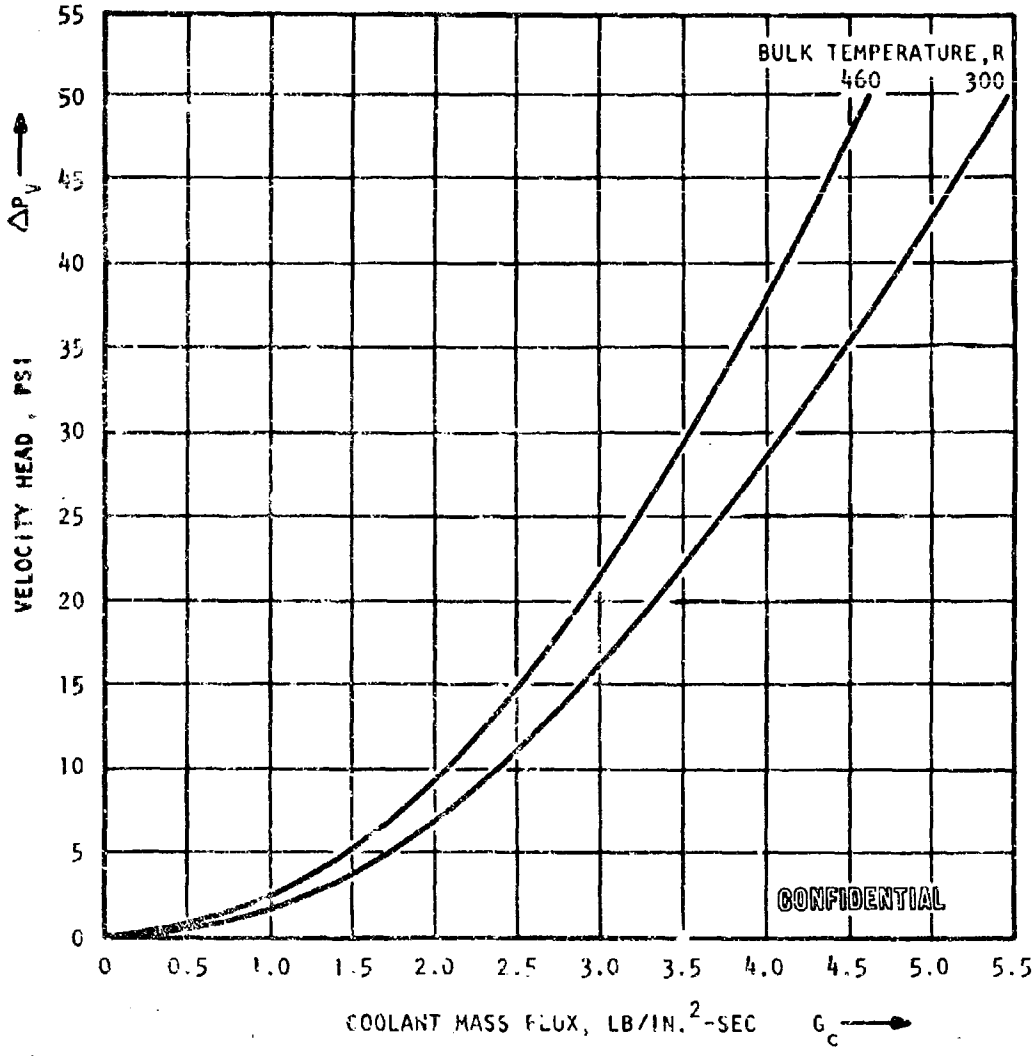

Figure 95. Hydrogen Velocity Head as a Function of Mass Flux for Transfer Passage Design

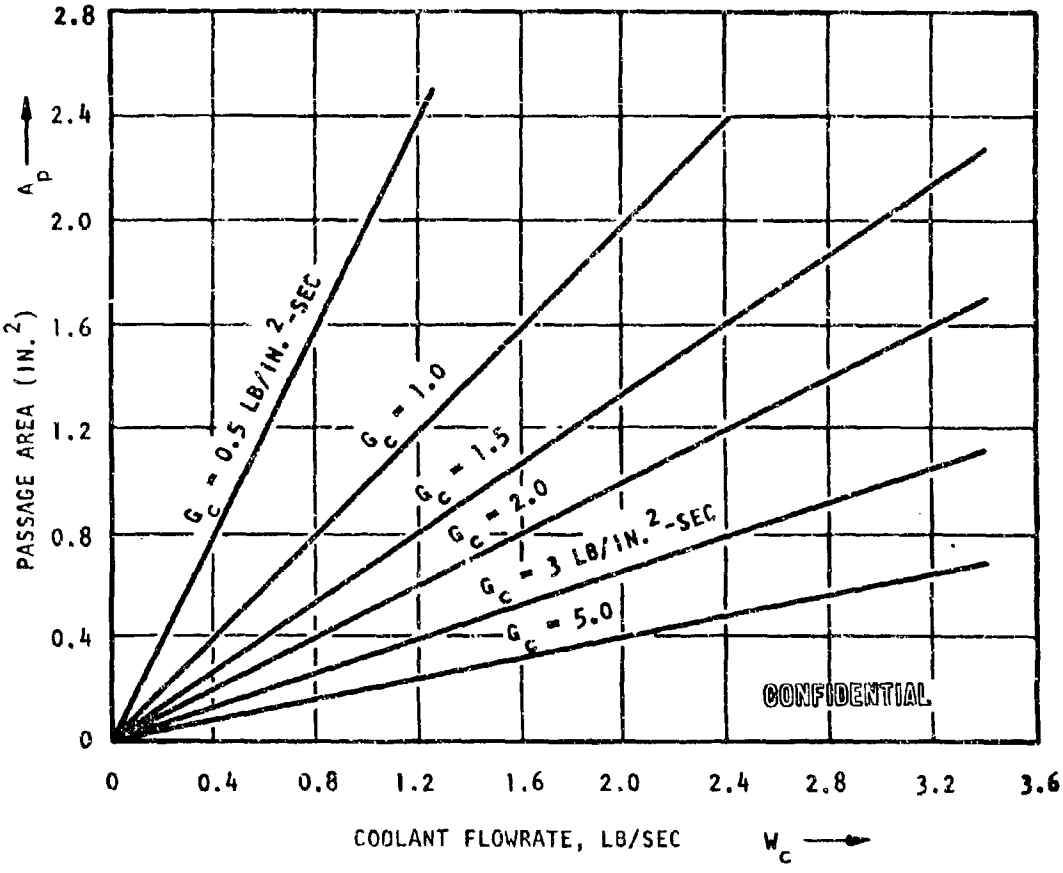

Figure 96. Coolant Passage Area vs Flowrate for Selected Mass Flux

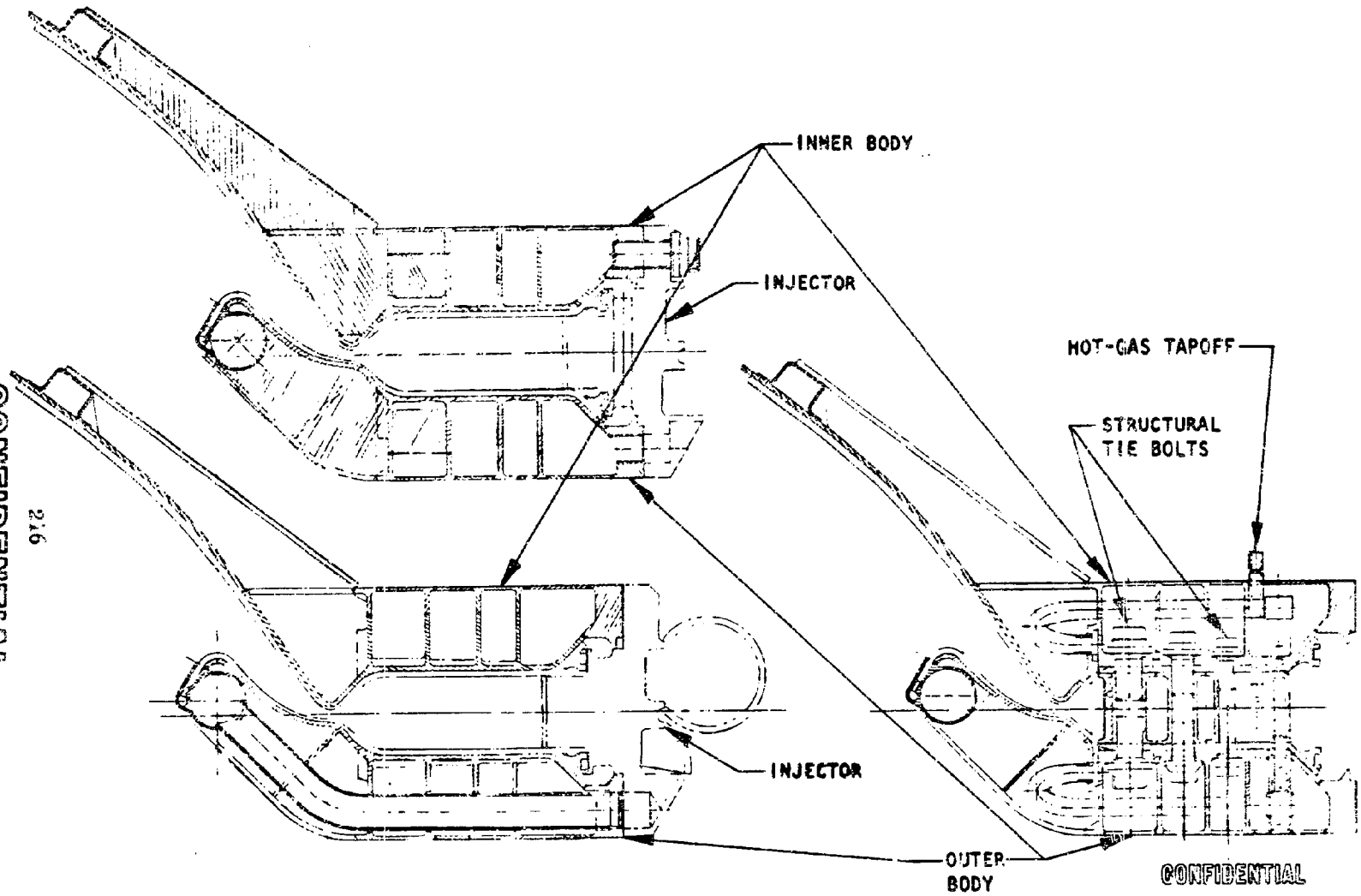

Figure 97. Conventional Inconel 718 Structural Concept, 250K Aerospike Thrust Chamber Demonstrator Module

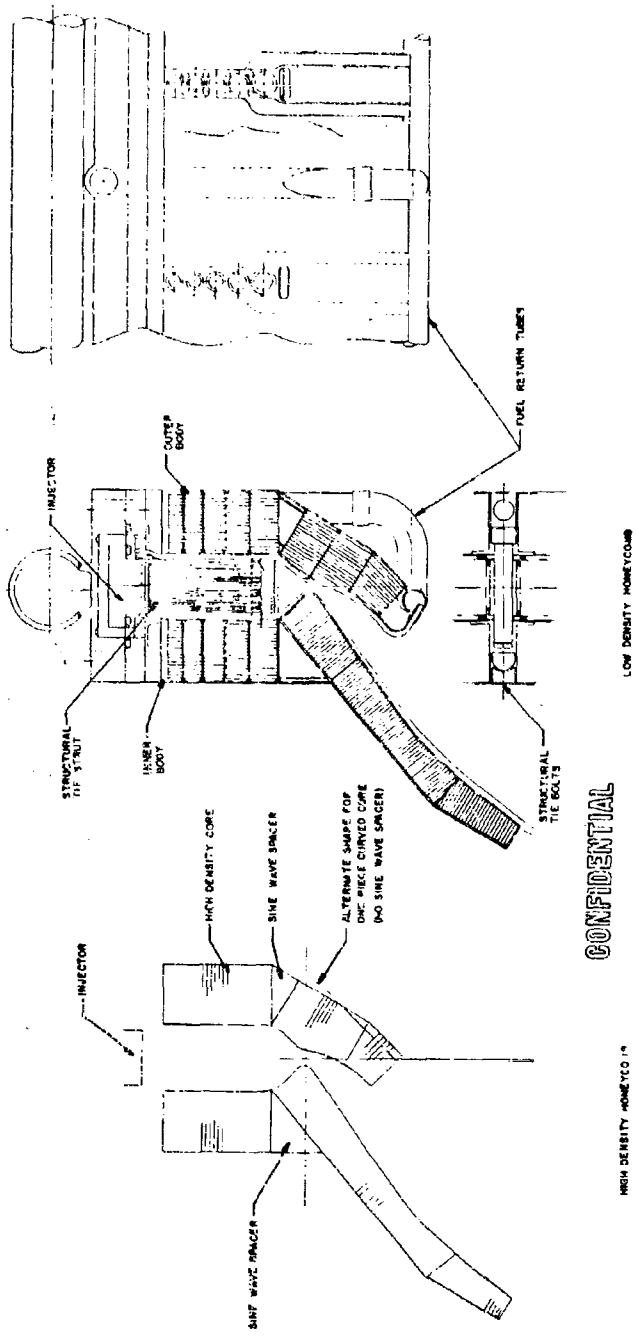

Figure 98. Demonstrator Chamber Study (Honeycomb Structure)

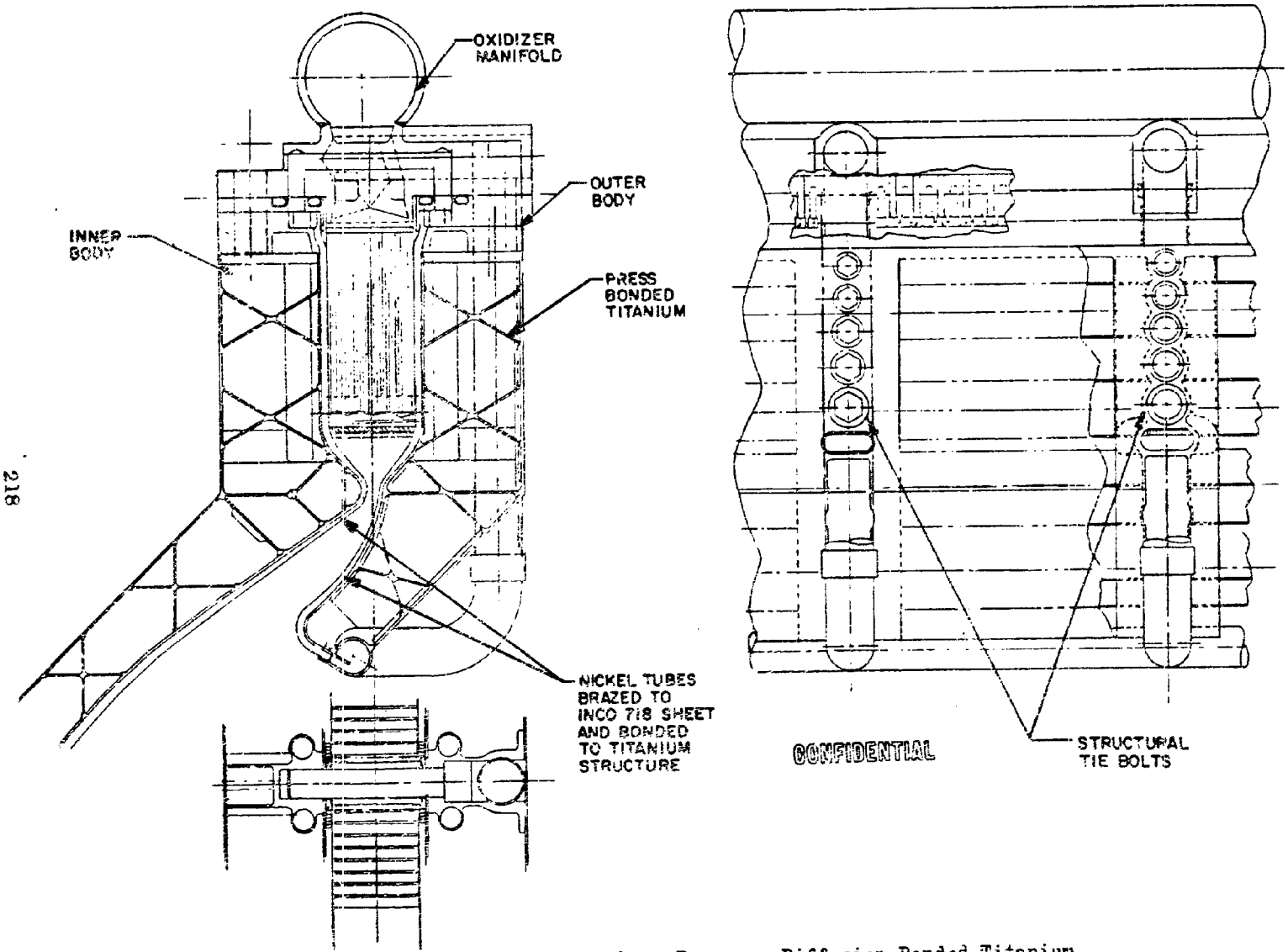

Figure 99 Demonstrator Chamber, Pressure Diffusion-Bonded Titanium

fabrication method, which would require more time than available for the demonstrator module. They were, therefore, eliminated for the demonstrator and 20K segment. They do point out the potential of advanced fabrication techniques for the Flight Module.

(U) Titanium was selected for the chamber wall structure because of its extremely high strength-to-weight ratio. A weight saving of approximately 200 pounds can be realized with titanium over an INCO 718 configuration. Fabrication of the titanium wall will be achieved by machining a ring forging to the configuration required to yield the highest strength-to-weight design. This method was selected over a machined and welded assembly because it can be designed to higher stress levels because of the absence of welding.

(C) TABLE 25

DESIGN COMPARISON STUDY

Design	Chamber Weight	Experience	Manufacture and Assembly	Cost
Machined INCO 718	990	State-of-the-Art	Difficult to machine	Moderate
Machined Titanium	750	Semiadvanced	New assembly techniques required for epoxy assembly	Moderate
Titanium Honeycomb	650	Advanced	Difficult to machine and assembly	High
Diffusion-Bonded Honeycomb	600	Advanced	Extremely difficult to assemble	High

(U) Assembly Techniques. An assembly concept using 360-degree continuous titanium structure for inner and outer bodies and segmented tube sections was compared to the chosen 360-degree brazed tube bundle and segmented titanium structure. The former combination made mandatory braze

and weld operations after adhesive application and magnified segment tolerance and fit-up problems. Until technology in these areas is advanced, the adoption of the potentially lower-cost, segmented-tube bundle concept will be deferred.

(U) Mechanical joining of segments has been substituted for the electron-beam welding which had been considered earlier. This was done despite a potential weight increase, because of manufacturing and processing problems defined in a more detailed investigation. Among these are dimensional control of the segment fit to ensure a satisfactory joint penetration control of the electron beam to preclude adhesive and tube damage, and control of the welding atmosphere in the presence of adhesive to ensure a sound joint. The mechanical joint contemplated employs tensile bolts between the titanium segment flanges and line-drilled shear pins for alignment and shear-carrying capability.

(U) Two concepts (Fig. 100) were studied for the structural tie between the inner and outer bodies. The first was the selected tie through the chamber baffles, while the second was to employ separate structural ties in the subsonic portion of the combustor immediately upstream of the throat (Fig. 100a). Chamber stability baffles would still be required with this design.

(C) The initial results of this study indicated that 80 subsonic ties together with 40 stability baffles would yield the lightest-weight chamber assembly. Detailed design and analysis revealed that with 80 preloaded ties, the predicted weight increased, while the amount of chamber blockage increased the heat flux on this tie from approximately 15 Btu/in.^{2}-sec to 28 Btu/in.^{2}-sec, and therefore increased the coolant pressure drop required to cool the tie. Furthermore, with both a subsonic tie and a stability baffle to cool, the hydrogen coolant circuit became undesirably complex. For these reasons, the 80 separate structural tie design was abandoned in favor of using bolts through the 40 baffles.

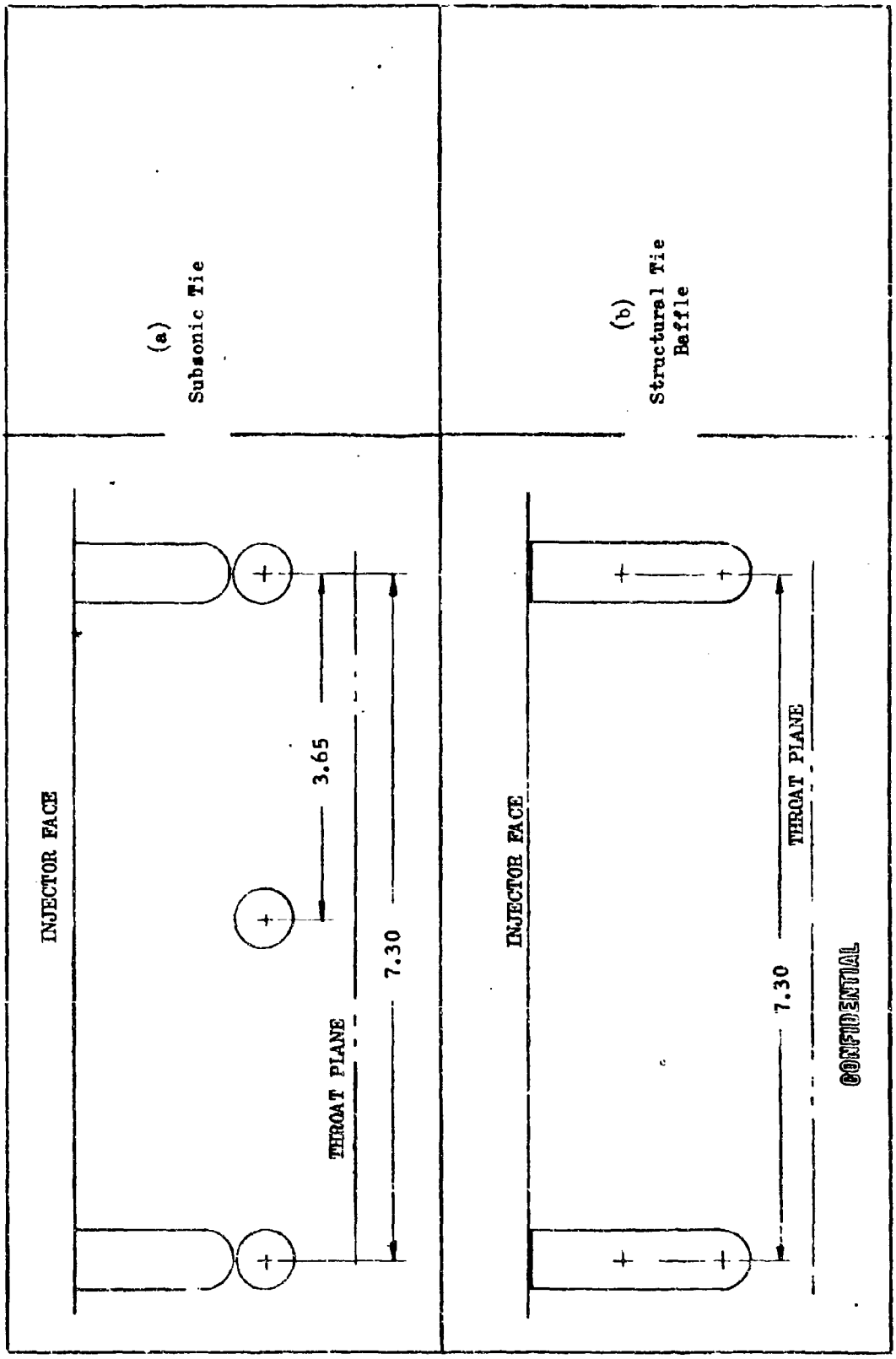

Figure 100. Structural Tie Concepts

(U) Coolant Circuit Alternatives. Several different cooling circuit designs were studied before the final series circuit was selected. The two initial candidates were a separate baffle cooled with the flow intercepted by the baffle seat and the remainder of the inner body tube flowrate crossing over to the outer body through the injector (Fig. 101A) and an integral baffle cooled by all of the fuel collected in a manifold in the injector (Fig. 101A). These two designs are shown together with the final design in Fig. 101B). The final design incorporates a separate baffle with all of the flow crossing over from the inner body to the outer body through the baffle and using a portion of this flow to cool the baffle. The circuit ΔP's shown in Fig. 101 represent the increase in cooling circuit pressure loss over a reference circuit which has no baffles. The selected circuit combines the most desirable features of the two configurations shown. In this design, both the pressure drop and bulk temperature rise of the separate flow paths have been balanced before they are combined in cooling of the outer wall immediately upstream of the throat. Furthermore, the baffle is separated from the injector assembly, which ensures easier installation of the injector on the chamber wall assembly, and the injector is smaller because it does not have to provide room for crossover passages.

(U) Tube Splice. Two configurations were considered for the inner tube wall: 4240 single tubes extending from injector end to the exit, and 4240 single tubes in the combustor to a point approximately 4.0 inches downstream of the throat, which are then spliced (two to one) to 2120 tubes extending to the exit. Both configurations were evaluated with respect to pressure drop, fabricability, weight, and cost with the following results.

(C) The use of single tubes extending the full length of the inner chamber wall imposes a pressure drop penalty of 100 psi over the spliced configuration. In addition, the "splice" subassembly affords a weight reduction of approximately 50 pounds. These advantages are tempered, however, by added fabrication and tooling costs required to braze and flow check the three-piece subassembly in addition to each individual section. The 2:1 splice joint configuration shown in Fig. 67 and located approximately 4.0 inches below the throat plane was selected for the inner wall of the Demonstrator Module thrust chamber based on pressure drop and weight factors.

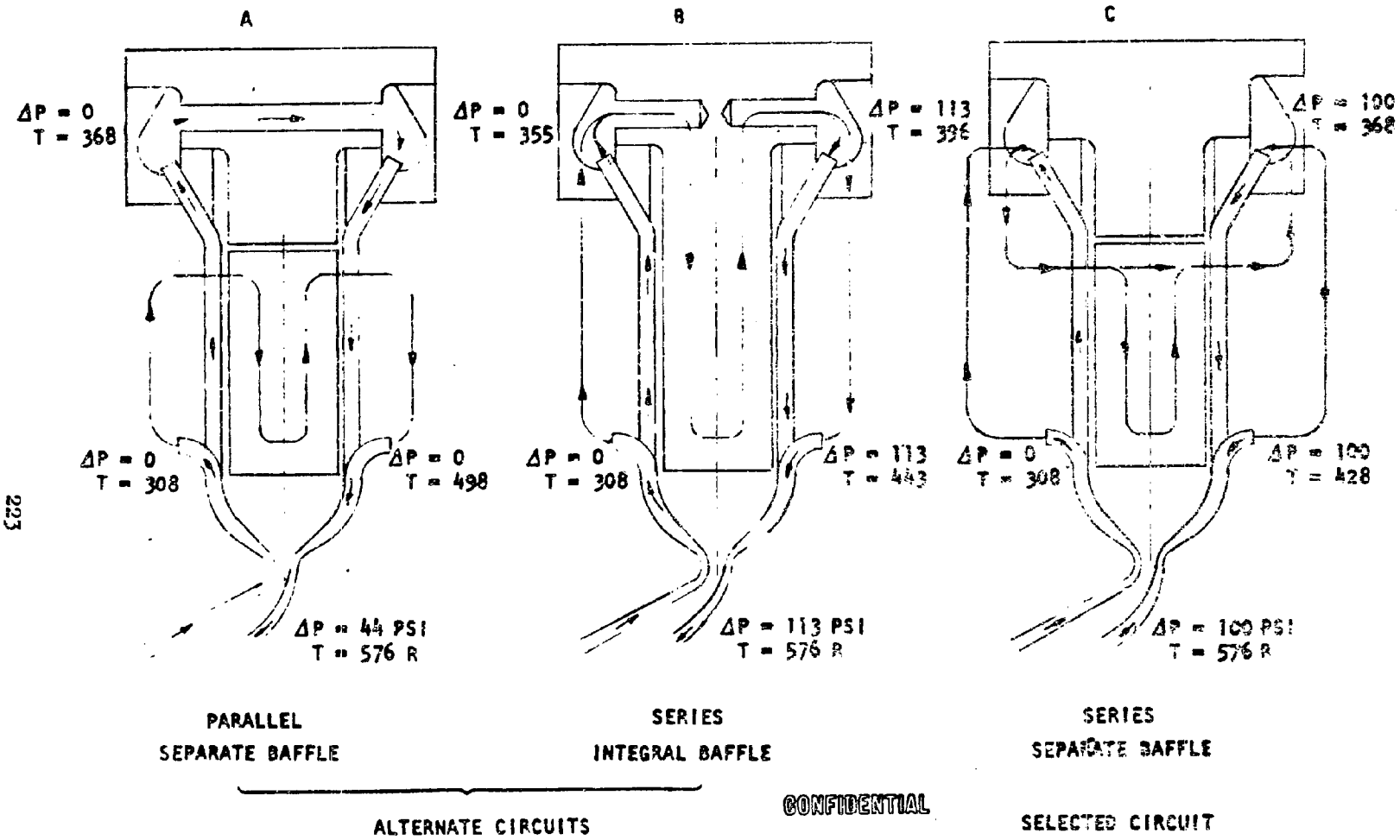

Figure 101. 250K Flow Circuits

(U) Injector Design Description. The injector forms the forward closure of the combustion chamber and is an assembly of copper-orifice strips, LO_2 and GH_2 propellant manifolding, and a structural body (Fig. 67).

(U) The injector is designed to resist thermal contraction loads by piloting on the upper seal rings of inner and outer bodies. Internal pressure-separating loads are carried through the attaching bolts to the inner and outer bodies. External loads induced by differential thrust are taken through the subsonic struts, and thus do not affect the injector. Several configurations were considered for the Demonstrator Module injector, all of which were based on the 40-compartment combustor and the orifice strip design demonstrated during Task II testing. The design aspects of the selected injector are shown in Table 26.

(C) TABLE 26

INJECTOR DESIGN PARAMETERS

Mean Injector Diameter, inches	93.0
Injector Face Width, inches	2.0
Number Injector Compartments	40
Number Strips Per Compartment	6
Total Number Injector Strips	240
Diameter, Fuel Orifices, inch	0.085
Diameter, Oxidizer Orifices, inch	0.040
Injection Pattern	Triplet, two oxidizer

(C) The injector face is divided into 40 compartments, 2 inches wide by 7 inches long, physically separated by structural subsonic struts when assembled to the thrust chamber. Each compartment thus formed is composed of six copper strips (which contain both LO_2 and LH_2 injection orifices) extending radially across the width of the combustor compartment. Figure 102 is a detail drawing of the Demonstrator Engine Injector Assembly.

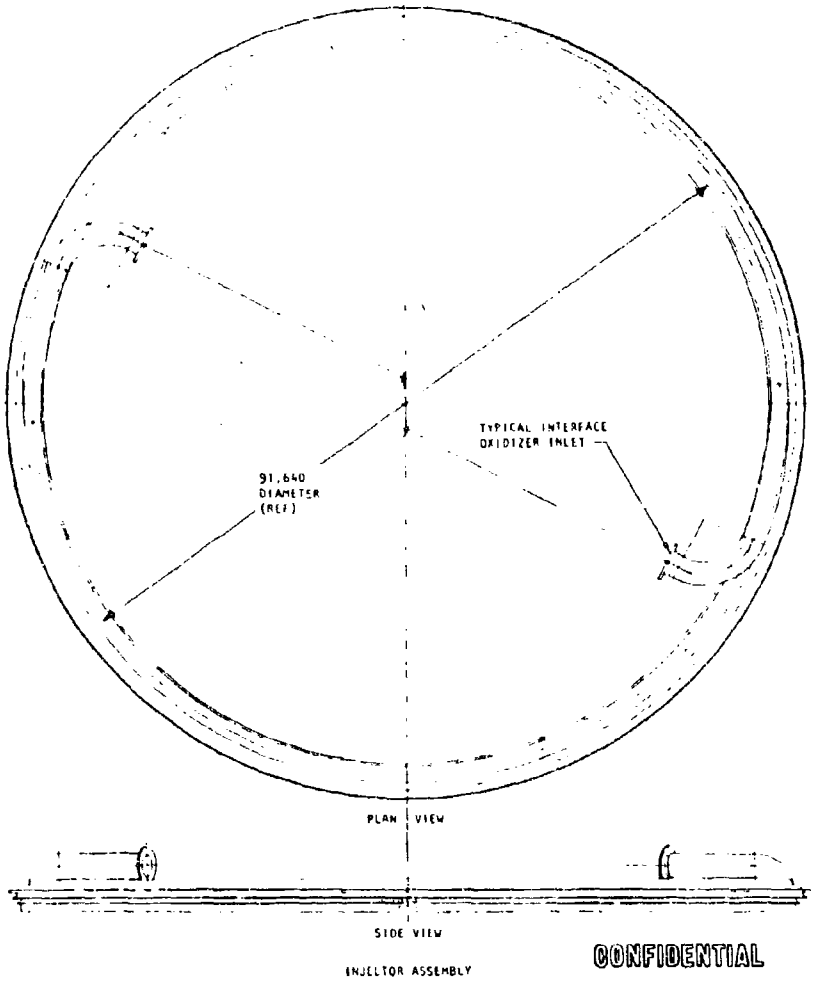

Figure 102A. 250K Demonstrator Engine Injector Assembly

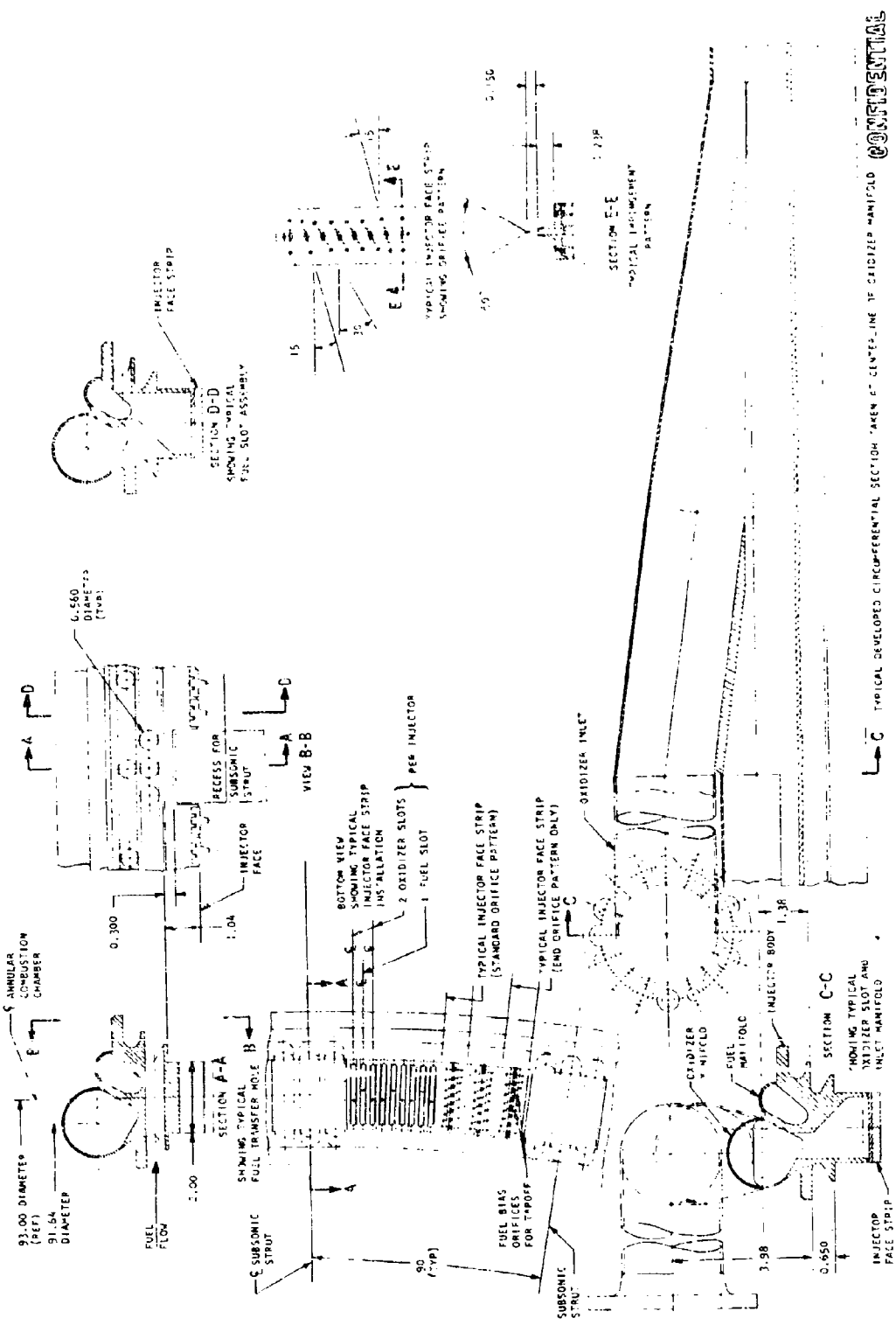

Figure 102m. 250K Demonstrator Engine Injector Assembly

(C) The injector face pattern is similar to those used in Phase I. Each strip contains eight triplet patterns (two oxidizers on one fuel). LH_2 is injected through the center of each orifice strip from the apex of the "steeples." Two LO_2 orifices in the flat surface on either side direct oxidizer which impinges with LH_2 streams 0.160 inch downstream of the "steeple." The triplet pattern formed utilizes the injected hydrogen to atomize the LO_2 streams through shear action (momentum exchange). The raised "steeple" prevents injector face burning by reducing hot-gas recirculation against the face. The "baffle" effect formed by this geometry is also an aid in stabilizing combustion.

(U) Electrical discharge machined flow passages in the injector body connect the fuel and oxidizer manifolds directly to the orifice strips. Entrance to the LO_2 toroidal manifold is made through two tangential inlets to ensure good distribution under all operating conditions. The smaller LH_2 toroidal manifold is fed by 40 "riser" tubes bringing flow from the outer body exit manifold. The LO_2 toroidal manifold is fabricated from INCO 718 shells welded to the central body.

(U) Fuel transfer holes are provided in the central body through which jacket coolant flows from the inner body to the outer body. These passages are located over each strut between compartments. A small deflector on the outboard side aids in curbing the flow with minimum turbulence.

(U) Provision is made on the injector body in a manner similar to that used on Task II hardware for installation of instrumentation in critical locations. Oxidizer manifolding will contain bosses for installation of such instrumentation to record inlet pressures and temperatures and gradients from inlets to the remotest distribution point. Provision for recording chamber pressure in several compartments is made through a hydrogen strip by means of 0.125 diameter pressure probes, secured to the body exterior. The probes are inserted through the body, an H_2 electrical discharge-machined (EDM) feed slot, and through the strip, and then are sealed against external leakage.

(U) Injector Assembly Analysis. An experimental study was conducted (using 2.5K toroidal combustion chamber segments that resulted in: (1) achievement of performance and operational goals, and (2) selection of an injector pattern for a full-scale (250K) injector design for the Aerospike Engine. The pattern chosen was the result of experimental screening through hot firing of numerous candidate injector patterns, all of which were applications of basic injector design principles to the requirements listed in Table 27. Further design considerations of the injector and the LO_2 manifold are discussed in the following paragraphs.

(C) TABLE 27

DESIGN REQUIREMENTS—INJECTOR

c* Efficiency	
at Maximum Thrust (250K at MR = 6:1)	99.6
at Minimum Thrust (50K at MR = 6:1)	98.5
Propellant	
Oxidizer	LO_2
Fuel	GH_2
Oxidizer Flowrate, lb/sec	
Maximum	523.6
Minimum	90.4
Injector Inlet Pressure, Oxidizer, psia	
Maximum	2126
Minimum	335
Fuel Flowrate, lb/sec	
Maximum	86.2
Minimum	14.0
Injector Inlet Pressure, Fuel, psia	
Maximum	2033.0
Minimum	396
Ignition Medium	Hot gas
Ignition Flowrate, lb/sec	3.69

(C) Injector Performance. By use of a fan triplet pattern, c* efficiencies greater than 98 percent at low chamber pressures (325 to 937 psia) and better than 99 percent at high chamber pressures (up to 1500 psia) were demonstrated with strip injectors in the 2.5K segment tests in Task II, "Injector Performance Investigation."

(U) Ignition and Tapoff Considerations. The injector was designed on the basis of requirements imposed by the use of hot-gas tapoff and hot-gas ignition. The injector design selected is ideal in this respect in that the orifices in each strip adjacent to the struts, through which the hot gases flow, can be adjusted to provide a low mixture ratio bias for low-temperature tapoff gases and yet not obstruct the hot-gas ignition source. This strip adjustment was initially accomplished by plugging LO_2 orifices and adding hydrogen orifices. Further adjustment of these features and of stream location and angle is possible. Since these changes are made on only two strips per compartment, and in a local zone, no significant change in overall performance results is anticipated.

(U) Stability Considerations. Combustion stability is an important criterion for injector design. In general, three types of combustion instability can be identified as oscillations driven by energy sources in: (1) the combustion chamber alone (so-called acoustic instability), (2) the feed system alone, and (3) both of these subsystems with coupling between them (so-called chugging instability). The first and third types are not only the most frequent, but can be influenced by the injector design.

(C) Because of the short length of the annular combustion chamber, cross-sectional modes of acoustic instability are all of such high frequencies

that they are not expected to occur. The first longitudinal mode for the 6-inch-long chamber is approximately 5500 cps; liquid rocket instabilities at frequencies greater than 4000 cps are usually nonexistent. No instances of sustained cross-sectional modes have been recorded in all annular combustion chamber tests accomplished to date.

(C) Circumferential (race track) modes, which are acoustic instabilities of the lowest frequency that can occur in an annular combustion chamber, have been computed to be approximately 220 cps, based upon a mean diameter of 93 inches and a sonic velocity of 5500 ft/sec for the combustion gas. Higher-order resonances will have frequencies which are integral multiples of 220 cps. It is in this mode that an injector design, if prone to acoustic instability, will manifest itself in the annular combustion chamber. The subsonic struts, which are to be used for structural support, will serve as damping devices for this mode.

(C) Recent tube-wall thrust chamber testing has also shown thrust chamber and LO_2 torus pressure oscillations in the 220 cps frequency range. Examination of the torus pressure reveals a phase shift which definitely identifies a circumferential pressure wave in the system. The frequency of 220 cps corresponds to a propagation time of 4.5 milliseconds. Since LO_2 has an acoustic velocity of 3000 ft/sec, and the torus mean circumference is 24.3 feet, a wave propagated through the torus will require approximately 8.1 milliseconds to complete one cycle. The observed 4.5-millisecond propagation time is therefore a reflection of the first acoustic mode in the thrust chamber combustor. It appears very probable that incomplete compartment separation was the cause of the circumferential pressure oscillations. The Demonstrator Module will utilize the subsonic struts as an integral part of the structure and all gaps will be closed.

(U) Chugging instability is a coupled phenomenon between the thrust chamber combustion process and the propellant feed system. Of the several types of combustion instability, chugging is probably the best understood and therefore the easiest to predict and eliminate. In a thrust chamber utilizing hydrogen as a regenerative coolant, hydrogen becomes very compressible near the injector face and will not participate in chugging instabilities. The oxidizer then becomes the propellant which is of interest when discussing chugging. Chugging has been observed during both solid- and tube-wall, full-scale testing.

(U) For the Demonstrator Module injector configuration, two effective areas exist for controlling chugging threshold. The first concerns the oxidizer injection velocity and is often referred to in terms of injector pressure drop. Increasing the velocity will reduce the chugging tendency. A second area of effective control involves the feed passages from the oxidizer torus to the injector. A smaller diameter increases the fluid inertance and tends to decouple the combustor from the LO_2 torus.

(U) LO_2 Manifold. The design requirements for the 250K Demonstrator Module LO_2 manifold have been developed based on the following generalized oxidizer manifold design criteria:

Item	Criterion
Oxygen Quality for Ignition	Gas
Differential Priming Time	Balanced ignition
Design	No pockets for gas or dead ends
Static Pressure Distribution	±4 percent
Torque	No additional system weight
Roll Impulse (volume), ft-lb sec	1000

(C) These criteria are based on experimental cold-flow (LN_2) and water-flow results of a full-scale, four tangential inlet manifold, and 1/4-scale transparent models of the four tangential, the two tangential, and the two radial inlet types tested under the NASA System and Dynamics Investigation Advanced Engine Aerospike. Based on these criteria, the following specific design requirements for the 250K Demonstrator Module LO_2 manifold have been developed:

1. The manifold torus should be a constant cross-section manifold.
2. There should be no dead ends in any section. With a constant cross-section manifold this would imply complete circulation from one sector to the other.
3. The inlets should be of the tangential type.
4. The number of inlets to the torus depends on the desired volume of the manifold, the maximum velocity, and the allowable differential prime time.
5. The inlets may be located on either the top or the inside of the manifold, and the inlet should intersect the manifold torus in a tangential manner.
6. The inlet should have the same diameter as the manifold torus, and the transition zone between the inlet and the torus should occur in a minimum of 25 degrees of arc.
7. Central location for the origin of the inlet ducts or a uniform length of all lines will not be required. Acceptability of a given design will be based on an evaluation on the individual merits of the design. However, as a general ground rule, all inlet line configurations should have one-half engine symmetry, and the differential line length between the shortest and longest pair should not differ by more than 30 percent.
8. To maintain a ±4 percent static pressure distribution, the maximum manifold velocity should be 60 ft/sec.

9. The number of "downcomers" will be controlled by the injector requirements. For the current injector design, three downcomers per baffled compartment should be employed.

10. The downcomers should be located in the outside section of the manifold.

11. The mass of the manifold with respect to the vapor-forming potential must be considered and maintained at a minimum.

(U) The specific design requirements were based on criteria developed from LN_2 cold-flow testing of the LO_2 manifold. It is possible that hot-firing engine data could modify these criteria, which could lead, in turn, to modification of the specific design requirements. One of the more stringent requirements, from the standpoint of engine system design, is the number of inlets. In general, more inlets produce smaller manifold volumes and/or lower manifold velocities. In addition, the greater number of inlets produces the smaller differential prime times. (The differential prime time is defined as the time between ignitable quantities of oxidizer discharged through all orifices.) While there is strong experimental evidence to indicate that the minimum number of inlets (from an operational standpoint) should be no less than four (and possibly more), final evaluation of both the minimum number of inlets and the minimum manifold volume will depend on the complete hot-firing test results.

(U) Injector Alternatives Studied. Several materials were appraised for use as the structural body of the Demonstrator Module injector. Design considerations included: (1) minimizing weight, (2) providing assurance of primary leak path repair by hand brazing, and (3) minimizing manufacturing development by utilizing techniques developed during the Phase I program. Materials considered were INCO 718, Inconel 625, and CRES 347. The Inconels presented problems in either TIG braze repair or confidence in attaining adequate braze of strip to body. CRES 347 was chosen as the material offering the best compromise between fabricability, repairability, and weight.

(U) The injector configuration was fixed as an axially bolted design with separate baffles. The injector body is held in place by two titanium retainer rings which are axially bolted to the combustor body. The concept is shown in Fig. 103a in comparison to an alternate method of attaching the injector, as shown in Fig. 103b. In the latter design, the axial bolts are placed through a steel flange extension of the injector. The retainer ring design was selected in preference to the steel body flange design because of lower weight and cost estimates.

(U) The decision to use the axially bolted concept was made after comparison with an integral baffle-injector design which utilized the upper structural tie bolt as a shear connection. The integral concept provided restraint against hydraulic and pneumatic separating loads and offered a potential large weight reduction. The concept, shown in Fig. 104, will be analyzed for growth from the bolted concept for application on the flight configuration. Alignment, the necessity for injector preload and line drilling for installation, and questionable component interchangeability are problems which must be solved before this lightweight configuration can be adopted.

(U) Base Closure Description. The perforated base closure used with aerospike thrust chambers provides the means for introduction and distribution of turbine exhaust gases into the inner-body base region to increase base thrust. Criteria for design of the base closure included:

1. Compatibility with engine system components regarding deflections and dimensional variations due to temperature and vibration
2. Efficient dispersion of turbine gas flow for uniform secondary flow injection

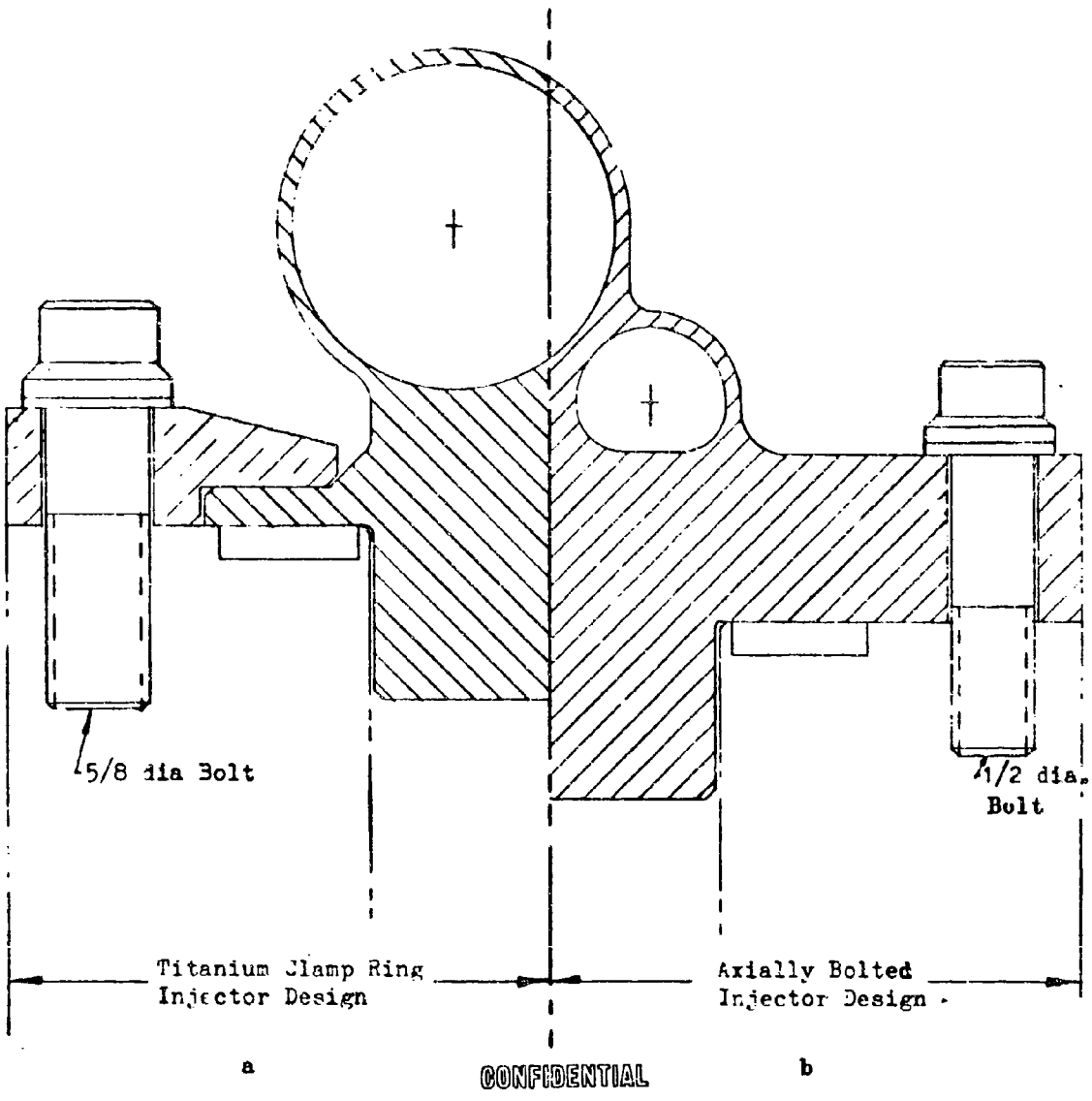

Note: AISI 347 used for injector body in both configurations

Figure 103. Axial Bolted Injector Design Concepts

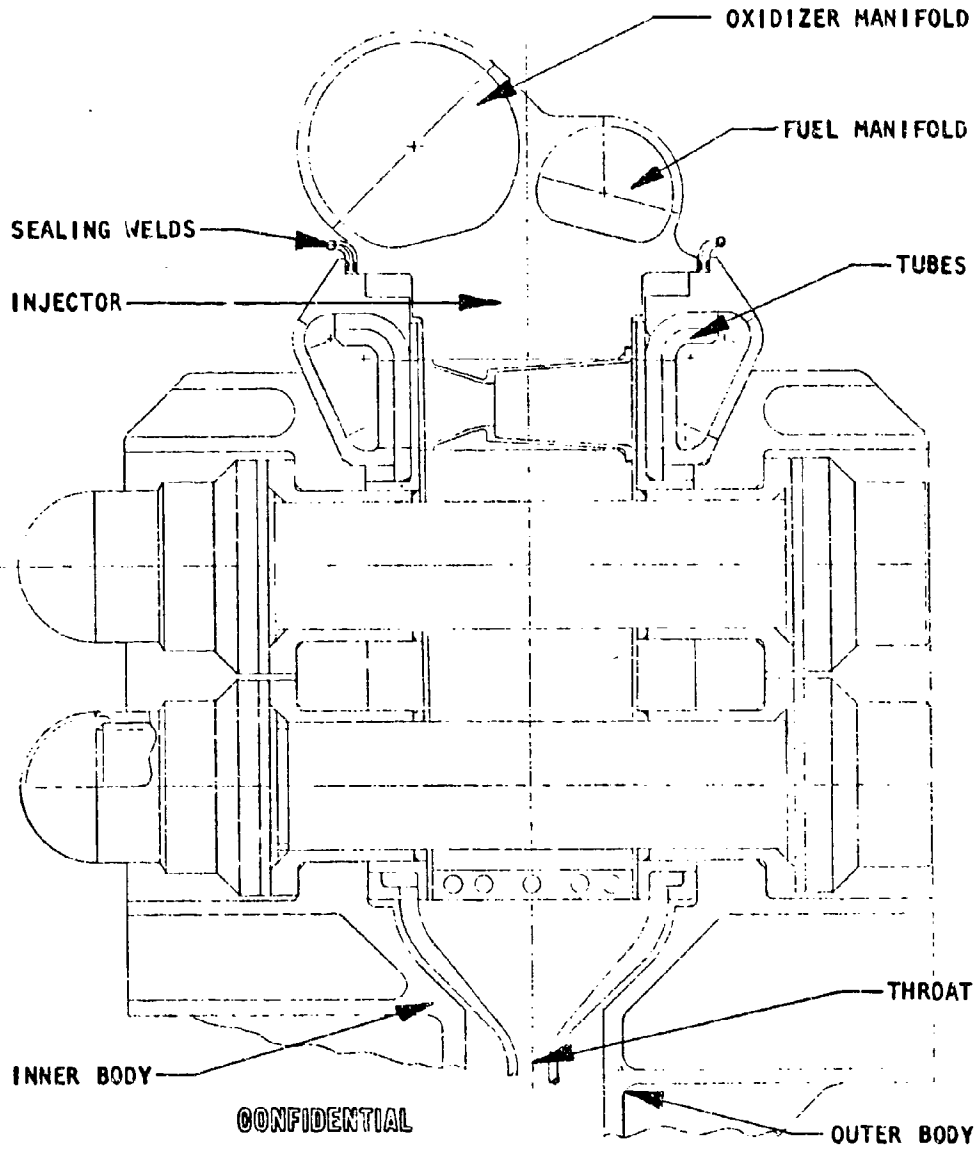

Figure 104. Integral Baffle Injector

3. Minimum weight
4. Capability for removal of closure to facilitate component accessibility and repair
5. Adequate cooling

(U) The nozzle base closure design (Fig. 105) is a membrane-type INCO 718 structure using an oblate spheroid configuration. This closure is mounted directly to the pump turbine flanges, thereby transmitting the closure thrust directly through the pumps into the thrust structure. Such a design minimizes any loads imposed on the thrust chamber nozzle exit. A flexible omega joint seals the connection between the bottom of the chamber and the base closure.

(U) The minor-to-major axis ratio of the spheroid was selected after conducting a trade study analyzing pressure vessel head shape and weight. A minor axis dimension of 6 inches was determined to provide a minimum weight compatible with envelope considerations. The aft surface of the closure extends 5.0 inches below the nozzle exit plane; however, this additional height does not affect the gimbal excursion, while the weight and internal flow advantages offset the increased height.

(U) An internal bolting arrangement between the turbine exhaust ducts and the base closure flanges is used with access provided by holes in the shell for intersection of the bolts.

(U) The aft portion of the shell is perforated with orifices that comprise 125 sq in. of the flow area (10 percent porosity). A representative orifice size and spacing would consist of 0.257-inch-diameter orifices, 0.875 inch apart.

(U) Base Closure Analysis. Design studies were made to determine the best base closure configuration to ensure high performance of the secondary

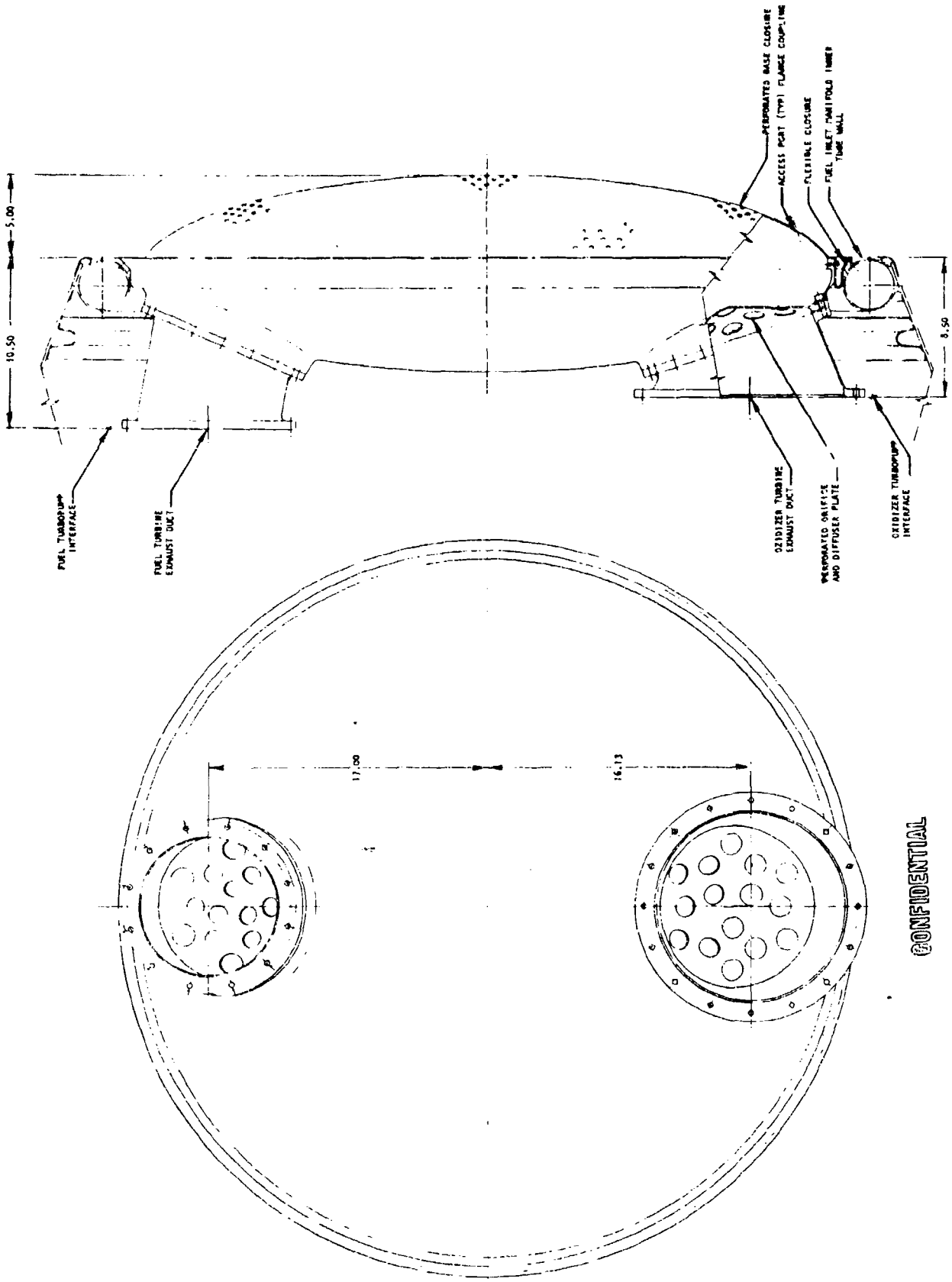

Figure 105. 250K Demonstrator Module Porous Base Closure Assembly

flowrate. Additional analysis was made to study the base heating to determine temperature requirements imposed upon the base structure. These studies are discussed in the following paragraphs.

(U) Performance Considerations. Secondary gas flow is introduced in the wake region of separated supersonic flow to improve the interaction with the surrounding primary flow and thus increase base pressure. In the application of this principle to the Aerospike Engine, Rocketdyne experiments have been conducted under NASA Contract NAS8-19. This program undertook evaluation of bleed injection methods, cavity depth, and base geometry. The results of this investigation showed conclusively that injection through a perforated base closure (either flat or curved) located at the exit plane achieved performance equal to deep-cavity injection over a wide range of secondary flowrates, all other nozzle parameters remaining consistent with the principle of low axial momentum. In a short distance downstream of the closure, the gases from the individual perforations undergo a sudden expansion, thereby ensuring a uniform subsonic secondary flow distribution in the wake region formed by the separated primary flow.

(C) Base Heating. The base closure for the Aerospike nozzle consists of a perforated oblate spheroid through which the turbine gas (secondary flow) passes. The holes are spaced to produce recirculatory flow of the secondary gases in the vicinity of the perforated base, thereby protecting the closure with a low-temperature secondary flow blanket. The maximum secondary gas temperature is approximately 1300 F; therefore, the temperature of the perforated base closure will not exceed this value. The base surface temperature measured as a function of time during uncooled chamber tests is shown in Fig. 106 for a zero-base bleed condition. Maximum wall temperature for the solid base closure (no secondary flow) at the end of the 600-millisecond test was 200 F, indicating no heating problems in that region as seen by the small surface temperature rise with time. The

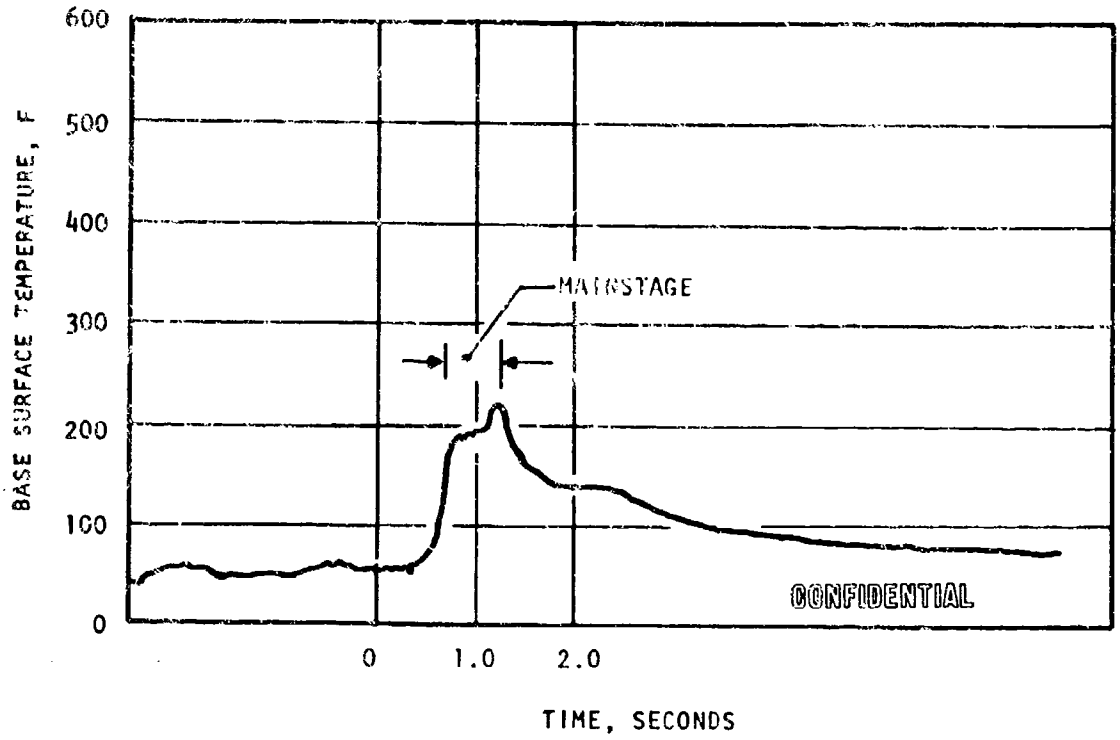

Figure 106. Base Closure Temperature, Phase I Solid Wall (Test No. 006, P_c = 900 psia)

Demonstrator Module will operate with a large base bleed, which is introduced in the base cavity. The base bleed will consequently maintain the base structure at that temperature.

(C) Base Closure Design Alternative Studies. The two basic concepts studied for the module base closure design are shown in Fig. 107 and 108. The first was a conventional flat plate base closure (similar to that used in the experimental chamber), attached rigidly to the LH_2 thrust chamber manifold at the nozzle exit (Fig. 107). A thrust load of approximately 7400 pounds would be transmitted through the closure to the thrust chamber. The necessity of flexible connections between the closure and the pump turbines required the assumption that a modification of the oxidizer turbine flange was feasible. Even with the assumed diminishing of the oxidizer turbine flange diameter, available space precluded the effective utilization of a bellows section. A slip joint was less desirable but could be made to fit in the space limitation. The 7-inch depth of

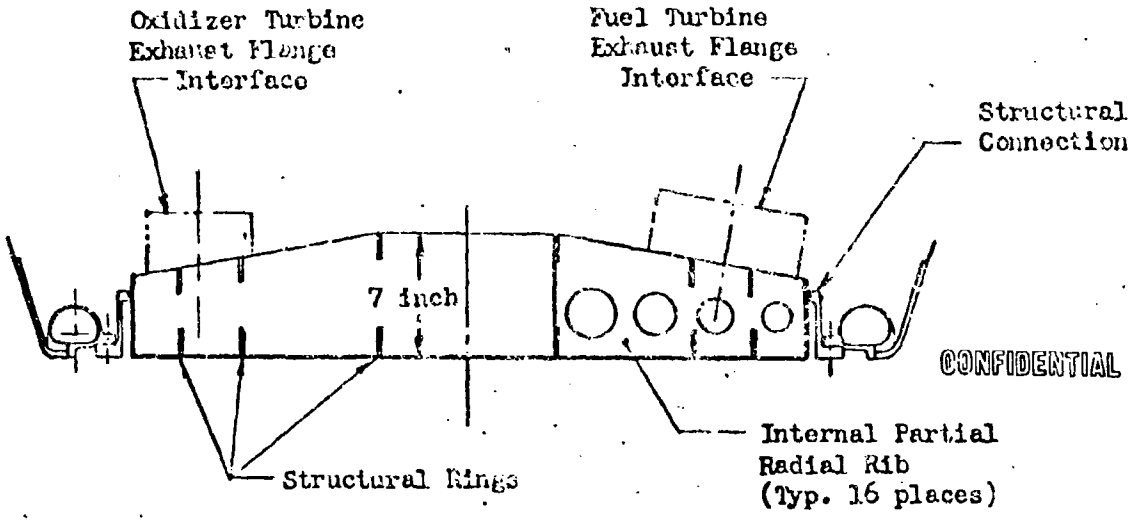

Figure 107. Flat Plate Base Closure

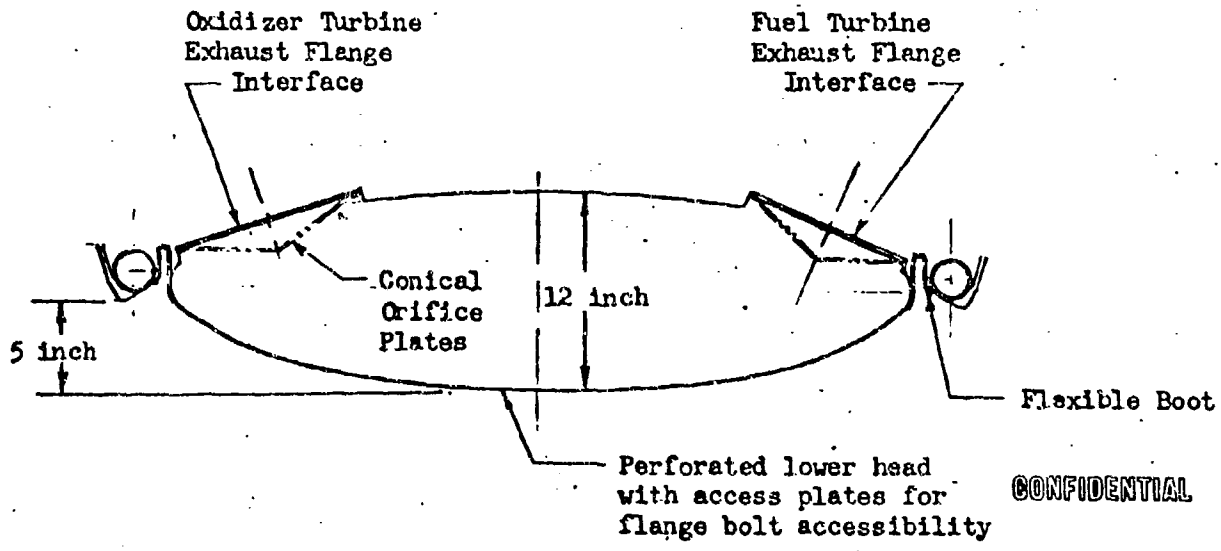

Figure 108. Oblate Spheroidal Membrane Base Closure

the base closure was determined by the available geometry. The configuration itself contained a flat predrilled bottom plate and an upper dish-shaped plate of INCO 718. The internal reinforcing structure consisted of eight radial ribs and 16 partial radial ribs. The ribs were connected by three circumferential rings at the bottom and three circumferential ribs at the top. All radial ribs contained large orifices to allow the distribution of the internal gases. Plate stress considerations determined the rib and ring spacing. The estimated weight of 251 pounds for this configuration significantly exceeded its budget 190 pounds. Furthermore, there was difficulty in dispersing turbine gases because of the restrictive internal structure.

(U) The second design was the oblate spheroid shown in Fig. 105 and 108. This design was selected over the flat plate because of its ability to meet the targeted weight of 90 pounds and simplified configuration eliminating extensive welding of internal support structure.

(U) Two methods for attaching the base closure to the chamber assembly were evaluated: (1) attachment directly to the chamber nozzle with expansion couplings provided at the turbine duct interfaces, and (2) attachment directly to the turbopumps with a flexible coupling between the closure and nozzle to contain the secondary flow base pressure and to provide an aft support for the pumps. Because of the limited space available between the closure and turbine discharge flanges and the simplicity of design with a rigid connection of the base closure to the turbines. the second configuration was incorporated in the final system design.

Turbomachinery Design

(U) A preliminary design of the engine turbomachinery was undertaken to establish the component performance and weight, to provide more accurate envelopes for the module design system integration, and to define the requirements for long-lead items which would require action at the onset of Phase II. Two individual turbopump units were studied, one for the fuel and one for the oxidizer, each of which includes a pump, preinducer, and turbine. The separate designs, analyses, and tradeoff studies are discussed in detail below.

(C) Fuel Turbopump Design Requirements. The initial fuel turbopump design requirements were derived from the contract thrust, performance, and operational requirements listed in Table 9 together with the pressure requirements defined by the system analyses. The Demonstrator Module Fuel Turbopump design must meet the requirements listed in Table 28 and provide not less than a maximum pump efficiency of 75 percent over the mixture ratio excursion at full thrust.

(U) The turbine was designed based upon gases having the properties listed in Table 29. These properties correspond to those of gas generator gases and not tapoff gases. This assumption was made to ensure an adequate turbine design before definite tapoff properties have been established. A turbine designed for gas generator properties will not suffer a performance loss when operated with tapoff gases; however, the converse is not true.

(C) TABLE 28

TURBOPUMP DESIGN CONDITIONS

Parameter	Nominal (MR=6:1)	Maximum Off Nominal	3σ Tolerance	Maximum Design Requirement
Pump Q_f, gpm	8450	9560	483	10,043
Pump P_D, psia	2766	2942	210	3152
NPSH, feet	60			
Pump Inlet Pressure, psia	32.0			
Pump Inlet Temperature, R	41.7			
Turbine W_f, lb/sec	10.5	12.2	1.3	13.5
P_{in} (Turbine Inlet Pressure), psia	1000	1165 (MR=5)	117	1282
P_o (Turbine Discharge Pressure), psia	70	76.9 (MR=5)	8.23	85.13
T_{in} (Turbine Inlet Gas Temperature), F	1960	1960	152	2112
Turbine Efficiency	62.2			

For turbopump operating characteristics at off-design mixture ratios see Table 10, page 78.

(C) TABLE 29

TURBINE GAS PROPERTIES

Mixture Ratio	1.12
Molecular Weight	4.272
Temperature, F	1960
C_p, btu/lb F	1.802
Specific Heat Ratio	1.348

(U) Fuel Turbopump Alternatives Studied. Several tradeoff studies were conducted before the final turbopump design concept was established. These included a study of pump types, preinducer drives, number of turbine wheels, turbine disk configuration, and the aft turbine bearing carrier. These trade off studies are discussed in the following paragraphs.

(C) Configuration Selection. Establishment of the maximum operation head of 96,970 feet for the fuel pump required a re-evaluation of the selection of the type of pump best able to meet this requirement. The three types re-evaluated were: (1) a single-stage, inducer/centrifugal pump (one and one-half stagesP; (2) a single-stage, multivaned centrifugal pump (multistaged radial); and (3) a two-stage centrifugal pump. Pump parameters at the design point used for comparison are shown in Table 30 and the head and efficiency curves for the three types are shown in Fig. 109.

(U) The evaluation of the pumps was made on the basis of life, weight, hydrodynamic performance, uprating capability, manufacturing difficulty, efficiency, off-design performance, structural design, maximum bearing DN, maximum seal speed, and overall dimensions.

(C) TABLE 30

LIQUID HYDROGEN PUMP PARAMETERS AT DESIGN POINT,
MIXTURE RATIO = 6

Parameter	One and One-Half-Stage	Two-Stage	Multistage Radial
Impeller Speed, rpm	36,000	36,000	36,000
Preinducer Speed, rpm	14,600	14,600	14,600
Impeller Discharge Diameter, inches	11.4	9.30	11.4
Impeller Inlet Diameter, inches	6.75	6.0	5.5
Preinducer Inlet Diameter, inches	9.0	9.0	9.0
Preinducer Head, feet	700	700	700
Impeller Required NPSH, feet	600	600	600
Overall Head Coefficient	0.820	1.23	0.820

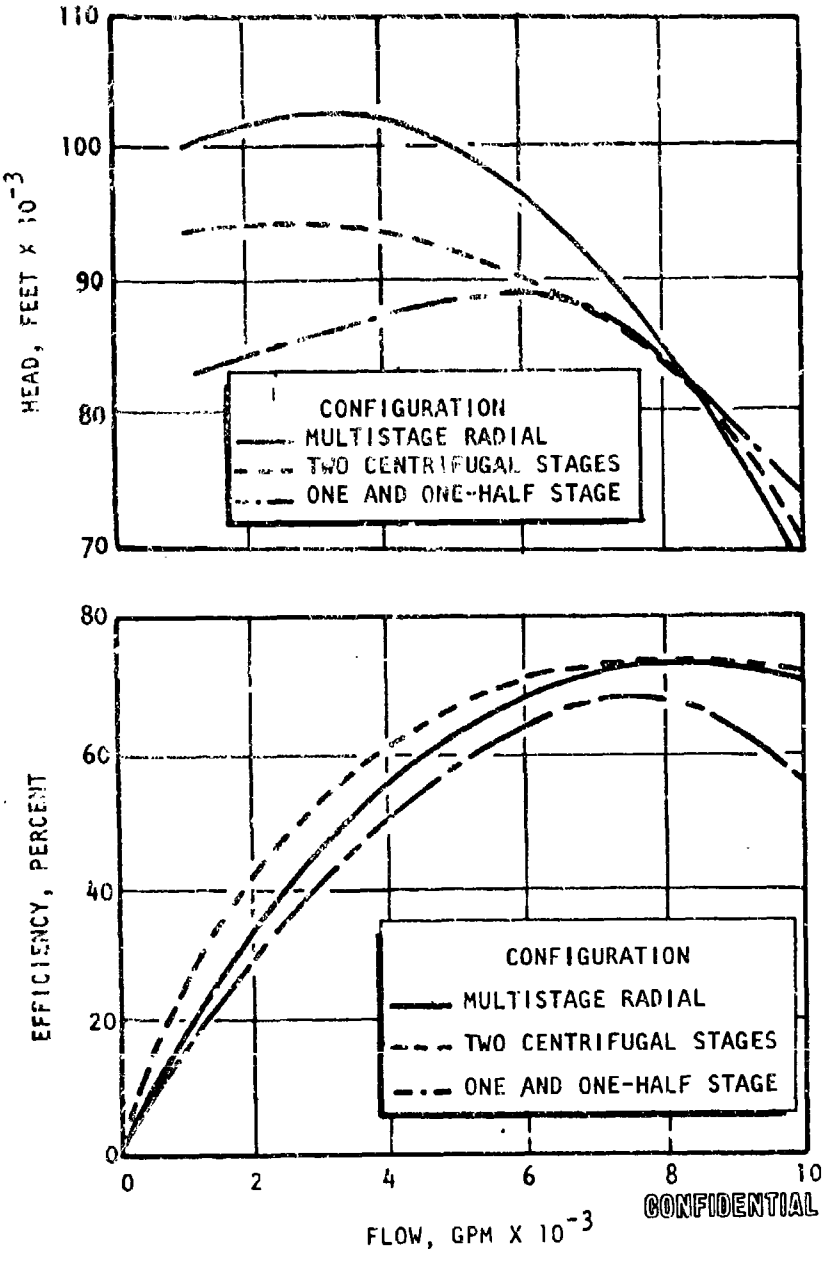

Figure 109. Head and Efficiency vs Flow (Pump Speed = 36,000 rpm)

(U) A summary of the comparison of the three fuel pump configurations is shown in Table 31. Based on weight, efficiency, uprating capability, and off-design performance characteristics, the one and one-half stage pump was eliminated from further consideration.

(U) The choice between the two-stage centrifugal and the radial stage pump was more difficult. Weight and efficiency were about equal. Reliability and long life, achieved through the design approach of a minimum of parts, a minimum number of joints and high-pressure leak paths, elimination of stress areas, and material selection for adequate strength, were roughly equivalent. The difficulty of casting crossover lines on the two-stage design was balanced by the effort required to maintain rotor tip clearances on the multistage radial concept. Seal speeds and bearing DN valves were almost identical. However, data on the operating characteristics of the radial design was extremely limited and on this basis, the two-stage centrifugal configuration was selected.

(U) Preinducer Drive Selection. Requirements of minimum weight and size, high overall efficiency, and reliability for the preinducer drive generated a design study in which six configruations, shown schematically in Fig.110, were investigated.

(U) The through-flow, hydraulic turbine drive was selected for the fuel pump, while the high-pressure hydraulic hub turbine drive was selected for the oxidizer pump. The tradeoffs leading to these decisions are presented below.

(U) The gear-driven preinducer offered the advantages of relatively high efficiency (gear box efficiency of approximately 97 percent) and a constant speed ratio. The gear drive is an attractive solution to the problem; gear

TABLE 31

TURBOPUMP COMPARISON

	One and One-Half Stage	Two Stage	Multistage
1. Life, hours	10	10	10
2. Weight (less turbine), pounds	171 (titanium impeller)	150 (aluminum impeller)	152 (titanium impeller
3. rpm (maximum)	38,900	38,900	38,900
4. Impeller Tip Speed, rpm (38,900 maximum)	1940 (shrouded radial)	1575	1940 (unshrouded)
5. Head Coefficient	0.795	1.2	0.795
6. Hydrodynamic Performance	Depends on one-half stage performance	Least number of problems	Depends on maintaining blade clearance; stall characteristic unknown
7. Uprating Capability	None (unless impeller is made unshrouded)	Yes	Yes
8. Manufacturing	Difficult to machine vanes	Casting of cross-over lines difficult	No problem
9. Efficiency, percent	69	74	74
10. Off-Design	Flat because of radial vanes	In between	Steepest
11. Structural Design	Impeller marginal	No problem	Stiff structure required to maintain clearance
12. Maximum Bearing DN	1.556	1.556	1.576
13. Maximum Seal Speed, ft/sec	760	760	760

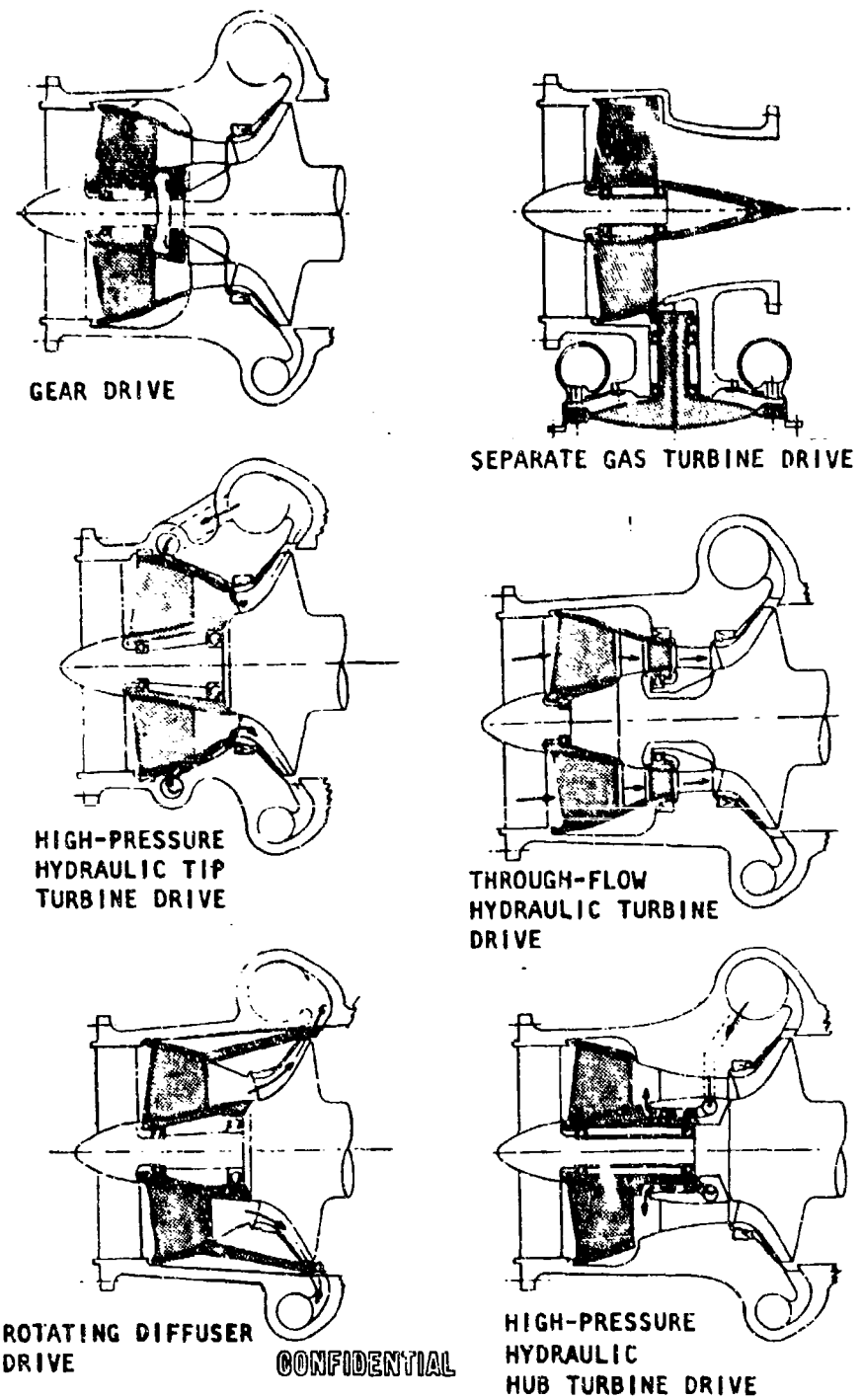

Figure 110. Candidate Preinducer Configurations

face loads are low (approximately 800 lb/in.) and pitch line velocities are only 3900 ft/min. Additionally, previous experience has indicated success in operating gears in both oxidizer and fuel. It is believed, however, that the added complexity of the gear box may increase development time, and therefore this concept is less attractive than others investigated.

(U) The separate gas turbine-driven preinducer offers the highest potential overall pump efficiency, provided hot gas is available with no performance penalty to the system. Low-pressure turbine exhaust gases are a possible source for this purpose. The disadvantages of this system are that both complexity and weight are markedly increased. In essence, it means adding a third turbopump with its own turbine, bearings, seals and attendant inlet and discharge piping. It was believed that these disadvantages out-weighed the pump performance advantages to be gained, and therefore, it was not considered further.

(U) The high-pressure hydraulic tip turbine drive operates by recirculating high-pressure fluid from the discharge of the main pump through a staged hydraulic turbine mounted in the tip of the preinducer. The efficiency of this design was somewhat lower than the through-flow design, partly because of the recirculation, but mainly because the large turbine pitch diameter resulted in extremely short blades and stators and the ratio of leakage area to through-flow area was large. Sealing at the large diameter also presented a problem, and as a result, this design was dropped.

(C) The through-flow, hydraulic turbine drive system is designed integrally between the low-speed preinducer and the high-speed impeller. A high-speed preinducer mounted directly on the pump shaft provides the head rise to drive the hydraulic turbine, which is directly linked to the low-speed inducer. This design offers a relatively high overall turbopump efficiency, a minimum of mechanical complexity, and it can be developed independently of the main pump. The main drawback to the through-flow hydraulic turbine design is a possible loss in performance at off-design operation. An analytical investigation was performed to determine the off-design performance of this candidate.

It was found that if the speed ratio (ratio of main inducer speed to preinducer speed) was approximately 2 to 1, there was very little drift (ratio stayed constant) at off-design conditions. The speed ratio is determined by vector diagrams covering inducer blade leaving angle, passage flow area and therefore velocity, rotor entrance and leaving blade angle, turbine entrance and leaving angle, and a factor for friction losses. Because the ratio of the fuel pump inducer to main inducer was approximately 2 to 1, the throughflow, hydraulic turbine drive preinducer was selected for the fuel turbopump.

(C) However, the speed ratio for the oxidizer pump is approximately 4 to 1, and thus, the through-flow drive would result in an adverse drift at off-design. Also, an axial thrust analysis in the oxidizer pump through-flow inducer resulted in the requirement for either a balance piston or a large-diameter balance drum. Because both conditions were undesirable, the through-flow inducer was eliminated from consideration on the oxidizer pump.

(C) The rotating diffuser drive, in which a set of rotating vanes at the main pump discharge is used to drive the preinducer, was investigated as an alternate to the oxidizer pump through-flow inducer to eliminate the axial balance problem introduced by the through-flow hydraulic turbine. This design allowed the balance drum diameter to be reduced, reducing the rubbing velocity from 700 to 600 ft/sec at the nominal operating point.

(U) Since the stator has to operate over a considerable range of incidence angles as the pump is throttled, stalling may occur, with a resulting performance loss. With the rotating diffuser design, stalling, should it occur, could not be alleviated because there is no method of adjusting preinducer speed.

(U) As a solution to possible stalling problmes of the rotating diffuser design, the high-pressure hydraulic hub turbine drive was analyzed. Its operation is similar to the high-pressure hydraulic tip turbine drive except that the hydraulic turbine is mounted in the hub instead of at the tip. This allows the turbine to be designed with adequate blade heights and reduces the sealing requirements (two seals compared to five for the rotating diffuser). Furthermore, the preinducer can be developed independently of the main pump, in contrast to the rotating diffuser design. Because the hydraulic turbine is physically separated from the main pump in the preinducer hub, this design can accommodate preinducer speed controls which will provide the capability to vary the inducer discharge flow angle. Then, should a stall region be encountered during throttling, it would be only necessary to place a speed control valve in the hydraulic turbine inlet flow line to change the flow angle and alleviate the condition.

(C) Turbine Selection. Since the turbine flowrate in an aerospike engine is used as the secondary flow in the base region of the nozzle, it becomes desirable to optimize the magnitude of this flow. The amount of secondary flow as a ratio of the primary flow was shown in the performance analysis section to have a direct effect upon the engine specific impulse. While the magnitude of this effect does not change total specific impulse more than 1 percent, it is nevertheless worthwhile to attempt to achieve maximum engine performance. For the 1500-psi chamber pressure demonstrator engine, the turbine flowrate is larger than the desired optimum secondary flow. Therefore, efforts were made to improve the turbine performance and reduce the required turbine flowrate.

(U) The required pump horsepower establishes the turbine power requirement which, in turn, is the product of three primary elements:

$$HP_{turbine} = \text{turbine efficiency} \times \text{usable available energy} \times \text{flowrate}$$

(U) To minimize the flowrate, both of the other elements must be maximized. The usable available energy is a function of the turbine drive gas temperature and the turbine pressure ratio. These parameters are fixed at their maximum values by stress considerations and the system pressure balance. The turbine efficiency is a function of the pitch line velocity and the number of blade rows. The first of these two design parameters, pitch line velocity, is established by the pump speed and stress limitations on the turbine disk and rotor blades.

(U) Therefore, the only design variable remaining is the number of blade rows. Efficiency will increase with added turbine wheels; however, an associated weight and envelope penalty is incurred. The optimum turbine design is then determined from a total system specific impulse-weight tradeoff. This was done for both the fuel and oxidizer turbines, employing the performance index tradeoff factors in the applications study section of this report.

(U) Figure 111 shows the variation in fuel turbine flowrate as a function of the number of blade rows, together with the corresponding change in turbine weight and the average change in performance index for the six vehicles in the applications study. These data were used to complete the turbine wheel tradeoff optimization which is also shown in this figure. This figure shows the three-wheel turbine to have a slight performance index advantage for the fuel turbine. Furthermore, the three-wheel design has a lower development and fabrication cost than a four-wheel configuration.

(C) The oxidizer turbine study involved an additional tradeoff with pump speed. The maximum pump efficiency occurs at about 20,000 rpm; however, it was not possible to obtain satisfactory turbine performances at this speed because a 50-percent admission design was necessary. Therefore, the pump speed was increased to 25,000 rpm, which allowed the diameter to be decreased from 12 to 10 inches which increased the blade height from 0.260 to 0.320 inch.

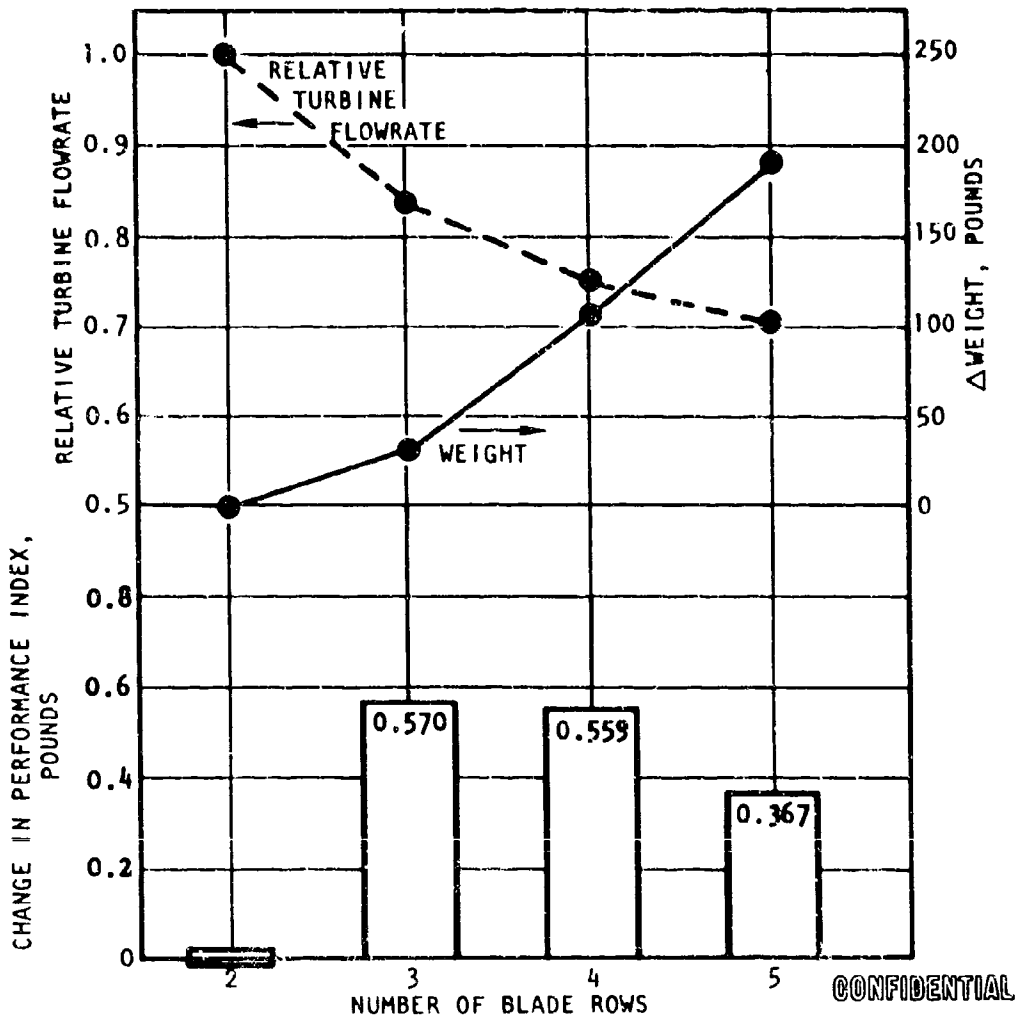

Figure 111. Fuel Turbine Weight and Flowrate Tradeoffs

(C) The oxidizer turbine study involved an additional tradeoff with pump speed. The maximum pump efficiency occurs at about 20,000 rpm; however, it was not possible to obtain satisfactory turbine performances at this speed, because a 50-percent admission design was necessary. Therefore, the pump speed was increased to 25,000 rpm, which allowed the diameter to be decreased from 12 to 10 inches which increased the blade height from 0.260 to 0.320 inch.

(U) Fuel Turbine Disks. A number of turbine disk profiles were analyzed to determine the required thicknesses for various configurations based on estimated rotor blade profiles and turbine disk temperature distributions.

(U) Fir tree and integrally machined blades with welded and bolted curvic disc connections were considered in various combinations. The selected disc profiles and corresponding stresses for discs having integral blades with curvic connections are shown in Fig. 112 through 115 . A summary of stresses and allowable operating speeds is shown in Table 32 .

(U) The curves of Fig. 116 show the results of the configuration investigation. The allowable operating speed vs center thickness for various disc configurations is presented. The blades can be changed from integrally machined to fir tree attached blades for the same disc center thickness, provided the wheels are attached by welding rather than by curvic coupling.

(U) Natural frequencies and critical running speeds will be calculated, and the profile will be modified as required to remove these from the operating speed range.

(U) Aft Bearing Carrier. Both the LO_2 and LH_2 turbopumps have an outboard aft bearing. The bearings must be rigidly supported by members which

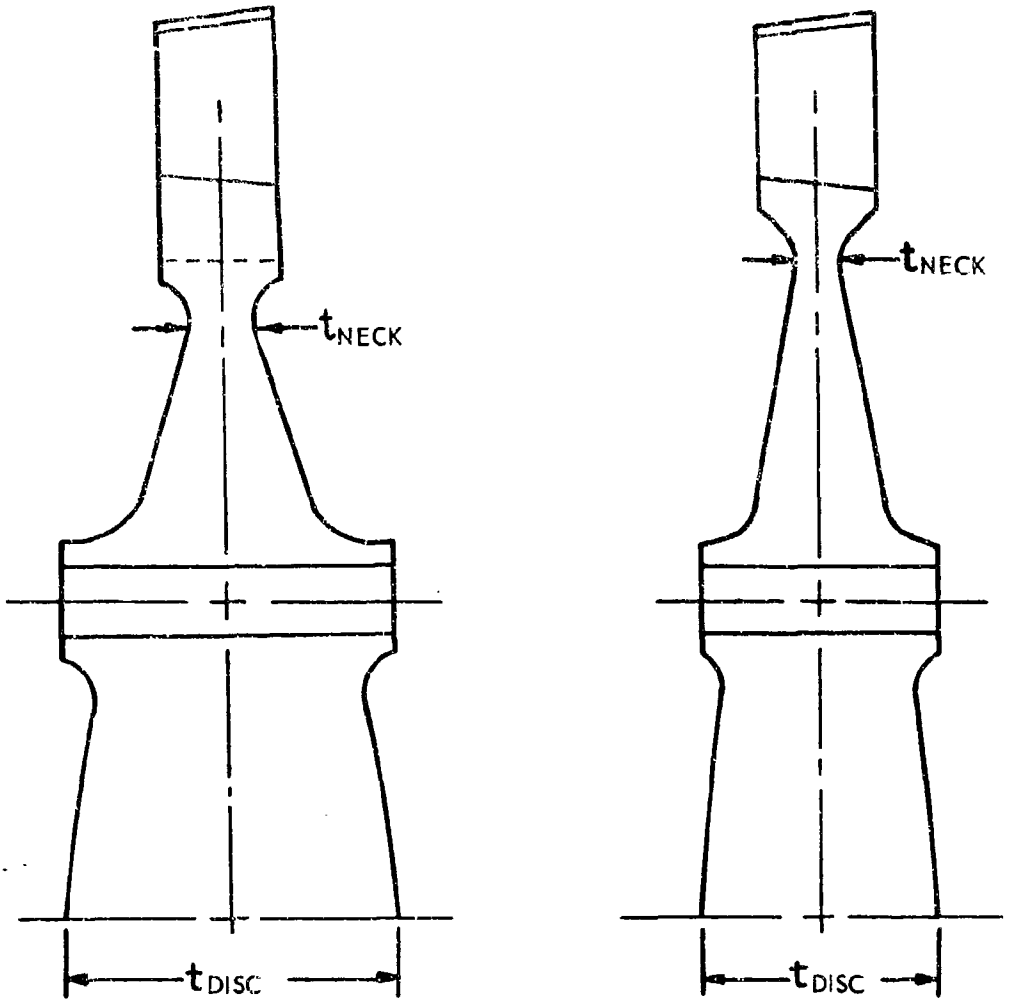

FIR TREE BLADES

CONFIDENTIAL

INTEGRAL BLADES

DESIGN CRITERIA :
MATERIAL: INCO 718
RM TEMP F_{tu} 180 KSI
ELONGATION 15 PERCENT
MAX RPM 38,900

MAXIMUM ALLOWABLE OPERATING SPEED=75-PERCENT BURST SPEED

* UNSHROUDED DESIGN

	FIR-TREE BLADES			INTEGRAL BLADES		
	FIRST STAGE	SECOND STAGE	THIRD STAGE	FIRST STAGE	SECOND STAGE	THIRD* STAGE
t_{NECK}	0.36	0.37	—	0.25	0.26	0.37
t_{DISC}	2.0	1.75	—	1.4	1.25	1.4
GAS TEMP F	1320	1100	—	1320	1100	945

Figure 112. Mark 30 Turbine Disc Profiles

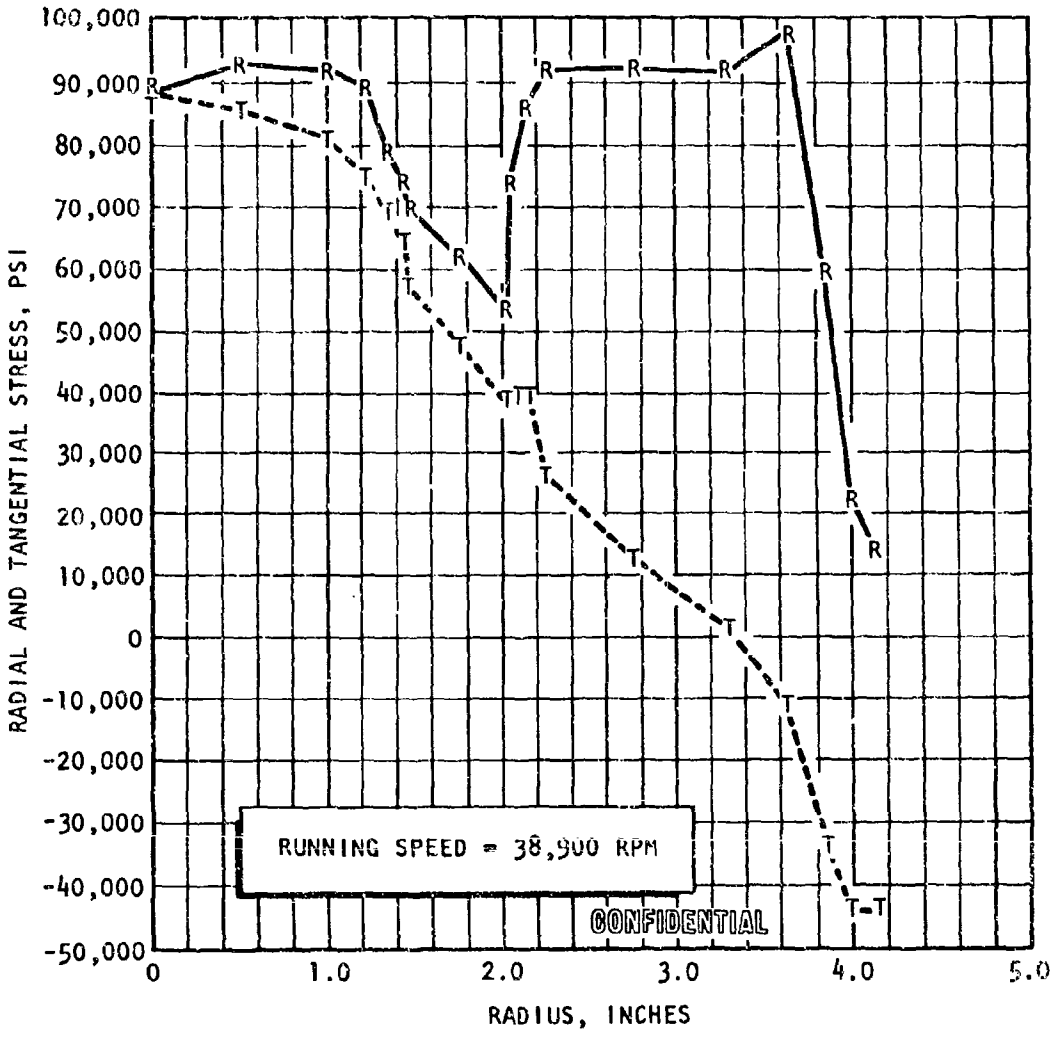

Figure 113. First-Stage Fuel Turbine Disc Stress vs Radius

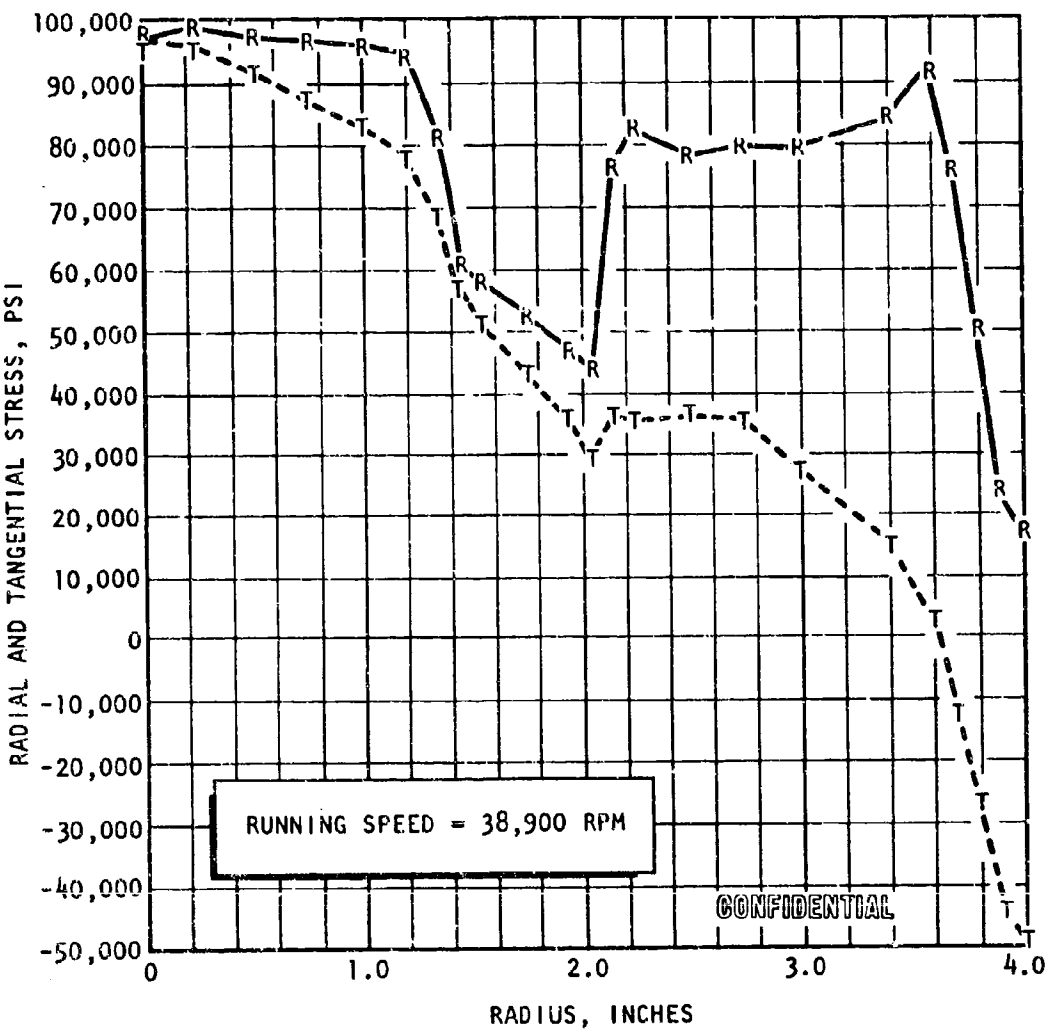

Figure 114. Second-Stage Fuel Turbine Disc Stress vs Radius

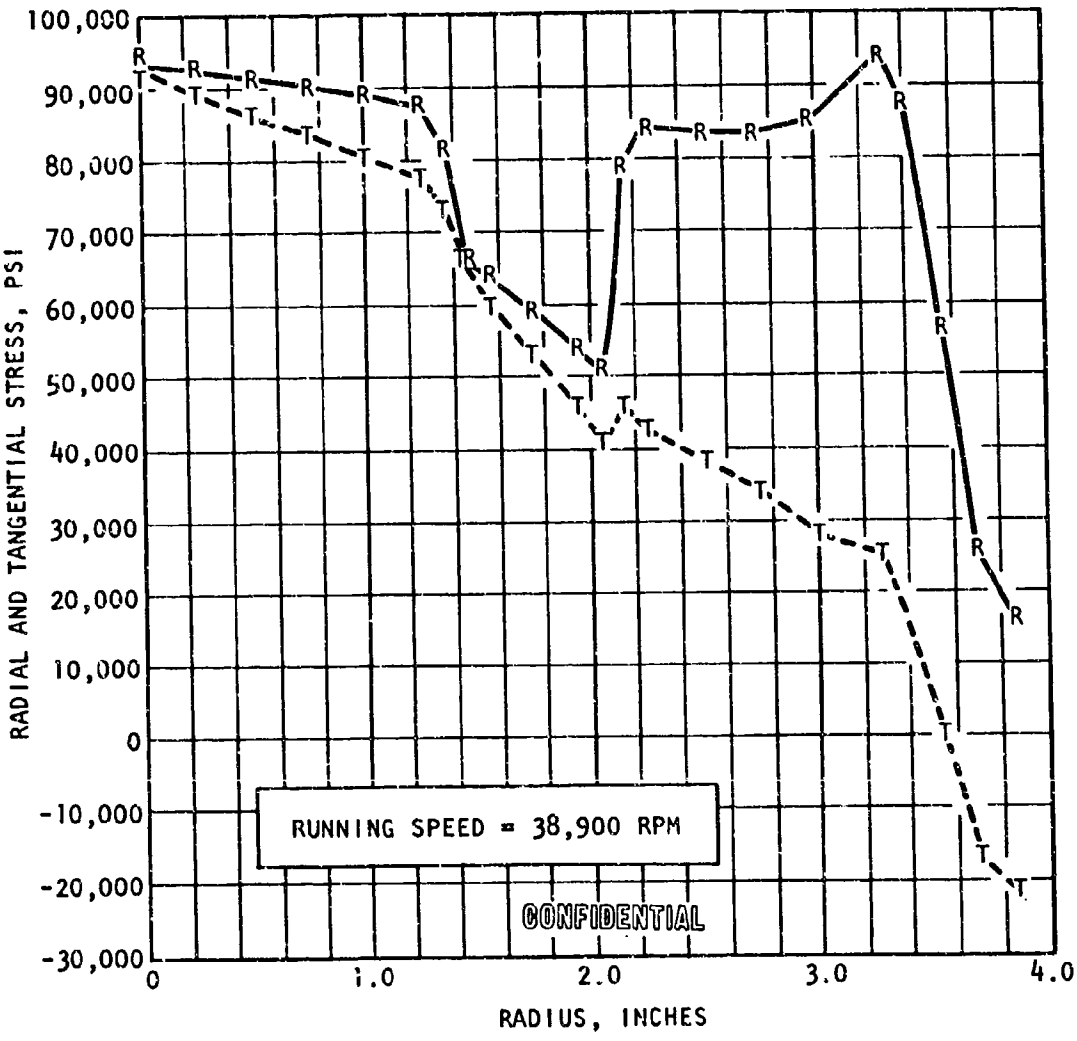

Figure 115. Third-Stage Fuel Turbine Disc Stress vs Radius

TABLE 32

(C) MARK 30-F TURBINE DISK DATA

	Stage		
	1	2	3
Required Center Thickness, inches	1.4	1.25	1.4
Center Thickness for Numbers in This Table, inches	1.5	1.25	1.4
Neck Thickness, inches	0.25	0.26	0.37
Rim Thickness, inch	0.65	0.65	0.86
Blade Attachment	Integral	Integral	Integral
Wheel Attachment	Curvic	Curvic	Curvic
Average Tangential Stress, psi	62,500	67,400	68,900
Maximum Tangential Stress, psi	88,100	97,300	93,000
Maximum Radial Stress, psi	98,000	99,000	94,000
Burst Speed, rpm	52,880	51,100	51,100
Allowable Operating Speed, rpm	39,600	38,400	38,400
Materials Properties for INCO 718			
F_{tu}, psi	156,000	160,000	161,000
F_{ty}, psi	125,000	126,000	127,000
Elongation, percent	15	15	15
Weighted Average Temperature, F	800	680	590

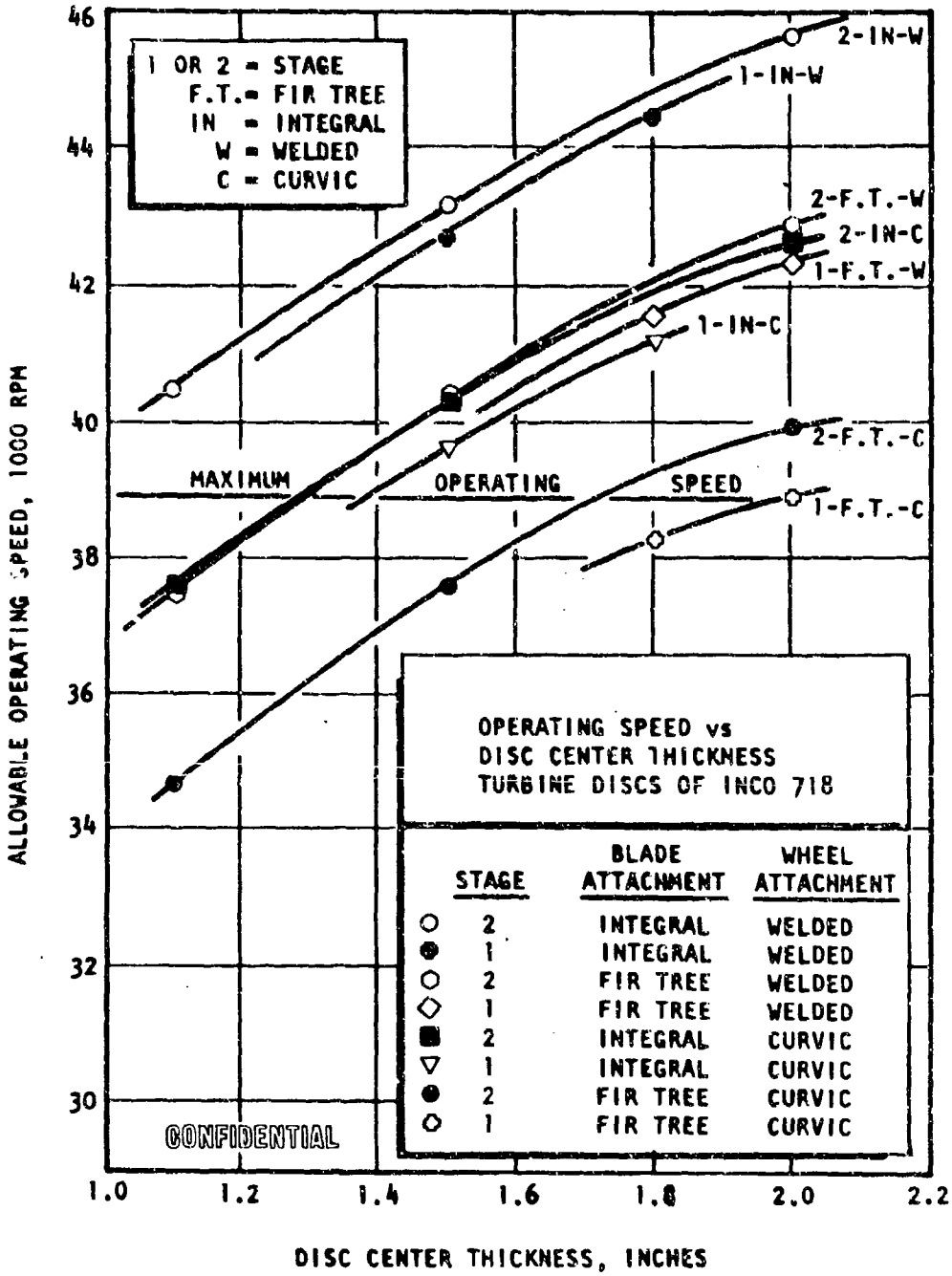

Figure 116. Allowable Operating Speed vs Disc Center Thickness (Turbine Disk of Inconel 718)

will be exposed to the turbine hot-gas environment and must block only a limited portion of the gas flow area. The thermal stresses and distortions caused by these gases could be very high. The struts are enclosed by sheet metal shrouds to protect them from direct gas impingement and to serve as turbine discharge gas flow straighteners. The struts have pinned ends to minimize the thermal stresses. A study was conducted to determine thermal stress and structure flexibility for various strut configurations. The results are tabulated in Fig. 117 and 118 and Table 32. By using pinned end struts, the bearing carrier flexibility can be easily varied by changing the strut dimensions. The thickness of the fixed end struts is limited because of the thermally induced bending stresses. The limiting thickness values are shown at the bottom of Table 33. The selection of pinned end struts virtually eliminates the thermal stress problem.

(U) The chosen configuration of six 0.15- by 1.75-inch cross-section struts on a nine-strut pattern will have a radial spring rate of 5.96×10^6 lb/in.

(U) Fuel Turbopump Description. The fuel turbopump consists of a two-stage centrifugal pump mounted on a common shaft with a three-row turbine with a concentric integral, hydraulic turbine driven preinducer. Turbopump axial thrust is handled by means of a hydraulic balance piston located between the two main impellers. A layout of the complete assembly is shown in Fig. 119, and the subcomponents are discussed further in the following paragraphs.

(U) Pump. The fuel pump assembly consists of the preinducer, the impellers, the balance piston, and the housing.

(C) The preinducer, designed to meet the NPSH condition of 60 feet, has as axial flow design with four vanes at the inlet increasing to eight vanes at the discharge. The higher solidity at the discharge is to provide a

	$A = 0.15 \times 1.0 = 0.15$ in.^{2} $I = 2.81 \times 10^{-4}$ in.^{4}			$A = 0.4 \times 2.25 = 0.90$ in.^{2} $I = 1.20 \times 10^{-2}$ in.^{4}		
	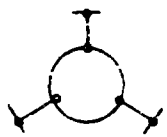		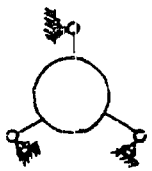	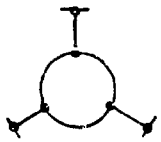	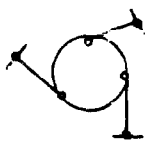	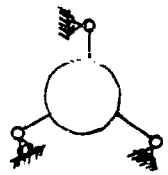
k_{xx} k_{yy} $k_{xy}=k_{yx}$	Unstable	1.71×10^6 1.71×10^6 ∞	0.00094×10^6 0.00094×10^6 -0.135×10^6	Unstable	10.23×10^6 10.23×10^6 ∞	0.040×10^6 0.040×10^6 ∞
Thermal Stress*	258,000 psi	0	0	258,000 psi	0	0
Stress Due to 1000 lb F_x, F_y, F_{45} Load	Unstable	4350 psi 4220 psi 4440 psi	620,000 psi 516,000 psi 559,000 psi	Unstable	725 psi 703 psi 740 psi	83,800 psi 72,500 psi 80,900 psi

CONFIDENTIAL

*Assumes a radial thermal gradient only

Figure 117. Summary of Springrates for Pinned-Pinned Struts

	$A = 0.15 \times 1 = 0.15$ in.^{2} $I = 2.81 \times 10^{-4}$ in.^{4}			$A = 0.4 \times 2.25 = 0.90$ in.^{2} $I = 1.20 \times 10^{-2}$ in.^{4}		
	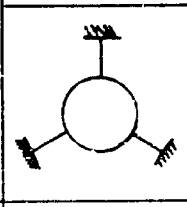	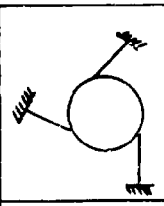	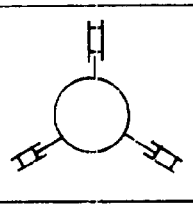	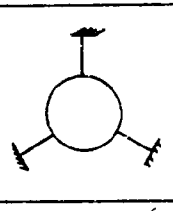	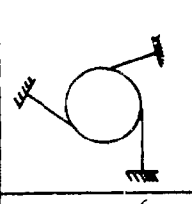	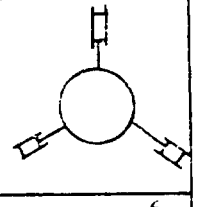
k_{xx} k_{yy} $k_{xy}=k_{yx}$	1.89×10^6 1.89×10^6 ∞	1.71×10^6 1.71×10^6 ∞	0.0037×10^6 0.0037×10^6 ∞	11.46×10^6 11.46×10^6 ∞	10.34×10^6 10.34×10^6 ∞	0.161×10^6 0.161×10^6 ∞
Thermal Stress*	258,000 psi	155,000 psi	0	258,000 psi	413,000 psi	0
Stress Due to 1000 lb F_x, F_y, F_{45} Load	3800 psi 4440 psi 4560 psi	4350 psi 3610 psi 2980 psi	298,000 psi 268,000 psi 287,000 psi	767 psi 730 psi 777 psi	770 psi 700 psi 610 psi	41,900 psi 36,300 psi 40,400 psi

CONFIDENTIAL

*Assumes a radial thermal gradient only

Figure 118. Summary of Springrates for Fixed-Fixed Struts

(C) TABLE 33

AFT BEARING SUPPORT

SPRINGRATE SUMMARY

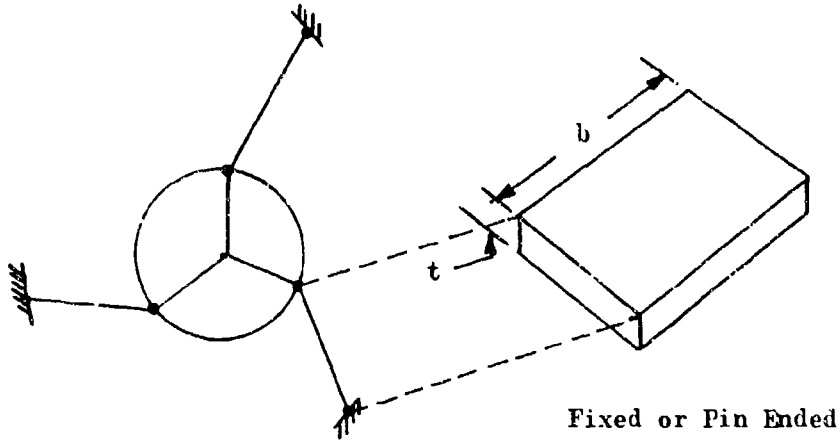

Fixed or Pin Ended

t	b	3 Struts	6 Struts	9 Struts
0.15	1.00	1.71×10^6	3.42×10^6	5.13×10^6
0.40	2.25	10.23×10^6	20.46×10^6	30.69×10^6
0.07	2.25	1.80×10^6	3.60×10^6	5.40×10^6
0.10	2.25	2.57×10^6	5.14×10^6	7.71×10^6
0.15	1.75	2.98×10^6	5.96×10^6	8.94×10^6

NOTE: For the configuration, the springrates are approximately proportional to the area, where

A = x-sectional area of strut

$= t \times b$

b_{max} = maximum allowable width of strut = 2.25 inches

t_{max} = Maximum allowable thickness of strut

= 0.07 inch for Hastelloy-C

= 0.10 inch for Inconel-X

= Determined by Thermal Stress

} Fixed End Only

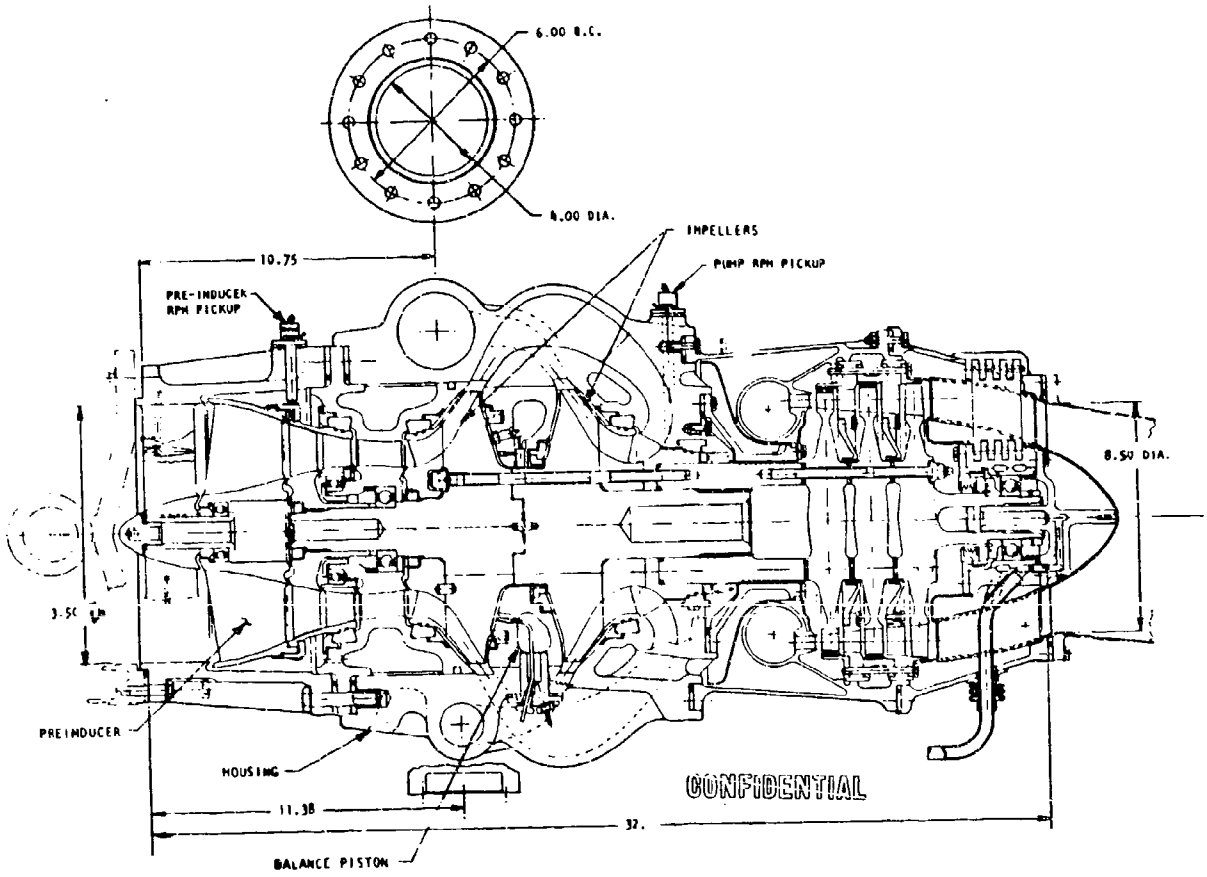

Figure 119. Demonstrator Engine Fuel Turbopump

more uniform flow distribution to the high-speed rotor just aft of the preinducer. It operates at approximately 42 percent of the main pump speed (14,535 rpm) and produces a head rise of 883 feet. The preliminary configuration of the high-speed inducer has seven blades, is machined from a titanium forging, and is splined to the main shaft. It operates at a tip speed of 1160 ft/sec (driven by the main turbine at 35,000 rpm) and produces a head rise of 4000 feet. The flow then passes through a single-stage impulse hydraulic turbine which drives the low-speed preinducer because the two are coupled together through their shrouds. The turbine head drop is 1692 feet, which means that the overall head rise in the preinducer section (head available to the main impellers) is approximately 3200 feet. The preinducer design parameters are shown in Table 34.

(C) The two pump impellers are mounted back-to-back and the flow from the first-stage impeller passes through five crossover tubes to the inlet to the second-stage impeller. The impellers are made of titanium and fully shrouded to improve impeller efficiency and minimize variations in developed head because of axial clearance. The rear shrouds are tilted so the exit angle is approximately 60 degrees from the axes to permit the vanes to be nearly radial elements with discharge vane angles of 60 degrees from tangential. With the preinducer, the required impeller suction specific speed of 7313 is easily attainable and no cavitation problems are anticipated.

The basic impeller geometry is presented in Table 35.

(U) The axial thrust loads of the pump and turbine are controlled by means of a balance piston which is located between the two impellers for two reasons: (1) there is no external leakage, i.e., balance piston flow path is from the discharge of the second stage (high-pressure impeller) through the balance piston and then into the discharge of the first-stage impeller, and (2) the leakage is the same as would result with the normal interstage seal between the two impellers. That is, if the balance piston was not located between the two impellers, a labryinth seal would have to be installed between the two impellers, and the leakage across the labyrinth would be approximately the same as the flow required by the balance piston.

(C)

TABLE 34

DESIGN PARAMETERS AND FUEL PREINDUCER
OFF-DESIGN OPERATING CONDITIONS

	Mixture Ratios		
	5	6	7
Preinducer			
Speed, rpm	15,300	14,535	13,950
Head Rise, feet	941	883	829
Inlet Flow Coefficient	0.0755	0.07	0.0663
Inlet Tip Diameter, inches	9.5	9.5	9.5
Discharge Tip Diameter, inches	7.83	7.83	7.83
High Speed Inducer			
Speed, rpm	36,800	35,000	33,600
Head Rise, feet	4250	4000	3760
Inlet Flow Coeficient	0.0373	0.081	0.0767
Inlet Tip Diameter, inches	7.6	7.60	7.6
Discharge Tip Diameter, inches	6.9	6.90	6.9
Suction Specifi. Speed	19,300	18,900	18,500
Turbine			
Speed, rpm	15,300	14,535	13,950
Head Drop, feet	1795	1692	1590
Inlet Tip Diameter, inches	6.83	6.83	6.83
Discharge Tip Diameter, inches	6.5	6.50	6.5

(C)

TABLE 35

FUEL PUMP IMPELLER DESIGN PARAMETERS

Number of Stages	2
Impeller Head Rise/Stage, feet	39,000
Impeller Discharge Diameter, inches	9.5
Impeller Tip Width (Normal to Flow), inches	0.45
Rear Shroud Angle at Discharge (from axis), degrees	60
Discharge Blade Angle from Tangential, degrees	60
Impeller Inlet Eye Diameter, inches	6.28
Inlet Hub Diameter, inches	4.5
No. of Blades at Inlet	6.0
No. of Blades at Discharge	24.0
Head Coefficient (stage)	0.597
Suction Specific Speed	7313

(U) The pump inlet housing and volutes are made of cast Tens 50 aluminum alloy and include the first- and second-stage discharge volutes and crossover tubes. The flow from the second-stage impeller passes through five crossover tubes between the first-stage tubes and into a volute mounted forward of the first-stage impeller. This produces a rigid casting with a minimum diameter. The main pump housing is bolted to the preinducer housing at one end and to the turbine inlet manifold at the other end.

(C) Turbine. The fuel turbine is a three-row, essentially velocity-compounded impulse turbine; however, there is a small change in static pressure across each blade row. All three turbine discs are machined from Inconel 718 with integral blades to minimize turbopump length and weight. In the first two rows the blades are shrouded; the third row has an unshrouded blade to allow maximum blade height to utilize as much of the

available energy in the gas as possible. The turbine discs are fastened together with through bolts and torque is transmitted through curvic couplings. Honeycomb seals are utilized at the blade tip and on the between stage stator elements to decrease losses. The turbine manifold is kept at a minimum diameter to obtain the lightest possible weight. Power from the turbine is supplied to the second-stage impeller through a spline drive and then to the first-stage impeller which is fastened to the second stage with through bolts. The turbine nozzle is welded integral with the turbine manifold with a conical support between the manifold and housing. The individual turbine stator vanes are supported by rings bolted to the housing and to the inner diaphragm. The turbine outboard bearing is mounted to six struts with pinned ends 15 degrees off radial to maintain bearing alignment when subjected to thermal gradients. There are nine discharge turbine vanes, six fair around the bearing support struts, and the other three are utilized to provide propellant cooling to the outboard turbine bearing. The turbine gas path and design parameters are shown in Fig. 120.

(U) Bearings. The liquid hydrogen turbopump employs two hydraulically coupled rotating elements, each supported on two ball bearings. For purposes of tabulation, they will be designated starting at the inlet to the preinducer 1F, 2F, 3F, and 4F. The design requirements of the fuel turbopump bearings are shown in Table 36.

(U) Ball bearings were chosen throughout because of their inherent ability to start quickly without prepressurization, to survive lube coolant and successfully ingest some contamination. Furthermore, a large body of successful test experience has been gained for propellant-lubricated turbopump ball bearings.

(C) The LH_2 preinducer operates at 14,500 rpm mounted on two outer race rotating ball bearings (1F and 2F). This approach reduces the bearing

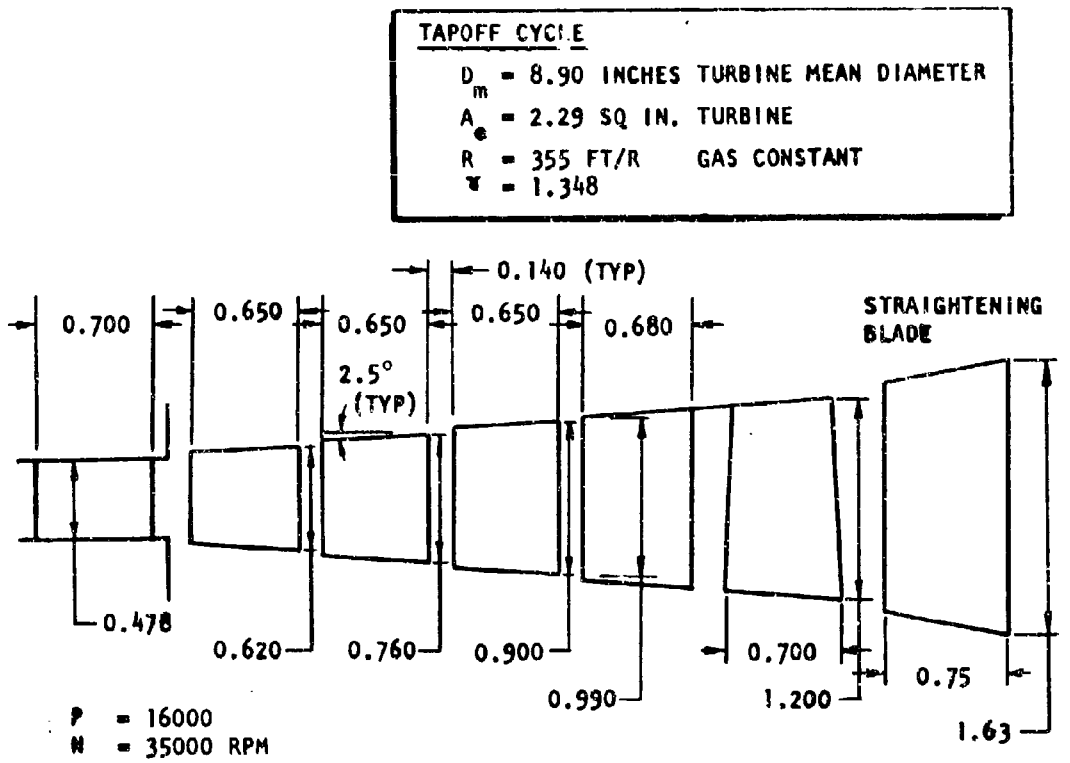

Figure 120. Mark 30-F Turbine Gas Path Sketch

(C) TABLE 36

LH_2 TURBOPUMP BEARING DESIGN REQUIREMENTS

Position	Type	Coolant	Load Axial	Radial	rpm	DN, Millions	Bearing Dimension, millimeters	
							Bore	OD
1F	Conrad Ball	LH_2	Spring Preload	Shaft Unbalance and Hydraulic	14,535*	0.44	30	45
2F	Conrad Ball	LH_2	Preinducer Thrust	Shaft Unbalance and Hydraulic	14,535*	1.09	75	100
3F	Angular Contact Ball	LH_2	Spring Preload	Shaft Unbalance and Hydraulic	35,000	1.40	40	80
4F	Angular Contact Ball	GH_2	Spring Preload	Shaft Unbalance and Hydraulic	35,000	1.40	40	80

*Outer Race Rotation

CONFIDENTIAL

size to the point that the application is considered state of the art. Both bearings are cooled by recirculation of LH_2 with the lubrication requirements defined by the cage material constituents.

(C) The inlet end bearing (3F) on the pump main shaft operates at 35,000 rpm and is also cooled with liquid fuel. The bearing is preloaded axially by a spring with the rotor thrust carried by a balance piston. This application, except for the long life required, is considered state of the art.

(U) The preliminary design of the fuel turbine shows ball bearings located at the aft end of the turbopump in the turbine discharge area (4F) which are preloaded with springs and cooled with gaseous hydrogen. Selection of this design is not firm and the subject is discussed further in the Analysis section.

(U) Seals. The liquid hydrogen turbopump has two main seal areas. One between the second-stage pump impeller and the turbine, designated AF, and the other between the outboard bearing and the turbine exhaust, designated as BF. Hydrostatic liftoff seals with the design requirements shown in Table 37 were selected for both applications.

(U) Materials. The materials selected for the primary turbopump components are based on Rocketdyne experience in the design and production of pump assemblies for rocket engines. This experience, which includes an extensive past history of service together with continuous material testing and structural testing, has provided the detailed background necessary for the material selections which meet the performance, reliability, and long operating life requirements of the module.

(C)

TABLE 37

LIQUID HYDROGEN TURBOPUMP SEAL DESIGN REQUIREMENTS

Position	Seal Type	Upstream, or High Pressure Side			Low Pressure Side			Speed	
		Fluid	Pressure, psig	Temperature, F	Fluid	Pressure, psig	Temperature, F	Nominal, rpm	Average Relative Speed, ft/sec
AF	Lift-off Face	LH_2	1600	-420	GH_2 + steam	270	1000	35,000	735
BF	Lift-off Face	GH_2	100	-250	GH_2 + steam	66	850	35,000	356

CONFIDENTIAL

(U) Tens-50 aluminum alloy castings are the primary selection for the LH_2 and LOX volutes and inlet housings. This material provides satisfactory strength at minimum weight and can be cast in complex forms. Foundry technology required to cast complex structures has been acquired through extensive development and production usage, and guaranteed minimum mechanical properties for Premium Strength Tens 50-T60 at room temperature and -423 F have been easily met.

(U) Forged titanium 5.0Al-25Sn is used for the inducer, preinducer, and main impeller. This selection was based on material testing and actual service experience. The material has demonstrated that the conservative minimum properties used in the design can be easily met if normal metallurgical control is enforced at the suppliers.

(U) The use of the same alloys for the major components of the Demonstrator Module turbine as are used for the corresponding components in the J-3 engine fuel pump turbine is contemplated. For the manifold and nozzle block, Hastelloy C alloy will be used; for the integral turbine disk and blades, Inconel 718 will be used.

(C) Considerable design and fabrication experience has been gained on these alloys in the production of the J-2 fuel pump turbine. However, the increase in operating time and number of starts of the turbine over that of the H-2 turbine will require the development of additional material properties design data. The design parameter of 300 starts makes it necessary to consider thermal fatigue properties in the design. The approach here will be to generate low cycle isothermal fatigue data which can be applied to the thermal fatigue design problem. The 10-hour firing life requirement also requires that creep and stress-rupture data be developed.

(U) The requirements of propellant-cooled bearings for LO_2 and LH_2 turbopumps have been satisfactorily filled by ball bearings with 440 C races and balls, equipped with glass fabric supported Teflon (GTFE) cages.

(U) Testing of other cage materials (including polyimides, Chemloy 719 and Rulon A) for LO_2 and LH_2 cooled bearings did not demonstrate any to be superior to GTFE (Armalon). For this reason, Armalon is the first choice for use in all bearing cages.

(U) Fuel Turbopump Analysis. The following paragraphs discuss the performance, hydrodynamic, and stress analyses made in connection with the fuel turbopump design.

(C) Pump Performance. Pump hydrodynamic performance is predicted by use of a digital computer program which calculates the performance and losses through the pump for each pump element. All losses are calculated in the dimensionless form of head loss times gravitational constant divided by tip speed squared. The program evaluates losses of inducers, stators, impellers, varied diffusers, volutes, and volute exit diffusers. Types of losses include incidence, skin friction, diffusion, disk friction, balance rib power, recirculation loss, clearance loss, wear ring leakage, and momentum loss. The coefficients and equations used in the program have been found to give reliable preliminary design performance predictions of both H-Q performance and power. To assure meeting the NPSH requirement of 60 feet, a design input value of 30 feet was used in the hydrodynamic analysis for the preinducer. The overall performance of the fuel pump, including its preinducer, is shown in Fig. 121, and the estimated pump operating line throttling down to 5:1 is shown.

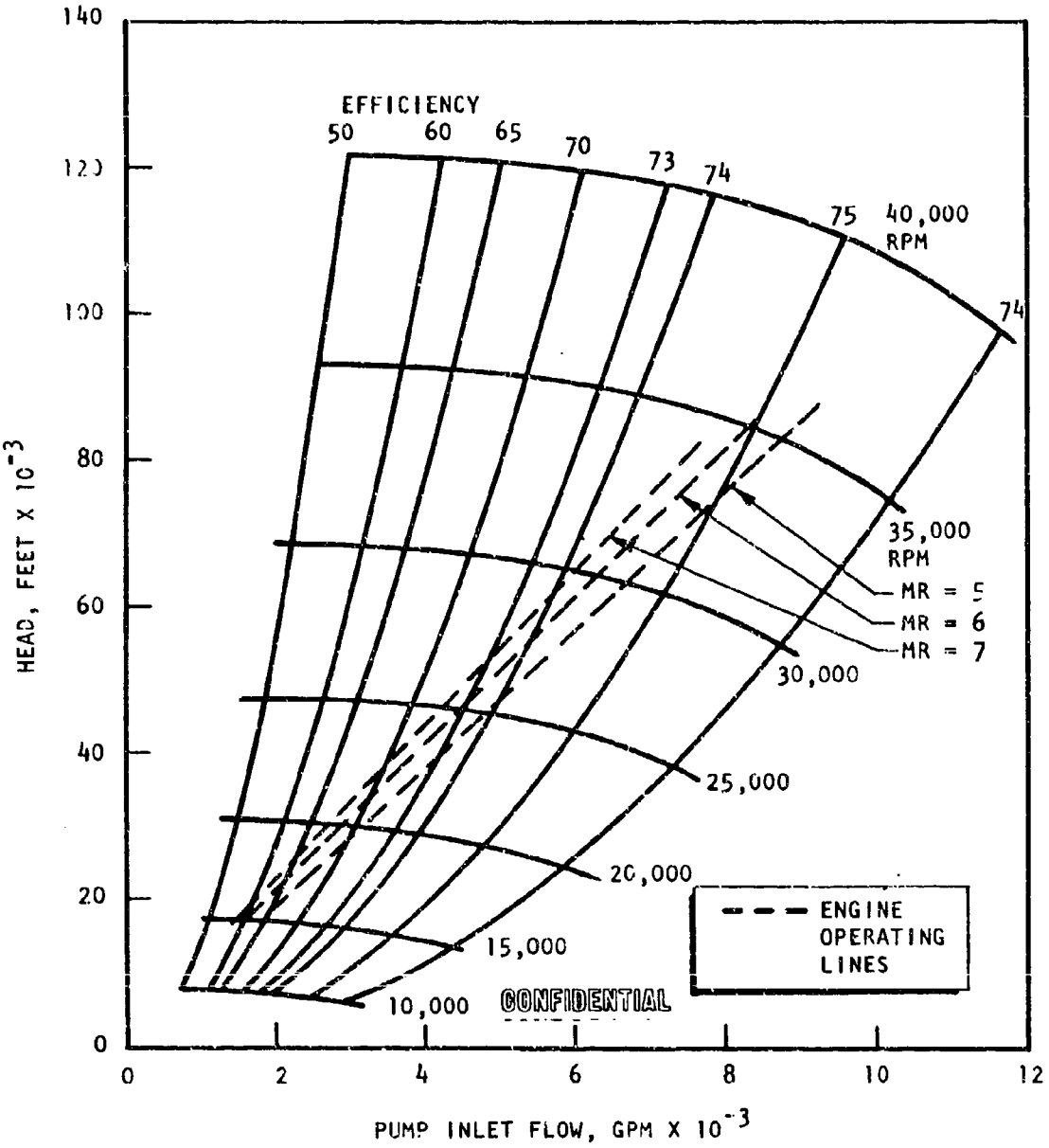

Figure 121. Mark 30 Fuel Pump Performance Map

(C) Volute Hydrodynamic Analysis. The first-stage impeller discharge flow system consists of five flow passages which drop the velocity and direct the flow to the second-stage impeller inlet. The diffusion occurs in the elliptical difusing passages which diffuse the flow while turning it. Such a design has been shown experimentally to be capable of producing higher efficiencies than straight elliptical diffusers (Ref. 4).

(C) The second-stage impeller discharges also into five elliptical flow passages with a velocity ratio of 2.34. These passages then discharge into a collector which leads to a single discharge flange. A clay model of a portion of the volute is shown in Fig. 122.

(C) Main Inducer. The main high-speed fuel inducer provides a head rise of 4000 feet, which imposes substantial centrifugal and hydrodynamic loads. Therefore, a preliminary structural analysis was performed for the estimated blade geometry. The maximum calculated vane steady stress is 31,350 psi (25,700-psi centrifugal stress and 5,650-psi pressure bending stress) which is satisfactory for titanium. The two lowest blade bending mode natural frequencies are approximately 3900 cps and 14,200 cps. These are sufficiently removed from the 1550-cps excitation frequency produced by the preinducer blades.

(U) Fuel Impeller. Preliminary structural calculations of several proposed impeller backplate configurations have been performed. The geometry and maximum allowable tip velocities are presented in Table 38 for various materials.

Figure 122. Volute Mockup

(C) TABLE 38

GEOMETRY AND MAXIMUM ALLOWABLE TIP VELOCITIES

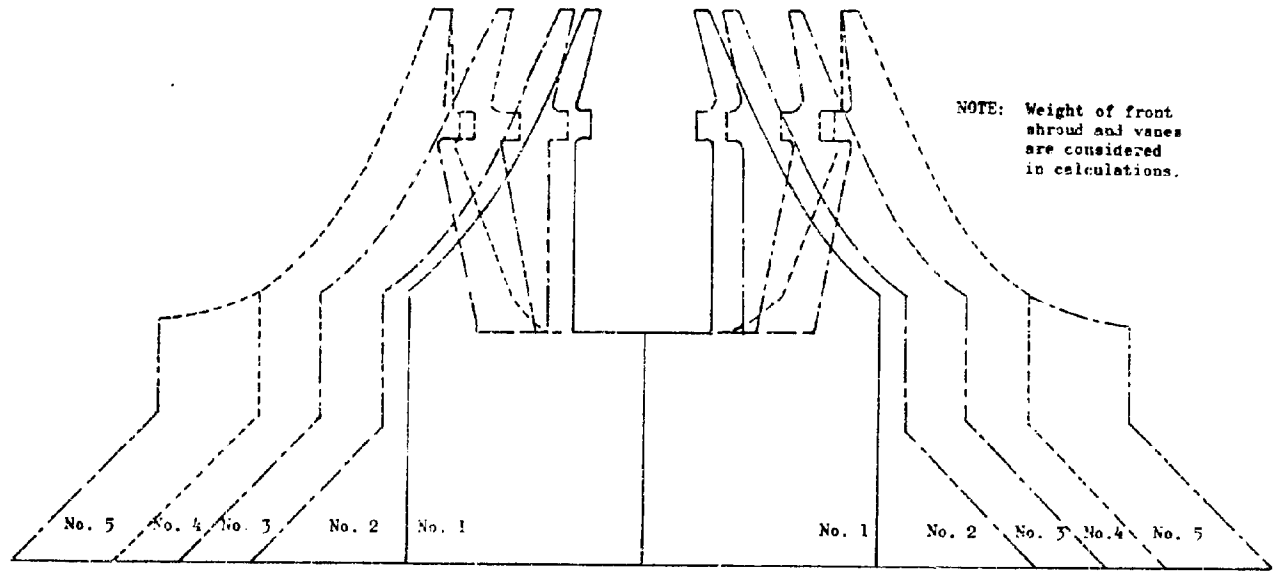

NOTE: Weight of front shroud and vanes are considered in calculations.

Aerospike H_2 Impeller Design Tip Speed = 1709 fps

AEROSPIKE 2 STAGE H_2 IMPELLER BACKPLATE MAXIMUM ALLOWABLE TIP SPEEDS IN FPS (-200 F MATERIAL PROPERTIES USED)

Configuration Number	Materials					
	Tens-50 T60 (Premium) Aluminum, fps	7075 T/3 Aluminum, fps	6061 T6 Aluminum, fps	6061 T6R Aluminum, fps	6070 T6 Aluminum, fps	A110-AT-ELI (5Al-2.5Sn) Titanium, fps
1	1280	1400	1370	1480	1580	1830
2	1360	1460	1460	1590	1690	1950
3	1410	1540	1510	1670	1770	2030
4	1430	1560	1550	1690	1790	2050
5 (cast)	1490					

Does not meet 1700 fps tip speed requirements

(U) Titanium and several aluminum alloys were considered as possible impeller materials because of their favorable strength-to-weight ratio. Ductility, ease of fabrication, and history of successful use as impeller material were also considered. The allowable tip speeds were calculated in accordance with established Rocketdyne burst speed policy; i.e., the maximum allowable operating speed equal to 75 percent of the calculated burst speed.

(C) As shown in Table 38 , 6070-T6 aluminum and A110-AT-EL1 titanium alloy impellers can be fabricated to meet the 1700 ft/sec maximum tip speed requirement. A weight comparison of the impeller configurations for aluminum and titanium is shown in Table 39. An aluminum impeller is seen to have the weight advantage; however, the maximum tip speeds are marginal even for the thicker profiles.

(U) The vanes are perhaps the most critical area of the impeller because of the high speed requirements of the hydrogen pump. Structurally, a thick vane is desirable to carry the centrifugal loads; hydrodynamically, a thin vane is desirable for performance. To compare the effect of these conflicting requirements for aluminum and titanium impeller materials, the minimum possible vane thicknesses required for structural adequacy (the thickness for a vane having no bending stresses) were calculated. These vane thickness profiles along the mean streamline are shown in Fig. 123. The aluminum vane requires approximately twice the thickness of the titanium vane for structural adequacy.

(C) TABLE 39

TWO-STAGE IMPELLER WEIGHT COMPARISON

Configuration	Aluminum Weight, pounds			Titanium Weight, pounds		
	Pre-Impeller	Impeller	Total	Pre Impeller	Impeller	Total
1	2.1*	7.8*	9.9*	3.4	12.6	16.0
2	2.1*	7.9*	13.0*	↓	12.7	16.1
3	2.1	8.9	11.0	↓	14.3	17.7
4	2.1	10.3	12.4	↓	16.6	20.0
5	2.1*	9.3*	11.4*	↓	15.0	18.4

*Does not meet 1700-fps tip speed requirement

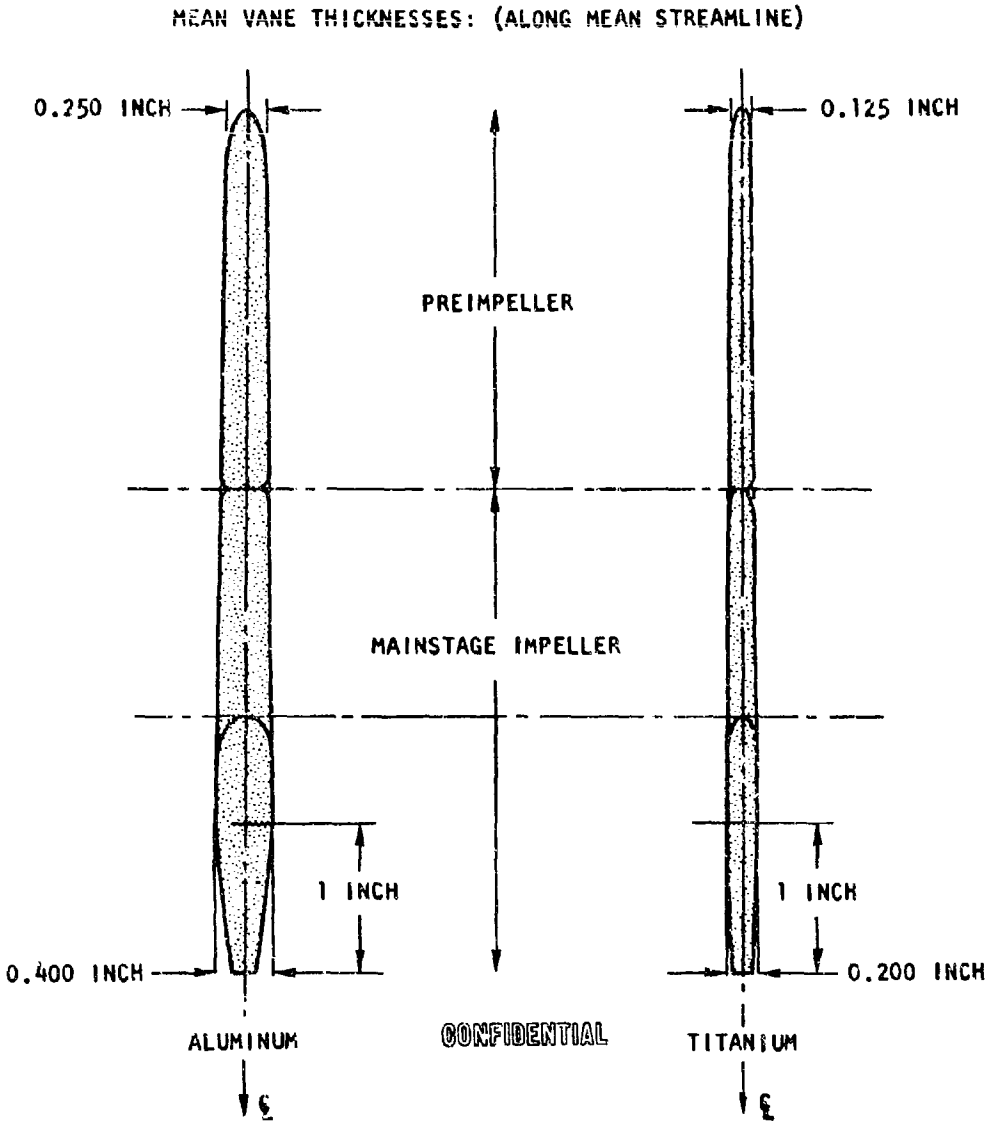

THESE ARE THE VALUES OF THE ABSOLUTE MINIMUM VANE THICKNESS REQUIRED - THESE ARE TO BE USED ONLY FOR PRELIMINARY HYDRODYNAMIC ANALYSIS. BENDING STRESS AND TAPERS WERE NOT CONSIDERED.

Figure 123. Minimum Required Impeller Vane Thickness

(U) Titanium was chosen as the impeller material to permit the vanes to be thinner for increased hydrodynamic performance. The impellers will be integral with the shaft and will be joined with through bolts. The integral impeller-shaft design increases the strength of the backplate by eliminating the central splined bore. A portion of the impeller, the preimpeller, will be made separate from the main impeller to provide ease of fabrication. Shear pins will be used to distribute torsional and centrifugal loads into the main impeller backplate.

(C) The maximum allowable tip speed of the selected configuration, estimated from calculations of a number of proposed backplate configurations, is approximately 1800 ft/sec. A representative backplate stress distribution is shown in Fig. 124.

(U) Fuel Pump Rotor Studs. An analysis was conducted to determine the adequacy of the pump rotor bolting arrangement. The choice of titanium as the impeller material provides a marked advantage over aluminum insofar as the allowable impeller thrust separating load is concerned. This can be seen from Fig. 125. The allowable separating load increases with decreasing temperature for the selected impeller materials 5Al-2.5Sn ELI titanium. At liquid hydrogen temperatures, the separating load that the bolts can carry and still maintain an adequate margin on separation between components of the bolted stackup is approximately three times as large with titanium impeller material as with aluminum.

(U) The shear stress in the studs at the interfaces between the two impellers is 16,500 psi, well within the acceptable limit.

(U) The turbine torque is transmitted to the high-pressure impeller through a spline which is integral to the stub shaft of the impeller. This arrangement circumvents the problems resulting from driving with shear pins through

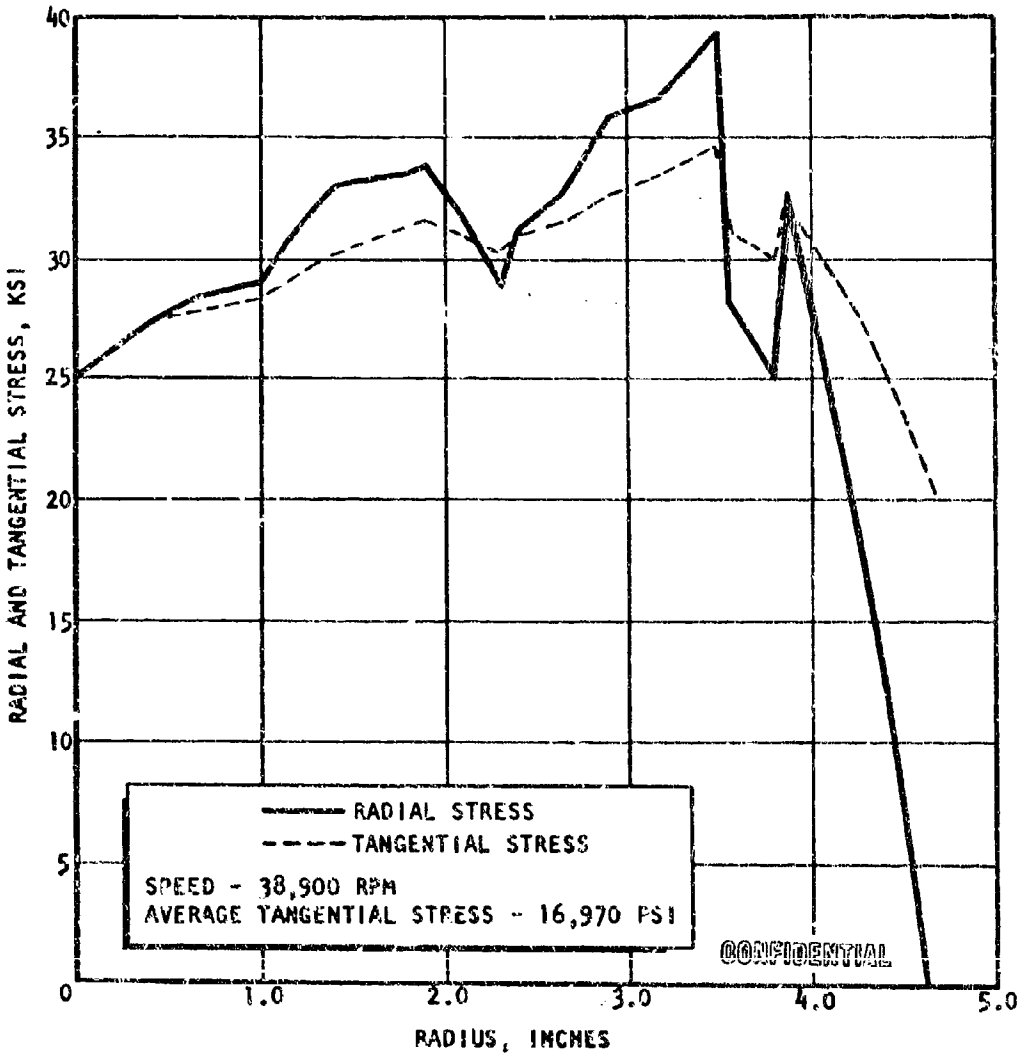

Figure 124. Fuel Impeller Representative Backplate Stress Distribution

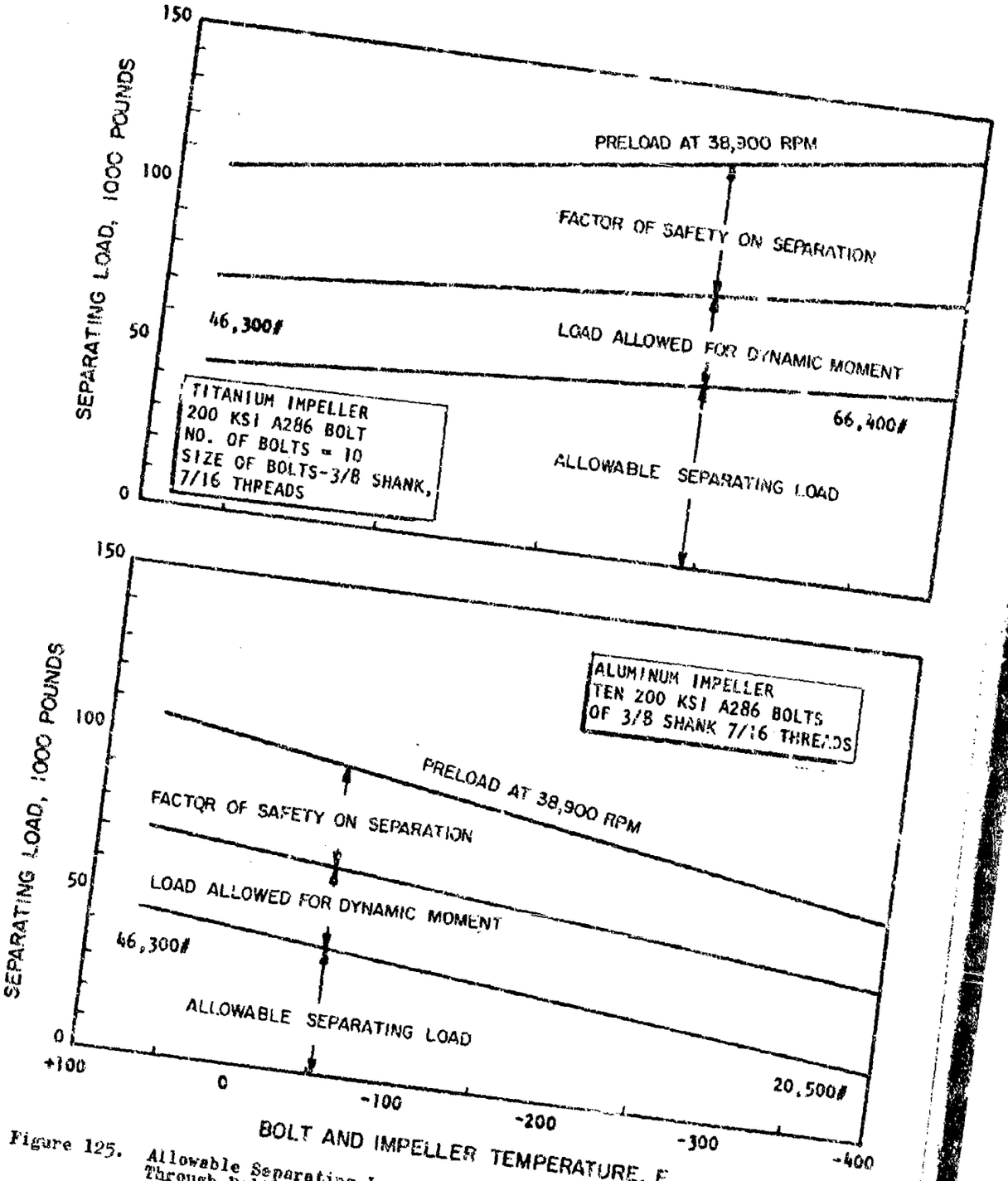

Figure 125. Allowable Separating Load vs Temperature for Fuel Impeller Through Bolts.

two relatively thin intermediate members. However, the torsional wind-up of the stub shaft introduces excessive bending stresses in the pump rotor studs if they are supported in the tangential direction. A design which allows tangential freedom but provides radial support for the studs will minimize these bending stresses.

(U) The spline shear stresses are low and at the minimum section the shaft is adequate to carry the torsional load.

(U) Fuel Pump Balance Piston Backplate. The balance piston backplate will be made of titanium to minimize thermal differential movements between it and the impellers. The deflections and stresses for the worst load conditions; i.e., with the high-pressure orifice closed, are shown in Fig. 126.

(U) The maximum tangential stress is approximately 11,000 psi. The maximum principal stress in the r-z (radial-axial) plane is 16,000 psi. These stresses are within the acceptable limits for titanium.

(U) Fuel Volute Structural Analysis. The volute will be designed to minimize the deflections in the discontinuity areas, near the tongues. In keeping with current Rocketdyne policy, the volutes will be subjected to a proof-pressure test during manufacture. This proof test will serve two purposes. First, high localized discontinuity stresses will be preyielded, and second, a partial measure of quality assurance will be accomplished. Volutes of similar design have been subjected to 500 proof-pressure cycles without failure.

(U) Preliminary calculations were performed to determine the required wall thicknesses of the interstage crossover ducts. The large separating load created by the fluid pressures is carried by the walls of these passages.

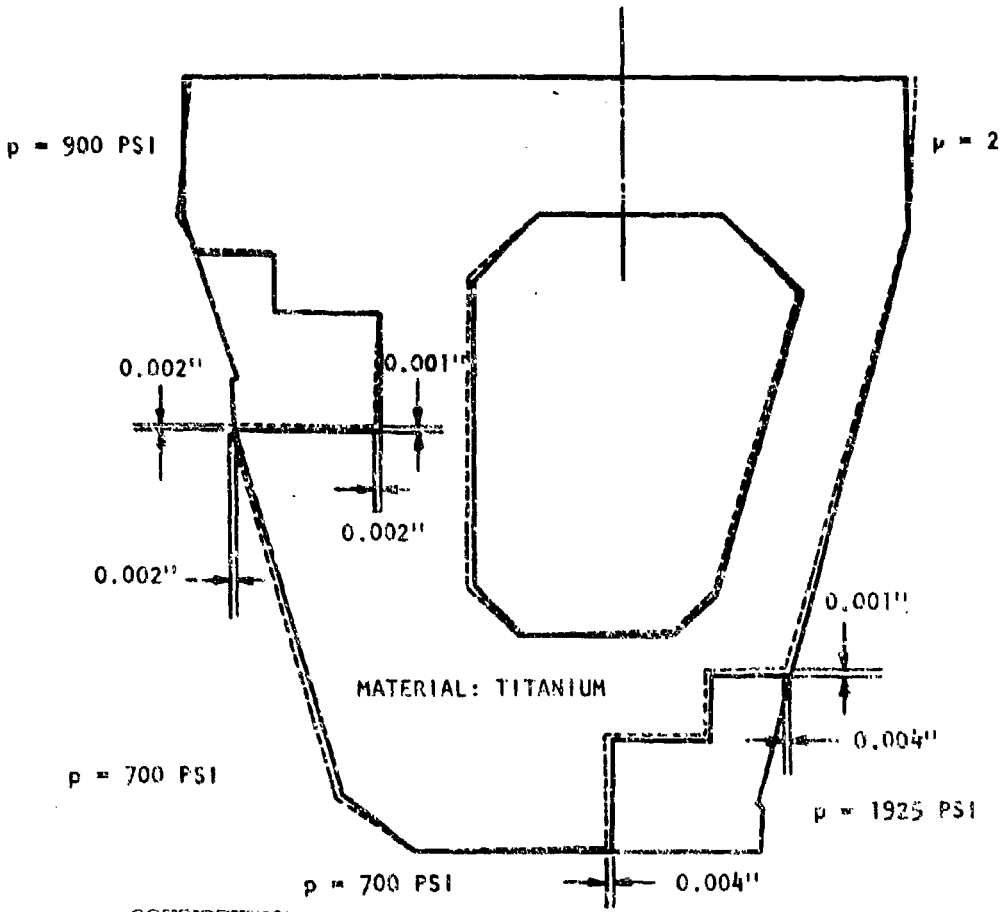

Figure 126. Balance Piston Backplate

The volute has 10 crossover ducts (5 per stage), hence 10 tongues. The required wall thickness varies from 0.60 inch at the entrance of one passage to 0.90 inch immediately upstream of the entrance to the next. The required wall thickness for the high-pressure collector scroll is 0.75 inch at the volute discharge.

(U) Turbine Performance. The estimated performance map for the fuel turbine is shown in Fig.127. This map was developed by reducing the available energy in accordance with turbine energy loss coefficients that have evolved from design and development of previous turbines. These coefficients adjust the available energy for primary friction losses caused by gas flow and expansion within the individual blade passages and for secondary losses resulting from blade path geometry, incidence, Mach number, trailing edge thickness, and leakage within each nozzle-rotor stage. These loss coefficients were derived from correlations of preliminary performance estimates with the final test data for previous turbines that have been built and tested. These turbines have been tested over an operating range of speed and pressure ratio far greater than the turbine was intended to operate to accurately determine both design and off-design performance. After testing the complete turbine, individual rotors and stators were systematically removed and tests were conducted to determine performance with and without these elements. The resulting overall and staging test data were then compared with the preliminary performance estimates and the energy loss coefficients used in the design were revised, if required, according to the test results.

(U) This method of design and development and the considerable amount of test data accumulated allowed the refinement of design coefficients to a high degree of confidence.

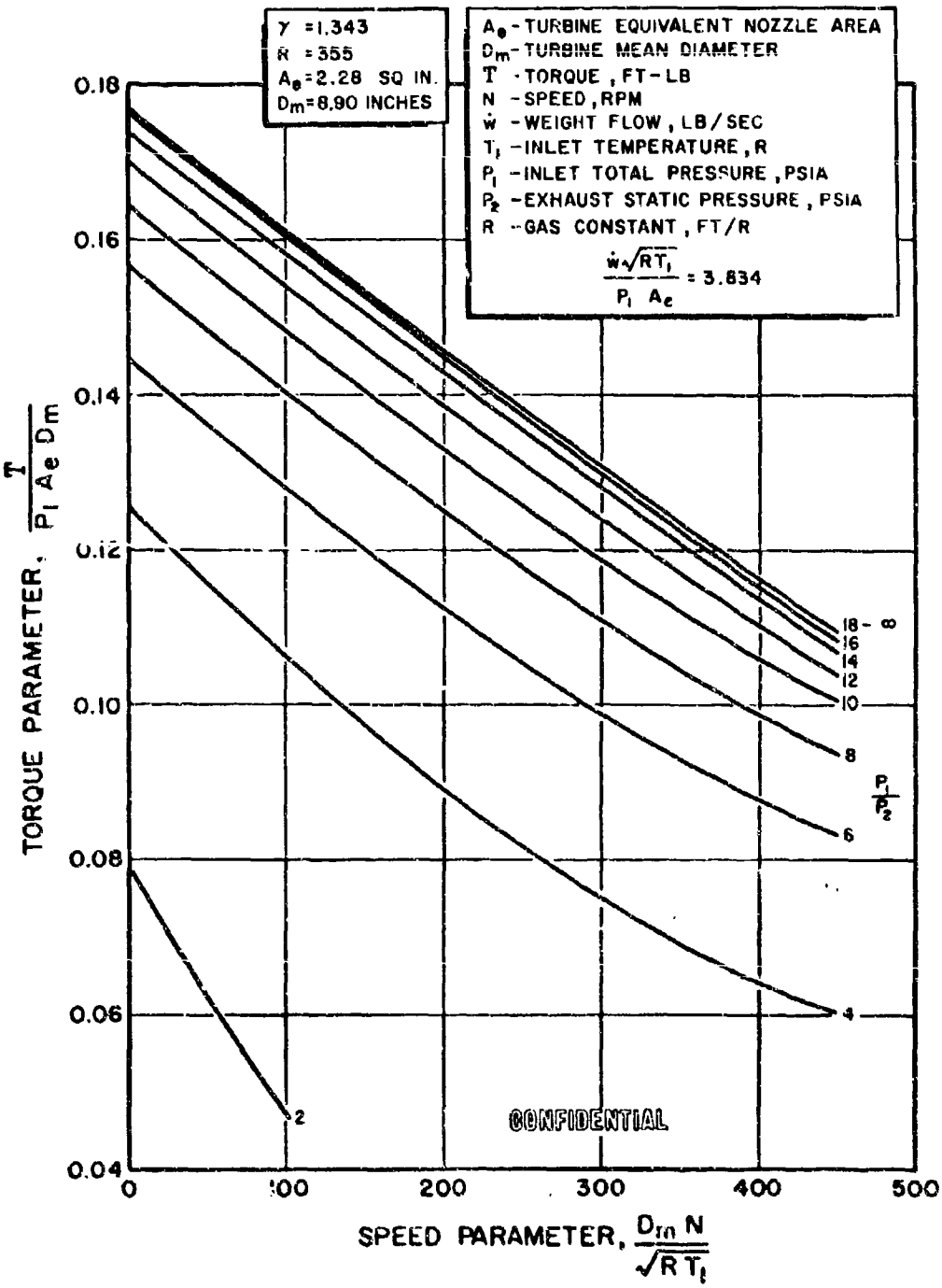

Figure 127. Turbine Estimated Performance, Three-Stage Version

(U) The fuel turbine staging, impulse with velocity compounding, is quite similar to staging that has previously been evaluated. Therefore, the final fuel turbine hardware is expected to perform in close conformance with the estimated performance map.

(U) Fuel Turbine Rotor Blades. Turbine blade stresses were estimated based on similar blades in existence. The first- and second-stage blades are hollowed and shrouded. The third stage is tapered and twisted and will probably be shrouded to reduce vibration induced stresses. The estimated steady-state stresses are shown in Table 40. The values shown do not include stresses caused by twist or stacking. Optimum fillet radii, having minimum stress concentrations, were assumed.

(U) Vibration natural frequencies were estimated for the third-stage blade, which is expected to be the most critical stage. An interference diagram for this stage is shown in Fig. 128. If the blades are unshrouded, a resonant frequency will be experienced within the operating speed range. A number of approaches to minimize the severity of this potential problem area will be considered. A selection of geometry and numbers of nozzles to remove the resonant frequencies from the operating speed range is a possible but not probable solution. A continuous tip shroud may raise the first tangential bending frequency above the operating speed range.

(U) If the resonant frequencies cannot be removed from the operating speed range, the geometry may be selected so that they occur in the lower speed (low stress) range, and the intermediate and high-speed ranges are free from resonances. An additional alternative is available. A change in geometry to fir tree attachments can be made without affecting the overall package size, providing the discs are welded together rather than bolted, as mentioned previously. Tests will be conducted to verify the blade natural frequencies. Studies will be made to optimize the design for the vibration

(C) TABLE 40

LH_2 TURBINE BLADE STRESSES

	First Stage (Shrouded)	Second Stage (Shrouded)	Third Stage (Unshrouded)
MAXIMUM STRESSES (at leading and trailing edges), psi			
Without Stress Concentration			
Centrifugal*	30,500	44,100	42,170
Power Bending	5,360	5,560	5,190
Total	35,860	49,660	47,360
With Stress Concentration			
Centrifugal*	37,900	54,900	52,300
Power Bending	6,700	6,900	6,400
Total	44,600	61,800	58,700
MATERIAL PROPERTIES FOR INCO 718			
Ultimate Strength, psi	124,000	153,000	156,000
10 Hour Rupture Strength, psi	83,000	140,000	150,000
Temperature, F	1,320	1,100	945

NOTE: Speed 38,900 rpm
Power 22,585 hp
Torque 36,500 in.-lb

*Centrifugal bending stresses are not included.

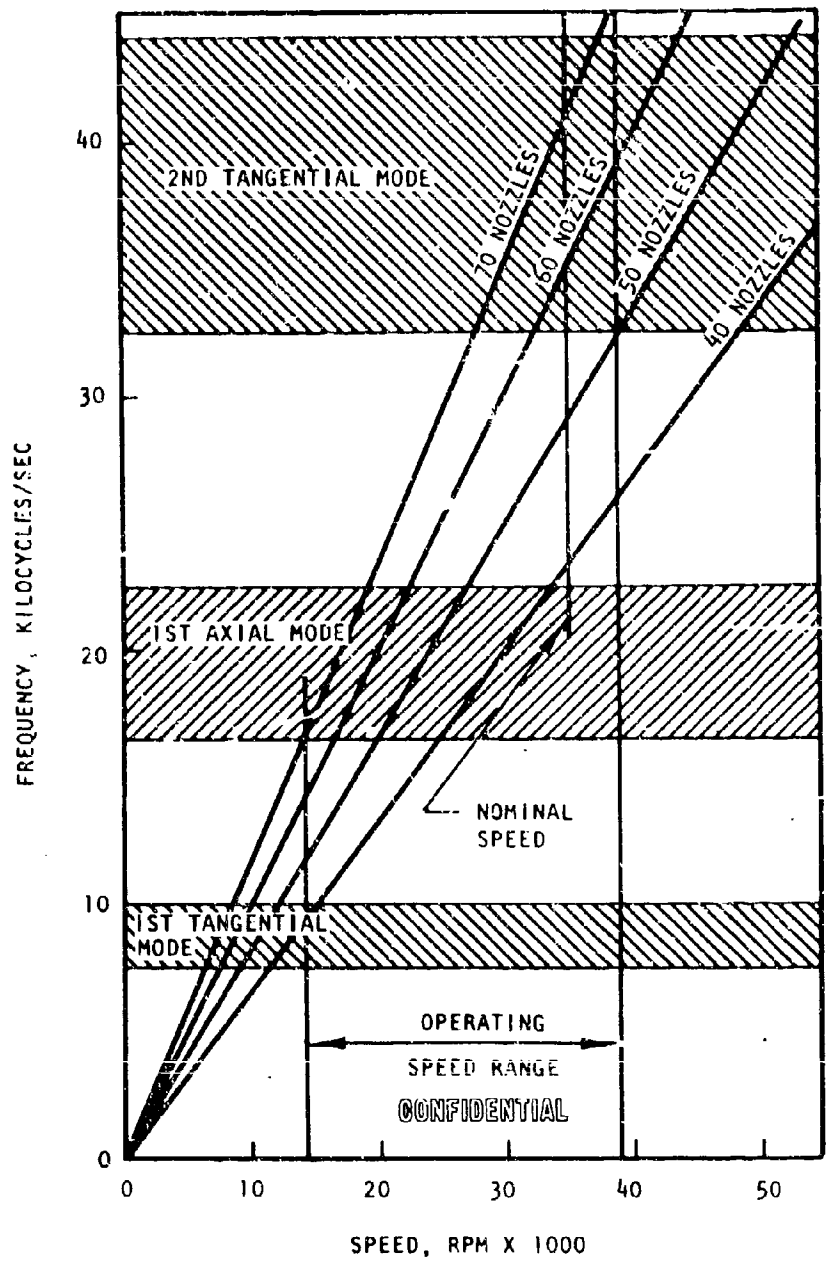

Figure 128. Third-Stage Turbine Blade Interference Diagram

consideration. The vibration considerations are expected to be less critical in the first- and second-stage blades with integral continuous shrouds. The thermal duty cycle will be defined for operating conditions. Thermal stresses and the attendant low cycle fatigue will also be a consideration in determining the airfoil and shroud cross-sectional geometries.

(U) Fuel Turbine Inlet Manifold. The turbine inlet manifold will be made of Hastelloy C. Use of Hastelloy C eliminates the need for a heat treated weldment and provides adequate rupture strength and good ductility. The thermal duty cycle will be defined and low cycle fatigue considered in the sizing of the manifold and turbine stationary parts.

(C) Seal Analysis. The function of the main liquid hydrogen pump seal package is to prevent excessive leakage of liquid hydrogen into the turbine. The package consists of three flow restrictions in series between the 1600-psig fluid at the inlet to the second stage and 270-psig turbine downstream pressure. The first and third restrictions are labyrinth seals which must flow a substantial amount of fluid to create a pressure drop seals which must flow a substantial amount of fluid to create a pressure drop, and so are considered mainly as backup seals. The second seal is the main flow restriction and is a positive-type shaft seal, which will be referred to as the primary LH_2 seal.

(C) The most advanced seal application in the LH_2 pump is the high-pressure primary LH_2 seal which will be required to operate outside present experience and state of the art for both speed (735 ft/sec) and pressure (1600 psig).

(U) In order to attain the life required, seal concepts other than two contacting flat rubbing surfaces will be required because of the high heat generation and resulting wear. An attractive alternative is the liftoff seal, in

which the sealing faces are separated, eliminating wear. Testing to date had indicated that hydrostatic liftoff seals can perform satisfactorily at high speeds for LH_2 service. It is felt that the hydrostatic seal is adaptable to higher pressures and speeds because of its noncontacting feature.

(U) The hydrostatic seal is self-compensating, in that face geometry is designed so that the seal is hydraulically in balance with the faces separated slightly. Further opening drops the pressure between the seal faces, and hydraulic forces tend to close the seal. The seal then operates at a small controlled gap with a small steady leakage. Because the hydrostatic seal remains lifted off as long as the applied pressure exceeds the design liftoff pressure, this type of seal should be insensitive to speed, higher pressure, or operational time. The remaining design goal is then to provide a secondary seal (most probably a bellows) capable of withstanding the seal pressure.

(C) Bearing Analysis. The most significant new technology area in the turbopumps is the turbine bearings which must operate at 35,000 rpm (LH_2 pump) and 25,000 rpm (LO_2 pump) lubricated and cooled by gaseous hydrogen. A limited amount of testing was conducted in which ball bearings were cooled with gaseous hydrogen. Two sets of 45-mm bore bearings were run at 34,500 rpm to 38,800 rpm for 212 minutes total test time. Three sets of 60-mm bore bearings were operated for accumulated test times of 481, 301, and 507 seconds, respectively. In general it was concluded that more cage pocket wear, lower load and speed capacity, and more ball and race surface degradation occur with GH_2-cooled bearings when compared to LH_2-cooled bearings.

(U) Two potential solutions are considered; the final choice will depend upon test results. Preliminary tests will be conducted to determine uprating limits with gaseous hydrogen coolant. As an alternative, a lubrication system with gaseous hydrogen plus an additive such as tributyl phosphate will be tested. This system has been used for gear and bearing lubrication in another application. The anticipated lubrication requirements for the turbine bearings are less severe than those for gears, and it is therefore expected that an additive system, if needed, will comprise a satisfactory solution of operational problems.

(U) The preliminary designs of both turbopumps show ball bearings preloaded with springs. Consideration will be given during the detail design to the use of roller bearings in the turbine position. The roller bearings are expected to have the following advantages:

1. No sliding of outer race required
2. High radial stiffness

It is expected, however, that roller bearings will require additives in the gaseous hydrogen to prevent excessive roller end wear.

(U) The choice among the alternative systems will be based on design analyses including shaft dynamic analysis and upon bearing test results.

(U) Rotordynamics. Several critical speed analyses were performed for various configurations of LH_2 turbopump rotating assembly. Each rotating assembly was idealized as a system of lumped mass stations. The inertia properties and elastic characteristics for each station were then approximated. The system simulated was then evaluated by a transfer matrix scheme yielding the critical speeds. The analysis procedure was performed using digital programs operating on the IBM system 360. Critical speed variations for changes of bearing radial spring rates were studied. The final configuration analyzed exhibited at least one critical speed within the operating speed range for any practical range of bearing spring rate. Figure 129 displays a plot of critical speeds vs bearing radial spring rate. Bearing spring rates in excess of 1.3 (10^6) lb/in. are recommended to minimize critical speed problems; i.e., for such values only one critical speed will exist within the desired operating speed range. Figure 130 shows the first critical speed shaft normalized mode shape. Although the rotor analysis indicates the first critical speed to be within the throttling speed range, it is predominantly a bearing critical speed (most of the deflection due to bearing flexibility). Experience with similar types of rotating assemblies, with proper balancing of the physical rotor and damping by the fluid forces, show that this critical speed mode is not apparent in experimental data. However, the analysis does point out a potential area to be cognizant of, during development testing, should problems arise.

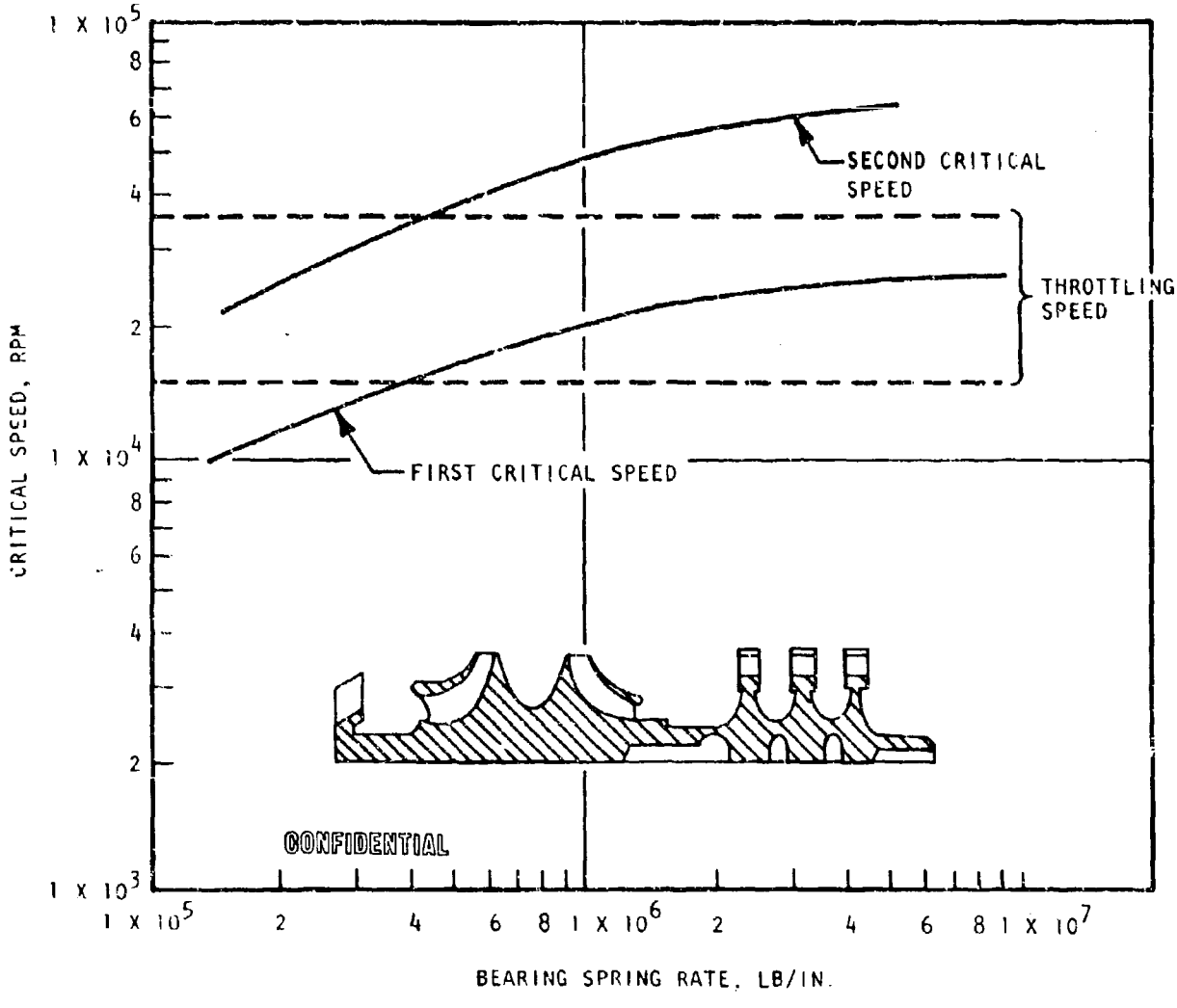

Figure 129. LM_2 Turbopump Critical Speed vs Bearing Spring Rate

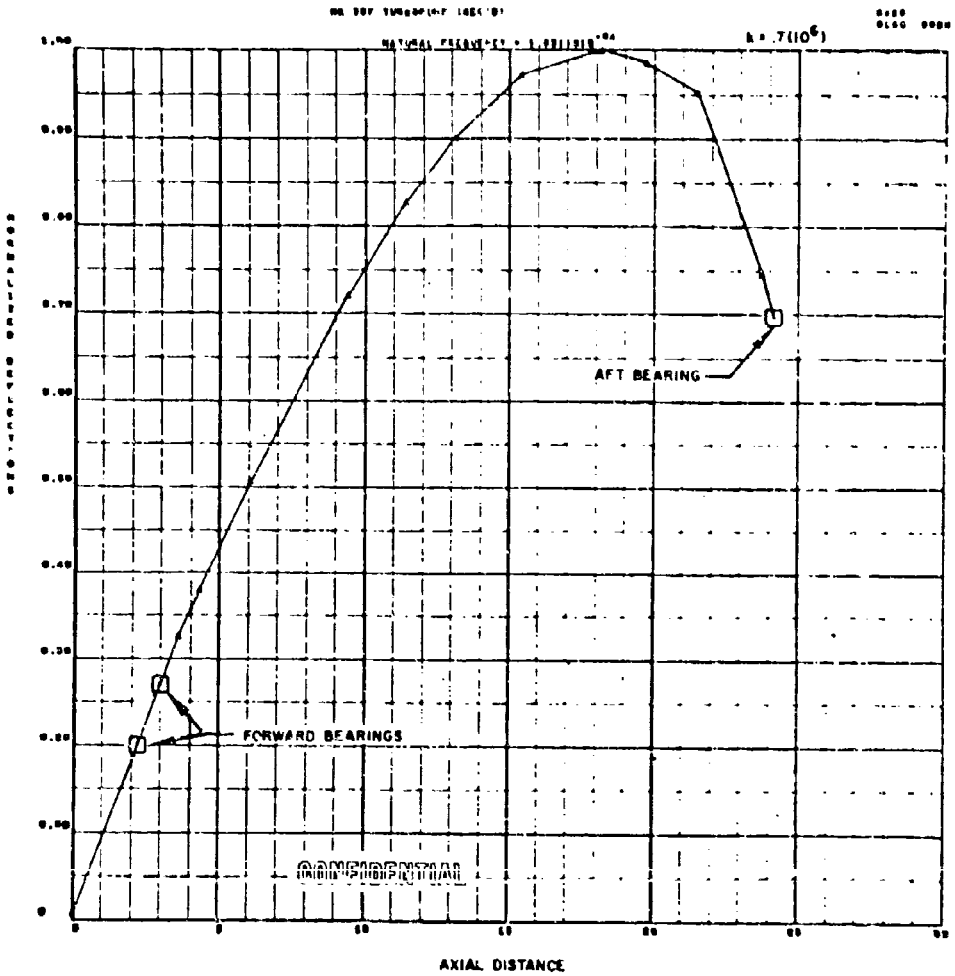

Figure 130. Turbopump First Critical Speed Mode Shape

(C) Oxidizer Turbopump Design Requirements. The initial oxidizer turbopump design requirements were derived from the thrust, performance, and operational requirements listed in Table 9, together with the pressure requirements defined by the system analyses. The demonstrator module oxidizer pump design must meet the requirements listed in Table 41 and provide a maximum efficiency not less than 73 percent over the mixture ratio excursion at full thrust.

(C) TABLE 41

OXIDIZER TURBOPUMP DESIGN CONDITIONS

Parameter	Nominal (MR=6:1)	Maximum Off Nominal	3 σ Tolerance	Maximum Design Requirement
Pump Q_o, gpm	3126	3295	160	3455
Pump P_D, psia	2060	2118	166	2284
NPSH, feet	16			
Pump Inlet Pressure, psia	40.0			
Pump Inlet Temperature, R	175.6			
Turbine W_f, lb/sec	3.91	4.13	0.47	4.6
P_{in} (Turbine Inlet Pressure), psia	750	791	92	883
P_o (Turbine Discharge Pressure), psia	40	44.1 (MR=5)	4.32	48.42
T_{in} (Turbine Inlet Gas Temperature), F	1960	1960	152	2112
Turbine Efficiency	47.4			

(U) The turbine was designed based on the gas generator properties listed in Table 29 . For turbopump operating characteristics at off-design mixture ratios see Table 10 , page 78.

Oxidizer Turbopump Alternatives Studied.

(C) Pump Configuration. Because of the high density of LO_2, the required pump head is relatively low (H 4610 feet maximum). The low head, when combined with high speed (to minimize weight and envelope), results in a high specific speed design. The high specific speed and medium volume flow of 3100 gpm, combined with the requirement for throttling, make this pump ideally suited to a centrifugal design. Such a pump has the characteristics of high efficiency, low weight, design simplicity, and wide off-design performance. Therefore, no other candidate configurations were investigated for the main centrifugal stage. The analysis for the selection of a hydraulic turbine mounted in the preinducer hub to drive the preinducer was presented with the fuel pump preinducer drive analysis, page 248.

(U) Oxidizer Turbine Disk Configuration. A study was conducted to determine the required turbine disk configurations. The selected profiles and corresponding stresses are shown in Fig. 131 through 134. The disc material is Inconel 718 and the blades are fir tree attached. During the initial portion of this study, the required sizes were calculated for the third-stage disc with and without a central hole. The results are shown in Fig. 131 and 135. This study was conducted considering blades with fir tree attachments. The thickest hollow disc considered (Fig. 135) did not have an adequate allowable speed. From a comparison of Fig. 131 and 135 it can be observed that the solid disc offers advantages in turbine assembly and weight. During the detail design of the turbine disc, analysis will

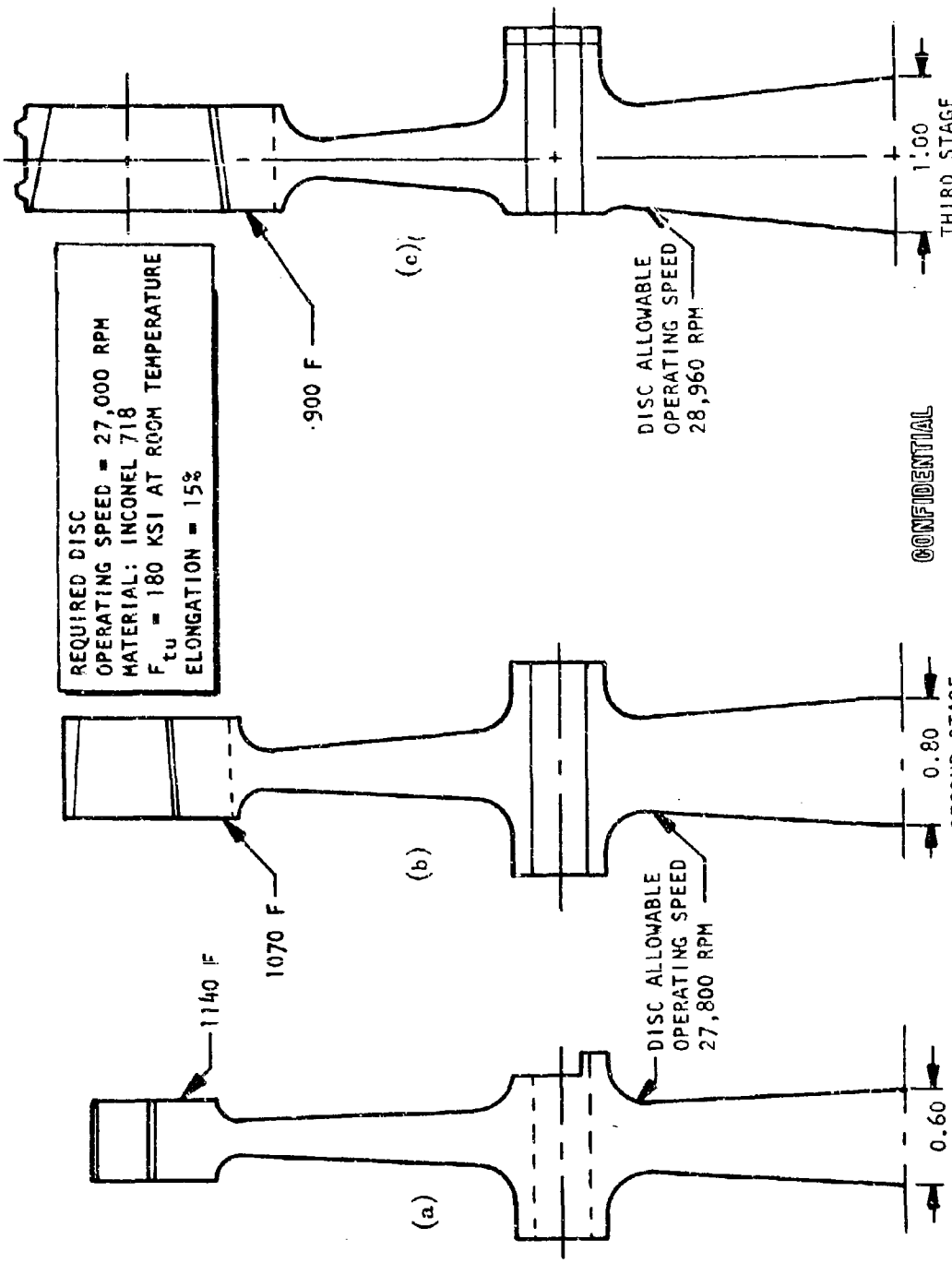

Figure 131. Oxidizer Turbine Disc Sizing (With Shrouded Fir Tree Blades)

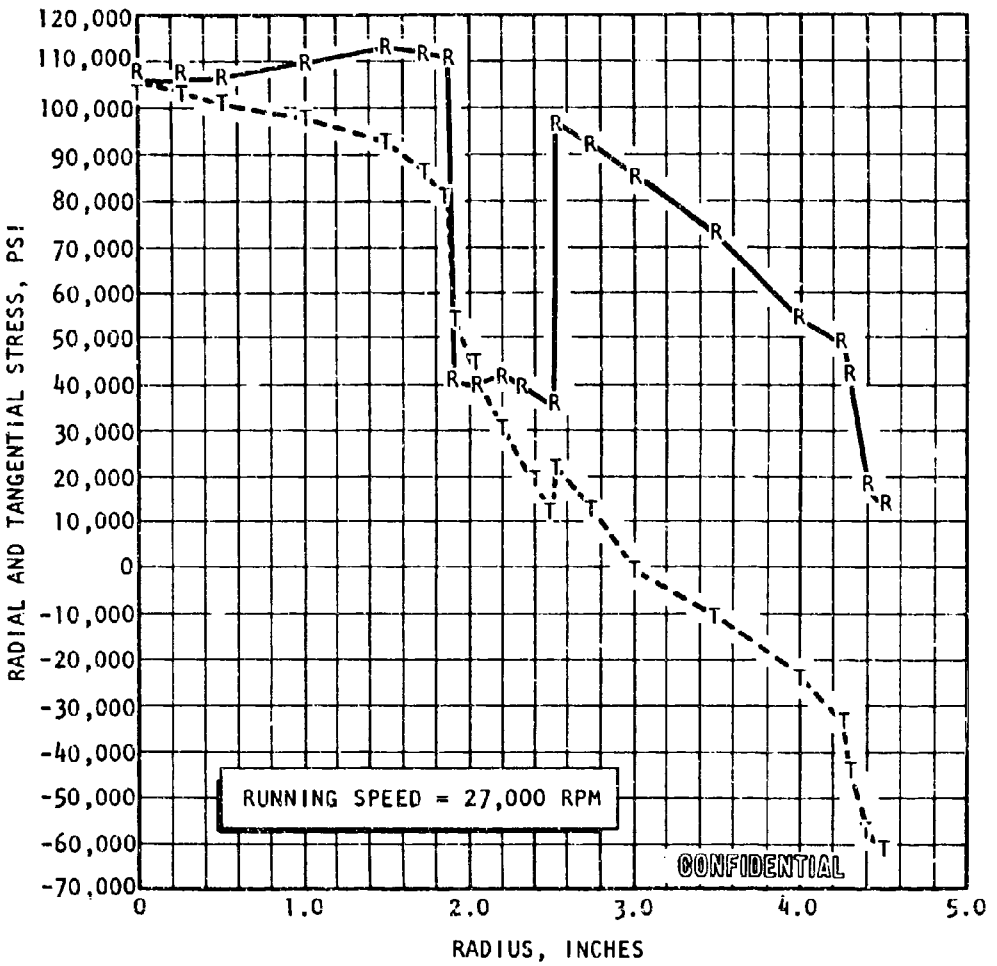

Figure 132. First-Stage Oxidizer Turbine Disc Stress vs Radius

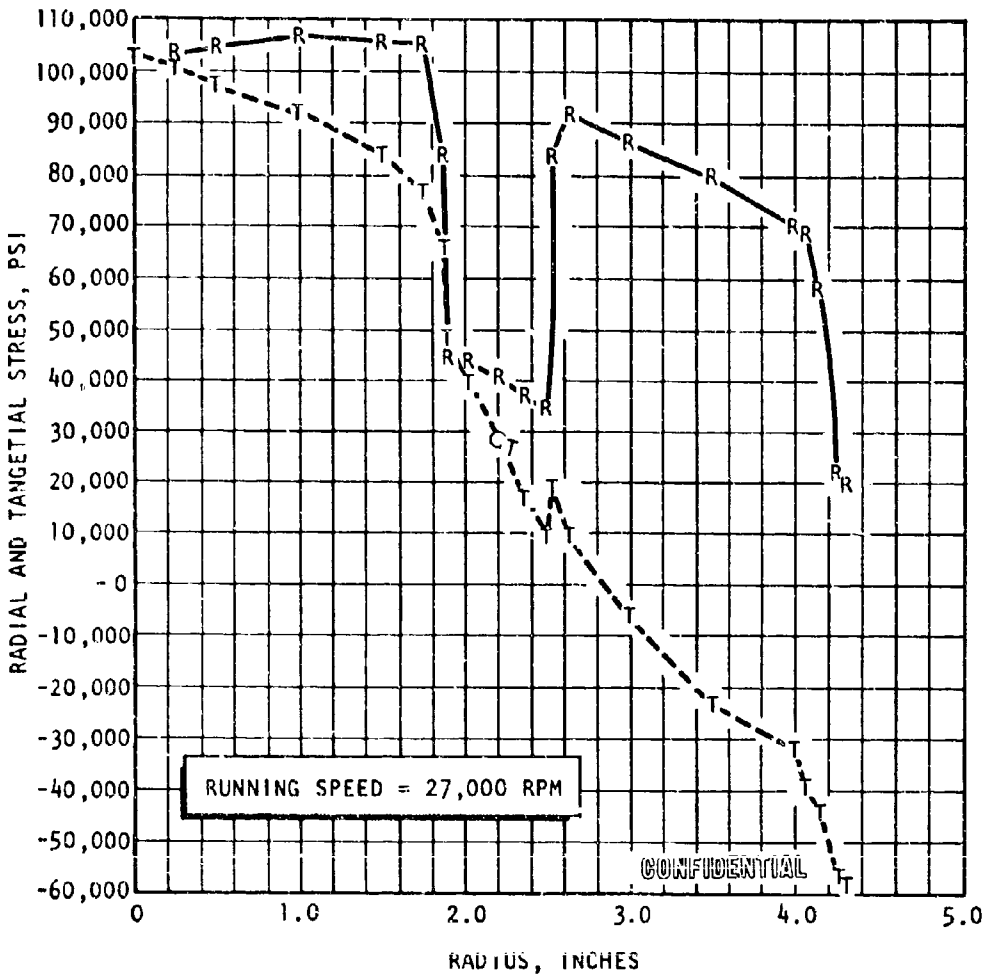

Figure 133. Second-Stage Oxidizer Turbine Disc Stress vs Radius

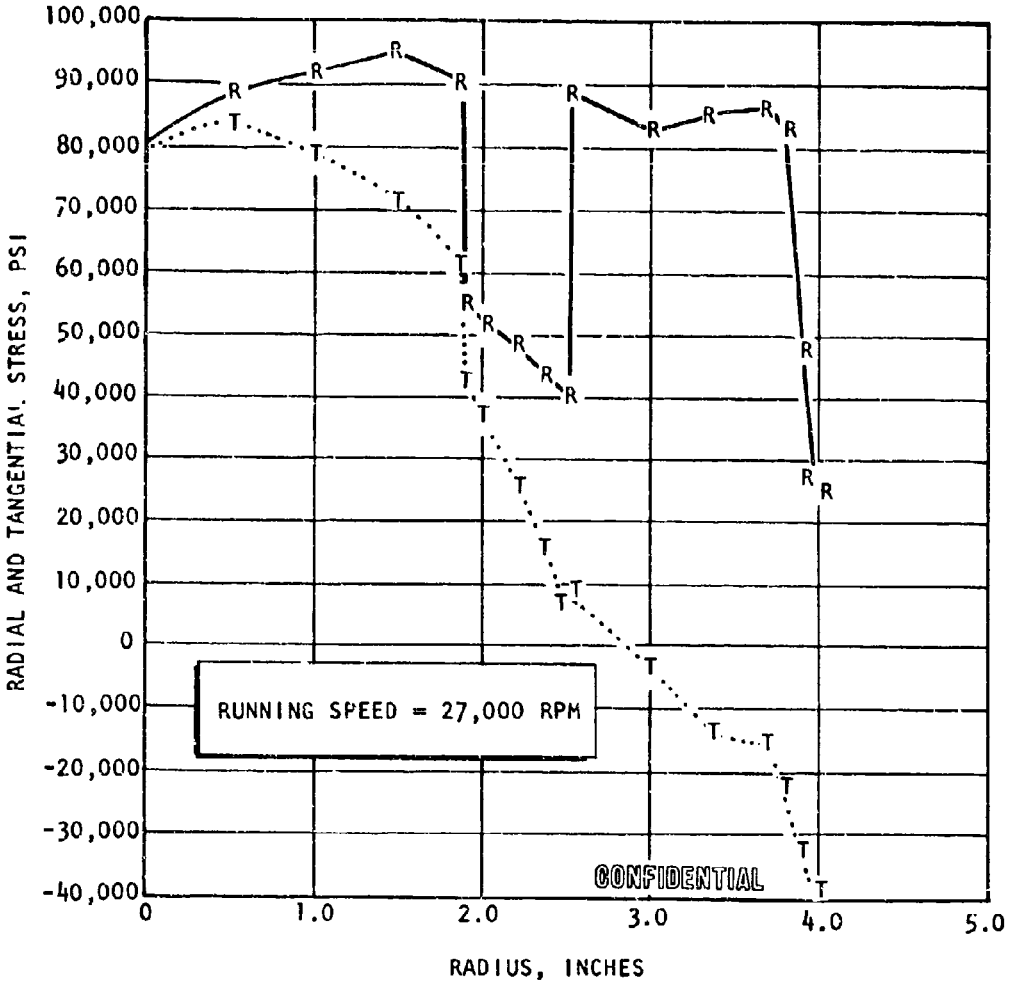

Figure 134. Third-Stage Oxidizer Turbine Disc Stress vs Radius

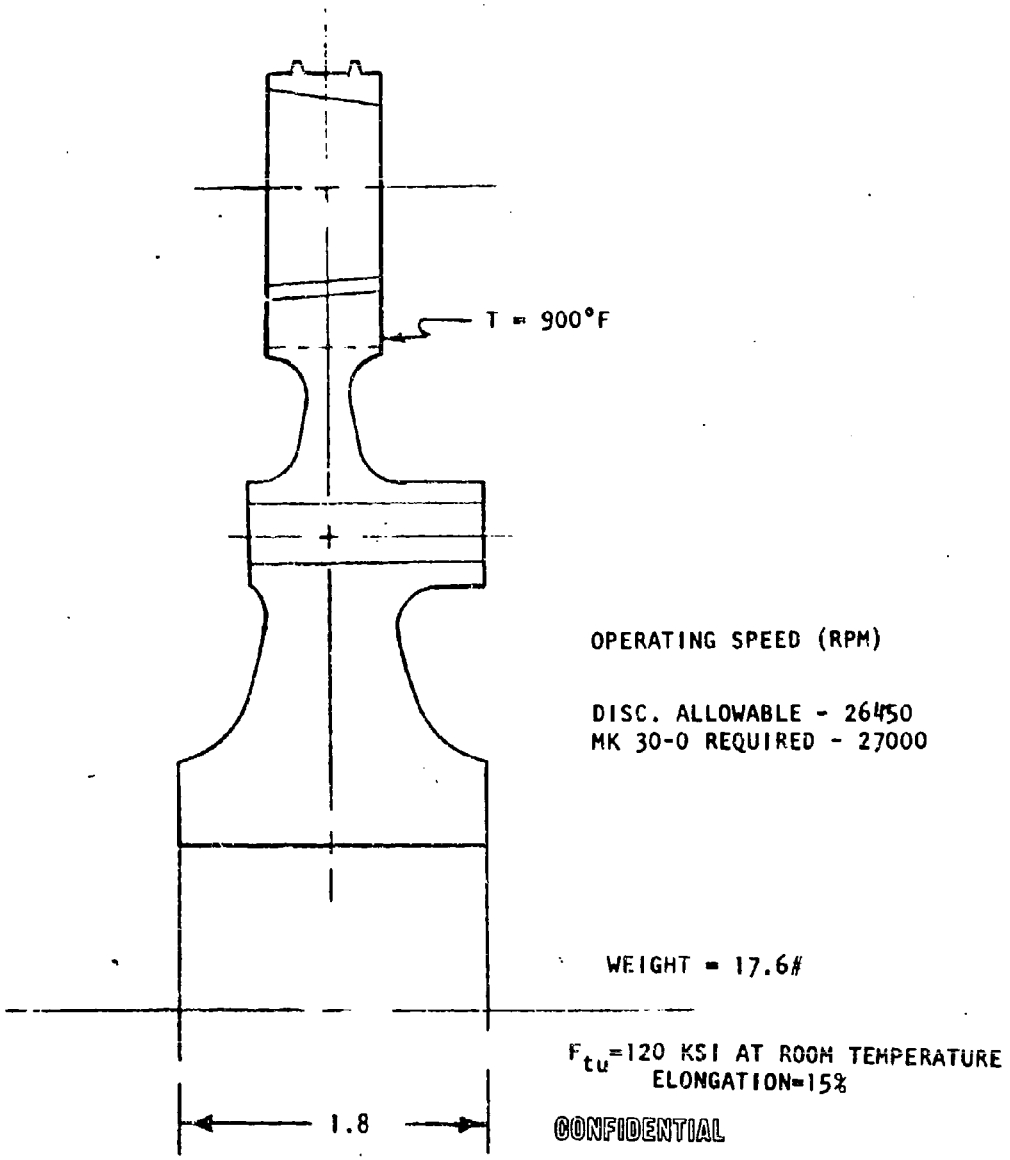

Figure 135. Mark 30-0 Turbine Third Stage Disc Preliminary Sizing Disc With Hole (Shrouded Fir Tree Blades)

be performed to determine the disc natural frequencies and critical running speeds. Disc profiles will be modified as required to remove the critical running speeds from the operating speed range.

(U) Oxidizer Turbopump Description. The oxidizer turbopump consists of a single-stage, centrifugal pump mounted on a common shaft with a three-row turbine, with a concentric, integral, hydraulic turbine driven preinducer. A layout of the complete assembly is shown in Fig. 136.

(U) Pump. The oxidizer pump assembly consists of the preinducer, the impeller, and the housing.

(C) The preinducer, designed to meet the NPSH condition of 16 feet, is similar to the fuel pump preinducer, with four vanes at the inlet increasing to eight at the discharge. It operates at approximately 25 percent of the main pump speed (6000 rpm), and produces a head rise of 320 feet, which requires that the following high-speed inducer operate at a very moderate suction specific speed of 17,900. The oxidizer preinducer drive differs from the fuel preinducer drive in that a four-stage hydraulic turbine is located in the inducer hub rather than a single-stage in the main hydrodynamic passage. It is driven by high-pressure (2000 psia) liquid oxygen tapped from the pump discharge, and returned to the main pump flow between the preinducer and the main inducer. At the nominal design point the recirculated flow is approximately 15 percent of the total oxidizer flowrate. A fifth stage could be added, which would reduce the hydraulic turbine flow to 12 percent if a higher efficiency became necessary. The hub turbine drive also offers the possibility of separate speed control of the preinducer by including a throttle valve in the hydraulic turbine supply line. The preinducer design parameters are shown in Table 42.

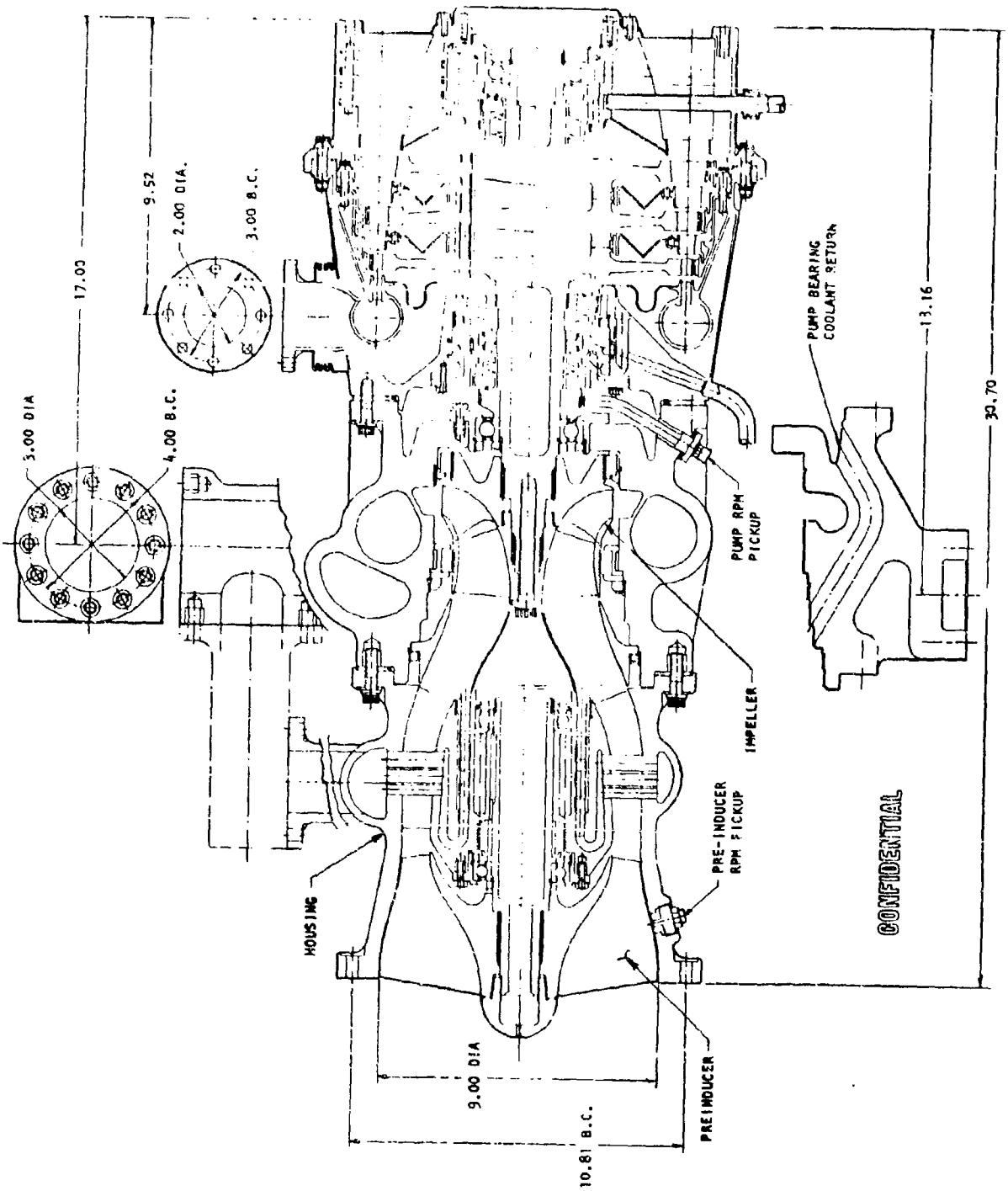

Figure 136A. Demonstrator Engine Oxidizer Turbopump

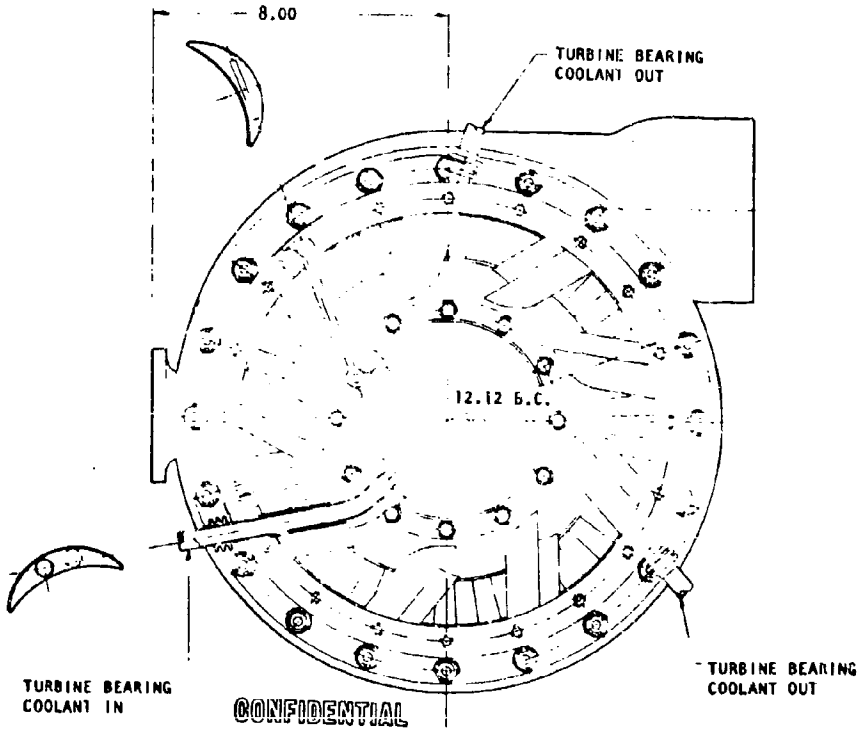

Figure 136B. Demonstrator Engine Oxidizer Turbopump

(C) TABLE 42

OXIDIZER PREINDUCER DESIGN PARAMETERS AND OFF-DESIGN OPERATING CONDITIONS

	Mixture Ratios		
	5	6	7
Preinducer			
Speed, rpm	5800	6000	6300
Inducer Inlet Flow Coefficient	0.069	0.07	0.0706
Head Rise, feet	310	320	330
Inducer Inlet Tip Diameter, inches		9	
Blade Number 4 Plus 4 Splitters			
Inducer Discharge Tip Diameter, inches		7.75	
Inducer Head Coefficient		0.250	
Stator Inlet Tip Diameter, inches		7.75	
Stator Discharge Tip Diameter, inches		6.75	
Hydraulic Turbine			
Hub Turbine Pitch Diameter, inches		3.75	
Passage, Height, inch		0.29	
Number of Stages		4 to 5	

(C) The high-speed inducer has blades machined from K-monel and splined to the main shaft. It operates at a tip speed of 507 ft/sec (at 25,000 rpm) and provides a head rise of 716 feet.

(C) The selected impeller design results in a centrifugal stage head coefficient of 0.357 and a stage efficiency of 80 percent. The impeller is made of Tens-50 aluminum and is shrouded to permit large clearances between metal surfaces to minimize explosion hazard. The impeller seals, which operate with close clearances, are fabricated of fluorocarbon material, which has been experimentally demonstrated to be safe for this application during operation in H-1, J-2, and F-1 oxidizer pumps supplied to the NASA. The basic impeller geometry is presented in Table 43.

(U) The pump housing is made of cast Tens 50 aluminum alloy and incorporates a double-tongue volute with the two passages joined upstream of a single discharge. The volute construction minimizes radial bearing loads at off-design conditions and reduces volute friction losses by cutting the flow path length. A port is provided upstream of the discharge flange for the preinducer turbine drive fluid supply.

(U) Turbine. The oxidizer turbine is a three-row, essentially velocity compounded impulse turbine similar to the fuel turbine.

(U) Turbine discs are mounted similar to the LH_2 turbine, and torque is transmitted to the pump impeller through a splined, integral turbine shaft. Since turbine length is not dictated by disc stress considerations, discs will be machined independently of the blades and the cast blades will be attached to the discs with fir trees. Blades on all three rows are shrouded, and honeycomb seals are provided both at the blade tips and at the interstage diaphragm. The turbine gas path and design parameters are shown in Fig. 137.

(C) TABLE 43

OXIDIZER CENTRIFUGAL PUMP STAGE GEOMETRY

High Speed Inducer	
Speed, rpm	25,000
Inducer inlet flow coefficient	0.201
Inducer heat rise, feet	716
Inducer inlet tip diameter, inches	4.65
Inducer discharge tip diameter, inches	4.4
Inducer head coefficient	0.100
Suction specific speed	17,900
Impeller	
Impeller inlet eye diameter, inches	4.4
Impeller tip diameter, inches	5.5
Impeller tip width, inches	0.9
Centrifugal stage head coefficient	0.357

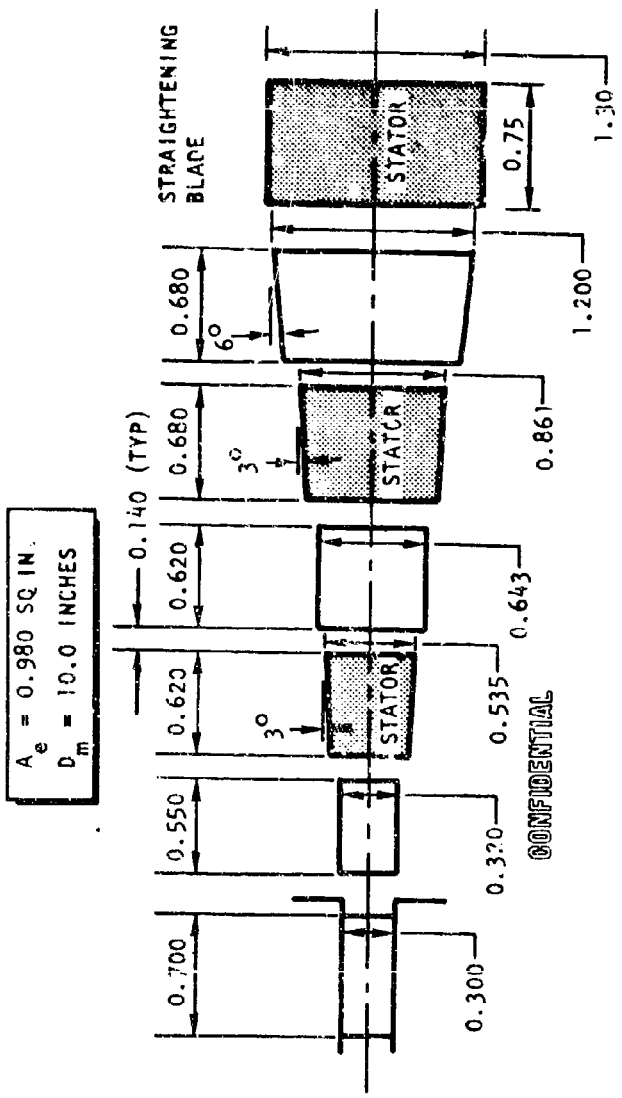

Figure 137. Turbine Gas Path Sketch

(U) Bearings. The liquid oxygen turbine employs two hydraulically coupled rotating elements each supported on two ball bearings. For purposes of tabulation they will be designated 1φ, 2φ, 3φ, and 4φ. The design requirements of the oxidizer turbopump bearings are shown in Table 44.

(C) The LO_2 pump employs four propellant-lubricated ball bearings for component location: two on the hydraulically driven preinducer and two on the turbine and pump shaft. The preinducer operates at 6000 rpm, with both bearings cooled and lubricated by recirculation of LO_2. Both bearings have 40-millimeter bores, operate at nominal speed, and are considered to be a state-of-the-art applications that will pose no design and development problems.

(C) The inlet end bearing on the pump shaft (50-millimeter bore) will operate at 25,000 rpm, cooled by LO_2, and will support any net hydraulic pump thrust loads. Recent testing on an IRD program has demonstrated the capability of a similar bearing to operate at 25,000 rpm at a thrust load of 600 pounds for 15 hours. To attain bearing reliability with no further developments, the net turbopump thrust must be balanced to the ±600 pound range. Assuming that this is done, the 3φ bearing application is considered within successful test experience.

(U) Since the environment downstream of the outboard turbine bearing seal is hydrogen-rich, this bearing is lubricated and cooled with gaseous hydrogen tapped from the thrust chamber inlet manifold. A discussion of this application was presented in the Hydrogen Turbopump Bearings section of this report.

(U) Seals. The most sensitive seal application is the oxidizer seal package, whose function is separation of LO_2 and hydrogen-rich steam used in the turbine. Mixing of these fluids can result in an explosion. The oxidizer pump will employ a redundant seal arrangement, in which failure

(C) TABLE 44

OXIDIZER BEARING DESIGN REQUIREMENTS

Position	Type	Coolant	Load Axial	Radial	rpm	DN	Bearing Dimensions, millimeters	
							Bore	OD
1φ	Conrad Ball	LO_2	Spring Preload	Shaft Unbalance and Hydraulic	6,000	0.24	40	70
2φ	Conrad Ball	LO_2	Preinducer Thrust	Shaft Unbalance and Hydraulic	6,000	0.24	40	70
3φ	Angular Contact Ball	LO_2	Spring Preload	Shaft Unbalance and Hydraulic	25,000	1.25	50	87
4φ	Angular Contact Ball	GH_2	Spring Preload	Shaft Unbalance and Hydraulic	25,000	1.0 1.125	40 45	80 85

CONFIDENTIAL

of any one of three seals will not result in mixing of the sealed fluids. The package will consist of a primary LO_2 face seal, designated A, a purged shaft riding intermediate seal (B), and a turbine face seal (C). The purge gas will be introduced into the interior of the shaft riding seal, where it will be maintained at a pressure higher than that existing in either of the drain lines, thus preventing any leakage of either seal from entering the purged area. The purge gas leaking across the shaft-riding segments carries leakage with it from both seals out the drain lines. This seal arrangement has been used successfully on the H-1, F-1, and J-2 turbopumps.

(U) The design requirements for the above seals and also the outboard turbine seal (D) are summarized in Table 45.

(U) Materials. The oxidizer pump does not have stress levels as high as the fuel pump, and therefore aluminum alloys are used wherever possible. The preinducer is made of machined 6061-T6 aluminum and the impeller of cast Tens-50 aluminum. These materials provide the required strength for the pressure bending loads and have long been used successfully as a cryogenic inducer material. However, wrought K-Monel was selected for the high-speed inducer because of its cavitation resistance properties. The pump inlet housing and volute are made of cast Tens-50 aluminum just as in the fuel pump.

(U) Because the turbine blades are machined separately and attached to the discs with fir trees, it is possible to use a different material than that of the disc. Therefore, Inconel 713C was used for the blades because of its better machinability, and Inconel 718 was used for the turbine discs as in the fuel turbine. The turbine manifold and nozzle block are both made of Hastelloy C.

(C)

TABLE 45

OXIDIZER SEAL PACKAGE DESIGN REQUIREMENTS

Seal Identification		Upstream (or High-Pressure Side)			Downstream (or Low-Pressure Side)				
Seal Position	Seal Type	Fluid	Pressure, psig	Temperature, F	Fluid	Pressure, psig	Temperature, F	Speed, rpm	Average Relative Speed, ft/sec
Aϕ	Liftoff Face	LO_2	200	-297	GO_2 + GN_2 or GHe	10 max 0 min	-200	25,000	276
Bϕ	Purged Shaft Rider	GN_2 or GHe	30	Ambient	GO_2/ H_2 + steam	10 max 0 min	-200/800	25,000	245
Cϕ	Liftoff Face	GH_2 + steam	140	870	GN_2 or GHe + GH_2 + steam	10 max 0 min	800 max	25,000	350
Dϕ	Liftoff Face	GH_2	100	-250	GH_2 + steam	40	820	25,000	260

CONFIDENTIAL

(U) Oxidizer Turbopump Analysis. The following paragraphs discuss the performance, hydrodynamic, and stress analyses made in connection with the oxidizer turbopump design.

(C) Pump Performance. A hydrodynamic analysis similar to that discussed under the fuel pump was used to generate the pump performance shown in Fig. 138. This map also includes the estimated pump operating line throttling down to 5:1. For the oxidizer preinducer, a NPSH of 12 feet was used to ensure meeting the requirement of 60 feet.

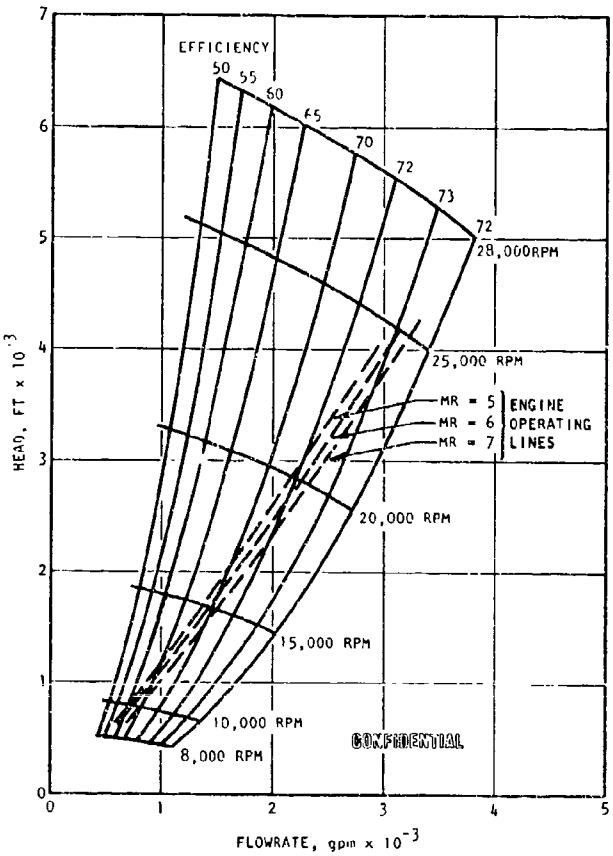

Figure 138. Mark 30 Oxidizer Pump Performance Map (With Engine Operating Lines)

(U) Axial Thrust Balance. The turbopump axial thrust balance will be accomplished by setting the front and rear impeller seal diameters to balance the pump and turbine loads within values which can be sustained by the bearings. The axial thrust can be maintained within ±500 pounds after

a development program, and the initial load values will permit the test program required to finalize the axial thrust system. Trimming of axial thrust will be accomplished by use of antivortex ribs inside the impeller rear seal. The stationary ribs control the pressure gradient inside the wear ring, and varying the diameter will vary the impeller thrust. This system has proved effective on the J-2 oxidizer pump and the F-1 fuel pump.

(C) Pump Structural Analysis. The fluid turbine preinducer assembly for the LOX pump will have a maximum operating speed of 6750 rpm. At this speed, the proposed aluminum hub and shroud assemblies will be structurally adequate to support the centrifugal loads without excessive deflections.

(C) The LO_2 pump main inducer will operate at a maximum speed of 27,000 rpm. The calculated maximum allowable safe operating speed for the K-Monel splined hub configuration is 31,500 rpm.

(C) The LO_2 impeller backplate (Fig. 139) is satisfactory for the 27,000-rpm maximum operating speed. The impeller will be made of premium strength Tens-50 aluminum with Grade 1 properties in the critical areas. The calculated backplate burst speed is 41,800 rpm, resulting in an allowable operating speed of 31,400 rpm. The radial and tangential stress distributions are also shown in Fig. 139.

(U) The critical section of the shaft between the impeller drive spline and the turbine (the spline relief) is structurally adequate. The shaft is sized to withstand the applied torsional and bending stresses.

(U) This volute, like the fuel volute, will be made of high-strength Tens-50 aluminum, and will be proof tested to pre-yield the material in the higher stress regions and to provide a partial measure of quality assurance.

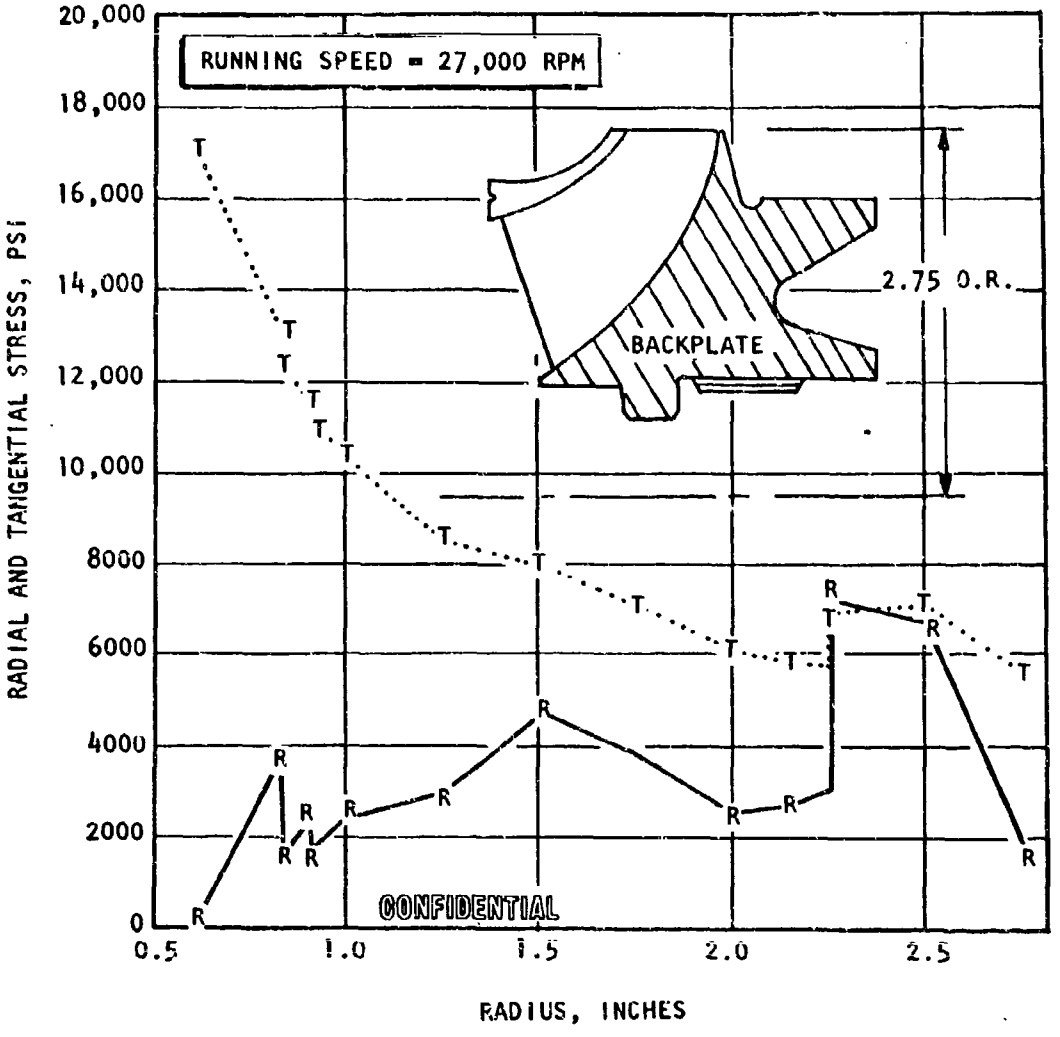

Figure 139. Oxidizer Impeller Stress vs Radius

(C) Turbine Performance. The estimated performance map of the oxidizer turbine is shown in Fig. 140. This map was developed in a manner similar to the fuel turbine map discussed on page 290. Because of the system control requirements, the turbine inlet pressure for the oxidizer turbine is 750 psia. This is 250 psi lower than the fuel turbine inlet pressure because of the series hot-gas valve arrangement. However, higher inlet pressures were not found to be advantageous for the oxidizer turbine because they require a reduction in the first-stage blade height, with an associated loss in efficiency.

(U) LO_2 Turbine Rotor Blades. Turbine blade stresses were estimated from data on similar Rocketdyne turbine blades. The blades will be hollow and shrouded. The steady-state stresses are shown in Table 46. The blades will be designed with optimum fillets to minimize stress concentrations.

(U) The blades will be tilted to partially compensate for the power bending moment, and hence reduce the leading and trailing edge stresses.

(U) Vibration natural frequencies were estimated for the first- and third-stage blades. Although the configuration shown on the layout has fir tree blade attachments, frequencies were estimated for integrally machined blades. This was done to see whether there was any possibility of designing the unshrouded blades such that no natural frequencies would fall within the operating speed range, i.e., if the first tangential bending mode could be raised above the maximum operating speed. The interference diagram resulting from this study is shown in Fig. 141. As can be seen from this figure, the first cantilever bending natural frequency of an unshrouded integral blade falls within the operating speed range.

(U) Incorporating a fir tree blade attachment lowers the natural frequencies. It is likely that there will be some natural frequency excited within the

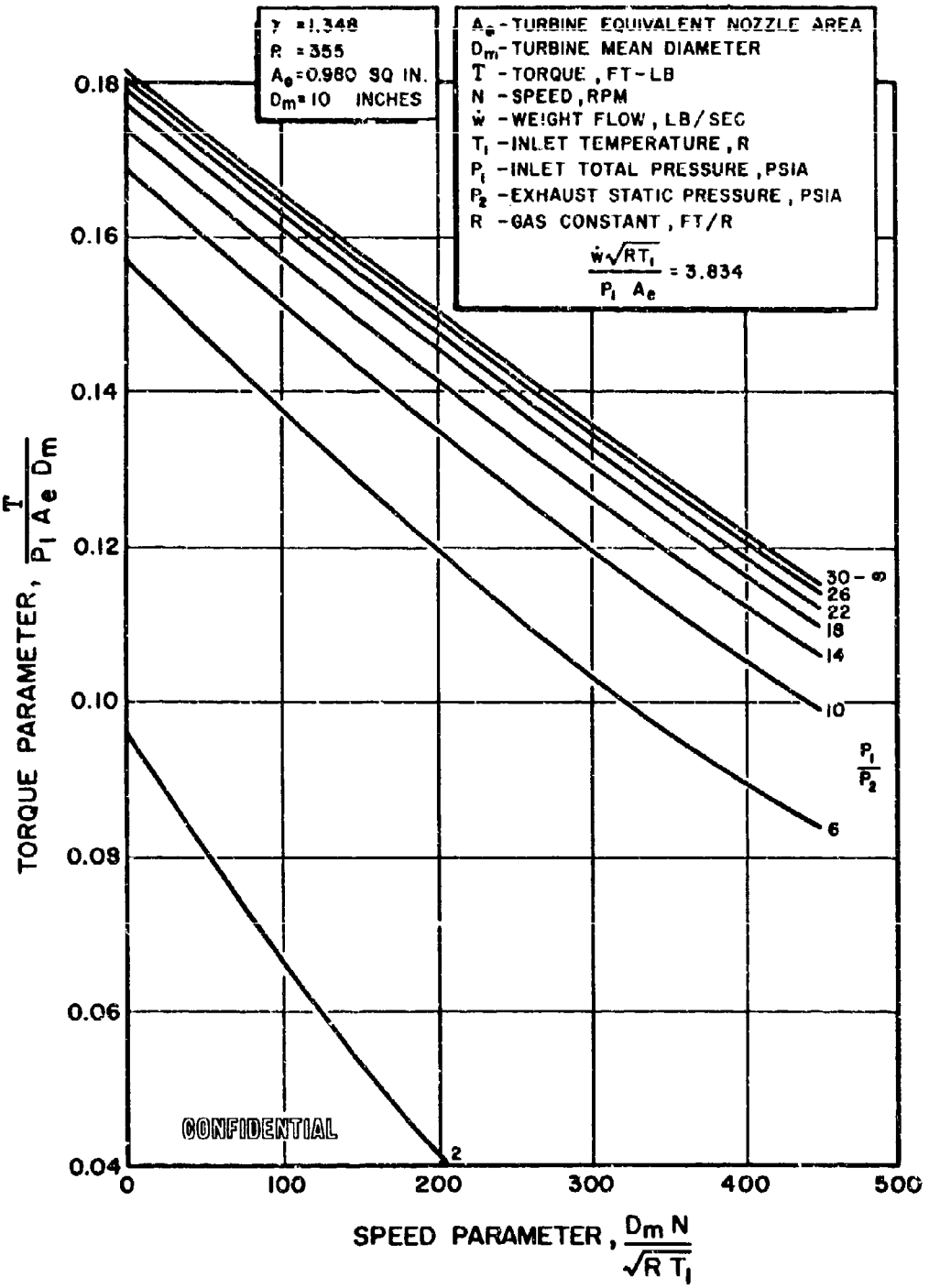

Figure 140. Mark 30-0 Turbine Estimated Performance, Tapoff Cycle, Parallel Operation, Three-Stage Version

(C) TABLE 46

LO_2 TURBINE BLADE STRESSES

	First Stage (Shrouded)	Second Stage (Shrouded)	Third Stage (Unshrouded)
MAXIMUM STRESSES, psi			
Without Stress Concentration			
Centrifugal Stress	8,280	20,000	31,900
Power Bending Stress	2,080	3,370	3,300
Total	10,360	23,370	35,200
With Stress Concentration			
Centrifugal Stress	10,250	24,800	39,600
Power Bending Stress	2,580	4,180	4,090
Total	12,830	28,980	43,690
MATERIAL PROPERTIES, INCO 713C			
Ultimate Strength, psi	106,000	107,000	100,000
10 Hour Rupture Strength, psi	85,000	100,000	104,000
Temperature, F	1,330	1,120	890

NOTE: Speed 27,000 rpm
Power 6,258 hp
Torque 14,650 in.-lb

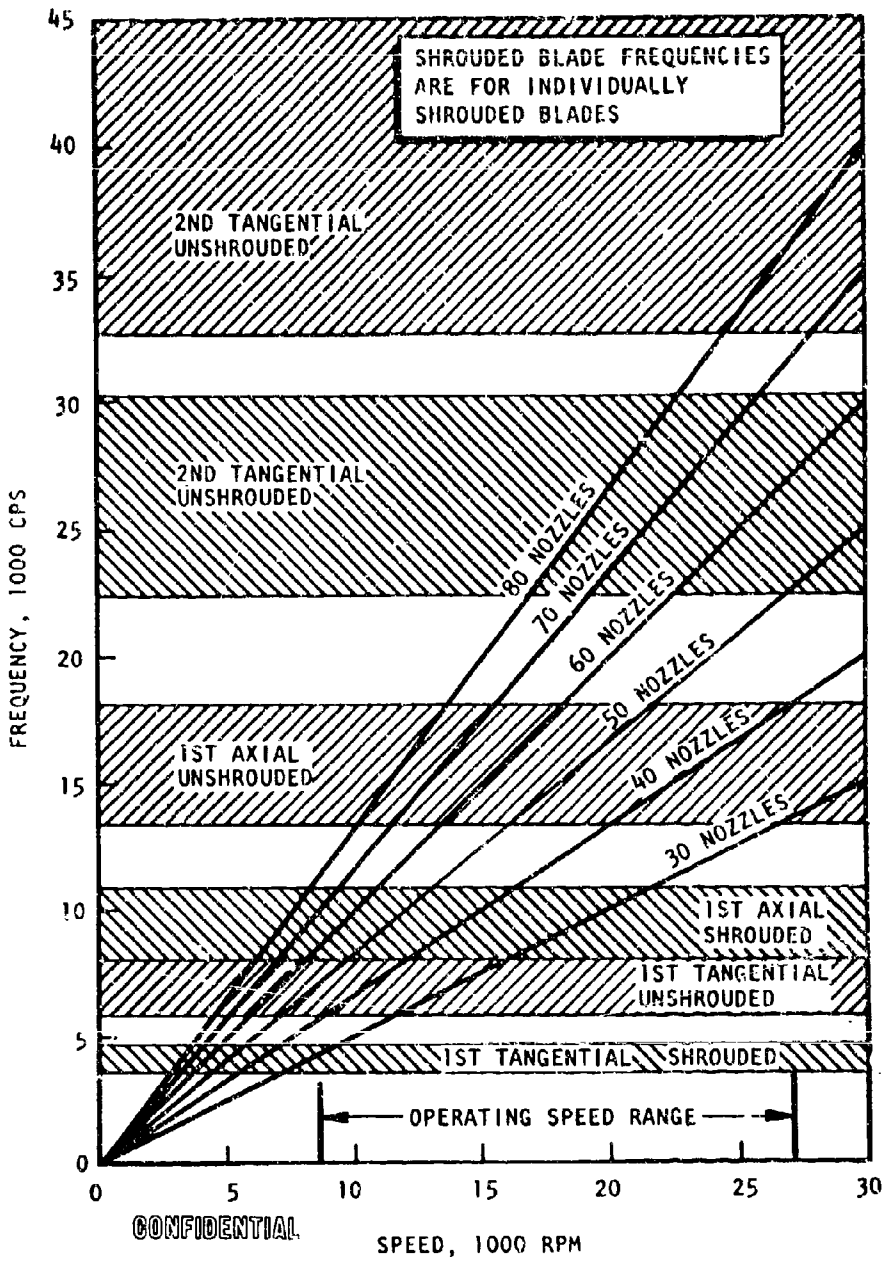

Figure 141. LO_2 Third-Stage Turbine Rotor Blade Interference Diagram Blade Machined Integral

operating speed range. Several alternatives will be considered. Choosing the number of nozzles such that the first tangential and first axial mode natural frequencies are excited below the minimum steady operating speed, and the second tangential mode is excited above the maximum steady operating speed, is a possible alternative. Another consideration is to allow the blades to be in resonance at low speeds (low stress) such that the blade is free of resonance in the middle and higher end of the operating speed range. Still another consideration is to cast the turbine blades in clusters with continuous root and tip shrouds joining the blades within the cluster. This would raise the tangential frequencies considerably.

(U) The most probable solution to the frequency problem would be to machine the blades integral with the disc with a continuous integral shroud. This would possibly raise all major natural frequencies above the maximum operating speed if the number of nozzles could also be minimized. Other problems, such as damping, thermally induced stresses and anticipated scrap rates would also have to be considered for this type of design.

(U) Liquid Oxygen Turbine Manifold. The turbine manifold is made of Hastelloy C. Use of Hastelloy C is desirable because no heat treatment is required. This facilitates fabrication and welding. The thermal duty cycle will be defined, and this part will be designed to meet the life requirement as dictated by low-cycle fatigue and stress rupture considerations.

(C) Rotordynamics. Several critical speed analyses were performed for various preliminary configurations of the LO_2 turbopump rotating assembly. The final configuration considered consisted of pump mainshaft and preinducer rotating assemblies. Figures 142 and 143 display the variation of critical speed vs bearing radial spring rates for both the inducer and main shaft. The analysis indicates that, for bearing radial rates in excess of 2 (10^6)

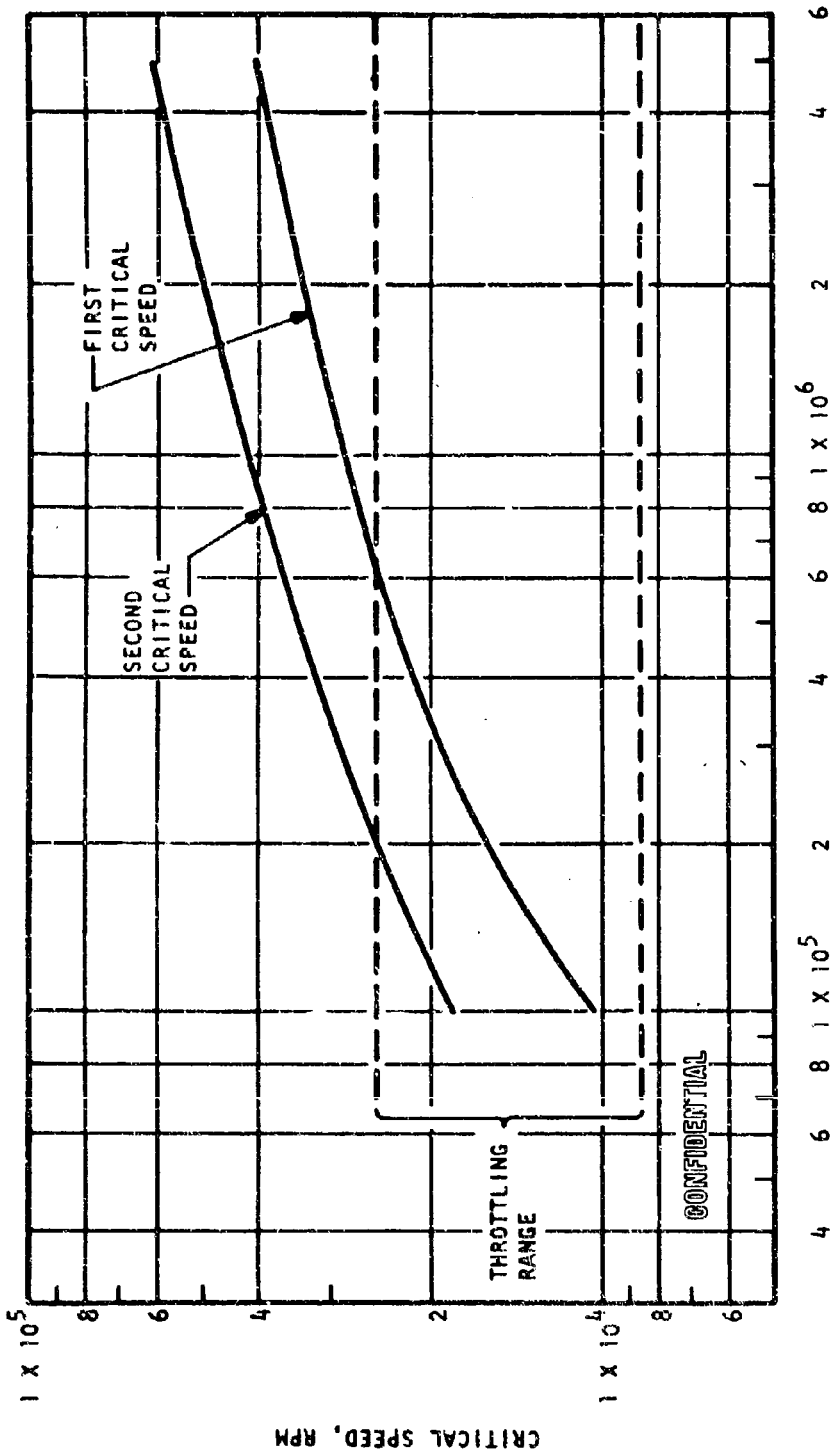

Figure 142. Critical Speed vs Bearing Spring Rate for Mainshaft

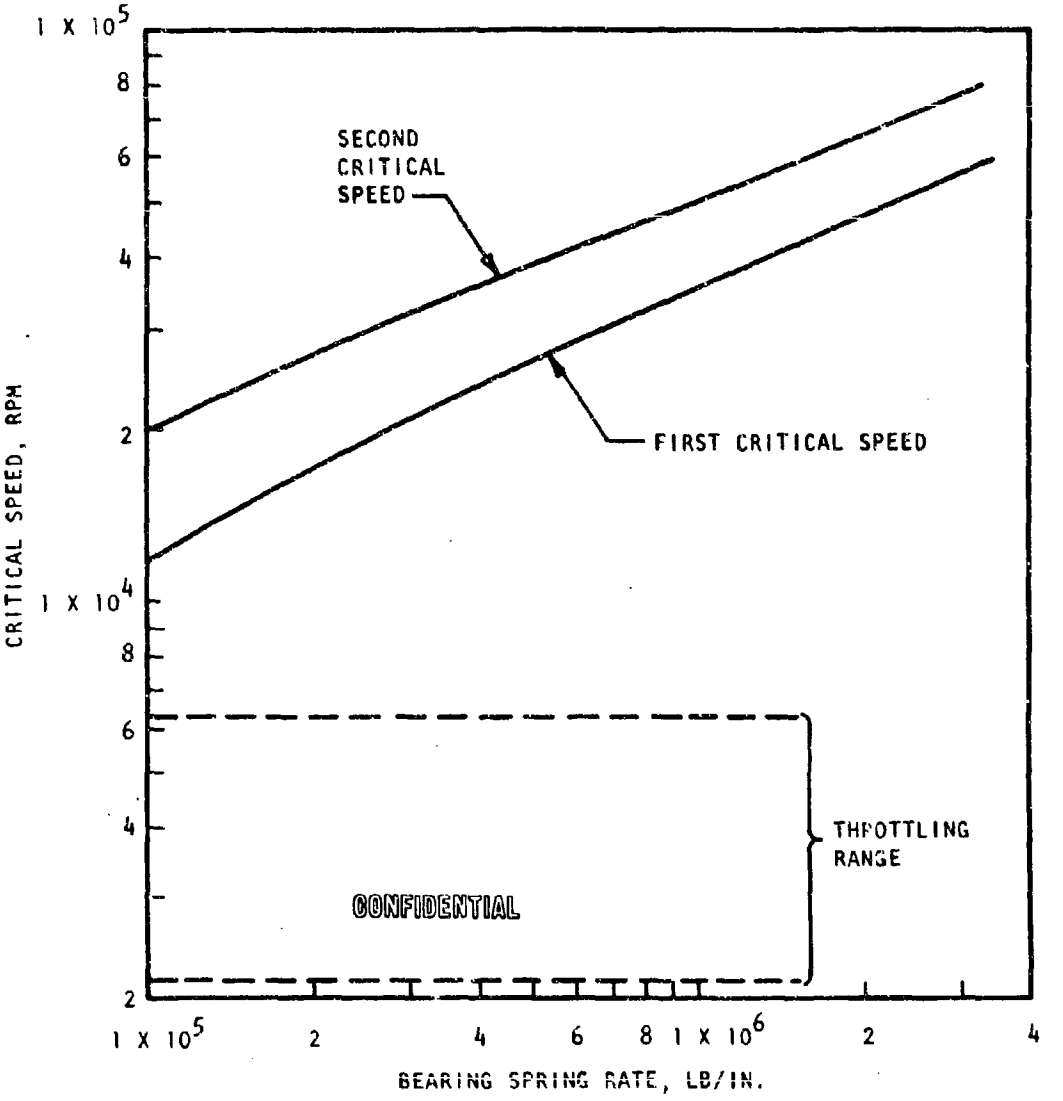

Figure 143. Critical Speeds of LO_2 Inducer

lb/in., on both mainshaft and preinducer, no critical speed problems will exist within the operating speed range (8,600 to 25,000 rpm). Figure 144 shows the first critical speed shaft mode shape.

(U) Oxidizer Turbopump Seals. The high speed of the LO_2 turbopump leads to the choice of a hydrodynamic or hydrostatic liftoff seal for the primary LO_2 seal.

(C) Testing accomplished under company sponsorship at similar speeds indicates that a hydrodynamic seal outperformed a conventional rubbing contact face seal for LO_2 service; a modified hydrodynamic seal operated for 14 hours at 25,000 rpm, whereas a conventional seal was limited to approximately 2 hours. The tests simulated turbopump speed, but at low pressures. Since test conditions approaching turbopump pressure levels induced high wear rates, it is concluded that improvements must be made to the existing design before considering it suitable for turbopump use. Three seal designs will be considered for the primary position:

1. Commercially designed hydrodynamic similar to the type tested
2. Spiral land hydrodynamic designed by Rocketdyne
3. Commercially designed hydrostatic seal

(U) A segmented shaft-riding seal is used for the intermediate pump seal, which is typical of turbopump secondary seals and turbine seals. A major anticipated problem associated with the use of shaft-riding seals in high-speed applications is the heat generation at the mating surface. To achieve the life requirements of the Mark 30 pump, some means of reducing the seal friction, such as pressure balancing or reducing shaft forces by arch-binding of the segments must be employed. Another approach is to design a seal similar to an orifice-compensated hydrostatic bearing with pressure pads. Design analyses of these concepts should be part of any future program.

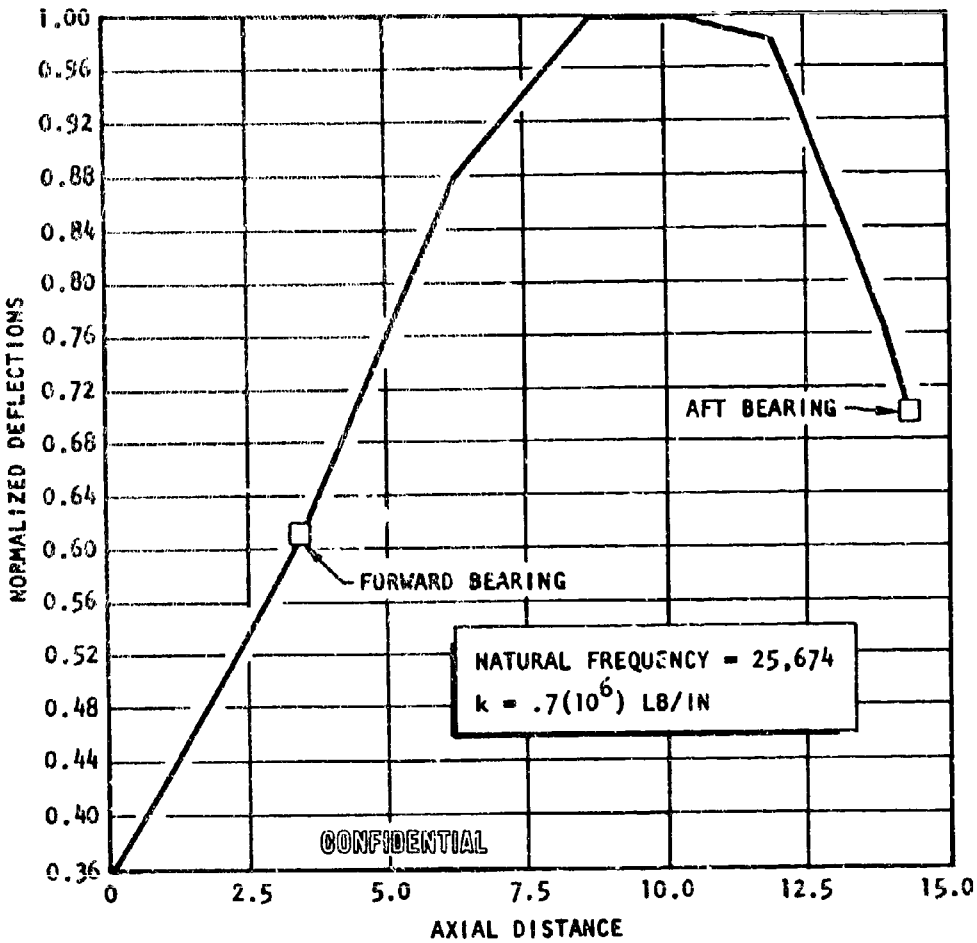

Figure 144. Turbopump First Critical Speed Mode Shape

(U) The turbine seal design will be similar to the primary oxidizer seal, and it is expected that a lift-off seal will be required to avoid excessive wear rates. The comments made on the primary oxidizer seal will, in general, apply to the turbine seal as well.

(U) Oxidizer Turbine Bearing Analysis. A discussion of the oxidizer turbine bearings was included in the fuel turbine bearing analysis, page .

Control Design

(U) The controls design effort was conducted in two distinct areas, performance controller logic and valve mechanical design. Some of the basic trade studies leading to the selection of the control system (open loop vs closed loop) and the control valve location (hot-gas vs liquid valves and series vs parallel arrangement) were discussed under the System Analysis section. The Controls Design section therefore covers a more detailed description of the selection system (closed loop, series hot-gas valves) and the design of the control valves.

(U) Control System Description. The selected performance controls system is shown schematically in Fig. 145; facility-type components are distinguished from engine-type components by a dashed line.

(U) Control over engine thrust and mixture ratio is obtained by proper positioning of two hot-gas valves in the turbine-drive subsystem. One of these valves is located in the tapoff gas line common to both turbines; the other is located in the hot-gas supply line to the oxidizer turbine. The first of these valves, the tapoff throttle valve, is primarily for thrust level control; the second, the oxidizer turbine valve, is primarily for mixture ratio control; however, there is some interaction between the valves so that neither valve is functionally exclusive. These valves will be driven by integral hydraulic actuators, which will be positioned by hydraulic servovalves. Integral with the valve actuators will be variable reluctance-type position transducers producing modulated carrier signal feedback.

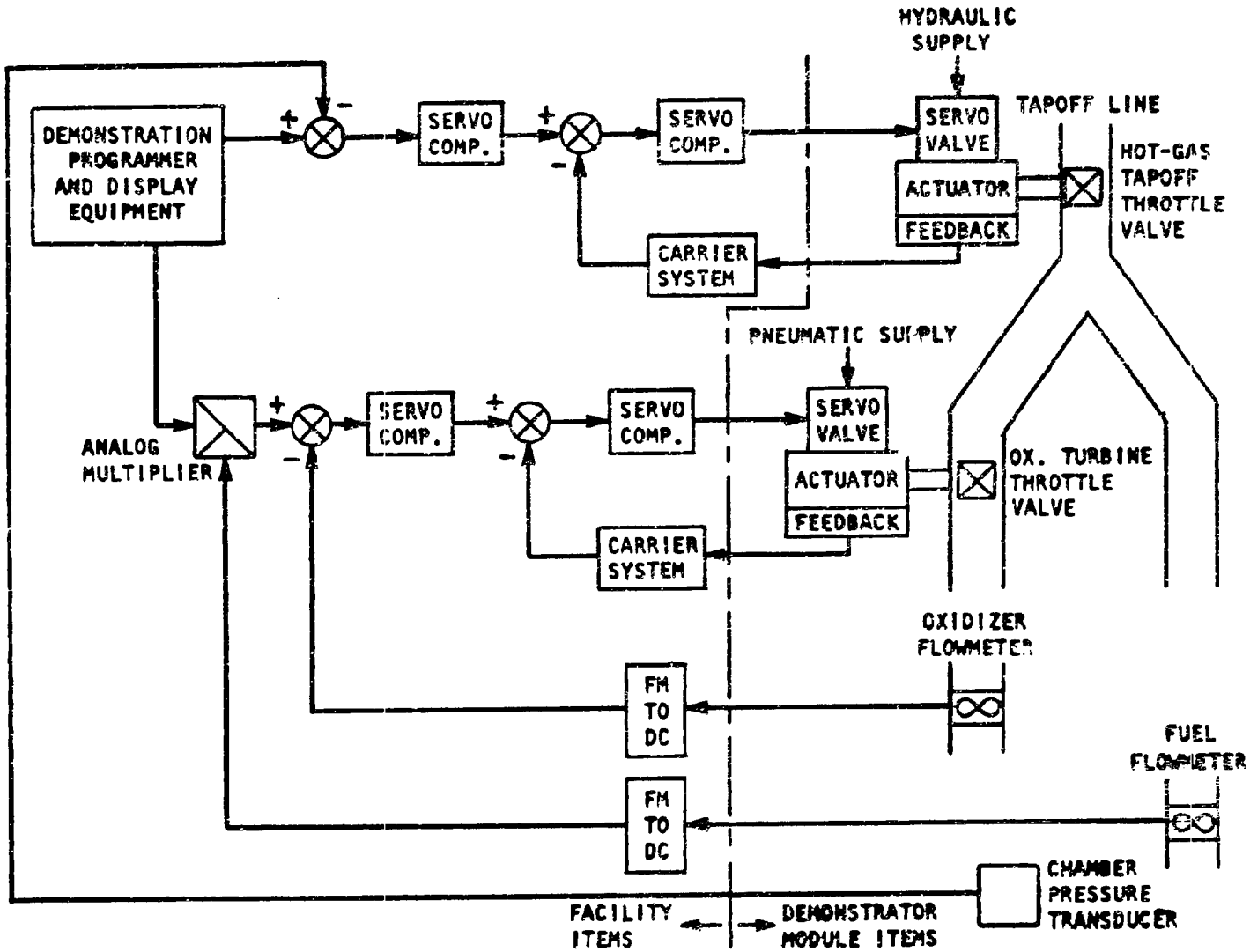

Figure 145 Functional Diagram, Demonstrator Module Performance Controls

(U) The signals from the variable reluctance position transducers will be demodulated and compared to a valve position reference signal. The error between these two signals, if any, will be passed through a dynamic shaping network, amplified, and applied to the hydraulic servovalve during the appropriate hot-gas valve for correction of the error.

(U) Demonstrator Module thrust will be measured by a chamber pressure transducer (which may consist of several units to obtain an average). The signal from this transducer will be compared to the desired signal. The error resulting from this comparison (if any) will be used, after appropriate dynamic shaping, to produce an appropriate change in the valve position reference signal.

(U) Engine fuel flow and engine oxidizer flow will be measured volumetrically by turbine flowmeters. FM to DC converters will be used to process the flowmeter pulses to a level proportional to flow. The signal from the fuel flowmeter converter will be multiplied by the desired mixture ratio and this product compared to the oxidizer flow signal. The error resulting from this comparison will be used, after appropriate dynamic shaping, to produce an appropriate change in the valve position reference signal.

(U) Should studies show the desirability of adding either pressure or temperature compensation to the volumetric flow measurements, a term can be added to the error signal for correction of the constant-density assumptions made.

(U) Control System Analysis. A nonlinear analog computer model of the Demonstrator Module was constructed and developed for control studies. This model was used to evaluate dynamic performance of several control schemes for the trade studies and to provide a design tool for the closed-loop control system.

(U) Engine components simulated by the model are the fuel and oxidizer turbopumps, fuel regenerative-coolant circuit, thrust chamber, control valves, and the fluid flow ducts. Pump performance was simulated by

curve fits of the head-capacity and torque-capacity curves. Turbine performance was simulated by programming the turbine performance maps which relate turbine torque to turbine speed, drive gas properties, and pressure ratio. Simulation of the fuel regenerative-cooling circuit required consideration of heat transfer and hydrogen properties. The cooling circuit was divided into two lumps. For each lump, the heat input was determined as a function of the temperature difference between the thrust chamber gases and the coolant, chamber pressure, and mixture ratio. Specific volume and specific internal energy of the hydrogen coolant were determined from mass and energy balances across the two "lumps." Pressure and temperature are determined as a function of specific volume and specific internal energy from hydrogen properties curve fits. The thrust chamber was represented as a sonic nozzle with the characteristic velocity a function of mixture ratio. The control valves were simulated as compressible flow orifices with pneumatic position control systems on valve area. Friction and threshold nonlinearities were included. Fluid flow lines were treated as lumped resistances only with the appropriate choice of compressible or incompressible flow.

(U) A special device used to assist in obviating the requirements for large numbers of function generators was a multiplexor. This device allows high-speed switching of input and output to a function generator, thereby eliminating the need for large numbers of gas flow functions and hydrogen properties functions. The speed of operation was far outside the bandwidth of dynamic interest.

(U) A linearized version of the engine equations was also developed for digital computer use. The purpose of this effort was to develop an optimization design tool so that various control optimization techniques could be applied and then verified by insertion in the nonlinear analog computer model.

(U) The required transfer functions for the Demonstrator Module control system are illustrated in Fig. 146, which is a block diagram of the system. The design differs somewhat from conventional servomechanism design in that two interacting loops are present. Nevertheless, a design procedure can be developed for this case and used for optimum control search and synthesis.

(C) The "fixed" part(s) of the block diagram (all those blocks that do not have the key word "compensation") were determined by using the nonlinear analog computer model to obtain frequency or Bode plots at various operating conditions. A Bode plot of the hydraulic valve position control loops is shown in Fig. 147. This plot shows commanded valve position, θ_c, as input, and valve area, A_{tov}, as output. The presence of nonlinearities is obvious from the steep dropoff of the gain curve at 80 rad/sec. The engine transfer functions were also determined from Bode plots made from the analog model, two of which are shown in Fig. 148 and 149 . Transfer functions have been determined at the four extremes of the operating region (100 and 20 percent thrust; 5:1 and 7:1 MR) and for the "cross" blocks shown in Fig. 146.

(C) The curves of Fig. 148 and 149 show frequency responses for both nominal and 20-percent engine thrust levels. The gain is not normalized for purposes of comparison with the ditital linear model, and for obtaining influence coefficients directly at low frequency. Both curves show that up to 50 rad/sec, the particular transfer function may be approximated by a single-order lag term.

(C) Results from the linear digital model for the 100- and 20-percent thrust level operating points give the following transfer functions for the engine, where P_c is chamber pressure, MR is mixture ratio of the thrust chamber, A_{ttv} is tapoff throttle valve area, A_{otv} is oxidizer turbine throttle valve area, and s is the Laplace operator.

$$dP_c/dA_{ttv} = 440(s/116 - 1)/(s/12.5 + 1) \qquad P_c = 1500 \text{ psia, MR} = 6$$

$$dMR/dA_{otv} = 5.96/(s/24 + 1) \qquad P_c = 1500 \text{ psia, MR} = 6$$

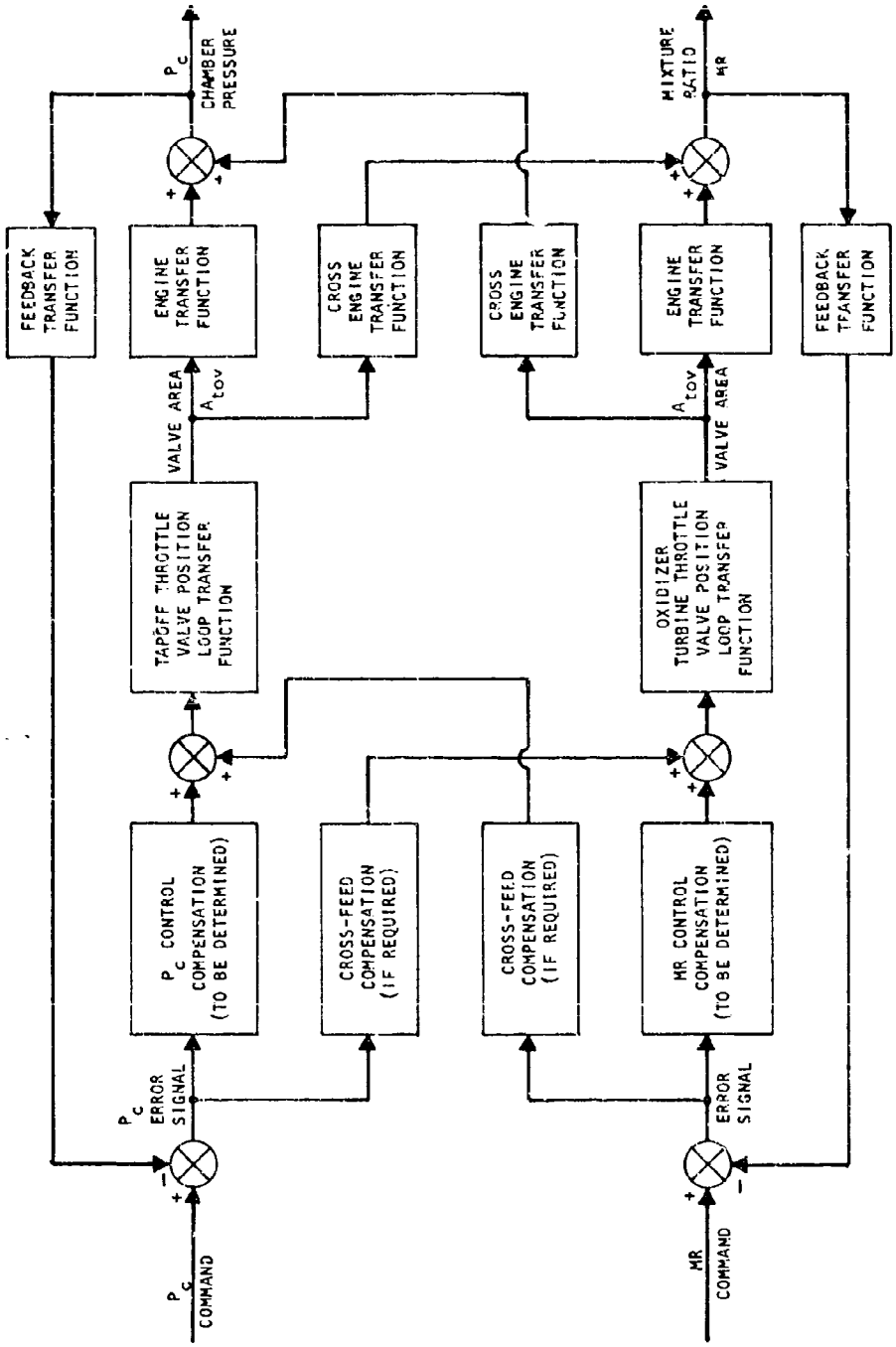

Figure 146. Performance Controls System Block Diagram

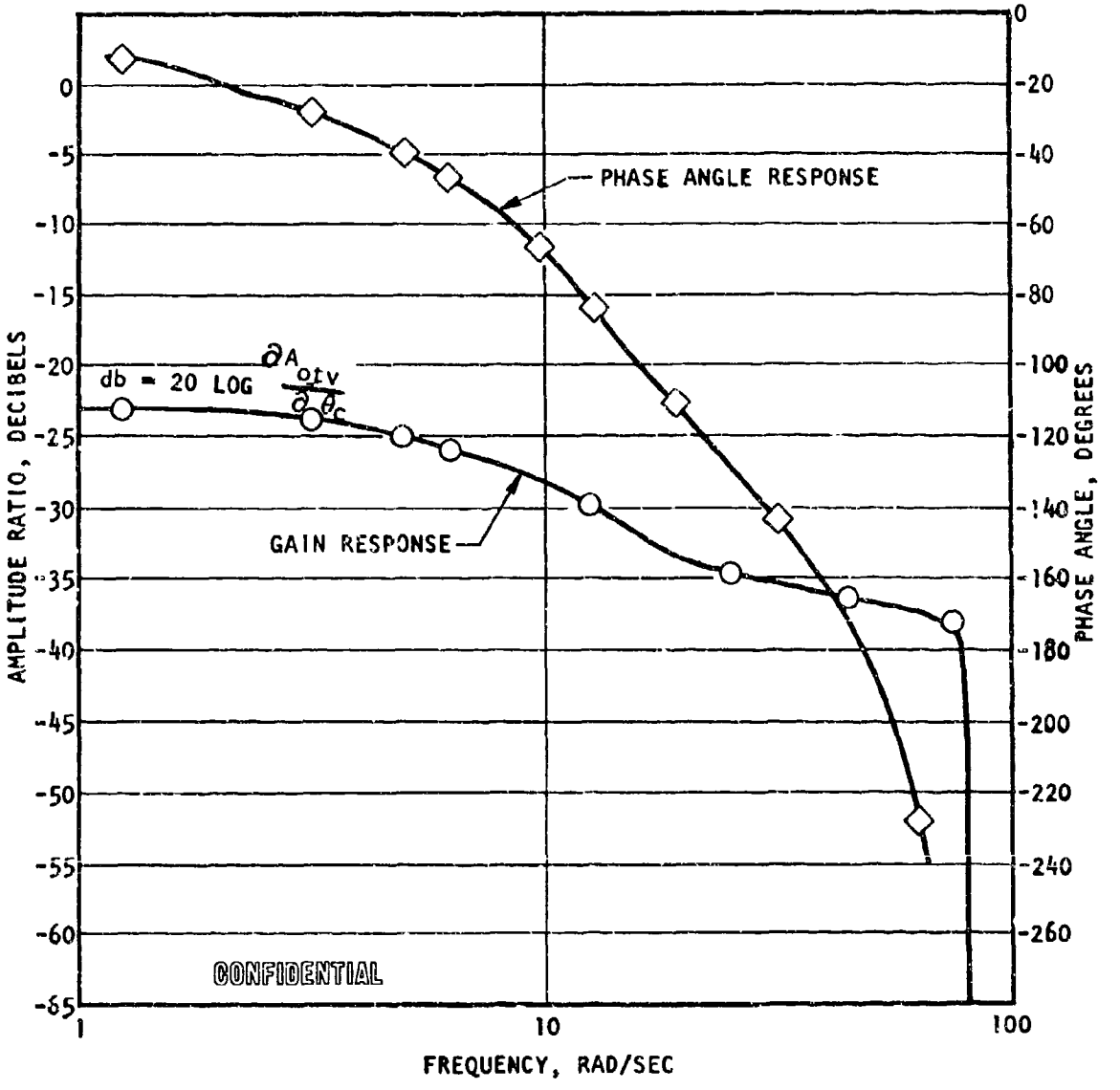

Figure 147. Throttle Valve Position Transfer Function (Closed-Loop Frequency Response)

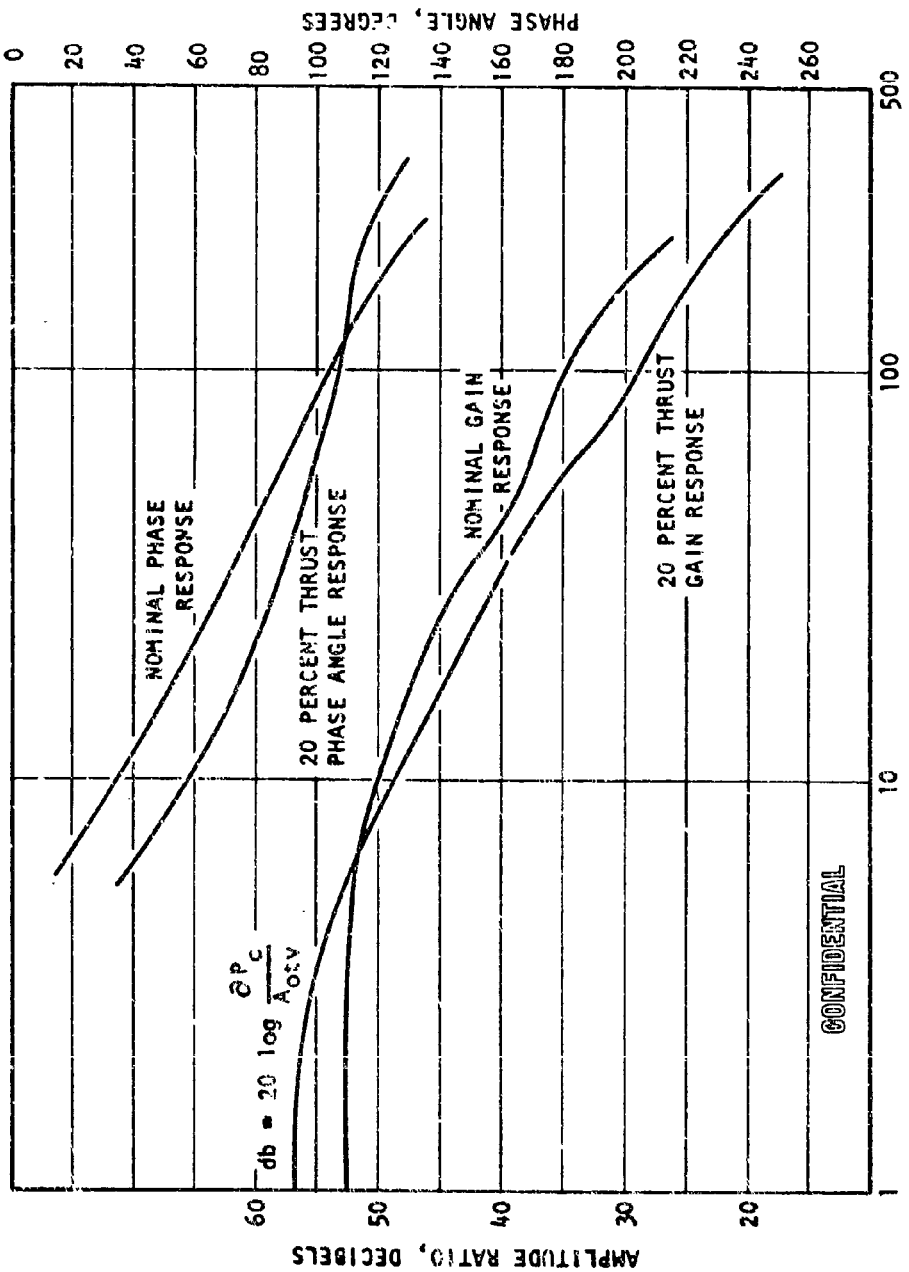

Figure 148. Demonstrator Module Response Chamber Pressure as a Function of Tapoff Throttle Valve Area at Constant Oxidizer Turbine Throttle Valve Area (Nominal and 20-Percent Thrust Levels)

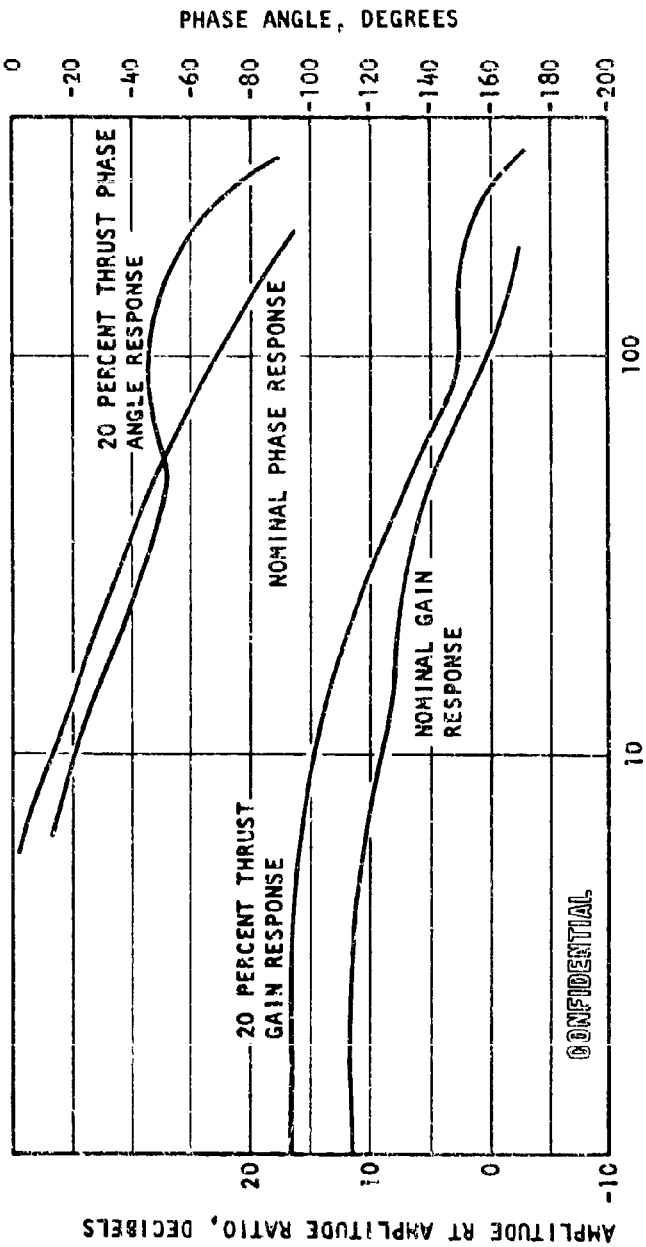

Figure 149. Demonstrator Module Response Mixture Ratio as a Function of Oxidizer Turbine Throttle Valve Area at Constant Tapoff Throttle Valve Area (Nominal and 20 percent Levels)

$dP_c/dA_{ttv} = 583(s/275 - 1)/(s/7.2 + 1)$ $\quad P_c = 325$ psia, MR = 6

$dMR/dA_{otv} = 9.11/(s/16 + 1)$ $\quad P_c = 325$ psia, MR = 6

(U) No attempt to compare the results obtained from the digital model and the analog computer model other than a cursory examination has been tried. It should be noted that the analog computer model includes many nonlinearities not found in the digital system equations.

(U) The final step in the control system design is the establishment of the compensation and feedback transducer functions needed to complete the description of the system shown in Fig. 146. For purposes of performing studies during Task I, this was accomplished by insertion of a proportional plug integral compensation network into the analog computer model and start model. Servoloop operation was found to be satisfactory for the study purposes, but design and optimization remains to be accomplished using updated component and system data and an exact solution for the missing transfer functions.

(U) The dynamic control compensation terms added can be minimized to reduce equipment complexity and improve reliability, and the "cross" transfer function terms can be utilized as necessary to reduce control system interaction and improve the speed of response. To illustrate the design procedure for determining the compensation transfer functions, consider the following method. The system is defined by the block diagram of Fig. 150 . The equations may be written without cross compensation as:

$$P_c(1 + G1C1H1) + MR(G2C2H2) = G1C1R1 + G2C2R2$$

$$-P_c(G3C1H1) + MR(1 + G4C2H2) = G4C2R2 - G3C1R1$$

with the solution:

$$P_c = \frac{C1R1(G1 + G1G4C2H2 + G2G3C2H2) + C2R2G2}{1 + G4C2H2 + G1C1H1 + G1C1H1G4C2H2 + G2C2H2G3C1H1}$$

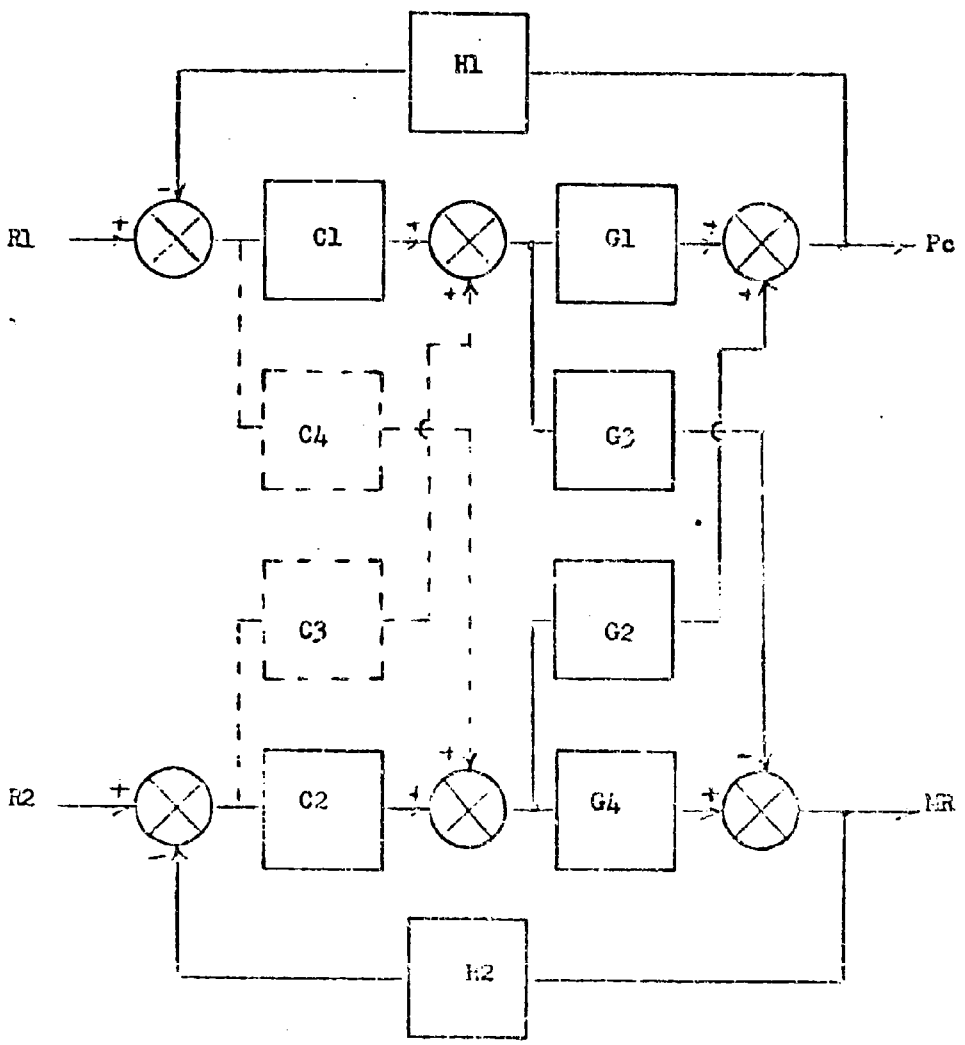

Figure 150. Control System Block Diagram

$$MR = \frac{C2R2(G4 + G1G4C1H1 + G2G3C1H1) - C1R1G3}{1 + G4C2H2 + G1C1H1 + G1C1H1G4C2H2 + G2C2H2G3C1H1}$$

which can be manipulated algebraically by choices of C1 and C2 to get stable acceptable dynamic response, although this is cumbersome. A fruitful approach is to include the cross-compensation terms:

$$P_c(1 + G1C1H1) + MR(G1C3H2 + G2C2H2) = R1G1C1 + R2(G1C3 + G2C2)$$

$$P_c(G4C4H1 - G3C1H1) + MR(1 + G4C2H2) = R2G4C2 + R1(G4C4 - G3C1)$$

If the cross-compensation terms are especially selected:

$$C4 = G3C1/G4$$

$$C3 = G2C2/G1$$

then the solution becomes:

$$P_c = \frac{G1C1R1}{1 + G1C1H1}$$

$$MR = \frac{G4C2R2}{1 + G4C2H2}$$

which is more tractable in that conventional root locus techniques can be applied separately to each loop.

(U) Final determination of the compensation and the transducer feedback transfer functions can then be accomplished by consideration of singularity location over the entire range of engine operation. Compensation singularities will be added according to modified root locus techniques illustrated by the procedure listed.

(U) The servocompensation obtained can then be inserted into the analog computer model of the throttling system for verification of design goals and for trimming, and to obtain plots of expected response characteristics of the closed-loop engine system. Start and shutdown characteristics can also be obtained by insertion of system equations into the digital start model.

(U) Control System Alternatives Studied. Studies investigating a control system with no cross-transfer functions, and the desirability of different feedback point measurements for system control were conducted. These are presented in the following paragraphs.

(U) Simplified Control System. A control system without interrelating valve function generators was initially considered; however, such a system does not permit throttling at constant mixture ratio. The throttling paths of this design are shown in Fig. 151. It can be seen in this figure that throttling, using one valve without modifying the position of the other, will probably lead to an undesirable operating region, or, at least, away from the desired point. This is largely because of differences in the steady-state operating parameters of the pumps and turbines. Because specification of these parameters will compromise design of the pumps and turbines, it will be necessary to provide trimming in the form of function generators. There are a number of ways to provide these functions, such as electronically, cam linkage, etc., but they all share the requirement for calibration to one particular set of hardware.

(U) The effect of variations in turbomachinery hardware is also shown in Fig. 151 by the dotted paths. These data were based upon a turbomachinery design which has, roughly, a 10-percent change in the pump H-Q curves and the turbine efficiency -U/C curves from the design represented by the solid lines. The figure reveals the controls sensitivity to the turbomachinery characteristics because a three-unit change in mixture ratio at low thrust occurs between the two designs. Although the expected variations in pump curves from engine-to-engine is a factor of 3 less than shown, and the

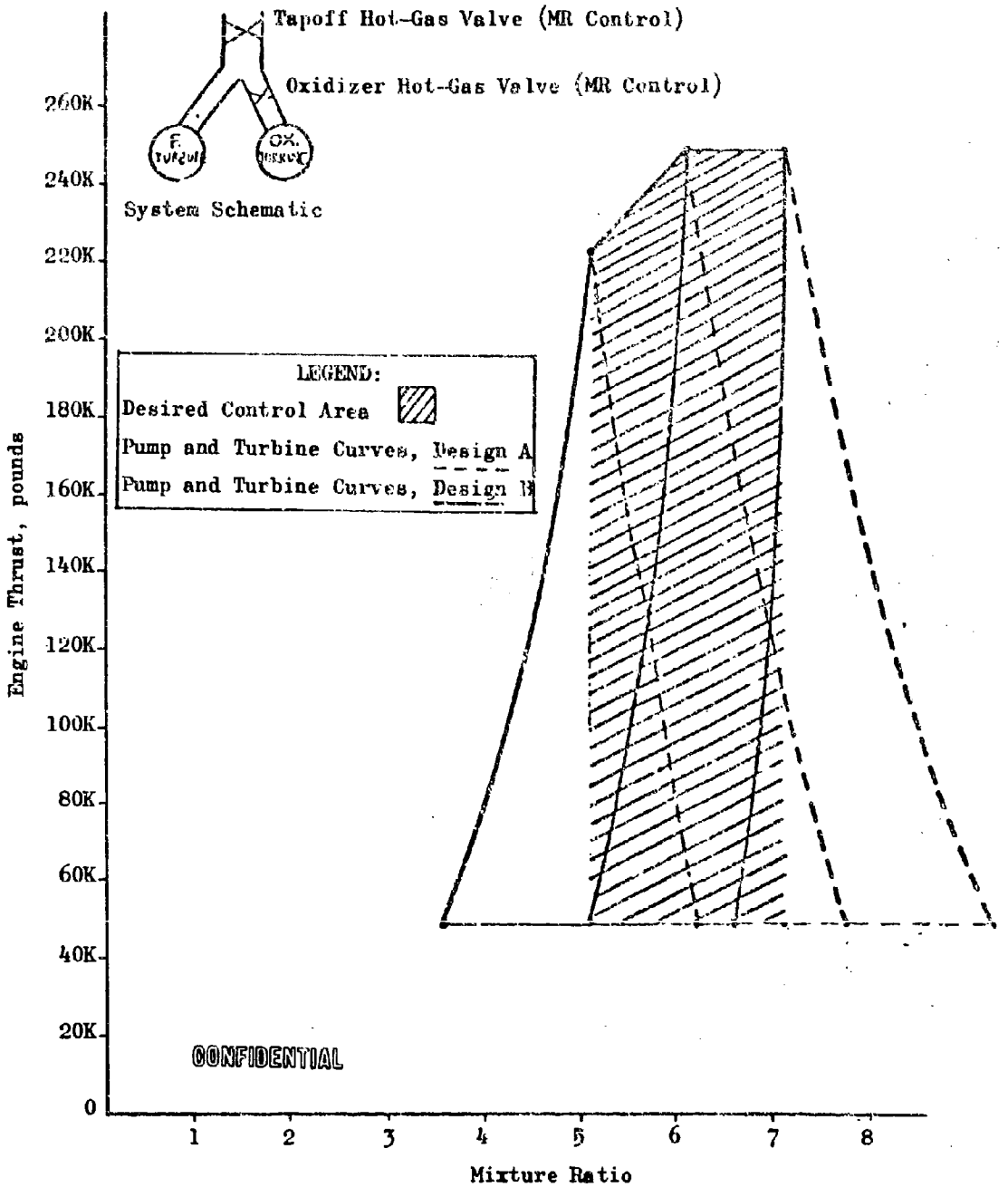

Figure 151. Effect of Pump and Turbine Curves on Open-Loop Mixture Ratio Control System

expected variation in turbine elficiency is a factor of 5 less than shown, this will nevertheless produce an intolerable variation in mixture ratio during throttling.

(U) It was therefore concluded that a cross-function generator was required in the system.

(U) Feedback Point Selection. The following parameters were considered in a feedback point study to select the optimum measured parameters for the control system: fuel turbopump speed, oxidizer turbopump speed, fuel pump discharge pressure, oxidizer pump discharge pressure, fuel pump outflow, oxidizer pump outflow, fuel manifold inlet pressure, oxidizer manifold inlet pressure, chamber pressure, chamber temperature, tapoff gas temperature, and thrust. The parameter that most accurately measures thrust is evidently thrust, and those which most accurately measure mixture ratio are the two pump out mass flows.

(U) Actual thrust measurement is unacceptable for several reasons. First, thrust will vary some with altitude, although less than conventional bell engines. Programming will therefore have to be adjusted for ambient conditions for demonstration. Secondly, thrust is an interface parameter between the engine and vehicle mounting while chamber pressure is an engine parameter. Flight pressure transducer technology also leads flight load cell technology. And last, high-accuracy control for flight purposes is not required because the vehicle guidance computer will supply the "trimming" in an outer control loop. A thrust control based on calculations using the pump out mass flows was also considered. However, this method has inherent inaccuracies because of the difficulty in measuring the mass flows. Volumetric flow measurements must have temperature and pressure corrections to compute the mass flowrate. Therefore, a chamber pressure feedback was considered. This parameter can be measured with transducers which are state of the art, reliable, and independent of the mounting scheme. A failure rate of 0.0021 per exposure for pressure transducers in a similar application was experienced over the period of June 1964 to

April 1966 (about one-half of these were out-of-calibration only). Repeatability of 3/4 percent of full scale has been demonstrated. Furthermore, it was shown in the Systems Analysis section that chamber pressure control is superior to thrust control from a vehicle system standpoint.

(U) Ideally, it should be possible to select one additional measurement and provide the required mixture ratio feedback signal for the control loop. This could theoretically be chamber temperature, because it is a strong function of mixture ratio. Unfortunately, this measurement is beyond the state of the art. It is expected that tapoff gas temperature will also vary with mixture ratio, although with less pronounced effect, because the tapoff design objective is to minimize this variation. The present reliability of hot-gas temperature measurement is not enough for a man-rated control system, so this also was considered beyond the state of the art.

(U) All other means feasible to measure mixture ratio require two measurements. The use of turbine-type volumetric flow meters, with correction for density if required, was indicated by Rocketdyne experience. According to flight instrumentation systems reliability data for the J-2 engine (which is a similar application), the failure rate is 0.004 per exposure for turbine flow meters for the period of June 1964 through April 1966. Repeatability of 1/4 percent of the operating level has been demonstrated. A special study was therefore conducted with the volumetric flow meters and possible correction parameters using the computer model over the operating region of the engine. Variations in density due to variations in temperature and pressure were taken into account. The following table summarizes the results of the study:

Measured Parameters	Error Over Operating Envelope in Mixture Ratio, percent
Two Volumetric Flows	±5
Two Volumetric Flows and Chamber Pressure	±2
Two Volumetric Flows and Fuel Pump Outlet Pressure	±2
Two Volumetric Flows and Fuel Pump Out Temperature	±3
Two Volumetric Flows, Fuel Pump Out Temperature and Pressure	±0.5

(U) As implied by the table, variations in the oxidizer system over the operating envelope have little effect upon the mixture ratio calculation. These variations are predictable, and, therefore, can be taken into account when programming the system. Use of the two volumetric flows and chamber pressure was found to meet the engine accuracy requirements (±3 percent) with a minimum of instrumentation, and these were therefore selected for the Demonstrator Module.

(U) Main Propellant Valve Alternatives Studied. A design tradeoff study was performed to optimize the main propellant valve configuration to meet system requirements. The valve types considered were a butterfly valve, a poppet valve, and a modified ball valve (visor valve).

(U) The butterfly valve is essentially a rotating blade which is operated by a linear actuator through a link-level mechanism. The blade or butterfly is fabricated as a section of sphere, and sealing is accomplished with a pressure-actuated lip seal. The major advantage of this valve type is shortness in line length and relatively low weight and pressure drop. The major problem areas are shaft bearings and gate seal design.

(U) The poppet design is a conventional balanced poppet configuration. The advantages of this type of valve are that a minimum of seals is required and that a direct link is provided between the actuator and the poppet. The poppet valve, however, is the heaviest configuration and has the highest pressure loss. The major development problem in the poppet valve is optimization of the poppet balancing to minimize the actuation force required at all poppet positions.

(U) The visor valve utilizes a segment of a ball which is rotated by a linear actuator through a link lever arrangement. This configuration rotates the ball out of the flow stream in the full-open position and provides minimum pressure drop. A bellows-loaded plastic seal provides

the primary propellant seal. The valve weight falls between the butterfly and poppet valves. The major advantage is low pressure loss, and the disadvantages are the number of dynamic seals required and the need for rotating bearings.

(U) A tradeoff study comparison is shown in Table 47 with the larger number representing the most desirable configuration. Category A, Primary Considerations, has been weighed twice as heavily as the other areas because of its impact upon system performance. The visor valve resulted in the best rating with superior characteristics in pressure loss and performance, and was therefore selected for the Demonstrator Module. Table 48 shows the specific weight and pressure loss characteristics for each valve.

(U) Main Propellant Valve Description and Analysis. Because the line sizes are nearly the same, one basic design was used for both the main oxidizer and main fuel valves. One major layout was prepared, and where necessary, minor changes were made to define differences between the valves which were required because of component location in the system. Although initial system design studies were based on an oxidizer line size of 3.00-inch diameter and fuel line of 2.50-inch diameter, subsequent engine balances required a 4.00-inch diameter for the oxidizer high-pressure feed system and 3.74-inch diameter for the fuel.

(U) The layouts for the two valves are shown in Fig. 152 and 153, with no detail presented for the facility-provided actuator. A hollow ball is used to minimize the flow forces acting on the ball and to minimize the shaft stresses from the inertia of the ball on closing. The bearings are designed to run wet in order to locate them as close to the ball as possible and minimize the shaft overhang and bending loads. Naflex seals are provided for the exterior seals, and machined plastic pressure-actuated seals are planned for the shaft. The ball seal is a pressure-loaded bellows seal, with low-pressure sealing provided by the bellows-installed spring load. The flow direction of the fuel valve is opposite from that of the oxidizer valve to provide moisture protection for the primary seal bellows.

TABLE 47

MAIN PROPELLANT VALVE TRADE STUDY* SUMMARY

Features	Poppet	Visor	Butterfly
A. Primary Considerations			
1. Reliability	9	8	5
2. Δ P Penalty	1	10	5
3. Weight	6	7	9
4. Cost	9	6	7
Subtotal	25	31	26
B. Performance Characteristics			
1. Stability, Position-Flow, Pressure	1	5	3
2. Actuation Control Time	2	4	3
3. Ramping (Oxidizer Valve)	1	4	3
4. Downstream Flow Profile	3	4	2
5. Perferred Position, Penalty	4	3	2
Subtotal	11	20	13
C. Malfunction, Resistance to			
1. Seal Leakage, Actuator	3	4	4
2. Seal Leakage, Propellant	4	3	2
3. Galling	3	4	4
4. Vibration	3	3	3
5. Pressure Surges	2	4	3
6. Freezing	4	3	4
7. Seal Confidence, High Pressure	4	3	2
Subtotal	23	24	22
D. Construction			
1. Number of Parts	5	3	2
2. Number of Dynamic Seals	2	4	3
3. Number of Static Seals	4	2	3
4. Bearing Required, Penalty	5	2	2
5. Structural Stability	5	3	2
Subtotal	21	14	12
E. Production			
1. Producibility (Complex Parts)	5	3	4
2. Special Fabrication Technique	4	3	3
Subtotal	9	6	7
F. Time			
1. Design	4	3	4
2. Development	3	3	4
3. Manufacturing	4	3	4
4. Servicing	4	4	4
Subtotal	15	13	16
Total	104	108	96

*Point value 1 to 10 Category A; 1 to 5 Categories B to F

NOTE: High total is most desirable

TABLE 48

MAIN PROPELLANT VALVE PRESSURE LOSS SUMMARY

BASIC VALUES

Valve Type	Fuel			Oxidizer		
	ΔP	Weight	Line	ΔP	Weight	Line
Visor	9.2	51	4.0	16.9	51	4.0
Butterfly	22.0	45	4.0	45.0	45	4.0
Poppet	54.2	55	4.0	110.0	55	4.0

LINE LOSS

	Fuel	Oxidizer
Line, psi/ft	1.12	2.05
Elbow, psi	5.13	9.45
Velocity, ft/sec	220	73

CONFIDENTIAL

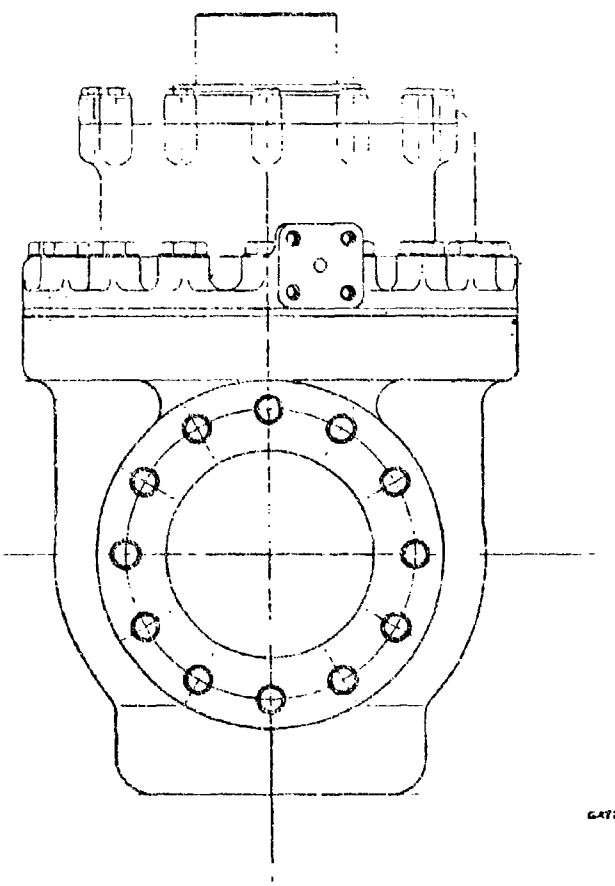

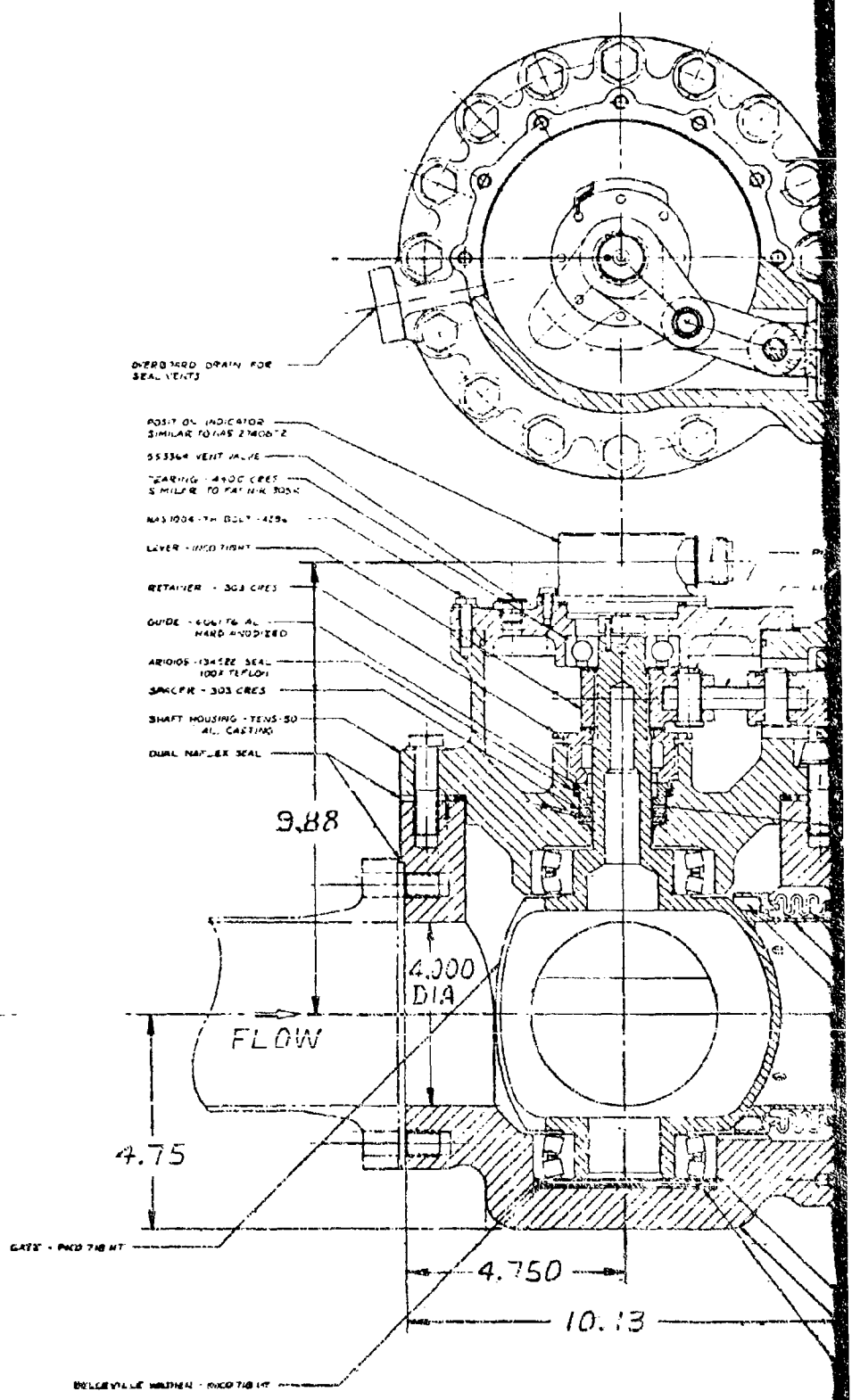

1

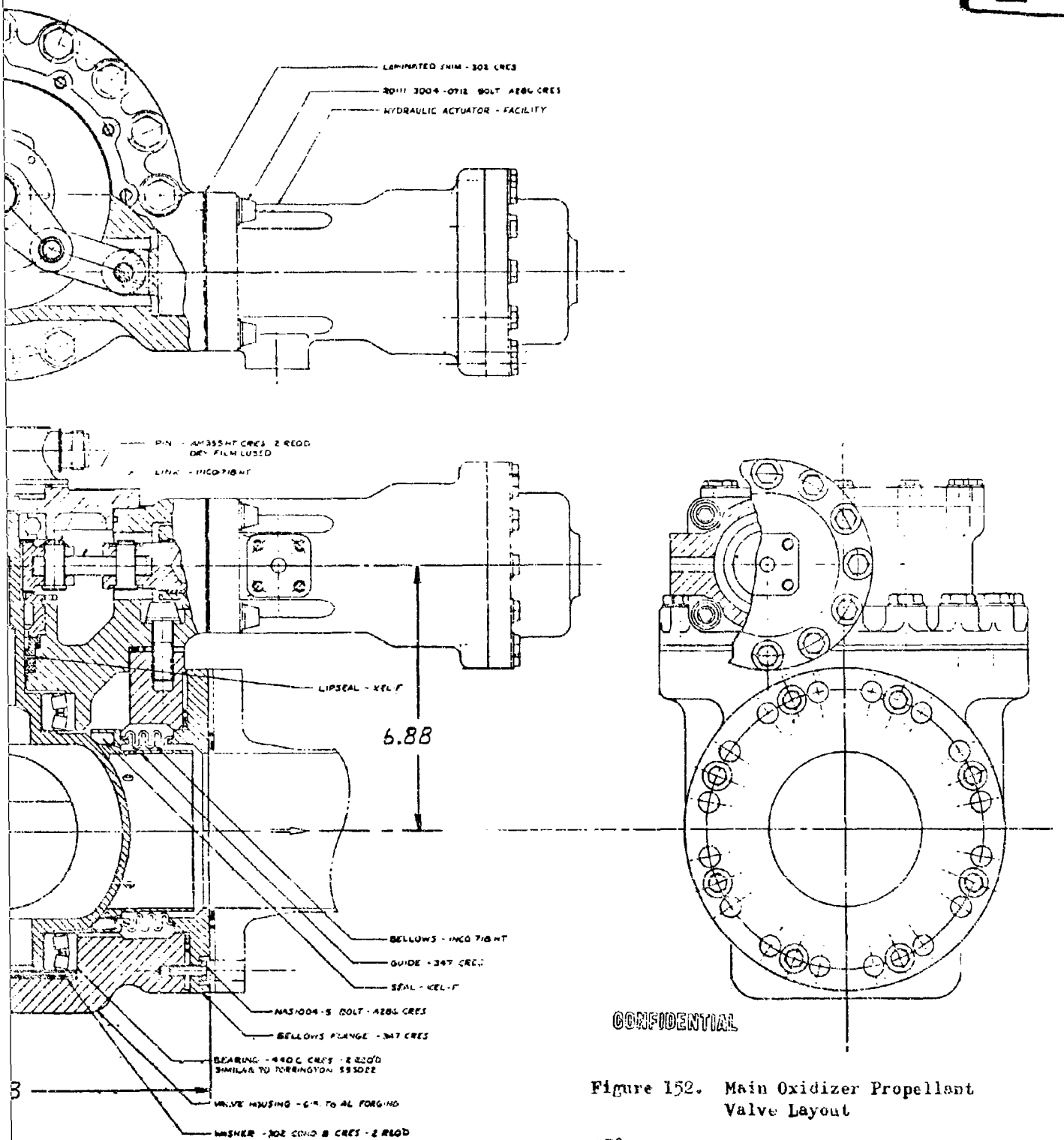

Figure 152. Main Oxidizer Propellant Valve Layout

CONFIDENTIAL

1

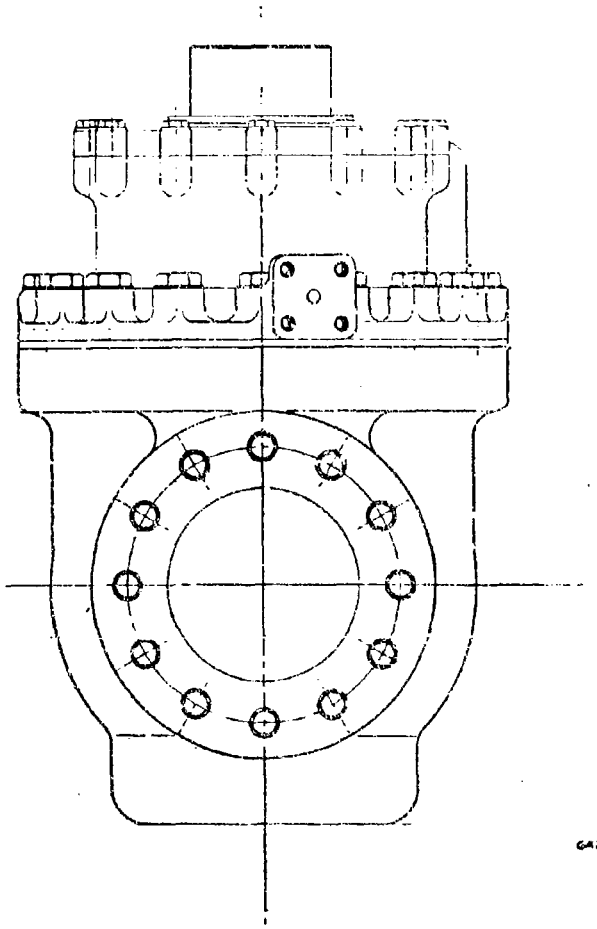

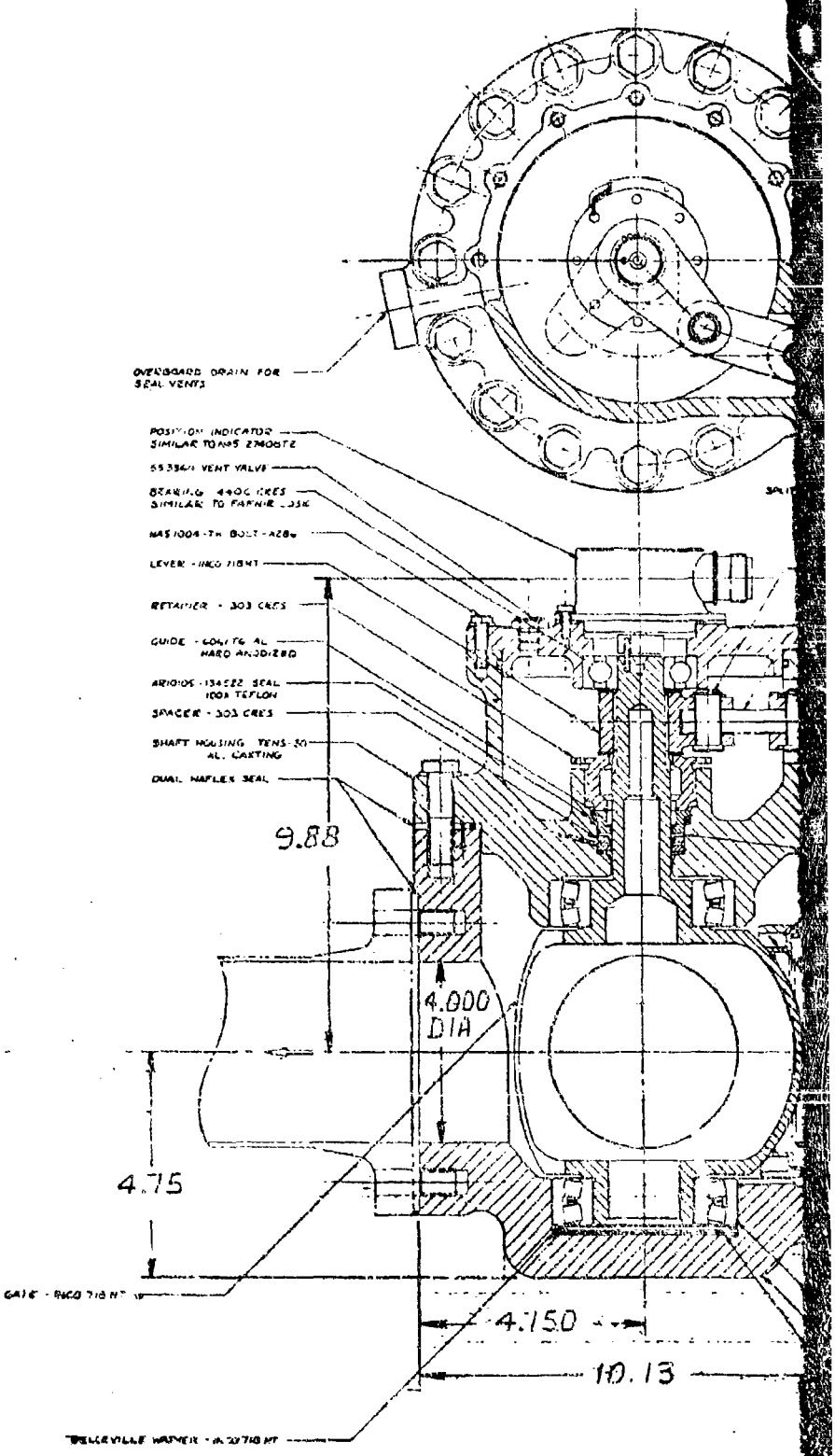

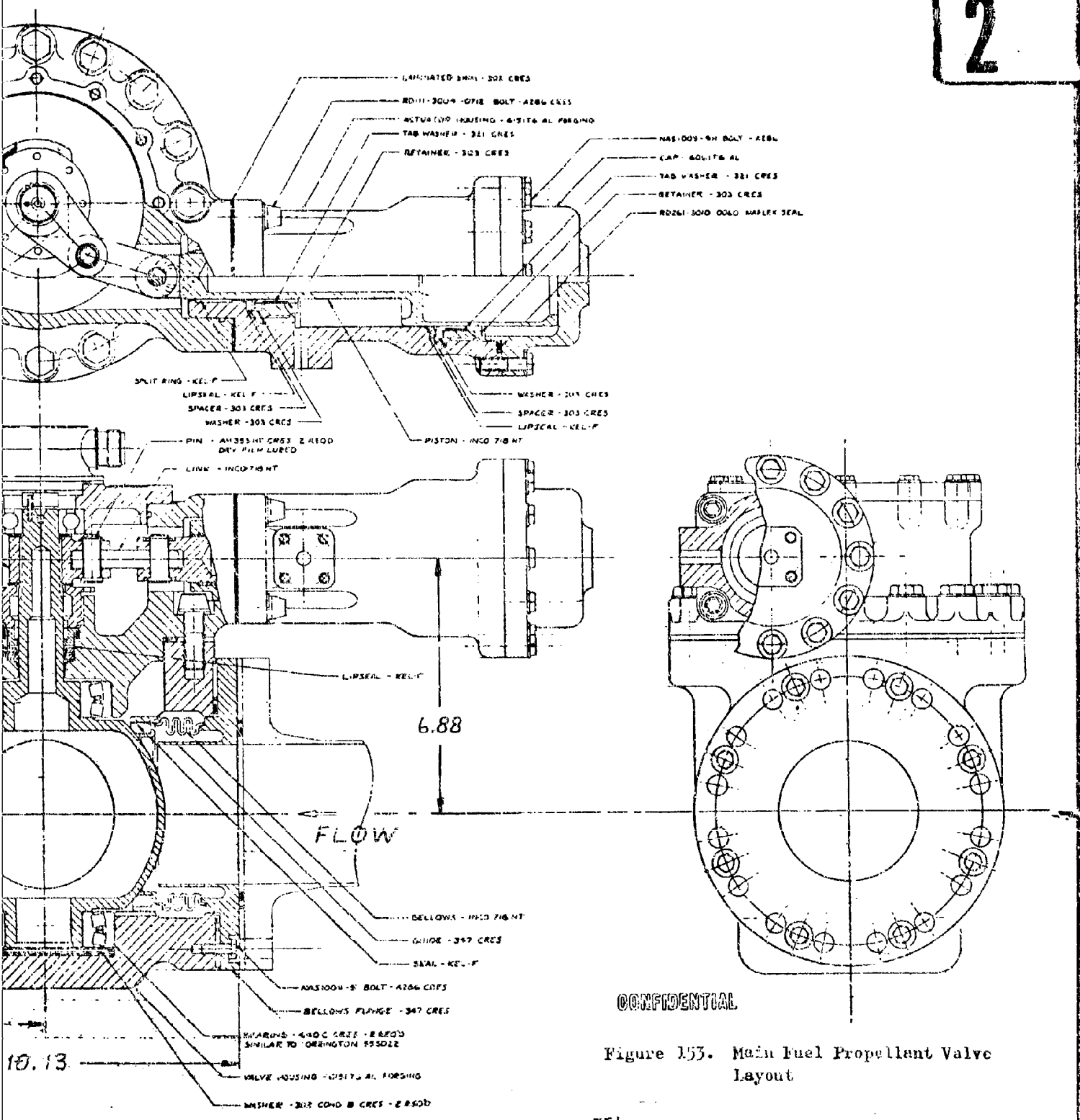

Figure 153. Main Fuel Propellant Valve Layout

(U) Each valve is oriented so as to place the bellows area downstream of the gate from the moisture source to prevent moisture from collecting in the area of the bellows and subsequent seal leakage problems. From studies of the valve locations and feed system plumbing configurations, it was determined that the most probable source of moisture for the oxidizer valve was downstream of the valve through the thrust chamber injector. On the fuel side, because the location of the fuel valve is below the pump, the major source of moisture was considered upstream of the fuel valve. Furthermore, the fuel valve is protected from downstream ambient moisture sources by the thrust chamber tube bundle. By reversing the flow direction of the fuel valve, the bellows area of each valve is thereby protected from moisture by the primary gate seal. However, for the gate seal to function satisfactorily with the new flow direction, a minor modification in the bellows seal design to change the relationship of the bellows neutral axis and the seal area on the ball was necessary. No other design modifications are required to provide for the reversed flow, and no significant change in valve performance or sealing characteristics is anticipated.

(U) Tapoff Hot-Gas Throttle Valve Alternatives. A design tradeoff study was performed to evaluate hot-gas valve types and to select the optimum configuration. Four configurations were evaluated in the study, one butterfly design, two poppet designs, and a ball or visor design.

(U) The butterfly valve design (A) consists of: (1) a flat or contoured disk that may be adjusted about an axis perpendicular to flow to close entirely or open to any desired position, (2) a gate housing, (3) an actuator mechanism, (4) a servocontrol valve, and (5) position indication feedback and instrumentation devices. A butterfly hot-gas valve has been successfully used for a similar application on the J-2 engine at a lower operating temperature.

(U) The first poppet valve design (B) consists of a poppet which is virturally pressure balanced and provides linear flow area as a function of actuator position, and indication feedback and instrumentation devices. The second poppet valve design (D) is similar to case (B) except that the poppet is of convertional type, i.e., not pressure balanced.

(U) The last design studied was a ball or visor design (C). This type of valve utilizes a hollow ball segment which is located in the housing to provide a small clearance between the housing inlet flow port and the ball. As the ball is rotated, the hole through the ball passes across a tube which is aligned with the inlet and outlet ports. Under these conditions, the visor valve reacts similarly to a blade valve, relative to its flow-area characteristics. The design features considered in the tradeoff study are tabulated and evaluated in Table 49. The higher number indicates the preferred design.

(U) The evaluation indicated a potentially higher reliability for the poppet valve because the design is basically more simple. A balanced poppet design requires a relatively small actuation force and the force does not change appreciably with ΔP. The butterfly and ball valve require rotating bearings which are subjected to loads which are a direct function of valve ΔP and, therefore, experience major changes in load and actuator force requirement. The poppet valve provides a direct connection between the actuator piston and poppet, whereas, the ball and butterfly valve require a bell crank mechanism to convert linear piston motion to rotating ball or blade motion. The poppet valve also produces a linear change in flow area as a function of actuator position, while the ball and butterfly valves have a nonlinear relationship which can be made linear only by complex contouring of the ball element or valve body. These considerations all make the poppet valve desirable from the standpoint of basic design considerations.

TABLE 49

HOT-GAS VALVE TRADE STUDY SUMMARY

	Design / Weight	Butterfly A	Pressure-Balanced Poppet B	Visor C	Simple Poppet D
Performance					
1. Linearity of Throttling	5	3	5	4	4
2. Pressure Unbalance on Throttling Element	3	1	3	2	1
3. Temperature Insulation of Servo	5	4	3	4	3
4. Vibration	5	4	3	3	3
5. Pressure Drop	10	7	6	10	5
6. Leakage, Main Valve Throttling Element	2	1	1	2	1
	30	20	21	25	17
Complexity and Problem Areas					
1. External Seals	3	1	3	0	1
2. Dynamic Seals	6	4	3	3	2
3. Bearings	5	2	5	1	5
4. Rack and Pinion or Linkage	5	2	5	2	5
5. Bellows	5	5	5	3	2
6. Sliding Surfaces	5	3	3	4	2
7. Position Indicator	5	4	3	4	3
8. State-of-Art Development, No. of Areas	8	4	6	4	5
9. Moisture and Contamination	3	2	2	1	1
	45	27	35	22	27
Cost					
1. Main Housing	4	4	2	3	1
2. Actuator	3	2	3	2	1
3. Throttling Element	3	2	3	1	2
	10	8	8	6	4
Size and Weight					
1. Size	5	3	4	3	3
2. Weight	10	7	7	6	6
	15	10	11	9	9
Total	100	65	75	62	57

NOTE: Higher number indicates a superior design

(U) The major drawback of the poppet valve is the high-pressure drop in the full-open position. Evaluation of the overall system, however, indicated that the valve can be incorporated in a converging "Y" in the hot-gas duct, and the overall system allowable pressure drop will not be exceeded. The balanced poppet valve design was therefore selected for the tapoff throttle valve.

(U) Tapoff Hot-Gas Throttle Valve Description. The tapoff hot-gas throttle valve is a pressure-balanced poppet type located in the "Y" joint of the two ducts. It is a normally open valve which is actuated by a pneumatic actuator. The actuator piston is attached directly to the poppet by a piston rod which eliminates all backlash, while pressure balance holes in the poppet minimize the control forces necessary to actuate the valve. Some contouring of the poppet is incorporated to reduce the rate of change of area with stroke as the valve approaches the closed position. The relationship of flow area and poppet position throughout the operating limits is shown in the tapoff hot-gas throttle valve drawing (Fig. 154).

(C) Material selection for the hot-gas throttle valve is limited because of the 1960 R operating temperature and 1490-psia pressure level. These conditions combined with the requirement for minimum weight dictate the use of high-temperature alloys. Hastelloy-C was chosen for the housing for good high-temperature mechanical properties and because it can be used as a casting. Stellite 21 was selected for the poppet because of its resistance to erosion with high-velocity hot gas. Stellite 21 may also be welded on the edge of the housing next to the poppet if further evaluation indicates that it is necessary. The piston rod is Rene 41, which was selected because it is somewhat easier to machine and is satisfactory for areas not directly in the flow stream. The piston rod bearing is a silver-graphite material and it also acts as the rod seal. Any gas which leaks through the bushing is bled off. The actuator is protected from the hot-gas temperature by insulation and air cavities.

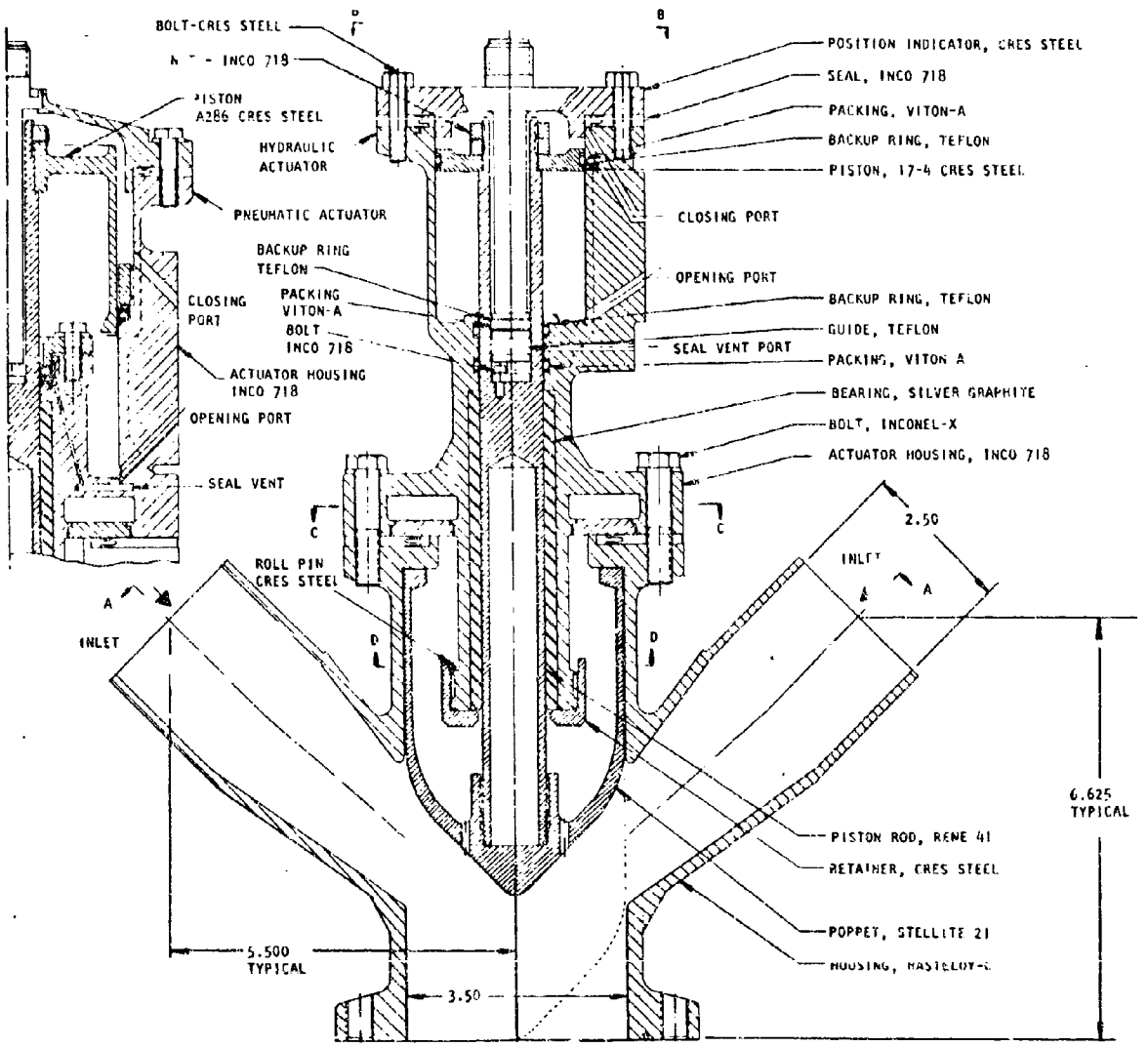

Figure 154A. Hot-Gas Tapoff Throttle Valve Assembly

(This page is Unclassified)

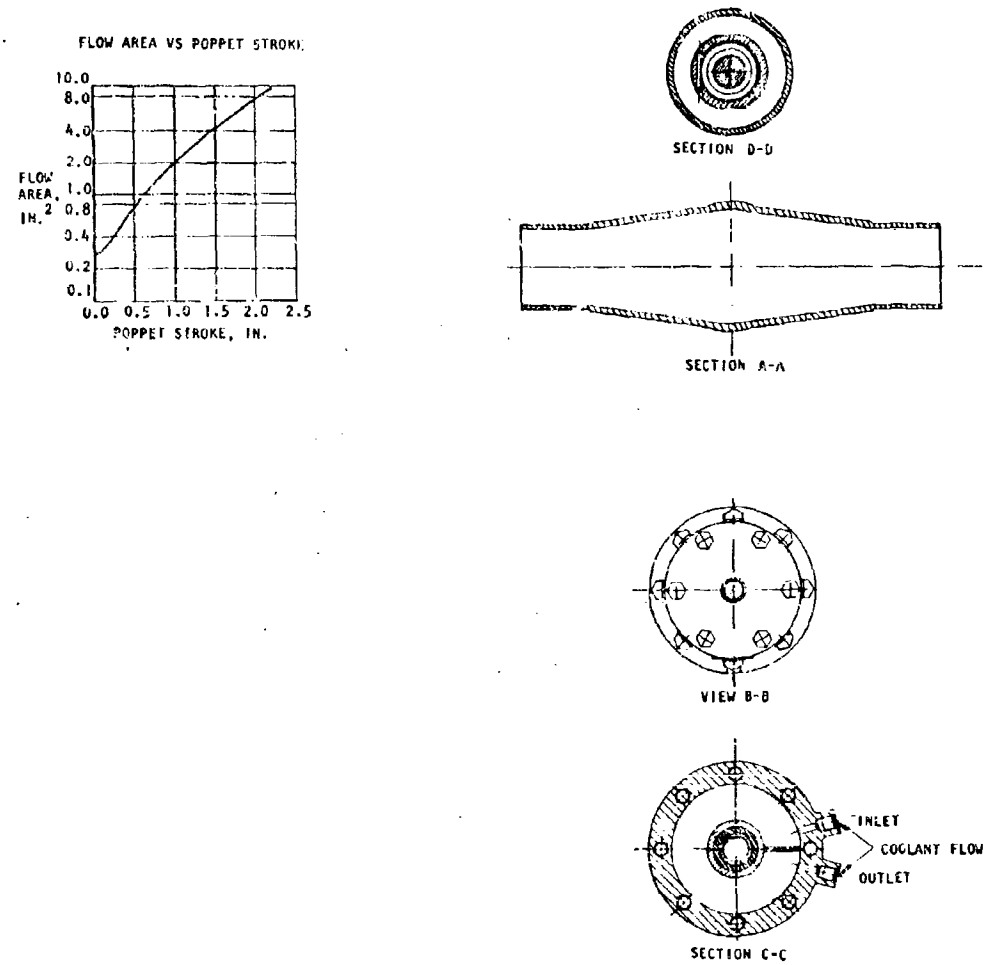

Figure 154D. Hot-Gas Tapoff Throttle Valve Assembly

(This page is Unclassified)

(U) A design layout was initiated and the maximum and minimum valve flow areas were established to meet the engine operating limits. The poppet nose was contoured to reduce turbulence as the hot gas flows around the poppet. In addition, a slight taper was incorporated to reduce the rate of change of area with stroke as the poppet approaches the closed position.

(C) Tapoff Hot-Gas Throttle Valve Analysis. Engine balance studies were performed to establish the operating requirements (flow and ΔP) for the tapoff throttle valve at 20- and 100-percent thrust through a mixture ratio range of 5:1 to 7:1. These data, presented in Fig. 155, represent the extreme operating limits for the valve. The tapoff throttle valve was designed to meet the most critical flow/ΔP relationship, which is the 100-percent thrust and 5:1 mixture ratio condition.

(C) A design study was conducted to determine the poppet and body profiles which result in a relationship between valve resistance and actuator stroke that will provide satisfactory throttling characteristics through the entire thrust and mixture ratio range. Curves showing the relationship of relative value resistance as a function of mixture ratio for 20- and 100-percent thrust are shown in Fig. 156. These data cover a mixture ratio range of 5:1 to 7:1. The relative resistance is based on the following expression:

$$\Delta P = \frac{R \dot{W}^2}{\rho}$$

where

ΔP = pressure drop, psi

R = valve resistance, $sec^2/in.^5$

$\dot{W}$ = flowrate, lb/sec

ρ = specific weight ($lb/in.^3$)

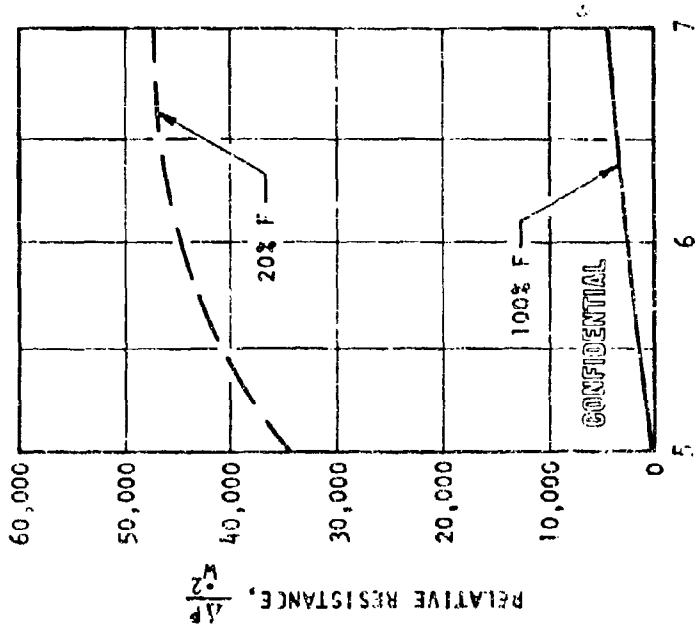

Figure 154. Tapoff Throttle Valve Relative Resistance

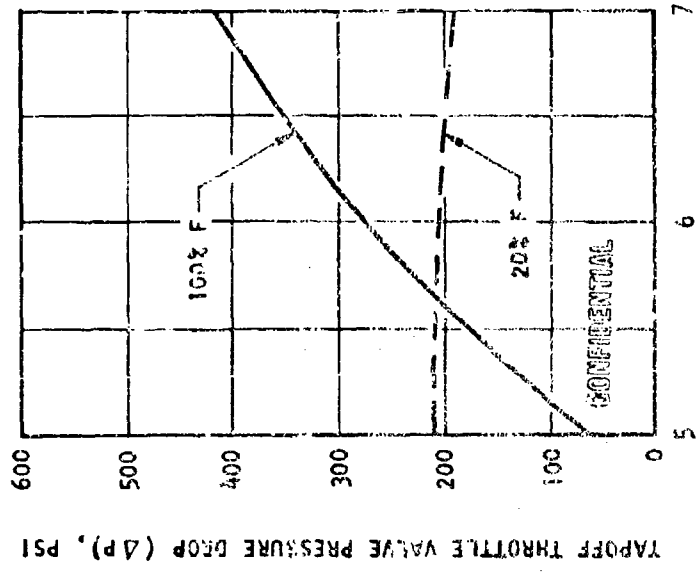

Figure 155. Tapoff Throttle Valve Pressure Drop Requirements

Because the tapoff gas properties are assumed to be constant over the entire operating range, the specific weight is directly proportional to the total pressure ($\rho = P/RT$), and a relative resistance can be computed:

$$R_{REL} = \frac{P\Delta P}{\dot{W}^2}$$

(U) This parameter is then used in the poppet design vs stroke analysis.

(C) A preliminary steady-state heat transfer analysis was made to evaluate the transient heat transfer from the poppet into the actuator. Assuming a heat transfer path through steel, the temperature at the approximate location of the actuator O-rings (assumed to be 6 inches away from a 1500 F heat source) is 81 F after 300 seconds of engine operation with an initial temperature of 70 F. After engine cutoff, this temperature will continue to rise for some time as the component tends toward temperature equilibrium. The heat transfer analysis did not include the transient effect after shutdown; however, the calculations made through cutoff appear to indicate that the maximum tolerable temperature of 350 F will not be approached, and therefore, the service life of 10 hours should not present a design problem relative to the actuator O-rings.

(U) Several areas related to the high temperature of the hot gas which should be studied further became apparent during the design. The materials required because of the high operating temperature are difficult to machine by conventional methods, which precludes the use of threads. Therefore, the joint between the piston rod and poppet cannot utilize a threaded fastener. Brazing appears to be satisfactory; however, some additional analysis is required to ensure that sufficient braze area is provided.

(U) Because the valve will operate with a high degree of throttling with high-temperature gas, erosion of the housing may be critical. This area must be analyzed thoroughly, and if necessary, a material such as Stellite 21 which is more resistant to erosion can be welded into the critical area.

(U) Heat transfer from the valve housing and poppet into the actuator may also be higher than desirable. Hydraulic fluid circulation can be provided in the facility actuator, insulation can be used wherever possible, and the configuration of the parts in the heat transfer path can be studied to optimize the heat transfer and heat-capacity relationship.

(U) Oxidizer Turbine Hot-Gas Throttle Valve Requirements. While no design study was conducted to select and lay out a configuration for the oxidizer turbine throttle valve, analysis was conducted to define the operating range of the valve. This study was similar to the tapoff throttle valve analysis and resulted in the operating requirements (ΔP and $\dot{W}$) shown in Fig. 157, and the relative resistance requirements shown in Fig. 158.

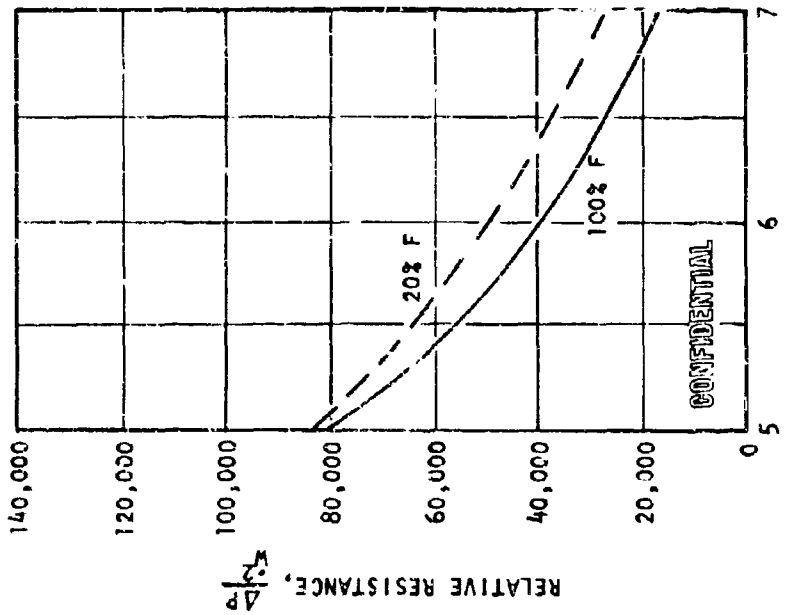

Figure 158. Oxidizer Turbine Throttle Valve Relative Resistance

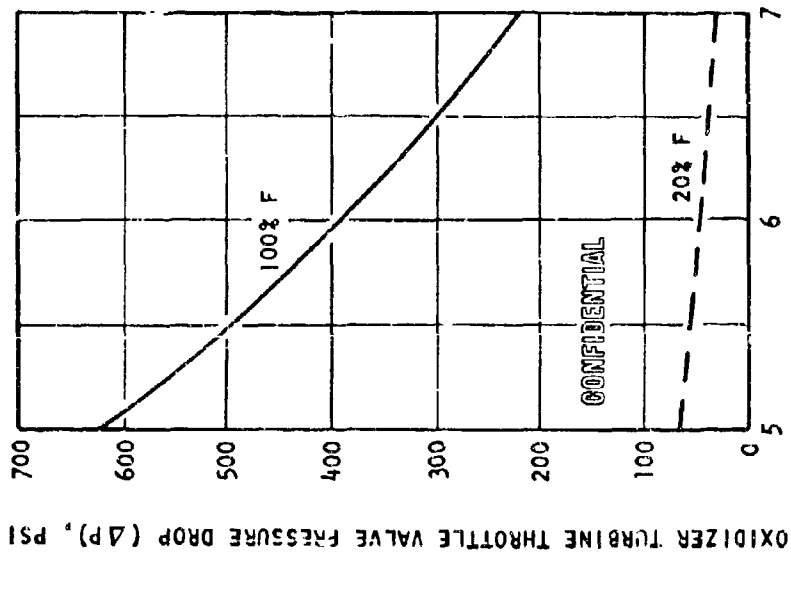

Figure 157. Oxidizer Turbine Throttle Valve Pressure Drop Requirements

FLIGHT MODULE DESIGN

Objectives and Requirements

(U) The objective of the Phase I Flight Module Design and Analysis Task was to prepare a preliminary layout of a 100-inch 250K module, which defined the basic module configuration, envelope, and weight, and to determine the predicted performance of this module. Parametric weight, performance, and envelope data were then to be generated for use in performing the Applications Study. The design was to be an advanced configuration that could result from an engineering development program subsequent to the Phase II Demonstration Program. Advanced component technologies not necessarily demonstrated during Phase I nor intended to be demonstrated during Phase II, but which were considered reasonable projections for an engineering development program, were assumed.

Summary of Work Accomplished

(U) The effort expended on this task resulted in the preparation of a preliminary layout of an advanced flight module, the calculation of the module weight, and the prediction of the module performance. Parametric weight and performance data were also predicted for thrust levels from 100K to 350K, diameters from 50 to 160 inches, and chamber pressures from 750 to 2000 psia.

Summary of Flight Module Design

(U) The Flight Module design is conceptually the same as the Demonstrator Module. The same power cycle, types of pumps and turbines, structural concept, and operational sequence are used. The preliminary layout is shown in Fig. 159.

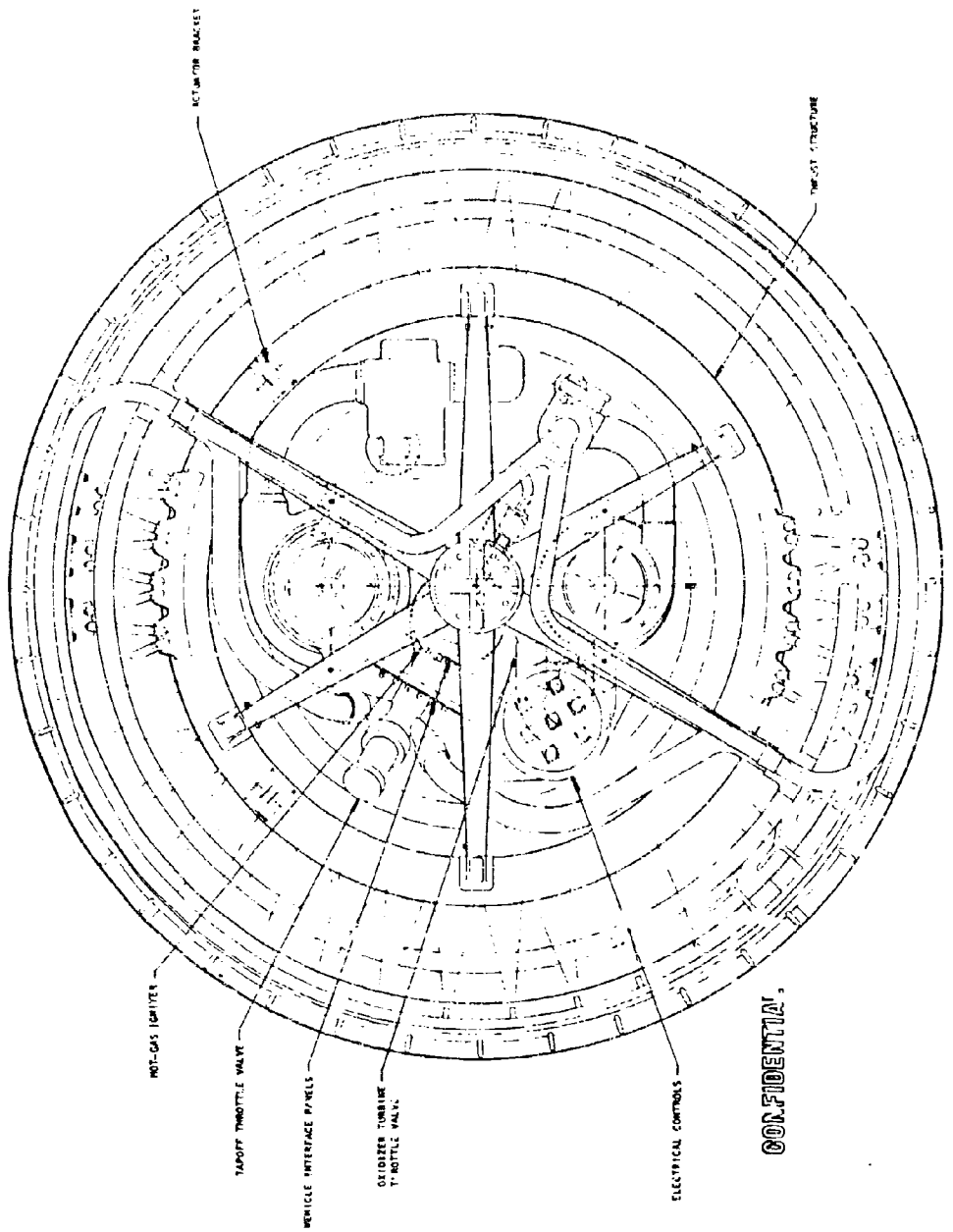

Figure 159A. 250K Flight Engine

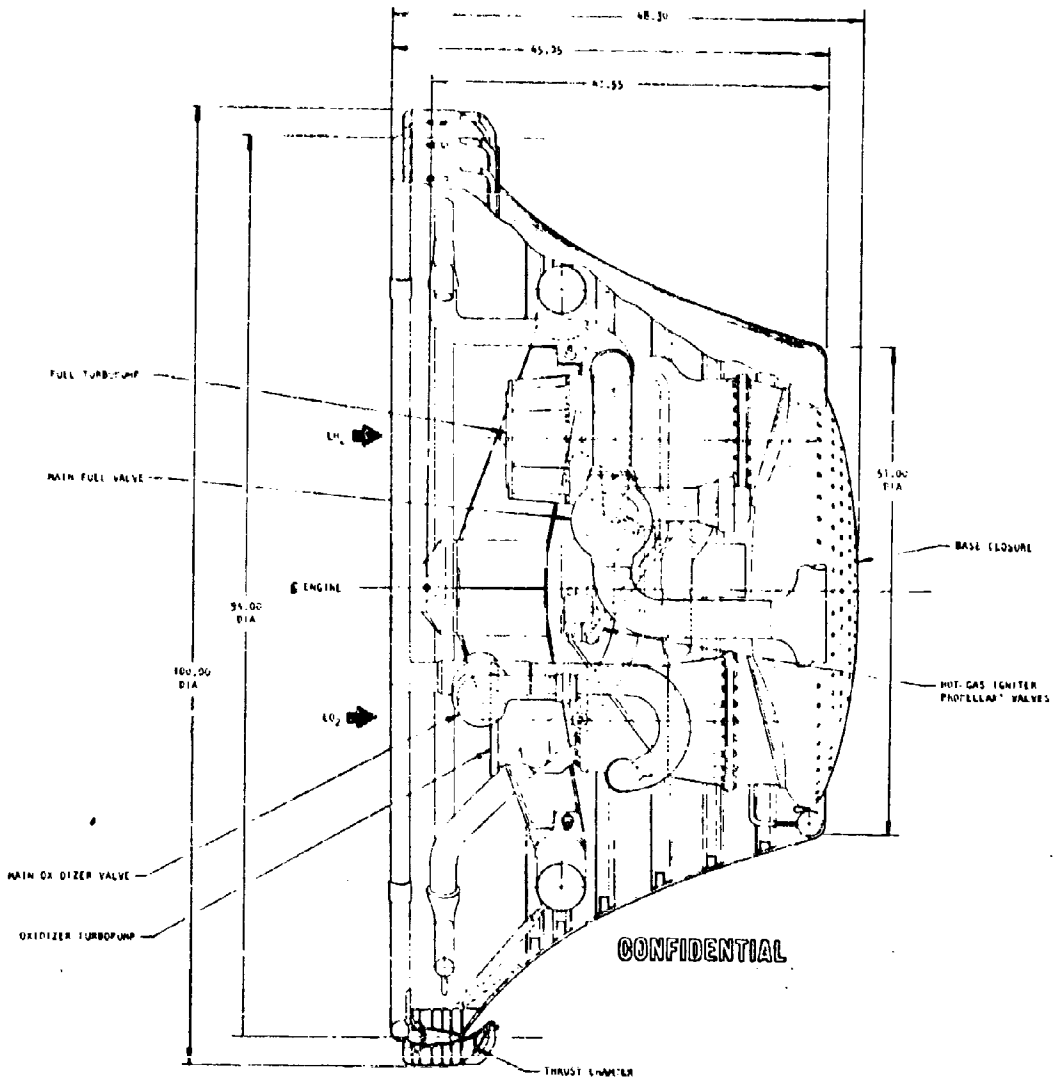

Figure 159B 250K Flight Engine

(C) The Flight Module differs from the Demonstrator Module in that nearly all subsystems and components employ welded interconnects and assemblies to minimize system weight and improve reliability. Component arrangements within the engine have been modified to reflect the technological improvements and refinements characterizing the Flight Module. The configuration thus evolved employs a greater degree of symmetry regarding propellant feed ducting, hot-gas tapoff ducting, and engine thrust mount. The separate turbine exhaust ducts are eliminated as a result of improvement modifications to the turbopumps, which allows recessing the turbopumps lower into the engine cavity, and which also aids in attaining engine thrust mount symmetry. The result is a shorter, lighter engine than the Demonstrator Module. The overall diameter remains the same at 100 inches; however, the length is reduced to 48.3 inches, and the weight is reduced to 2939 pounds. An advanced, tapered-wall combustion chamber geometry (1-1/2 by 4 inches) was evolved from the parallel wall Demonstrator Module, which permits an increase in the centerline diameter to 94.0 inches, and a resultant area ratio increase to 75.8:1.

(C) Small improvements in the turbopump efficiencies are projected which, together with advancements in other component and system designs, result in an improvement in engine specific impulse to 452.0 seconds at an engine mixture ratio of 6:1.

(C) The Flight Module configuration is projected based on a development effort designed to reach the lighter-weight component configurations and to ensure the durability life goals. Tube and segment tests conducted during Phase I have already indicated the feasibility of the 300 thermal cycles for the thrust chamber (315 operating cycles were achieved on a 2.5K segment), and turbopump seal and bearing tests have exceeded the 10-hour TBO requirement (15 hours for two sets of LO_2-lubricated bearings, and 14 hours on a hydrodynamic seal).

System Analysis

(U) Because of the changes in engine design between the Flight and Demonstrator Modules, some changes in performance have been projected.

(C) Combustion Chamber Performance. The Flight Module combustion chamber efficiency for the short-length combustor (4-inch) is estimated to be at least as high as for the longer (6-inch) Demonstrator Module. Even though past test programs have indicated that c^* efficiencies fall off slightly with shorter combustor lengths, the compact design permits regenerative cooling pressure loss reductions which can be used to provide a larger injector ΔP. This higher injector pressure drop will result in higher hydrogen injection velocities and permit atomization of the liquid oxygen to occur in a shorter distance. This improvement, combined with improved injector design as a result of the Phase II development effort, should result in combustion efficiencies at least as high as those reported for the Demonstrator Module. Therefore, the combustion efficiency of the Flight Module was predicted to be the same as the Demonstrator Module.

(C) Improved design of the combustion chamber and nozzle contour is expected to increase specific impulse of the Flight Module. The improved combustion chamber design for the Flight Module (1-1/2 by 4 inches) will allow an effective engine diameter (measured to shroud tip) of 90.5 inches, as compared to 89.5 inches for the Demonstrator Module. This results in a corresponding increase in expansion area ratio of 74.1 to 75.8. In addition, a method has been formulated to optimize further the nozzle contour and base pressure for the Flight Module.

(U) A truncated ideal contour was selected for the Demonstrator Module nozzle because the method for designing a mathematical optimum aerospike nozzle with base bleed was not developed at that time. The truncated ideal contour had been shown both theoretically and experimentally to

give high nozzle efficiencies; however, it is not an optimum configuration. Preliminary estimates indicate that a gain in thrust coefficient of 0.2 percent could be obtained from a contour which optimizes the effects of both the primary flow and the secondary flow in the base region.

(U) The method recently formulated generalizes the nozzle contour calculation method to include a nonzero base pressure in addition to the present area ratio and length constraints. The optimization procedure then used an iteration on base pressure to reach the final design. First, an optimum nozzle contour is calculated for an assumed base pressure, then the base bleed rate required to produce this pressure is computed and compared to the actual engine turbine flowrate. The procedure is repeated until the calculated required base bleed rate is found equal to the actual engine turbine flowrate, which is used as the bleed-flow in the aerospike engine.

(U) Turbomachinery Performance. The Flight Module turbomachinery concept is basically the same configuration as that of the Demonstrator Module. However, performance improvement through increased efficiencies is a major area of projected improvement for the flight turbomachinery. Improvement in turbomachinery efficiencies will require the evaluation of the major pressure leakage and power-absorbing losses in the various components. Analytical studies must be conducted, supplemented by a comprehensive test program, to improve designs where required.

(U) Table 50 shows a comparison between the Demonstrator Module pump and turbine efficiencies at the nominal operating point and the target efficiencies for the nominal operating point of the Flight Module. In order to improve turbine efficiencies, it will be necessary to experimentally isolate each of the losses and evaluate the magnitude of this

(C) TABLE 50

COMPARISON OF TURBOPUMP EFFICIENCIES FOR DEMONSTRATOR MODULE AND TARGET EFFICIENCIES FOR FLIGHT MODULE

Component	Demonstrator Module, percent	Flight Module, percent
Fuel Pumps	75	77
Oxidizer Pumps	73	75
Fuel Turbine	62	65
Oxidizer Turbine	47	55

loss experimentally and compare this value with the analytical prediction of its magnitude. In general, these losses are as follows:

1. Expansion Energy Coefficient
2. Kinetic Energy Coefficient
3. Incidence Loss Coefficient
4. Mach Number Coefficient
5. Edge Coefficient
6. Nozzle Deviation Coefficient

(U) Additional parameters are considered for evaluating the stage efficiency losses as follows:

1. Stage Work From Diagram Calculations
2. Stage Available Energy
3. Rotor Reaction
4. Nozzle Height Corrections

5. Average Rotor Height Correction
6. Tip Clearance Losses
7. Rotor Opening Coefficient

(U) The experimental determination of these various losses will be done by making surveys afer each blade row and finding the radial and circumferential variation of the static pressure and/or total pressure and the velocities including magnitude and direction.

(U) Engine Performance. The Flight Module operating characteristics (Table 51) were established utilizing the Flight Module thrust chamber and turbomachinery improvements (area ratio and efficiencies) and the same component tolerances as used in the Demonstrator Module.

(U) Parametric Data. Parametric Flight Module performance and weight data have been generated for use in applications studies which are useful in optimizing engine design and performance characteristics. The parametric data show the effect of all significant design parameters including thrust, chamber pressure, mixture ratio, and diameter (area ratio) on engine performance and weight.

(C) Parametric engine specific impulse, geometry, and weight, based on Flight Module design criteria, were generated for the combinations of parameters shown in Table 52. Over 180 curves of parametric data have been prepared. A few of these curves are presented in the following pages; the bulk of them are contained in the Special Applications Study Report, AFRPL-TR-67-269. The data presented are for a fixed design at a nominal mixture ratio of 6:1 with mixture ratio excursions made at

(C) TABLE 51

FLIGHT MODULE OPERATING CHARACTERISTICS

	Mixture Ratio, o/f=5		Mixture Ratio, o/f=6		Mixture Ratio, o/f=7	
	Rated Thrust	20% Thrust	Rated Thrust	20% Thrust	Rated Thrust	20% Thrust
Vacuum Thrust, pounds	244,100	48,700	250,000	50,000	254,700	50,860
Vacuum Specific Impulse, seconds	454.6	447.6	452.0	445.5	443.7	433.4
Chamber Pressure, psia	1500	325	1500	325	1500	325
Engine Diameter, inches	100	100	100	100	100	100
Expansion Area Ratio	75.8	81.5	75.8	81.5	75.8	81.5
Percent Length of 15-degree Cone	25	25	25	25	25	25
T/C Mixture Ratio, o/f *	5.36	5.15	6.45	6.19	7.55	7.28
Characteristic Velocity, fps	7805	7665	7553	7421	7264	7092
Thrust Coefficient	1.849	1.841	1,899	1,894	1.938	1.930
Base Pressure, psia	4.27	0.71	4.02	0.67	3.86	0.68
Sea Level Thrust, pounds	202,000		206,000		208,000	
Sea Level Specific Impulse, seconds	377		372		363	
Geometric Throat Area, $in.^2$	84.8	80.0	84.8	80.0	84.8	80.0
Engine Oxidizer Flowrate, lb/sec	447.5	90.7	474.1	96.2	502.2	102.7
Engine Fuel Flowrate, lb/sec	89.5	18.1	79.0	16.0	71.7	14.7
Thrust Chamber Thrust, pounds	235,289	47,230	241,700	48,600	246,668	49,450
Thrust Chamber LO_2 Flowrate, lb/sec	442.1	90.2	469.3	95.8	497.8	102.2
Thrust Chamber Fuel Flowrate, lb/sec	82.5	17.5	72.8	15.5	65.9	14.0
Base Thrust, pounds	8833	1471	8300	1405	7983	1410
LO_2 Pump Inlet Pressure, psia	37.5	37.5	37.5	37.5	37.5	37.5
LH_2 Pump Inlet Pressure, psia	32.0	32.0	32.0	32.0	32.0	32.0
LO_2 Pump Discharge Pressure, psia	1996	348	2060	350	2118	352
LH_2 Pump Discharge Pressure, psia	2942	601	2766	567	2642	546
LO_2 Pump Horsepower, bhp	4451	185	4865	192	5315	200
LH_2 Pump Horsepower, bhp	19,272	970	16,061	848	14,021	796
LO_2 Turbine Inlet Temperature, R	1960	1960	1960	1960	1960	1960
LH_2 Turbine Inlet Temperature, R	1960	1960	1960	1960	1960	1960
LO_2 Turbine Discharge Temperature, R	1407	1628	1382	1622	1365	1729
LH_2 Turbine Discharge Temperature, R	1295	1608	1312	1618	1327	1643
LO_2 Turbine Pressure Ratio	16.2	15.1	18.8	16.2	20.5	17.7
LH_2 Turbine Pressure Ratio	15.2	13.8	15.0	13.6	14.6	13.1
LO_2 Turbine Flowrate, lb/sec	2.7	0.19	2.8	0.19	3.0	0.29
LH_2 Turbine Flowrate, lb/sec	9.6	0.91	8.2	0.82	7.4	0.83

*Injector MR and flowrate are the same as for the engine. Differences between engine flowrates and MR above and primary nozzle shown below reflect tapoff requirements.

(c) TABLE 52

FLIGHT ENGINE PARAMETRIC DESIGN PARAMETERS

Thrust, pounds	Chamber Pressure, psia	Engine Mixture Ratio	Engine Diameter, inches
100,000	1000, 1500	5.0, 5.5 6.0, 6.5, 7.0	50, 70 80, 90
150,000	1000, 1500	5.0, 5.5, 6.0, 6.5, 7.0	55, 80 100, 110
200,000	1000, 1500	5.0, 5.5 6.0, 6.5, 7.0	60, 80, 100, 120
250,000	750, 1000, 1250 1500, 1750, 2000	5.0, 5.5, 6.0 6.5, 7.0	68.5, 80, 100 120, 130
300,000	1000, 1500 2000	5.0, 5.5, 6.0 6.5, 7.0	70, 100, 120, 140
350,000	750, 1000, 1250 1500, 1750, 2000	5.0, 5.5, 6.0 6.5, 7.0	80, 100, 120 140, 160

constant chamber pressures. Therefore, the thrust will vary with the mixture ratio excursion in a manner similar to that of the Demonstrator Module. Subsequent curve callouts of thrust refer to the design point thrust level at MR = 6:1.

(C) Figure 160 shows a plot of engine specific impulse vs engine diameter for several chamber pressures. This plot is for a vacuum thrust of 250K and engine mixture ratio of 6.0.

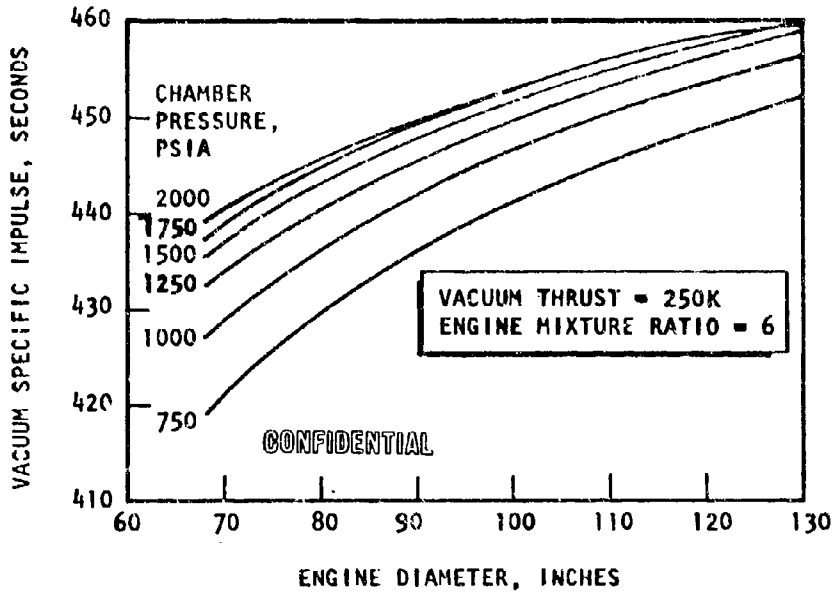

Figure 160. Specific Impulse vs Diameter

(U) The increase in parametric Flight Module performance over that shown early in the contract effort is the result of an increased area ratio achieved by a reduced chamber width and backup structure thickness, improved tapoff gas properties (discussed in the Demonstrator Module Performance subsection, page 99),and projected improvements in turbomachinery efficiencies.

(U) The thrust chamber cooling pressure drop was estimated from parametric heat transfer studies using nickel cooling tubes. This imposes certain heat transfer limits of chamber pressure and engine diameter which are reflected in the performance curves. Extension of the chamber pressure limits may be achieved by the use of beryllium-copper or other advanced tube materials.

(U) It will be noted that, for diameters above 100 inches, the performance reaches a maximum value before the maximum chamber pressure is reached. This occurs because the effect of the increased secondary flow offsets the gain in specific impulse available at the increased area ratio. Figure 161 presents a plot of nozzle area ratio vs engine diameter for parametric chamber pressure. Figure 162 shows a plot of engine length vs engine

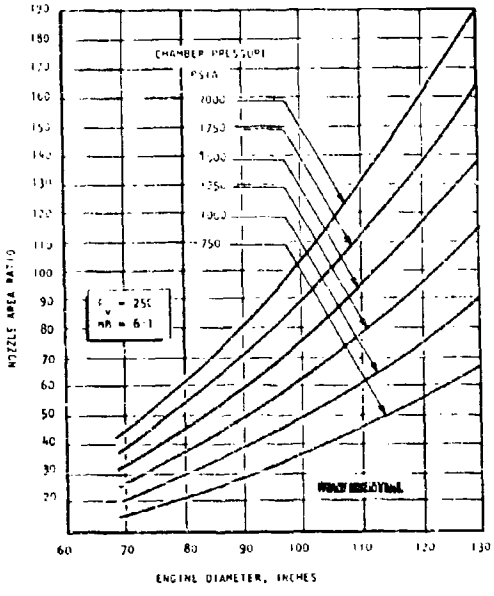

Figure 161. Effect of Engine Diameter on Nozzle Area Ratio

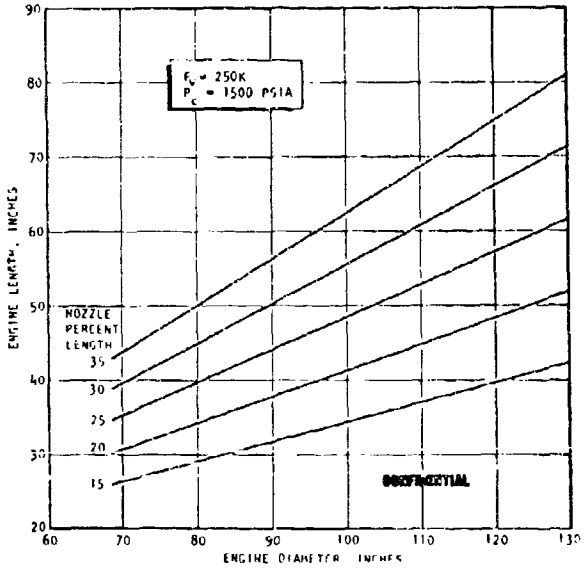

Figure 162. Engine Length vs Engine Diameter

diameter for several percent lengths. Variations in engine length with thrust, chamber pressure, and engine mixture ratio are negligible.

System Design

(U) Because the Demonstrator Module design requirements were based on expected Flight Module requirements, there is little difference between the design considerations for the two systems. The primary differences lie in a reduction in weight and an extension in the operating life of the Flight Module, with a small improvement in performance. A layout of the Flight Module was shown in Fig. 159, and the significant differences between the demonstrator and flight systems are discussed in the following paragraphs.

(U) Thrust Subsystem. The thrust subsystem is conceptually identical to the proposed demonstrator thrust subsystem and is comprised of the same basic elements. The thrust chamber assembly has the same maximum diameter of 100 inches, but the overa l length of 48.3 inches is 8.25 inches shorter than the demonstrator length. As opposed to the demonstrator thrust subsystem, the tapoff manifold is integrally welded to the injector, and the injector is attached to the combustion chamber structure by bolts passing through the 40 subsonic struts that are integrally welded to the injector.

(C) Thrust Chamber. With additional development, it is probable that the thrust chamber combustor configuration can be changed from the parrallel-wall configuration (2 inches wide by 6 inches long) to a smaller, tapered-wall design (1-1/2 inches wide at the injector by 4 inches long). This combustor geometry is an advanced concept evolved from the Demonstrator Module design and test analysis which offers improvements in weight and performance. The annular combustion chamber centerline diameter is 94.0 inches (1 inch larger than the Demonstrator Module), resulting from

the smaller combustion width. At 37.8 inches, the nozzle is 0.8 inch longer than the Demonstrator Module nozzle from throat to exit plane (slightly higher area ratio), while the exit plane diameter has been changed from 49.64 inches to 51.0 inches.

(U) The combustion chamber structure, fabricated from cast aluminum, is a smaller, refined version of the Demonstrator Module concept to provide a lighter-weight, more efficient means of supporting the combustor tube bundle. The low-pressure portion of the nozzle is supported by hoop compression bands fabricated from Inconel 718. The truss portion of the thrust mount is welded to the inner periphery of the combustion chamber structure near the throat plane rather than bolted at 40 points.

(C) The inner nozzle tube bundle still incorporates a 2:1 splice 4 inches below the throat; however, 0.008-inch wall Inconel 625 is used for the tubes below the splice, replacing the nickel tubes of the Demonstrator Module.

(C) Injector. The Flight Module injector incorporates a similar triplet orifice pattern as the Demonstrator Module; however, the injector face has been reduced from a width of 2 inches to 1-1/2 inches, and the centerline diameter increased from 93.0 inches to 94.0 inches. In contrast to the Demonstrator Module, the hot-gas passages from the tapoff ports extend through the injector to the common tapoff manifold instead of through the combustor inner-body structure, thus eliminating the hot-gas seals required on the demonstrator. The flight injector body is attached to the combustion chamber structure by the bolts passing through the 40 subsonic struts. A tapered oxidizer inlet manifold with two tangential inlets is welded to the top of the injector.

(U) Base Closure. The flight thrust chamber base closure is identical to the demonstrator with the exception of a smaller depth (11 inches as opposed to 12 inches) and relocation further into the thrust chamber cavity, which decreases overall engine length.

(U) Thrust Structure. The thrust structure for the Flight Module will be identical in concept to the demonstrator structure. The Flight Module thrust mount, however, is refined from the demonstrator in that the radial beams are arranged symmetrically (a direct result of a decrease in turbopump size), and the truss portion is welded to the periphery of the combustor inner body. The symmetrical arrangement results in a minimum weight. A spherical gimbal bearing block of the type used on the J-2 engine system rather than the nonrotating mount of the demonstrator is attached to the thrust mount hub at the engine longitudinal centerline and transmits thrust loads to the vehicle structure. The gimbal bearing allows the engine thrust vector to be varied 7 degrees in any direction from the neutral position.

(U) Propellant Feed Subsystem. The Flight Module propellant feed subsystem is comprised of the same basic components as the demonstrator subsystem. All components within the system are functionally identical to the components employed on the demonstrator and are mounted in the same manner. Component refinements and modifications have been incorporated to save weight, increase reliability, and adapt the system to vehicle operation. All components and plumbing are joined by welding, thus eliminating the bolted flange connections used on the Demonstrator Engine.

(U) The fuel and oxidizer turbopumps are shorter units than those employed on the Demonstrator Module, resulting in a decrease in engine weight and, also, allowing the fuel pump discharge manifold to be located below the thrust mount beam, which minimizes the fuel duct length and routing complexity. A 3-inch reduction in the fuel pump length was projected based

upon improved hydrodynamic passage design and reduction in the pump impeller and turbine rotor lengths. A 1-1/2-inch reduction in the oxidizer pump length was projected for similar reasons.

(U) The external line used on the demonstrator oxidizer turbopump for supplying oxidizer power to drive the low-speed preinducer turbine was replaced by an internal flow passage in the pump assembly housing, thus minimizing package envelope.

(U) The Flight Module main propellant valves differ from the Demonstrator Module valves in that they are individually sized to their respective feed line diameters and pressures, and the valve bodies are designed to provide the capability of welded assembly, thus eliminating seals and minimizing system weight. Helium pneumatic supply is used for the actuators.

(U) Turbine Drive Subsystem. The turbine drive subsystem fuel and oxidizer turbine discharge ducts formerly used on the Demonstrator Module have been eliminated by relocating the turbopumps deeper into the engine cavity. Thus, the turbines discharge directly into the base closure. All other component configurations are similar to those used on the Demonstrator Module except that welded joints replace the bolted connections.

(U) Hot-Gas Ignition Subsystem. The Flight Module hot-gas ignition subsystem is conceptually identical to the demonstrator subsystem, with the only differences being that welded connections are employed between component and subsystem interfaces, and pneumatic power is used for the valve actuators.

(U) Throttling and Mixture Ratio Control. The Flight Module control system and actuation power subsystem are functionally identical to those used on the Demonstrator Module, with the exception that pneumatic power is used for the valve actuators.

(U) Mass Properties. The Flight Module center of gravity location, moment of inertia properties, and weight are outlined below. A detail summary of module system and subsystem component weights is presented on page 380.

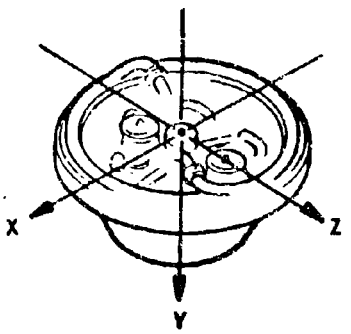

ENGINE WEIGHT, POUNDS	CENTER OF GRAVITY, INCHES			MOMENT OF INERTIA, SLUG FT^2		
	Y	X	Z	I_{YY}	I_{XX}	I_{ZZ}
2939	+10.7	+0.5	+0.3	735	624	588

(U) Weight. The Flight Module weights were projected on the assumption that development efforts and design refinements that would be impractical for the Demonstrator Module could be made for the Flight Module. For example, flanged fittings are used throughout the Demonstrator Module to reduce development cost and time. The Flight Module will have all welded fittings, resulting in a significant weight saving. Advanced technologies beyond the scope of the demonstrator program, but which could be realized in a Flight Module development program, have also contributed to a weight reduction. A comparison of the Demonstrator and Flight module weights is presented in Table 53. A summary of the basic reasons behind the indicated weight differences for each of the components is shown in Table 54.

(U) Interface and Environmental Requirements. The vehicle connection points for the module are the gimbal block, actuator attach points, propellant inlets, and the electrical and penumatic supply. The dimensional location of the required interfeces for these connections is listed in Table 55. Because the Demonstrator Module was designed to meet the Flight Module environmental conditions, no changes in design are projected in this area.

(C) TABLE 53

SUMMARY COMPARISON OF DEMONSTRATOR AND FLIGHT ENGINE WEIGHTS

	Demonstrator Engine		Flight Engine	
Thrust Subsystem	(2675)*		(1726)**	
Injector and Manifold	352		210	
Injector Clamp Rings	144		-	
Structural Tie	474		228	
Inner Body	(772)		(547)	
Inner Body Structure		258		258
Tubes and Braze		159		159
Nozzle Structure		100		100
Inlet Manifold		30		30
Outer Body	(431)		(341)	
Outer Body		267		267
Tubes and Braze		52		52
Return Manifold		22		22
Base Closure	72		72	
Tapoff Manifold	60		58	
Thrust Structure	300		270	
Attach Parts	70		-	
Turbine Drive Subsystem	(106)		(76)	
Tapoff Lines	26		23	
Inlet Duct Oxidizer Turbine	6		2	
Exhaust Duct, Turbine	18		-	
Tapoff Throttle Valve	36		34	
Oxidizer Turbine Throttle Valve	18		15	
Calibration Orifices	2		2	
Hot-Gas Igniter Subsystem	(112)		(105)	
Combustor and Injector	47		46	
Hot-Gas Distribution Manifold	33		32	
Hot-Gas Igniter Isolation Valve	28		23	
Propellant Feed Line	2		2	
Oxidizer Pressure Regulator	2		2	
Propellant Feed Subsystem	(1028)		(833)	
Oxidizer Turbopump	(343)		(258)	
Preinducer		54		43
Pump Assembly		91		76
Turbine Assembly		198		139
Fuel Turbopump	(453)		(347)	
Preinducer		41		30
Pump Assembly		204		168
Turbine Assembly		208		149
Propellant Ducting	61		59	
Propellant Flow Sensors	9		9	
Main Oxidizer Valve	60		59	
Main Fuel Valve	59		58	
Igniter Propellant Control Valve	11		11	
Mounts Turbopump	32		32	
Vent and Purge Subsystem	(29)		(27)	
Gimbal Bearing			(81)	
Controls Electrical			(39)	
Controls Pneumatic			(52)	
Total Engine Weight	(3950)		(2939)	

*Thrust chamber assembly weight (thrust subsystem minus thrust structure) = 2375 pounds
**Thrust chamber assembly weight (thrust subsystem minus thrust structure) = 1456 pounds

(C) TABLE 54

SUMMARY EXPLANATION OF DIFFERENCES BETWEEN DEMONSTRATOR AND FLIGHT ENGINE WEIGHTS

Item	Demonstrator Engine	Flight Engine
Thrust Subsystem		
Injector and Manifold	Bolt on injector, 2 x 6 inch chamber	Drop-in injector, 1.5 x 4 inch chamber
Clamp Rings	Required	Not required
Structural Tie	2 x 6 inch straight wall chamber	1.5 x 4 inch taper wall chamber
Inner Body Structure	2 x 6 inch chamber -- material, titanium 44 ksi ultimate tensile strength	1.5 x 4 inch chamber, material, aluminum 55 ksi ultimate tensile strength
Tubes and Braze	All Nickel: 0.012 wall, inner 0.010 wall, outer	Nickel to splice, 0.012 inner wall and 0.010 outer wall 625 aft of splice, 0.008 wall
Nozzle Structure	7 bands lower strength Nickel tubes	5 bands: high-strength Inconel tubes
Inlet Manifold	Low-strength material, no heat treat, constant diameter	New design; high-strength material heat treat after weld, tapered
Outer Body Structure		
Return Manifolds		Higher strength, thinner wall material
Tapoff Manifold	Constant diameter	Elimination of flanges, bolts and seals, tapered
Thrust Structure	Unsymmetrical	Symmetrical
Attach Parts	Required	Not required
Turbine Drive Subsystem		
Tapoff Line		Elimination of flanges, bolts, and seals
Inlet Duct Oxidizer		Elimination of flanges, bolts, and seals
Exhaust Ducts Turbine	Two ducts	Incorporated with turbine body
Tapoff Valve		Eliminate flanges, excess cast material removed
Oxidizer Turbine Throttle Valve		Eliminate flanges, excess cast material removed
Hot-Gas Igniter Subsystem		
Combustor and Injector	Mechanically linked valves, bolted assembly	Integrated valves, all-welded assembly
Hot-Gas Distribution Manifold		Eliminate flanges, excess cast material removed
Hot-Gas Isolation Valve		Eliminate flanges, excess cast material removed
Propellant Feed Subsystem		
Oxidizer Pump Fuel Pump		Overall component weight reduction program to be conducted on all parts
Propellant Ducting Main Oxidizer Valve Main Fuel Valve		Eliminate flanges, bolts, seals; remove excess cast material

CONFIDENTIAL

(C) TABLE 55

INTERFACE LOCATION

	X, in.	Y, in.	Z, in.
Gimbal Center	0	0	0
Gimbal Attach	0	+3.5	0
Fuel Pump	0	+9.5	+15.5
Oxidizer Pump	0	+7.5	-13.75
Actuator Attach Points	On thrust structure ring (two at 90 degrees)		
Electrical and Pneumatic	To be determined		

APPLICATION STUDY

(U) The prime objective of this study was to define a single engine module which provides a high performance index for the vehicle applications defined by the Air Force. Six vehicles were defined for a 250K vacuum thrust level (Ref. 5), and six vehicles were defined for a 350K vacuum thrust level (Ref. 6).

(C) It was concluded from this study that the common module for the 250K vehicles should have a diameter of 78 inches and a rated thrust chamber pressure of 1300 psia. Table 56 summarizes the engine and installation data of the common module in the six vehicles. The module defined in this study is truly common in that there are no changes or modifications required from vehicle to vehicle.

(C) The common module parameters for the 350K vehicles were determined to be a diameter of 96 inches and a rated thrust chamber pressure of 1370 psia. The engine and installation data summary is shown in Table 57.

(C) The parameters for optimum and common modules for all vehicles at both thrust levels are summarized in Fig. 163. In general, the lower-stage vehicle modules optimize at higher chamber pressure than the modules for the upper-stage vehicles, and the recoverable vehicle modules optimize at significantly lower chamber pressures than do those in the expendable vehicles. The optimum chamber pressure never exceeds 1900 psia. It is seen that for each case (250K and 350K), the optimum pressures are approximately the same, and as anticipated the optimum diameters are larger for the 350K modules. This same trend appears in the common modules; namely, approximately the same chamber pressure for both, and the 250K common module has a diameter of 78 inches compared to the 96 inches diameter for the 350K common module.

(C) TABLE 56

PERFORMANCE INDEX OPTIMIZATION RESULTS OF THE 250K COMMON MODULE

Parameters	Case No. 1 Expendable First Stage	Case No. 2 Expendable Second Stage	Case No. 3 Expendable Single Stage To Orbit	Case No. 4 Recoverable First Stage VTOHL	Case No. 5 Recoverable Second Stage (Pickaback)	Case No. 6 Recoverable Second Stage (Tandem)
Performance Index (W_x), pounds	229,600	62,470	40,990	299,400	76,700	37,400
Engine Description						
Vacuum Thrust, lb/engine	250,900	248,500	250,900	252,300	251,400	253,080
Number of Modules	5	1	5	8	2	1
Chamber Pressure, psia	1,300	1,300	1,300	1,300	1,300	1,300
Area Ratio	36	36	36	36	36	36
Module Diameters, inches	78	78	78	78	78	78
Module Length, inches	36	36	36	36	36	36
Mixture Ratio	6.2	5.7	6.2	6.5	6.3	6.7
I_s vacuum, seconds	439	441	439	437	438	435
I_s sea level, seconds	372	---	372	370	---	---
Vehicle Mount Height, inches	112	70	100	83	54	35
Module Gimbal Point Radius	81	---	81	107	---	---
Installation Weight (W_e), pounds	18,233	3,332	18,437	28,360	7,330	3,261
Feed System	1,945	230	1,855	3,300	845	227
Thrust Structure	2,520	396	2,780	3,142	975	328
Heat Shield	238	---	262	270	98	---
TVC System	1,300	260	1,300	2,080	520	260
Pressurization System	165	33	165	264	66	33
Instrumentation and Malfunction Detection System	315	63	315	504	126	63
Module(s)	11,750	2,350	11,750	18,800	4,700	2,350
Fairing Area (A_f), ft^2	680	---	680	1,550	1,900	222
Interstage Area (A_i), ft^2	---	577	---	---	---	574

CONFIDENTIAL

(C) TABLE 57

PERFORMANCE INDEX OPTIMIZATION RESULTS OF THE 350K COMMON MODULE

Parameters	Case No. 1 Expendable First Stage	Case No. 2 Expendable Second Stage	Case No. 3 Expendable Single Stage To Orbit	Case No. 4 Recoverable First Stage VTOHL	Case No. 5 Recoverable Second Stage (Pickaback)	Case No. 6 Recoverable Second Stage (Tandem)
Performance Index (W_x), pounds	259,500	89,800	48,450	314,800	48,910	51,380
Engine Description						
Vacuum Thrust, lb/engine	351,498	349,375	350,749	353,745	353,745	353,745
Number of Modules	4	1	4	6	1	1
Chamber Pressure, psia	1,370	1,370	1,370	1,370	1,370	1,370
Area Ratio	46	46	46	46	46	46
Module Diameter, inches	96	96	96	96	96	96
Module Length, inches	46	46	46	46	46	46
Mixture Ratio	6.2	5.9	6.1	6.5	6.5	6.5
Is vacuum, seconds	442	444	443	440	440	440
Is sea level, seconds	376	---	377	373	---	---
Vehicle Mount Height, inches	118	68	100	77	100	35
Module Gimbal Point Radius	72	---	72	102	---	---
Installation Weight (W_e), pounds	6,668	1,282	6,611	8,019	1,897	1,193
Feed System	1,722	240	1,290	2,450	465	240
Thrust Structure	2,990	598	3,330	2,623	988	509
Heat Shield	180	---	215	282	---	---
TVC System	1,384	346	1,384	2,076	346	346
Pressurization System	140	35	140	210	35	35
Installation and Malfunction Detection System	252	63	252	378	63	63
Module(s)	13,640	3,410	13,640	20,460	3,410	3,410
Fairing Area (A_f), ft^2	713	---	706	1,705	1,710	245
Interstage Area (A_i), ft^2	---	653	---	---	---	688

CONFIDENTIAL

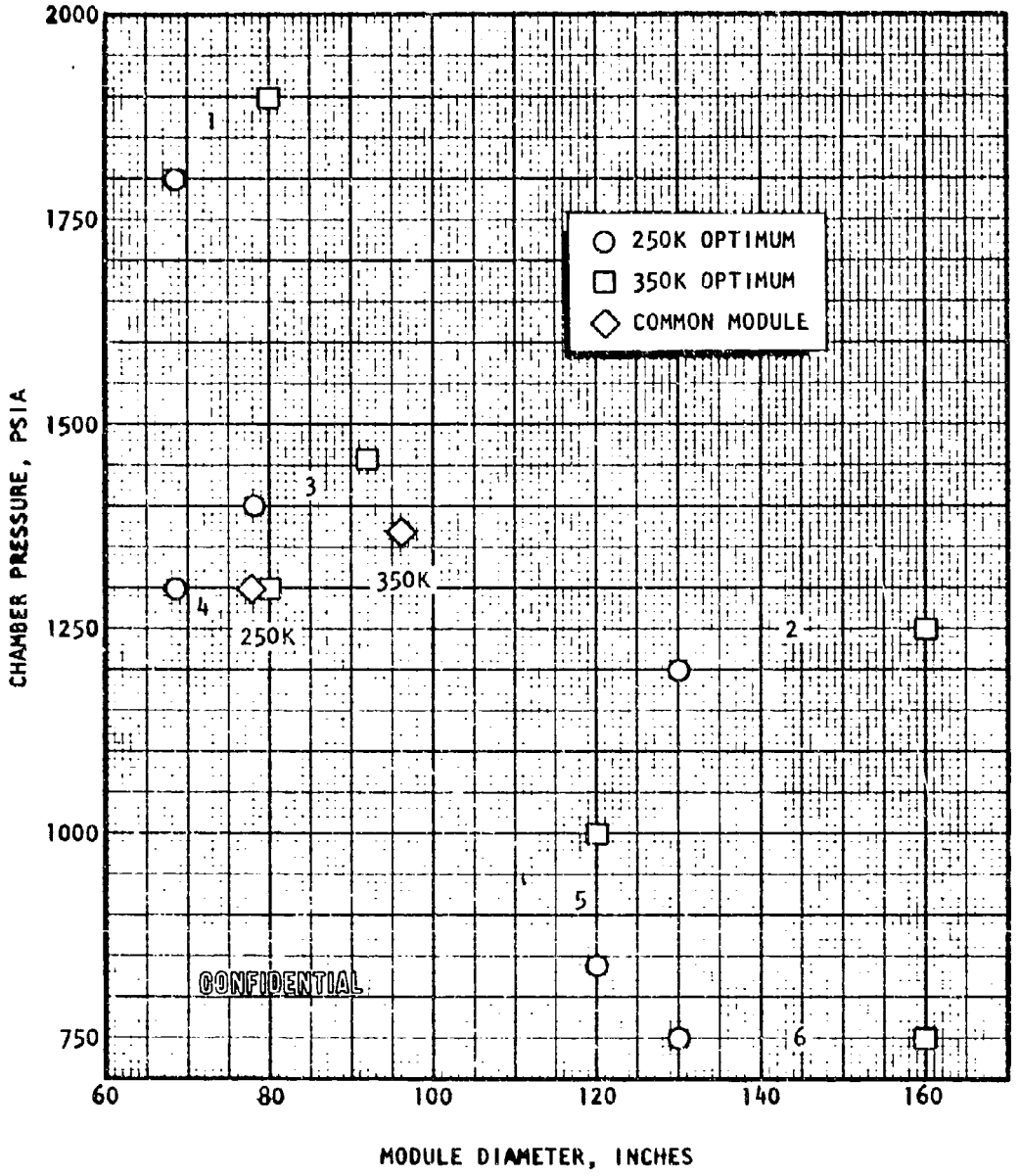

Figure 163. Application Study Parameters for Optimum and Common Modules (Six Cases), MR = 6

(U) The area ratios for the optimum and common modules are presented in Fig. 164. The area ratio for each vehicle at both thrust levels are approximately the same. This is also true for the common modules.

(U) A summary of weight, maximum diameter, and performance for the optimum and common modules is presented in Tables 58 and 59.

(U) This study has shown that performance index is quite insensitive to chamber pressure. In general a rather wide variation in chamber pressure and/or module diameter can be accommodated with a resulting performance index loss of less than one percent. An exception to this is Case 4 for both thrust levels. Even though the loss for this case is farily insensitive to a large change in chamber pressure, because of the geometry of the given configuration, a small increase in module diameter leads to a large loss in performance index. This has a strong influence on the diameter of the common module.

(C) The results of the special studies based on the selected common module for the 250K thrust class vehicles are summarized below:

1. Constant Thrust Mode in lieu of the Selected Constant Chamber Pressure Control Mode - the study indicates that when the constant vacuum thrust mode is used:
   a. The peak mixture ratio shifts slightly to a lower value
   b. There is no noticeable change in the maximum performance index
   c. The optimum operating parameters remain essentially unaffected
2. Nozzle Percent Length Variation - The study shows that the increase in performance index is extremely small as the nozzle percent length is increased from the designed value of 25 percent.

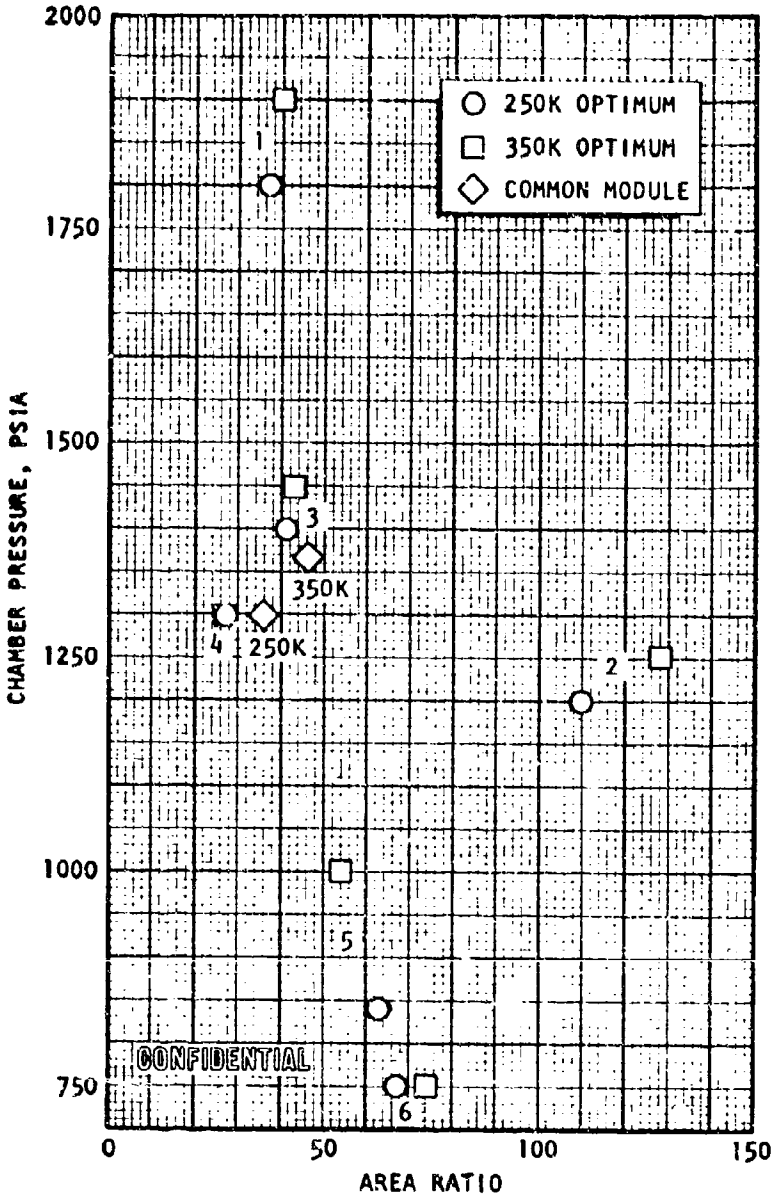

Figure 164. Area Ratio for Optimum and Common Modules, Six Cases (M.R. = 6.0)

(C) TABLE 58

250K MODULES

Parameter	Optimum Modules Case No. 1	2	3	4	5	6	Common Module
Diameter, inches	68.5	130	78	68.5	120	130	78
Chamber Pressure, psia	1800	1200	1400	1300	840	750	1300
Area Ratio	37	109	41	27	63	67	36
Weight, pounds	2600	3170	2420	2130	2450	2450	2350
I_s vacuum, seconds MR = 6.0	439	459	441	433	451	453	440
I_s sea level, seconds MR = 6.0	385	-	377	378	-	-	373
$F_{sea\ level}$, pounds MR = 6.0	220,000	-	214,000	219,000	-	-	212,000

CONFIDENTIAL

(C) TABLE 59

350K MODULES

Parameter	Optimum Modules Case No. 1	2	3	4	5	6	Common Module
Diameter, inches	80	160	92	80	120	160	96
Chamber Pressure, psia	1900	1250	1460	1300	1000	750	1370
Area Ratio	40	127	43	27	53	74	46
Weight, pounds	3660	4560	3360	2940	3260	3500	3410
$I_{s\ vacuum}$, seconds MR = 6.0	440	461	443	434	448	454	444
$I_{s\ sea\ level}$, seconds MR = 6.0	385	-	378	377	-	-	374
$F_{sea\ level}$, pounds MR = 6.0	306,000	-	299,000	304,000	-	-	294,000

3. Programmed Mixture Ratio - Small gains in performance index can be achieved in the booster vehicles through use of programmed mixture ratio. The largest potential gain in performance was realized in the single stage to orbit vehicle. In this case, the increase in performance index amounted to approximately 2 to 3 percent.

4. The Use of a Side Gas Injection Thrust Vector Control System in lieu of a Mechanical Gimbaling System - The comparative study indicates that mechanically gimbaling the engine results in the highest performance index for all vehicles.

(U) A study was conducted to determine the effect of stage weight-growth constants which were specified for each vehicle on the optimum module parameters as the constants for the recoverable vehicles approached unity. The conclusion was that as the constants approached unity the optimum chamber pressures for the recoverable vehicles approached the chamber pressures for the expendable vehicles.

(C) Listed below are the significant conclusions reached in the Phase 1, Applications Study.

1. The common 250K aerospike engine to meet all six Air Force applications should have a design chamber pressure of 1300 psia and a diameter of 78 inches. The common 350K aerospike engine should have a design chamber pressure of 1370 psia and a diameter of 96 inches.

2. There is no significant performance index advantage to increasing the 250K or 350K aerospike engine design chamber pressure to a value greater than 1500 psia for any of the six Air Force defined vehicles and missions.

3. Based on the Air Force defined missions and vehicles, there is no need to throttle the common aerospike engine deeper than 3:1, nor operate over a mixture ratio range greater than 5.7:1 to 6.7:1, except for possible propellant utilization requirements.

4. The Air Force defined reusable vehicles all require significantly lower engine chamber pressures to maximize performance index than do the expendable vehicles.